frontiers | Research Topics

Recent advances in diagnosis and treatment of brain tumors: from pediatrics to adults

Edited by
John Bianco, Dimitrios N. Kanakis, Cesare Zoia,
Archya Dasgupta and Majaz Moonis

Published in
Frontiers in Oncology
Frontiers in Neurology
Frontiers in Pediatrics

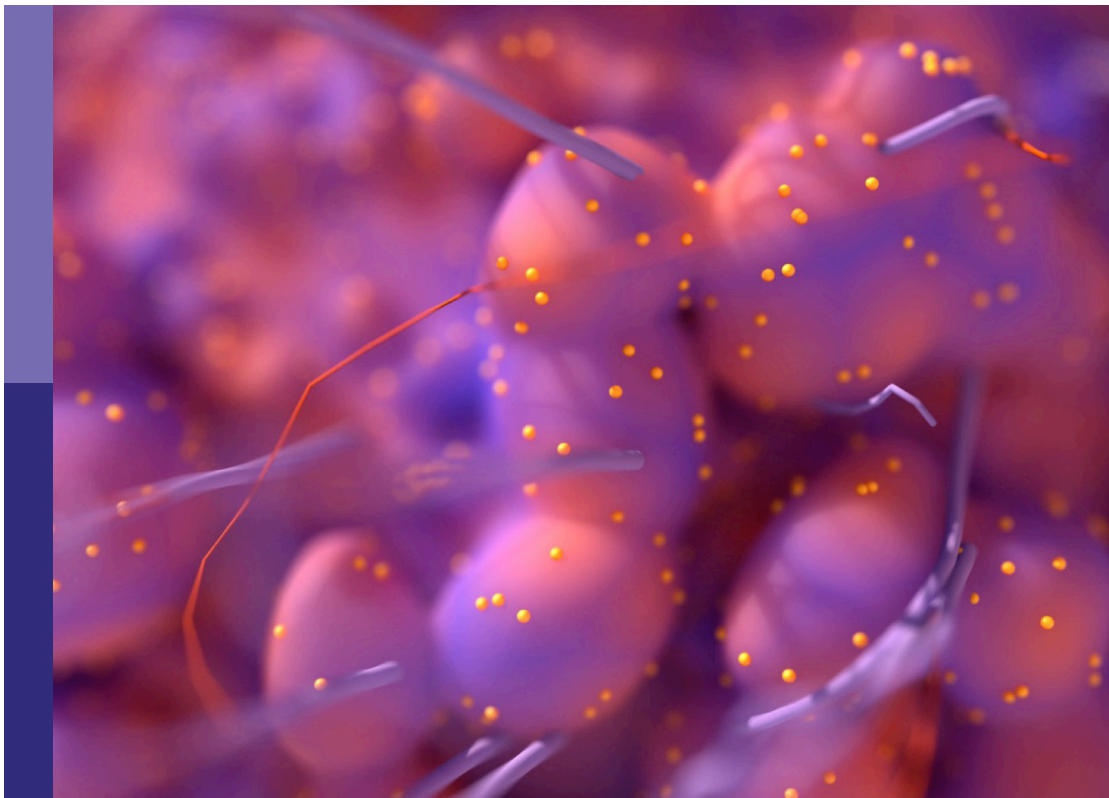

ISSN 1664-8714
ISBN 978-2-8325-6438-7
DOI 10.3389/978-2-8325-6438-7

About Frontiers

Frontiers is more than just an open access publisher of scholarly articles: it is a pioneering approach to the world of academia, radically improving the way scholarly research is managed. The grand vision of Frontiers is a world where all people have an equal opportunity to seek, share and generate knowledge. Frontiers provides immediate and permanent online open access to all its publications, but this alone is not enough to realize our grand goals.

Frontiers journal series

The Frontiers journal series is a multi-tier and interdisciplinary set of open-access, online journals, promising a paradigm shift from the current review, selection and dissemination processes in academic publishing. All Frontiers journals are driven by researchers for researchers; therefore, they constitute a service to the scholarly community. At the same time, the *Frontiers journal series* operates on a revolutionary invention, the tiered publishing system, initially addressing specific communities of scholars, and gradually climbing up to broader public understanding, thus serving the interests of the lay society, too.

Dedication to quality

Each Frontiers article is a landmark of the highest quality, thanks to genuinely collaborative interactions between authors and review editors, who include some of the world's best academicians. Research must be certified by peers before entering a stream of knowledge that may eventually reach the public - and shape society; therefore, Frontiers only applies the most rigorous and unbiased reviews. Frontiers revolutionizes research publishing by freely delivering the most outstanding research, evaluated with no bias from both the academic and social point of view. By applying the most advanced information technologies, Frontiers is catapulting scholarly publishing into a new generation.

What are Frontiers Research Topics?

Frontiers Research Topics are very popular trademarks of the *Frontiers journals series*: they are collections of at least ten articles, all centered on a particular subject. With their unique mix of varied contributions from Original Research to Review Articles, Frontiers Research Topics unify the most influential researchers, the latest key findings and historical advances in a hot research area.

Find out more on how to host your own Frontiers Research Topic or contribute to one as an author by contacting the Frontiers editorial office: frontiersin.org/about/contact

Recent advances in diagnosis and treatment of brain tumors: from pediatrics to adults

Topic editors

John Bianco — Princess Maxima Center for Pediatric Oncology, Netherlands
Dimitrios N. Kanakis — University of Nicosia, Cyprus
Cesare Zoia — San Matteo Hospital Foundation (IRCCS), Italy
Archya Dasgupta — Advanced Centre for Treatment, Research and Education in Cancer (ACTREC), India
Majaz Moonis — UMass Memorial Medical Center, United States

Citation

Bianco, J., Kanakis, D. N., Zoia, C., Dasgupta, A., Moonis, M., eds. (2025). *Recent advances in diagnosis and treatment of brain tumors: from pediatrics to adults*. Lausanne: Frontiers Media SA. doi: 10.3389/978-2-8325-6438-7

Table of contents

frontiers | Frontiers in Neurology

TYPE Editorial
PUBLISHED 27 May 2025
DOI 10.3389/fneur.2025.1606149

OPEN ACCESS

EDITED AND REVIEWED BY
David D. Eisenstat,
Royal Children's Hospital, Australia

*CORRESPONDENCE
Cesare Zoia
✉ gioiaoffice@gmail.com

RECEIVED 04 April 2025
ACCEPTED 12 May 2025
PUBLISHED 27 May 2025

CITATION
Bianco J, Kanakis DN, Dasgupta A, Moonis M and Zoia C (2025) Editorial: Recent advances in diagnosis and treatment of brain tumors: from pediatrics to adults.
Front. Neurol. 16:1606149.
doi: 10.3389/fneur.2025.1606149

Editorial: Recent advances in diagnosis and treatment of brain tumors: from pediatrics to adults

John Bianco[1], Dimitrios N. Kanakis[2], Archya Dasgupta[3], Majaz Moonis[4] and Cesare Zoia[5]*

[1]Image Sciences Institute, University Medical Center Utrecht, Utrecht, Netherlands, [2]School of Medicine, University of Nicosia, Nicosia, Cyprus, [3]Advanced Centre for Treatment, Research and Education in Cancer (ACTREC), Mumbai, India, [4]UMass Memorial Medical Center, Worcester, MA, United States, [5]Unit of Neurosurgery, Department of Surgical Sciences, San Matteo Hospital Foundation (IRCCS), Pavia, Italy

KEYWORDS

brain tumor, neuro oncology, pediatric neurosurgery, diagnosis, treatment

Editorial on the Research Topic
Recent advances in diagnosis and treatment of brain tumors: from pediatrics to adults

Introduction

In the last few years, an impressive development has been achieved in the arena of new diagnostic and therapeutic approaches for brain tumors, both in children and adults. This has in turn led to the recognition of new tumor entities as well as to better categorization of the existing ones. The recent WHO classification of the CNS tumors (2021) has been entirely revised, and the term "integrated diagnosis" has since been applied, which refers to a combination of the classical histopathological diagnosis with the accompanying molecular results of some of the most common tumors. In addition, further progress has been made in the field of imaging, with the invention of more accurate methods and the improvement of previously established diagnostic modalities. As a result of the aforementioned achievements in the diagnosis of brain tumors, new treatment options have been introduced, cultivating in improved therapeutic response in several tumor entities.

Due to the immense progress not only in the field of diagnosis but also in the treatment of brain tumors, it is of utmost importance to present newly identified biomarkers and innovative techniques, which allow on the one hand more accurate diagnoses and on the other hand more precise therapeutic interventions. Since much research is conducted at present with this regard, the result of these investigations should be shared with the broader research community, in order to improve thereafter both the available diagnostic methods in the fields of histopathology and imaging and the therapeutic techniques in the areas of neurosurgery and chemo-/radio-therapy. Undoubtfully, this will contribute to accomplishing the target of "personalized medicine" in the public. This Research Topic assembles 23 contributions—spanning original research, reviews, case reports, methods, and clinical trials—to illuminate the multidisciplinary frontiers of brain tumor science, bring together new discoveries in the diagnosis and therapy of pediatric and adult brain

tumors, where the evolving landscape of glioma management continues to integrate innovative diagnostic tools and therapeutic strategies.

Evaluating biomarkers distribution, surgical intervention, and magnetic resonance spectroscopic imaging in the prognosis, differentiation, and diagnosis of brain tumors

According to Hu and Zhang, advanced multiparametric MRI (DSC, DWI, DTI, MRS) had the potential to non-invasively predict Ki-67 labeling index, a marker of tumor proliferation, in a cohort of 109 glioma patient. Their model, combining rCBVmax, rCBFmax, rADCmin, rFAmax, and Cho/Cr ratio, achieved high accuracy ($R^2 = 0.80$), correlating with tumor grade. This approach could enhance preoperative planning by identifying high-proliferation gliomas, predicting prognosis before surgery, though validation in larger cohorts is needed. In another study by Yang et al., the cost effective diagnostic potential of peripheral blood parameters, including neutrophil-lymphocyte ratio (NLR), systemic immune-inflammation index (SII), and pan-immune-inflammation value (PIV), where gliomas could be distinguished from benign tumors, underscores their role in malignancy assessment. Supplementing these two studies, Lange et al. identified a 7-gene glutamatergic panel differentiating glioblastomas (GBMs) from brain metastases with 88% accuracy. Although larger validation is needed, this tool could supplement pathology in ambiguous cases, reducing reliance on invasive biopsies. Guo et al. developed a scoring system predicting ventriculoperitoneal shunt need post-pediatric tumor resection. They show that factors such as age (< 3 years), midline location, preoperative hydrocephalus, and total resection stratify risk, aiding postoperative monitoring, providing a practical evaluation. Scores ranging from 6 to 14 points indicate high risk, while the model also emphasizes blood loss as a novel, objective predictor linked to inflammation and CSF dynamics. The grim prognosis of diffuse intrinsic pontine gliomas (DIPGs), nowadays referred to as diffuse midline gliomas (DMGs) was reinforced by Boukaka et al., showing that benign brainstem tumors treated surgically display a survival rate of over 90%, compared to 3-year survival of just 2% for diffuse pontine gliomas. While stereotactic biopsy is not part of the standard of care in DMG of the pons, the heterogeneity of this disease advocated their use in providing critical on molecular and genetic characteristics that can guide treatment decisions, including entry into clinical trials. They advocate for individualized treatments based on molecular profiling to guide emerging therapies, stressing the urgency for targeted drug development, and highlighting the balance between aggressive resection (for benign lesions) and quality of life, and more biomolecular and genetic research for DMG. Future efforts must prioritize validating these tools in diverse cohorts and integrating molecular data into clinical algorithms, ensuring precision medicine becomes a tangible reality for glioma patients.

Clinical trials assessing feasibility, efficacy and benefit of therapies in glioblastoma and craniopharyngioma

Two clinical trials presented in this Research Topic explore adjuvant strategies in glioma treatment, addressing duration of standard therapy and novel drug repurposing. Anvari et al. challenges the utility of extended temozolomide dosing (12 vs. 6 cycles) in high-grade gliomas. Despite comparable survival rates, the authors demonstrate that extended therapy showed no survival benefit, as well as lower completion rates, where toxicity, cost, and potential reduced salvage response underscore 6 cycles as standard. However, molecularly defined subgroups may warrant tailored approaches, necessitating further study. Pace et al. investigate drug repurposing, where they evaluated chlorpromazine combined with temozolomide in unmethylated MGMT GBM. In a phase II clinical trial, a median progression free survival of 8 months was achieved (vs. historical 5 months), with an overall survival of 15 months, meeting primary endpoints. They also found that the safety profile of chlorpromazine was manageable, and its repurposing to disrupt neuron-GBM signaling and therapeutic resistance merits phase III evaluation. What these studies do is to highlight the need of optimizing existing protocols, and the importance of exploring repurposed drugs to overcome resistance in glioma therapy. Similarly, in their brief research report, Hedrich et al. retrospectively document the feasibility of intracystic treatment with peginterferon alfa-2a in five patients (4 patients <12 years, 1 adult patient) with cystic craniopharyngioma, observing cyst reduction with minimal toxicity, while also reducing hospital visits. Although some challenges such as cyst leakage need to be addressed, this approach aligns with the paradigm of treating craniopharyngioma as a chronic condition, prioritizing quality of life over aggressive interventions.

Rare cases of CNS tumors and the importance of molecular profiling

The diagnosis and management of central nervous system tumors presents unique challenges, frequently requiring integration of advanced molecular profiling and multidisciplinary collaboration. Recent case reports presented in this Research Topic highlight these complexities, offering insights into diagnostic pitfalls, molecular advancements, and therapeutic strategies. Liu et al. present a case of intraventricular Rosai-Dorfman disease (RDD), a rare histiocytic disorder, in a young patient with no recurrence at 10-year follow-up following resection. Six similar cases in the literature were reviewed and showed that, although treatment guidelines for RDD have not been established, individualized surgical interventions and vigilant postoperative monitoring offer a favorable prognosis for this rare condition. The authors highlight the importance of considering RDD, though rare, in the differential diagnosis of intraventricular masses in pediatric patients. Wu et al. present a case of pleomorphic xanthoastrocytoma (PXA, WHO 2) with an NTRK fusion and a CDKN2A deletion in a 2-year-old patient with spontaneous intracranial hemorrhage. This case is one of few pediatric PXA reports that offers molecular profiling

and illustrates the role of genomic testing in identifying targetable alterations, while underscoring hemorrhage as a rare presentation of low-grade gliomas. A case of synchronous IDH-NOS grade II (frontal) and IDH-mutant grade IV (parietal) astrocytomas is presented by Jia et al., which challenges the norms of glioma progression through molecular analysis revelations of divergent clonal origins, where an EGFR amplification in the parietal lesion was observed. This case highlights the necessity of comprehensive molecular workup in multifocal gliomas to inform surgical and adjuvant strategies. Edelbach et al. presents a case of glioblastoma in the brainstem, the diagnosis of which relied on molecular profiling after inconclusive biopsy. Although radiotherapy with concomitant and adjuvant temozolomide improved symptoms, this report stresses the dismal prognosis of infratentorial GBM and highlights the challenges of managing diffuse primary pontine glioblastoma, stipulating the need for more effective treatment options for this rare subtype of GBM. In another study, the Todai OncoPanel was used to analyse recurrent meningioma, revealing NF2 loss, CDKN2A deletion, and subclonal TRAF7 mutations. Ohara et al. highlighted the limitations of current meningioma therapies by showing that although high-risk markers were identified with this panel, no actionable targets were found. This case study advocates for expanded molecular panels and trials targeting pathways like PI3K or CDK inhibitors. A case of polymorphous low-grade neuroepithelial tumor of the young (PLNTY), harboring a FGFR3-TACC3 fusion and a TERT promoter mutation, was presented by Golub et al. showing that this entity mimics high-grade glioma in histological and molecular features. This case emphasizes the need for attentive follow-up of low-grade lesions such as PLNTY and the diagnostic value of methylation profiling to help elucidate the role and timing of adjuvant treatment. Consoli et al. presents two GBM cases which were misdiagnosed as autoimmune encephalitis due to atypical MRI features and false-positive onconeural antibodies, but later confirmed as GBM following biopsies prompted by unresponsiveness to immunosuppression treatment. This report warns against overreliance on serological markers in atypical presentations and advocates early biopsy in ambiguous cases. These case studies highlight that there is a need to prioritize efforts in validating molecular biomarkers in clinical trials, to expand targeted therapies, and to refine guidelines for rare entities. As molecular diagnostics evolve, so too must therapeutic paradigms, ensuring precision medicine transcends common tumors to address the full spectrum of CNS malignancies. For both pediatric DIPG/DMG and adult GBM, the future hinges on bridging diagnostic accuracy with innovative treatments, ensuring aggressive interventions are balanced against quality of life and the promise of tailored therapies.

Reviewing technological advancements and patient centricity in diagnosing and treating CNS malignancies

The evolving landscape of neuro-oncology demands innovative diagnostic and therapeutic strategies, particularly for rare or complex CNS tumors. This Research Topic also contains a number of reviews that shed light on critical advancements, highlighting that improved outcomes can be achieved by integrating technology, molecular insights, and patient-centered care. Through a bibliometric analysis of 179 studies from the Web of Science core database, Abudueryimu et al. reveal the pivotal role of MRI surgical planning and recurrence monitoring following spinal schwannoma diagnosis, while highlighting disparities in terms of research quality between Eastern and Western institutions. They point out that while China leads in publication volume, institutes in Europe and America dominate in citation impact. To bridge quantity and quality, future efforts must prioritize standardized imaging protocols and translational studies to refine feature analysis, enhancement studies, and quantitative assessments. Progress in these domains raises the bar for diagnostic and therapeutic approaches for spinal intradural schwannomas, improving patient care and outcomes. Yu et al. performed a meta-analysis comparing [^{1}8F]FET and [^{1}8F]FDOPA PET for glioma recurrence diagnosis. They found that while both demonstrate similar specificity, [^{1}8F]FDOPA shows superior sensitivity, attributed to its dual targeting of dopamine pathways and amino acid metabolism, although sample sizes were limited. As limited availability and higher costs hinder widespread adoption of [^{1}8F]FDOPA, the authors advocate using hybrid approaches combining PET's molecular sensitivity with MRI's anatomical specificity. A narrative review by Chen et al. explores the evolving landscape of treatment efficacy of the complex intracranial tumor adamantinomatous craniopharyngioma. The take home message of this review is that alternative approaches for sustained disease control, such as subtotal resection paired with radiotherapy, which achieves comparable tumor control with fewer complications, could pose a paradigm shift away from radical resection, while emerging targeted therapies and cyst-directed treatments offer promise. Namiot et al. investigated brain tumor diagnosis by exploring the potential of *in situ* hybridization (ISH) techniques. By cross-referencing 513 records with the OMIM database, a large number of mutations suitable for ISH were pinpointed, such as amplifications in EGFR, MDM2, and MDM4, and deletions of PTEN, CDKN2/p16, TP53, and DMBT1 that correlate with poor prognosis in glioma patients, as well as other chromosomal anomalies across different non-glioma brain tumors. Though highlighting the potential of this technique in diagnosing and prognosticating various brain tumors, the authors concede that while ISH enhances subclassification, its inability to resolve small mutations limits standalone use, urging integration with next-generation sequencing for comprehensive profiling. Many therapeutics fail in the clinic because of the blood-brain barrier (BBB) disallowing chemo-/immune-therapies to reach the target site. Recent research analyzing the application of ultrasound for therapeutic purposes has highlighted the role of focused ultrasound (FUS) as a treatment modality for gliomas, as presented by Nwafor et al.. FUS has emerged as a dual tool for thermal ablation and blood-brain barrier disruption (BBBD), enhancing chemotherapeutic delivery beyond the BBB. While challenges remain and further investigation is still needed, early clinical trials show promising results in enhanced drug delivery in brain tumors using this non-invasive approach. The reviews outlined above map a path forward where technology and patient-centricity converge,

urging clinicians and researchers to embrace multidisciplinary collaboration for transformative progress in neuro-oncology.

Liquid biopsies and artificial intelligence for identifying tumor burden and monitoring progression

Technological advancements that promise to refine diagnostics, enhance treatment efficacy, and support clinical decision-making continue to evolve, where novel strategies such as liquid biopsies and artificial intelligence (AI) integration underline the field's trajectory toward precision medicine. Barber et al. investigated techniques for enriching circulating tumor cells (CTCs) by comparing four CTC enrichment methods to address GBM's diagnostic challenges. The authors found that the ScreenCell® system emerged as the most viable for clinical use due to its simplicity, speed, and biomarker-agnostic approach, achieving CTC isolation via size-based filtration, with minimal cell loss, while having compatibility with downstream analysis. Dheepak et al. introduce a novel imaging framework that integrates Gray-Level Co-occurrence Matrix (GLCM) and Local Binary Pattern (LBP) features, augmented by interaction features derived from their outer product. By using this approach in classifying gliomas, meningiomas, and pituitary tumors using a linear SVM classifier, they were able to achieve an accuracy rate of 98.84%. These methods have the potential to improve the precision of medical image processing significantly, in turn assisting clinicians to provide more accurate diagnoses and treatments for brain tumors. Along these lines, Mut et al. explored the role of AI in GBM surgery, highlighting its strengths in tumor segmentation and resection extent prediction via radiomics and connectomics. However, the authors go on to report that predicting post postoperative outcomes was limited due to data variability and less quantifiable patient-related factors. As such, they advocate for standardized datasets, multimodal imaging integration, and ethical AI frameworks, and conclude that while AI can aid in training, it cannot yet replicate the nuanced judgment of experienced neurosurgeons.

Conclusions and future perspectives

This Research Topic combines 23 studies spanning diagnostics, therapeutics, and emerging technologies in neuro-oncology, emphasizing the multidisciplinary advances in brain tumor diagnosis and therapy and progress toward precision medicine. Key advancements include non-invasive diagnostic tools that can predict glioma proliferation, differentiate gliomas from benign tumors, and provide molecular profiles that further refine diagnostics. Therapeutic innovations also challenge conventional protocols, questioning the benefit on overall survival of extended treatment in patients with newly diagnosed GBM, advocating for molecularly tailored approaches. Repurposing of drugs was also shown to hold promise by demonstrating improved progression free survival in unmethylated MGMT GBM, warranting further phase III trials. For rare tumors, adapted treatment protocols, prioritizing quality of life over aggressive surgery, has been shown to be effective and well tolerated. The complexity of diagnosis, where different entities can give rise to ambiguities, shows the need for advancing genomic testing and molecular profiling, where imaging, liquid biopsies and artificial intelligence have emerged as potentially transformative tools for tumor classification and intraoperative decision-making. Drug delivery enhancement through FUS mediated BBB-opening could increase efficacy, reduce toxicity, and improve overall quality of life. These studies collectively promote the shift toward minimally invasive diagnostics, targeted therapies, and data-driven tools, where molecular insights can be integrated with multidisciplinary care, balancing aggressive intervention with patient-centered outcomes. While challenges such as validation requirements, lack of druggable targets for rare subtypes, as well as cost barriers and availability remain, technological breakthroughs in neuro-oncology as outlined in this Research Topic can bridge the gap between innovation and impactful outcomes, delivering innovation and cutting-edge therapies that bring the field closer to personalized medicine for both common and rare CNS malignancies.

Author contributions

JB: Writing – review & editing, Writing – original draft. DK: Writing – original draft, Writing – review & editing. AD: Writing – review & editing, Writing – original draft. MM: Writing – original draft, Writing – review & editing. CZ: Writing – original draft, Writing – review & editing.

Conflict of interest

The authors declare that the research was conducted in the absence of any commercial or financial relationships that could be construed as a potential conflict of interest.

Publisher's note

frontiers | Frontiers in Oncology

TYPE Case Report
PUBLISHED 24 August 2023
DOI 10.3389/fonc.2023.1254674

OPEN ACCESS

EDITED BY
Cesare Zoia,
San Matteo Hospital Foundation (IRCCS), Italy

REVIEWED BY
Naci Balak,
Istanbul Medeniyet University Goztepe Education and Research Hospital, Türkiye
Giorgio Mantovani,
University of Ferrara, Italy

*CORRESPONDENCE
Fedele Dono
fedele.dono@unich.it

RECEIVED 07 July 2023
ACCEPTED 18 July 2023
PUBLISHED 24 August 2023

CITATION
Consoli S, Dono F, Evangelista G, Corniello C, Onofrj M, Thomas A and Sensi SL (2023) Case Report: Brain tumor's pitfalls: two cases of high-grade brain tumors mimicking autoimmune encephalitis with positive onconeuronal antibodies.
Front. Oncol. 13:1254674.
doi: 10.3389/fonc.2023.1254674

Case Report: Brain tumor's pitfalls: two cases of high-grade brain tumors mimicking autoimmune encephalitis with positive onconeuronal antibodies

Stefano Consoli[1,2], Fedele Dono[1,2]*, Giacomo Evangelista[1,2], Clarissa Corniello[1,2], Marco Onofrj[1], Astrid Thomas[1] and Stefano L. Sensi[1,3,4]

[1]Department of Neuroscience, Imaging and Clinical Science, "G. d'Annunzio" University of Chieti-Pescara, Chieti, Italy, [2]Epilepsy Center, "SS Annunziata" Hospital, Chieti, Italy, [3]Behavioral Neurology and Molecular Neurology Units, Center for Advanced Studies and Technology (CAST), University "G. d'Annunzio" of Chieti-Pescara, Chieti, Italy, [4]Institute for Advanced Biomedical Technologies, University of Chieti-Pescara, Chieti, Italy

Background: Glioblastoma (GBM) is the most common primary brain tumor in adulthood. Initial diagnosis is generally based on clinical and MRI findings, which may be misinterpreted as other neurological pictures, including autoimmune encephalitis (AE). AE is a heterogeneous group of neuroinflammatory diseases due to the presence of auto-antibodies targeting antigens on neuronal synaptic or cell surface. In the present report, we describe two peculiar cases of GBM initially misdiagnosed as AE, focusing on the diagnostic pitfalls and the treatment strategies.

Methods: We report the case of two patients with high-grade brain tumors, initially misdiagnosed and treated for AE. Clinical, laboratory, and neuroradiological data are discussed in terms of differential diagnosis between AE and GBM.

Results: The presence of atypical brain MRI findings and the unresponsiveness to immunosuppressive treatment are major red flags in the differential diagnosis between AE and GBM. In these cases, a brain biopsy is necessary to confirm the diagnosis.

Conclusions: Atypical brain tumor presentation causes a diagnostic and therapeutic delay. A positive onconeural autoantibodies result should always be interpreted cautiously, considering the possibility of a false-positive test. A brain biopsy is mandatory for a definite diagnosis.

KEYWORDS

glioblastoma, autoimmune encephalitis, diagnosis, neuroimaging, epilepsy

1 Introduction

Glioblastomas (GBMs) are the most common primary brain tumors in adulthood, with a peak incidence between 65 and 75 years of age (1) and a median lifespan ranging from 8 to 14 months. According to tumor localization, GBM clinical manifestations spread from asymptomatic to severe neurological pictures. They may include neuropsychological changes, new-onset seizures, motor and/or sensory deficits, gate instability, cerebellar signs, and parkinsonism (2, 3). According to the 2021 CNS Classifications (4), the molecular characterization of primary brain tumors is critical for accurate diagnosis. Generally, GBMs are defined as IDH-wildtype tumors which may be associated with several further mutations, including telomerase reverse transcriptase (TERT) promoter mutations, epidermal growth factor receptor (EGFR) amplification, and concurrent gain of chromosome 7/loss of chromosome 10 [+7/-10] (5). Molecular changes are crucial for both therapeutic and prognostic purposes. It has been shown that temozolomide (TMZ) treatment is more effective in patients with peculiar molecular fingerprinting. In addition, some molecular findings, like unmethylated methylguanine-DNA methyltransferase (MGMT) and TERT gene promoter mutation, are generally related to poorer prognosis (5, 6).

Magnetic resonance imaging (MRI) of the brain is mandatory for GBM diagnosis (7). Typical brain MRI findings include: 1) hypointense to isointense lesions on T1-weighted sequences, 2) heterogeneous contrast enhancement uptake with a rim shape pattern indicative of necrosis, 3) hyperintense lesions on T2-weighted and fluid-attenuated inversion recovery (FLAIR) sequences associated with surrounding vasogenic edema (8). Moreover, advanced MRI techniques such as perfusion-weighted imaging (PWI) and magnetic resonance spectroscopy (MRS) could add further details. Indeed, PWI generally shows an increased relative cerebral blood volume, whereas MRS shows an increased choline and lactate pick with decreased N-acetyl-aspartate (9). Notwithstanding, MRI findings may sometimes be atypical and mimic various neurological conditions, including autoimmune encephalitis (AE) (10, 11).

AE is an antibody-mediated brain inflammatory process prompted by antibodies against intracellular or extracellular antigens (12). The AEs encompass a broad clinical spectrum that ranges from neurological and neuropsychiatric symptoms (e.g., changes in behavior or cognition, psychosis, abnormal movements, gate instability, aphasia, and depression) to subtle cognitive decline and seizures (13, 14). Diagnosis of AE is supported by several laboratory and neuroradiological findings (12, 15). Cerebrospinal fluid (CSF) analysis may highlight lymphocytic pleocytosis, increased proteins, or oligoclonal bands (OCBs) positivity, though patients with unremarkable findings have also been reported (15). Brain MRI generally shows T2/FLAIR hyperintense signal on the bilateral mesial temporal lobes or, less frequently, the lateral temporal lobe and the insula (16). However, heterogeneous patterns with multifocal brain lesions involving the cerebral cortex, the basal ganglia, or the brainstem have also been reported (17).

The differential diagnosis between GBM and AE may be challenging due to the possible unspecific clinical and neuroradiological findings which can be associated with both conditions. In the present report, we describe two peculiar cases of GBM initially misdiagnosed as AE, focusing on the diagnostic pitfalls and the treatment strategies.

2 Case presentation

2.1 Case 1

A 40-year-old, right-handed man was admitted to the emergency room (ER) due to the recurrence of focal impaired awareness seizures with behavioral arrest. The patient's past medical history revealed a subtle amnesic cognitive impairment with brief episodes of amnesia and behavioral disorders (i.e., agitation and crying spells) started about 3 months before the seizure onset, concomitantly to the administration of the second dose of the Sars-CoV2 vaccine (Comirnaty, Pfizer-BioNTech COVID-19 Vaccine). The patient underwent a brain MRI, which showed diffuse cortico-subcortical T2 and FLAIR hyperintense lesions involving the bilateral hippocampal and fusiform gyri, the right frontoparietal cortex, the left thalamus, and the right pulvinar (Figures 1A–F). In the suspicion of an AE, a lumbar puncture was performed, which was unremarkable. In addition, the autoimmune panel for surface and intracellular neuronal antibodies, executed on both CSF and serum, was negative. A possible post-SARS-CoV-2 vaccine acute disseminated encephalomyelitis (ADEM) was therefore diagnosed. Corticosteroid (methylprednisolone 1 g for 5 days) and anti-seizure (Levetiracetam 1500 mg/day) therapies were started, which led to a gradual improvement of the seizure frequency and the behavioral disturbance. However, a further neuropsychological evaluation revealed the persistence of cognitive deficits with executive functions and short- and long-term memory involvement.

After five months, the patient's cognitive symptoms worsened. A new lumbar puncture showed no pathological findings. Nevertheless, the autoimmune autoantibodies panel for AE showed the positivity of anti-recoverin antibodies in the serum (titer 1:32) (Table 1). A brain MRI and MSR (Figures 1G, H) were performed, which revealed T2 and FLAIR diffuse hyperintense lesions with high signals in diffusion-weighted imaging (DWI) and increased Choline/N-acetyl-aspartate ratio (Ch/Naa>2). Thus, a neuroradiological diagnosis of gliomatosis cerebri was made. A stereotactic brain biopsy and subsequent neuropathological evaluations were performed, resulting in a glioma tumor isocitrate dehydrogenase 1 (IDH-1) and 2 (IDH-2) wild type, glial fibrillary acidic protein (GFAP) and oligodendrocyte transcription factor 2 (Olig2) positive. The proliferation index, indexed by Mindbomb Homolog-1 (MIB-1) antibody, was 10% associated with an area of necrosis. Therefore, the molecular and histological characteristics resulted in a diagnosis of glioblastoma (grade 4, WHO 2021). Due to the MRI characteristics of the lesion, a neurosurgical approach was ruled out in favor of combined treatment with radiotherapy (2 Gy per day, total 60 Gy) and chemotherapy (temozolomide, 75 mg/m^2 during radiotherapy followed by 6 cycles of 200 mg/m^2 for 5 days each 28-day cycle), in line with the Stupp Protocol.

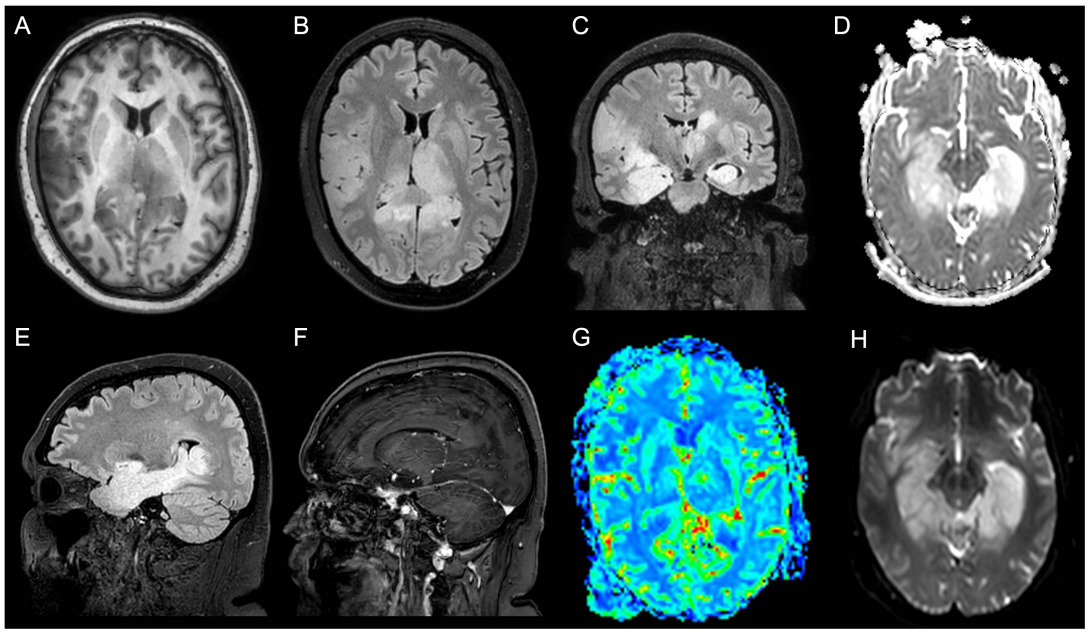

FIGURE 1
Patient 1 MRI scan of the brain shows diffuse cortico-subcortical T2 and Fluid Attenuated Inversion Recovery (FLAIR) images hyperintense lesions involving the bilateral hippocampal, the fusiform gyri, the right frontoparietal cortex, the left thalamus, and the right pulvinar. **(A)** Axial T1-weighted image; **(B)** Axial FLAIR image; **(C)** Coronal FLAIR image; **(D)** Axial apparent diffusion coefficient (ADC) image; **(E)** Sagittal FLAIR image; **(F)** Sagittal made of contrast positive T1-weighted image; **(G)** Axial perfusion weighted (PWI) image; **(H)** Axial diffusion weighted image (DWI).

At the 1-year visit follow-up, the patient was autonomous in daily activities but could not resume work (Karnofsky score: 70%). The patient did not complain of any severe adverse effects related to CT/RT regimens. However, persistent short-term memory deficits and depressive symptoms were reported. Furthermore, the patient referred recurrent daily episodes of epigastric sensation and dejà-vu, which were otherwise interpreted as focal aware seizure. A concomitant EEG showed sporadic diphasic high-amplitude sharp waves on the left anterior temporal lobe regions. A treatment with Lamotrigine 200 mg/die was then introduced with moderate benefit on the depressive symptoms and a reduction of>50% of seizure frequency. The MRI scan of the brain showed no modification of the neuroradiological picture.

The patient's time-line events are summarized in Figure 2A.

2.2 Case 2

A 35 years-old, right-handed man was admitted to the ER for persistent (i.e., 30 days) and slowly progressive hearing loss and postural instability. The patient's past medical history was unremarkable. At the admission, the patient showed a right sensorineural hearing loss and nystagmus in all directions of gaze, associated with slight weakness of the right lower limb.

Thus, the patient underwent a brain MRI, which showed a T2/FLAIR hyperintense blurred lesion on the right pontine-bulbar portion and the ipsilateral superior and middle cerebellar peduncles. The PWI, as well as the MRS, were unremarkable (Figures 3A–H). In the suspicion of rhombencephalitis, a lumbar puncture was performed, which showed normal cell and protein levels as well as no bacterial (i.e., Listeria, Tuberculosis, and Mycoplasma) and viral (e.g., Herpes simplex virus 1 and 2, and Cytomegalovirus) infection. However, the autoimmune panel for surface and intracellular neuronal antibodies revealed positivity for anti-GluR3 antibodies both in the CSF (titer 1:2) and in the serum (titer 1:200) (Table 1). On the contrary, serum Myelin Oligodendrocyte Glycoprotein (MOG) and Aquaporin 4 (AQP4) antibodies resulted in normal. Thus, the patient was treated with methylprednisolone (1 g/day for 5 days) followed by oral prednisolone at 50 mg/day, and a moderate improvement of neurological symptoms was observed.

After 3 months, a worsening of the clinical picture occurred. In particular, the patient developed right hemiparesis and appeared more confused and irritable. A brain lesion biopsy revealed a high-grade infra-tentorium IDH-1 and IDH-2 wild-type glial tumor, GFAP and Olig2 positive and histone H3-K27M mutation-negative (glioblastoma, grade 4 WHO 2021). The proliferation index (MIB-1) was 35%.

A surgical approach and adjuvant radiotherapy (2 Gy per day, total 60 Gy) and chemotherapy (temozolomide, 75 mg/m^2 during radiotherapy followed by 6 cycles of 200 mg/m^2 for 5 days each 28-day cycle) in line with the Stupp Protocol were then attempted. However, due to a severe reduction in platelet count, chemotherapy was discontinued after six weeks.

The last follow-up was performed one year after surgery. The patient showed persistent right sensorineural hypoacusia, conjugate rightward gaze paralysis, and diplopia with inexhaustible nystagmus in leftward lateral gaze. In addition, personal self-sufficiency was severely affected by walking difficulties and right-side weakness (Karnofsky score: 60%). The MRI scan of the brain showed no modification of the neuroradiological picture.

The patient's time-line events are summarized in Figure 2B.

10.3389/fonc.2023.1254674

TABLE 1 Patients' cerebrospinal fluid (CSF) and serum analysis characteristics.

Cerebrospinal fluid analysis				
Patient 1	*Cytochemical examination*	*Result*	*Autoimmune panel*	*Titer*
	Appearance	Clear	*Anti Ca^{2+} Channel Ab*	Negative
	White cells	3 cells/mm^3	*Aanti VGCK Ab*	Negative
	Glucose	60.4 mg/dl	*Anti GLUR3 Ab*	Negative
	Proteins	31.8 mg/dl	*Anti AMPAR1,2 Ab*	Negative
	Microbiological panel		*Anti CASPR2 Ab*	Negative
	HSV-1	Negative	*Anti LGI1 Ab*	Negative
	HSV-2	Negative	*Anti NMDAR Ab*	Negative
	HHV-6	Negative	*Anti GABAR Ab*	Negative
	HHV-7	Negative	*Anti GAD65 Ab*	Negative
	HHV-8	Negative	*Anti MOG Ab*	Negative
	CMV	Negative	*Anti AQP4 Ab*	Negative
	EBV	Negative	*Oligoclonal bands*	Negative
	VZV	Negative		
Patient 2	*Cytochemical examination*	*Result*	*Autoimmune panel*	*Titer*
	Appearance	Clear	*Anti Ca^{2+} Channel Ab*	Negative
	White cells	1 cells/mm^3	*Aanti VGCK Ab*	Negative
	Glucose	54 mg/dl	*Anti GLUR3 Ab*	**1:2**
	Proteins	26 mg/dl	*Anti AMPAR1,2 Ab*	Negative
	Microbiological panel		*Anti CASPR2 Ab*	Negative
	HSV-1	Negative	*Anti LGI1 Ab*	Negative
	HSV-2	Negative	*Anti NMDAR Ab*	Negative
	HHV-6	Negative	*Anti GABAR Ab*	Negative
	HHV-7	Negative	*Anti GAD65 Ab*	Negative
	HHV-8	Negative	*Anti MOG Ab*	Negative
	CMV	Negative	*Anti AQP4 Ab*	Negative
	EBV	Negative	*Oligoclonal bands*	Negative
	VZV	Negative		
Serum analysis				
Patient 1	*Autoimmune panel*	*Titer*		
	Anti Ca^{2+} Channel Ab	Negative	Anti-Ma1 Ab	Negative
	Anti VGCK Ab	Negative	Anti-Ma2/Ta Ab	Negative
	Anti GLUR3 Ab	Negative	Anti-CV2/CRMP5 Ab	Negative
	Anti AMPAR1,2 Ab	Negative	Anti-Hu Ab	Negative
	Anti CASPR2 Ab	Negative	Anti-Ri p54 Ab	Negative
	Anti LGI1 Ab	Negative	Anti-Yo Ab	Negative
	Anti NMDAR Ab	Negative	Anti-recoverin Ab	***1:32***
	Anti GABAR Ab	Negative	Anti-amphiphysin Ab	Negative
	Anti GAD65 Ab	Negative	Anti-SOX1 Ab	Negative

(Continued)

TABLE 1 Continued

Serum analysis				
	ANA	Negative	Anti-Zic4 Ab	Negative
	ENA	Negative	Anti-titin Ab	Negative
	Antiphospholipid antibodies	Negative	Anti-Tr Ab	Negative
Patient 2	*Autoimmune panel*	*Titer*		
	Anti Ca^{2+} Channel Ab	Negative	Anti-Ma1 Ab	Negative
	Anti VGCK Ab	Negative	Anti-Ma2/Ta Ab	Negative
	Anti GLUR3 Ab	**1:200**	Anti-CV2/CRMP5 Ab	Negative
	Anti AMPAR1,2 Ab	Negative	Anti-Hu Ab	Negative
	Anti CASPR2 Ab	Negative	Anti-Ri p54 Ab	Negative
	Anti LGI1 Ab	Negative	Anti-Yo Ab	Negative
	Anti NMDAR Ab	Negative	Anti-recoverin Ab	Negative
	Anti GABAR Ab	Negative	Anti-amphiphysin Ab	Negative
	Anti GAD65 Ab	Negative	Anti-SOX1 Ab	Negative
	ANA	Negative	Anti-Zic4 Ab	Negative
	ENA	Negative	Anti-titin Ab	Negative
	Antiphospholipid antibodies	Negative	Anti-Tr Ab	Negative

AMPAR, alpha-amino-3-hydroxy-5-methyl-4-isoxazolepropionic acid receptor; ANA, antinuclear antibody; AQP4, aquaporin-4; CASPR2, anti-contactin-associated protein-like 2; CMV, cytomegalovirus; CV2/CRMP5, collapsin response mediator protein; EBV, Epstein-Barr virus; GABAR, anti-y-aminobutyric acid-beta-receptor 1; ENA, extractable nuclear antigen; GAD65, glutamic acid decarboxylase 65; GLUR3, glutamate receptor 3; HSV, herpes simplex virus; HHV, human herpes virus; LGI1, leucine-rich glioma inactivated 1; MOG, myelin oligodendrocyte glycoprotein; NMDAR, N-methyl-D-aspartate receptor; SOX1, superoxide dismutase 1; Tr, thyrotropin; VGCK, voltage-gated potassium channel; VZV, varicella-zoster virus; Zic4, zinc finger protein. Bold numbers are used to identify pathological findings.

3 Discussion

GBM's presentation may be very heterogeneous in terms of imaging and clinical findings, sometimes mimicking other neurological conditions such as AE (18).

In the two cases we reported, patients presented atypical neuroradiological and clinical features that did not immediately lead to a brain tumor diagnosis. In the first case, a diffuse cortico-subcortical involvement, as demonstrated by brain MRI scans, strongly supported the diagnosis of inflammatory encephalitis

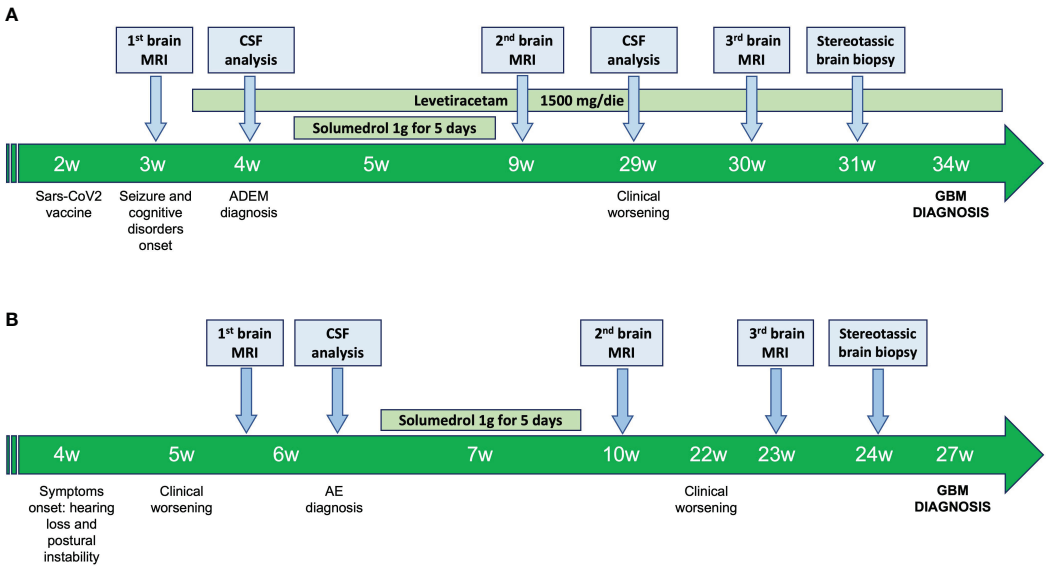

FIGURE 2
Patient 1 **(A)** and patient 2 **(B)** time-line events. ADEM, Acute disseminated encephalomyelitis; AE, Autoimmune encephalitis; CSF, Cerebrospinal Fluid; GBM, Glioblastoma; MRI, Magnetic Resonance Image of the brain.

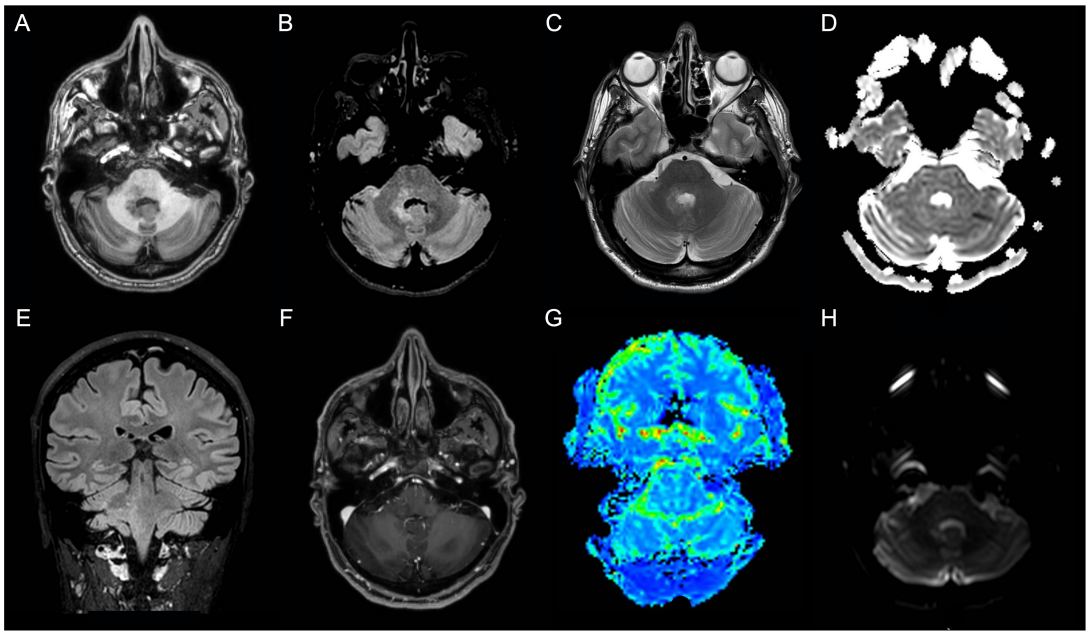

FIGURE 3
Patient 2 MRI scans of the brain shows T2-weighted and Fluid Attenuated Inversion Recovery (FLAIR) images hyperintense blurred lesion on the right pontine-bulbar portion and the ipsilateral superior and middle cerebellar peduncles **(A)** Axial T1-weighted image; **(B)** Axial FLAIR image; **(C)** Axial T2-weighted image; **(D)** Axial apparent diffusion coefficient (ADC) image; **(E)** Sagittal FLAIR image; **(F)** Axial made of contrast positive T1-weighted image; **(G)** Axial perfusion weighted (PWI) image; **(H)**) Axial diffusion weighted image (DWI).

(11). Indeed, to date, less than 2% of individuals with malignant gliomas have been documented to have multicentric GBMs showing a pattern of *gliomatosis cerebri* (19). In the second case, the specific localization of the brain lesion raised some doubts regarding its actual etiology. Adults rarely develop primary infra-tentorial glioblastoma, and cerebropontine angle (CPA) location is estimated to be even rarer (incidence range from 1.5% to 4.1%) (20, 21). Unfortunately, in both cases, the employment of advanced MRI techniques (i.e., PWI and MRS) failed to help elucidate the specific etiology.

From a clinical point of view, both patients presented several neurological symptoms with a subacute onset mimicking the presentation of an AE. In particular, the new-onset seizures associated with subacute neuropsychological deficits observed in the first patient agreed with the AE diagnosis according to Grauss' criteria (12). On the other hand, the signs of cerebellar and pontine-bulbar involvement observed in the second patient raised the suspicion of inflammatory rhombencephalitis (22, 23). However, laboratory tests performed on serum and CSF partially confirmed the diagnosis of AE. Although both patients showed serum and/or CSF positivity for onconeural autoantibodies, there was a discrepancy between the specific antibodies-related syndrome and the actual clinical features. Anti-amphiphysin antibodies are typically associated with stiff-person syndrome (SPS) (i.e., a neurological syndrome characterized by axial rigidity, muscle stiffness, and startle reflex) (24, 25) whereas anti-GluR3 antibodies are generally observed in Rasmussen encephalitis, untreatable epilepsy and, less frequently, rhombencephalitis (26, 27). Thus, while the second patient showed some clinical symptoms which could fit with an anti-GluR3 encephalitis diagnosis, the first patient did not show any manifestations which could even raise suspicion of SPS.

However, in the first patient, some anamnestic data supported the hypothesis of an inflammatory brain process. Indeed, the close correlation between the SARS-CoV-2 vaccine administration and the onset of the symptoms raised suspicion of post-vaccine acute disseminated encephalomyelitis (ADEM) (28). ADEM usually affects younger patients, but several cases during adulthood have also been described specifically in the context of SARS-CoV-2 vaccination (29).

In both cases, immunosuppressive therapy with high-dose corticosteroids was started, with mild-to-moderate effects on neurological symptoms. However, due to the atypical radiological presentation and the successive worsening of the clinical picture, we sought to perform a stereotactic brain biopsy by which a histological and molecular diagnosis of glioblastoma (GBM grade 4, WHO 2021) was ascertained. It has to be pointed out that though the use of corticosteroids is allowed in patients suffering from GBM due to the well-known anti-edema effects (30), more aggressive immunosuppressive treatment (e.g., azathioprine, cyclophosphamide, anti-CD20 monoclonal antibodies), commonly used to treat AE refractory to corticosteroids, should be avoided given the possible detrimental effects on tumor progression.

However, in our cases, the brain biopsy led to the correct diagnosis, allowing the most appropriate therapies and avoiding invasive and potentially harmful treatments.

4 Conclusion

Glioblastomas (GBMs) could present with similar clinical and radiological findings that can be seen in autoimmune encephalitis (AE), leading to diagnostic and treatment delays. A positive onconeural autoantibodies result should always be interpreted with caution, taking into account the possibility of a false-positive test. A biopsy should be performed before starting a potentially harmful therapy, especially in case of unusual symptoms and radiological features. Neurologists should always consider the possibility of an atypical presentation of a relatively common disease, keeping in mind the heterogeneous clinical and radiological behavior of glioblastoma.

Data availability statement

The raw data supporting the conclusions of this article will be made available by the authors, without undue reservation.

Ethics statement

Ethical approval was not provided for this study on human participants because written informed consent was obtained from the patient to publish this case report and any accompanying images. The paper is exempt from ethical committee approval because it is not necessary for the publication of the case report. We confirm that we have read the Journal's position on issues involved in ethical publication and affirm that this report is consistent with those guidelines. The patients/participants provided their written informed consent to participate in this study. Written informed consent was obtained from the patient to publish this case report and any accompanying images.

Author contributions

SC: Conceptualization, Data curation, Writing – original draft. FD: Conceptualization, Data curation, Formal Analysis, Investigation, Methodology, Project administration, Resources, Supervision, Validation, Visualization, Writing – original draft, Writing – review & editing. GE: Data curation, Investigation, Writing – review & editing, Data curation, Investigation, Writing – review & editing. CC: Investigation, Writing – review & editing. MO: Resources, Supervision, Validation, Visualization, Writing – review & editing. AT: Supervision, Validation, Visualization, Writing – review & editing. SS: Data curation, Supervision, Validation, Visualization, Writing – review & editing.

Funding

This work was supported by non-profit agencies [Italian Department of Health (RF-2013– 02358785 and NET-2011-02346784-1), the AIRAlzh Onlus (ANCC-COOP), European Union's Horizon 2020 research and innovation program under the Marie Skłodowska-Curie grant agreement iMIND – no. 84166, the Alzheimer's Association – Part the Cloud: Translational Research Funding for Alzheimer's Disease (18PTC-19-602325), and the Alzheimer's Association – GAAIN Exploration to Evaluate Novel Alzheimer's Queries (GEENA-Q-19- 596282)].

Conflict of interest

The authors declare that the research was conducted in the absence of any commercial or financial relationships that could be construed as a potential conflict of interest.

Publisher's note

References

1. Omuro A, DeAngelis LM. Glioblastoma and other Malignant gliomas: a clinical review. *JAMA* (2013) 310(17):1842–50. doi: 10.1001/jama.2013.280319

2. Alentorn A, Hoang-Xuan K, Mikkelsen T. Presenting signs and symptoms in brain tumors. *Handb Clin Neurol* (2016) 134:19–26. doi: 10.1016/B978-0-12-802997-8.00002-5

3. Hadidchi S, Surento W, Lerner A, Liu CJ, Gibbs WN, Kim PE, et al. Headache and brain tumor. *Neuroimaging Clin N Am* (2019) 29(2):291–300. doi: 10.1016/j.nic.2019.01.008

4. Louis DN, Perry A, Wesseling P, Brat DJ, Cree IA, Figarella-Branger D, et al. The 2021 WHO classification of tumors of the central nervous system: a summary. *Neuro Oncol* (2021) 23(8):1231–51. doi: 10.1093/neuonc/noab106

5. Melhem JM, Detsky J, Lim-Fat MJ, Perry JR. Updates in IDH-wildtype glioblastoma. *Neurotherapeutics* (2022) 19(6):1705–23. doi: 10.1007/s13311-022-01251-6

6. Śledzińska P, Bebyn MG, Furtak J, Kowalewski J, Lewandowska MA. Prognostic and predictive biomarkers in gliomas. *Int J Mol Sci* (2021) 22(19):10373. doi: 10.3390/ijms221910373

7. Fathi Kazerooni A, Bakas S, Saligheh Rad H, Davatzikos C. Imaging signatures of glioblastoma molecular characteristics: A radiogenomics review. *J Magn Reson Imaging.* (2020) 52(1):54–69. doi: 10.1002/jmri.26907

8. Shukla G, Alexander GS, Bakas S, Nikam R, Talekar K, Palmer JD, et al. Advanced magnetic resonance imaging in glioblastoma: a review. *Chin Clin Oncol* (2017) 6(4):40. doi: 10.21037/cco.2017.06.28

9. Fink JR, Muzi M, Peck M, Krohn KA. Multimodality brain tumor imaging: MR imaging, PET, and PET/MR imaging. *J Nucl Med* (2015) 56(10):1554–61. doi: 10.2967/jnumed.113.131516

10. Macchi ZA, Kleinschmidt-DeMasters BK, Orjuela KD, Pastula DM, Piquet AL, Baca CB. Glioblastoma as an autoimmune limbic encephalitis mimic: A case and review of the literature [published online ahead of print, 2020 Mar 7]. *J Neuroimmunol* (2020) 342:577214. doi: 10.1016/j.jneuroim.2020.577214

11. Khandwala K, Mubarak F, Minhas K. The many faces of glioblastoma: Pictorial review of atypical imaging features. *Neuroradiol J* (2021) 34(1):33–41. doi: 10.1177/1971400920965970

12. Graus F, Titulaer MJ, Balu R, Benseler S, Bien CG, Cellucci T, et al. A clinical approach to diagnosis of autoimmune encephalitis. *Lancet Neurol* (2016) 15(4):391–404. doi: 10.1016/S1474-4422(15)00401-9

13. Dono F, Evangelista G, Consoli S, Scorrano G, Russo M, di Pietro M, et al. Anti-N-methyl-D-aspartate receptor (NMDAr) encephalitis during pregnancy: A case report. *Epilepsy Behav Rep* (2022) 19:100535. doi: 10.1016/j.ebr.2022.100535

14. Uy CE, Binks S, Irani SR. Autoimmune encephalitis: clinical spectrum and management. *Pract Neurol* (2021) 21(5):412–23. doi: 10.1136/practneurol-2020-002567

15. Ramanathan S, Al-Diwani A, Waters P, Irani SR. The autoantibody-mediated encephalitides: from clinical observations to molecular pathogenesis. *J Neurol* (2021) 268(5):1689–707. doi: 10.1007/s00415-019-09590-9

16. Liang C, Chu E, Kuoy E, Soun JE. Autoimmune-mediated encephalitis and mimics: A neuroimaging review. *J Neuroimaging* (2023) 33(1):19–34. doi: 10.1111/jon.13060

17. Štourač P, Bednářová J, Zicháček P, Čermáková Z, Pavelek Z, Vališ M. Autoimmune and limbic encephalitis: case series with some atypical variables in clinical practice. *Neurol Sci* (2022) 43(1):687–90. doi: 10.1007/s10072-021-05563-x

18. Bradley D, Rees J. Brain tumor mimics and chameleons. *Pract Neurol* (2013) 13 (6):359–71. doi: 10.1136/practneurol-2013-000652

19. Yan Y, Dai W, Mei Q. Multicentric glioma: an ideal model to reveal the mechanism of glioma. *Front Oncol* (2022) 12:798018. doi: 10.3389/fonc.2022.798018

20. Lee JH, Kim JH, Kwon TH. Primary glioblastoma of the cerebellopontine angle: case report and review of the literature. *J Korean Neurosurg Soc* (2017) 60(3):380–4. doi: 10.3340/jkns.2015.0303.006

21. Kasliwal MK, Gupta DK, Mahapatra AK, Sharma MC. Multicentric cerebellopontine angle glioblastoma multiforme. *Pediatr Neurosurg* (2008) 44 (3):224–8. doi: 10.1159/000121380

22. Jubelt B, Mihai C, Li TM, Veerapaneni P. Rhombencephalitis / brainstem encephalitis. *Curr Neurol Neurosci Rep* (2011) 11(6):543–52. doi: 10.1007/s11910-011-0228-5

23. Campos LG, Trindade RA, Faistauer Â, Pérez JA, Vedolin LM, Duarte JÁ. Rhombencephalitis: pictorial essay. *Radiol Bras* (2016) 49(5):329–36. doi: 10.1590/0100-3984.2015.0189

24. Newsome SD, Johnson T. Stiff person syndrome spectrum disorders; more than meets the eye. *J Neuroimmunol* (2022) 369:577915. doi: 10.1016/j.jneuroim.2022.577915

25. Geis C, Weishaupt A, Hallermann S, Grünewald B, Wessig C, Wultsch T, et al. Stiff person syndrome-associated autoantibodies to amphiphysin mediate reduced GABAergic inhibition. *Brain* (2010) 133(11):3166–80. doi: 10.1093/brain/awq253

26. Varadkar S, Bien CG, Kruse CA, Jensen FE, Bauer J, Pardo CA, et al. Rasmussen's encephalitis: clinical features, pathobiology, and treatment advances. *Lancet Neurol* (2014) 13(2):195–205. doi: 10.1016/S1474-4422(13)70260-6

27. Cucuzza ME, Pavone P, D'Ambra A, Finocchiaro MC, Greco F, Smilari P, et al. Autoimmune encephalitis and CSF anti-AMPA GluR3 antibodies in childhood: a case report and literature review. *Neurol Sci* (2022) 43(9):5237–41. doi: 10.1007/s10072-022-06170-0

28. Permezel F, Borojevic B, Lau S, de Boer HH. Acute disseminated encephalomyelitis (ADEM) following recent Oxford/AstraZeneca COVID-19 vaccination. *Forensic Sci Med Pathol* (2022) 18(1):74–9. doi: 10.1007/s12024-021-00440-7

29. Kalita IR, Singh HV, Sharma S. Acute abducens nerve palsy with acute disseminated encephalomyelitis-like presentation following COVID-19 vaccination. *Indian J Ophthalmol* (2023) 71(5):2279–81. doi: 10.4103/ijo.IJO_1778_22

30. Esquenazi Y, Lo VP, Lee K. Critical care management of cerebral edema in brain tumors. *J Intensive Care Med* (2017) 32(1):15–24. doi: 10.1177/0885066615619618

frontiers | Frontiers in Oncology

TYPE Original Research
PUBLISHED 17 October 2023
DOI 10.3389/fonc.2023.1248553

OPEN ACCESS

EDITED BY
Archya Dasgupta,
Tata Memorial Hospital, India

REVIEWED BY
Michel Roethlisberger,
University Hospital of Basel, Switzerland
Mario Ganau,
Oxford University Hospitals NHS Trust, United Kingdom

*CORRESPONDENCE
Feng Chen
chenfenghuanle@163.com
Yang Liu
yangliuat@yeah.net

†These authors have contributed equally to this work

RECEIVED 27 June 2023
ACCEPTED 02 October 2023
PUBLISHED 17 October 2023

CITATION
Guo Z-Y, Zhong Z-A, Peng P, Liu Y and Chen F (2023) A scoring system categorizing risk factors to evaluate the need for ventriculoperitoneal shunt in pediatric patients after brain tumor resection. *Front. Oncol.* 13:1248553. doi: 10.3389/fonc.2023.1248553

A scoring system categorizing risk factors to evaluate the need for ventriculoperitoneal shunt in pediatric patients after brain tumor resection

Zhong-Yin Guo[1,2†], Zi-An Zhong[1†], Peng Peng[1], Yang Liu[1*] and Feng Chen[1*]

[1]Department of Neurosurgery, Xiangyang Central Hospital, Affiliated Hospital of Hubei University of Arts and Science, Xiangyang, Hubei, China, [2]Department of Neurosurgery, Tongji Hospital, Tongji Medical College, Huazhong University of Science and Technology, Wuhan, Hubei, China

Objectives: To develop a scoring system based on independent predictors of the need for ventriculoperitoneal (VP) shunt after brain tumor resection in pediatric patients.

Methods: A total of 416 pediatric patients (≤ 14 years old) with brain tumors who underwent surgery were randomly assigned to the training (n = 333) and validation cohorts (n = 83). Based on the implementation of VP shunt, the training cohort was divided into the VP shunt group (n = 35) and the non-VP shunt group (n = 298). Univariate and multivariate logistic analyses were performed. A scoring system was developed based on clinical characteristics and operative data, and scores and corresponding risks were calculated.

Results: Age < 3 (p = 0.010, odds ratio [OR] = 3.162), blood loss (BL) (p = 0.005, OR = 1.300), midline tumor location (p < 0.001, OR = 5.750), preoperative hydrocephalus (p = 0.001, OR = 7.044), and total resection (p = 0.025, OR = 0.284) were identified as independent predictors. The area under the curve (AUC) of the scoring system was higher than those of age < 3, BL, midline tumor location, preoperative hydrocephalus, and total resection (0.859 vs. 0.598, 0.717, 0.725, 0.705, and 0.555, respectively; p < 0.001). Furthermore, the scoring system showed good performance in the validation cohort (AUC = 0.971). The cutoff value for predictive scores was 5.5 points, which categorized patients into low risk (0-5 points) and high risk (6-14 points) groups.

Conclusions: Our scoring system, integrating age < 3, BL, midline tumor location, preoperative hydrocephalus, and total resection, provides a practical evaluation. Scores ranging from 6 to 14 points indicate high risk.

KEYWORDS

pediatric patient, age, blood loss, midline tumor location, preoperative hydrocephalus, tumor resection, risk factor

Introduction

Brain tumors have the highest morbidity and mortality among pediatric patients with solid tumors throughout all stages of childhood (1, 2). The rapid growth and development of the nervous system in childhood make radiotherapy and chemotherapy relatively contraindicated for children with brain tumors (3). As a result, surgery remains the predominant treatment for pediatric brain tumors (1, 3, 4).

Hydrocephalus is a serious postoperative complication in children with brain tumors, characterized by pathological ventricular expansion and increased intracranial pressure. Its pathogenesis may be related to an imbalance between the production and absorption of cerebrospinal fluid (CSF) (5–7). The incidence of preoperative hydrocephalus in children with brain tumors is approximately 50%, while postoperative hydrocephalus can range from 16% to 35% (7) (8, 9). Hydrocephalus can cause many symptoms and sequalae depending on the age of the child such as speech impairment, neuropsychiatric disorders and life-threatening events (7, 10, 11). Prompt ventriculoperitoneal (VP) shunt placement is typically necessary since hydrocephalus tends to be progressive (7). Therefore, it is crucial to identify the risk factors for postoperative hydrocephalus and provide appropriate treatment.

Several studies have emphasized the significant role of age, preoperative hydrocephalus, total resection, and tumor pathologies to predict postoperative hydrocephalus in children with brain tumors, while inconsistent findings prevented from comprehensively evaluating risks (8, 12, 13). Factors such as limited sample sizes, variations in variables, different tumor locations (supratentorial or infratentorial), varying age definitions (ranging from < 16 to < 20 years old), and differences in statistic methods (univariate or multivariate), might contribute to these inconsistencies (9, 14). Moreover, Hu et al. has made a novel discovery regarding the blood loss (BL) as an independent predictor for hydrocephalus in the children with infratentorial tumors (15). In the present work, we comprehensively involved related variables using multivariate analysis and developed a scoring system to assess the occurrence or progression hydrocephalus that needed a VP shunt in children with brain tumors.

Methods

Patients and data

The flowchart of patient selection is presented in Figure 1. The study was approved by Tongji hospital's institutional ethics committee (TJ_JRB20211271), and data were collected after obtaining consent from the patients' parents or guardians. From November 2020 to January 2021, a total of 436 patients under 14 years of age were diagnosed with brain tumors and underwent tumor resection at our hospital. Twenty patients were excluded as follows: (a) refusal to undergo surgery or opting for biopsy only (n = 5); (b) previous history of VP shunt treatment (n = 7); (c) poor postoperative outcome, such as death or coma lasting over 2 weeks (n = 8). Next, 416 patients were randomly categorized into the training cohort (n = 333) and validation cohort (n = 83) based on 4:1 ratio. Based on the implementation of VP shunt, the training cohort were divided into a VP group (n = 35) and a non-VP group (n = 298). Hydrocephalus was diagnosed using magnetic resonance imaging, symptoms, and an Evans' ratio > 0.3 (16) (Figure 2F). VP shunts were

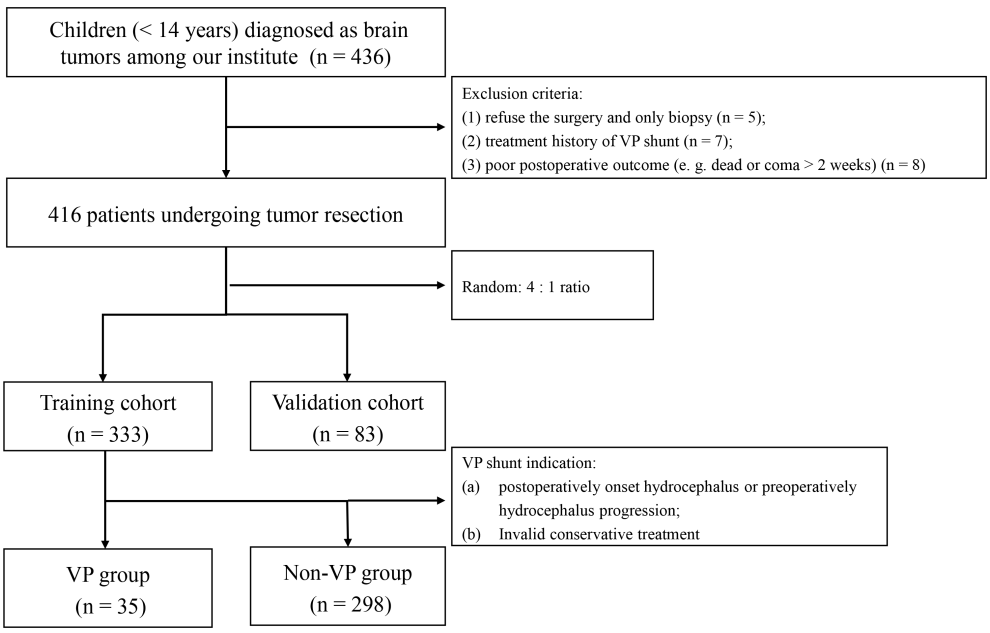

FIGURE 1
The flow chart of patient selection. VP, ventriculoperitoneal.

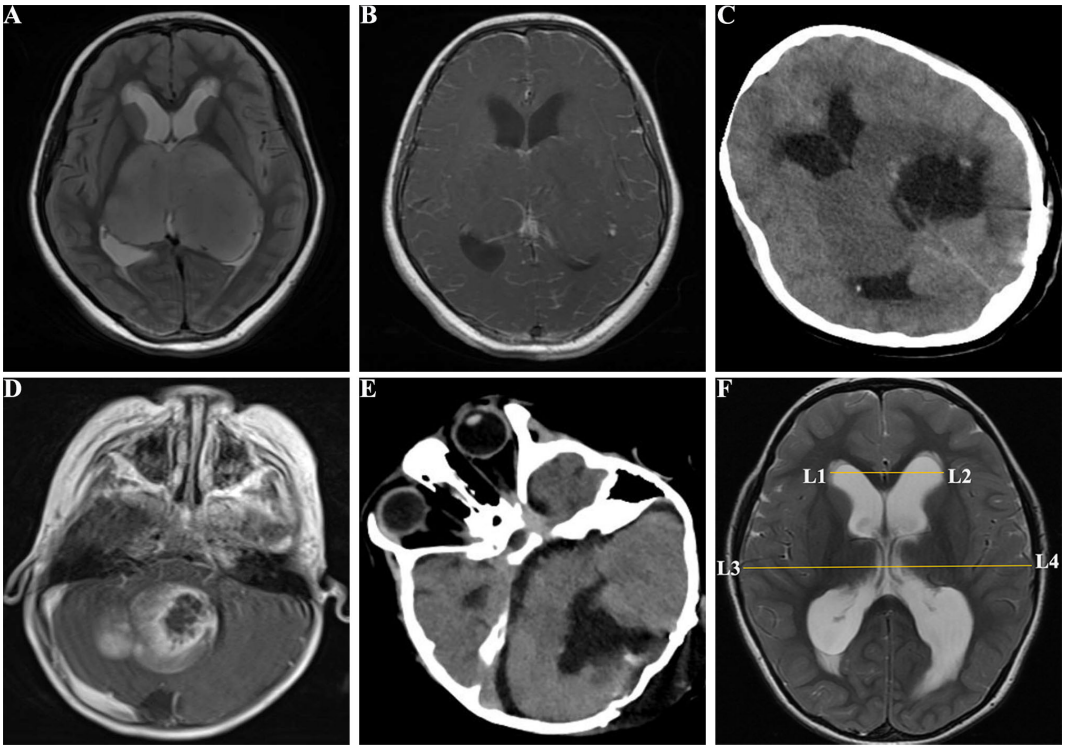

FIGURE 2
Images of pediatric patients with brain tumors. **(A)**, a 10 years old female with supratentorial tumors in the T2 FSE of MRI before surgery; **(B)**, enhanced MRI T1 FSE+C showed bilateral supratentorial tumors before surgery; **(C)**, CT image of the supratentorial tumor with incomplete total resection; **(D)**, a 3 years old male with infratentorial tumors in the enhanced MRI T1 FSE+C before surgery; **(E)**, CT image of the infratentorial tumor after tumor resection; **(F)**, Postoperative hydrocephalus with Evan's index > 0.3. FSE, fast spin echo; CT, compute tomography; MRI, magnetic resonance imaging; Evan's index = L1L2/L3L4.

required for the following indications: (a) postoperative onset of hydrocephalus or progression of preoperative hydrocephalus; (b) failure of conservative treatment.

Clinical characteristics and operative data were collected from medical records in our hospital. The collected variables included operative time, BL (quantified by the intraoperative blood transfusion volume), age (< 3 or ≥ 3 years old), tumor size (≤ 30 mm or > 30 mm), Ki 67 index (≥ 5 or< 5), tumors locations, gender, symptom duration (≤ 1 months or > 1 months), World Health Organization (WHO) grade (I–II [low-grade] and III–IV [high-grade]), presence of preoperative hydrocephalus, extent of tumor resection, American Society of Anesthesiologists (ASA) scale (classified as I–II [low risk] and III–IV [high risk]; patients in V–VI were ineligible to undergo surgery), tumor recurrence, and pathology: medulloblastoma, astrocytoma, ependymoma, and others (primitive neuroectodermal tumor [PNET], oligodendroglioma, choroid plexus papilloma [CPP], choroid plexus carcinoma [CPC], meningioma, neuroblastoma, schwannoma, hemangioblastoma, germ cell tumor [GCT], dysembryoplastic neuroepithelial tumors [DNT], atypical teratoid/rhabdoid tumor [AT/RT], and atypical rhabdomyosarcoma), and infratentorial tumors' characteristics were outlined in the study conducted by D'Arco F et al. (17). Based on the spatial relationship of tumors to the ventricle and tentorium, tumor locations were classified into two categories: (a) supratentorial (Figures 2A–C) or infratentorial tumors (Figures 2D, E) as defined by Corti et al. (18); (b) midline tumor location (including tumors located at basal ganglia, diencephalon, third ventricle, lateral ventricles, fourth ventricle, pineal body, cerebellar vermis, and brainstem) or other locations.

Statistical analysis

Statistical analysis was performed using SPSS 26.0 (IBM Inc, Chicago, IL). Continuous variables were presented as median ± interquartile range, while categorical variables were expressed as frequencies (percentages). The normal distribution of the parameter dataset was assessed using the Kolmogorov-Smirnov test. Univariate logistic analysis was performed to analyze all variables between two groups. Using the stepwise method, significant variables in univariate analysis (operative time, BL, age < 3, Ki-67 index, midline tumor location, infratentorial tumors, WHO grade, preoperative hydrocephalus, total resection, ASA scale, and pathology) were then entered into a multivariate logistic regression (19). A logistic model (Model-Logit) was constructed based on independent risk factors. Risk factor categories were employed to develop a scoring system. Receiver operating characteristic (ROC) curves were generated to calculate significant variables of areas under the curve (AUCs) and cutoffs. The Delong test was performed to compare the AUCs of scoring system in training cohort with in validation cohort. In accordance with the

literature, predictive scores and corresponding risk estimate were calculated (20, 21). Differences with $p < 0.05$ were considered statistically significant.

Results

Patient demographics

The flow chart of patient selection is shown in Figure 1. The training cohort of 333 pediatric patients (< 14 years old) included 196 males and 137 females; 65 patients were under the age of 3, accounting for 20% of the total approximately. Within the training cohort, 173 patients (52%) presented with preoperative hydrocephalus and 299 patients (90%) underwent total resection. Following tumor resection, 35 children underwent VP shunt placement, resulting in an incidence rate of 11%. In the VP group, 5 cases (14%), including 3 children with infratentorial tumors, had obstructive hydrocephalus. The remaining 30 cases (86%) presented with communicating hydrocephalus. The median value of BL was 2.00 U. The pathology of the 155 supratentorial tumors included 84 cases (54%) of low-grade glioma, 15 cases (10%) of ependymoma, 1 case (1%) of medulloblastoma, and 55 cases (35%) categorized as other types including AT/RT, CPP, CPC, cavernous hemangioma, DNT, craniopharyngioma, GCT, meningioma, neuroblastoma, high-grade glioma, PNET, and schwannoma. Among the 178 infratentorial tumors, 73 cases (41%) were diagnosed as medulloblastoma, 59 cases (33%) as astrocytoma, 25 cases (14%) as ependymoma, and 21 patients (12%) presented with other types including PNET, oligodendroglioma, CPP, meningioma, schwannoma, atypical rhabdomyosarcoma, and hemangioblastoma. Besides, 104 cases (31%) were midline tumors. In the VP group, 28 cases (80%), including 2 with postoperative onset hydrocephalus, underwent VP shunt due to hydrocephalus progression within 2 weeks of tumor resection. 3 patients (9%) required the procedure between 2 weeks and 2 months after tumor resection, while two patients (6%) needed it after tumor resection, and another two patients (6%) required it over 2 months later. The demographic differences between the VP and non-VP groups are displayed in Table 1.

TABLE 1 Univariate analysis of the predictive factors for VP shunt.

Variables	VP group (n = 35)	Non-VP group (n = 298)	*p* value
Operation time	5.34 ± 2.62	4.55 ± 1.41	**0.001**
Blood loss	3.00 ± 2.00	2.00 ± 1.00	**0.002**
Age			
< 3 y	13 (37%)	52 (17%)	**0.007**
≥ 3 y	22 (63%)	246 (83%)	Reference
Size			
≤30 mm	10 (29%)	109 (37%)	Reference
> 30 mm	25 (71%)	189 (63%)	0.352
Ki 67 index			
≧ 5	23 (66%)	136 (46%)	**0.028**
< 5	12 (34%)	162 (54%)	Reference
Midline tumor location	25 (71%)	79 (27%)	< **0.001**
Infratentorial tumors	24 (68%)	154 (52%)	0.062
Male	20 (57%)	176 (59%)	0.827
Symptom duration			
≤ 1 months	24 (69%)	207 (69%)	Reference
> 1 months	11 (31%)	91 (31%)	0.914
WHO grade			
I-II	12 (34%)	156 (52%)	Reference
III-IV	23 (66%)	142 (48%)	**0.028**
Preoperative hydrocephalus			
Yes	31 (89%)	142 (48%)	< **0.001**
No	4 (11%)	156 (52%)	Reference
Total resection			
Yes	28 (80%)	271 (91%)	**0.049**
No	7 (20%)	27 (9%)	Reference
ASA scale			
I-II	24 (69%)	247 (83%)	Reference
III-IV	11 (31%)	51 (17%)	**0.044**
Tumor recrudesce	4 (11%)	35 (12%)	0.956
Pathology			**0.020**
Medulloblastoma	12 (34%)	62 (21%)	**0.004**
Astrocytoma	6 (17%)	137 (46%)	Reference
ependymoma	7 (20%)	33 (11%)	**0.007**
Others	10 (29%)	66 (22%)	**0.021**

Significance level where p < 0.05 were in bold. ASA, American Society of Anesthesiologists; WHO, World Health Organization; VP, ventriculoperitoneal.

Predictive factors for VP shunt and scoring system

The univariate logistic regression results of the predictive factors for VP shunt are shown in the Table 1. To further explore the independent predictors, we used the stepwise forward method to incorporate significant variables in univariate analysis into multivariate analysis, as presented in Table 2. The age < 3 (p = 0.010, OR = 3.162, CI = 1.314 – 7.608), BL (p = 0.005, OR = 1.300, CI = 1.084 – 1.560), midline tumor location (p < 0.001, OR = 5.750, CI = 2.406 – 13.742), preoperative hydrocephalus (p = 0.001, OR = 7.044, CI = 2.120 – 23.405), and total resection (p = 0.025, OR = 0.284, CI = 0.095 – 0.855) were the independent predictors. Based on these findings, we established the Model-Logit and developed a corresponding scoring system, which is presented in Table 3. The scoring system provides the corresponding points and risk estimates, as outlined in Table 4.

10.3389/fonc.2023.1248553

TABLE 2 Results of multivariate logistic regression.

Variables	β value	*p-value*	OR value	95% CI
Age < 3	1.151	0.010	3.162	1.314 – 7.608
Blood loss	0.262	0.005	1.300	1.084 – 1.560
Midline tumor location	1.749	< 0.001	5.750	2.406 – 13.742
Preoperative Hydrocephalus	1.952	0.001	7.044	2.120 – 23.405
Total resection	-1.258	0.025	0.284	0.095 – 0.855
Constant	-4.341	< 0.001	0.013	

OR, odds ratio; CI, confidence interval; OR, odds ratio; CI, confidence interval.

Model-logit and scoring system

The Model-Logit could be established: Logit (P) = -4.341 + 1.151 * age (< 3: yes = 1, no = 0) + 0.262 * BL + 1.749 * midline tumor location (yes = 1; no = 0) + 1.952 * preoperative hydrocephalus (yes = 1, no = 0) – 1.258 * total resection (yes = 1, no = 0). This model was accurate but inconvenient for clinical use. Therefore, we establish a scoring system to assess the need for a VP shunt, whose method is similar to Wilson et al. (20). The scoring system was shown in the Table 3. Risk factors were categorized and reference values (W_{ij}) were set. We set the basic risk value ($W_{i\mathrm{REF}}$) of age < 3, BL, midline tumor location, preoperative hydrocephalus, and total resection as 0, 1U, 0, 0, 1, respectively. When parameters exceeded the $W_{i\mathrm{REF}}$, the greater points represented higher risks. The distance (D) was calculated based on the equation: $D = \beta_i*(W_{ij} - W_{REF})$. We set the constant B change of each risk factor for each point in the model. We regarded every increase of 2 U of BL as one point, as follows: B = 2 * β_{BL}, $\mathrm{Points}_j = D_i/B$. Finally, the risk estimate corresponding to the total score was based on the following equation: $P = \frac{1}{1+exp(-\sum_{i=0}^{p}\beta_i\chi_i)}$; $\sum_{i=0}^{p}\beta_i\chi_i = \beta_{constant} + \beta_{Age}*W_{1REF} + \beta_{BL}*W_{2REF} + \beta_{TM}*W_{3REF} + \beta_{PH}*W_{4REF} + \beta_{TR}*W_{5REF} + B*Total\ \ score = 0.524*Total\ \ score - 5.337$. Total cores ranged from 0 to 14 points. The total point and risk estimates are displayed in the Table 4.

To evaluate the performance of our scoring model, we generate ROC curves for independent predictors and models, respectively (Figure 3A). Our model demonstrated a significantly higher AUC

TABLE 3 Predictive model using risk factor categories.

Risk factor	Categories	Reference value	W_{ij}-$W_{i\mathrm{REF}}$	D	Points
Age					
	< 3	1	1	1.151	2
	≥ 3	0 = $W_{1\mathrm{REF}}$	0	0	0
Blood loss					
	BL ≤ 2.00	1 = $W_{2\mathrm{REF}}$	0	0	0
	2< BL ≤ 4	3	2	0.524	1
	4< BL ≤ 6	5	4	1.048	2
	BL > 6	7	6	1.572	3
Midline tumor location					
	Yes	1	1	1.749	3
	No	0 = $W_{3\mathrm{REF}}$	0	0	0
Preoperative Hydrocephalus					
	Yes	1	1	1.952	4
	No	0 = $W_{4\mathrm{REF}}$	0	0	0
Total resection					
	Yes	1 = $W_{5\mathrm{REF}}$	0	0	0
	No	0	-1	1.258	2

W_{ij}, reference value; W_{REF}, the basic risk value; D, distance, $D = \beta*(W_{ij} - W_{i\mathrm{REF}})$; $\mathrm{Points}_i = D_i/B$.

10.3389/fonc.2023.1248553

TABLE 4 Estimate of risk corresponding to total scores.

Total scores	Estimate of risk	Total scores	Estimate of risk
0	0.48%	8	24.14%
1	0.81%	9	34.96%
2	1.35%	10	47.58%
3	2.26%	11	60.52%
4	3.77%	12	72.13%
5	6.20%	13	81.38%
6	10.04%	14	88.07%
7	15.86%		

compared to age < 3, BL, midline tumor location, preoperative hydrocephalus, and total resection (0.859 vs. 0.598, 0.717, 0.725, 0.705, and 0.555, $p < 0.001$, respectively). Besides, AUC of the scoring system was close to Model-Logit (0.859 vs. 0.856, $p = 0.487$). Based on a cutoff value of 5.5 points, the predictive scores classified patients into low-risk (0-5 points) and high-risk (6-14 points) categories. Furthermore, the scoring system demonstrated excellent performance in an independent dataset consisted of 83 pediatric patients with brain tumors (AUC = 0.971) (Figure 3B).

Discussion

Brain tumors are commonly diagnosed in pediatric patients, and surgical resection is the primary treatment (22). However, postoperative hydrocephalus can significantly increase mortality and morbidity, especially in children (15). Previous studies investigating predictors of postoperative hydrocephalus in children with brain tumors have yielded inconsistent findings due to variations in inclusion criteria, statistical methods, limited variables, and sample sizes (1, 9, 12, 23). Most previous studies enrolled patients aged between 16 and 20 years old. However, we believe that including pediatric patients under 14 years old is justified as it allows for a more representative reflection of the patient population, considering tumor spectrum and CSF pathophysiology (15, 24, 25).

In our study, we conducted a comprehensive analysis of correlated parameters in pediatric patients with brain tumors using multivariate analysis. We included patients under 14 years old and analyzed various factors associated with postoperative hydrocephalus. We observed that most cases of postoperative hydrocephalus progression occurred within two weeks. Additionally, we developed a scoring system based on independent risk predictors, including ag e< 3, BL, preoperative hydrocephalus, midline tumor location, and tumor resection. The scoring system exhibited an AUC comparable to that of the Model-Logit (0.859 vs. 0.856, $p = 0.486$) and outperformed any single variable in both the training and validation cohorts.

Consistent with our findings, previous analyses have shown that younger age is associated with a higher risk of postoperative or progressive hydrocephalus requiring a VP shunt (9, 15, 23). The incidence of preoperative and postoperative hydrocephalus is significantly higher in younger children compared to adults (26). Approximately 50% of children are reported to have hydrocephalus at the time of diagnosis, which aligns closely with the rate observed in our training cohort (9). Preoperative hydrocephalus has been found to be significantly associated with the need for VP shunt implementation following tumor resection in children with brain tumors. Surgical trauma, combined with the immature function of CSF circulation, exaggerated intracranial hypertension, and ventricular dilatation, contribute to the increased formation or acute progression of hydrocephalus. Furthermore, the unique

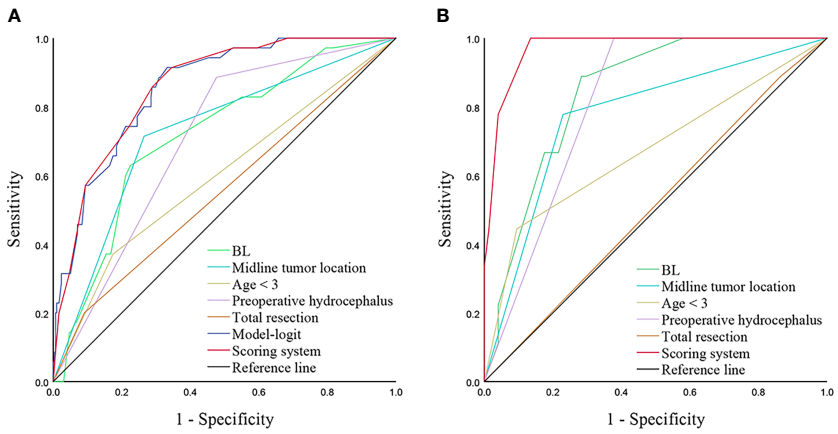

FIGURE 3
ROC curves analyzing scoring system and independent predictors in training cohort **(A)** and validation cohort **(B)**. A, AUCs of the scoring system, Model-Logit, BL, Midline tumor location, age < 3, preoperative hydrocephalus, and total resection are 0.859, 0.856, 0.717, 0.725, 0.598, 0.705 and 0.555, respectively in the training cohort. B, AUCs of scoring system, BL, Midline tumor location, age < 3, preoperative hydrocephalus, and total resection are 0.971, 0.841, 0.774. 0.675, 0.811, and 0.512, respectively in the validation cohort. ROC, receiver operator characteristic; AUC, area under the curve, BL, blood loss.

anatomical structure of posterior cranial fossa has led to increased interest in exploring the influence of preoperative hydrocephalus on postoperative hydrocephalus in children with infratentorial tumors (9, 23). It is noteworthy that while the incidence of preoperative hydrocephalus is higher in infratentorial tumors compared to supratentorial tumors, the location itself is not significantly associated with postoperative hydrocephalus. It implied another category (midline tumor location and others) may better explain the cause of postoperative hydrocephalus.

Midline tumor location have been identified as an independent predictor of postoperative hydrocephalus formation or progression, which is consistent with previous studies (9, 22, 23). This association may be attributed to the inflammatory reaction of surrounding tissues caused by surgical resection adjacent to the midline. Consequently, adhesion and obstruction of the interventricular foramen, third ventricle, midbrain aqueduct, and fourth ventricle can exacerbate hydrocephalus (27). Additionally, surgical damage to the ventricular zone, blood-brain barrier, and subarachnoid space may contribute to the development or progression of hydrocephalus (27). While the supratentorial or infratentorial categories did not yield significant results, this lack of significance can be partly attributed to the proportion of cerebellar hemisphere tumors. In contrast, the significance of midline tumors underscores its close proximity to the ventricles, subsequently influencing CSF. This observation aligns with existing literature that has emphasized the proximity of infratentorial tumors to the fourth ventricle as a notable risk factor (15). Besides, our data showed that the histology was not an independent predictor of postoperative hydrocephalus. This finding may be explained by the correlation observed between histology and typical midline tumors such as medulloblastoma and ependymoma. Therefore, we recognized the impact of surgical procedures on postoperative hydrocephalus and included the extent of tumor resection in our analyses. Analysis of postoperative images in the VP group revealed that 7 children had not undergone total resection, and among them, 5 cases, including 4 with midline tumors, developed postoperative obstructive hydrocephalus. This underscores the clinical importance of total resection. Furthermore, total resection played an independent protective role, which is consistent with certain studies (14, 22) although some studies have reported conflicting results (9, 15, 23). This discrepancy could potentially be attributed to the limited number of cases involving incomplete total resections.

We introduced a novel predictive variable, BL, which we estimated using intraoperative blood transfusion volume to mitigate the subjective bias of the operator and anesthetist in calculating BL during surgery (15). This approach provides a relatively objective reflection of intraoperative blood volume and maintenance of blood circulation in children. Evaluating intraoperative BL indirectly provides insight into the blood supply, tumor size, and the difficulty of resection, thus offering predictive value for the prognosis of children with brain tumors. Intraoperative hemorrhage can induce an inflammatory reaction and local tissue adhesion in the surgical area. Consequently, this can disrupt the connections between choroid plexus cells and corresponding cells, leading to impaired CSF flow and decreased ventricular volume maintenance function (28). Karimy et al. explored the pathophysiological mechanisms of intraoperative hemorrhage leading to the progression of hydrocephalus and found that hemorrhage can stimulate choroid plexus epithelial cells to produce an inflammatory response through factors like Toll-like receptor 4 and nuclear factor-κB (29). Thus, timely control of bleeding and blood loss management are crucial in children with brain tumors.

Rationale for scoring system

Although any single markers presented good predictive performance, they were only highlighted by their significance and applied thresholds. Numerous factors contributed to the results. Our scoring system showed the better predictive performance than any single marker both in the training cohort and validation cohort. The risk estimate corresponding to the total point could also be used in future studies. The optimal cutoff value of the scoring system was 5.5 points, which defined patients with low risks (0-5 points) and high risks (6-14 points).

Limitations of the study

There were several limitations in our study that should be acknowledged. It was retrospective and conducted in a single center, potentially limiting generalizability. Validation using data from other centers would have been preferable. We did not include postoperative CSF tests, and surgical position and imaging characteristics were not accounted for in our analysis. Additionally, BL calculation was challenging due to intraoperative factors, leading us to estimate BL based on transfusion volume. Further research is necessary to validate the findings and address the limitations.

Conclusions

Most postoperative hydrocephalus progresses within two weeks. The scoring system integrating age < 3, midline tumor location, preoperative hydrocephalus, total resection, and BL could apply practical evaluations. Children with total scores from 6 to 14 points had a high-risk level and need careful attention after surgery.

Data availability statement

The raw data supporting the conclusions of this article will be made available by the authors, without undue reservation.

Ethics statement

The studies involving humans were approved by Tongji hospital's institutional ethics committee. The studies were

conducted in accordance with the local legislation and institutional requirements. The human samples used in this study were acquired from primarily isolated as part of your previous study for which ethical approval was obtained. Written informed consent for participation was not required from the participants or the participants' legal guardians/next of kin in accordance with the national legislation and institutional requirements.

Author contributions

Z-YG and Z-AZ collected data and wrote the draft. PP: analyzed data. YL and FC: designed, revised, and supervised the study. All authors contributed to the article and approved the submitted version.

Conflict of interest

The authors declare that the research was conducted in the absence of any commercial or financial relationships that could be construed as a potential conflict of interest.

Publisher's note

References

1. Udaka YT, Packer RJ. Pediatric brain tumors. *Neurologic Clinics* (2018) 36 (3):533–56. doi: 10.1016/j.ncl.2018.04.009

2. Pollack IF, Agnihotri S, Broniscer A. Childhood brain tumors: current management, biological insights, and future directions. *J Neurosurg Pediatr* (2019) 23(3):261–73. doi: 10.3171/2018.10.Peds18377

3. Wang WH, Sung CY, Wang SC, Shao YJ. Risks of leukemia, intracranial tumours and lymphomas in childhood and early adulthood after pediatric radiation exposure from computed tomography. *CMAJ Can Med Assoc J = J l'Association medicale Can* (2023) 195(16):E575–e83. doi: 10.1503/cmaj.221303

4. Ghajar-Rahimi G, Kang KD, Totsch SK, Gary S, Rocco A, Blitz S, et al. Clinical advances in oncolytic virotherapy for pediatric brain tumors. *Pharmacol Ther* (2022) 239:108193. doi: 10.1016/j.pharmthera.2022.108193

5. Alois CI, Luntz A. Recognizing and managing hydrocephalus in children. *JAAPA Off J Am Acad Physician Assistants* (2023) 36(4):18–26. doi: 10.1097/01.Jaa.0000921260.32212.39

6. Schneider M, Schuss P, Güresir Á, Borger V, Vatter H, Güresir E. Surgery for posterior fossa meningioma: elevated postoperative cranial nerve morbidity discards aggressive tumor resection policy. *Neurosurgical Rev* (2021) 44(2):953–9. doi: 10.1007/s10143-020-01275-6

7. Tully HM, Doherty D, Wainwright M. Mortality in pediatric hydrocephalus. *Dev Med Child Neurol* (2022) 64(1):112–7. doi: 10.1111/dmcn.14975

8. Dewan MC, Lim J, Shannon CN, Wellons JC 3rd. The durability of endoscopic third ventriculostomy and ventriculoperitoneal shunts in children with hydrocephalus following posterior fossa tumor resection: A systematic review and time-to-failure analysis. *J Neurosurg Pediatr* (2017) 19(5):578–84. doi: 10.3171/2017.1.Peds16536

9. Foreman P, McClugage S 3rd, Naftel R, Griessenauer CJ, Ditty BJ, Agee BS, et al. Validation and modification of a predictive model of postresection hydrocephalus in pediatric patients with posterior fossa tumors. *J Neurosurg Pediatr* (2013) 12(3):220–6. doi: 10.3171/2013.5.Peds1371

10. Bell H, Ownsworth T, Lloyd O, Sheeran N, Chambers S. A systematic review of factors related to children's quality of life and mental health after brain tumor. *Psycho-oncology* (2018) 27(10):2317–26. doi: 10.1002/pon.4850

11. Grønbæk JK, Wibroe M, Toescu S, Frič R, Thomsen BL, Møller LN, et al. Postoperative speech impairment and surgical approach to posterior fossa tumours in children: A prospective European multicentre cohort study. *Lancet Child Adolesc Health* (2021) 5(11):814–24. doi: 10.1016/s2352-4642(21)00274-1

12. Thompson EM, Bramall A, Herndon JE 2nd, Taylor MD, Ramaswamy V. The clinical importance of medulloblastoma extent of resection: A systematic review. *J neuro-oncology* (2018) 139(3):523–39. doi: 10.1007/s11060-018-2906-5

13. Bognár L, Borgulya G, Benke P, Madarassy G. Analysis of csf shunting procedure requirement in children with posterior fossa tumors. *Child's nervous system ChNS Off J Int Soc Pediatr Neurosurg* (2003) 19(5-6):332–6. doi: 10.1007/s00381-003-0745-x

14. Teske N, Chiquillo-Domínguez M, Skrap B, Harter PN, Rejeski K, Blobner J, et al. Shunt dependency in supratentorial intraventricular tumors depends on the extent of tumor resection. *Acta Neurochir (Wien)* (2023) 165(4):1053–64. doi: 10.1007/s00701-023-05532-7

15. Hu SQ, Guo ZY, Wan LJ, Chen ZR, Wan F. Blood loss in operation is independently predictive of postoperative ventriculoperitoneal shunt in pediatric patients with posterior fossa tumors. *Pediatr Neurol* (2023) 144:119–25. doi: 10.1016/j.pediatrneurol.2023.04.023

16. Zhou X, Xia J. Application of evans index in normal pressure hydrocephalus patients: A mini review. *Front Aging Neurosci* (2021) 13:783092. doi: 10.3389/fnagi.2021.783092

17. D'Arco F, Khan F, Mankad K, Ganau M, Caro-Dominguez P, Bisdas S. Differential diagnosis of posterior fossa tumours in children: new insights. *Pediatr Radiol* (2018) 48(13):1955–63. doi: 10.1007/s00247-018-4224-7

18. Corti C, Urgesi C, Massimino M, Gandola L, Bardoni A, Poggi G. Effects of supratentorial and infratentorial tumor location on cognitive functioning of children with brain tumor. *Child's nervous system ChNS Off J Int Soc Pediatr Neurosurg* (2020) 36(3):513–24. doi: 10.1007/s00381-019-04434-3

19. Turhon M, Kang H, Li M, Liu J, Zhang Y, Zhang Y, et al. Treatment of fusiform aneurysms with a pipeline embolization device: A multicenter cohort study. *J neurointerv Surg* (2023) 15(4):315–20. doi: 10.1136/neurintsurg-2021-018539

20. Wilson PW, D'Agostino RB, Levy D, Belanger AM, Silbershatz H, Kannel WB. Prediction of coronary heart disease using risk factor categories. *Circulation* (1998) 97 (18):1837–47. doi: 10.1161/01.cir.97.18.1837

21. Hu SQ, Hu JN, Chen RD, Yu JS. A predictive model using risk factor categories for hospital-acquired pneumonia in patients with aneurysmal subarachnoid hemorrhage. *Front Neurol* (2022) 13:1034313. doi: 10.3389/fneur.2022.1034313

22. Anetsberger S, Mellal A, Garvayo M, Diezi M, Perez MH, Beck Popovic M, et al. Predictive factors for the occurrence of perioperative complications in pediatric posterior fossa tumors. *World Neurosurg* (2023) 172:e508–e16. doi: 10.1016/j.wneu.2023.01.063

23. Helmbold LJ, Kammler G, Regelsberger J, Fritzsche FS, Emami P, Schüller U, et al. Predictive factors associated with ventriculoperitoneal shunting after posterior fossa tumor surgery in children. *Child's nervous system ChNS Off J Int Soc Pediatr Neurosurg* (2019) 35(5):779–88. doi: 10.1007/s00381-019-04136-w

24. Won SY, Gessler F, Dubinski D, Eibach M, Behmanesh B, Herrmann E, et al. A novel grading system for the prediction of the need for cerebrospinal fluid drainage following posterior fossa tumor surgery. *J Neurosurg* (2019) 132(1):296–305. doi: 10.3171/2018.8.Jns181005

25. Ostrom QT, Adel Fahmideh M, Cote DJ, Muskens IS, Schraw JM, Scheurer ME, et al. Risk factors for childhood and adult primary brain tumors. *Neuro-oncology* (2019) 21(11):1357–75. doi: 10.1093/neuonc/noz123

26. Marx S, Reinfelder M, Matthes M, Schroeder HWS, Baldauf J. Frequency and treatment of hydrocephalus prior to and after posterior fossa tumor surgery in adult patients. *Acta Neurochir (Wien)* (2018) 160(5):1063–71. doi: 10.1007/s00701-018-3496-x

27. Hochstetler A, Raskin J, Blazer-Yost BL. Hydrocephalus: historical analysis and considerations for treatment. *Eur J Med Res* (2022) 27(1):168. doi: 10.1186/s40001-022-00798-6

28. Sevensky R, Newville JC, Tang HL, Robinson S, Jantzie LL. Cumulative damage: cell death in posthemorrhagic hydrocephalus of prematurity. *Cells* (2021) 10(8):1911. doi: 10.3390/cells10081911

29. Karimy JK, Zhang J, Kurland DB, Theriault BC, Duran D, Stokum JA, et al. Inflammation-dependent cerebrospinal fluid hypersecretion by the choroid plexus epithelium in posthemorrhagic hydrocephalus. *Nat Med* (2017) 23(8):997–1003. doi: 10.1038/nm.4361

frontiers | Frontiers in Neurology

TYPE Original Research
PUBLISHED 23 October 2023
DOI 10.3389/fneur.2023.1297835

OPEN ACCESS

EDITED BY
Cesare Zoia,
San Matteo Hospital Foundation (IRCCS), Italy

REVIEWED BY
Giorgio Mantovani,
University of Ferrara, Italy
Naci Balak,
Istanbul Medeniyet University Goztepe Education and Research Hospital, Türkiye

*CORRESPONDENCE
Yuan Ma
✉ Tianfu_47@163.com
Qing Ou-Yang
✉ oyq911@126.com

†These authors have contributed equally to this work

RECEIVED 20 September 2023
ACCEPTED 02 October 2023
PUBLISHED 23 October 2023

CITATION
Yang Y, Hu F, Wu S, Huang Z, Wei K, Ma Y and Ou-Yang Q (2023) Blood-based biomarkers: diagnostic value in brain tumors (focus on gliomas). *Front. Neurol.* 14:1297835. doi: 10.3389/fneur.2023.1297835

Blood-based biomarkers: diagnostic value in brain tumors (focus on gliomas)

Yuting Yang[1,2], Fei Hu[2], Song Wu[2], Zhangliang Huang[1,2], Kun Wei[2], Yuan Ma[1,2*†] and Qing Ou-Yang[2*†]

[1]Institute of Biomedical Engineering, College of Medicine, Southwest Jiaotong University, Chengdu, Sichuan, China, [2]Department of Neurosurgery, Affiliated Hospital of Southwest Jiaotong University, The General Hospital of Western Theater Command, Chengdu, Sichuan, China

Background: Brain tumors, especially gliomas, are known for high lethality. It is currently understood that the correlations of tumors with coagulation and inflammation have been gradually revealed.

Objective: This study aimed to explore the potential value of several reported peripheral blood parameters as comprehensively as possible, with preoperative diagnosis and identification of brain tumors (focus on gliomas).

Methods: Patients with central nervous system tumors (craniopharyngioma, ependymoma, spinal meningioma, acoustic neuroma, brain metastases, meningioma, and glioma) or primary trigeminal neuralgia admitted to our hospital were retrospectively analyzed. The results of the routine coagulation factor test, serum albumin test, and blood cell test in peripheral blood were recorded for each group of patients on admission. Neutrophil–lymphocyte ratio (NLR), derived NLR (dNLR), platelet–lymphocyte ratio (PLR), lymphocyte–monocyte ratio (LMR), prognostic nutritional index (PNI), the systemic immune-inflammation index (SII), pan-immune-inflammation value (PIV), and their pairings were calculated. Their ability to identify brain tumors and their correlation with glioma grade were analyzed.

Results: A total of 698 patients were included in this retrospective case–control study. Glioma patients had higher NLR, SII, and PIV but lower LMR. The NLR in the brain metastasis group was lower than that in the control, meningioma, and acoustic neuroma groups, but the SII and PIV were higher than those in the ependymoma group. Fibrinogen, white blood cell count, neutrophil count, NLR, SII, and PIV in the GBM group were higher than those in the control group. In all comparisons, NLR and NLR + dNLR showed the greatest accuracy, with areas under the curve (AUCs) of 0.7490 (0.6482–0.8498) and 0.7481 (0.6457–0.8505), respectively. PIV, dNLR + PIV, and LMR + PIV ranked second, with AUCs of 0.7200 (0.6551–0.7849), 0.7200 (0.6526–0.7874), 0.7204 (0.6530–0.7878) and 0.7206 (0.6536–0.7875), respectively.

Conclusion: NLR, PIV, and their combinations show high sensitivity and specificity in the diagnosis of brain tumors, especially gliomas. Overall, our results provide evidence for these convenient and reliable peripheral blood markers.

KEYWORDS

brain tumors, glioma, pan-immune-inflammation value, neutrophil–lymphocyte ratio, diagnostic indicator

Introduction

Approximately 300, 000 people worldwide are diagnosed with brain tumors each year, and approximately 250, 000 died (1). According to the classification published by the WHO, common central nervous system (CNS) tumors include acoustic neuroma, meningioma, brain metastases, glioma, and some other tumors (2). The most common primary brain tumor is meningioma (39% of all brain tumors and 54.5% of non-malignant brain tumors), followed by tumors of the saddle area (craniopharyngioma, pituitary tumors, etc.) (3). Among primary malignant tumors of the brain, glioblastoma (GBM) has the highest incidence [14.3% of all tumors, 49.1% of malignant tumors, and 81% of glioma (4)], with a five-year survival rate of only 6.8% (3). The incidence of ependymoma is approximately 0.2 to 0.4 per 100, 000 individuals (5). The treatment of brain tumors includes surgery, radiotherapy, and chemotherapy (temozolomide adjuvant chemotherapy). Most patients died of progressive disease. Thus, accurate grading has a huge impact on the way of treatment.

The identification of brain tumors has long been based on histological examination (the patient undergoes surgery, and the diagnosis is confirmed by a pathologist). Sometimes clinical presentation and radiological methods (visualization with contrast-enhanced magnetic resonance imaging, X-rays, etc.) can also make a simple distinction. However, histological and radiological tests are invasive and expensive. Recently, liquid biopsies based on circulating tumor cells (CTCS) in peripheral blood samples have been recognized as superior technological advances (6), but the test remains expensive, and routine screening is not available in most institutions. We still lack more economical, convenient, and widely available diagnostic biomarkers.

Cancer has long been reported to be associated with chronic inflammation (7). Recently, some peripheral blood-based indicators, neutrophil–lymphocyte ratio (NLR), derived NLR (dNLR), platelet–lymphocyte ratio (PLR), lymphocyte–monocyte ratio (LMR), prognostic nutritional index (PNI), the systemic immune–inflammation index (SII), and pan–immune–inflammation value (PIV) have been reported to be associated with the prognosis or stratification of several tumors, such as glioma (8–10), lung cancer (11), and colorectal cancer (12–14). However, only a few studies have reported their diagnostic value in brain tumors, particularly glioma (15, 16). At the same time, tumor patients are characterized by a dysregulated coagulation system and a systemic hypercoagulable state (17). Different degrees of activation of the coagulation system seem to be associated with tumor aggressiveness (18). Therefore, some coagulation parameters and inflammatory indicators may be valuable in tumor diagnosis. Among them, PIV, a novel immune indicator recently created, has been shown to have an independent and significant association with poor outcomes in GBM patients, who received postoperative radiotherapy and concomitant addition of temozolomide adjuvant therapy (19).

In this study, we compared differences in coagulation parameters, serum albumin levels, and peripheral blood cell counts among primary trigeminal neuralgia, ependymoma, craniopharyngioma, acoustic neuroma, brain metastases, meningiomas, and gliomas. Furthermore, the diagnostic value of NLR, dNLR, PLR, LMR, PNI, SII, PIV, and their combinations in brain tumors was further evaluated, especially in GBM.

Methods

Study design

A descriptive case–control design was adopted, and to ensure the research quality, the STROBE checklist was used to report findings (Supplementary Table S1).

Setting

The medical records of patients with brain tumors (craniopharyngioma, ependymoma, spinal meningioma, acoustic neuroma, brain metastases, meningioma, or glioma) and trigeminal neuralgia (NT) patients admitted to the Neurosurgery Department of the General Hospital of Western Theater Command in Chengdu from January 2017 to December 2022 were retrospectively analyzed.

Participants

Patients included in this study had to meet the following criteria: (1) craniopharyngioma, ependymoma, spinal meningioma, acoustic neuroma, brain metastases, and meningioma, or glioma confirmed by biopsy or postoperative pathological examination; (2) complete preoperative routine coagulation parameters, serum albumin level, and peripheral blood cell count data; (3) no previous hypertension, hyperlipidemia, diabetes, metabolic syndrome, heart disease, liver and kidney dysfunction, hematologic disorders, autoimmune diseases, no preoperative fever, infectious diseases, and no use of preoperative anti-infective drugs and steroids; (4) no previous brain tumors, currently has only one type of brain tumor and no tumor-specific treatment history such as radiotherapy or chemotherapy (except brain metastases); (5) informed consent.

As for the control group, patients admitted to our neurosurgery department for trigeminal nerve microvascular decompression or facial nerve microvascular decompression during the same period, and the requirements were as follows: (1) complete preoperative information on routine coagulation parameters, serum albumin levels, and peripheral blood cell counts; (2) no previous tumor, hypertension, hyperlipidemia, diabetes, metabolic syndrome, heart disease, liver and kidney dysfunction, hematologic disorders, autoimmune diseases, no preoperative fever, infectious diseases, and no anti–infective drugs; (3) informed consent.

Data collection

Demographic parameters and pathological information were retrieved and recorded from the medical record, including gender, age, diagnosis, tumor grade, histological type, and primary site of brain metastasis. Patients were routinely examined upon admission for coagulation parameters [prothrombin time (PT), fibrinogen (FIB) level, activated partial thromboplastin time (APTT), and thrombin time (TT)], serum albumin levels, and peripheral blood cell counts [platelet count, white blood cell (WBC) count,

neutrophil count, lymphocyte count, monocyte count, eosinophil count, and basophil count]. All tests were performed at our hospital testing department.

Data measurement

In addition, the above data were used to calculate NLR (neutrophil/lymphocyte count), dNLR ([white blood cell count – neutrophil count]/lymphocyte count), PLR (platelet count/lymphocyte count), LMR (lymphocyte count/monocyte count), PNI (albumin count + lymphocyte count *5), SII (platelet count * neutrophil count/lymphocyte count), and PIV (neutrophil count * platelet count * monocyte count/lymphocyte count). Furthermore, these data were used to calculate NLR + dNLR, NLR + PLR, NLR + LMR, NLR + PNI, NLR + SII, NLR + PIV, dNLR + PLR, dNLR + LMR, dNLR + PNI, dNLR + SII, dNLR + PIV, PLR + LMR, PLR + PNI, PLR + SII, PLR + PIV, LMR + PNI, LMR + SII, LMR + PIV, PNI + SII, PNI + PIV, and SII + PIV.

Statistical analysis

Statistical analysis was performed using GraphPad Prism 9.4.1. First, the Kruskal–Wallis test was used to analyze the normality of the variables. We used the median (range) to represent all data. The Mann–Whitney *U*-test was used for comparison between groups. The Spearman correlation test was used to analyze the correlation among variables. The diagnostic efficacy of peripheral blood inflammatory markers in subjects was evaluated by the area under the curve (AUC) obtained from the receiver operating characteristic (ROC) curve. A *P*-value of <0.05 was considered to be statistically significant.

Results

Participants' characteristics

A total of 698 patients were included in this study, including 66 patients with trigeminal neuralgia, 14 patients with craniopharyngioma, 15 patients with ventricular meningioma, 17 patients with chordoma, 93 patients with auditory neuroma, 39 patients with brain metastases, 313 patients of meningioma, and 141 patients with glioma (grade I, 1 case; grade II, 50 cases; grade III, 20 cases; and grade IV, 69 cases). The selection flowchart is demonstrated in Figure 1.

Glioma patients [48 (8–74)] were significantly younger than control patients [58.5 (19–82)], acoustic neuroma patients [54.5 (15–83)], brain metastases patients [59 (39–78)], and meningioma patients [53 (5–81)]. Patients in the meningioma group were also significantly younger than the control group. The majority of patients with meningioma were female [232, (74.12%)]. Detailed demographic information is listed in Table 1.

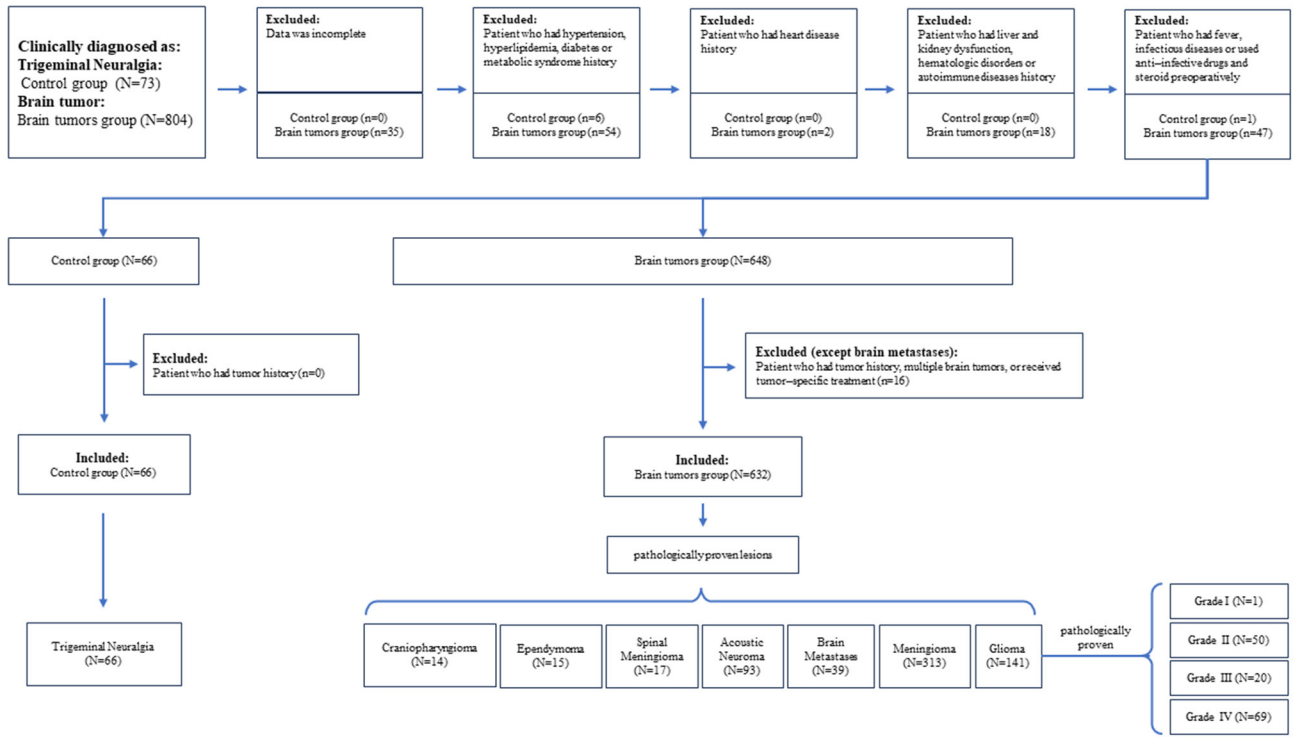

FIGURE 1
Selection flowchart of participants.

TABLE 1 Preoperative characteristics of patients with brain tumors.

Parameter	Trigeminal neuralgia	Craniopharyngioma	Ependymoma	Spinal meningioma	Acoustic neuroma	Brain metastases	Meningioma	Glioma
Age	58.5 (19–82)	49 (19–66)	47.5 (4–76)	55.5 (22–83)	54.5 (15–83)	59 (39–78)	53 (5–81)*	48 (8–74)*+§#
No. of patients	66	14	15	17	93	39	313	141
Male (*n*, %)	27 (40.91%)	6 (42.86%)	6 (40%)	14 (82.35%)	36 (38.71%)‡	19 (48.72%)	81 (25.88%)‡	85 (60.28%)+§
Female (*n*, %)	39 (59.09%)	8 (57.14%)	9 (60%)	3 (17.65%)	57 (61.29%)‡	20 (51.28%)	232 (74.12%)‡	56 (39.72%)+§
Albumin (g/L)	42.9 (37.3–49.6)	42.95 (39.6–46.4)	44.4 (31.2–49.9)	42.8 (39.9–53.9)	43.3 (34–54)	41.9 (31.8–50)	42.8 (34.9–53.2)	43 (35.1–55)
PT (s)	10.6 (9–12.9)	10.25 (9.8–12)	10.7 (9.6–12.5)	10.5 (9.6–11.5)	10.6 (9.2–12.3)	10.8 (9.4–12.4)	10.6 (8.7–13.3)	10.7 (9–13.2)
FIB (g/L)	2.35 (1.71–6.5)	2.58 (1.87–5.34)	2.58 (2.11–5.1)	2.63 (1.86–3.77)	2.59 (1.52–4.86)	2.63 (2–5.6)	2.63 (1.18–9.27)	2.56 (1.62–6.85)
APTT (s)	26.2 (18.1–42.6)	25.35 (21.6–34.7)	29.3 (22.8–46.5)	28 (23.2–42)	26.8 (19.2–32.3)	25.8 (19.6–33.6)	26.3 (15.1–39.3)	25.95 (17.4–36)
TT (s)	17.8 (15.3–22.3)	18.9 (16.2–21.9)	17.9 (11.72–20.2)	18.2 (16.6–20.3)	17.8 (15.3–25.9)	18.3 (16.1–20.6)	18 (15.1–21.6)	18.15 (14.1–23.6)
Platelets (10^9/L)	166 (88–314)	155 (113–243)	204 (110–402)	190 (118–254)	180 (74–406)	179.5 (50–395)	174 (64–517)	188 (83–426)
WBCs (10^9/L)	5.41 (3.3–14.62)	6.32 (3.53–11.33)	7.11 (4.57–11.33)	5.53 (3.82–10.78)	5.56 (3.22–16.7)	6.24 (2.61–21.48)	5.65 (3.08–20.88)	6.82 (3–15.26)*+#
Neutrophils (10^9/L)	3.48 (1.57–13.79)	3.72 (1.75–10.05)	4.03 (2.17–12.76)	3.46 (2.12–7.41)	3.46 (1.69–7.93)	4.43 (1.71–13.98)*+	3.57 (1.32–12.5)§	4.35 (1.8–14.37)*+#
Lymphocytes (10^9/L)	1.48 (0.74–3.01)	2.04 (0.63–2.75)	1.68 (1–5.54)	1.57 (0.94–2.81)	1.62 (0.76–2.9)	1.28 (0.42–2.69)^	1.55 (0.37–4.34)	1.56 (0.49–3.19)
Monocytes (10^9/L)	0.34 (0.06–0.77)	0.32 (0.2–0.6)	0.34 (0.24–0.79)	0.36 (0.16–0.79)	0.32 (0.12–0.75)	0.35 (0.09–1.2)	0.34 (0.13–1.2)	0.39 (0.03–1.31) +#
Eosinophils (10^9/L)	0.12 (0–0.66)	0.18 (0.03–0.45)	0.12 (0–0.46)	0.1 (0.02–0.23)	0.11 (0–0.62)	0.07 (0–0.67)^	0.1 (0–0.8)	0.08 (0–0.92)^#
Basophils (10^9/L)	0.02 (0–0.08)	0.02 (0–0.1)	0.02 (0.01–0.07)	0.03 (0.01–0.07)	0.02 (0–0.08)	0.02 (0.01–0.07)	0.02 (0–0.13)	0.02 (0–0.08)
NLR	2.11 (0.97–18.39)	1.74 (0.9–15.95)	2.22 (0.93–8.92)	2.13 (0.84–4.29)	2.11 (0.83–4.79)	3.65 (1.2–16.38)*^+	2.13 (0.6–18.89)§	2.81 (0.97–28.74)*^+#
dNLR	1.32 (1.11–2.32)	1.28 (1.16–2.03)	1.29 (1.11–1.58)	1.27 (1.21–1.75)	1.3 (1.14–1.72)	1.34 (1.09–1.97)	1.29 (1.1–2.32)	1.33 (1.1–2.13)
PLR	107.8 (48.81–409.5)	75.58 (43.64–350.8)	87.48 (40.2–226)	134(63.6–204.8)	110.09 (44.71–476.32)	127.8 (27.59–278.6)	110.32 (33.33–395.24)	119.48 (41.25–776)
LMR	4.42 (0.96–12.5)	6.4 (1.05–8.59)	4.75 (2.64–10.45)	5.64 (2.24–7.81)	4.71 (1.72–9.83)	3.87 (0.38–12.56)^+	4.91 (0.92–12.06)§	4.02 (0.92–16.33)^+#
PNI	50.2 (41–60.6)	54.17 (44.55–56.85)	52.45 (39.65–75.5)	52.6 (45.3–60.1)	51.7 (40.55–62.35)	49.7 (33.9–58.75)	51.3 (41.4–66.15)	51.1 (40.55–66.65)
SII	366.67 (151.31–3934.75)	245.08 (106.6–3525.48)	407 (130.25–1684.7)	420.2 (145.65–1089.74)	369.77 (144.46–1733.79)	545.5 (18.97–3411.13)^	358.5 (86.23–3235.63)	514.8 (152.58–3142.07)^+#
PIV	124.8 (26.99–2462)	92.82 (35.18–2115)	157.7 (60.66–551.5)	114.1 (57.91–590.4)	131.0 (26.37–603.4)	222.2 (23.54–3445)^	120.8 (21.72–2394)§	196.5 (21.63–4126)*^+#

Values are median (range). *$p < 0.05$, compared to trigeminal neuralgia. ^$p < 0.05$, compared to craniopharyngioma. †$p < 0.05$, compared to ependymoma. ‡$p < 0.05$, compared to spinal meningioma. + $p < 0.05$, compared to acoustic neuroma. §$p < 0.05$, compared to brain metastases. #$p < 0.05$, compared to meningioma.

10.3389/fneur.2023.1297835

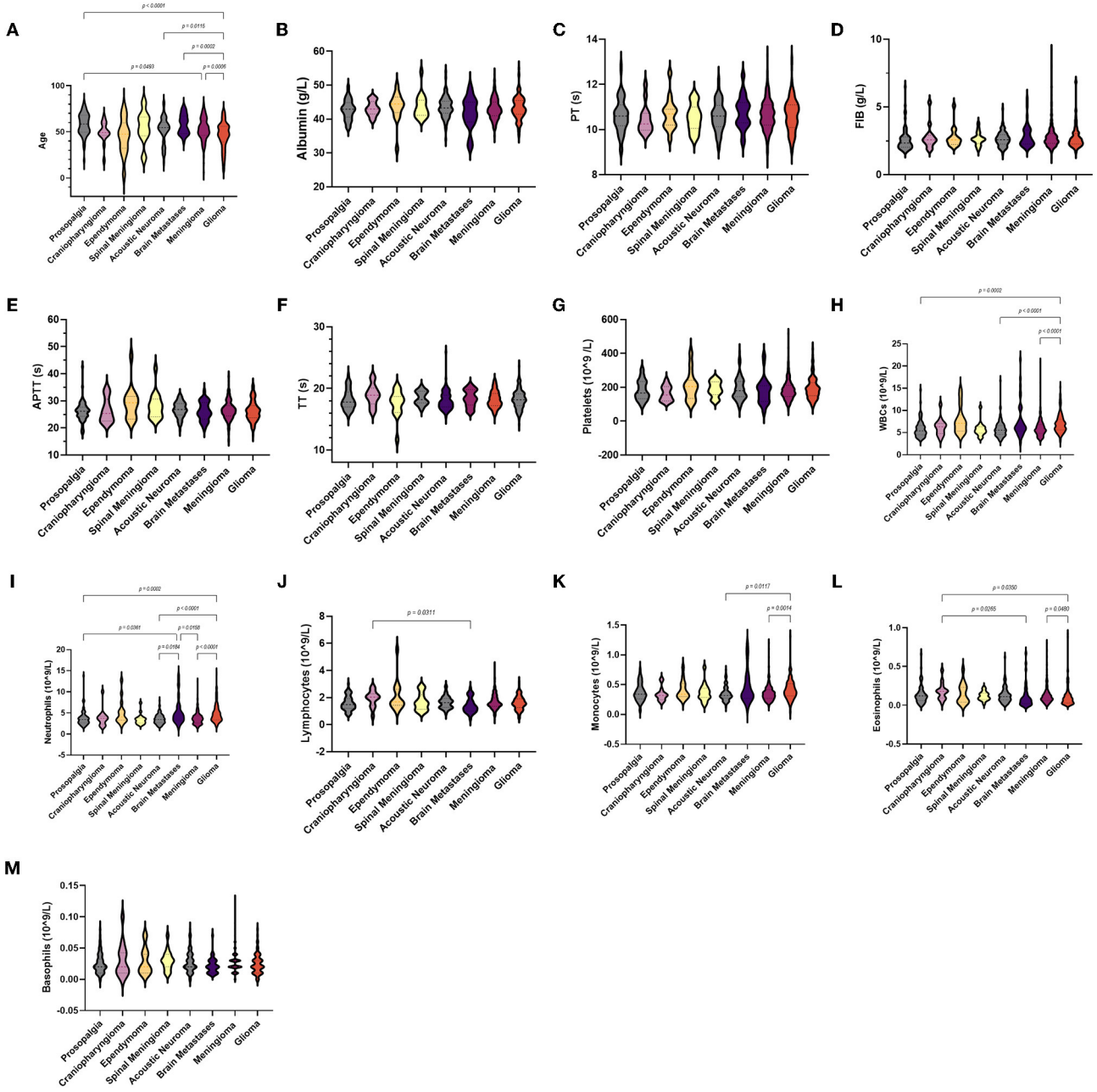

FIGURE 2
Violin diagram showing comparative results of characteristics in the trigeminal neuralgia group, craniopharyngioma group, ependymoma group, acoustic neuroma group, brain metastases group, meningioma group, and glioma group (the dashed line in the middle represents the median and the dashed lines on both sides represent the interquartile range). **(A)** Age, **(B)** albumin, **(C)** PT, **(D)** FIB, **(E)** APTT, **(F)** TT, **(G)** platelets, **(H)** WBCs, **(I)** neutrophils, **(J)** lymphocytes, **(K)** monocytes, **(L)** eosinophils, **(M)** basophils.

Comparison of preoperative blood markers between the control group and the tumor group

In all groups, no significant differences were observed in albumin, basophil count, and coagulation parameters (Figure 2). For neutrophils, the brain metastasis group [4.43 (1.71–13.98)] was higher than the trigeminal neuralgia [3.48 (1.57–13.79)], acoustic neuroma [3.46 (1.69–7.93)], and meningioma groups [4.43 (1.71–13.98)]. Compared with the control group, the acoustic neuroma group, the meningioma group, and the glioma group had much higher white blood cell counts [6.82 (3–15.26)] and neutrophil counts [4.35 (1.8–14.37)]. Meanwhile, the monocyte count of glioma patients [0.39 (0.03–1.31)] was higher than that of acoustic neuroma [0.32 (0.12–0.75)] and meningioma patients [0.34 (0.13–1.2)].

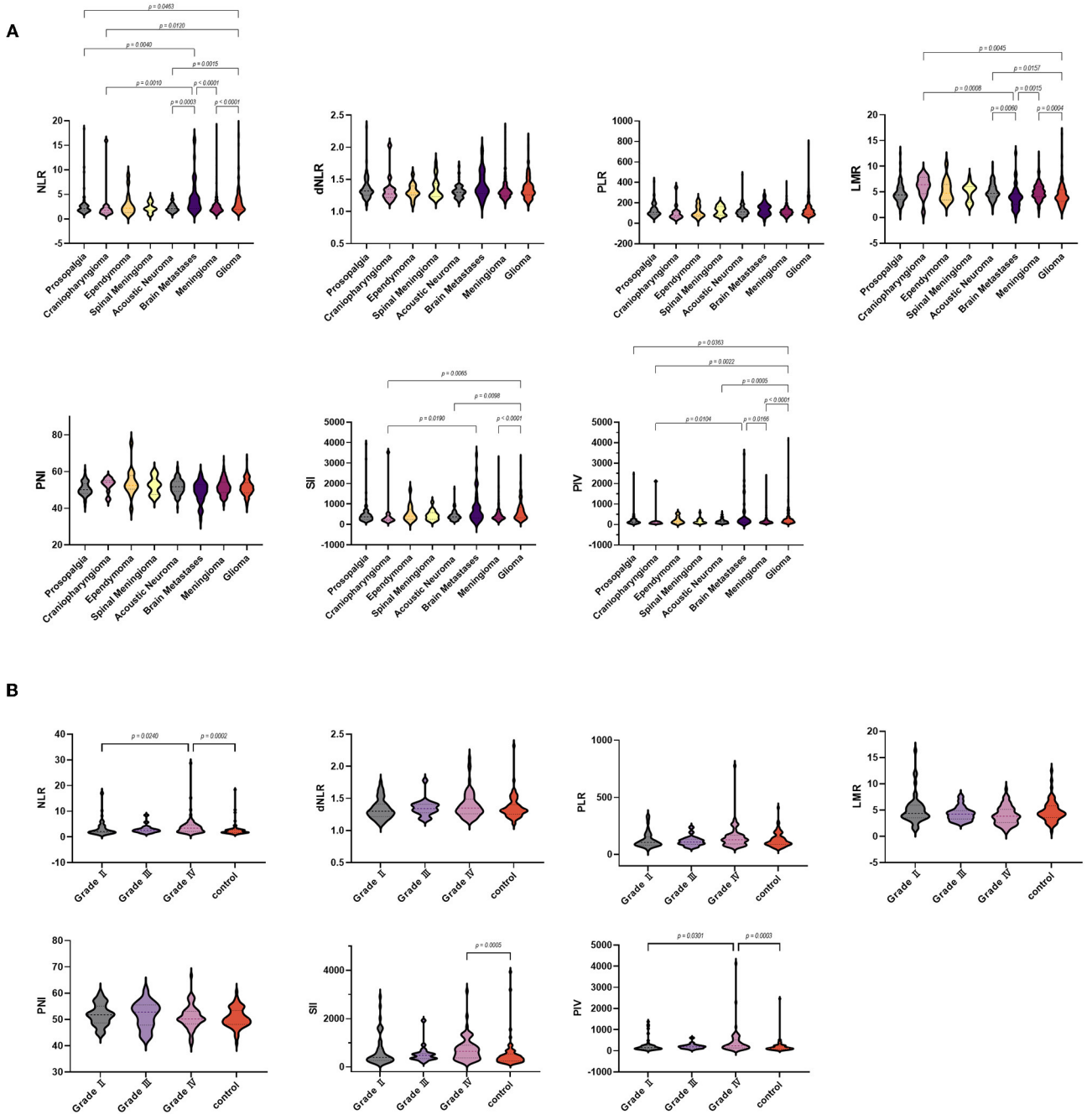

FIGURE 3
Violin diagram showing comparative results of preoperative inflammatory markers in different groups (the dashed line in the middle represents the median and the dashed lines on both sides represent the interquartile range). **(A)** Comparison of preoperative blood markers between the control group and the tumor group, **(B)** Comparison of preoperative blood markers for glioma of different grades.

As for laboratory parameters (Figure 3A), NLR and PIV were higher in the brain metastasis group than in the acoustic neuroma group, but the data were not significant. The NLR, SII, and PIV of glioma patients [2.81 (0.97–28.74), 514.8 (152.58–3142.07), and 196.5 (21.63–4126)] were significantly higher than the trigeminal neuralgia, craniopharyngioma, acoustic neuroma, and meningioma. We also observed lower LMR in the glioma group [4.02 (0.92–16.33)]. Moreover, NLR was lower in the brain metastasis group than in the control, meningioma, and acoustic neuroma groups, but the SII and PIV were higher than in the ependymoma group. Surprisingly, there were no differences in dNLR, PLR, and PNI among all groups.

Comparison of preoperative blood markers for glioma of different grades

We further analyzed these parameters in different grades of glioma according to the WHO (Table 2). Among the coagulation

TABLE 2 Correlations between preoperative inflammatory markers and glioma grade.

Marker	Trigeminal neuralgia	Glioma grade			
		I ($n = 1$)	II ($n = 50$)	III ($n = 20$)	IV ($n = 69$)
Age	58.5 (19–82)	44	42.5 (8–71)*	46.5 (21–72)*	52 (10–74)*†
Albumin in g/L	42.9 (37.3–49.6)	41.8	43.4 (37.5–52.8)	44.6 (35.3–49.3)	42.7 (35.1–55)
PT	10.6 (9–12.9)	10.8	1055 (9.2–11.8)	10.55 (9.2–11.8)	10.8 (9–13.2)
FIB	2.35 (1.71–6.5)	2.14	2.41 (1.7–4.25)	2.52 (2–3.44)	2.67 (1.62–6.85)*†
APTT	26.2 (18.1–42.6)	28.7	26.55 (19.7–36)	24.5 (19.8–31.4)	25.9 (17.4–34.9)
TT	17.8 (15.3–22.3)	17	18.55 (16.3–23.6)	18.9 (16.2–21.2)	17.9 (14.1–21.4)†
Platelets (10^9/L)	166 (88–314)	139	181.5 (83–362)	172 (97–299)	193 (90–426)
WBCs (10^9/L)	5.41 (3.3–14.62)	5.12	5.99 (3.9–13.37)	6.86 (4.29–9.39)	7.1 (3–15.26)*
Neutrophils (10^9/L)	3.48 (1.57–13.79)	3.07	3.61 (1.9–11.07)	4.23 (2.24–8.08)	5.1 (1.8–14.37)*
Lymphocytes (10^9/L)	1.48 (0.74–3.01)	1.46	1.71 (0.49–2.71)	1.54 (0.95–2.96)	1.52 (0.5–3.19)
Monocytes (10^9/L)	0.34 (0.06–0.77)	0.37	0.38 (0.03–0.84)	0.38 (0.25–0.64)	0.42 (0.17–1.31)
Eosinophils (10^9/L)	0.12 (0–0.66)	0.19	0.08 (0–0.92)	0.11 (0.01–0.47)	0.07 (0–0.44)
Basophils (10^9/L)	0.02 (0–0.08)	0.03	0.02 (0–0.08)	0.03 (0–0.08)	0.02 (0.01–0.06)
NLR	2.11 (0.97–18.39)	2.1	2.09 (0.97–17.31)	2.59 (1.31–8.51)	3.42 (0.98–28.74)*†
dNLR	1.32 (1.11–2.32)	1.4	1.3 (1.1–1.75)	1.34 (1.17–1.78)	1.35 (1.15–2.13)
PLR	107.8 (48.81–409.5)	95.21	105.67 (41.25–342.86)	108.9 (61.78–237.89)	128.76 (61.44–776)
LMR	4.42 (0.96–12.5)	3.95	4.35 (1.44–16.33)	4.22 (2.63–7.59)	3.82 (0.92–9)
PNI	50.2 (41–60.6)	49.1	51.78 (44.5–60.3)	52.73 (43.2–61)	50.18 (40.55–66.65)
SII	366.67 (151.31–3934.75)	292.28	397.48 (152.58–2907.43)	476.32 (202.52–1922.19)	646.7 (170.91–3142.07)*
PIV	124.8 (26.99–2462)	108.1	154.2 (21.36–1381)	191.5 (50.63–615.1)	243.0 (32.47–4126)*†

Values are median (range). *$p < 0.05$, compared to trigeminal neuralgia. ^$p < 0.05$, compared to glioma grade I glioma patients. †$p < 0.05$, compared to glioma grade II glioma patients. ‡$p < 0.05$, compared to glioma grade III glioma patients.

parameters (Figure 4), the FIB of GBM [2.67 (1.62–6.85)] was significantly higher than the control group and glioma grade II. For inflammation markers, white blood cell counts and neutrophils were both significantly higher in gliomas [7.1 (3–15.26) and 5.1 (1.8–14.37)] than in the control group. Differences in lymphocyte counts, monocytes, eosinophils, and basophil counts were not observed.

As for laboratory parameters (Figure 3B), NLR and PIV were higher in GBM than in controls and glioma grade II, and SII was higher than in controls. The differences in dNLR, PLR, LMR, and PNI were not significant.

Correlation of blood markers and their pairs with glioma grade

To study the correlation between laboratory parameters and glioma grade better, we respectively analyzed the correlation among NLR, dNLR, PLR, LMR, PNI, and SII in GBM, glioma grade I–III, and control group (Figure 5, Supplementary Tables S2–S4).

In the GBM group, NLR and SII ($r = 0.8411$, $p < 0.0001$) showed the strongest correlation. In the glioma grade I-III group, PLR and SII ($r = 0.8376$, $p < 0.0001$) showed a significant positive correlation, but little difference with NLR and SII, SII and PIV. SII and PIV ($r = 0.8778$, $p < 0.0001$) is the highest positive correlation in the control group. In contrast, the negative correlation between dNLR and LMR was the strongest in all three groups.

Although NLR and dNLR, NLR and PLR, NLR and SII, NLR and PIV, dNLR and PIV, PLR and SII, PLR and PIV, and SII and PIV were positively correlated in all three groups, the degree of correlation was inconsistent. Among the eight pairs of markers, NLR and dNLR, NLR and SII, NLR and PIV, and dNLR and PIV were higher in the GBM group than the glioma grade I-III group than the control group.

Diagnostic value of blood markers and their pairs in glioma diagnosis and glioma grading

Since the different performances of these indicators in our various tests, we further evaluated the clinical value of these markers and their pairs (Table 3, Figure 6).

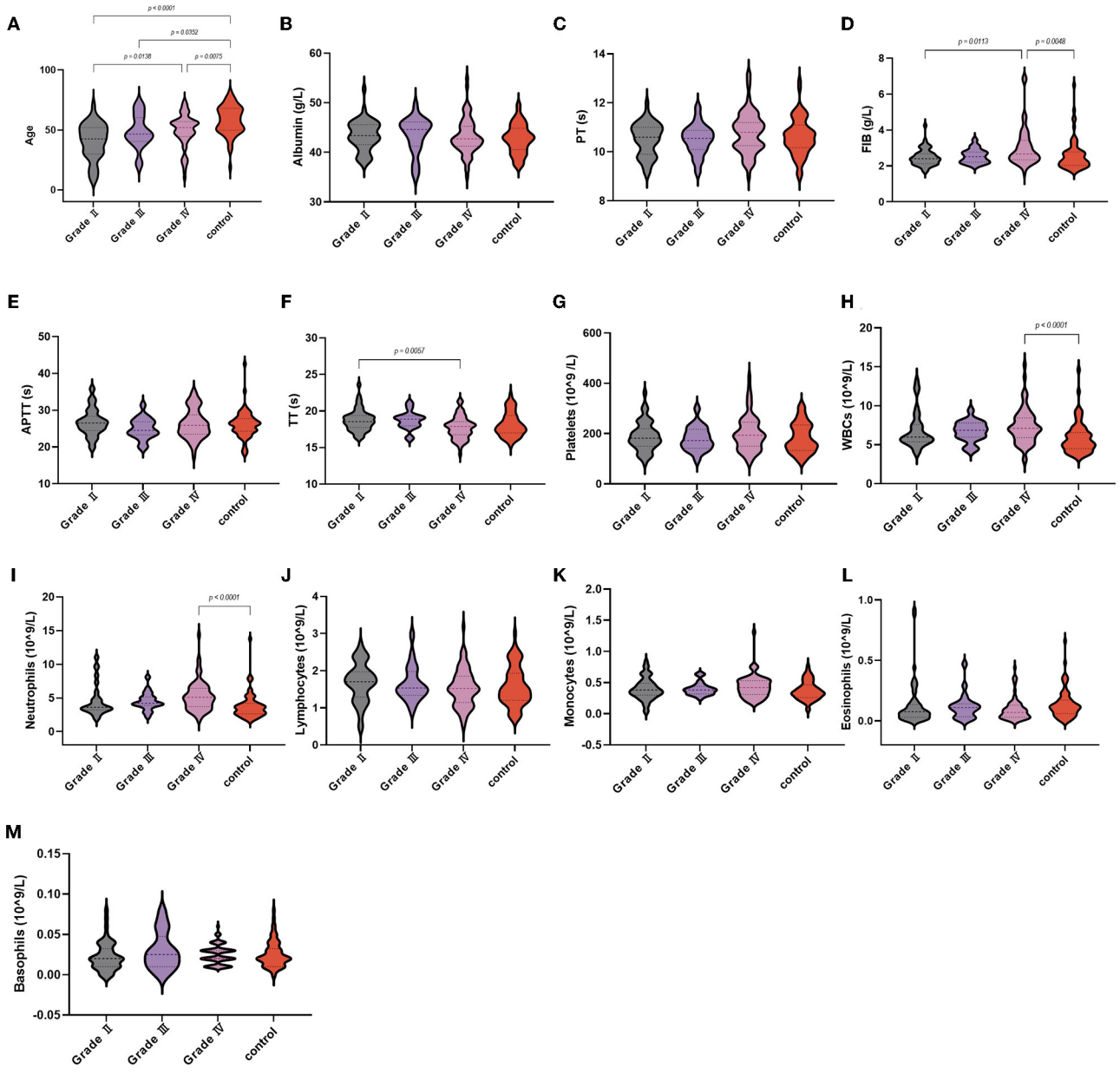

FIGURE 4
Violin diagram showing comparative results of characteristics in the trigeminal neuralgia group, glioma grade I, glioma grade II, glioma grade III, and glioma grade IV group (the dashed line in the middle represents the median and the dashed lines on both sides represent the interquartile range). **(A)** Age, **(B)** albumin, **(C)** PT, **(D)** FIB, **(E)** APTT, **(F)** TT, **(G)** platelets, **(H)** WBCs, **(I)** neutrophils, **(J)** lymphocytes, **(K)** monocytes, **(L)** eosinophils, **(M)** basophils.

When the acoustic neuroma group was compared with the brain metastatic tumor group (Figure 6A), NLR [0.7490 (0.6482–0.8498)] and NLR + dNLR [0.7481 (0.6457–0.8505)] performed well, but there was little difference between NLR single and paired. When glioma was compared with meningioma (Figure 6B), our results showed that NLR [0.6505 (0.5947–0.7068)] ranked second, next to PIV [0.6726 (0.6178–0.7274)]. NLR + PIV [0.6743 (0.6196–0.7289)], LMR + PIV [0.6745 (0.6201–0.7290)], and PIN + PIV [0.6739 (0.6192–0.7287)] showed higher AUCs. When GBM was compared with glioma grade I– III (Figure 6C), most markers showed lower AUCs overall. Among them, PIV [0.6444 (0.5522–0.7367)] and NLR + SII [0.6565 (0.5999–0.7130)] are relatively higher. When GBM was compared with other brain tumors (excluding brain metastases), NLR [0.7200(0.6551–0.7849)] and PIV [0.7200 (0.6526–0.7874)] performed similarly. Here, a number of markers and pairs show higher diagnostic predictive value, such as NLR + PIV [0.7199 (0.6522–0.7876], dNLR + PIV [0.7204 (0.6530–0.7878)], and PNI + PIV [0.7187 (0.6512–0.7862)]. Among the combined parameters, only NLR + LMR, NLR + PNI, and dNLR + PNI were not significant.

Regrettably, PNI did not perform well enough. In general, NLR, SII, PIV, and their pairing gave remarkable results, which showed significant predictive value in all subgroups.

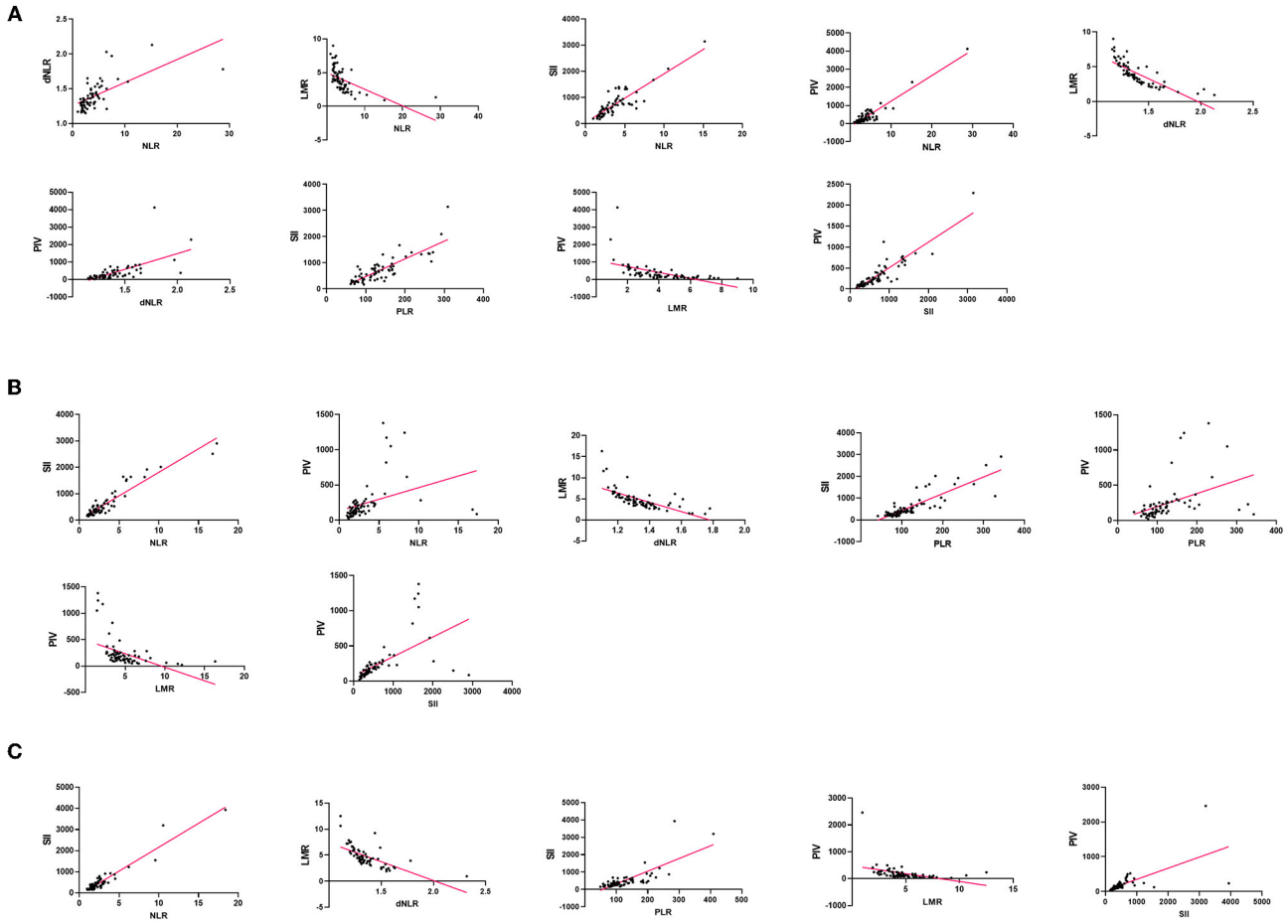

FIGURE 5
Correlation of blood markers and their pairs: **(A)** in the GBM group, **(B)** in the glioma grade I– III group, **(C)** in the control group.

Discussion

A growing number of studies have shown that inflammation is clearly present in the early stages of tumor progression, which may promote tumor progression and lead to poor prognosis (7, 20, 21). Peripheral blood biomarkers such as NLR and PLR have attracted widespread attention, but the discriminatory ability of such single biomarkers has always been limited. For this reason, excluding factors that may affect coagulation parameters, inflammatory markers, and albumin in the blood, we analyzed all previously reported parameters (NLR, dNLR, PLR, LMR, PNI, SII, and PIV) as comprehensively as possible and aimed to find the most specific and accurate blood-based biomarkers.

Whether the thrombotic disease without foundation is a clinical marker of occult cancer has been controversial (22, 23). Recently, it has also been reported that venous thromboembolism usually occurs shortly after diagnostic surgery for glioma (24). Therefore, in the present study, we are also concerned with partial coagulation parameters and speculate whether tumors could be detected early by abnormal coagulation parameters. Our data show that FIB levels were elevated in the GBM group relative to patients with trigeminal neuralgia and glioma grade II patients. At the same time, TT was shorter in the GBM group. FIB is a sensitive biochemical index, and its increase reflects not only an imbalance of coagulation or fibrinolytic system but also systemic inflammatory syndrome when inflammation is present in the body. Because of this, abnormal coagulation parameters, including FIB, may contribute to the determination of the malignancy of glioma but may also be related to the inflammatory response of the organism caused by cancer. Thus, we need more studies to discuss this issue.

In this study, significantly elevated white blood cell counts were observed in glioma patients compared to patients with trigeminal neuralgia, acoustic neuroma, and meningioma. Although white blood cell count is not currently considered a blood marker for glioma, elevated neutrophil counts have long been associated with tumor growth. Many studies about neutrophils have focused on angiogenesis, a characteristic of high-grade gliomas (25, 26). Our data also suggest that glioma had a higher neutrophil count than trigeminal neuralgia, acoustic neuroma, and meningioma. Some researchers have proposed that neutrophils, on the one hand, inhibit the anticancer activity of other immune cells by releasing reactive oxygen species (ROS) (27, 28), thus promoting tumor occurrence; on the other hand, they promote tumor proliferation and combat tumor cell senescence through various paracrine signaling pathways (29).

TABLE 3 Diagnostic value of NLR, dNLR, PLR, LMR, PNI, and pairs.

Marker	Acoustic neuroma vs. brain metastases		Glioma vs. meningioma		GBM vs. WHO I–III		GBM vs. others (exclude brain metastases)	
	AUC (95% CI)	*p*-value	AUC (95% CI)	*p*-value	AUC (95% CI)	*p*-value	AUC (95% CI)	*p*-value
NLR	0.7490 (0.6482–0.8498)	<0.0001*	0.6505 (0.5947–0.7068)	<0.0001*	0.6409 (0.5489–0.7330)	0.0040*	0.7200 (0.6551–0.7849)	<0.0001*
dNLR	0.6450 (0.5322–0.7577)	0.0090*	0.5709 (0.5109–0.6308)	0.0159*	0.5706 (0.4758–0.6655)	0.1493	0.5979 (0.5217–0.6740)	0.0078*
PLR	0.5972 (0.4843–0.7101)	0.0815	0.5510 (0.4910–0.6109)	0.0828	0.6048 (0.5102–0.6994)	0.0323*	0.6071 (0.5330–0.6811)	0.0036*
LMR	0.7065 (0.6004–0.8127)	0.0002*	0.6300 (0.5716–0.6883)	<0.0001*	0.6137 (0.5200–0.7070)	0.0203*	0.6675 (0.5937–0.7412)	<0.0001*
PNI	0.6409 (0.5341–0.7477)	0.0108*	0.5061 (0.4487–0.5635)	0.8360	0.5683 (0.4726–0.6640)	0.1633	0.5504 (0.4817–0.6190)	0.1707
SII	0.6589 (0.5434–0.7745)	0.0040*	0.6441 (0.5866–0.7015)	<0.0001*	0.6346 (0.5407–0.7285)	0.0062*	0.7089 (0.6407–0.7771)	<0.0001*
PIV	0.6646 (0.5533–0.7760)	0.0035*	0.6726 (0.6178–0.7274)	<0.0001*	0.6444 (0.5522–0.7367)	0.0032*	0.7200 (0.6526–0.7874)	<0.0001*
NLR + dNLR	0.7503 (0.6484–0.8522)	<0.0001*	0.6485 (0.5925–0.7045)	<0.0001*	0.6457 (0.5891–0.7023)	<0.0001*	0.7125 (0.6462–0.7789)	<0.0001*
NLR + PLR	0.5946 (0.4772–0.7120)	0.1036	0.5541 (0.4943–0.6140)	0.0654	0.5705 (0.5114–0.6296)	0.0169*	0.6120 (0.5385–0.6855)	0.0023*
NLR + LMR	0.6052 (0.4914–0.7189)	0.0703	0.5245 (0.4656–0.5833)	0.4053	0.5476 (0.4899–0.6052)	0.1073	0.5591 (0.4892–0.6291)	0.1079
NLR + PNI	0.5219 (0.4024–0.6414)	0.7059	0.5706 (0.5139–0.6274)	0.0162*	0.5615 (0.5046–0.6183)	0.0373*	0.5333 (0.4647–0.6019)	0.3651
NLR + SII	0.6607 (0.5447–0.7768)	0.0057*	0.6396 (0.5818–0.6973)	<0.0001*	0.6471 (0.5901–0.7040)	<0.0001*	0.6988 (0.6288–0.7689)	<0.0001*
NLR + PIV	0.6627 (0.5497–0.7758)	0.0059*	0.6743 (0.6196–0.7289)	<0.0001*	0.5448 (0.4838–0.6059)	0.1291	0.7199 (0.6522–0.7876)	<0.0001*
dNLR + PLR	0.5894 (0.4721–0.7066)	0.1240	0.5510 (0.4910–0.6109)	0.0827	0.5669 (0.5075–0.6262)	0.0236*	0.6072 (0.5333–0.6812)	0.0035*
dNLR + LMR	0.6659 (0.5550–0.7769)	0.0043*	0.6307 (0.5725–0.6890)	<0.0001*	0.6203 (0.5612–0.6794)	<0.0001*	0.6702 (0.5967–0.7437)	<0.0001*
dNLR + PNI	0.6349 (0.5244–0.7454)	0.0202*	0.5026 (0.4452–0.5600)	0.9301	0.5050 (0.4472–0.5629)	0.8646	0.5457 (0.4774–0.6139)	0.2140
dNLR + SII	0.6596 (0.5434–0.7758)	0.0060*	0.6395 (0.5817–0.6972)	<0.0001*	0.6469 (0.5899–0.7038)	<0.0001*	0.6987 (0.6286–0.7688)	<0.0001*
dNLR + PIV	0.6645 (0.5514–0.7776)	0.0055*	0.6737 (0.6190–0.7283)	<0.0001*	0.5443 (0.4833–0.6054)	0.1333	0.7204 (0.6530–0.7878)	<0.0001*
PLR + LMR	0.5851 (0.4674–0.7028)	0.1430	0.5470 (0.4869–0.6071)	0.1095	0.5634 (0.5038–0.6231)	0.0317*	0.6029 (0.5280–0.6778)	0.0051*
PLR + PNI	0.5723 (0.4529–0.6916)	0.2135	0.5530 (0.4930–0.6130)	0.0712	0.5694 (0.5101–0.6287)	0.0188*	0.6060 (0.5314–0.6805)	0.0039*
PLR + SII	0.6570 (0.5401–0.7740)	0.0069*	0.6347 (0.5765–0.6929)	<0.0001*	0.6458 (0.5888–0.7028)	<0.0001*	0.7032 (0.6351–0.7712)	<0.0001*
PLR + PIV	0.6573 (0.5406–0.7739)	0.0078*	0.6440 (0.5853–0.7028)	<0.0001*	0.5505 (0.4897–0.6113)	0.0871	0.7002 (0.6271–0.7732)	<0.0001*
LMR + PNI	0.6590 (0.5499–0.7682)	0.0062*	0.5382 (0.4804–0.5960)	0.1937	0.5417 (0.4834–0.5999)	0.1583	0.5974 (0.5269–0.6678)	0.0081*
LMR + SII	0.6589 (0.5427–0.7751)	0.0063*	0.6390 (0.5812–0.6968)	<0.0001*	0.6467 (0.5898–0.7037)	<0.0001*	0.6985 (0.6283–0.7686)	<0.0001*
LMR + PIV	0.6580 (0.5443–0.7718)	0.0075*	0.6745 (0.6201–0.7290)	<0.0001*	0.5437 (0.4826–0.6047)	0.1391	0.7206 (0.6536–0.7875)	<0.0001*
PNI + SII	0.6574 (0.5406–0.7741)	0.0068*	0.6390 (0.5812–0.6968)	<0.0001*	0.6474 (0.5904–0.7043)	<0.0001*	0.6989 (0.6288–0.7691)	<0.0001*
PIN + PIV	0.6547 (0.5406–0.7688)	0.0088*	0.6739 (0.6192–0.7287)	<0.0001*	0.6521 (0.5955–0.7087)	<0.0001*	0.7187 (0.6512–0.7862)	<0.0001*
SII + PIV	0.6757 (0.5605–0.7909)	0.0030*	0.6374 (0.5779–0.6969)	<0.0001*	0.6060 (0.5106–0.7015)	0.0310*	0.6991 (0.6243–0.7738)	<0.0001*

Others include patients with trigeminal neuralgia, craniopharyngioma, ependymoma, acoustic neuroma, meningioma, and glioma grade I–III. *P < 0.05.

10.3389/fneur.2023.1297835

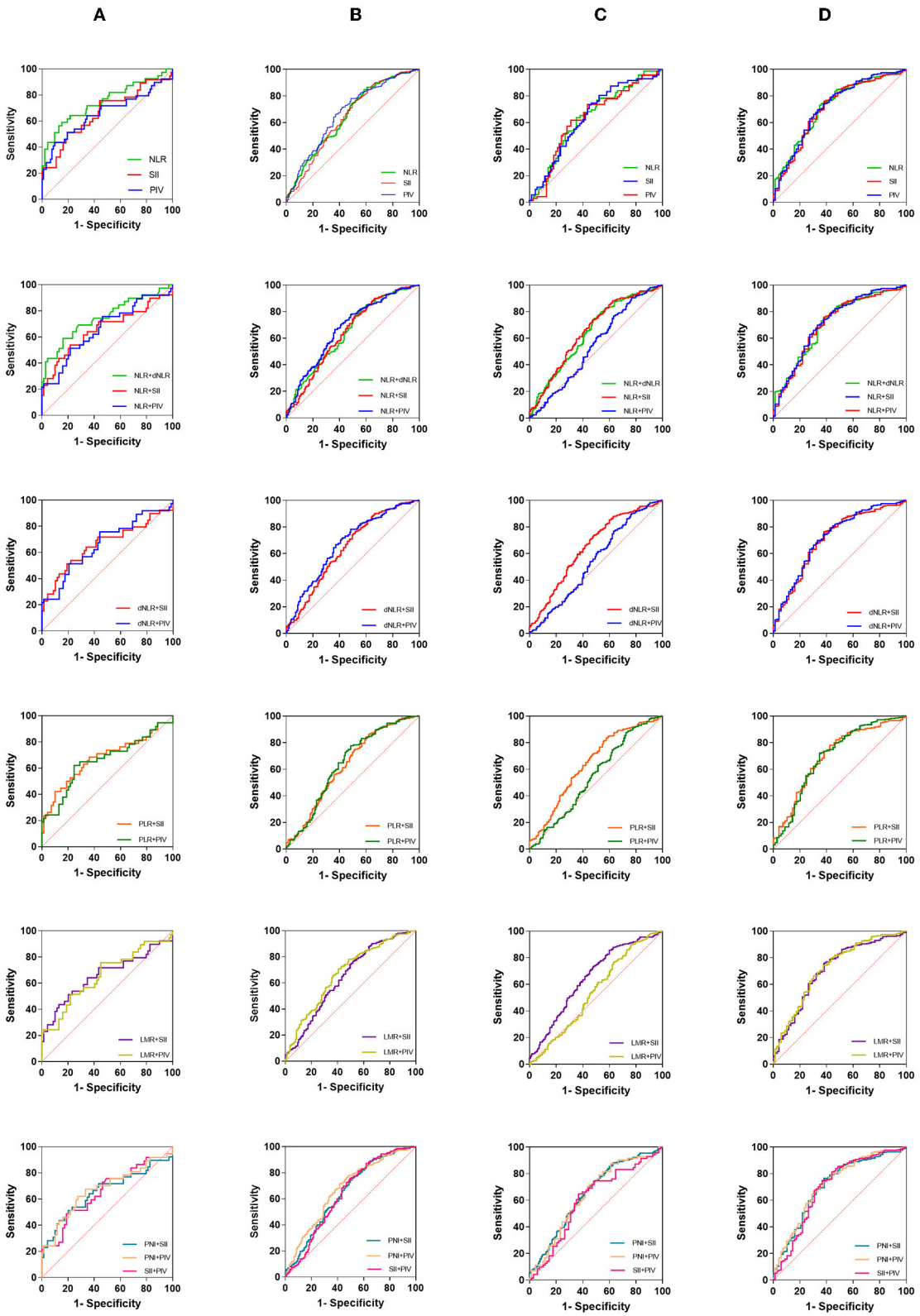

FIGURE 6
The diagnostic value of preoperative inflammatory markers in glioma diagnosis and glioma grading. **(A)** Acoustic neuroma vs. brain metastases, **(B)** glioma vs. meningioma, **(C)** GBM vs. WHO I–III, **(D)** GBM vs. others (exclude brain metastases).

NLR has been confirmed to be associated with glioma prognosis in several studies (8–10). The almost overwhelming data also suggest that NLR is associated with glioma identification and grading (14, 15). NLR also ranked first in our study with an AUC of 0.7490 (0.6482–0.8498). The combination of NLR and dNLR ranked second, which strongly confirmed their predictive ability. SII levels provide prognostic evidence for many solid tumors, such as prostate cancer (30), breast cancer (31), and gastric cancer (32). In our results, SII levels were significantly elevated in brain metastases and GBM. When compared with brain tumors other than brain metastases, SII and all combinations with it are highly accuracy in GBM, including NLR + SII, dNLR + SII, PLR + SII, LMR + SII, and PNI + SII. Consistent with the results of a recent meta-analysis (33), the strong discriminatory potential of SII for malignancies was also demonstrated in this study. The accuracy of PIV and all its pairs is higher. The strong correlation between PIV and the other five indicators also indicates that PIV has more diagnostic value when combined. As in most studies, differences in platelet count and lymphocyte count were not significant in the classification of brain tumors and the grading of gliomas (15, 34). In parallel, the changes in dNLR were not significant in our study. Therefore, we prefer that the changes in the levels of these laboratory parameters be mainly reflected in the elevation of neutrophils. Significant differences were mainly concentrated in brain metastases and gliomas compared with other non-malignant tumors, so we believe that the results of this study will be more helpful in judging the malignancy of brain tumors. The significant difference between glioma and other tumors stems from the highly malignant characteristics of GBM.

Limitations

In addition, there are some limitations in our study: (1) Small sample types and numbers. Among the patients included in our study, craniopharyngioma, ependymoma, chordoma, and glioma grade I samples were small, and other brain tumors, such as pituitary tumors and lymphomas, were not included. (2) The case group is quite heterogeneous, which may lead to bias. (3) Lack of healthy human samples. We had to use trigeminal neuralgia samples as a control group for brain tumors, but we cannot exclude that trigeminal neuralgia disease itself causes alterations in these markers. (4) A single combination approach. We only use addition to combine the various indicators and more combinations that deserve subsequent exploration. (5) False-positive may exist. A lot of positive results in our study, but there are many factors that we are not aware of that could be contributing to this result.

Conclusion

In summary, our data suggest that NLR, SII, PIV, and their pairs are promising biomarkers to help determine tumor type, grade, and malignancy degree of brain tumors. Additionally, larger samples and more categorized studies should be conducted for clinical practice.

Data availability statement

The raw data supporting the conclusions of this article will be made available by the authors, without undue reservation.

Ethics statement

The requirement of ethical approval was waived by the General Hospital of Western Theater Command for the studies involving humans because of the retrospective nature of the study and due to all procedures being performed as part of routine care. The studies were conducted in accordance with the local legislation and institutional requirements. Written informed consent for participation in this study was provided by the participants' legal guardians/next of kin.

Author contributions

YY: Data curation, Writing—original draft, Writing—review and editing. FH: Data curation, Writing—original draft. SW: Data curation, Writing—original draft. ZH: Data curation, Writing—original draft. KW: Data curation, Writing—original draft. YM: Funding acquisition, Methodology, Writing—review and editing. QO-Y: Funding acquisition, Methodology, Writing—review and editing.

Funding

The author(s) declare financial support was received for the research, authorship, and/or publication of this article. The present study was supported by grants from the Research Project of the General Hospital of Western Theater Command (2021–XZYG–A13 and 2021–XZYG–C37) and the Spark Talent program to QO-Y of General Hospital of the Western Theater Command.

Conflict of interest

The authors declare that the research was conducted in the absence of any commercial or financial relationships that could be construed as a potential conflict of interest.

Publisher's note

All claims expressed in this article are solely those of the authors and do not necessarily represent those of their affiliated organizations, or those of the publisher, the editors and the reviewers. Any product that may be evaluated in this article, or claim that may be made by its manufacturer, is not guaranteed or endorsed by the publisher.

Supplementary material

The Supplementary Material for this article can be found online at: https://www.frontiersin.org/articles/10.3389/fneur.2023.1297835/full#supplementary-material

References

1. Sung H, Ferlay J, Siegel RL, Laversanne M, Soerjomataram I, Jemal A, et al. Global cancer statistics 2020: GLOBOCAN estimates of incidence and mortality worldwide for 36 cancers in 185 countries. *CA Cancer J Clin.* (2021) 71:209–49. doi: 10.3322/caac.21660

2. Louis DN, Ohgaki H, Wiestler OD, Cavenee WK, Burger PC, Jouvet A, et al. The 2007 WHO classification of tumours of the central nervous system. *Acta Neuropathol.* (2007) 114:97–109. doi: 10.1007/s00401-007-0243-4

3. Ostrom QT, Cioffi G, Waite K, Kruchko C, Barnholtz-Sloan JS. CBTRUS statistical report: primary brain and other central nervous system tumors diagnosed in the United States in 2014-2018. *Neuro Oncol.* (2021) 23: 1–105. doi: 10.1093/neuonc/noab200

4. Ostrom QT, Gittleman H, Liao P, Rouse C, Chen Y, Dowling J, et al. CBTRUS statistical report: primary brain and central nervous system tumors diagnosed in the United States in 2007-2011. *Neuro Oncol.* (2014) 16:1–63. doi: 10.1093/neuonc/nou223

5. Schaff LR, Mellinghoff IK. Glioblastoma and other primary brain malignancies in adults: a review. *JAMA.* (2023) 329:574–87. doi: 10.1001/jama.2023.0023

6. Ring A, Nguyen-Strauli BD, Wicki A, Aceto N. Biology, vulnerabilities and clinical applications of circulating tumour cells. *Nat Rev Cancer.* (2023) 23:95–111. doi: 10.1038/s41568-022-00536-4

7. Coussens LM, Werb Z. Inflammation and cancer. *Nature.* (2002) 420:860–7. doi: 10.1038/nature01322

8. Yang T, Mao P, Chen X, Niu X, Xu G, Bai X, et al. Inflammatory biomarkers in prognostic analysis for patients with glioma and the establishment of a nomogram. *Oncol Lett.* (2019) 17:2516–22. doi: 10.3892/ol.2018.9870

9. Ali H, Harting R, de Vries R, Ali M, Wurdinger T, Best MG. Blood-based biomarkers for glioma in the context of gliomagenesis: a systematic review. *Front Oncol.* (2021) 11:665235. doi: 10.3389/fonc.2021.665235

10. Zhang X, Li C, Xiao L, Gao C, Zhao W, Yang M, et al. Predicting individual prognosis and grade of patients with glioma based on preoperative eosinophil and neutrophil-to-lymphocyte ratio. *Cancer Manag Res.* (2020) 12:5793–802. doi: 10.2147/CMAR.S260695

11. Smith D, Raices M, Cayol F, Corvatta F, Caram L, Dietrich A. Is the neutrophil-to-lymphocyte ratio a prognostic factor in non-small cell lung cancer patients who receive adjuvant chemotherapy? *Semin Oncol.* (2022) 49:482–9. doi: 10.1053/j.seminoncol.2023.01.006

12. Li Y, Xu T, Wang X, Jia X, Ren M, Wang X. The prognostic utility of preoperative neutrophil-to-lymphocyte ratio (NLR) in patients with colorectal liver metastasis: a systematic review and meta-analysis. *Cancer Cell Int.* (2023) 23:39. doi: 10.1186/s12935-023-02876-z

13. Fuca G, Guarini V, Antoniotti C, Morano F, Moretto R. The pan-immune-inflammation value is a new prognostic biomarker in metastatic colorectal cancer: results from a pooled-analysis of the Valentino and TRIBE first-line trials. *Br J Cancer.* (2020) 123:403–9. doi: 10.1038/s41416-020-0894-7

14. Guven DC, Sahin TK, Erul E, Kilickap S, Gambichler T, Aksoy S. The association between the pan-immune-inflammation value and cancer prognosis: a systematic review and meta-analysis. *Cancers.* (2022) 14:675. doi: 10.3390/cancers14112675

15. Chen F, Chao M, Huang T, Guo S, Zhai Y, Wang Y. The role of preoperative inflammatory markers in patients with central nervous system tumors, focus on glioma. *Front Oncol.* (2022) 12:1055783. doi: 10.3389/fonc.2022.1055783

16. Zheng SH, Huang JL, Chen M, Wang BL, Ou QS, Huang SY. Diagnostic value of preoperative inflammatory markers in patients with glioma: a multicenter cohort study. *J Neurosurg.* (2018) 129:583–92. doi: 10.3171/2017.3.JNS161648

17. Bauer AT, Gorzelanny C, Gebhardt C, Pantel K, Schneider SW. Interplay between coagulation and inflammation in cancer: Limitations and therapeutic opportunities. *Cancer Treat Rev.* (2022) 102:102322. doi: 10.1016/j.ctrv.2021.102322

18. Moik F, Chan WE, Wiedemann S, Hoeller C, Tuchmann F, Aretin MB. Incidence, risk factors, and outcomes of venous and arterial thromboembolism in immune checkpoint inhibitor therapy. *Blood.* (2021) 137:1669–78. doi: 10.1182/blood.2020007878

19. Topkan E, Kucuk A, Selek U. Pretreatment pan-immune-inflammation value efficiently predicts survival outcomes in glioblastoma multiforme patients receiving radiotherapy and temozolomide. *J Immunol Res.* (2022) 2022:1346094. doi: 10.1155/2022/1346094

20. Qian BZ, Pollard JW. Macrophage diversity enhances tumor progression and metastasis. *Cell.* (2010) 141:39–51. doi: 10.1016/j.cell.2010.03.014

21. Efendioglu M, Sanli E, Turkoglu C, Balak N. Reduced serum sRANKL and sTREM2 levels in high-grade gliomas: association with prognosis. *Noro Psikiyatr Ars.* (2021) 58:133–6. doi: 10.29399/npa.27536

22. Robin P, Otten HM, Delluc A, van Es N, Carrier M, Salaun PY. Effect of occult cancer screening on mortality in patients with unprovoked venous thromboembolism. *Thromb Res.* (2018) 171:92–6. doi: 10.1016/j.thromres.2018.09.055

23. Sorensen HT, Mellemkjaer L, Steffensen FH, Olsen JH, Nielsen GL. The risk of a diagnosis of cancer after primary deep venous thrombosis or pulmonary embolism. *N Engl J Med.* (1998) 338:1169–73. doi: 10.1056/NEJM199804233381701

24. Eisele A, Seystahl K, Rushing EJ, Roth P, Le Rhun E, Weller M. Venous thromboembolic events in glioblastoma patients: an epidemiological study. *Eur J Neurol.* (2022) 29:2386–97. doi: 10.1111/ene.15404

25. Quail DF, Joyce JA. The microenvironmental landscape of brain tumors. *Cancer Cell.* (2017) 31:326–41. doi: 10.1016/j.ccell.2017.02.009

26. Lin YJ, Wei KC, Chen PY, Lim M, Hwang TL. Roles of neutrophils in glioma and brain metastases. *Front Immunol.* (2021) 12:701383. doi: 10.3389/fimmu.2021.701383

27. Jackstadt R, van Hooff SR, Leach JD, Cortes-Lavaud X, Lohuis JO, Ridgway RA. Epithelial NOTCH signaling rewires the tumor microenvironment of colorectal cancer to drive poor-prognosis subtypes and metastasis. *Cancer Cell.* (2019) 36:319–36. doi: 10.1016/j.ccell.2019.08.003

28. Gong L, Cumpian AM, Caetano MS, Ochoa CE, De la Garza MM, Lapid DJ. Promoting effect of neutrophils on lung tumorigenesis is mediated by CXCR2 and neutrophil elastase. *Mol Cancer.* (2013) 12:154. doi: 10.1186/1476-4598-12-154

29. Hedrick CC, Malanchi I. Neutrophils in cancer: heterogeneous and multifaceted. *Nat Rev Immunol.* (2022) 22:173–87. doi: 10.1038/s41577-021-00571-6

30. Meng L, Yang Y, Hu X, Zhang R, Li X. Prognostic value of the pretreatment systemic immune-inflammation index in patients with prostate cancer: a systematic review and meta-analysis. *J Transl Med.* (2023) 21:79. doi: 10.1186/s12967-023-03924-y

31. Zhang Y, Sun Y, Zhang Q. Prognostic value of the systemic immune-inflammation index in patients with breast cancer: a meta-analysis. *Cancer Cell Int.* (2020) 20:224. doi: 10.1186/s12935-020-01308-6

32. Zhang Y, Lin S, Yang X, Wang R, Luo L. Prognostic value of pretreatment systemic immune-inflammation index in patients with gastrointestinal cancers. *J Cell Physiol.* (2019) 234:5555–63. doi: 10.1002/jcp.27373

33. Zhang S, Ni Q. Prognostic role of the pretreatment systemic immune-inflammation index in patients with glioma: a meta-analysis. *Front Neurol.* (2023) 14:1094364. doi: 10.3389/fneur.2023.1094364

34. Subeikshanan V, Dutt A, Basu D, Tejus MN, Maurya VP, Madhugiri VS. A prospective comparative clinical study of peripheral blood counts and indices in patients with primary brain tumors. *J Postgrad Med.* (2016) 62:86–90. doi: 10.4103/0022-3859.180551

frontiers | Frontiers in Pediatrics

TYPE Original Research
PUBLISHED 23 October 2023
DOI 10.3389/fped.2023.1193474

OPEN ACCESS

EDITED BY
Archya Dasgupta,
Tata Memorial Hospital, India

REVIEWED BY
Flavio Giordano,
University of Florence, Italy
Gerardo Caruso,
University Hospital of Policlinico G. Martino, Italy

*CORRESPONDENCE
Carmine Mottolese
✉ carmine.mottolese@chu-lyon.fr

RECEIVED 10 June 2023
ACCEPTED 10 October 2023
PUBLISHED 23 October 2023

CITATION
Boukaka RG, Beuriat P-A, Di Rocco F, Vasiljevic A, Szathmari A and Mottolese C (2023) Brainstem tumors in children: a monocentric series in the light of genetic and bio-molecular progress in pediatric neuro-oncology. Front. Pediatr. 11:1193474. doi: 10.3389/fped.2023.1193474

Brainstem tumors in children: a monocentric series in the light of genetic and bio-molecular progress in pediatric neuro-oncology

Rel Gerald Boukaka[1], Pierre-Aurélien Beuriat[1,2], Federico Di Rocco[1,2], Alexandre Vasiljevic[3], Alexandru Szathmari[1] and Carmine Mottolese[1]*

[1]Department of Pediatric Neurosurgery, Hôpital Femme Mère Enfant, Hospices Civils de, Lyon, France, [2]Université Claude Bernard, Lyon 1, Lyon, France, [3]Department of Pathology and Neuropathology, Groupement Hospitalier Est, Hospices Civils de Lyon, Lyon, France

Introduction: Brainstem tumors represent a challenge. Their management and prognosis vary according to anatomopathological findings and genetic and bio-molecular fingerprints. We present our experience with pediatric brainstem tumors.

Material and methods: All patients admitted for a brainstem tumor at the Pediatric Neurosurgical Unit at Hôpital Femme Mère Enfant hospital between January 1997 and December 2019 were considered. Patients data were obtained through a retrospective review of the medical records; follow-up was from the last outpatient consultation.

Results: One hundred and twelve patients were included. Eighty-five patients (75.9%) had open surgery or stereotactic biopsy. Thirty-five patients were treated for hydrocephalus. Sixty-six received an adjuvant treatment. Several protocols were adopted according to the SFOP and SIOP during this time period. The overall survival rate was 45% with a median follow-up of five years (range 1–18 year). However, the survival rate was very different between the diffuse intrinsic pontine gliomas (DIPG) and the others tumor types. If we exclude the DIPG (59 patients), of which only 1 was alive at 3 years, the survival rate was 90.6% (only 5 deaths over 53 patients) with a median follow up of 5 years.

Conclusions: Our series confirms that benign tumors of the brainstem have a good survival when treated with surgical removal ± adjuvant therapy. Diffuse pontine gliomas continue to have a dismal prognosis. Individualized treatment based on molecular fingerprints may help to select the best adjuvant therapy and hence potentially improve survival.

KEYWORDS

pediatric, brainstem, dipg, benign, surgery

Introduction

Brainstem tumors represent 15% of children brain tumors; 80% of children brainstem tumors are diffuse intrinsic pontine gliomas (DIPG) that have a dismal prognosis. Brainstem tumors were first described by Kummel in 1881 (1) and Monakow (2). The first nosological classification was reported in 1926 by Bailey and Cushing who emphasized, for the first time, that brainstem gliomas could develop from certain

embryological cells (3). The dismal history of brainstem tumors and their catastrophic evolution was already noted in their report.

In 1989, a report of the French Speaking Society of Neurosurgery on Brainstem Tumors showed the progress achieved in term of radiological diagnosis using MRI, histological classification and genetic knowledge. The role of surgery to treat exophytic lesion of the mesencephalon, of the bulbo-medullary region or focal lesions anywhere in the brainstem was also recognized. However, the survival rate of diffuse intrinsic gliomas did not improve (4). The purpose of this paper is to share our experience with a consecutive series of 112 children with brainstem tumors treated from 1997 to 2019 and to emphasize the role of recent genetic and bio-molecular progress.

Material and methods

All patients who were admitted and diagnosed with a brainstem tumor in the Pediatric Neurosurgical Unit at the "Hôpital Femme Mère Enfant" (Hospices Civils de Lyon, Lyon, France) between January 1997 and December 2019 were included in this study. Patient data were obtained through a retrospective review of the medical records from our data base; follow-up data was from the last outpatient visit. All patients without a clinical history or radiological images and without a documented post-surgical follow-up were excluded from this study.

The study protocol was approved by the local ethics committee.

One hundred and twelve patients were included in this study. All patients were diagnosed with a cranio-medullary MRI with and without gadolinium. The male/female ratio was 0.94 and the age varied from 6 months to 18 years with a median age of 8.9 years. The symptomatology that led to the diagnosis was unknown in 44 patients (39.3%), progressive in 63 patients (56.2%), acute in 2 patients (1.8%) and incidental in 3 patients (2.7%). At diagnosis, 14% of patients presented a deficit of the mixed cranial nerves, 21% cerebellar troubles with balance disorders, 16% nystagmus and torticollis, 10% impaired consciousness while 38% presented with a mild intracranial hypertension. According to the classification of Choux (5), 59 patients were classified as belonging to the group I (52.7%), 25 to the group II (22.3%), 26 to group III (23.2%), and 2 to group IV (1.8%).

Table 1 shows the different tumor locations. The surgical removal was definite as Growth total Resection (GTR), when the post-operative MRI showed a total removal, as Near Total resection (NTR) when the removal was at least of 90% of the pre-operative volume, and subtotal removal (STR) when less of 90% of the tumor was removed (6).

TABLE 1 Tumors localisation.

Localization	*N* = 112 (100%)
Pons	59 (53%)
Tectal region	15 (12.5%)
Bulbo-medullary region	16 (14.3)%
Latero-bulbar region	8 (7.1%)
Ponto-cerebellar angle	4 (3.6%)
Bulb	3 (2.6%)
Ponto-bulbar region	6 (5.3%)

Out of the 34 patients with DIPG the histological diagnosis were a grade IV diffuse malignant glioma in 24 patients, a grade III astrocytary glioma in 3 patients, an anaplastic gliomas in one patient, a grade III oligo-astrocytary glioma in one patient, an AT/RT in two patients and an ETANTR in one patient. The radiological findings were not different between the different tumor types (**Figure 1**).

Histology of focal and exophytic brainstem tumors were a grade I pilocytic astrocytoma (**Figure 2**) in 63% of cases of, a ganglioglioma (**Figure 3**) in 29% and a oligo-astrocytary tumors in 8% of cases.

Results

Eighty-five patients (75.9%) had open surgery or biopsy (open or stereotactic). For DIPGs, the biopsy was proposed to the family but in 27 patients the biopsy was refused so the diagnosis was based on neuroradiological criteria. **Table 2** details the histopathological findings. Forty-four of the surgical procedures were biopsies either open (23 patients), frame-based (16 patients) or frameless (5 patients). The other surgical procedures were a direct surgical approach aimed at tumor removal. Three patients were operated for a recurrence and no patient received a third surgical procedure. One patient was re-operated for a new biopsy because the first procedure did not permit a diagnosis. Forty-two patients had surgery for tumor removal with a total surgical resection in 20 cases (47.6%), a subtotal resection in 13 patients (30%), and a partial resection in 9 patients (22.4%). Thirty-five patients were treated for hydrocephalus during forty-eight surgical procedures. Thirty of these procedures were ventriculo-peritoneal (VP) shunt while 18 endoscopic third ventriculocisternostomy (ETV). Hydrocephalus needed to be treated after surgery in 12 patients. Four patients needed VP shunt after surgery despite a previous ETV and three patients had new ETV after the direct approach on the tumor.

We tabulated the post-operative complications separately for patients who underwent biopsy and for those who underwent tumor removal. In the biopsy group, 29% of the patients (14/48) had postoperative complications. One patient died after a diffuse edematous reaction of the brainstem, 2 patients presented a reversible bradycardia, one patient had respiratory troubles that regressed after the administration of corticoids, 2 patients had worsening of the pre-operative cerebellar syndrome, 3 patients had worsening of the pre-operative motor deficit (complete deficit in one case), 5 patients presented new cranial nerves deficit (3 facial nerve palsy and 2 swallowing problems). 29% (12/41) of patients who had surgery aimed at tumor removal had postoperative complications: 12 had a new cranial nerve deficit (7 swallowing troubles, 2 VIth nerve palsy, 3 peripheral facial nerve palsy), 2 patients presented a Parinaud syndrome, 2 patients had worsening of the pre-operative cerebellar syndrome, one patient developed a left hemiparesis and 2 patients developed tetraparesis with respiratory troubles. In one case a small intratumoral hemorrhage was visualized without clinical

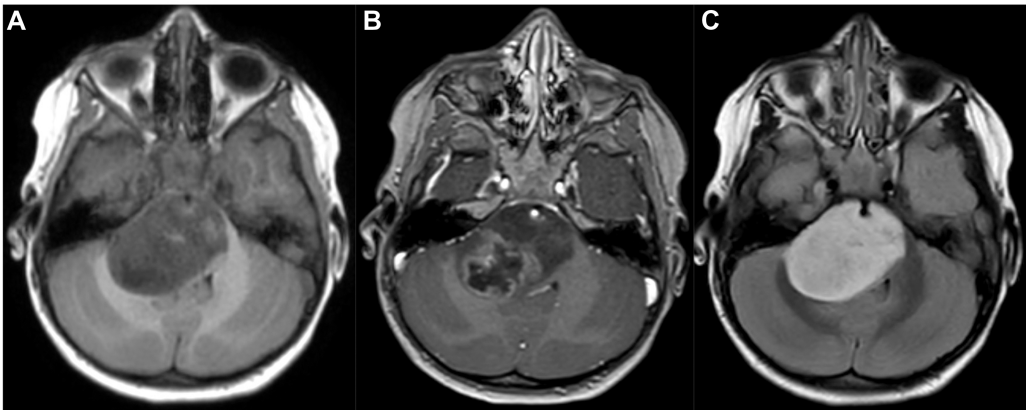

FIGURE 1
MRI scan in an axial 3D T1-weighted contrast (**A**), 3D T1-weighted contrast after gadolinium injection (**B**) and 3D T2 Flair-weighted contrast (**C**) showing a typical diffuse intrinsic pontine glioma (DIPG).

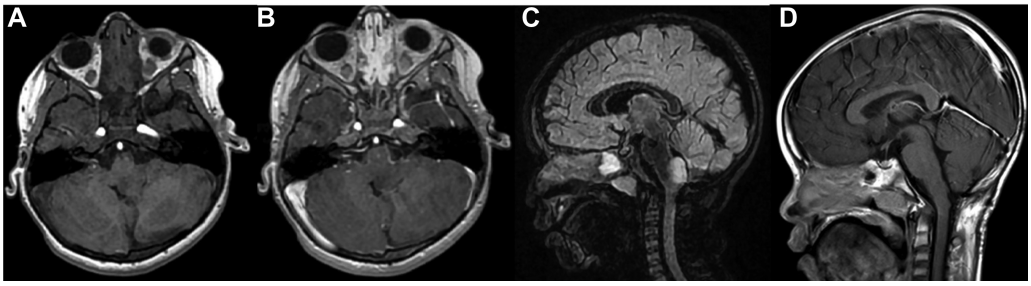

FIGURE 2
Pre operative MRI scan in an axial 3D T1-weighted contrast (**A**), 3D T1-weighted contrast after gadolinium injection (**B**) and sagital 3D T2 Flair-weighted contrast (**C**) showing a typical typical exophytic bulbo-medullar ganglioglioma. D is the post operative control in a sagital 3D T1-weighted contrast after gadolinium injection showing a complete removal.

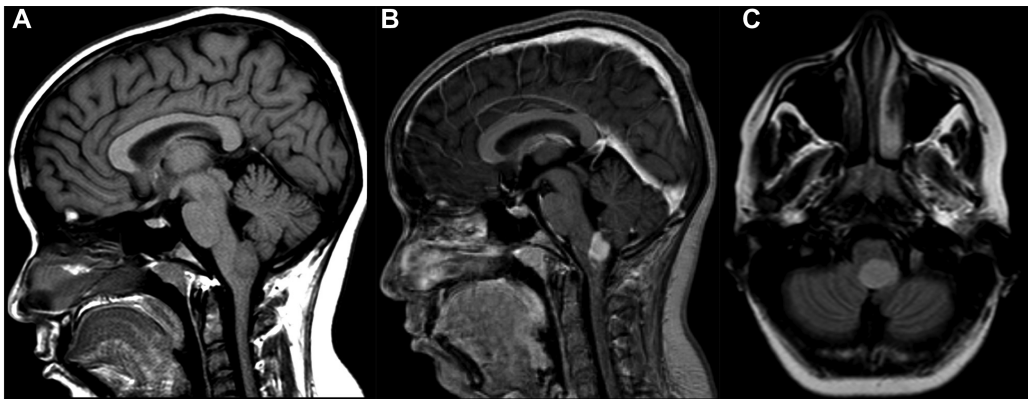

FIGURE 3
MRI scan in a sagital 3D T1-weighted contrast (**A**), 3D T1-weighted contrast after gadolinium injection (**B**) and 3D T2 Flair-weighted contrast (**C**) showing a typical typical exophytic bulbo-medullar ganglioglioma.

symptoms, 2 patients developed an epidural hematoma that didn't need a surgical treatment, and two patients developed a pseudo-meningocele treated with furosemide.

Five patients with a DIPG without histone mutation presented a metastatic evolution in spite of two different chemoterapic treatment.

TABLE 2 Anatomopathological findings.

Anatomopathological findings	$N = 85$ (100%)
Pilocytic Astrocytoma	31
Grade IV astrocytoma	26
Ganglioglioma	8
Grade III astrocytoma	7
Gangliocytoma	5
Grade II astrocytoma	3
AT/RT	2
ETANTR	1
PNET	1
Malignant glioneuronal tumor	1

ETANTR, Embryonal tumor with abundant neuropil and true rosettes; AT/RT, Atypical Teratoid Rhaboid Tumor; PNET, primitive neuroectodermal tumor.

Molecular genetic characteristic

We obtained complete histopathological and biomolecular analysis in 40 patients out of the 85 operated patients.

In patients with a diffuse gliomas, a mutation K27M of the histone H3.3 (H3K27M) was found in 18 cases. This mutation is characterized by the substitution of a lysine (K) with the methionin (M). It was absent in 10 cases. Amplification of PDGFRA was seen in two cases.

Among 15 tested circumscribed benign gliomas, the presence of BRAF molecular alterations was recorded in 9 cases. BRAF alterations included KIAA1549-BRAF fusion that is more specific of pilocytic astrocytomas (5 cases) and the BRAF V600E mutation that is more frequent in ganglioglioma (4 cases).

Two patients were diagnosed as AT/RT. One patient had an embryonal tumor with multi-layered rosettes (ETMR) with an ETANTR phenotype.

We were able to define five groups of patients (Table 3): diffuse gliomas with H3K27M mutation (18 patients), diffuse gliomas without H3K27M mutation (10 patients), circumscribed benign focal gliomas with BRAF alterations (9 patients), and embryonal tumors (3 patients). The presence of the H3K27M mutation allowed the inclusion of patients with DIPG in specific therapeutic protocols such as BIOMEDE. The presence of BRAF-V600E mutation and KIAA1549-BRAF fusion favoured the use of targeted therapy in patients with partial removal or recurrence.

Complementary treatment

Sixty-six patients (59%), had postoperative chemotherapy according to the indications of our neuro oncological team and according to the protocol of the SFOP. Several types of protocol were used (BIOMEDE, LGG, TRONC 98, TARCEVA, CILENT, STUPP, BB SFOP, VELBE, PNET HR) following recommendations of the local neuro-oncological team. All patient with DIPGs received a complementary treatment.

Table 4 shows the different protocols used, and the survival at one, two and five years. Twenty-six patients were treated with only chemotherapy at beginning and 31 patients were treated with chemotherapy followed by radiotherapy. Three patients received chemotherapy after a new surgical procedure for tumor recurrence. Six more patients received chemotherapy for tumor progression on the follow-up MRI scan. Five patients with a DIPG received only radiotherapy due to rapid progressing neurological deterioration.

Survival

At last follow-up, the overall survival rate was 45% with a median follow-up of 7.5 years (range from 1 to 23 years). However, this survival rate was very different between DIPG and circumscribed/exophytic gliomas. For DIPG, the median survival is inferior to one year (10.7 months) with a range between 4 months and 36 months. The DIPG with a survival of 36 months was H3.1 mutated with the lost of PTEN. If we exclude the 59 DIPG (with only 1 patient alive after 3 years of follow-up), the survival rate of the non-DIPG tumors of our cohort was 90.6% (only 5 deaths over 53 patients) showing that benign tumors of the brainstem can have a good survival. The median survival for all patients with benign focalized or exophytic brainstem tumors was 13 years with a range varying from two to 23 years. Eleven patients had a survival superior to fifteen years with a range between 15 and 23 years.

The mortality was 14.3% ($n = 2$) for the tectal plate tumors (Grade IV astrocytoma and 1 patient not operated), 6.25% ($n = 1$) for the bulbo-medullary region tumors (ganglioglioma), 0% for the ponto-bulbar and ponto-mesencephalic region exophytic tumors, 9.1% ($n = 1$) for the latero-bulbar and bulbar region tumors and 25% ($n = 2$) for the ponto-cerebellar tumors (AT/RT). Figure 4 shows the survival curve of all the brainstem tumors highlighting the different evolution between the DIPG and the non-DIPG tumors.

Discussion

Brainstem tumors still represent a great challenge for paediatric neurosurgeons and neuro- oncologists because the survival rate remains low despite the recent progress in genetic and molecular knowledge (7–9). The balance is always between the lesions

TABLE 3 Summary of the molecular findings.

Radiology/histopathology	Diffuse glioma		Circumscribed/exophytic glioma		Embryonal tumors	No detected BRAF alterations
Molecular data	H3K27M+	H3K27M−	BRAF V600E	KIAA1549-BRAF fusion	AT/RT, ETANTR	No detected BRAF alterations
Number of patients	18	10	4	5	3	6

10.3389/fped.2023.1193474

TABLE 4 Summary of all treatment protocol used for high grade tumor with the corresponding survival rate.

Protocol	Number of patients	1-year survival (%)	2-year survival (%)	3-year survival (%)
BIOMEDE	16	64	6.1	6.1
TRONC 98	15	53	20	0
CILENT	3	33	0	0
TARCEVA	4	0	0	0
TEMODAL	4	0	0	0
PNET HR	2	0	0	0

accessible to a surgical removal and the more infiltrating lesions such as DIPGs that are characterized by a dismal prognosis. Brainstem tumors were already described in the 50s and a French monograph reported the first modern classification and description of these insidious lesions (10). After the first report of Kummel in the US in 1881 (1), Monakow (2), Bailey and Cushing (3) reported the first modern description of this pathology in 1926 and stated that it was impossible to treat these tumors. Moreover, Matson, the father of the modern pediatric neurosurgery, stated that surgery was not indicated for treatment of this tumors (11). Brainstem tumors represent 15% of tumors of the central nervous system in children and 80% are located in the pontine region. There is no preference of sex and the mean age at diagnosis is between 7 and 9 years. In 1989, Guy, Jan and Guegan pointed out the progress in the field of radiology, electrophysiology and in the surgical removal of exophytic brainstem tumors (4). This report confirmed the dismal outcome in terms of clinical results and survival for DIPG in comparison with circumscribed or exophytic brainstem tumors that are generally histologically more benign and accessible to large surgical resection (4).

Stroink (1986) classified brainstem lesion in 4 differents groups: exophytic lesions (group I), intrinsic lesions without enhancement (group II a), intrinsic lesions with lateral or ventral extension (group II b), intrinsic lesion with enhancement (group III); focal lesions (group IV) (5). We have used the classification of Choux (12) that separates the lesion in diffuse, intrinsic focal, extrinsic focal, and cervico-medullary tumors. This classification was used in because it is a French classification. The diffuse forms of this classification correspond to the DIPG tumors that represent a particular form of brainstem tumors not eligible for a surgical resection and characterized by their dismal prognosis.

All these classifications should be improved by including MRI and molecular analysis of the tumor in order to decide the best oncological treatment and assess their possible prognostic evolution. Indeed, to-date the main progress is represented by the bio-molecular and genetic knowledge of the Central Nervous System tumors. For brainstem tumors, two main oncogenic pathways have been individualized: the BRAF pathway that is usually associated with benign tumors and the histone pathway that characterizes malignant neoplasms. Diffuse midline glioma and DIPG are mostly characterized by the presence of the H3.3K27M or H3.1K27M mutation of the histone genes H3F3A and HIST1H3B respectively. The mutation inhibits the PCR2 complex and regulates gene expression via the global reduction in demethylation and trimethylation of lysine 27 residue of histone sub-unit (13, 14). For benign brainstem tumors, the identification of BRAF alterations permits to use new anti – BRAF drugs such as dabrafenid or vemurafenid or anti—MEK as trametinib or selumetinib. Previous studies have shown that gangliogliomas with BRAF-V 600E mutation have an increased risk for progression or recurrence especially in tumor located in

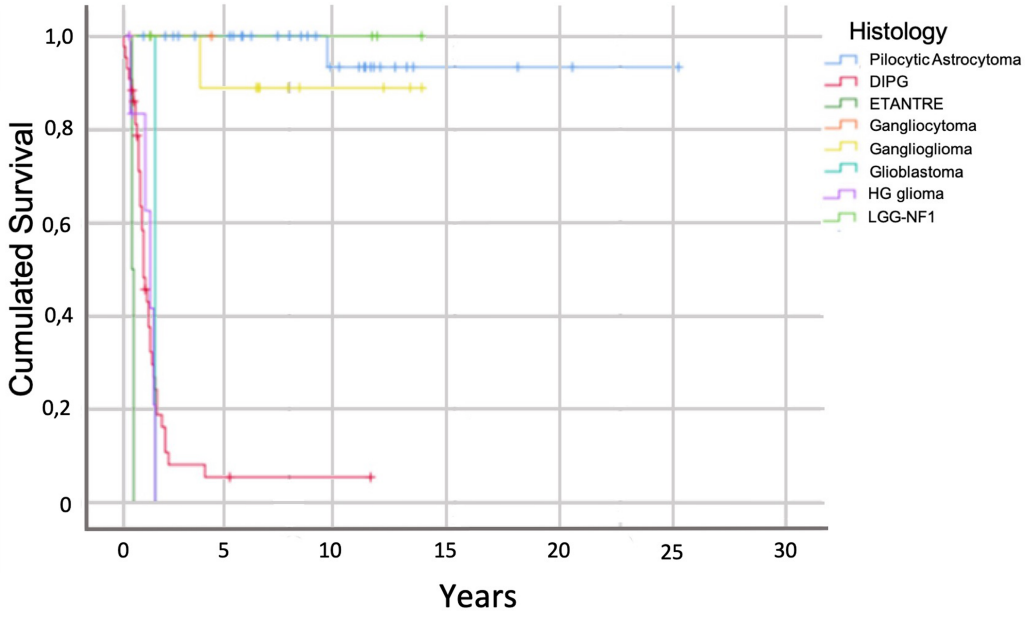

FIGURE 4
Survival analysis of the different histology types.

the brainstem with a shorter progression free survival compared to BRAF wild-type gangliogliomas (15). Bio-molecular and genetic markers are even more important for DIPG in order to find new targeted drugs to improve the survival.

Castel et al. in a biomolecular study concerning 62 patients, showed the loss of H3K27 trimethylation in 95% of the DIPG samples (16). Beside the H3K27M mutation, H3.1 K27M and H3.3 K27I mutations were found in pontine tumors. An oligodendroglial differentiation was observed more frequently in H3.3K27M DIPG. The H3.1K27M mutation was associated with the presence of large areas of necrosis and a better response to radiotherapy with a better survival rate of 15 months compared to a survival of 9.2 months for H3.3 mutated patients. These findings are consistent with the literature (17).

In our experience the treatment with targeted chemotherapy did not significantly change the rate of survival for DIPG because the median survival was inferior to one year (10.7 months) in patients with and without the mutation. Considering only patients treated with the BIOMEDE program and patients treated with the TRONC 98, there was no significant difference in the median survival with a survival of 13.7 months for the group (BIOMEDE) and 13.5 months for the TRONC 98 group. We have to stress that, in our cohort, biomolecular analysis was available only in a limited number of patients. This prevented us to establish significant statistical differences regarding the survival as these technologies were available only from 2015 onward.

The necessity to include patients in targeted chemotherapy protocols was at the origin of trials encouraging to perform biopsies and we share this attitude.

The importance of the biopsy for brainstem tumors has been highlighted by the progress on molecular targets for many general cancers (18) and by the need of establishing a correct histopathological and molecular diagnosis. Indeed no less than 10% of patient with presumed brainstem gliomas had different post-biopsy diagnoses such as demyelinating disease, vascular lesions, infectious disease like rhombencephalitis etc (19). The second strong argument for biopsy is the inclusion of patients in new tailored protocols with new targets according to the genetic constitution of the tumor as the French Biomede study (20). However, to date, the stereotactic biopsy has been criticized because the sample was taken in a limited region and thus could not represent the entire volume of the tumor. Therefore, it was debatable to expose patients to the risk of surgery in such a critical anatomical structure (21). To avoid the possible clinical complications, post mortem biopsies have been proposed and performed (21). Analysis of post –mortem tissue and some surgical biopsies have suggested that identifiable genetic and molecular alterations can be found and may serve as therapeutics targets (22). However, post-mortem tissue samples could no reproduce valid bio-molecular tumor markers (23, 24).

If a biopsy has to be done, different surgical techniques can be used: direct approach, stereotactic technique with a frame or frameless, stereotactic biopsy using image guidance. We have switched from a frame-based to a frameless biopsy technique (Medtronic) without losing precision and without increasing the rate of complications. We have not observed significant statistical differences concerning the rate of sequels with the different techniques used except for a slight increase with the direct approach because it was associated to a more extended surgical removal. In the literature, the rate of transient and permanent deficits following biopsy varies from 4% to 1% with a rate of 94.9% of diagnostic yield (25), 4.9% of morbidity and 0.7% of mortality (26). Roujeau et al. reported a rate of 8% of complications without non-diagnostic biopsies (27). In a later paper, Puget raised the question if it was really worthy performing biopsies of brainstem lesions (28). Schumacher stressed that the diagnosis of brainstem tumors could be done with images criteria, laboratory data and clinical and laboratory data alone (27–29). Paugh underlined that with limited specimen it is not always possible to have a representative element of the tumor and also of its genetic constitution (27, 30).

In the future, it may be possible that the PET/MRI scans may help to establish a diagnosis of these tumors with the study of their own metabolism avoiding the need of a surgical biopsy.

Our rate of post-surgical complications for biopsies for brain stem tumors was 22%. This higher rate of complications could be explained with the higher number of biopsies realized with a direct open approach with an attempt to remove a volume of tumor as large as possible avoiding clinical sequelae.

The other reason of our high rate of complications may be due to the fact that we reported also transitory complications as cardiac rhythm troubles and respiratory failures during the procedures that were completely reversible; if we remove these short-lived complications our rate of post-biopsy complications goes down to 6.5% as in other series. Regarding the mortality rate, our 2.2% rate confirm that the location of this tumor exposes the patients to a real risk.

In the future, liquid biopsy and liquid biome can take a great importance not only to establish the diagnosis but also to have an evaluation of treatments in the follow-up of the disease. Liquid biopsy is a developing technique in cancer studies using saliva, blood, urine, CSF to detect cells free tumors DNA (Ct DNA), circulating tumor cells (CTC) and tumor extracellular vesicles (31, 32). CSF –derivates have better sensibility compared with circulating tumor cells (33). In 2017, Huang could show Sanger sequencing and mutation—specific PCR to detect H3 mutations in CSF- derivate tumor DNA (34). However, these techniques need highly specialized laboratories. The main limitations are the calculation of allele frequency and the lack of sensitivity. However, this could in the future guarantee a precise histological and genetic diagnosis representing a real alternative to the surgical biopsy.

Surgical considerations

The first direct surgical approaches for a brainstem tumor were reported in the 1960s (35). Then, Hoffman and Epstein reported in the 80s their experience with the exophytic forms located at level of the bulbo-medullary region and at level of the quadrigeminal plate (21, 36, 37). Bricolo et al. also described some entry points to

approach brainstem tumors reducing the risk of sequelae for patients and increasing the rate of surgical resection (38). Generally respecting these well definite entry zones help to reduce sequels. However, for us, it is important to approach the tumor either where it is visible at level of the anatomical surface or choising the shorter distance to join the tumor with short opening incision trying to respect the anatomical structures.

Progresses of surgical techniques were useful to remove focalized brainstem tumors, bulbo-medullary and latero-bulbar tumors or exophytic mesencephalic lesions that could benefit from a large resection. The use of neurovavigation, intra-operative neurophysiology and ultrasonic aspirator have also permitted a better surgical outcome. Nevertheless, the surgical approach has to be chosen based on the anatomical localization of the tumor, its exophytic extension and the axis of the tumor's growth. In our center, we generally use the sitting position except in cases of subtemporal approach to expose the lateral portion of the mesencephalic region or the lateral portion of the pontine region. The Mayfield headrest is used in patient older than three years old to avoid complication with the pins penetrating into the fragile bone of younger patients. The CUSA cavitron permits to remove tumors staying inside the tumor and with a weak power of aspiration and fragmentation it is possible to reduce the tumoral mass also on critical area as the floor of the fourth ventricle. We advocate an aggressive surgery for benign tumors such as pilocytic astrocytomas and ganglioglioma even if complete surgical removal was possible in only twenty patients of our cohort. A complete removal can be possible also at the level of the bulbo-medullary junction. A subtotal surgical resection was possible in 13 patients. In case of ganglioglioma of the latero-bulbar or latero bulbo-pontine region, a large removal can favor a quiescence of the tumor with a good evolution also for long time. For exophytic tectal plate tumors, we prefer the sub-occipital trans-tentorial approach, as for pineal tumors, that permits a very large exposure of the posterior mesencephalic region. We already reported our experience with tectal plate tumors (39). When tumors are benign the clinical results are satisfying and the surgical mortality is nihil as long as we follow a safe surgical strategy (40). The results of exophytic brain stem tumors are reported in the **Tables 1–3**. The indication of surgery for tectal plate tumors was relate to their volumetric progression, and to the fact that they were exophytic and associated with a documented clinical evolution. The rate of complication in 42 patients operated for exophytic or localized benign gliomas with a direct approach was 14% and involved principally the cranial nerves with mild swallowing troubles in a patient, a peripheral facial palsy in three patients, gait troubles in a child and a cerebellar syndrome in another case. A pseudo meningocele disappeared after treatment with furosemide and in two cases a skin infection was treated with antibiotics. One patient died of a cardio-respiratory complication one year after tumor removal (pilocytic astrocytoma) at level of the bulbo-medullary junction. Our experience confirmed that surgery of the brainstem tumors is possible as reported by others authors (21, 41). The respect of safe entry zone already described by different authors permits a more aggressive surgery with a low rate of sequelae and an acceptable mortality rate (6, 42, 43). Surgical removal of benign tumors, even with partial surgical resection can be able to stop their evolution for a long time.

On the other hand, surgery has limited possibilities for DIPG. We believe that in the future new radiological tools could allow a diagnosis without surgical procedures and also that the individualization of tumoral targets with tailored chemotherapies and radiotherapy could help to improve the prognosis of these tumors. The bio-molecular studies and tailored chemotherapic treatment in our experience did not permit an improved survival rate of patients with diffuse brainstem gliomas.

Conclusions

Our series confirms that histologically benign tumors have a good survival with surgical removal and adjuvant treatment. DIPG still have a dismal prognosis despite recent biomolecular characterizations and new chemotherapeutic regimens that have not been able to significantly improve their survival rate and the quality of life. Still, we believe that it is necessary to perform biopsies to obtain tissue for diagnosis and to perform molecular studies to improve the efficacy of adjuvant treatment. A better classification of brainstem tumors in children with the bio-molecular understanding of the oncogenic process will be in the future responsible for further improvement of more personalized treatment.

The future depends mainly on the discovery of more effective drugs that could change the dismal evolution of infiltrating brainstem tumors. The better overall prognosis of exophytic lesions may be due to the fact that these lesions are less aggressive and consequently more accessible to an extensive surgical resection that needs to be balanced with morbidity prevention and with the ability to maintain z good quality of life.

Data availability statement

The raw data supporting the conclusions of this article will be made available by the authors, without undue reservation.

Ethics statement

Ethical approval was not required for the study involving humans in accordance with the local legislation and institutional requirements. Written informed consent to participate in this study was not required from the participants or the participants' legal guardians/next of kin in accordance with the national legislation and the institutional requirements.

Author contributions

RB: Data collection, Statistics. PB: Write manuscript, Data collection, Statistics. FR: Revise Manuscript. AV: Data collection, Revise manuscript. AS: Data collection, Supervision, Revise manuscript, Statistics. CM, Supervision, Write manuscript, Data

collection. All authors contributed to the article and approved the submitted version.

Conflict of interest

The authors declare that the research was conducted in the absence of any commercial or financial relationships that could be construed as a potential conflict of interest.

Publisher's note

References

1. Kummel B. *Beitrag Zur Kasuistik Der Gliom Des Pons Und Der Medulla Oblongata*. Klin Medizin. (1881).

2. Monakow C. Histoire naturelle des tumeurs cérébrales, en particulier du gliome. *Encéphale*. (1926):117–89.

3. Bailey P, Cushing H. *A classification of tumors of the glioma group on a hystogenesis basis*. Philadelphia: Lippincot (1926).

4. Guegan Y, Guy G, Guegan Y. Les lésions chirurgicales du tronc cérébral. Rapport de la société de neurochirurgie de langue française. *Neurochirurgie*. (1989).

5. Stroink AR, Hoffman HJ, Hendrick EB, Humphreys RP. Diagnosis and management of pediatric brain-stem gliomas. *J Neurosurg*. (1986) 65:745–50. doi: 10.3171/jns.1986.65.6.0745

6. Klimo P, Nesvick CL, Broniscer A, Orr BA, Choudhri AF. Malignant brainstem tumors in children, excluding diffuse intrinsic pontine gliomas. *J Neurosurg Pediatr*. (2016) 17:57–65. doi: 10.3171/2015.6.PEDS15166

7. Hossain MJ, Xiao W, Tayeb M, Khan S. Epidemiology and prognostic factors of pediatric brain tumor survival in the US: evidence from four decades of population data. *Cancer Epidemiol*. (2021) 72:101942. doi: 10.1016/j.canep.2021.101942

8. Sun T, Xu Y, Pan C, Liu Y, Tian Y, Li C, et al. Surgical treatment and prognosis of focal brainstem gliomas in children: a 7 year single center experience. *Medicine (Baltimore)*. (2020) 99:e22029. doi: 10.1097/MD.0000000000022029

9. Joud A, Stella I, Klein O. Diffuse infiltrative pontine glioma biopsy in children with neuronavigation, frameless procedure: a single center experience of 10 cases. *Neurochirurgie*. (2020) 66:345–8. doi: 10.1016/j.neuchi.2020.05.007

10. Guillain G, Bertrand I, Gruner J. *Les gliomes infiltrés du tronc cérébral*. Masson. (1945).

11. Ingraham FD, Matson DD. *Neurosurgery of infancy*. (1954).

12. Choux M, Lena G, Do L. Brain stem tumors. In: Choux M, Di Rocco C, Hockley A, editors. *Pediatric neurosurgery*. New York: Churchill Livingstone (200). p. 471–91.

13. Lewis PW, Müller MM, Koletsky MS, Cordero F, Lin S, Banaszynski LA, et al. Inhibition of PRC2 activity by a gain-of-function H3 mutation found in pediatric glioblastoma. *Science*. (2013) 340:857–61. doi: 10.1126/science.1232245

14. Rashed WM, Maher E, Adel M, Saber O, Zaghloul MS. Pediatric diffuse intrinsic pontine glioma: where do we stand? *Cancer Metastasis Rev*. (2019) 38:759–70. doi: 10.1007/s10555-019-09824-2

15. Dahiya S, Haydon DH, Alvarado D, Gurnett CA, Gutmann DH, Leonard JR. BRAFV600E Mutation is a negative prognosticator in pediatric ganglioglioma. *Acta Neuropathol*. (2013) 125:901–10. doi: 10.1007/s00401-013-1120-y

16. Castel D, Philippe C, Calmon R, Le Dret L, Truffaux N, Boddaert N, et al. Histone H3F3A and HIST1H3B K27M mutations define two subgroups of diffuse intrinsic pontine gliomas with different prognosis and phenotypes. *Acta Neuropathol*. (2015) 130:815–27. doi: 10.1007/s00401-015-1478-0

17. Wu G, Diaz AK, Paugh BS, Rankin SL, Ju B, Li Y, et al. The genomic landscape of diffuse intrinsic pontine glioma and pediatric non-brainstem high-grade glioma. *Nat Genet*. (2014) 46:444–50. doi: 10.1038/ng.2938

18. Warren KE. Diffuse intrinsic pontine glioma: poised for progress. *Front Oncol*. (2012) 2:205. doi: 10.3389/fonc.2012.00205

19. Dellaretti M, Touzet G, Reyns N, Dubois F, Gusmão S, Pereira JLB, et al. Correlation among magnetic resonance imaging findings, prognostic factors for survival, and histological diagnosis of intrinsic brainstem lesions in children. *J Neurosurg Pediatr*. (2011) 8:539–43. doi: 10.3171/2011.9.PEDS1167

20. Grill J. Biological medicine for diffuse intrinsic pontine gliomas eradication (BIOMEDE): results of the three-arm biomarker-driven randomized trial in the first 230 patients from Europe and Australia.

21. Epstein F, Wisoff JH. Surgical management of brain stem tumors of childhood and adolescence. *Neurosurg Clin N Am*. (1990) 1:111–21. doi: 10.1016/S1042-3680(18)30827-1

22. Angelini P, Hawkins C, Laperriere N, Bouffet E, Bartels U. Post mortem examinations in diffuse intrinsic pontine glioma: challenges and chances. *J Neurooncol*. (2011) 101:75–81. doi: 10.1007/s11060-010-0224-7

23. Robison NJ, Kieran MW. Diffuse intrinsic pontine glioma: a reassessment. *J Neurooncol*. (2014) 119:7–15. doi: 10.1007/s11060-014-1448-8

24. Taylor KR, Mackay A, Truffaux N, Butterfield Y, Morozova O, Philippe C, et al. Recurrent activating ACVR1 mutations in diffuse intrinsic pontine glioma. *Nat Genet*. (2014) 46:457–61. doi: 10.1038/ng.2925

25. Samadani U, Judy KD. Stereotactic brainstem biopsy is indicated for the diagnosis of a vast array of brainstem pathology. *Stereotact Funct Neurosurg*. (2003) 81:5–9. doi: 10.1159/000075097

26. Pincus DW, Richter EO, Yachnis AT, Bennett J, Bhatti MT, Smith A. Brainstem stereotactic biopsy sampling in children. *J Neurosurg*. (2006) 104:108–14. doi: 10.3171/ped.2006.104.2.108

27. Roujeau T, Machado G, Garnett MR, Miquel C, Puget S, Geoerger B, et al. Stereotactic biopsy of diffuse pontine lesions in children. *J Neurosurg Pediatr*. (2007) 107:1–4. doi: 10.3171/PED-07/07/001

28. Puget S, Beccaria K, Blauwblomme T, Roujeau T, James S, Grill J, et al. Biopsy in a series of 130 pediatric diffuse intrinsic pontine gliomas. *Childs Nerv Syst*. (2015) 31:1773–80. doi: 10.1007/s00381-015-2832-1

29. Schumacher M, Schulte-Mönting J, Stoeter P, Warmuth-Metz M, Solymosi L. Magnetic resonance imaging compared with biopsy in the diagnosis of brainstem diseases of childhood: a multicenter review. *J Neurosurg Pediatr*. (2007) 106:111–9. doi: 10.3171/ped.2007.106.2.111

30. Paugh BS, Broniscer A, Qu C, Miller CP, Zhang J, Tatevossian RG, et al. Genome-wide analyses identify recurrent amplifications of receptor tyrosine kinases and cell-cycle regulatory genes in diffuse intrinsic pontine glioma. *J Clin Oncol*. (2011) 29:3999–4006. doi: 10.1200/JCO.2011.35.5677

31. Caretti V, Jansen MHA, Vuurden Dv, Lagerweij T, Bugiani M, Horsman I, et al. Implementation of a multi-institutional diffuse intrinsic pontine glioma autopsy protocol and characterization of a primary cell culture. *Neuropathol Appl Neurobiol*. (2013) 39:426–36. doi: 10.1111/j.1365-2990.2012.01294.x

32. Alix-Panabières C, Pantel K. Clinical applications of circulating tumor cells and circulating tumor DNA as liquid biopsy. *Cancer Discov*. (2016) 6:479–91. doi: 10.1158/2159-8290.CD-15-1483

33. Pan C, Diplas BH, Chen X, Wu Y, Xiao X, Jiang L, et al. Molecular profiling of tumors of the brainstem by sequencing of CSF-derived circulating tumor DNA. *Acta Neuropathol*. (2019) 137:297–306. doi: 10.1007/s00401-018-1936-6

34. Huang TY, Piunti A, Lulla RR, Qi J, Horbinski CM, Tomita T, et al. Detection of histone H3 mutations in cerebrospinal fluid-derived tumor DNA from children with diffuse midline glioma. *Acta Neuropathol Commun*. (2017) 5:28. doi: 10.1186/s40478-017-0436-6

35. Alvisi C, Cerisoli M, Maccheroni ME. Long-term results of surgically treated brainstem gliomas. *Acta Neurochir (Wien)*. (1985) 76:12–7. doi: 10.1007/BF01403823

36. Epstein F, Constantini S. Practical decisions in the treatment of pediatric brain stem tumors. *Pediatr Neurosurg*. (1996) 24:24–34. doi: 10.1159/000121011

37. Vandertop WP, Hoffman HJ, Drake JM, Humphreys RP, Rutka JT, Amstrong DC, et al. Focal midbrain tumors in children. *Neurosurgery*. (1992) 31:186–94. doi: 10.1227/00006123-199208000-00003

38. Bricolo A, Turazzi S. Surgery for gliomas and other mass lesions of the brainstem. *Adv Tech Stand Neurosurg*. (1995) 22:261–341. doi: 10.1007/978-3-7091-6898-1_5

39. Mottolese C, Szathmari A, Beuriat PA, Frappaz D, Jouvet A, Hermier M. Tectal plate tumours. Our experience with a paediatric surgical series. *Neurochirurgie*. (2015) 61:193–200. doi: 10.1016/j.neuchi.2013.12.007

40. Lapras C, Bognar L, Turjman F, Villanyi E, Mottolese C, Fischer C, et al. Tectal plate gliomas. Part I: microsurgery of the tectal plate gliomas. *Acta Neurochir (Wien)*. (1994) 126:76–83. doi: 10.1007/BF01476414

41. Cavalheiro S, Yagmurlu K, da Costa MDS, Nicácio JM, Rodrigues TP, Chaddad-Neto F, et al. Surgical approaches for brainstem tumors in pediatric patients. *Childs Nerv Syst*. (2015) 31:1815–40. doi: 10.1007/s00381-015-2799-y

42. Ogata N, Yonekawa Y. Paramedian supracerebellar approach to the upper brain stem and peduncular lesions. *Neurosurgery*. (1997) 40:101–4; discussion 104–105. doi: 10.1097/00006123-199701000-00023

43. Kyoshima K, Kobayashi S, Gibo H, Kuroyanagi T. A study of safe entry zones via the floor of the fourth ventricle for brain-stem lesions. Report of three cases. *J Neurosurg*. (1993) 78:987–93. doi: 10.3171/jns.1993.78.6.0987

frontiers | Frontiers in Oncology

TYPE Case Report
PUBLISHED 21 November 2023
DOI 10.3389/fonc.2023.1307591

OPEN ACCESS

EDITED BY
Dimitrios N. Kanakis,
University of Nicosia, Cyprus

REVIEWED BY
Kensuke Tateishi,
Yokohama City Universit, Japan
Prit Benny Malgulwar,
University of Texas MD Anderson Cancer Center, United States

*CORRESPONDENCE
Danielle Golub
dgolub1@northwell.edu

RECEIVED 04 October 2023
ACCEPTED 02 November 2023
PUBLISHED 21 November 2023

CITATION
Golub D, Lynch DG, Pan PC, Liechty B, Slocum C, Bale T, Pisapia DJ and Juthani R (2023) Polymorphous low-grade neuroepithelial tumor of the young with FGFR3-TACC3 fusion mimicking high-grade glioma: case report and series of high-grade correlates.
Front. Oncol. 13:1307591.
doi: 10.3389/fonc.2023.1307591

Polymorphous low-grade neuroepithelial tumor of the young with FGFR3-TACC3 fusion mimicking high-grade glioma: case report and series of high-grade correlates

Danielle Golub[1,2*], Daniel G. Lynch[3], Peter C. Pan[4,5], Benjamin Liechty[6], Cheyanne Slocum[6], Tejus Bale[7], David J. Pisapia[6] and Rupa Juthani[1]

[1]Department of Neurosurgery, Weill Cornell Medicine, New York, NY, United States, [2]Department of Neurosurgery, Northwell Health, Manhasset, NY, United States, [3]Zucker School of Medicine at Hofstra/Northwell Health, Hempstead, NY, United States, [4]Department of Neurology, Weill Cornell Medicine, New York, NY, United States, [5]Department of Neurology, Columbia University, New York, NY, United States, [6]Department of Pathology, Weill Cornell Medicine, New York, NY, United States, [7]Department of Pathology, Memorial Sloan Kettering Cancer Center, New York, NY, United States

Background: Polymorphous low-grade neuroepithelial tumor of the young (PLNTY) is a recently described entity that can mimic high-grade glioma (HGG) in histologic and molecular features; however, factors predicting aggressive behavior in these tumors are unclear.

Methods: We present an indolent neuroepithelial neoplasm in a 59-year-old female with imaging initially suggestive of HGG, and a series of adult patients with HGG harboring FGFR3-TACC3 fusions are also presented for comparison.

Results: Pathology in the case patient revealed low-grade cytomorphology, microcalcifications, unusual neovascularization, and a low proliferation index. The lesion was diffusely CD34+ and harbored an FGFR3-TACC3 fusion and TERT promoter mutation. A diagnosis of PLNTY was therefore favored and the patient was observed with no progression at 15-month follow-up. In patients with HGG with FGFR3-TACC3 fusions, molecular findings included IDH-wildtype status, absence of 1p19q codeletion, CDKN2A loss, TERT promoter mutations and lack of MGMT promoter methylation. These patients demonstrated a median 15-month overall survival and a 6-month progression-free survival.

Conclusion: PLNTY is a rare low-grade entity that can display characteristics of HGG, particularly in adults. Presence of FGFR3-TACC3 fusions and other high-grade features should raise concern for a more malignant precursor lesion when a diagnosis of PLNTY is considered.

KEYWORDS

FGFR fusion, glioblastoma, glioma molecular drivers, high-grade glioma, PLNTY

1 Introduction

Low-grade epilepsy-associated neuroepithelial tumors (LEATs) are a diverse set of epileptogenic neurodevelopmental lesions along a broad histological glial—glioneuronal spectrum that has made them historically difficult to classify (1, 2). Polymorphous low-grade neuroepithelial tumor of the young (PLNTY) represents the most recently recognized LEAT entity in the latest WHO classification, defined by oligodendroglioma-like cellular features, an infiltrative growth pattern, diffuse CD34 immunoreactivity, and frequent MAPK pathway aberrations—in particular, BRAF V600E and FGFR isoform fusion alterations (3, 4). On MRI, PLNTY can be difficult to distinguish from oligodendroglioma, DNET, or focal cortical dysplasia; it typically presents as a focal FLAIR hyperintensity with rare nodular enhancement and/or cystic components (5, 6). On CT, however, distinctive macrocalcifications are frequently observed (6). Increasing reports of LEATs consistent with PLNTY have helped to refine these defining characteristics, but the majority of reports to date have presented pediatric and young adult patients. Rare reports of PLNTY in middle-aged patients are partially explained by the lesions' localization in the non-dominant hemisphere, likely prolonging the asymptomatic period (7, 8). Additionally, the differential diagnosis of heterogeneously enhancing cortical lesions in older patients generally prioritizes higher-grade gliomas over low-grade congenital lesions, further complicating the correct diagnosis of PLNTY in adults.

The FGFR3-TACC3 fusion, seen in a variety of solid tumors, produces a constitutively active fibroblast growth factor 3 receptor that leads to the upregulation of RAS-MAPK, PI3K-AKT, and JAK/STAT pathways responsible for increased cellular proliferation, migration, and angiogenesis (9). In high-grade glioma (HGG), this fusion alteration has been associated with amplification of cell cycle-related genes and decreased survival (10), however the fusion's impact on survival invasiveness of low-grade pathologies such as PLNTY is not well-understood. Furthermore, it is unclear if the presence of the FGFR3-TACC3 fusion in an adult patient with PLNTY confers increased malignant potential, warranting adjuvant therapy. The concomitant presence of molecular findings common to HGGs with histologic findings and a clinical course consistent with a low-grade pathology such as PLNTY is unique and highlights some of the potential limitations of current molecular diagnostic criteria.

In this series, we describe an unusual case of adult PLNTY with an FGFR3-TACC3 fusion alteration that harbored histological and molecular features associated with HGG, but displayed a benign clinical course. We compare findings in this case to a review of published PLNTY cases to identify common and unique histologic and molecular features. We further contrast the molecular similarities and differences in this case of PLNTY to a corresponding series of 8 gliomas harboring FGFR3-TACC3 fusions identified by targeted sequencing panels. Finally, we assess the clinical outcomes including progression-free and overall survival in patients with glioblastoma (GBM) harboring the FGFR3-TACC3 fusion. This series aims to highlight a unique case of PLNTY and to identify potential limitations in our molecular diagnostic criteria for GBM.

2 Case presentation: PLNTY with high-grade features

A 59-year-old, right-handed female presented with new onset generalized tonic-clonic seizures. CT demonstrated multiple masses associated with calcification in the right frontal lobe with vasogenic edema (Figure 1F). Subsequent magnetic resonance imaging (MRI) revealed multifocal enhancing lesions with associated areas of susceptibility involving the right frontal lobe, cingulate, and underlying white matter, with partial calcification containing intrinsic T1 hyperintensity. There was infiltrative appearing T2 signal hyperintensity extending across the midline along the corpus callosum with mild associated mass effect (Figures 1A-E). No T2-FLAIR mismatch was apparent. Radiological findings were reviewed at a multi-disciplinary tumor board, and favored to represent a glial neoplasm, either oligodendroglioma or high-grade astrocytoma. The patient underwent surgical resection, with post-operative MRI demonstrating a gross total resection of enhancing disease.

Initial frozen section was concerning for high-grade infiltrating glioma due to the presence of glial features, hyperplastic appearing vasculature, and necrosis. Permanent histologic sections, however, showed a moderately cellular neuroepithelial neoplasm with abundant microcalcification, with perivascular, perineuronal, and subpial growth (Figures 2C, D). Regions of necrosis and neovascularization were thought to represent intra-tumoral infarction rather than true tumoral necrosis or microvascular proliferation (Figures 2A, B). The remainder of the tumor appeared cytologically bland with cytoplasmic clearing and branched capillaries resembling oligodendroglioma (Figure 2E). Immunohistochemistry demonstrated strong staining for GFAP in some portions of the tumor and synaptophysin reactivity in other portions (Figures 2F-H). Notably, the tumor was diffusely, strongly positive for CD34 (Figure 2I). Tumor cells were non-reactive for both $IDH1^{R132H}$ and p53, and showed preservation of ATRX. The Ki-67 proliferation index was <1% (Figure 2J). Of note, TERT promoter mutation and polysomy 7 without EGFR amplification was identified, and the MGMT promoter was unmethylated. Due to the unusual low-grade nature of this tumor, methylation array profiling was performed using the DKFZ brain tumor classifier (11). No match was obtained, and copy number analysis revealed polysomy of chromosomes 7 and 8 with monosomy of chromosome 10 (Figure 2K). Subsequent fusion analysis identified FGFR3-TACC3 fusion. Based on the low-grade morphology with oligodendroglioma-like components, CD34 immunopositivity, IDH-wildtype status, and absence of a match by methylation array profiling, an interpretation of a low-grade tumor such as PLNTY was favored (12).

The patient was discharged home on postoperative day 3 with no neurological deficits. Other than a single seizure episode two months postoperatively that resolved with the addition of a second anti-epileptic medication, she did well clinically with no recurrent symptomatology. She has been followed closely with MRIs every 3 months without evidence of recurrent or progressive disease with most recent follow-up at 15 months postoperatively.

10.3389/fonc.2023.1307591

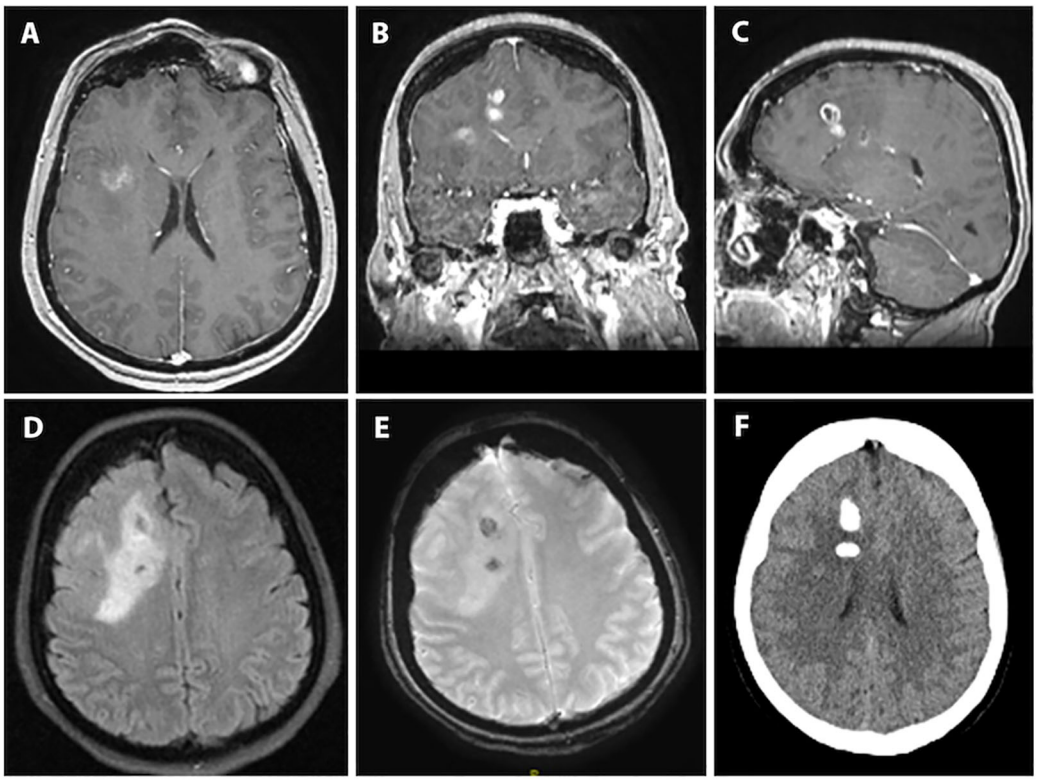

FIGURE 1
Preoperative imaging for index case of PLNTY with high-grade features. **(A–C)**: T1-weighted axial, coronal and sagittal sequences with contrast demonstrating multifocal enhancement involving the right frontal lobe and cingulate gyrus. **(D)**: T2/FLAIR-weighted axial sequence showing the bulk of the lesion to be T2/FLAIR hyperintense with clear mass effect and some surrounding vasogenic edema. **(E)**: Susceptibility-weighted imaging showing two areas susceptibility likely corresponding to intralesional calcification given the matching hyperdensities seen on **(F)**: axial computed-tomography imaging.

3 Case series: FGFR3-TACC3 fusions in HGG

3.1 Methods

All HGGs treated at Weill Cornell Medicine found to have FGFR3-TACC3 fusion by targeted sequencing (Oncomine Comprehensive Panel v2, FoundationOne) were included in this study under an IRB-approved protocol. Tumor characteristics (including radiographic features, location, histopathology, and molecular analysis), treatment characteristics (including extent-of-resection, chemotherapy, and radiation therapy), and clinical outcomes (including progression-free survival and overall survival), were retrospectively reviewed and evaluated.

3.2 Results

A total of eight cases of GBM with FGFR3-TACC3 fusion were identified including two male and six female patients. Median age at diagnosis was 64 years (range 41-74). Seven of these tumors met histopathologic criteria for GBM on initial tissue analysis. All were IDH-wildtype, and 7/8 (87.5%) were MGMT unmethylated, while 1/8 (12.5%) harbored MGMT promoter methylation. Five tumors were located in the frontal lobe, 2 tumors in the parietal lobe, and 1 tumor in the temporal lobe. Gross total resection was achieved in 5 cases; the remainder were either sub-totally resected (1) or biopsied (2). All cases were treated with standard external beam radiotherapy and concurrent temozolomide following surgery. Half of the cases were treated with 59.4-60 Gy in 30-33 fractions, and the other half were treated with a hypofractionated course of 40.05 Gy in 15 fractions.

Median progression-free survival in this cohort was 6 months (Figure 3), while median overall survival was 15 months (Figure 4). Three patients progressed rapidly after initial chemoradiation and were not treated further with adjuvant temozolomide chemotherapy: A 63-year-old man with a left frontal GBM who underwent subtotal resection followed by temozolomide and a radiation dose of 59.4 Gy in 33 fractions, who elected hospice care at 3 months postoperatively and ultimately died 15 months postoperatively, and two other patients who were lost to follow-up after transitioning to hospice; a 71-year-old woman with a gross totally-resected right frontal GBM and a 61-year-old woman with a biopsied left parietal GBM. Both received temozolomide with radiation dose of 40.05 Gy in 15 fractions and transitioned to hospice before adjuvant chemotherapy.

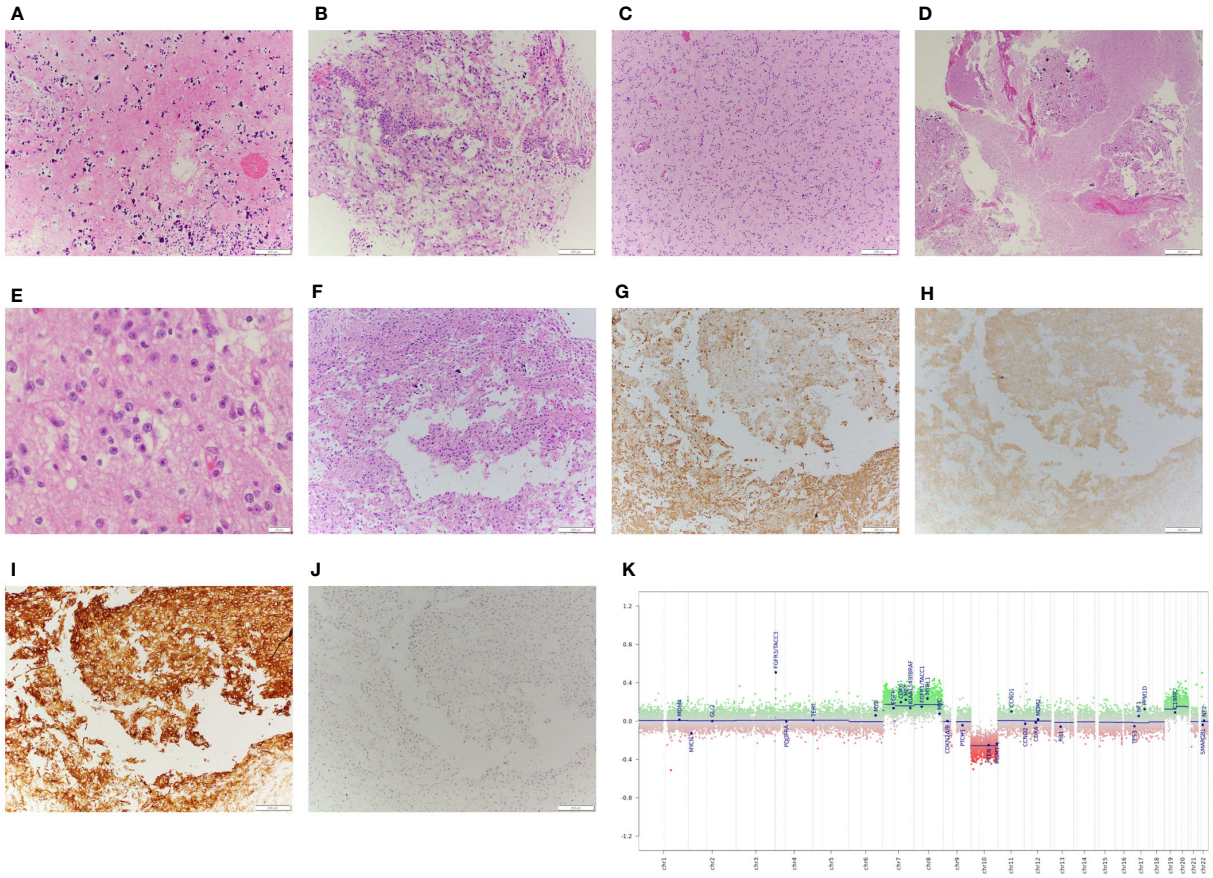

FIGURE 2
Pathological examination of surgical specimen including DNA methylation analysis. **(A)**: Histologic examination with geographic regions of necrosis with **(B)**: adjacent regions of sinusoidal neovascularization. The majority of tumor tissue demonstrated a cytologically bland neoplasm, **(C)**: comprised of regions with an infiltrative and **(D)**: occasionally more demarcated growth pattern, often associated with microcalcification. **(E)**: High power images of the tumor demonstrate some features suggestive of neurocytic differentiation, including open chromatin and prominent nucleoli. **(F)**: The greatest degree of nuclear atypia was seen in regions adjacent to the necrosis, which demonstrated variable immunoreactivity for **(G)**: GFAP and **(H)**: synaptophysin, with **(I)**: strong, diffuse staining for CD34. **(J)**: Of note, the Ki-67 proliferative index was low, <1% in atypical cells. **(K)**: Copy number analysis obtained from methylation array profiling data demonstrates whole chromosome gains of chromosomes 7, 8, 19, and 20, and loss of chromosome 10, and copy number gain of the FGFR3-TACC3 locus, consistent with the underlying fusion identified.

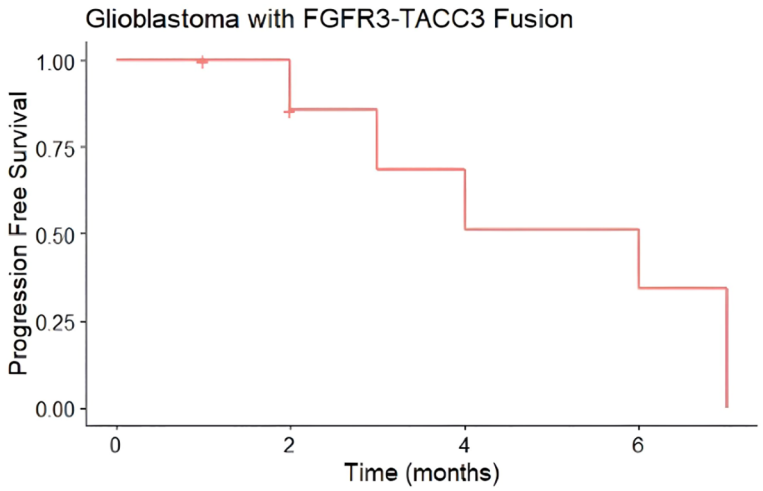

FIGURE 3
Progression-Free Survival (PFS) of glioblastomas from case series with FGFR3-TACC3 fusion. Median progression-free survival was 6 months (n = 8, 6 events). Hashmark indicates censored.

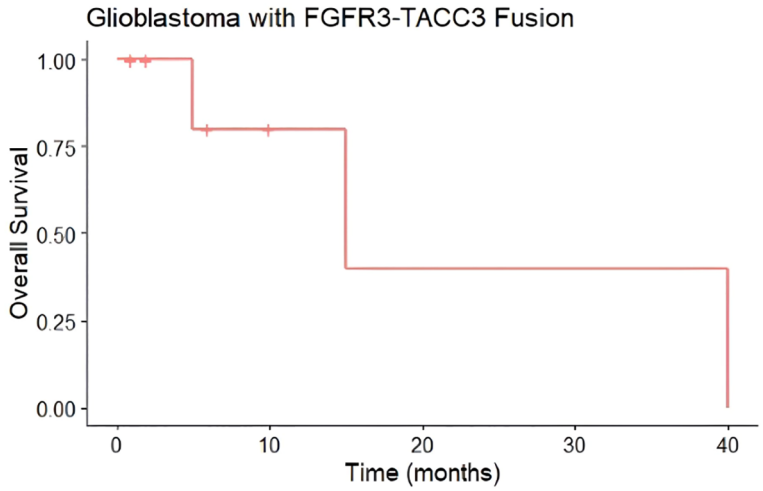

FIGURE 4
Overall Survival (OS) of glioblastomas from case series with FGFR3-TACC3 fusion. Median overall survival of 15 months (n=8, 3 events). Hashmark indicates censored.

4 Discussion

4.1 Histological and molecular characteristics of PLNTY

The term "polymorphous" was originally ascribed to PLNTYs because of their significant histological heterogeneity; while consistently demonstrating areas of oligodendroglioma-like cells with round nuclei and perinuclear halos, some PLNTY samples also have areas of vague perivascular ependymoma-like pseudorosetting and patchy regions of fibrillary, spindled astrocytic components (4). A consistent finding across PLNTY lesions is strong, diffuse CD34 immunoreactivity (4). CD34, a well-known intercellular adhesion protein and marker of hematopoietic stem cells, is also transiently expressed in early neural development (13). In addition to PLNTY, ganglioglioma, DNET, and pleomorphic xanthroastrocytoma (PXA) are often focally CD34+, albeit in a more heterogeneous distribution (14). The expression of CD34 across multiple pediatric lesions, particularly LEATs, suggests that these lesions may involve developmentally arrested or dysregulated neural progenitors. In fact, most of these CD34+ lesions, including PLNTY, are also frequently associated with regional cortical dysplasia (15). Accordingly, one of the largest series examining LEATs found that CD34 expression was associated with a significantly longer duration of epilepsy—further suggesting a congenital or developmental structural cause (16).

PLNTY also exhibits a collectively distinct genetic and epigenetic signature. Huse et al.'s original series identified frequent mutually exclusive genetic aberrations involving the MAP kinase pathway including BRAF V600E and FGFR2 or FGFR3 fusion transcripts (4). Since this seminal work, mutually exclusive BRAF and FGFR2 or FGFR3 mutations have been identified in nearly all reported cases of PLNTY (Table 1) (4, 6–8, 17–23). BRAF V600E is a constitutively active downstream effector in the MAPK pathway that is a widely implicated oncogenic driver in several cancers and an established pharmacogenetic target. Similarly, the FGFR2 and FGFR3 fusion transcripts constitutively dimerize to activate the MAPK pathway and are also potential therapeutic targets (24). While MAPK pathway alterations clearly play a critical driver role in PLNTY, the same can be said of a majority of LEATs (5) and of several other types of cancers. However, genome-wide methylation profiling has established that PLNTY exhibits a distinct DNA methylation signature most closely related to that of ganglioglioma; in fact, when applied to a wider set of previously profiled tumors, Huse et al. found that two additional lesions initially diagnosed as ganglioglioma and low-grade glioma, NOS actually clustered best with the PLNTY methylation signature, and furthermore harbored consistent FGFR2 fusion alterations (4). While most LEAT subtypes, including PLNTY, rely on MAPK pathway activation, distinct DNA methylation signatures and histological characteristics suggest etiological differences based on the differentiation state of the lesional cell of origin.

4.2 FGFR3-TACC3 fusions in GBM

The FGFR3-TACC3 fusion identified in our index PLNTY case can been seen in 3-8% of GBMs (25, 26). Like its manifestation in PLNTY, FGFR3-TACC3 fusion is mutually exclusive with the more common receptor tyrosine kinase mutations in GBM such as EGFR, PDGFR, or MET (27). In glioma and GBM, FGFR3-TACC3 is also associated with wild-type IDH status, homozygous deletion of CDKN2A, amplification of CDK4 and MDM2, and decreased survival—sometimes despite lower grade features such as low proliferation indices (10, 28, 29). These characteristics were consistent in our FGFR3-TACC3-positive GBM series in which all 8 lesions were IDH-wildtype and were predominantly MGMT promoter unmethylated. In our series, survival was comparable to the median survival reported by Stupp et al., without clearly conferring a poorer prognosis (30). However, this comparison is

TABLE 1 Review of Cases of PLNTY in the Literature.

Studies	No. of Cases	Age	Gender	Onset of Epilepsy	Lesion Localization	Histological Features	OLIG2+	GFAP+	CD34+	Ki67	BRAF Mutation	FGFR Fusion Transcript
Huse et al. (2017) (4)	10	4-32	4M, 6F	3-22	6 R temporal 1 L temporal 2 R occipital 1 R frontal	* All: Oligodendroglioma-like cells with compact nuclei and perinuclear halos * 9: Patchy fibrillary and spindled astrocytic features * All: Patchy perivascular pseudorosettes * 9: Calcifications	All: Strong	All: Patchy	All: Strong, diffuse; +regional cortex	8: <1% 1: 3% 1: 5%	3 BRAF V600E	1 FGFR3-TACC3 1 FGFR2-KIAA1598 1 FGFR2-CTNNA3
Bitar et al. (2018) (17)	1	31	M	10	R temporal	* Oligodendroglioma-like cells with compact nuclei and perinuclear halos * Patchy fibrillary and spindled astrocytic features * Rare eosinophilic granular bodies		Patchy	Strong, diffuse; +regional cortex	1-2%	BRAF V600E	
Riva et al. (2018) (8)	1	57	M	No seizures	R frontal	* Oligodendroglioma-like cells with compact nuclei and perinuclear halos * Patchy perivascular pseudorosettes	Yes	Yes	Strong, diffuse; +regional cortex	2-3%		FGFR3-TACC3
Gupta et al. (2019) (18)	1	30	M	22	R middle temporal gyrus	* Oligodendroglioma-like cells with compact nuclei and perinuclear halos		Moderate staining between tumor cells	Strong, diffuse; +regional cortex	<1%	BRAF V600E	
Johnson et al. (2019) (6)	9	5-34	2M, 7F		3 R temporal 3 L temporal 1 R parietal 1 L parietal 1 3rd ventricle	* All: Oligodendroglioma-like cells with compact nuclei and perinuclear halos * 8: Calcifications	All: Yes	All: Patchy	Diffuse in most cases, focal or patchy in some cases		4 BRAF V600E 1 BRAF fusion	2 FGFR2-KIAA1598 1 FGFR2 rearrangement
Lelotte et al. (2019) (19)	1	33	F	31	R temporal	* Oligodendroglioma-like cells with compact nuclei and perinuclear halos * Astrocytic and pilocytic regions * Patchy perivascular pseudorosettes	Yes	Yes	Strong, diffuse; +regional cortex	<1%	BRAF V600E	
Sumdani et al. (2019) (20)	1	19	M	19	R parietal	* Oligodendroglioma-like cells with compact nuclei and perinuclear halos * Calcifications			Strong, diffuse	<1%	BRAF V600E	
Surrey et al. (2019) (21)	6	7-16	4M, 2F		3 temporal 1 parietal 1 temporo-parietal 1 temporo-occipital	* All: Oligodendroglioma-like cells with compact nuclei and perinuclear halos * All: variable astrocytic features * 2: Rare eosinophilic granular bodies * 4: Calcifications			All: Strong, diffuse		3 BRAF V600E	1 FGFR2-CTNNA3 2 FGFR2-INA

(Continued)

10.3389/fonc.2023.1307591

TABLE 1 Continued

Studies	No. of Cases	Age	Gender	Onset of Epilepsy	Lesion Localization	Histological Features	OLIG2+	GFAP+	CD34+	Ki67	BRAF Mutation	FGFR Fusion Transcript
Benson et al. (2020) (7)	1	44	F		L temporal	* All: Oligodendroglioma-like cells with round-to-ovoid nuclei and perinuclear halos * Calcifications	Strong		Strong, diffuse	<1%	BRAF V600E	
Chen et al. (2020) (22)	3	14-16	2M, 1F	13-14	1 R temporal 1 L temporal 1 R frontal	* All: Oligodendroglioma-like cells * All: Patchy spindled astrocytic features * All: Calcifications	All: Yes		All: Strong, diffuse		1 BRAF V600E	1 FGFR3-TACC3
Bale et al. (2021) (23)	1	15	F	15	L temporal	* Oligodendroglioma-like cells * Patchy perivascular pseudorosettes * Calcifications			Strong, diffuse	<2%		FGFR3-TACC3

limited by the small sample size in this study; larger series are necessary to make meaningful conclusions regarding the implication of the FGFR3-TACC3 fusion on survival in GBM.

In the first description of the subset of GBMs harboring the FGFR3-TACC3 fusion, Singh et al. suggested that the fusion alteration also played a role in increasing chromosomal instability and aneuploidy (26). Soon after, Parker et al. identified a critical loss of a 3'-untranslated region of FGFR3 in the fusion construct that confers resistance to regulation by microRNAs, and demonstrated constitutive activity of the receptor itself that engages downstream MAPK and PI3K signaling (27). Shared histological features of GBMs harboring FGFR3-TACC3 include nuclear monomorphism (similar to what is classically observed in oligodendroglioma), frequent microcalcifications, perivascular pseudorosettes, and CD34 ramified labeling—features also seen in PLNTY (28). Such distinctive similarities between PLNTY and GBM with FGFR3-TACC3 fusions may confound diagnosis and associated prognostic implications; it is conceivable that PLNTY with FGFR3-TACC3 fusion, particularly in adult patients, may act more aggressively, making correct diagnosis and determination of subsequent treatment critical. Indeed, FGFR rearrangements in the setting of CDKN2A/B loss and ATRX loss have been associated with more aggressive behavior in classically lower grade tumors such as pilocytic astrocytoma (31).

The FGFR3-TACC3 fusion has also been studied as a targetable mutation in GBM. In addition to positive data from a handful of preclinical studies (10, 26, 27), at least two pan-FGFR tyrosine kinase inhibitors, Erdafitinib (JNJ-42756493) and Dovitinib (TKI258), have demonstrated safety and some limited but promising clinical efficacy in phase I studies (32, 33). Whether there is a role for these adjuvant treatments in PLNTY remains to be determined.

4.3 Unique characteristics in late presentation of PLNTY: implications for molecular diagnoses and clinical management

This case of PLNTY demonstrates multiple irregularities not previously reported in the literature, with a comprehensive review of previously published cases summarized in Table 1. PLNTY is rare in the adult population, making this a unique case of PLNTY in a 59-year-old patient. Histologically, the areas of intra-tumoral infarct and regions mimicking neovascularization in the setting of an infiltrative-appearing tumor may initially suggest the diagnosis of a HGG or GBM. Moreover, the tumor was found to harbor a TERT promoter mutation, which in the setting of IDH-wildtype diffuse astrocytoma is now thought to be sufficient for a diagnosis of GBM (3, 34). However, given the remarkably low Ki-67 proliferation index, abundant microcalcifications suggestive of a long-standing process, oligodendroglioma-like features, strong and diffuse CD34 positivity, and the presence of an FGFR3-TACC3 fusion, a diagnosis of PLNTY was ultimately chosen in light of the latest diagnostic criteria from the fifth edition of the WHO Classification of Tumors of the Central Nervous System (3, 35).

Additionally, while there were no high confidence matches in DNA methylation array analysis using the latest Heidelberg classifier (v12.5), the tumor matched closest to the methylation class "Low-grade glial/glioneuronal/neuroepithelial tumors" (calibration score 0.46).

While PLNTY is still rare enough that the associated literature and experience are still insufficient to confidently guide clinical management, the available cases do support an indolent course compared to GBM. Clinically, the patient has shown no evidence of recurrence despite lack of adjuvant treatment over a 15-month period, which strongly supports the diagnosis of a lower grade entity. Interestingly, the only other report of PLNTY in a patient over 50 also identified an FGFR3-TACC3 fusion and found a Ki-67 index of 2-3% (8). These similarities with respect to subtle high-grade features raise the possibility of a unique entity of PLNTY in adults that may require a more individualized approach including increased surveillance. Nevertheless, the misclassification of a high-grade tumor can be devastating, and extensive multi-institutional, multi-disciplinary discussion including neuropathology, neuroradiology, neuro-oncology, neurosurgery, and radiation oncology was employed prior to the determination that the tumor in this index case would be followed without adjuvant therapy. The patient and family were counseled on the rarity of this entity, and the possibility of a recurrence necessitating further treatment.

The identification of malignant behavior in FGFR3-altered low-grade tumors is likely multifactorial and may involve identifying additional alterations in DNA damage signaling and telomere maintenance. Interestingly, in our comprehensive review of reported PLNTY cases (Table 1), there was no previous report of a concomitant TERT promoter mutation as observed in our index case. Analysis of the MSK-IMPACT glioma cohort revealed no significant difference survival between FGFR3-altered gliomas with or without the TERT mutation; however, a statistically insignificant trend towards reduced median survival was observed when concurrent alterations in CDKN2A were present (Supplementary Figure 1) (36–38). Furthermore, no significant differences in survival were noted in this cohort with mutations in genes associated with p16-RB1 signaling (Supplementary Figure 2), p14-p53 signaling (Supplementary Figure 3), or telomere maintenance (Supplementary Figure 4). These analyses are limited both by small sample size and the multiple alterations included for each gene considered.

There has been one previous report in a pediatric patient of malignant transformation of a lesion with an FGFR3-TACC3 fusion originally diagnosed as PLNTY based on histological findings (23). Interestingly, despite the recurrent lesion's glioblastoma-like features, the patient responded well to proton-based radiotherapy and temozolomide and remained recurrence-free at 34 months. The potential aggressiveness of PLNTY with FGFR-TACC fusion alterations contrasts the existing literature on PLNTY with BRAF V600E mutations. Although more often seen in adult male patients, BRAF V600E positive PLNTY cases have not demonstrated an increased propensity for recurrence or aggressiveness (39, 40). Furthermore, our literature review (Table 1) generally supports a pathological correlation between BRAF V600E expression and a lower mitotic index (all <1%). Nonetheless, while stability at 15-month follow-up is reassuring, it remains possible that recurrence could refute the original interpretation of the case lesion as PLNTY. Given that this tumor is rarely seen in the adult population and not previously described collectively with FGFR3-TACC3 fusion alteration, TERT promoter mutation, and polysomy 7, the potential for a more aggressive clinical course remains and necessitates close follow-up and counseling.

5 Conclusions

PLNTY is a rare entity that clinically and histologically can mimic HGG. While more commonly seen in the pediatric population, it should be considered in the differential for adult primary tumors. Characteristic genetic alterations may predispose to malignant transformation, in contrast to pediatric cases. Lesions found to have FGFR3-TACC3 fusions with histopathologic features most consistent with HGG clinically may be associated with a worse prognosis when coupled with mutations such as TERT promoter, but further studies are needed to better define potential differences in overall and progression-free survival based on the presence of this fusion with and without concurrent molecular alterations. Close attention to follow-up in low-grade lesions, such as PLNTY, is recommended, especially in adult patients with high-grade molecular characteristics given the potential consequences of withholding adjuvant therapy in the event of a truly higher-grade entity. A larger series of such cases with long-term follow-up and attention to molecular alterations may help elucidate the role and timing of adjuvant treatment.

Data availability statement

The original contributions presented in the study are included in the article/Supplementary Material. Further inquiries can be directed to the corresponding author.

Ethics statement

The studies involving humans were approved by Weill Cornell Institutional Review Board. The studies were conducted in accordance with the local legislation and institutional requirements. The participants provided their written informed consent to participate in this study. Written informed consent was obtained from the individual(s) for the publication of any potentially identifiable images or data included in this article.

Author contributions

DG: Conceptualization, Formal Analysis, Methodology, Supervision, Visualization, Writing – original draft, Writing – review & editing. DL: Data curation, Formal Analysis, Methodology, Writing – original draft, Writing – review & editing. PP: Formal Analysis, Investigation, Resources,

Supervision, Writing – review & editing. BL: Data curation, Formal Analysis, Supervision, Visualization, Writing – review & editing. CS: Data curation, Investigation, Writing – original draft. TB: Conceptualization, Data curation, Formal Analysis, Resources, Writing – review & editing. DP: Conceptualization, Formal Analysis, Investigation, Methodology, Supervision, Writing – review & editing. RJ: Conceptualization, Data curation, Methodology, Project administration, Supervision, Writing – original draft, Writing – review & editing.

Funding

The author(s) declare that no financial support was received for the research, authorship, and/or publication of this article.

Acknowledgments

The authors would like to acknowledge Dr. Michael Schulder (Northwell Health) for his support of the primary authors during the writing and revision process.

Conflict of interest

The authors declare that the research was conducted in the absence of any commercial or financial relationships that could be construed as a potential conflict of interest.

Publisher's note

Supplementary material

The Supplementary Material for this article can be found online at: https://www.frontiersin.org/articles/10.3389/fonc.2023.1307591/full#supplementary-material

References

1. Blumcke I, Aronica E, Urbach H, Alexopoulos A, Gonzalez-Martinez JA. A neuropathology-based approach to epilepsy surgery in brain tumors and proposal for a new terminology use for long-term epilepsy-associated brain tumors. *Acta Neuropathol* (2014) 128:39–54. doi: 10.1007/s00401-014-1288-9

2. Kasper BS, Kasper EM. New classification of epilepsy-related neoplasms: The clinical perspective. *Epilepsy Behav* (2017) 67:91–7. doi: 10.1016/j.yebeh.2016.12.020

3. Board WCoTE. *World Health Organization Classification of Tumours of the Central Nervous System. 5th Edition*. Lyon: International Agency for Research on Cancer (2021).

4. Huse JT, Snuderl M, Jones DT, Brathwaite CD, Altman N, Lavi E, et al. Polymorphous low-grade neuroepithelial tumor of the young (PLNTY): an epileptogenic neoplasm with oligodendroglioma-like components, aberrant CD34 expression, and genetic alterations involving the MAP kinase pathway. *Acta Neuropathol* (2017) 133:417–29. doi: 10.1007/s00401-016-1639-9

5. Huse JT, Rosenblum MK. The Emerging Molecular Foundations of Pediatric Brain Tumors. *J Child Neurol* (2015) 30:1838–50. doi: 10.1177/0883073815579709

6. Johnson DR, Giannini C, Jenkins RB, Kim DK, Kaufmann TJ. Plenty of calcification: imaging characterization of polymorphous low-grade neuroepithelial tumor of the young. *Neuroradiology* (2019) 61:1327–32. doi: 10.1007/s00234-019-02269-y

7. Benson JC, Summerfield D, Carr C, Cogswell P, Messina S, Gompel JV, et al. Polymorphous Low-Grade Neuroepithelial Tumor of the Young as a Partially Calcified Intra-Axial Mass in an Adult. *AJNR Am J Neuroradiol* (2020) 41(4):573–8. doi: 10.3174/ajnr.A6500

8. Riva G, Cima L, Villanova M, Ghimenton C, Sina S, Riccioni L, et al. Low-grade neuroepithelial tumor: Unusual presentation in an adult without history of seizures. *Neuropathology* (2018) 38:557–60. doi: 10.1111/neup.12504

9. Nelson KN, Meyer AN, Wang CG, Donoghue DJ. Oncogenic driver FGFR3-TACC3 is dependent on membrane trafficking and ERK signaling. *Oncotarget* (2018) 9:34306–19. doi: 10.18632/oncotarget.26142

10. Di Stefano AL, Fucci A, Frattini V, Labussiere M, Mokhtari K, Zoppoli P, et al. Detection, Characterization, and Inhibition of FGFR-TACC Fusions in IDH Wild-type Glioma. *Clin Cancer Res* (2015) 21:3307–17. doi: 10.1158/1078-0432.CCR-14-2199

11. Capper D, Jones DTW, Sill M, Hovestadt V, Schrimpf D, Sturm D, et al. DNA methylation-based classification of central nervous system tumours. *Nature* (2018) 555:469–74. doi: 10.1038/nature26000

12. Brat DJ, Aldape K, Colman H, Holland EC, Louis DN, Jenkins RB, et al. cIMPACT-NOW update 3: recommended diagnostic criteria for "Diffuse astrocytic glioma, IDH-wildtype, with molecular features of glioblastoma, WHO grade IV". *Acta Neuropathol* (2018) 136:805–10. doi: 10.1007/s00401-018-1913-0

13. Lin G, Finger E, Gutierrez-Ramos JC. Expression of CD34 in endothelial cells, hematopoietic progenitors and nervous cells in fetal and adult mouse tissues. *Eur J Immunol* (1995) 25:1508–16. doi: 10.1002/eji.1830250606

14. Blumcke I, Aronica E, Becker A, Capper D, Coras R, Honavar M, et al. Low-grade epilepsy-associated neuroepithelial tumours - the 2016 WHO classification. *Nat Rev Neurol* (2016) 12:732–40. doi: 10.1038/nrneurol.2016.173

15. Palmini A, Paglioli E, Silva VD. Developmental tumors and adjacent cortical dysplasia: single or dual pathology? *Epilepsia* (2013) 54 Suppl 9:18–24. doi: 10.1111/epi.12438

16. Vornetti G, Marucci G, Zenesini C, de Biase D, Michelucci R, Tinuper P, et al. Relationship among clinical, pathological and bio-molecular features in low-grade epilepsy-associated neuroepithelial tumors. *J Clin Neurosci* (2017) 44:158–63. doi: 10.1016/j.jocn.2017.06.022

17. Bitar M, Danish SF, Rosenblum MK. A newly diagnosed case of polymorphous low-grade neuroepithelial tumor of the young. *Clin Neuropathol* (2018) 37:178–81. doi: 10.5414/NP301081

18. Gupta VR, Giller C, Kolhe R, Forseen SE, Sharma S. Polymorphous Low-Grade Neuroepithelial Tumor of the Young: A Case Report with Genomic Findings. *World Neurosurg* (2019) 132:347–55. doi: 10.1016/j.wneu.2019.08.221

19. Lelotte J, Duprez T, Raftopoulos C, Michotte A. Polymorphous low-grade neuroepithelial tumor of the young: case report of a newly described histopathological entity. *Acta Neurol Belg* (2019) 120(3):729–32. doi: 10.1007/s13760-019-01241-0

20. Sumdani H, Shahbuddin Z, Harper G, Hamilton L. Case Report of Rarely Described Polymorphous Low-Grade Neuroepithelial Tumor of the Young and Comparison with Oligodendroglioma. *World Neurosurg* (2019) 127:47–51. doi: 10.1016/j.wneu.2019.03.181

21. Surrey LF, Jain P, Zhang B, Straka J, Zhao X, Harding BN, et al. Genomic Analysis of Dysembryoplastic Neuroepithelial Tumor Spectrum Reveals a Diversity of Molecular Alterations Dysregulating the MAPK and PI3K/mTOR Pathways. *J Neuropathol Exp Neurol* (2019) 78:1100–11. doi: 10.1093/jnen/nlz101

22. Chen Y, Tian T, Guo X, Zhang F, Fan M, Jin H, et al. Polymorphous low-grade neuroepithelial tumor of the young: case report and review focus on the radiological features and genetic alterations. *BMC Neurol* (2020) 20:123. doi: 10.1186/s12883-020-01679-3

23. Bale TA, Sait SF, Benhamida J, Ptashkin R, Haque S, Villafania L, et al. Malignant transformation of a polymorphous low grade neuroepithelial tumor of the young (PLNTY). *Acta Neuropathol* (2021) 141:123–5. doi: 10.1007/s00401-020-02245-4

24. Bale TA. FGFR- gene family alterations in low-grade neuroepithelial tumors. *Acta Neuropathol Commun* (2020) 8:21. doi: 10.1186/s40478-020-00898-6

25. Babic I, Mischel PS. Multiple functions of a glioblastoma fusion oncogene. *J Clin Invest* (2013) 123:548–51. doi: 10.1172/JCI67658

26. Singh D, Chan JM, Zoppoli P, Niola F, Sullivan R, Castano A, et al. Transforming fusions of FGFR and TACC genes in human glioblastoma. *Science* (2012) 337:1231–5. doi: 10.1126/science.1220834

27. Parker BC, Annala MJ, Cogdell DE, Granberg KJ, Sun Y, Ji P, et al. The tumorigenic FGFR3-TACC3 gene fusion escapes miR-99a regulation in glioblastoma. *J Clin Invest* (2013) 123:855–65. doi: 10.1172/JCI67144

28. Bielle F, Di Stefano AL, Meyronet D, Picca A, Villa C, Bernier M, et al. Diffuse gliomas with FGFR3-TACC3 fusion have characteristic histopathological and molecular features. *Brain Pathol* (2018) 28:674–83. doi: 10.1111/bpa.12563

29. Granberg KJ, Annala M, Lehtinen B, Kesseli J, Haapasalo J, Ruusuvuori P, et al. Strong FGFR3 staining is a marker for FGFR3 fusions in diffuse gliomas. *Neuro Oncol* (2017) 19:1206–16. doi: 10.1093/neuonc/nox028

30. Stupp R, Mason WP, van den Bent MJ, Weller M, Fisher B, Taphoorn MJ, et al. Radiotherapy plus concomitant and adjuvant temozolomide for glioblastoma. *N Engl J Med* (2005) 352:987–96. doi: 10.1056/NEJMoa043330

31. Reinhardt A, Stichel D, Schrimpf D, Sahm F, Korshunov A, Reuss DE, et al. Anaplastic astrocytoma with piloid features, a novel molecular class of IDH wildtype glioma with recurrent MAPK pathway, CDKN2A/B and ATRX alterations. *Acta Neuropathol* (2018) 136:273–91. doi: 10.1007/s00401-018-1837-8

32. Bahleda R, Italiano A, Hierro C, Mita A, Cervantes A, Chan N, et al. Multicenter Phase I Study of Erdafitinib (JNJ-42756493), Oral Pan-Fibroblast Growth Factor Receptor Inhibitor, in Patients with Advanced or Refractory Solid Tumors. *Clin Cancer Res* (2019) 25:4888–97. doi: 10.1158/1078-0432.CCR-18-3334

33. Schafer N, Gielen GH, Kebir S, Wieland A, Till A, Mack F, et al. Phase I trial of dovitinib (TKI258) in recurrent glioblastoma. *J Cancer Res Clin Oncol* (2016) 142:1581–9. doi: 10.1007/s00432-016-2161-0

34. Diplas BH, He X, Brosnan-Cashman JA, Liu H, Chen LH, Wang Z, et al. The genomic landscape of TERT promoter wildtype-IDH wildtype glioblastoma. *Nat Commun* (2018) 9:2087. doi: 10.1038/s41467-018-04448-6

35. Louis DN, Wesseling P, Aldape K, Brat DJ, Capper D, Cree IA, et al. cIMPACT-NOW update 6: new entity and diagnostic principle recommendations of the cIMPACT-Utrecht meeting on future CNS tumor classification and grading. *Brain Pathol* (2020) 30(4):844–56. doi: 10.1111/bpa.12832

36. Cerami E, Gao J, Dogrusoz U, Gross BE, Sumer SO, Aksoy BA, et al. The cBio cancer genomics portal: an open platform for exploring multidimensional cancer genomics data. *Cancer Discovery* (2012) 2:401–4. doi: 10.1158/2159-8290.CD-12-0095

37. Gao J, Aksoy BA, Dogrusoz U, Dresdner G, Gross B, Sumer SO, et al. Integrative analysis of complex cancer genomics and clinical profiles using the cBioPortal. *Sci Signal* (2013) 6:pl1. doi: 10.1126/scisignal.2004088

38. Jonsson P, Lin AL, Young RJ, DiStefano NM, Hyman DM, Li BT, et al. Genomic Correlates of Disease Progression and Treatment Response in Prospectively Characterized Gliomas. *Clin Cancer Res* (2019) 25:5537–47. doi: 10.1158/1078-0432.CCR-19-0032

39. Baumgartner M, Lang S-S, Tucker A, Madsen P, Storm P, Kennedy B. Systematic review and cumulative analysis of clinical properties of BRAF V600E mutations in PLNTY histological samples. *Res Square* (2023). doi: 10.21203/rs.3.rs-3117717/v1

40. Furuta T, Moritsubo M, Muta H, Shimamoto H, Ohshima K, Sugita Y. Pediatric and elderly polymorphous low-grade neuroepithelial tumor of the young: Typical and unusual case reports and literature review. *Neuropathology* (2023) 43:319–25. doi: 10.1111/neup.12889

frontiers | Frontiers in Neurology

TYPE Case Report
PUBLISHED 23 November 2023
DOI 10.3389/fneur.2023.1270046

OPEN ACCESS

EDITED BY
Cesare Zoia,
San Matteo Hospital Foundation (IRCCS), Italy

REVIEWED BY
Nasser Khaled Yaghi,
Barrow Neurological Institute (BNI), United States
Giorgio Mantovani,
University of Ferrara, Italy

*CORRESPONDENCE
Satoru Miyawaki
✉ smiya-nsu@m.u-tokyo.ac.jp

RECEIVED 31 July 2023
ACCEPTED 18 October 2023
PUBLISHED 23 November 2023

CITATION
Ohara K, Miyawaki S, Nakatomi H, Okano A, Teranishi Y, Shinya Y, Ishigami D, Hongo H, Takayanagi S, Tanaka S, Shinozaki-Ushiku A, Kohsaka S, Kage H, Oda K, Miyagawa K, Aburatani H, Mano H, Tatsuno K and Saito N (2023) Case report and literature review: exploration of molecular therapeutic targets in recurrent malignant meningioma through comprehensive genetic analysis with Todai OncoPanel.
Front. Neurol. 14:1270046.
doi: 10.3389/fneur.2023.1270046

Case report and literature review: exploration of molecular therapeutic targets in recurrent malignant meningioma through comprehensive genetic analysis with Todai OncoPanel

Kenta Ohara[1], Satoru Miyawaki[1]*, Hirofumi Nakatomi[1], Atsushi Okano[1], Yu Teranishi[1], Yuki Shinya[1], Daiichiro Ishigami[1], Hiroki Hongo[1], Shunsaku Takayanagi[1], Shota Tanaka[1], Aya Shinozaki-Ushiku[2], Shinji Kohsaka[3], Hidenori Kage[4], Katsutoshi Oda[5], Kiyoshi Miyagawa[6], Hiroyuki Aburatani[7], Hiroyuki Mano[3], Kenji Tatsuno[7] and Nobuhito Saito[1]

[1]Department of Neurosurgery, Faculty of Medicine, The University of Tokyo, Tokyo, Japan, [2]Department of Pathology, The University of Tokyo Hospital, Tokyo, Japan, [3]Division of Cellular Signaling, National Cancer Center Research Institute, Tokyo, Japan, [4]Department of Next-Generation Precision Medicine Development Laboratory, Graduate School of Medicine, The University of Tokyo, Tokyo, Japan, [5]Division of Integrative Genomics, Graduate School of Medicine, The University of Tokyo, Tokyo, Japan, [6]Laboratory of Molecular Radiology, Center for Disease Biology and Integrative Medicine, Graduate School of Medicine, The University of Tokyo, Tokyo, Japan, [7]Genome Science and Medicine Laboratory, Research Center for Advanced Science and Technology, The University of Tokyo, Tokyo, Japan

Background: Despite accumulating research on the molecular characteristics of meningiomas, no definitive molecularly targeted therapy for these tumors has been established to date. Molecular mechanisms underlying meningioma progression also remain unclear. Comprehensive genetic testing approaches can reveal actionable gene aberrations in meningiomas. However, there is still limited information on whether profiling the molecular status of subsequent recurrent meningiomas could influence the choice of molecular-targeted therapies.

Case presentation: We report a case of meningioma with malignant progression and multiple recurrences. We performed matched tumor pair analysis using the Todai OncoPanel to investigate the possibility of additional standard treatments. The loss of several chromosomal regions, including *NF2* and *CDKN2A*, which is associated with aggressive meningiomas, was considered a significant driver event for malignant progression. Using additional matched tumor pair analysis, mutations in *TRAF7, ARID1A*, and *ERBB3* were identified as subclonal driver events at the time of recurrence. No genetic aberrations were found for which evidence-based targeted therapy was applicable. We also reviewed previous reports of molecular therapies in meningioma to discuss issues with the current molecular testing approach.

Conclusion: Gene panel testing platforms such as the Todai OncoPanel represent a powerful approach to elucidate actionable genetic alterations in various types of tumors, although their use is still limited to the diagnosis and prediction of prognosis in meningiomas. To enable targeted molecular therapy informed by gene-panel testing, further studies including matched tumor pair analyses

are required to understand the molecular characteristics of meningiomas and develop treatments based on genetic abnormalities.

KEYWORDS

malignant meningioma, malignant progression, Todai OncoPanel, comprehensive genomic analysis, actionable gene aberration

1 Introduction

The treatment of malignant meningioma remains challenging due to the absence of alternatives other than maximum surgical removal and radiation therapy (1). With recent advances in next-generation sequencing, several molecular approaches have been developed to understand the molecular characteristics of meningiomas. In addition to the well-known deletion of chromosome 22 and mutation of *NF2* (2–5), other driver gene mutations in *TRAF7*, *KLF4*, *AKT1*, *SMO*, and *POLR2A* have also been identified (6–10). Furthermore, DNA methylation and gene expression profiles have been studied in meningioma (11–14). Several molecularly targeted therapies for meningiomas have been attempted based on alterations identified in specific genes or their associated signaling pathways. Although some therapies are potentially effective (15–20), a definitive treatment has not yet been established. As reports analyzing acquired molecular aberrations with recurrent paired specimens have been limited (21, 22), molecular mechanisms underlying meningioma progression are still unclear.

Fortunately, large-scale genomic sequencing has identified numerous actionable gene aberrations in various tumor types (23–26). We have clinically applied the Todai OncoPanel (TOP) for the detection of cancer-related genes at our institution (26). This panel is characterized by a twin-panel system incorporating DNA and RNA that is effective in detecting fusion transcripts (26–28). However, the clinical utility of these panel tests for central nervous system tumors remains limited (29).

Here, we report a case of refractory malignant meningioma that was evaluated by comprehensive molecular testing to explore the potential indications for new targeted therapies. We focus on whether changes in the molecular profiles of matched recurrent meningiomas could influence the choice of molecular-targeted therapies. To better understand therapeutic approaches in meningiomas, this study reviewed the relevant literature or ongoing clinical trials based on potential therapeutic targets. We also discuss its usefulness and future issues associated with clinical panel sequencing in meningioma treatment.

2 Case description

A 55-year-old man had undergone initial tumor resection for a parasagittal meningioma, defined as World Health Organization (WHO) grade 1, at another hospital (Figure 1A). He had no significant medical history or family history of meningioma. After gamma knife radiosurgery for recurrence at the age of 61 years, a second resection had been performed at 65 years of age due to progressive tumor growth with histological transformation to a WHO grade 2 atypical meningioma (Figure 1B). At 68 years of age, he had been treated again with stereotactic radiosurgery for local recurrence. Due to tumor regrowth, he was referred to our hospital for a third surgery at 71 years of age (Figure 1C). On preoperative physical examination, he showed mild paralysis of the right lower limb. Manual muscle testing (MMT) of the right lower limb showed grade 4. His postoperative course was uneventful. The pathological specimen of the tumor indicated a diagnosis of malignant progression to anaplastic meningioma, WHO grade 3, with overt anaplasia and a high Ki-67 index (Figures 1D,E). Postoperative adjuvant radiation therapy was administered at a dose of 54 Gy. Two years later, a fourth surgical resection was required with progressive gait disturbance, and the patient was again diagnosed with an anaplastic meningioma (Figures 1F–H). After the surgery, his paralysis of the right lower limb worsened to MMT grade 3. With rehabilitation, his paralysis improved MMT grade4. He was able to walk with a cane and lead a largely independent life. Another recurrent lesion progressed toward the eloquent motor area at the posterior aspect of the tumor removal cavity (Figure 1I); however, surgical resection of the lesion was associated with a high risk of postoperative paralysis, and additional radiotherapy was ineffective. Considering that standard therapies were not viable, the patient wanted to explore the possibility of targeted molecular therapy. After thoroughly explaining that discovering a new treatment for meningioma with our panel analysis has yet to be established, he requested our genetic testing. Therefore, we performed comprehensive panel testing to elucidate whether this refractory meningioma possesses actionable gene aberrations suitable for targeted molecular therapies.

Todai OncoPanel analysis

We conducted comprehensive panel sequencing using TOP after obtaining the appropriate informed consent from the patient. The study was performed in accordance with the principles of the Declaration of Helsinki and was approved by the ethics committee of the University of Tokyo. The method of analysis has been reported previously (26). Briefly, this unique custom-made panel includes DNA and RNA components. The TOP DNA panel targets 464 genes to detect single-nucleotide variants (SNVs), small insertions/deletions, and copy number variations (CNVs). The TOP RNA panel detects 463 fusion genes using the junction capture method. In addition, various probes detect single nucleotide polymorphisms. By comparing tumor and normal reads, chromosomal gains and losses are visualized as a chromosomal copy number graph (Supplementary Tables 1, 2). The

Abbreviations: CNV, Copy number variation; SNV, Single nucleotide variant; TOP, Todai OncoPanel; VAF, Variant allele frequency; WHO, World Health Organization.

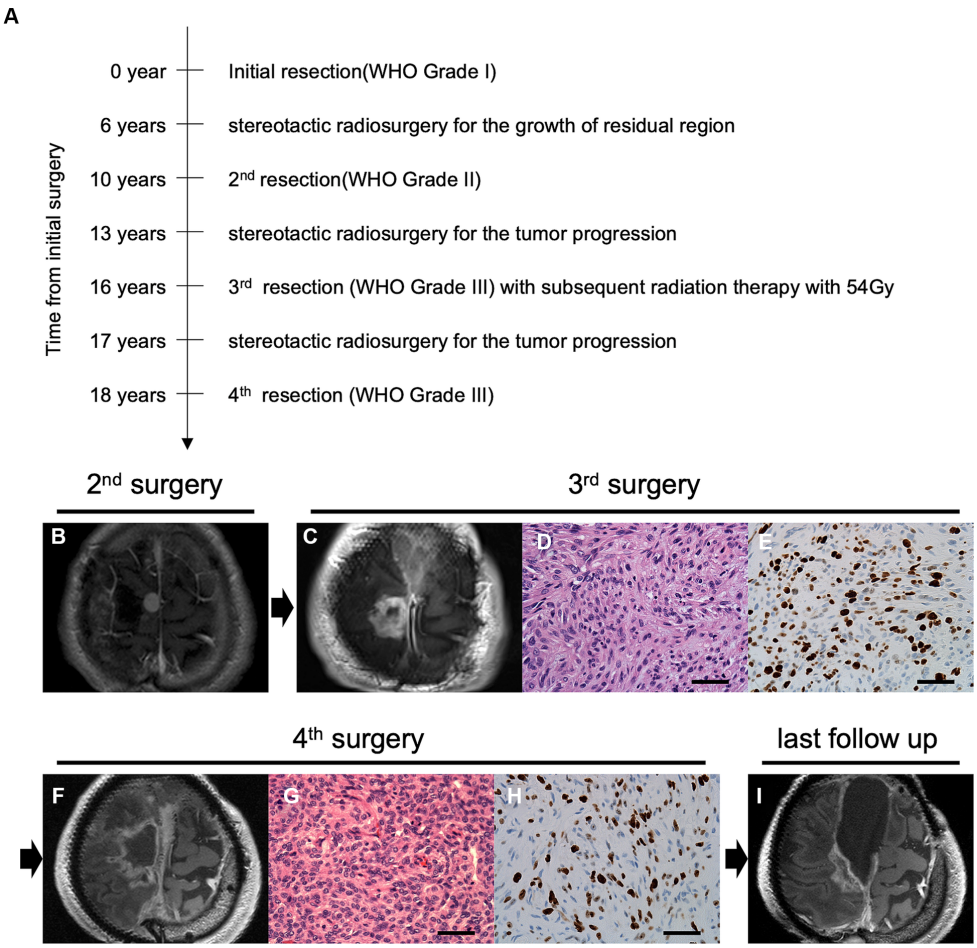

FIGURE 1
Time course and clinical findings of the progressive meningioma. **(A)** The diagram shows the time course of treatment and tumor progression. Preoperative magnetic resonance imaging (MRI) using gadolinium-enhanced T1 imaging (Gd-T1WI) of the parasagittal sinus meningioma at the second **(B)** and third **(C)** surgeries. Pathological features of the tumor at the third surgery indicate overt anaplasia by malignant progression with hematoxylin and eosin (H&E) staining **(D)** and high mitotic features in Ki-67 staining **(E)** under ×400 magnification (scale bar = 50 μm). Preoperative Gd-T1WI before the fourth tumor removal **(F)**. H&E staining **(G)** and Ki67 staining **(H)** at the fourth surgery (original magnification, ×400; scale bar = 50 μm). Postoperative follow-up imaging using Gd-T1WI shows tumor progression in the posterior cavity **(I)**.

tumor resected in the fourth surgery (Tumor S4) was mainly used to detect actionable gene aberrations, whereas the tumor resected in the third surgery (Tumor S3) was used for comparisons with Tumor S4. The detected genetic and transcriptional alterations were reviewed and classified according to the level of evidence and potential treatments by an expert panel consisting of physicians, pathologists, genetic counselors, molecular biologists, and cancer genome researchers.

2.2 Genetic findings

Both tumors were sequenced at a high depth in the TOP DNA panel (mean depth: 1196.4× for Tumor S3 and 1390.5× for Tumor S4). No significant difference was found in tumor purity (53.0% for Tumor S3 and 55.0% for Tumor S4, respectively; data not shown). Also, tumor cell compositions were similar in both histopathological images. We identified five non-synonymous mutations and one splice-site mutation in Tumor S4, with a detection threshold of variant allele frequency (VAF) > 5% (Table 1). The *TRAF7* mutation c.1168G > A (p.Gly390Arg), a frequent mutational hotspot in meningiomas, was detected. *ARID1A*, a component of the SWI/SNF complex that acts as a driver in high-grade meningiomas, was also mutated. We also found multiple chromosomal copy number losses, including 1p/22q co-deletion (Figure 2A). A 1q gain, which is associated with poor outcomes in meningiomas, was also observed. In addition, we identified various genetic CNVs, including *CDKN2A* deletions (Supplementary Table 3). TOP RNA testing revealed no fusion transcripts. We could not identify actionable gene aberrations that could be potential targets of approved drugs or clinical trials in expert panel reviews.

Next, we compared the genomic abnormalities of Tumor S3 with Tumor S4 to explore the differences that emerged during tumor progression. Tumor S4 showed six non-synonymous mutations with a VAF > 5%, whereas these mutations were detected with VAF less than 5% in Tumor S3. One mutation that was not detected in Tumor S4 was detected in S3 with VAF > 5% (Table 1). Genetic CNVs, including those in *CDKN2A*, were partially shared throughout tumor progression without notable changes (Supplementary Table 3).

10.3389/fneur.2023.1270046

TABLE 1 Tumor genetic variants identified using Todai OncoPanel.

Gene	CytoBand	Variant	Amino acid	Mutation type	VAF	
					Tumor S4	Tumor S3
TRAF7	16p13.3	c.1168G > A	p.G390R	Missense	28.8%	1.3%
ARID1A	1p36.11	c.1048 T > G	p.S350A	Missense	5.6%	3.3%
ERBB3	12q13.2	c.2938-38G > T	-	Splice-site	22.8%	1.9%
ERBB3	12q13.2	c.2954G > A	p.G985E	Missense	24.6%	1.5%
ERBB3	12q13.2	c.3010G > A	p.E1004K	Missense	26.2%	1.6%
ERBB3	12q13.2	c.3016G > A	p.E1006K	Missense	27.2%	1.8%
ERCC2	19q13.32	c.1034del	p.R345Lfs*14	Frameshift	Undetected	9.2%

VAF, Variant allele frequency.

Although the profile of the chromosomal CNVs of Tumor S3 was similar to that of Tumor S4, some chromosomal changes, such as the gain of 1q, 6p, and 14q and the loss of 4q and 10p, were additionally observed in Tumor S4 (Figure 2B), suggesting that Tumor S4 exhibits a pattern of branched clonal evolution from Tumor S3 (Figure 2C). Unfortunately, as no suitable molecularly targeted therapeutic agent exists for the patient's course, conservative follow-up was continued despite the continuously growing tumor.

3 Literature review of molecular targeted therapies for meningiomas

A search strategy was conducted according to the Preferred Reporting Items for Systematic Reviews and Meta-Analyses (PRISMA) guidelines (30). We searched using the term:("meningioma"[MeSH] AND "drug therapy") to identify relevant articles in MEDLINE[1] up to September 2023. We included articles that were original prospective phase II trials of molecular targeted therapies for meningiomas to demonstrate options for potentially applicable treatment in the future. To avoid missing relevant research efforts, we also hand-searched other articles on Phase II trials. Next, we searched for ongoing clinical trials for meningiomas on ClinicalTrials.gov to September 2023. We included ongoing phase II or III trials that focused only on meningioma.

4 Discussion

Here, we report a case of progressive meningioma that was evaluated by molecular profiling. Contrary to our expectations, no actionable genetic aberrations were detected. However, we obtained some implicative results via a genetic analysis of paired recurrent samples. In this progressive case, we identified the *TRAF7* mutation, which is typically found in benign meningiomas. Although this mutation was detected in both S3 and S4, the VAF of S3 was markedly low without differences in tumor purity. Tumor heterogeneity may have influenced the results, but this mutation may have been acquired as a subclonal driver event. *TRAF7* mutations are often associated with mutations in other genes, such as *AKT1*, *KLF4*, and *PIK3CA* (8, 9), and rarely with *NF2* alterations, suggesting that *TRAF7* mutation may not represent the earliest driver event, as in this case. Regarding the significance of the "add-on" *TRAF7* mutations, the accumulation of matched-pair analysis using recurrent specimens may help confirm this hypothesis.

Considering that the TOP test targeted sufficiently large genetic regions, we also identified *NF2* inactivation and chromosomal abnormalities, such as the loss of 1p, 6q, 10p, and 18q and deletion of *CDKN2A*, which indicated tumor aggressiveness in the present case (21, 31, 32). Interestingly, the 1q gain, which is harbored in the most aggressive types of meningioma, was acquired in Tumor S4 (33). High-grade meningiomas frequently exhibit *NF2* alterations (6, 8, 9). Furthermore, the number of genetic and chromosomal CNVs indicates the risk of recurrence and aggressiveness in malignant meningiomas and even a subset of benign WHO grade 1 tumors (22, 34). Although a variety of driver genetic events can be detected in a single genetic panel test in meningiomas (29, 35, 36), CNV analysis is also required to predict meningioma aggressiveness. Some reports have shown the usefulness of CNV analysis using DNA panel tests for meningiomas (29, 36). The behavior and recurrence risk of meningiomas are generally difficult to predict based on clinical features (e.g., the Simpson grading scale and WHO grading system) (37). Therefore, TOP analysis offers a significant advantage over other diagnostic tools by revealing the genetic profiles of meningiomas and identifying tumors associated with poor prognosis.

However, panel testing shows limitations in its therapeutic application. In multiple types of tumors, targeted gene panel testing cost-effectively clarifies the genetic background and identifies targetable gene aberrations. However, an unignorable discrepancy exists between the level of identified actionable gene aberrations and that of patients receiving accordingly targeted therapies. Actionable gene aberrations of various tumors are identified in 32.2%–59.4% of patients, whereas the level of patients who receive molecularly targeted therapy remains at approximately 10% (23–26). This discrepancy may be associated with the scarcity of established molecularly targeted therapies in comparison with the number of detectable genetic abnormalities. Even if a potentially effective therapeutic agent exists, the treatment cannot be administered without prior clinical validation. The presence of actionable gene mutations varies depending on the tumor type. Genomic panel testing is considered applicable for tumors for which molecularly targeted drugs are already available, whereas the applicability of molecularly targeted therapy is still limited in other tumors, including intracranial tumors.

1 www.pubmed.gov

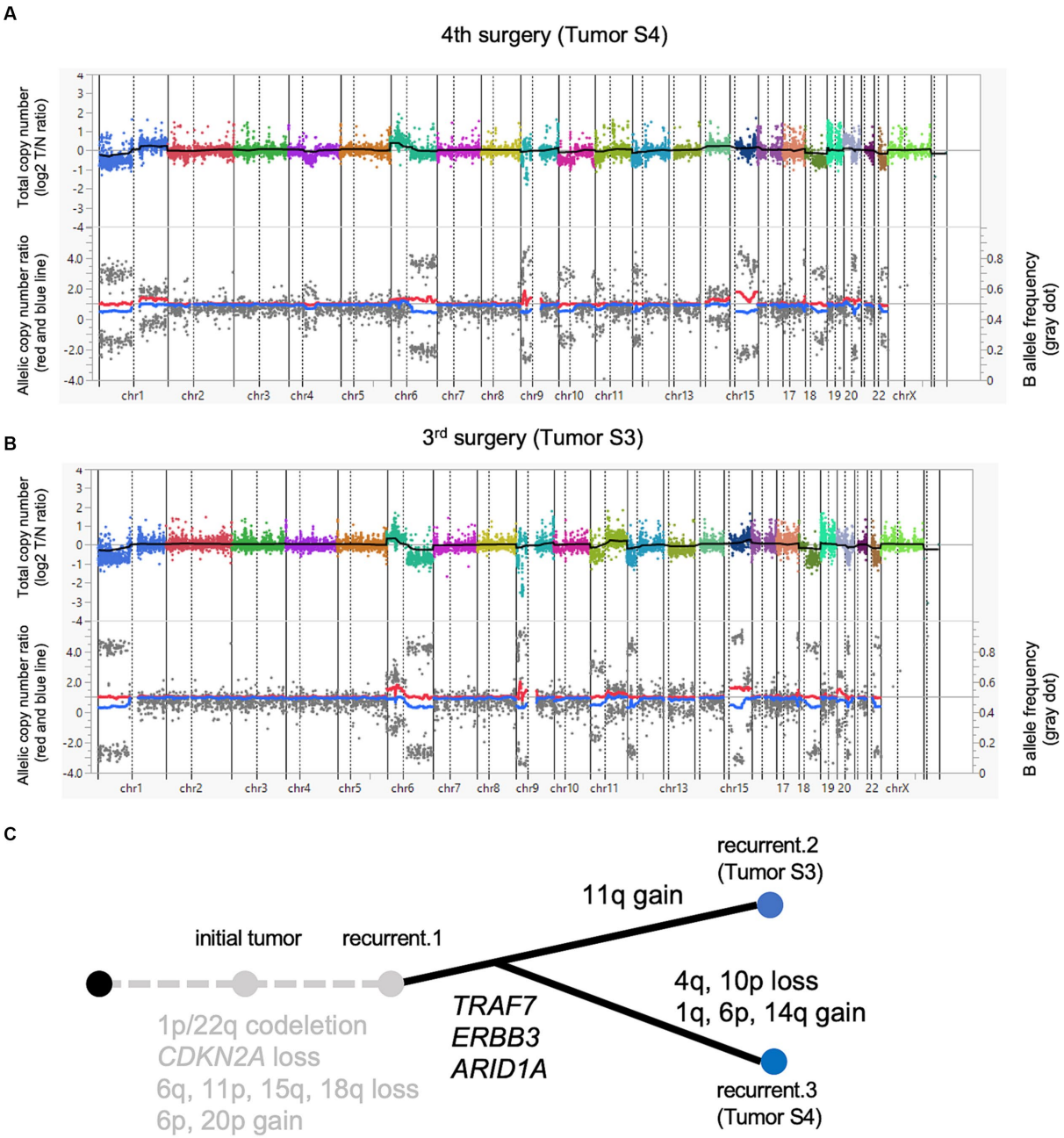

FIGURE 2
A paired analysis with Todai OncoPanel. Chromosomal copy number variations in anaplastic meningioma. The upper panel shows the total copy number, and the lower panel shows the allelic copy number ratio with B allele frequency at the fourth **(A)** and third surgeries **(B)**. Implications for driver events along with tumor progression **(C)**.

For meningiomas, which lack established molecular therapies, gene panel testing for therapeutic purposes remains challenging without the development of novel therapeutic agents. To our knowledge, several prospective studies have demonstrated the effects of molecular targeted therapies for meningiomas (Table 2). In the previous study, targeted agents such as anti-angiogenic inhibitors, mTOR inhibitors, and EGFR inhibitors were investigated based on the activation of intracellular signaling pathways in meningiomas (15, 17–20, 38, 39, 42). Also, other clinical trials based on potential targets in meningiomas are in progress. As major genetic drivers specific to meningiomas, *NF2*, *AKT1*, and *SMO* mutations could be targeted by FAK, AKT1, and SMO inhibitors, respectively (43, 44). As an immunotherapy, PD-1 inhibitor showed promising efficacy for immunosuppressive tumor microenvironment of high-grade meningiomas (40, 41). Previous large-scale studies have suggested the therapeutic potential of CDK inhibitors and histone deacetylase inhibitors in molecularly aggressive types of meningiomas (33, 45).

The prior studies suggest that those targeted therapies were expected to stabilize meningioma growth. However, as the results of these inhibitors are in Phase II trials, future investigations are still needed. Further, from a clinical perspective, the feasibility of these therapies is still limited because molecular testing for meningiomas is not part of routine practice. Even though well-recognized driver genetic events are not detected in some meningiomas (6–9), additional

TABLE 2 Review of molecular targeted therapy for meningiomas.

Previous studies of molecular targeted therapy for meningiomas								
References	*n*	WHO grade (*n*)	Intervention	Drug class	Molecular target	Phase	Radiographic response	6 M-PFS
Wen et al. (15)	23	1 (13) 2 (5) 3 (5)	Imatinib	PDGFR inhibitor	PDGFR	2	SD: 47.4%	29.40%
Norden et al. (19)	25	1 (8) 2 (9) 3 (8)	Gefitinib/erlotinib	EGFR inhibitor	EGFR	2	SD: 32%	28%
Reardon et al. (38)	21	1 (8) 2 (9) 3 (4)	Imatinib Hydroxyurea	PDGFR inhibitor	PDGFR	2	SD: 66.7%	61.90%
Raizer et al. (18)	25	1 (2) 2 (14) 3 (8)	Vatalanib	VEGFR inhibitor	VEGFR	2	SD: 68.2%	54.40%
Kaley et al. (17)	36	1 (4) 2 (30) 3 (6)	Sunitinib	Tyrosine kinase inhibitor	VEGFR, PDGFR, KIT	2	CR/PR: 5.6% SD: 69.4%	42%
Shih et al. (39)	17	1 (4) 2 (7) 3 (5)	Everolimus Bevacizumab	mTOR inhibitor VEGF inhibitor	mTOR VEGF	2	SD: 88%	69%
Graillon et al. (20)	20	1 (2) 2 (10) 3 (8)	Everolimus Octreotide	mTOR inhibitor	mTOR	2	N/A	55%
Brastianos et al. (40)	25	2 (22) 3 (3)	Pembrolizumab	PD-1 inhibitor	PD-1	2	SD: 72%	48%
Bi et al. (41)	25	2 (18) 3 (7)	Nivolumab	PD-1 inhibitor	PD-1	2	PR: 4% SD: 60%	42.40%
Kumthekar et al. (42)	42	1 (10) 2 (21) 3 (11)	Bevacizumab	VEGF binding monoclonal antibody	VEGF	2	PR:2% SD:86%	Grade1:90% Grade2/3:66%
Brastianos et al. (43)	36	1 (12) 2 (18) 3 (6)	GSK2256098	FAK inhibitor	*NF2*	2	PR: 2.8% SD: 66.7%	50%

Ongoing clinical trials of molecular targeted therapy for meningiomas							
NCT number	*n*	WHO grade(*n*)	Intervention	Drug class	Molecular target	Phase	Primary outcome
3071874	25	2, 3	Vistusertib	mTOR inhibitor	mTOR	2	PFS
5425004	24	2, 3	Cabozantinib	VEGF inhibitor	VEGF	2	PFS
5130866	89	-	AR-42 (OSU-HDAC42)	Histone deacetylase inhibitor	*NF2*	2, 3	PFS
2523014	124	-	Vismodeg	SMO inhibitor	*SMO*	2	PFS
			Capivasertib	AKT inhibitor	*AKT1*		
			Abemaciclib	CDK inhibitor	*CDKN2A* loss, *CDK* gain		

SD, stable disease; CR, complete response; PR, partial response; 6 M-PFS, 6-month progression-free survival; PFS, progression-free survival.

hidden molecular targets could be detected by further analysis of the increased number of these "apparently driver-negative" meningiomas.

Currently, genomic surveys with customized gene panel testing mainly contribute to personalized medicine by elucidating the genomic profile and allowing clinicians to select high-risk cases for closer follow-up. The number of analyzed cases needs to be increased to demonstrate the usefulness of TOP testing for meningiomas as a useful tool in future molecular therapy. At the same time, further molecular understanding of meningiomas and the development of therapeutic agents are required. Meningiomas show complicated diversity in their molecular landscapes, which can be identified by the integrated analysis of DNA methylation or gene expression profiles (11–14, 33, 45, 46). The correlation between molecular characteristics and specific genomic events requires elucidation. Combined panel testing such as TOP may yield comprehensive genetic profiles, including gene expression profiles, in the future. Also, matched tumor pair analysis may provide more detailed knowledge of molecular profiles.

In conclusion, gene panel analysis, including TOP, effectively elucidates various genetic alterations in meningiomas. However, panel testing is limited to diagnostic and prognostic prediction. The establishment of definitive treatments for meningiomas is essential for molecularly targeted therapy informed by genetic panel testing.

Data availability statement

The datasets presented in this article are not readily available because of ethical and privacy restrictions. Requests to access the datasets should be directed to the corresponding author.

Ethics statement

The studies involving humans were approved by the Institutional Review Board of the University of Tokyo. The studies were conducted in accordance with the local legislation and institutional requirements. The participants provided their written informed consent to participate in this study. Written informed consent was obtained from the individual(s) for the publication of any potentially identifiable images or data included in this article.

Author contributions

KOh: Data curation, Writing – original draft. SM: Writing – review & editing, Supervision. HN: Data curation, Writing – review & editing. AO: Data curation, Writing – review & editing. YT: Data curation, Writing – review & editing. YS: Data curation, Writing – review & editing. DI: Data curation, Writing – review & editing. HH: Data curation, Writing – review & editing. ShuT: Data curation, Formal analysis, Writing – review & editing. ShoT: Data curation, Formal analysis, Writing – review & editing. AS-U: Data curation, Formal analysis, Validation, Writing – review & editing. SK: Formal analysis, Writing – review & editing. HK: Formal analysis, Writing – review & editing. KOd: Formal analysis, Writing – review & editing. KM: Formal analysis, Writing – review & editing. HA: Formal analysis, Writing – review & editing. HM: Formal analysis, Writing – review & editing. KT: Formal analysis, Visualization, Writing – review & editing. NS: Project administration, Supervision, Writing – review & editing.

Funding

The author(s) declare financial support was received for the research, authorship, and/or publication of this article. We performed sequencing analysis and interpretation of the data under a grant from the Program for an Integrated Database of Clinical and Genomic Information (JP19kk0205016) from the Japan Agency for Medical Research and Development and a grant from Sysmex Corporation.

Acknowledgments

The authors gratefully thank the patient and his wife for permitting access to clinical and genetic data.

Conflict of interest

SK, HA, HK, and HM received research grants from Konica-Minolta outside of this study.

This study received funding from a grant from Sysmex Corporation. The funder had the following involvement with the study: Sequencing analysis and interpretation of the data. All authors declare no other competing interests.

Publisher's note

Supplementary material

The Supplementary material for this article can be found online at: https://www.frontiersin.org/articles/10.3389/fneur.2023.1270046/full#supplementary-material

References

1. Rogers L, Barani I, Chamberlain M, Kaley TJ, McDermott M, Raizer J, et al. Meningiomas: Knowledge Base, treatment outcomes, and uncertainties. A Rano Review. *J Neurosurg*. (2015) 122:4–23. doi: 10.3171/2014.7.JNS131644

2. Zankl H, Zang KD. Cytological and Cytogenetical Studies on Brain Tumors. 4. Identification of the missing G chromosome in human Meningiomas as no. 22 by fluorescence technique. *Humangenetik*. (1972) 14:167–9. doi: 10.1007/bf00273305

3. Ruttledge MH, Sarrazin J, Rangaratnam S, Phelan CM, Twist E, Merel P, et al. Evidence for the complete inactivation of the Nf2 gene in the majority of sporadic Meningiomas. *Nat Genet*. (1994) 6:180–4. doi: 10.1038/ng0294-180

4. De Vitis LR, Tedde A, Vitelli F, Ammannati F, Mennonna P, Bigozzi U, et al. Screening for mutations in the Neurofibromatosis type 2 (Nf2) gene in sporadic Meningiomas. *Hum Genet*. (1996) 97:632–7. doi: 10.1007/bf02281874

5. Teranishi Y, Okano A, Miyawaki S, Ohara K, Ishigami D, Hongo H, et al. Clinical significance of Nf2 alteration in grade I Meningiomas revisited; prognostic impact integrated with extent of resection, tumour location, and Ki-67 index. *Acta Neuropathol Commun*. (2022) 10:76. doi: 10.1186/s40478-022-01377-w

6. Abedalthagafi M, Bi WL, Aizer AA, Merrill PH, Brewster R, Agarwalla PK, et al. Oncogenic Pi3k mutations are as common as Akt1 and Smo mutations in meningioma. *Neuro Oncol*. (2016) 18:649–55. doi: 10.1093/neuonc/nov316

7. Brastianos PK, Horowitz PM, Santagata S, Jones RT, McKenna A, Getz G, et al. Genomic sequencing of Meningiomas identifies oncogenic Smo and Akt1 mutations. *Nat Genet*. (2013) 45:285–9. doi: 10.1038/ng.2526

8. Clark VE, Erson-Omay EZ, Serin A, Yin J, Cotney J, Ozduman K, et al. Genomic analysis of non-Nf2 Meningiomas reveals mutations in Traf7, Klf4, Akt1, and Smo. *Science*. (2013) 339:1077–80. doi: 10.1126/science.1233009

9. Clark VE, Harmanci AS, Bai H, Youngblood MW, Lee TI, Baranoski JF, et al. Recurrent somatic mutations in Polr2a define a distinct subset of Meningiomas. *Nat Genet*. (2016) 48:1253–9. doi: 10.1038/ng.3651

10. Okano A, Miyawaki S, Hongo H, Dofuku S, Teranishi Y, Mitsui J, et al. Associations of pathological diagnosis and genetic abnormalities in Meningiomas with the embryological origins of the meninges. *Sci Rep*. (2021) 11:6987. doi: 10.1038/s41598-021-86298-9

11. Patel AJ, Wan YW, Al-Ouran R, Revelli JP, Cardenas MF, Oneissi M, et al. Molecular profiling predicts meningioma recurrence and reveals loss of dream complex repression in aggressive tumors. *Proc Natl Acad Sci U S A*. (2019) 116:21715–26. doi: 10.1073/pnas.1912858116

12. Sahm F, Schrimpf D, Stichel D, Jones DTW, Hielscher T, Schefzyk S, et al. DNA methylation-based classification and grading system for meningioma: A multicentre, retrospective analysis. *Lancet Oncol*. (2017) 18:682–94. doi: 10.1016/s1470-2045(17)30155-9

13. Nassiri F, Mamatjan Y, Suppiah S, Badhiwala JH, Mansouri S, Karimi S, et al. DNA methylation profiling to predict recurrence risk in meningioma: development and validation of a nomogram to optimize clinical management. *Neuro Oncol*. (2019) 21:901–10. doi: 10.1093/neuonc/noz061

14. Prager BC, Vasudevan HN, Dixit D, Bernatchez JA, Wu Q, Wallace LC, et al. The meningioma enhancer landscape delineates novel subgroups and drives Druggable dependencies. *Cancer Discov*. (2020) 10:1722–41. doi: 10.1158/2159-8290.CD-20-0160

15. Wen PY, Yung WK, Lamborn KR, Norden AD, Cloughesy TF, Abrey LE, et al. Phase ii study of Imatinib Mesylate for recurrent Meningiomas (north American brain tumor consortium study 01-08). *Neuro Oncol*. (2009) 11:853–60. doi: 10.1215/15228517-2009-010

16. Nunes FP, Merker VL, Jennings D, Caruso PA, di Tomaso E, Muzikansky A, et al. Bevacizumab treatment for Meningiomas in Nf2: A retrospective analysis of 15 patients. *PLoS One*. (2013) 8:e59941. doi: 10.1371/journal.pone.0059941

17. Kaley TJ, Wen P, Schiff D, Ligon K, Haidar S, Karimi S, et al. Phase ii trial of Sunitinib for recurrent and progressive atypical and anaplastic meningioma. *Neuro Oncol*. (2015) 17:116–21. doi: 10.1093/neuonc/nou148

18. Raizer JJ, Grimm SA, Rademaker A, Chandler JP, Muro K, Helenowski I, et al. A phase ii trial of Ptk787/Zk 222584 in recurrent or progressive radiation and surgery refractory Meningiomas. *J Neuro Oncol*. (2014) 117:93–101. doi: 10.1007/s11060-014-1358-9

19. Norden AD, Raizer JJ, Abrey LE, Lamborn KR, Lassman AB, Chang SM, et al. Phase ii trials of Erlotinib or Gefitinib in patients with recurrent meningioma. *J Neuro Oncol*. (2010) 96:211–7. doi: 10.1007/s11060-009-9948-7

20. Graillon T, Sanson M, Campello C, Idbaih A, Peyre M, Peyriere H, et al. Everolimus and octreotide for patients with recurrent meningioma: results from the phase ii Cevorem trial. *Clin Cancer Res*. (2020) 26:552–7. doi: 10.1158/1078-0432.CCR-19-2109

21. Goutagny S, Yang HW, Zucman-Rossi J, Chan J, Dreyfuss JM, Park PJ, et al. Genomic profiling reveals alternative genetic pathways of meningioma malignant progression dependent on the underlying Nf2 status. *Clin Cancer Res*. (2010) 16:4155–64. doi: 10.1158/1078-0432.CCR-10-0891

22. Bi WL, Greenwald NF, Abedalthagafi M, Wala J, Gibson WJ, Agarwalla PK, et al. Erratum: genomic landscape of high-grade Meningiomas. *NPJ Genom Med*. (2017) 2:26. doi: 10.1038/s41525-017-0023-6

23. Sunami K, Ichikawa H, Kubo T, Kato M, Fujiwara Y, Shimomura A, et al. Feasibility and utility of a panel testing for 114 Cancer-associated genes in a clinical setting: A hospital-based study. *Cancer Sci*. (2019) 110:1480–90. doi: 10.1111/cas.13969

24. Zehir A, Benayed R, Shah RH, Syed A, Middha S, Kim HR, et al. Erratum: mutational landscape of metastatic Cancer revealed from prospective clinical sequencing of 10,000 patients. *Nat Med*. (2017) 23:1004. doi: 10.1038/nm0817-1004c

25. Meric-Bernstam F, Brusco L, Shaw K, Horombe C, Kopetz S, Davies MA, et al. Feasibility of large-scale genomic testing to facilitate enrollment onto Genomically matched clinical trials. *J Clin Oncol*. (2015) 33:2753–62. doi: 10.1200/JCO.2014.60.4165

26. Kohsaka S, Tatsuno K, Ueno T, Nagano M, Shinozaki-Ushiku A, Ushiku T, et al. Comprehensive assay for the molecular profiling of Cancer by target enrichment from formalin-fixed paraffin-embedded specimens. *Cancer Sci*. (2019) 110:1464–79. doi: 10.1111/cas.13968

27. Ando M, Kobayashi H, Shinozaki-Ushiku A, Chikuda H, Matsubayashi Y, Yoshida M, et al. Spinal solitary fibrous tumor of the neck: next-generation sequencing-based analysis of genomic aberrations. *Auris Nasus Larynx*. (2020) 47:1058–63. doi: 10.1016/j.anl.2019.12.001

28. Shinozaki-Ushiku A, Kohsaka S, Kage H, Oda K, Miyagawa K, Nakajima J, et al. Genomic profiling of multiple primary cancers including synchronous lung adenocarcinoma and bilateral malignant mesotheliomas: identification of a novel Bap1 germline variant. *Pathol Int*. (2020) 70:775–80. doi: 10.1111/pin.12977

29. Lorenz J, Rothhammer-Hampl T, Zoubaa S, Bumes E, Pukrop T, Kolbl O, et al. A comprehensive DNA panel next generation sequencing approach supporting diagnostics and therapy prediction in Neurooncology. *Acta Neuropathol Commun*. (2020) 8:124. doi: 10.1186/s40478-020-01000-w

30. Page MJ, McKenzie JE, Bossuyt PM, Boutron I, Hoffmann TC, Mulrow CD, et al. The Prisma 2020 statement: an updated guideline for reporting systematic reviews. *Syst Rev*. (2021) 10:89. doi: 10.1186/s13643-021-01626-4

31. Weber RG, Bostrom J, Wolter M, Baudis M, Collins VP, Reifenberger G, et al. Analysis of genomic alterations in benign, atypical, and anaplastic Meningiomas: toward a genetic model of meningioma progression. *Proc Natl Acad Sci U S A*. (1997) 94:14719–24. doi: 10.1073/pnas.94.26.14719

32. Guyot A, Duchesne M, Robert S, Lia AS, Derouault P, Scaon E, et al. Analysis of Cdkn2a gene alterations in recurrent and non-recurrent meningioma. *J Neuro Oncol*. (2019) 145:449–59. doi: 10.1007/s11060-019-03333-6

33. Nassiri F, Liu J, Patil V, Mamatjan Y, Wang JZ, Hugh-White R, et al. A clinically applicable integrative molecular classification of Meningiomas. *Nature*. (2021) 597:119–25. doi: 10.1038/s41586-021-03850-3

34. Harmanci AS, Youngblood MW, Clark VE, Coskun S, Henegariu O, Duran D, et al. Integrated genomic analyses of De novo pathways underlying atypical Meningiomas. *Nat Commun*. (2017) 8:14433. doi: 10.1038/ncomms14433

35. Pepe F, Pisapia P, Basso D, de Caro ML, Conticelli F, Malapelle U, et al. Next generation sequencing identifies novel potential actionable mutations for grade I meningioma treatment. *Histol Histopathol*. (2020) 35:741–9. doi: 10.14670/HH-18-195

36. Williams EA, Santagata S, Wakimoto H, Shankar GM, Barker FG 2nd, Sharaf R, et al. Distinct genomic subclasses of high-grade/progressive Meningiomas: Nf2-associated, Nf2-exclusive, and Nf2-agnostic. *Acta Neuropathol Commun*. (2020) 8:171. doi: 10.1186/s40478-020-01040-2

37. Simpson D. The recurrence of intracranial Meningiomas after surgical treatment. *J Neurol Neurosurg Psychiatry*. (1957) 20:22–39. doi: 10.1136/jnnp.20.1.22

38. Reardon DA, Norden AD, Desjardins A, Vredenburgh JJ, Herndon JE 2nd, Coan A, et al. Phase ii study of Gleevec(R) plus hydroxyurea (Hu) in adults with progressive or recurrent meningioma. *J Neuro Oncol*. (2012) 106:409–15. doi: 10.1007/s11060-011-0687-1

39. Shih KC, Chowdhary S, Rosenblatt P, Weir AB 3rd, Shepard GC, Williams JT, et al. A phase ii trial of bevacizumab and Everolimus as treatment for patients with refractory, progressive intracranial meningioma. *J Neuro Oncol*. (2016) 129:281–8. doi: 10.1007/s11060-016-2172-3

40. Brastianos PK, Kim AE, Giobbie-Hurder A, Lee EQ, Wang N, Eichler AF, et al. Phase 2 study of Pembrolizumab in patients with recurrent and residual high-grade Meningiomas. *Nat Commun*. (2022) 13:1325. doi: 10.1038/s41467-022-29052-7

41. Bi WL, Nayak L, Meredith DM, Driver J, Du Z, Hoffman S, et al. Activity of Pd-1 blockade with Nivolumab among patients with recurrent atypical/anaplastic meningioma: phase ii trial results. *Neuro Oncol*. (2022) 24:101–13. doi: 10.1093/neuonc/noab118

42. Kumthekar P, Grimm SA, Aleman RT, Chamberlain MC, Schiff D, Wen PY, et al. A multi-institutional phase ii trial of bevacizumab for recurrent and refractory meningioma. *Neurooncol Adv*. (2022) 4:123. doi: 10.1093/noajnl/vdac123

43. Brastianos PK, Twohy EL, Gerstner ER, Kaufmann TJ, Iafrate AJ, Lennerz J, et al. Alliance A071401: phase ii trial of focal adhesion kinase inhibition in Meningiomas with somatic Nf2 mutations. *J Clin Oncol*. (2023) 41:618–28. doi: 10.1200/JCO.21.02371

44. Brastianos PK, Galanis E, Butowski N, Chan JW, Dunn IF, Goldbrunner R, et al. Advances in multidisciplinary therapy for Meningiomas. *Neuro Oncol*. (2019) 21:i18–31. doi: 10.1093/neuonc/noy136

45. Choudhury A, Magill ST, Eaton CD, Prager BC, Chen WC, Cady MA, et al. Meningioma DNA methylation groups identify biological drivers and therapeutic vulnerabilities. *Nat Genet*. (2022) 54:649–59. doi: 10.1038/s41588-022-01061-8

46. Paramasivam N, Hübschmann D, Toprak UH, Ishaque N, Neidert M, Schrimpf D, et al. Mutational patterns and regulatory networks in epigenetic subgroups of meningioma. *Acta Neuropathol*. (2019) 138:295–308. doi: 10.1007/s00401-019-02008-w

frontiers | Frontiers in Oncology

TYPE Clinical Trial
PUBLISHED 14 December 2023
DOI 10.3389/fonc.2023.1320710

OPEN ACCESS

EDITED BY
Cesare Zoia,
San Matteo Hospital Foundation (IRCCS), Italy

REVIEWED BY
Alessia Pellerino,
University Hospital of the City of Health and Science of Turin, Italy
Soma Sengupta,
University of North Carolina at Chapel Hill, United States
Alberto Campione,
University of Insubria, Italy

*CORRESPONDENCE
Marco G. Paggi
marco.paggi@ifo.it

RECEIVED 12 October 2023
ACCEPTED 20 November 2023
PUBLISHED 14 December 2023

CITATION
Pace A, Lombardi G, Villani V, Benincasa D, Abbruzzese C, Cestonaro I, Corrà M, Padovan M, Cerretti G, Caccese M, Silvani A, Gaviani P, Giannarelli D, Ciliberto G and Paggi MG (2023) Efficacy and safety of chlorpromazine as an adjuvant therapy for glioblastoma in patients with unmethylated *MGMT* gene promoter: RACTAC, a phase II multicenter trial.
Front. Oncol. 13:1320710.
doi: 10.3389/fonc.2023.1320710

Efficacy and safety of chlorpromazine as an adjuvant therapy for glioblastoma in patients with unmethylated *MGMT* gene promoter: RACTAC, a phase II multicenter trial

Andrea Pace[1], Giuseppe Lombardi[2], Veronica Villani[1], Dario Benincasa[1], Claudia Abbruzzese[1], Ilaria Cestonaro[2], Martina Corrà[2], Marta Padovan[2], Giulia Cerretti[2], Mario Caccese[2], Antonio Silvani[3], Paola Gaviani[3], Diana Giannarelli[4], Gennaro Ciliberto[1] and Marco G. Paggi[1]*

[1]IRCCS - Regina Elena National Cancer Institute, Rome, Italy, [2]Veneto Institute of Oncology IOV-IRCCS, Padua, Italy, [3]IRCCS Besta Neurological Institute, Milan, Italy, [4]Fondazione Policlinico Universitario A. Gemelli, IRCCS, Rome, Italy

Introduction: Drug repurposing is a promising strategy to develop new treatments for glioblastoma. In this phase II clinical trial, we evaluated the addition of chlorpromazine to temozolomide in the adjuvant phase of the standard first-line therapeutic protocol in patients with unmethylated *MGMT* gene promoter.

Methods: This was a multicenter phase II single-arm clinical trial. The experimental procedure involved the combination of CPZ with standard treatment with TMZ in the adjuvant phase of the Stupp protocol in newly-diagnosed GBM patients carrying an unmethylated *MGMT* gene promoter. Progression-free survival was the primary endpoint. Secondary endpoints were overall survival and toxicity.

Results: Forty-one patients were evaluated. Twenty patients (48.7%) completed 6 cycles of treatment with TMZ+CPZ. At 6 months, 27 patients (65.8%) were without progression, achieving the primary endpoint. Median PFS was 8.0 months (95% CI: 7.0-9.0). Median OS was 15.0 months (95% CI: 13.1-16.9). Adverse events led to reduction or interruption of CPZ dosage in 4 patients (9.7%).

Discussion: The addition of CPZ to standard TMZ in the first-line treatment of GBM patients with unmethylated *MGMT* gene promoter was safe and led to a longer PFS than expected in this population of patients. These findings provide

10.3389/fonc.2023.1320710

proof-of-concept for the potential of adding CPZ to standard TMZ treatment in GBM patients with unmethylated *MGMT* gene promoter.

Clinical trial registration: https://clinicaltrials.gov/study/NCT04224441, identifier NCT04224441.

KEYWORDS

glioblastoma, drug repurposing, chlorpromazine, adjuvant treatment, *MGMT*

1 Introduction

Glioblastoma (GBM) is a frequent and severe brain tumor, characterized by poor response to treatment and an almost certainty of relapse. First-line GBM treatment, regardless of the molecular classification of the disease (1), consists in maximal surgical resection followed by radiotherapy with concomitant temozolomide (TMZ) treatment, followed by adjuvant TMZ. This scheme is however associated with a median overall survival (OS) of 14.6 months and a 5-year survival <5% (2), therefore leaving an unmet clinical need.

GBM presents high invasive and infiltrative properties (3), also coupled with a distinctive cellular heterogeneity, a prerequisite for a swift adaptation to treatment (4–7). Indeed, GBM has the ability to recover from genetic damages induced by radiotherapy and TMZ by means of an effective DNA repair system, especially in tumors characterized by unmethylated O6-methylguanine methyltransferase (*MGMT*) gene promoter (8). Of note, GBM is among the few tumors in which a single-drug treatment is currently in use: it may be possible to speculate that the addition of another therapy may help overcome resistance to TMZ (9).

An interesting characteristic of GBM is its responsiveness to neurotransmitters, as monoamines (10–12). The well-known interplay between neurons and tumors, especially GBM (11, 13), and the more recent identification of a synaptic neuron-GBM connectivity (14) confirms that neuron-secreted mediators are taken up by GBM cells, where they act as oncogenic stimuli (15). These findings paved the way for considering the addition of selected neuroleptic drugs as potential addition to GBM treatment (16). Indeed, many psychotropic drugs act on multiple postsynaptic receptors and display diverse pharmacological activity (16), including the ability to counteract GBM growth *in vitro* (17–19). Upon these assumptions, we evaluated the effects of one of the progenitors of neuroleptic medications, i.e., the antipsychotic drug chlorpromazine (CPZ), in use for about 70 years for psychiatric disorders in GBM patients. CPZ is a compound listed in the 2021 WHO Model List of Essential Medicines (20).

In an *in vitro* study, our group has already assayed CPZ effects on established and primary human GBM cells. The results defined the role of this drug in hindering GBM cell growth by acting at different levels through multimodal antitumor effects without any relevant action on non-cancer neuroepithelial cells (21, 22). In addition, CPZ acts synergistically with TMZ in hindering GBM vitality and stemness capabilities (21).

CPZ is a safe, low-cost and promptly available medication. All these conditions paved the way for repurposing CPZ as an add-on drug in GBM therapy. To this end, we planned the RACTAC (Repurposing the Antipsychotic drug Chlorpromazine as a Therapeutic Agent in the Combined treatment of newly diagnosed glioblastoma) phase II multicenter, single-arm study, in which CPZ is added to adjuvant TMZ in the first-line therapy of GBM patients whose tumor is characterized by an unmethylated *MGMT* gene promoter (8).

This study was designed with the purpose of investigating the clinical efficacy and safety of the addition of CPZ to the adjuvant TMZ administration in the first-line treatment of GBM patients carrying an unmethylated *MGMT* gene promoter.

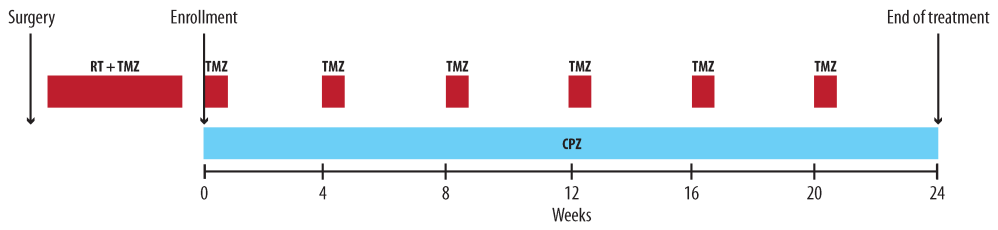

FIGURE 1
The RACTAC scheme: Scheme of the daily addition of CPZ during the adjuvant phase of the first line protocol for newly diagnosed GBM patients with unmethylated *MGMT* gene promoter. RT, radiotherapy; TMZ, temozolomide; CPZ, chlorpromazine.

2 Materials and methods

2.1 Study design

This was a multicenter, phase II single-arm clinical trial conducted in three Italian referral centers: the Regina Elena National Cancer Institute (Rome), the Veneto Institute of Oncology (Padua) and the Besta Neurological Institute (Milan).

The experimental procedure involved the combination of CPZ with standard treatment with TMZ in the adjuvant phase of the Stupp protocol (2) in newly diagnosed GBM patients carrying an unmethylated *MGMT* gene promoter. All patients received CPZ tablets ["Largactil", Teofarma S.R.L., Valle Salimbene (PV), Italy], during TMZ adjuvant treatment at a starting dose of 25 mg/day orally from day 1 onwards. The dosage was increased to 50 mg/day at the second cycle of treatment, if well tolerated, and continued for 6 cycles or until disease progression, death, unacceptable toxicity, or consent withdrawal (Figure 1).

This clinical trial has been approved by our Institutional Ethics Committee on September 6, 2019, and is registered as EudraCT #2019-001988-75 and ClinicalTrials.gov Identifier #NCT0422444.

2.2 Eligibility

Patients aged 18-75 years with newly diagnosed and histologically confirmed supratentorial GBM (World Health Organization 2016) and unmethylated *MGMT* gene promoter status were eligible. *MGMT* gene promoter methylation status was assessed in a local laboratory for each participating center by pyrosequencing or methylation-specific PCR. Additional inclusion criteria were: gadolinium (Gd)-enhanced MRI 48 h after surgery; stable or decreasing dose of steroids for 1 week before enrolment; Karnofski performance status (KPS) ≥70; satisfactory laboratory blood and biochemical results within 2 weeks prior to enrolment.

2.3 Endpoints

Progression-Free Survival (PFS) was the primary endpoint of this study. PFS was defined as the time from the start of the Stupp regimen (2) to the earliest documented date of disease progression, based on Response Assessment in Neuro-Oncology (RANO) criteria (23, 24), as determined by the investigator, death due to any cause, or censored at the date of the last assessment. Evaluating a meta-analysis of 91 GBM clinical trials, the choice of PFS as an endpoint can be considered appropriate as a surrogate endpoint for earlier evaluation. The 6-month PFS appears correlated with 1-year overall survival (OS) and median OS (25).

The secondary endpoints of this study were: (i) Overall survival (OS); defined as the time from diagnosis to the date of death from any cause or loss-to-follow-up); (ii) combination treatment toxicity. Adverse events (AEs) were evaluated according to the National Cancer Institute's Common Terminology Criteria for Adverse Events version 5.0. Safety assessments were performed from treatment initiation through 30 days after the last dose of chemotherapy with TMZ plus CPZ; (iii) Quality of Life (QoL), assessed by means of the EORTC QLQ C30+BN20 questionnaire at baseline and every 3 cycles (26, 27). Data on QoL are under evaluation at the time of drafting of this manuscript and will be presented in a separate paper.

2.4 Follow-up

Patients were followed-up monthly during adjuvant chemotherapy and every 3 months after completion of the standard treatment if the disease was stable. Radiological assessment was done by Gd brain MRI every 12 weeks from the first drug administration until progression.

Response assessment during study was based on investigators' evaluation using the RANO criteria (23, 24), which included blinded interpretation of MRI scans, assessment of neurological status, KPS scores, and steroid use.

2.5 Statistical analysis

All analyses were performed for the patients who received at least one dose of the study treatment. The primary objective of the study was to evaluate the proportion of patients free from progression after 6 months (PFS-6). Considering as unacceptable a percentage of PFS-6 (P0) equal to 35% and a desirable PFS-6 of 55% (P1), a minimum of 41 patients would be needed to guarantee a power of 80% at a significance level of 5% (one-sided) (28). If at least 20 patients were progression-free after 6 months, the treatment would be considered sufficiently active. All survival curves were estimated using the Kaplan-Meier method.

Clinical and demographic characteristics are reported as absolute counts and percentage when related to categorical items and as median and range if referred to quantitative variables.

3 Results

3.1 Patient characteristics

Between April 2020 and August 2022, 45 patients were screened; 41 received at least one cycle of treatment and were included in the final

TABLE 1 Baseline characteristics of the enrolled GBM patients.

Variables	Study population (n= 41)
Age at diagnosis (Median, y)	56 (range 20-75)
Gender	M 29 (70.7%); F 12 (29.3%)
KPS median	90 (range 70-100)
Extent of resection %	Gross Total Resection (GTR) 41.5; Partial Resection (PR) 56.1; Biopsy 2.4
Steroid treatment at baseline (%)	21 (51%)
Dexamethasone dose (mean)	4 mg

KPS, Karnofsky Performance status; GTR, Gross Total resection.

analysis. Study follow-up was closed on December 31, 2022. Patients' baseline characteristics and demographics are summarized in Table 1. The study was not adequately powered to determine whether there were any sex differences in clinical response to the treatment.

Twenty patients (48.7%) completed 6 cycles of treatment with TMZ at standard dose plus CPZ; twenty-one patients (51.2%) discontinued the treatment due to early progression (median cycles completed = 5.5, range 2-6). The median follow-up was 15 months (range 3-37).

3.2 Progression-free survival

At 6 months, 27 (65.8%) patients were alive and without progression: thus, the primary endpoint was achieved. Overall, 35 patients (85.4%) experienced disease progression, with a median PFS of 8.0 months (95% CI: 7.0-9.0) (Figure 2). PFS at different time points is reported in Table 2.

3.3 Overall survival

At study closure, 29 deaths (69.7%) have been observed, and median overall survival was 15.0 months (95% CI: 13.1-16.9). OS at different time-points is reported in Figure 2; Table 2.

3.4 Role of the extent of resection

Patients who underwent a gross total resection (GTR) had a longer PFS and OS than patients who underwent a partial resection (PR). As described (29), the extent of resection is an important prognostic factor for survival in glioblastoma (GBM) patients. This is also true in our case series, which was developed on a chronological basis and is representative of the general population of these patients, with a prevalence of PRs plus one case of biopsy.

3.5 Toxicity

The treatment scheme was associated with the onset of an expected dose-dependent sedation, especially at the beginning of the CPZ administration, and liver toxicity (1 serious case), however expected for both CPZ and TMZ. Treatment was well tolerated in all patients with mild somnolence (grade 1-2) in 8 (19.5%) and asthenia in 12 (29.2%) patients. In three patients, grade 3-4 hyper-transaminasaemia was observed (7%). Adverse events led to reduction or interruption of CPZ dosage in 4 patients (9.7%). Decreased platelets count grade 3 was observed in one patient and neutropenia grade 3 in one. All these data are summarized in Table 3.

4 Discussion

GBM patients with unmethylated *MGMT* gene promoter comprise 55-60% of total GBM cases and have a poorer prognosis due to their intrinsic resistance to alkylating agents. At present, while it is well recognized that TMZ brings a benefit in patients with methylated *MGMT* gene promoter, its use in cases of unmethylated *MGMT* gene promoter is still controversial. Indeed, EANO evidence-based guidelines on diagnosis and treatment of diffuse gliomas of adulthood report that TMZ might only be effective in GBM patients with methylated *MGMT* gene promoter, whereas its effectiveness on patients with unmethylated *MGMT* gene promoter is modest (8, 30).

Various therapeutic strategies have been investigated in phase II clinical trials to overcome drug resistance or bypass DNA repair pathways in GBM patients with unmethylated *MGMT* gene promoter (8, 31). In the same setting, addition of drugs other than TMZ alone in the first-line treatment did not lead to encouraging results (32–34). Other studies evaluated the efficacy of new agents as replacements for TMZ in the first-line treatment of GBM patients with unmethylated *MGMT* gene promoter. For example, in the EORTC 26082 phase II trial, temsirolimus was administered either during radiotherapy or as adjuvant treatment, showing no clinical benefit (35). In a single arm phase II trial, enzastaurin, a protein kinase C inhibitor, administered before, concomitantly with, and after radiotherapy in GBM patients with unmethylated *MGMT* gene promoter, did not achieve the primary endpoint of PFS at 6 months (36). On the other hand, in the same population of GBM patients, bevacizumab plus irinotecan provided a better PFS at 6 months than TMZ, but with no improvement in OS (37).

Our results show that the addition of CPZ to standard TMZ in the first-line treatment of GBM patients with unmethylated *MGMT* gene promoter was safe and led to a longer PFS, i.e., 8.0, than expected in this patient population. This finding met the primary endpoint of the study. A recent meta-analysis of five phase III clinical trials found that the standard-of-care treatment for GBM patients with unmethylated *MGMT* gene promoter results in a PFS of 4.99 months and an OS of 14.11 months (38).

In our study, however, median OS was 15 months, thus not representing a clinically relevant improvement over the data reported in this meta-analysis. Such an outcome could also relate to the administration of CPZ only in the adjuvant phase of treatment. Further studies are needed to investigate the concomitant association of CPZ also during radiotherapy.

The safety profile of CPZ was consistent with its well-known pharmacological profile, even when administered concomitantly with TMZ. In our study, the most frequent adverse event were mild somnolence (grade 1-2) in 18% of patients, usually in the first month of treatment, and fatigue, observed in 30% of patients, a symptom commonly reported within a range of 40-70% in primary brain tumor patients (39).

Quality of life (QoL) is an important outcome to be evaluated in these GBM patients. In our study, it has been measured by means of the EORTC QLQ-C30 and QLQ-BN20 questionnaires. These evaluations are currently in progress, and the results will be published shortly.

Most relevant limitations of the RACTAC trial are the small number of patients included in the study and the lack of a control group. However, the clinical characteristics of the patients at

10.3389/fonc.2023.1320710

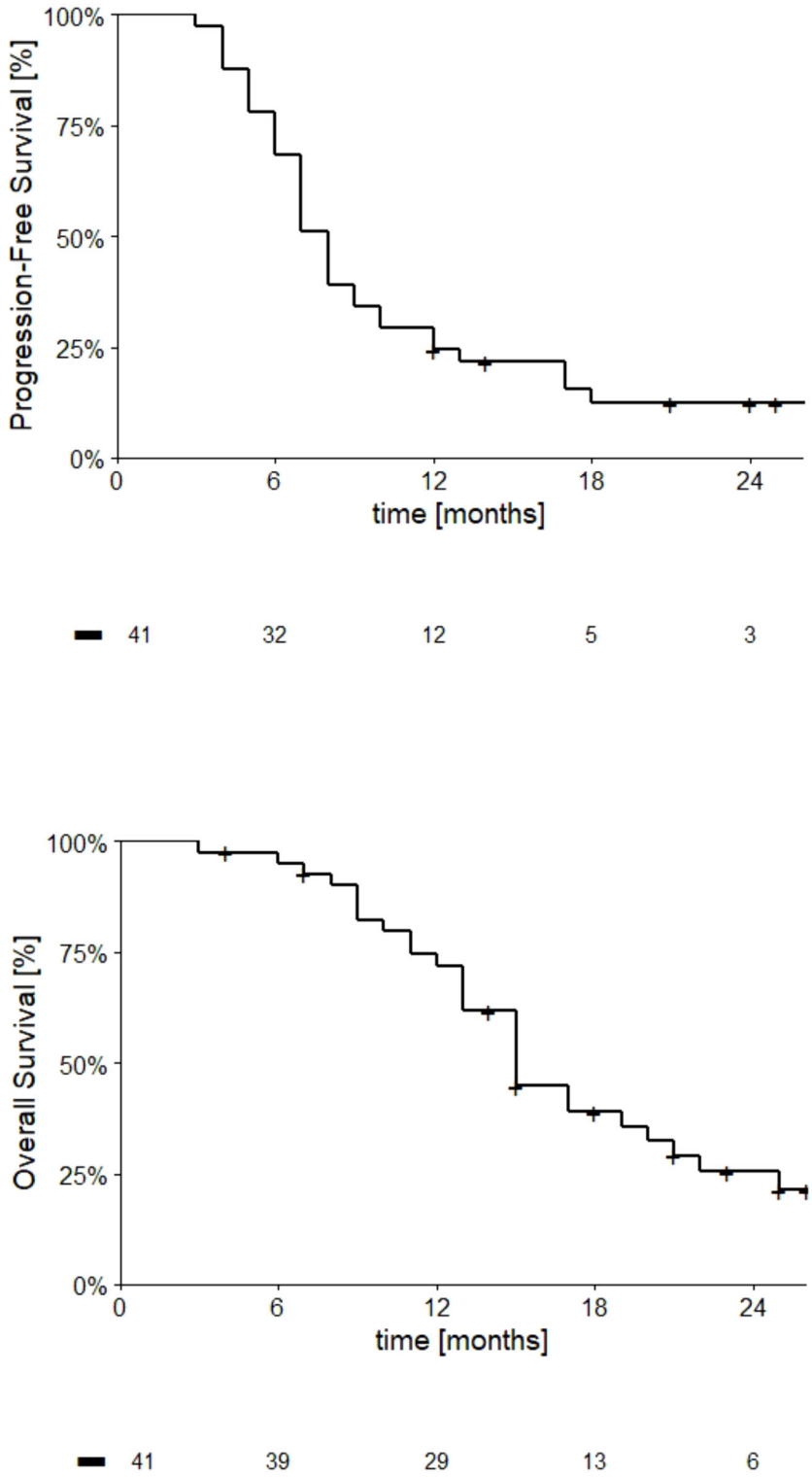

FIGURE 2
Kaplan-Meier curves describing PFS and OS trends (upper and lower charts, respectively) in GBM patients with unmethylated *MGMT* gene promoter treated according to the RACTAC protocol. The number of patients at risk at respective time points are indicated below the abscissa.

baseline appear representative of the real-world population of unmethylated *MGMT* gene promoter GBM. The PFS observed in this trial was 8.0 months and resulted promisingly longer than that reported in previous published trials in this population.

CPZ is a well-known DRD2 antagonist (40) and therefore has been successfully used in the treatment of psychiatric disorders. We intended to take advantage of its ability to interfere with the function of DRD2, as well as a number of other neuromediator receptors

TABLE 2 Progression-free survival (PFS) and overall survival (OS) in GBM patients with unmethylated *MGMT* gene promoter treated according to the RACTAC protocol.

	6 months	12 months	18 months	24 months
PFS	68.3%	24.4%	12.4%	12.4%
OS	95.1%	72.0%	38.9%	25.5%

TABLE 3 Drug-related adverse events.

Adverse events	Grade 1-2	Grade >2
Somnolence	8	0
Fatigue	11	1
Hypertransaminasemia	1	2
Thrombocytopenia	6	1
Neutropenia	1	1

(https://go.drugbank.com/drugs/DB00477), to hamper the pseudo-synaptic, oncogenic interplay between neurons and GBM. In addition, it should be considered that there is also a profound interplay between peripheral/central nervous systems and cancer, which acts through monoamine neuromediators and could represent a vulnerability targetable through the use of repurposed neuropsychiatric drugs in oncology and appliable to diverse cancer types (41, 42).

Evaluating the features of CPZ possibly useful in GBM treatment, we could also consider a number of studies showing the ability of this drug to hinder GBM malignant features in preclinical settings (43). In the same context, during the course of the RACTAC clinical trial, our group further refined the pharmacological effects of CPZ on GBM cells *in vitro*, demonstrating the ability of this medication to hinder GBM malignant features at multiple levels (21, 22) other than its known interference with the activity of neurotransmitters.

Since the plasticity of GBM and its ability to remodulate its cell population based on the selective pressure generated by therapies, we can state that this tumor cannot be defined as a "single-path disease", being therefore quite unsatisfying to treat it by means of targeted therapies. On these premises, it appears reasonable to consider the opportunity to use "dirty drugs", i.e., drugs that are not too targeted, but are able to hit some generalized vulnerabilities characterizing cancer cells.

Considering the escalation of the costs of novel anticancer medications, the long time it takes for them to reach the market and the consequent nonavailability for a great number of patients, the use of repurposed drugs can dramatically cut down time and drug expenses for effective medications to reach the bedside, with significant benefits for the patients and the Health Systems. In addition, the characteristics inherent in repositionable drugs represent a further therapeutic chance for GBM patients for which no second-line therapy is currently established as effective or for those that have already experienced all known therapeutic opportunities.

The RACTAC phase II clinical study was designed to investigate whether adding CPZ to the standard adjuvant TMZ in the Stupp protocol could improve therapeutic efficacy in patients with GBM with an unmethylated *MGMT* gene promoter. It also assessed the tolerability of adding a neuroleptic medication to GBM patients after neurosurgery and combined chemo-radiotherapy. This clinical trial is a proof-of-concept for the effectiveness of interfering with oncogenic monoamine signaling between neurons and GBM to inhibit tumor growth and malignancy, and, although not exhaustive, it can support the initiation of a subsequent phase III randomized clinical study.

Data availability statement

The datasets presented in this study can be found in online repositories. The names of the repository/repositories and accession number(s) can be found below: GARR repository at the following link: https://gbox.garr.it/garrbox/s/HZ2g4aBD26lJh1e.

Ethics statement

The studies involving humans were approved by Comitato Etico Centrale IRCCS – Sezione IFO-Fondazione Bietti, Roma (EudraCT # 2019-001988-75; ClinicalTrials.gov Identifier: NCT04224441). The studies were conducted in accordance with the local legislation and institutional requirements. The participants provided their written informed consent to participate in this study. Written informed consent was obtained from the individual(s) for the publication of any potentially identifiable images or data included in this article.

Author contributions

AP: Conceptualization, Data curation, Methodology, Resources, Supervision, Validation, Writing – original draft, Writing – review & editing. GL: Data curation, Resources, Validation, Writing – review & editing. VV: Data curation, Writing – review & editing. DB: Data curation, Writing – review & editing. CA: Data curation, Writing – review & editing. IC: Data curation, Resources, Writing – review & editing. MCo: Data curation, Resources, Writing – review & editing. MP: Data curation, Resources, Writing – review & editing. GCe: Data curation, Resources, Writing – review & editing. MCa: Data curation, Resources, Writing – review & editing. AS: Data curation, Writing – review & editing. PG: Data curation, Resources, Writing – review & editing. DG: Data curation, Formal analysis, Writing – review & editing. GCi: Funding acquisition, Supervision, Writing – review & editing. MGP: Conceptualization, Data curation, Funding acquisition, Methodology, Resources, Supervision, Validation, Writing – original draft, Writing – review & editing.

Funding

The author(s) declare financial support was received for the research, authorship, and/or publication of this article. Work partially financed by Funds Ricerca Corrente 2018-2019, 2020-2021, 2022-2023 from Italian Ministry of Health (GC, MGP) and by the European Union - NextGenerationEU through the Italian Ministry of University and Research under PNRR - M4C2-I1.3 Project PE_00000019 "HEAL ITALIA" to Marco G. Paggi, CUP H83C22000550006. This work was financially supported through funding from the institutional "Ricerca Corrente" granted by the Italian Ministry of Health. The views and opinions expressed are those of the authors only and do not necessarily reflect those of the European Union or the European Commission. Neither the European Union nor the European Commission can be held responsible for them.

Acknowledgments

This paper is dedicated to the memory of our friend and colleague Armando Felsani, who recently passed away and who contributed so much to the advancement of knowledge in the field of cell differentiation and cell cycle regulation. We thank Luca Giacomelli, PhD, for useful discussion. Editorial and graphical assistance were provided by Aashni Shah, Valentina Attanasio and Massimiliano Pianta (Polistudium SRL, Milan, Italy), and was supported by internal funds. We thank the patients who participated in the RACTAC trial and their families.

Conflict of interest

The authors declare that the research was conducted in the absence of any commercial or financial relationships that could be construed as a potential conflict of interest.

Publisher's note

References

1. Louis DN, Perry A, Reifenberger G, von Deimling A, Figarella-Branger D, Cavenee WK, et al. The 2016 World Health Organization classification of tumors of the central nervous system: a summary. *Acta Neuropathol* (2016) 131(6):803–20. doi: 10.1007/s00401-016-1545-1

2. Stupp R, Mason WP, van den Bent MJ, Weller M, Fisher B, Taphoorn MJ, et al. Radiotherapy plus concomitant and adjuvant temozolomide for glioblastoma. *N Engl J Med* (2005) 352(10):987–96. doi: 10.1056/NEJMoa043330

3. Rao JS. Molecular mechanisms of glioma invasiveness: the role of proteases. *Nat Rev Cancer* (2003) 3(7):489–501. doi: 10.1038/nrc1121

4. Lan X, Jorg DJ, Cavalli FMG, Richards LM, Nguyen LV, Vanner RJ, et al. Fate mapping of human glioblastoma reveals an invariant stem cell hierarchy. *Nature* (2017) 549(7671):227–32. doi: 10.1038/nature23666

5. Gimple RC, Bhargava S, Dixit D, Rich JN. Glioblastoma stem cells: lessons from the tumor hierarchy in a lethal cancer. *Genes Dev* (2019) 33(11-12):591–609. doi: 10.1101/gad.324301.119

6. Couturier CP, Ayyadhury S, Le PU, Nadaf J, Monlong J, Riva G, et al. Single-cell RNA-seq reveals that glioblastoma recapitulates a normal neurodevelopmental hierarchy. *Nat Commun* (2020) 11(1):3406. doi: 10.1038/s41467-020-17186-5

7. Hubert CG, Lathia JD. Seeing the GBM diversity spectrum. *Nat Cancer* (2021) 2 (2):135–7. doi: 10.1038/s43018-021-00176-x

8. Hegi ME, Diserens AC, Gorlia T, Hamou MF, de Tribolet N, Weller M, et al. MGMT gene silencing and benefit from temozolomide in glioblastoma. *N Engl J Med* (2005) 352(10):997–1003. doi: 10.1056/NEJMoa043331

9. Czarnywojtek A, Borowska M, Dyrka K, Van Gool S, Sawicka-Gutaj N, Moskal J, et al. Glioblastoma multiforme: the latest diagnostics and treatment techniques. *Pharmacology* (2023) 108(5):423–31. doi: 10.1159/000531319

10. Caragher SP, Hall RR, Ahsan R, Ahmed AU. Monoamines in glioblastoma: complex biology with therapeutic potential. *Neuro Oncol* (2018) 20(8):1014–25. doi: 10.1093/neuonc/nox210

11. Caragher SP, Shireman JM, Huang M, Miska J, Atashi F, Baisiwala S, et al. Activation of dopamine receptor 2 prompts transcriptomic and metabolic plasticity in glioblastoma. *J Neurosci* (2019) 39(11):1982–93. doi: 10.1523/JNEUROSCI.1589-18.2018

12. Venkataramani V, Tanev DI, Strahle C, Studier-Fischer A, Fankhauser L, Kessler T, et al. Glutamatergic synaptic input to glioma cells drives brain tumour progression. *Nature* (2019) 573(7775):532–8. doi: 10.1038/s41586-019-1564-x

13. Barygin OI, Nagaeva EI, Tikhonov DB, Belinskaya DA, Vanchakova NP, Shestakova NN. Inhibition of the NMDA and AMPA receptor channels by antidepressants and antipsychotics. *Brain Res* (2017) 1660:58–66. doi: 10.1016/j.brainres.2017.01.028

14. Hanahan D, Monje M. Cancer hallmarks intersect with neuroscience in the tumor microenvironment. *Cancer Cell* (2023) 41(3):573–80. doi: 10.1016/j.ccell.2023.02.012

15. Venkataramani V, Schneider M, Giordano FA, Kuner T, Wick W, Herrlinger U, et al. Disconnecting multicellular networks in brain tumours. *Nat Rev Cancer* (2022) 22 (8):481–91. doi: 10.1038/s41568-022-00475-0

16. Persico M, Abbruzzese C, Matteoni S, Matarrese P, Campana AM, Villani V, et al. Tackling the behavior of cancer cells: molecular bases for repurposing antipsychotic drugs in the treatment of glioblastoma. *Cells* (2022) 11(2):263. doi: 10.3390/cells11020263

17. Oliva CR, Zhang W, Langford C, Suto MJ, Griguer CE. Repositioning chlorpromazine for treating chemoresistant glioma through the inhibition of cytochrome c oxidase bearing the COX4-1 regulatory subunit. *Oncotarget* (2017) 8 (23):37568–83. doi: 10.18632/oncotarget.17247

18. Kang S, Lee JM, Jeon B, Elkamhawy A, Paik S, Hong J, et al. Repositioning of the antipsychotic trifluoperazine: Synthesis, biological evaluation and in silico study of trifluoperazine analogs as anti-glioblastoma agents. *Eur J Med Chem* (2018) 151:186–98. doi: 10.1016/j.ejmech.2018.03.055

19. Omoruyi SI, Ekpo OE, Semenya DM, Jardine A, Prince S. Exploitation of a novel phenothiazine derivative for its anti-cancer activities in Malignant glioblastoma. *Apoptosis* (2020) 25(3-4):261–74. doi: 10.1007/s10495-020-01594-5

20. World Health Organization. *World Health Organization Model List of Essential Medicines, 22nd List*. Geneva: World Health Organization (2021). Available at: https://www.who.int/publications/i/item/WHO-MHP-HPS-EML-2021.02.

21. Matteoni S, Matarrese P, Ascione B, Buccarelli M, Ricci-Vitiani L, Pallini R, et al. Anticancer properties of the antipsychotic drug chlorpromazine and its synergism with temozolomide in restraining human glioblastoma proliferation *in vitro*. *Front Oncol* (2021) 11:635472. doi: 10.3389/fonc.2021.635472

22. Matteoni S, Matarrese P, Ascione B, Ricci-Vitiani L, Pallini R, Villani V, et al. Chlorpromazine induces cytotoxic autophagy in glioblastoma cells via endoplasmic reticulum stress and unfolded protein response. *J Exp Clin Cancer Res* (2021) 40(1):347. doi: 10.1186/s13046-021-02144-w

23. Wen PY, Macdonald DR, Reardon DA, Cloughesy TF, Sorensen AG, Galanis E, et al. Updated response assessment criteria for high-grade gliomas: response assessment in neuro-oncology working group. *J Clin Oncol* (2010) 28(11):1963–72. doi: 10.1200/JCO.2009.26.3541

24. Radbruch A, Fladt J, Kickingereder P, Wiestler B, Nowosielski M, Baumer P, et al. Pseudoprogression in patients with glioblastoma: clinical relevance despite low incidence. *Neuro Oncol* (2015) 17(1):151–9. doi: 10.1093/neuonc/nou129

25. Han K, Ren M, Wick W, Abrey L, Das A, Jin J, et al. Progression-free survival as a surrogate endpoint for overall survival in glioblastoma: a literature-based meta-analysis from 91 trials. *Neuro Oncol* (2014) 16(5):696–706. doi: 10.1093/neuonc/not236

26. Aaronson NK, Ahmedzai S, Bergman B, Bullinger M, Cull A, Duez NJ, et al. The European Organization for Research and Treatment of Cancer QLQ-C30: a quality-of-life instrument for use in international clinical trials in oncology. *J Natl Cancer Inst* (1993) 85(5):365–76. doi: 10.1093/jnci/85.5.365

27. Osoba D, Aaronson NK, Muller M, Sneeuw K, Hsu MA, Yung WK, et al. The development and psychometric validation of a brain cancer quality-of-life questionnaire for use in combination with general cancer-specific questionnaires. *Qual Life Res* (1996) 5(1):139–50. doi: 10.1007/BF00435979

28. A'Hern RP. Sample size tables for exact single-stage phase II designs. *Stat Med* (2001) 20(6):859–66. doi: 10.1002/sim.721

29. Katsigiannis S, Grau S, Krischek B, Er K, Pintea B, Goldbrunner R, et al. MGMT-positive vs MGMT-negative patients with glioblastoma: identification of prognostic factors and resection threshold. *Neurosurgery* (2021) 88(4):E323–9. doi: 10.1093/neuros/nyaa562

30. Weller M, van den Bent M, Preusser M, Le Rhun E, Tonn JC, Minniti G, et al. EANO guidelines on the diagnosis and treatment of diffuse gliomas of adulthood. *Nat Rev Clin Oncol* (2021) 18(3):170–86. doi: 10.1038/s41571-020-00447-z

31. Weiler M, Hartmann C, Wiewrodt D, Herrlinger U, Gorlia T, Bahr O, et al. Chemoradiotherapy of newly diagnosed glioblastoma with intensified temozolomide. *Int J Radiat Oncol Biol Phys* (2010) 77(3):670–6. doi: 10.1016/j.ijrobp.2009.05.031

32. Nabors LB, Fink KL, Mikkelsen T, Grujicic D, Tarnawski R, Nam DH, et al. Two cilengitide regimens in combination with standard treatment for patients with newly diagnosed glioblastoma and unmethylated MGMT gene promoter: results of the open-label, controlled, randomized phase II CORE study. *Neuro Oncol* (2015) 17(5):708–17. doi: 10.1093/neuonc/nou356

33. Raizer JJ, Giglio P, Hu J, Groves M, Merrell R, Conrad C, et al. A phase II study of bevacizumab and erlotinib after radiation and temozolomide in MGMT unmethylated GBM patients. *J Neurooncol* (2016) 126(1):185–92. doi: 10.1007/s11060-015-1958-z

34. Asano K, Fumoto T, Matsuzaka M, Hasegawa S, Suzuki N, Akasaka K, et al. Combination chemoradiotherapy with temozolomide, vincristine, and interferon-beta might improve outcomes regardless of O6-methyl-guanine-DNA-methyltransferase (MGMT) promoter methylation status in newly glioblastoma. *BMC Cancer* (2021) 21 (1):867. doi: 10.1186/s12885-021-08592-z

35. Wick W, Gorlia T, Bady P, Platten M, van den Bent MJ, Taphoorn MJ, et al. Phase II Study of Radiotherapy and Temsirolimus versus Radiochemotherapy with Temozolomide in Patients with Newly Diagnosed Glioblastoma without MGMT Promoter Hypermethylation (EORTC 26082). *Clin Cancer Res* (2016) 22(19):4797–806. doi: 10.1158/1078-0432.CCR-15-3153

36. Wick W, Steinbach JP, Platten M, Hartmann C, Wenz F, von Deimling A, et al. Enzastaurin before and concomitant with radiation therapy, followed by enzastaurin maintenance therapy, in patients with newly diagnosed glioblastoma without MGMT promoter hypermethylation. *Neuro Oncol* (2013) 15(10):1405–12. doi: 10.1093/neuonc/not100

37. Herrlinger U, Schafer N, Steinbach JP, Weyerbrock A, Hau P, Goldbrunner R, et al. Bevacizumab plus irinotecan versus temozolomide in newly diagnosed O6-methylguanine-DNA methyltransferase nonmethylated glioblastoma: the randomized GLARIUS trial. *J Clin Oncol* (2016) 34(14):1611–9. doi: 10.1200/JCO.2015.63.4691

38. Alnahhas I, Alsawas M, Rayi A, Palmer JD, Raval R, Ong S, et al. Characterizing benefit from temozolomide in MGMT promoter unmethylated and methylated glioblastoma: a systematic review and meta-analysis. *Neurooncol Adv* (2020) 2(1): vdaa082. doi: 10.1093/noajnl/vdaa082

39. Valko PO, Siddique A, Linsenmeier C, Zaugg K, Held U, Hofer S. Prevalence and predictors of fatigue in glioblastoma: a prospective study. *Neuro Oncol* (2015) 17 (2):274–81. doi: 10.1093/neuonc/nou127

40. Beaulieu JM, Gainetdinov RR. The physiology, signaling, and pharmacology of dopamine receptors. *Pharmacol Rev* (2011) 63(1):182–217. doi: 10.1124/pr.110.002642

41. Magnon C, Hondermarck H. The neural addiction of cancer. *Nat Rev Cancer* (2023) 23:317–34. doi: 10.1038/s41568-023-00556-8

42. Chang A, Botteri E, Gillis RD, Lofling L, Le CP, Ziegler AI, et al. Beta-blockade enhances anthracycline control of metastasis in triple-negative breast cancer. *Sci Transl Med* (2023) 15(693):eadf1147. doi: 10.1126/scitranslmed.adf1147

43. Abbruzzese C, Matteoni S, Persico M, Villani V, Paggi MG. Repurposing chlorpromazine in the treatment of glioblastoma multiforme: analysis of literature and forthcoming steps. *J Exp Clin Cancer Res* (2020) 39(1):26. doi: 10.1186/s13046-020-1534-z

frontiers | Frontiers in Oncology

TYPE Review
PUBLISHED 21 December 2023
DOI 10.3389/fonc.2023.1326595

OPEN ACCESS

EDITED BY
Cesare Zoia,
San Matteo Hospital Foundation (IRCCS), Italy

REVIEWED BY
Alessandro Carretta,
University of Bologna, Italy
Matteo Zoli,
IRCCS Institute of Neurological Sciences of Bologna (ISNB), Italy

*CORRESPONDENCE
Ao Chen
neuro1993@163.com

RECEIVED 23 October 2023
ACCEPTED 06 December 2023
PUBLISHED 21 December 2023

CITATION
Chen A, Ai M and Sun T (2023) Advances in the treatment of Adamantinomatous craniopharyngioma: How to balance tumor control and quality of life in the current environment: a narrative review.
Front. Oncol. 13:1326595.
doi: 10.3389/fonc.2023.1326595

Advances in the treatment of Adamantinomatous craniopharyngioma: How to balance tumor control and quality of life in the current environment: a narrative review

Ao Chen[1]*, MingDa Ai[2] and Tao Sun[2]

[1]Department of Neurosurgery, Yueyang People's Hospital, Yueyang, China, [2]Department of Neurosurgery, The First Affiliated Hospital of Kunming Medical University, Kunming, China

Adamantinomatous craniopharyngioma (ACP) presents a significant challenge to neurosurgeons despite its benign histology due to its aggressive behavior and unique growth patterns. This narrative review explores the evolving landscape of ACP treatments and their efficacy, highlighting the continuous development in therapeutic approaches in recent years. Traditionally, complete resection was the primary treatment for ACP, but surgical -related morbidity have led to a shift. The invasive nature of the finger-like protrusions in the histological structure results in a higher recurrence rate for ACP compared to papillary craniopharyngioma (PCP), even after complete macroscopic resection. Given this, combining subtotal resection with adjuvant radiotherapy has shown potential for achieving similar tumor control rates and potentially positive endocrine effects. Simultaneously, adjuvant treatments (such as radiotherapy, intracystic treatment, and catheter implantation) following limited surgery offer alternative approaches for sustained disease control while minimizing morbidity and alleviating clinical symptoms. Additionally, advances in understanding the molecular pathways of ACP have paved the way for targeted drugs, showing promise for therapy. There is a diversity of treatment models for ACP, and determining the optimal approach remains a subject of ongoing debate in the present context. In order to achieve a good-term quality of life (QOL), the main goal of the cyst disappearance or reduction of surgical treatment is still the main. Additionally, there should be a greater emphasis on personalized treatment at this particular stage and the consideration of ACP as a potentially chronic neurosurgical condition. This review navigates the evolving landscape of ACP therapies, fostering ongoing discussions in this complex field.

KEYWORDS

Adamantinomatous craniopharyngioma (ACP), cystic craniopharyngioma, quality of life, cyst management, tumor control

1 Introduction

ACP, or adamantinomatous craniopharyngioma, is a benign tumor originating from residual epithelial cells of Rathke's pouch or the craniopharyngeal duct during the embryonic period (1, 2). Approximately 90% of ACP cases manifest as a cystic component (3), with incidence peaks observed in children aged 5 to 15 years and adults aged 45 to 60 years (4, 5). ACP stands as the prevalent non-neuroepithelial intracranial tumor in children, constituting approximately 5–11% of intracranial tumors within the pediatric age cohort (5). Despite being classified as a WHO Grade I tumor, ACP poses a significant challenge in neurosurgical treatment. This complexity arises from its proximity to vital structures like the optic nerve, thalamus, pituitary gland, and the circle of Willis. Additionally, at a histological level, the presence of finger-like protrusions facilitates tumor infiltration and circumferential growth, leading to indistinct boundaries (5–9). This distinctive anatomical and histological context underscores the surgical difficulty posed by ACP. Consequently, these factors contribute to a notable recurrence rate of ACP, persisting even after macroscopic total resection. This recurrence highlights the challenge of achieving complete eradication of the tumor. Even more concerning are the enduring sequelae stemming from surgical resection, encompassing hypothalamic syndrome, severe obesity, diabetes insipidus, visual impairments, and neurocognitive dysfunction (5, 10, 11). These persistent effects lead to a sustained decline in the overall QoL for affected patients.

While the concept of craniopharyngioma (CP) was initially proposed by Cushing in 1929 (12), its precise origin continues to be a subject of debate. Recent studies indicate that β-catenin and tumor stem cell markers are predominantly located within the histological finger-like protrusions (FP) (13). This observation suggests a potential association between FP, the origin of ACP, and the invasion of the hypothalamic-pituitary axis by the tumor. Nevertheless, this hypothesis requires additional empirical validation. Consequently, a comprehensive comprehension of ACP's biology and vigilant monitoring of the latest developments in treatment modalities hold paramount importance in enhancing the management of this highly complex tumor and ameliorating the quality of life for afflicted individuals.

2 Materials and methods

Studies included in this article were systematically searched in the PubMed and MEDLINE databases, with the last update conducted in November 2023. Keywords used in the search primarily consisted of "adamantinomatous craniopharyngioma," "cystic craniopharyngioma," "craniopharyngioma," "pediatric" and "childhood-onset" The screening process involved evaluating titles and abstracts, with full texts downloaded for further review if deemed necessary. Additionally, reference lists from extracted studies were thoroughly reviewed. Selection criteria focused on literature concerning advancements in ACP treatment, pathophysiology, tumor control, and patient quality of life, particularly emphasizing recent research, innovative methodologies, and therapeutic strategies. The goal was to provide a comprehensive and contemporary insight into clinical practices by examining the latest developments in ACP treatment and identifying optimal strategies to balance tumor control with quality of life.

Abbreviations: MRI, magnetic resonance imaging; ACP, Adamantinomatous craniopharyngioma; PCP, Papillary craniopharyngioma; CP, craniopharyngioma; GTR, Gross total resection; STR, Subtotal resection; EES, Endonasal endoscopic surgery; QoL, Quality of life; CSF, Cerebrospinal fluid; TCA, Transcranial approach; STLT, Suprachiasmatic endplate; PFS, progression-free survival.

3 Pathophysiology

3.1 Genetics and inflammation in ACP

Molecular studies have demonstrated that CTNNB1 exon 3 mutations, which encode β-catenin, are present in 57%-96% of ACP patients (14, 15). Importantly, these mutations are not detected in the adult-onset papillary histological CP subtype (PCP), underscoring their specificity to ACP. This mutation represents the sole known recurrent genetic aberration observed in ACP to date (10). CTNNB1 mutations have the capacity to impede the phosphorylation and degradation of β-catenin, resulting in its accumulation within the nucleus. This event triggers the subsequent activation of the WNT/β-catenin signal transduction pathway, ultimately culminating in tumorigenesis (16, 17). Studies have demonstrated that CTNNB1 mutations serve as oncogenic drivers in mouse models. Specifically, the expression of a functionally equivalent form of mutant β-catenin, akin to that observed in human ACP, in murine SOX2+ embryonic progenitors or adult stem cells leads to the development of tumors (17, 18). Additionally, these mouse models have unveiled novel targets that hold potential therapeutic value in the treatment of ACP (19).

The cystic and solid components of ACP both exhibit a wide array of cytokines, chemokines, and inflammatory mediators. This suggests that they likely share similar molecular characteristics and undergo common molecular events in the course of tumor pathogenesis (20). Elevated levels of cytokines including IL-6, IL-8, CXCL1, and IL-10 have been documented in the cystic fluid of ACP (21). Notably, IL-6 appears to play a role in instigating an inflammatory response in adjacent non-tumor tissues (19, 22). Furthermore, the expression patterns of these cytokines align with the activation of the inflammasome. This response may be initiated by the presence of cholesterol crystals within ACP (5, 23). The notable abundance of α-defensins identified in the cystic fluid implies that inflammation plays a crucial role in prompting the secretion of cyst fluid by epithelial cells lining the cyst wall. Additionally, this finding negates the possibility that the formation of ACP cyst fluid arises from blood-brain barrier disruption. Instead, it suggests that the innate immune response may be implicated in the pathological process of ACP cyst formation (24). These observations provide additional affirmation of the pivotal role played by inflammation in the pathogenesis of ACP.

3.2 Morphological and histological features

ACP shares similarities with adamantinoma and post-keratinized odontogenic cysts, typically presenting as calcified, cystic, and lobulated formations (25). From a macroscopic perspective, ACP can manifest as either purely cystic or cystic-solid structures. The solid portions exhibit an amorphous quality, containing numerous micro-calcifications. The cystic fluids are primarily composed of cholesterol crystals and cell fragments, imparting a distinctive "machine oil" appearance (20). The outer layer of the cystic wall comprises fibrous tissue, rendering it resilient and often challenging to puncture. Meanwhile, the inner layer is characterized by an incomplete stratified squamous epithelium, featuring scattered tumor cells extending into the cavity (26).

Histologically, tumors are distinguished by the presence of a peripheral basal cell layer of palisading epithelium, along with the aggregation of loosely arranged stellate cells. The solid components of the tumor typically exhibit distinctive accumulation of "wet" keratin and calcium salts (9, 27). The solid tumors have the propensity to infiltrate surrounding neural tissue in a finger-like manner. Consequently, this aggressive growth pattern can result in severe endocrine and visual dysfunction, as well as substantial surgical morbidity and high recurrence rates, rendering treatment highly challenging (5–9).

Unlike the diverse anatomical classification methods applied to PCP, the cystic nature of ACP facilitates tumor growth in various locations, including the anterior and middle cranial fossae, interpeduncular cisterna, ramus, cerebellar pontine region, and there have even been partial reports of ectopic ACP cases (28–31). Currently, there exists no pertinent literature on the anatomical classification of ACP. To establish a more precise anatomical classification for ACP, it is imperative to accumulate a substantial volume of case data and establish multi-center international registries. These efforts are crucial in providing guidance for clinical imaging identification and treatment approaches.

4 Evolution of visual function and endocrine status

Visual impairment in cases of ACP primarily stems from compression of the optic nerve pathway (8, 32, 33). Preoperative assessments have shown that deficits in visual acuity and visual field may reach levels as high as 70-80% (8, 34). The extent of visual impairment is contingent on the lesion's anatomical positioning in relation to the optic chiasma, with bitemporal hemianopia being a characteristic symptom. Recent studies have demonstrated that, even with straightforward cyst decompression, there can be a substantial improvement in visual function, with a response rate exceeding 75% (32, 35–37). This reaffirms that visual impairment predominantly arises from compression rather than direct tumor invasion. Nevertheless, following craniotomy, the occurrence of postoperative visual impairment may reach levels as high as 30% (38–40). This is primarily attributable to the tumor's close adherence to surrounding structures and its size (41).

It is imperative to measure hormones perioperatively and during follow-up to mitigate endocrine disorders (42). Preoperatively, the most prevalent endocrine deficiencies encompass growth hormone and gonadotropin deficits. Postoperatively, the most typical endocrine disorders include diabetes insipidus, hypothyroidism, adrenocortical dysfunction, and sexual dysfunction (43–47). The risk of endocrine deterioration is intricately tied to the type of surgical procedure (48–51). Craniotomy poses a higher risk compared to transsphenoidal sinus surgery (52–54), while partial resection carries a lower risk than total or subtotal resection (54). Minimally invasive cyst drainage yields a more favorable endocrine effect compared to surgical resection (31, 35–37, 55). While hormone replacement therapy continues to be the principal approach for addressing endocrine disorders, its administration requires circumspection, and a tailored treatment regimen must be devised (42).

5 Surgical strategy

Currently, surgery remains the foremost effective approach for treating ACP. The paramount objective of surgical intervention is to optimize resection safety while preventing irreversible harm to the hypothalamus. Nevertheless, surgical resection of ACP presents two significant challenges. Initially, while complete tumor resection may offer a potential cure for ACP, the recurrence rate remains elevated even after achieving full macroscopic removal. This is primarily due to the tissue structure of the finger-like projections, which can infiltrate and extend into critical neighboring structures like the hypothalamus and pituitary gland. Consequently, this often results in an indistinct demarcation between the tumor and healthy tissue. Attempting a broader resection can frequently lead to severe morbidity (5–9). Secondly, ACP can attain significant size, and not infrequently, its cyst wall becomes intimately attached to vital adjacent structures. Maintaining contact with the exceedingly thin cyst wall during surgery can be challenging, potentially leading to inadvertent detachment. Additionally, the cystic wall may have an ambiguous boundary with the arachnoid interface, further complicating complete resection (56–60). This challenge is particularly pronounced in cases where tumors reach a substantial size, possibly extending into the posterior cranial fossa and other regions. In such instances, employing a combination of approaches may be imperative to achieve complete cyst wall resection. However, this can potentially result in heightened surgical morbidity (61–65). A recent systematic review encompassing 17 studies on adult craniopharyngiomas was conducted (66). It involved 748 patients in the Gross Total Resection (GTR) cohort and 559 patients in the Subtotal Resection (STR) cohort. The findings indicated that GTR significantly reduced the likelihood of recurrence (OR, 0.106; 95% CI, 0.067-0.168; $P < 0.001$), albeit at the expense of an increased occurrence of postoperative panhypopituitarism (OR, 2.063; $P = 0.034$) and permanent diabetes insipidus (OR, 2.776; $P = 0.007$).

6 Endonasal endoscopic surgery

Over the last two decades, Endonasal Endoscopic Surgery (EES) has seen a growing utilization in the treatment of ACP, owing to its benefits of microinvasion and enhanced visualization (67–69). The 2020 EANS consensus statement on adult CP treatment advises utilizing the endonasal approach for midline CP, whereas transcranial approaches are suggested for lateral extension or purely intraventricular growth tumors (70). A recent systematic review comparing transcranial endoscopic and transcranial approaches to craniopharyngioma excision demonstrated that EES excision yielded a higher total excision rate and a greater likelihood of vision improvement (61.3% vs. 50.5%) in eight studies encompassing 376 patients. In cases where both approaches achieve complete tumor removal, EES exhibits superiority over TCA regarding GTR rate and visual outcomes. Additionally, it demonstrates positive effects on complications aside from cerebrospinal fluid (CSF) leakage, including hypopituitarism and diabetes insipidus (71). CSF leakage is a relatively prevalent complication following EES. However, this incidence is on a decreasing trend with the maturation of surgical proficiency and advancements in skull base repair techniques (71). In 2023, Qiao et al. conducted a comprehensive analysis of 364 craniopharyngioma patients who underwent EES over a span of ten years (72), representing the largest series to date. The study identified a larger dural defect size (OR 8.545, 95% CI 3.684-19.821, $p < 0.001$) and lower preoperative serum albumin levels (OR 0.787, 95% CI 0.673 to 0.919, $p = 0.002$) as independent risk factors for postoperative CSF leakage. Interestingly, CSF leakage was not associated with the opening of the third ventricle floor.

While Endonasal Endoscopic Surgery (EES) provides excellent visual field exposure to the subchiasmatic, postchiasmatic, and pituitary stalk-infundibular axes, its effectiveness is limited in cases of third ventricle ACP, particularly when the tumor extends bilaterally into the thalamus, leading to significant vaso-neurostructural lesions in its vicinity (73–75). Cavallo et al. (73) reported on a cohort of 103 patients with Craniopharyngioma, achieving a GTR rate of 68.9%. However, this rate decreased to 30% when the lesions extended bilaterally into the thalamus. In their another study (76), EES was employed to treat 13 patients primarily presenting with third ventricle ACP. Among them, GTR was achieved in 8 patients (66.7%). However, two patients experienced subdural hematomas, and one patient tragically succumbed to brain stem hemorrhage. Zhou et al. reported the utilization of EES in treating 14 patients with intrinsic third ventricle craniopharyngioma using the Suprachiasmatic Endplate (STLT) approach, 13 (92.8%) attained GTR, while the remaining patient achieved near-total resection (90%). Additionally, 3 patients necessitated hormone replacement therapy, and 1 patient experienced a decline in vision. The average follow-up period was 26.2 months, during which no instances of tumor recurrence were noted (74). While long-term follow-up data is lacking, their experience indicates that accessing the endplate offers superior exposure to the third ventricle environment and reduced surgery-related injury. This may present a novel neuroendoscopic option for treating third ventricle ACP (Figure 1, Figure 2).

7 Management of cyst (as a chronic neurosurgical disease)

7.1 Neuroendoscopic fenestration

Due to the benefits of endoscopic visualization, some earlier studies reported the safety and feasibility of employing endoscopic transventricular treatment for ACP. Over the past five years, a number of relatively small-scale series have serendipitously discovered that endoscopic fenestration for ACP has led to low surgical morbidity and a relatively extended period of disease control. Lauretti et al. reported that they achieved enduring tumor control by utilizing endoscopy to create a large opening in the upper section of the cyst and they attributed this mainly to the establishment of a permanent connection between the cyst cavity and the CSF space. Among the eight patients, there was a recurrence rate of 20% and a median progression-free survival (PFS) of 57 months. The authors identified endoscopy as an independent predictor of reduced cyst recurrence (37). Hollon et al. employed the "through-and-through" technique, conducting wide cyst fenestration at the top and bottom of the cyst for cystic retrochiasmatic craniopharyngiomas. Some patients received postoperative radiotherapy. The study had a mean follow-up of 2.5 ± 1.6 years, and a noteworthy decrease in postoperative cyst volume was noted. The patients experienced substantial enhancement in their quality of life, and there were no surgical complications (35). In a similar vein, Takano et al. accomplished long-term tumor control in 8 out of 9 patients (88.9%) over a mean follow-up of 72.9 months. This was achieved through fenestration and irrigation solely at the upper portion of the cyst, followed by segmental stereotactic radiotherapy. This led to significant alleviation of symptoms like cranial hypertension and visual impairment. No surgical complications arose (36).

7.2 Stereotactic cyst drainage

Steiert et al. conducted stereotactic-guided catheter implantation in 12 cases of cystic craniopharyngioma. Over an average follow-up period of 41 months, the cyst volume reduced by 64.2%. Additionally, post-radiotherapy, there was an average reduction of cyst volume by 92.0%. They also believe that establishing connection between the cyst cavity and the CSF space is an important factor in preventing the cyst reaccumulate. Furthermore, the patients experienced a significant improvement in visual function without incurring any new complications (77). Rachinger et al. conducted microsurgery and implemented stereotaxic "bidirectional drainage" in 79 cases of craniopharyngiomas. The median follow-up duration was 51 months (range: 14-188 months). The findings revealed that while the PFS for cystic tumors was relatively brief (5-year PFS: 53.6% vs 66.8%, $p = 0.10$), bidirectional drainage yielded significantly improved endocrine outcomes. The authors suggested that a majority of patients with cystic craniopharyngioma might not necessitate early radiotherapy post-drainage (32).

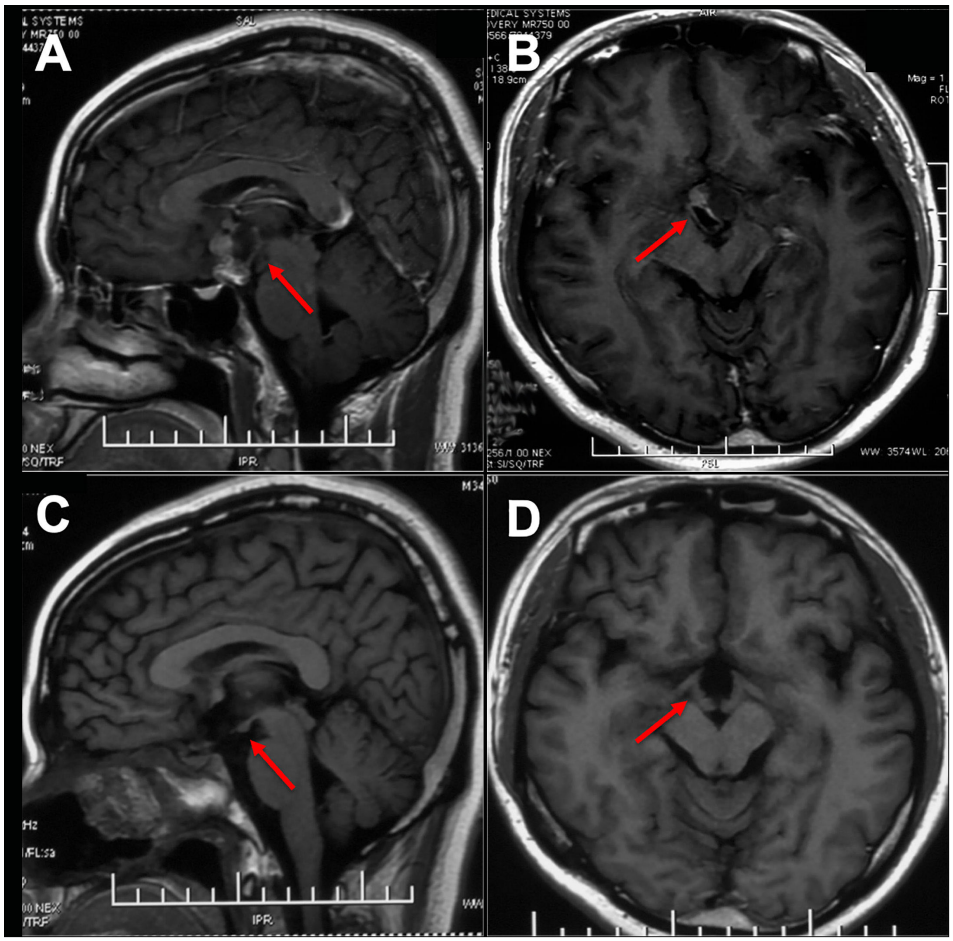

FIGURE 1
Preoperative and postoperative imaging of an intrinsic third ventricle craniopharyngioma with an intact mammillary body was documented ([aken reference from Zhou et al. (74)]. In images **(A, B)**, a cystic and solid lesion was observed in the suprasellar region, while postoperative MR images (**C, D)** displayed the intactness of the optic tract, third ventricle floor, and mammillary bodies.

Given the surgical resection's associated morbidity and the high recurrence rate of ACP post-operation, the amassed clinical data are progressively highlighting the constraints of traditional surgical approaches. Lately, there has been a growing interest in the management of cysts via tumor-focused methods (Table 1). This is primarily due to the potentially lower incidence rate compared to alternative surgical procedures, allowing patients to attain a satisfactory quality of life, particularly those with hydrocephalus (35–37, 75, 77). This staged treatment approach may be more strongly recommended. While the present treatment of ACP through cyst drainage, either independently or in conjunction with other modalities, recently observed clinical outcomes seems to have brought about notable improvements, especially in the patients' quality of life, but there are still some problems several problems. Firstly, the enduring effects on ACP may still be constrained, whether achieved through endoscopic cyst fenestration or basic drainage. The aftermath of these procedures is that cysts are prone to reaccumulate, solid tumors grow, and more importantly, recurrent tumors may complicate the initial treatment. Secondly, in theory, establishing a connection between the cyst cavity and the CSF space to use the CSF flow to reduce cyst reaccumulate may be an ideal way, but no studies have confirmed the exact effectiveness of this approach and it is uncertain whether the enlarged cyst opening will close. Thirdly, given the visual benefits of endoscopy, cysts can potentially be treated more comprehensively under direct visualization (Figure 3). Nevertheless, the extent to which endoscopy can conclusively be identified as a potential factor in reducing the recurrence rate of ACP remains uncertain, and there is still a lack of standardized guidelines for endoscopic therapy techniques. Additionally, there exists a diversity in the techniques for cyst drainage. The likelihood of cyst reformation and the safety of the procedure have not been thoroughly compared across different surgical approaches.

The limitations of the present literature on cyst management of ACP predominantly arise from the varying definitions of cystic recurrence in existing studies, making comparisons between different research endeavors challenging. Additionally, these clinical data primarily originate from patients treated in varying selective settings, often lacking extensive long-term follow-up (22), but these clinical experiences may open up a new potential avenue for the treatment of ACP.

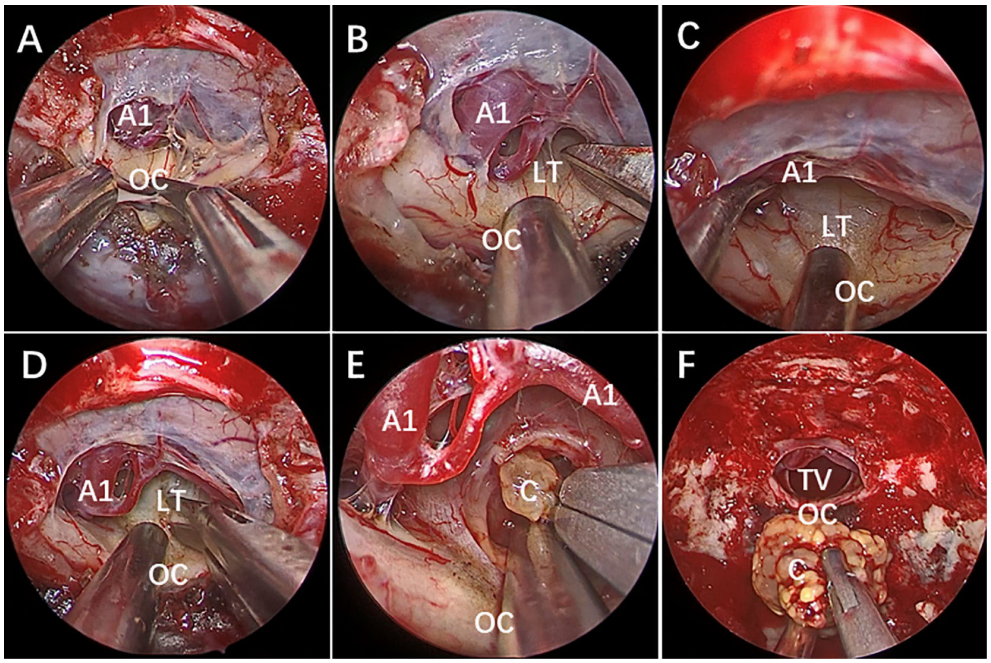

FIGURE 2
Endoscopic endonasal surgery (EES) was performed to remove the third ventricle Craniopharyngioma by STLT approach. [taken reference from Zhou et al. (74)]. **(A)** The optic chiasm exposure after the dura mater opening. **(B)** Lamina terminalis exposure after anterior longitudinal division and anterior circulation artery arachnoid membrane dissection. **(C)** Pulling the optic chiasm downward and the anterior circulation artery system upward to fully exposed the lamina terminalis and the surgical approach, and no tumor was found in the narrow infrachiasmatic space. **(D, E)** The anterior part of the third ventricle tumor was exposed after lamina terminalis incision, and the tumor was debulked and removed using suction tube and grasping forcep piece by piece; **(F)** Complete removal the third ventricle tumor without surgical-related injury. OC, optic chiasm; A1, A1 segment of anterior cerebral artery; LT, lamina terminalis; TV, third ventricle; C, craniopharyngioma.

7.3 Intracystic catheter and reservoir system

Given the potential reaggregation of cysts and the emergence of new clinical symptoms due to cystic occupation, an intracystic catheter and reservoir (such as a Rickham or Ommaya reservoir) are considered for implantation. In the majority of cases, it is feasible to establish a sustainable decompression regimen to address cyst progression (22, 82). Mouss et al. documented 52 patients with cystic craniopharyngioma, and with a minimum follow-up of 7 years, they were astounded to discover that 38 patients (73%) experienced no recurrence of cysts and necessitated no further treatment (81). Various methods for catheter implantation in the capsular cavity exist, encompassing neuroendoscopy, stereotactic techniques, neuronavigation, freehand placement, and intraoperative MRI, among others (81–85). The prevailing trend in development is the emphasis on precision and visualization in catheter placement. Nevertheless, catheter placement may give rise to infrequent complications like infection, bleeding, CSF leakage, catheter obstruction and displacement (32, 81, 82, 86–88). Lau et al. (87) undertook a systematic review of 43 studies and determined that the use of image guidance during implantation resulted in fewer complications compared to procedures without it. In our experience, it is challenging to completely aspirate the cyst contents during the initial surgery and accurately gauge the extent of cyst component removal in the absence of a clear visual field. It is important to note that the high viscosity of the "oil-like" cystic fluid, along with substantial calcification, can hinder later aspiration efforts, potentially necessitating catheter replacement after obstruction. Furthermore, even with precise preoperative positioning, certain rigid or elastic cyst walls may diminish the puncture fault tolerance rate (89), and forceful puncture may result in cystic bleeding (32, 48). However, visualization techniques like endoscopy can mitigate these issues, particularly in the case of polycystic or large craniopharyngiomas that extend into the posterior fossa. Employing a reservoir establishes a secure conduit for intracapsular irradiation and heightens sensitivity to subsequent radiation therapy by facilitating the removal of more fluid.

8 Radiotherapy

Radiotherapy serves as a crucial adjuvant therapy for ACP. Extensive clinical data and meta-analyses indicate that subtotal resection with radiotherapy (STR+RT) may yield tumor control rates similar to, or even superior to, those achieved by GTR, particularly in terms of endocrine outcomes (90–92). The 5-year PFS rates were 67-77% for GTR and 69-73% for STR in combination with radiotherapy (93, 94). Importantly, STR+RT did not elevate the risk of long-term onset or central diabetes insipidus. Notably, there is no substantial disparity in PFS across various radiological techniques (22). Proton therapy offers benefits

TABLE 1 Summary of Cyst Drainage for Cystic Craniopharyngiomas.

Study	Number of cases	Morphology	Drainage method	Radiotherapy	Follow-Up (months)	Recurrence Rate	Complications
Delitala et al., 2004 (78)	7	Cystic	Endoscopy	No	38	28%	No
Tirakotai et al., 2004 (79)	10	Mixed	Endoscopy	No	NA	20% (solid)	No
Schubert et al., 2009 (80)	7	Cystic	Stereotaxy	Yes	118	29%	No
Park et al., 2011 (48)	13	Cystic	Endoscopy	Yes	32	54%	No
Moussa et al., 2012 (81)	52	Cystic	Stereotaxy	No	54	27%	No
Takano et al., 2015 (36)	9	Cystic	Endoscopy	Yes	73	11%	No
Rachinger et al, 2016 (32)	31	Cystic	Stereotaxy	No	51	42%	Intratumo al bleeding (1)
Lauretti et al., 2017 (37)	8	Cystic	Endoscopy	No	56	12.5%	CSF leakage
Frio et al. 2019 (82)	11	Cystic	Endoscopy + Stereotaxy	No	41.4	27.3%	CSF leakage
Hollon et al. 2017 (35)	10	Cystic	Endoscopy	Yes	30	10% (solid)	No
Steiert et al. 2021 (77)	12	Cystic	Stereotaxy	Yes	41	0	Dislocation of the catheter
Chen et al. 2022 (55)	15	Cystic	Endoscopy	No	67	33%	No

CSF, cerebrospinal fluid.

over photon irradiation by minimizing the dosage received by closely situated critical structures, potentially ameliorating both acute and long-term toxic effects of radiation therapy. Findings from a recent single-arm Phase II clinical trial (NCT01419067) evaluating proton therapy in conjunction with limited surgery for craniopharyngioma (RT2CR) in children and adolescents demonstrated that proton therapy led to superior cognitive outcomes compared to photon therapy (95). However, no significant differences were observed in other aspects. However, there are several concerns associated with radiotherapy for ACP: (1) The ideal timing for radiotherapy remains uncertain—whether as an early adjuvant measure or as a salvage intervention. Limited-quality clinical evidence indicates that salvage radiotherapy may elevate the risk of visual and endocrine complications, although it does not confer a survival advantage. (2) Cyst growth is frequently an unpredictable phenomenon (61, 96, 97). Cysts can exhibit either rapid or gradual expansion at any given time, introducing instability in the potential coverage of the target region. Hence, periodic imaging throughout radiotherapy may be imperative to ascertain precise coverage. (3) Given the relative resistance of cysts to radiotherapy, surgical intervention or cyst drainage is often required in most cases to diminish the overall cyst volume, thereby enhancing the efficacy of radiotherapy (36, 48, 86). (4) In cases of mixed cystic and solid tumors, it is possible that solid and cystic components exhibit distinct responses to radiotherapy (98–100). Given the potential autonomy of these components, some studies have explored the combination of stereotactic radiotherapy (SRS) and endovascular radiotherapy as a therapeutic strategy for mixed ACP (101).

9 Intracavitary treatment

9.1 Intracavitary brachytherapy

Intracavitary Brachytherapy (IBT) has demonstrated effectiveness in ACP treatment while minimizing radiation exposure to adjacent normal tissue structures. A recent review (102) illustrated the favorable impact of IBT on cystic craniopharyngiomas. Among 228 patients with purely cystic lesions, 89% exhibited either complete or partial responses. This intervention led to visual and endocrine enhancements of 64% and 20%, respectively. In contrast, mixed cystic tumors showed less favorable outcomes. However, in the most extensive cohort (90 patients) with the lengthiest follow-up period (mean 121 months, ranging from 60 to 192 months), individual ACP patients treated with P32 brachyluminal irradiation exhibited significant results. Specifically, 56 cysts (43.4%) experienced complete regression or remained recurrence-free, while 47 cysts (36.4%) demonstrated a partial response. Five cysts (3.9%) remained stable. Additionally,

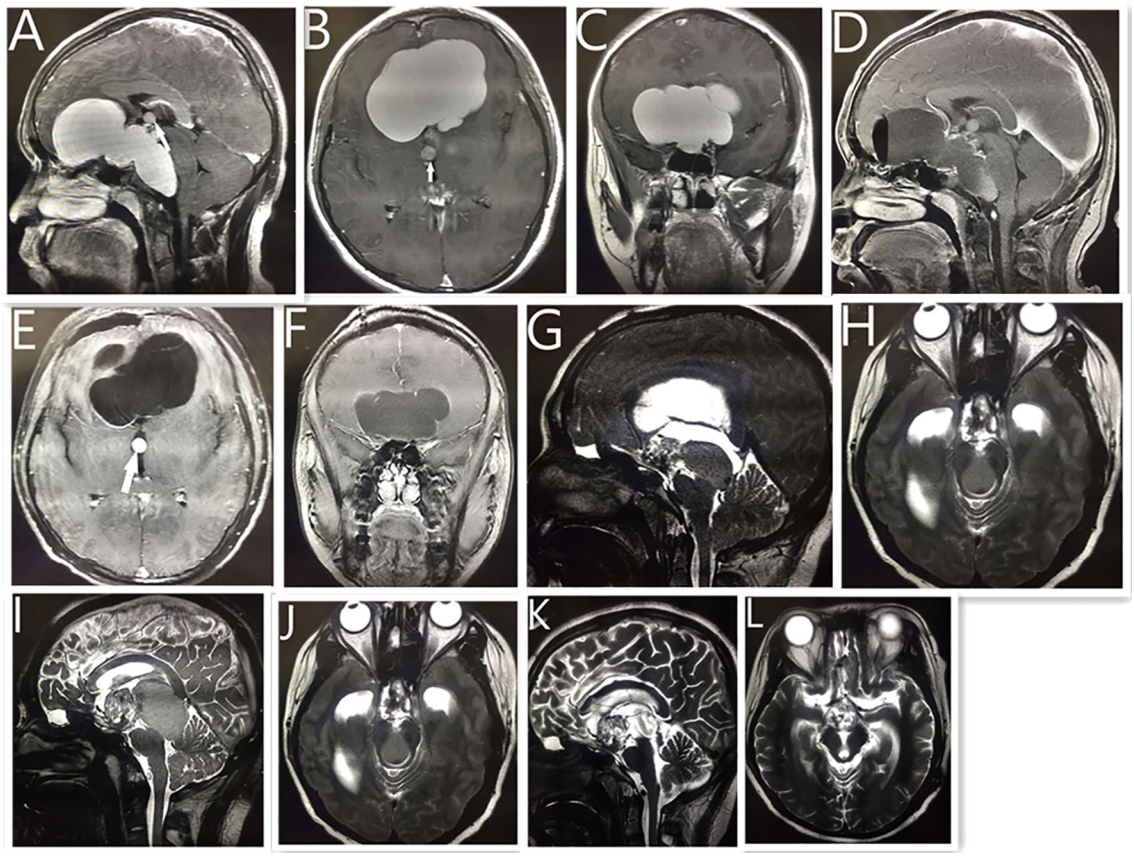

FIGURE 3
Neuroendoscopic treatment of giant cystic craniopharyngioma in a 15-year-old boy. MRI **(A–C)** showing a giant cystic lesion on the front middle, and posterior fossa. White arrow shows small cystic tumor of the third ventricle. Postoperative MRI reveals no obvious cystic tumor after neuroendoscopic surgery **(D–F)**. Five years later, the MRI reveals the previous tumor had disappeared, with a solid lesion on the suprasellar region **(G)** and a cystic lesion compressing the mid brain aqueduct **(H)**, which caused hydrocephalus. The patient received a ventriculoperitoneal shunt, and his condition improved. One year later, MRI reveals **(I, J)** that the tumor had become larger than before. Postoperative MRI reveals that **(K, L)** the cystic lesion disappeared and the midbrain aqueduct opened up after the neuroendoscopic surgery. As of 2 years into follow-up, the size of the remaining tumor had not changed, and the patient had continued to live a normal life.

complications arose in 7 patients (7.8%) (103). In two other extensive series (104, 105) encompassing 53 and 49 patients respectively, 5-year tumor control rates were 86% and 76%. Complications were observed in 5.9% and 6.1% of cases. The aforementioned comprehensive series of studies have demonstrated that IBT stands as a dependable method for treating ACP in the short to medium-term follow-up (Table 2). However, complications occur primarily stemming from radiation-induced damage due to nuclide leakage. Another constraint lies in IBT's reduced efficacy against the solid component of mixed tumors. This elucidates why IBT proves more efficacious in managing purely cystic tumors as opposed to mixed ones.

9.2 Intracavitary chemotherapeutic treatment

An alternative approach to enhance tumor control while minimizing radiation exposure involves exploring alternative intracapsular injection substances, including bleomycin and interferon. In several extensive retrospective studies employing bleomycin (112–114), Follow-up times ranged from 2 to 10 years. patients exhibited complete cyst disappearance rates ranging from 29% to 67%. Most cysts experienced varying degrees of reduction. Nonetheless, patients often experience complications such as headaches, nausea, and vomiting following administration. Simultaneously, nuclide leakage can potentially inflict damage on the hypothalamus and optic nerve, and in severe cases, lead to fatality (115–117). The clinical evidence from three consecutive reviews (118–120) does not favor the utilization of bleomycin in ACP, given the trade-off between benefits and complications. It is recommended that randomized controlled trials employing standardized dosing regimens be conducted to ascertain the safety and efficacy of bleomycin in tumor treatment. In contrast to bleomycin, which is linked to more prevalent adverse reactions in ACP treatment, a recent systematic review of intracapsular drugs for ACP indicated that intratumoral interferon alpha appeared to yield the most favorable response with minimal side effects in ACP treatment when compared to other drugs (121). Cavalheiro et al. conducted a prospective multi-center analysis involving 60 cases of ACP. Clinical and radiological improvements were observed in 76% of cases, with a small

TABLE 2 Review of the literature on Phosphorus-32 use in the treatment of cystic craniopharyngiomas.

Study	NO. of patients	Mean Age (years)	Radiation dose (mean)	Previous treatments	Response	Follow-Up (months)	Complications (N)
POLLACK, et al. 1988 (106)	9	–	200-300Gy	Surgery (22.2%)	Complete (22.2%) Partial (77.8%)	27	None
POLLOCK, et al., 1995 (107)	30	26	253Gy	Surgery (50%) RT (33.3%)	Complete (10%) Partial (83.3%) Stable (3%) Progression (20%)	37	VA (2), DI (2), AB (3)
Shahzadi et al. 2008 (108)	22	14	250Gy	Surgery (95.4%) RT (45.5%)	Complete (27.2%) Partial (45.5%) Stable (18.2%)	10.5	None
Zhao et al., 2009 (60)	20	6.2	400-500Gy	Surgery (58.8%)	Complete (30%) Partial (70%)	47.7	None
Barriger et al., 2011 (109)	19	20	290.5Gy	Surgery (63.2%) RT (5%)	Complete (5%) Partial (26.3%) Stable (10.5%) Progression (57.9%)	62	None
Hasegawa et al., 2011 (104)	41	29	224Gy	Surgery (52.8%) RT (24%)	Complete (17%) Partial (58.5 %) Stable (12.2 %) Progression (12.2%)	60	VA (3) DI (3)
Yu et al., 2014 (110)	20	6.7	150Gy	Surgery (15%) RT (5%)	Complete (60%) Partial (40%)	48.6	None
Maarouf, et al, 2015 (111)	17	15.4	200Gy	Surgery (58.8%) RT (17.6%)	Complete (5%) Partial (29.4%) Stable (17.6%) Progression (17.6%)	61.9	None
Kickingerer, et al., 2021 (105)	53	31.1	200Gy	Surgery (28) RT (18.9%)	Complete (29.4 %) Partial (52.9 %) Stable (5.9 %) Progression (11.8 %)	60.2	Hemiparesis (1) TNP (1)
Yu et al., 2021 (103)	90	36.6	250Gy	Surgery (61%) RT (15.6%)	Complete (43.4%) Partial (36.4%) Stable (3.9%)	121	VA (4), TNP (2), CAO (1)

VA, Visual abnormalities; TNP, Third nerve palsy; CAO, Carotid artery occlusion; DI, Diabetes insipidus; AB, Abnormal behaviour.

subset of patients experiencing minor side effects like mild headaches and eyelid edema (122). Kilday (123) et al. conducted a clinical trial involving 56 children from 21 international centers. Among them, 43 (77%) patients had received other treatments prior to interferon. Intracapsular interferon was found to impede further tumor progression compared to previous treatments. Following interferon therapy, 42 patients experienced progression (median time of 14 months; range of 0-8 years). The estimated median time to reach the final treatment after interferon therapy was 5.8 years (ranging from 1.8 to 9.7 years), and significant side effects were infrequent. However, the recently published National UK guidelines for the management of pediatric craniopharyngioma do not provide adequate evidence to endorse IFNα as the preferred first-line treatment option. Additionally, intracystic bleomycin and radioisotopes lack robust support as the primary strategies for ACP treatment (124).

10 Target therapies

As our understanding of ACP's pathogenesis advances, there is a growing optimism regarding the clinical application of targeted drugs aimed at the growth and molecular pathways associated with ACP. MEK inhibitors have demonstrated the ability to decrease tumor cell count, inhibit cell proliferation, and induce apoptosis by impeding the MAPK/ERK signal transduction pathways Park (125). In a compassionate treatment approach, a 26-year-old woman, previously subjected to multiple surgeries, received binimetinib for 8 months, resulting in a reduction in tumor volume. Although the reduction was not notably substantial, this case presents additional avenues for MEK as a potential target in ACP treatment (126). Simultaneously, drugs targeting IL-6 appear to elicit a more substantial reduction in volume during ACP treatment (127). Two patients with recurrent ACP experienced noteworthy reductions in tumor volume after receiving either tocilizumab or a combination of tocilizumab and bevacizumab. At present, the targeted therapy for the above targets has shown an optimistic attitude in the treatment of ACP for the time being, but further clinical and basic research is still needed to determine their specific efficacy in the treatment of ACP.

11 Childhood-onset craniopharyngioma

Childhood-onset craniopharyngioma predominantly manifests as Adamantinomatous Craniopharyngioma (ACP), showing a combination of cystic, solid, and calcified components (128). In contrast to the adult CP, its diagnosis often occurs late, featuring clinical indications like increased intracranial pressure, alongside endocrine deficits and visual impairment (5). Therapeutic strategies for childhood-onset CP encompass surgical resection, radiotherapy, cyst aspiration, and intracavitary chemotherapy. However, recent guidelines lack a clearly defined optimal treatment plan (124). Surgical outcome is often associated with a high recurrence rate. A comprehensive review (93) involving 109 studies and 532 cases of childhood-onset CP undergoing surgical resection revealed recurrences in 377 cases. The 5-year progression-free survival for GTR, STR+XRT, and STR alone stood at 77%, 73%, and 43%, respectively. GTR and STR+XRT exhibit similar tumor control rates, with GTR demonstrating relatively superior tumor control effects compared to STR alone. However, adjuvant radiotherapy is often employed as a salvage measure.

In the past, the use of the Endoscopic Endonasal Approach (EEA) in pediatric Craniopharyngioma (CP) appeared controversial due to unique considerations in children's nasal anatomy and the risk of CSF leakage. However, a recent systematic review of pediatric CP seems to challenge this perception (129). This review encompassed 835 patients underwent TCA (18 articles) and 403 patients underwent EEA (19 articles), indicating a rising preference for EEA in pediatric CP, showing favorable outcomes. Analysis from the study showed EEA as the preferred approach ($p = 0.006$, PI = 26.8-70.8, $I2 = 40\%$) for sellar-suprasellar CPs, while TCA was favored for purely suprasellar CPs ($p = 0.007$, PI = 13.5-81.1, $I2 = 61\%$). However, no significant difference was observed between the approaches for purely intrasellar lesions ($p = 0.94$, PI = 0-62.7, $I2 = 26\%$).

Recent two single-center retrospective studies further highlighted the feasibility and safety of EEA in treating pediatric midline CP (130, 131). In a cohort of 25 patients, a GTR reached 92%, with a tumor recurrence rate of 19% over a mean follow-up of 72 ± 67 months, and panhypopituitarism was the most common complication (92%) (130). Another study comparing EEA (35 patients) and TCA (16 patients) in pediatric midline CP found comparable tumor control and surgical complication rates between the approaches (131). Additionally, EEA may be associated with better visual and endocrine outcomes. This shifting preference underscores the increasing role and acceptance of EEA in managing pediatric CP.

While intracavitary chemotherapy or cyst aspiration generally show greater efficacy than conservative approaches, their PFS have not been well described compared to surgical resection in existing literature. In cases of childhood-onset CP accompanied by hydrocephalus, a staged approach involving minimally invasive cyst decompression followed by cyst aspiration or tumor resection is recommended to mitigate clinical risks and achieve effective tumor control (124).

CP invasion into the hypothalamus or surgical injury often leads to the development of hypothalamic syndrome, encompassing hypothalamic obesity and neuropsychological deficits (132). For patients with definite hypothalamic involvement, STR combined with postoperative radiotherapy is recommended to reduce the incidence of long-term obesity without increasing the recurrence rate (133). Accurate preoperative grading of hypothalamic involvement stands pivotal in shaping surgical strategies and preventing hypothalamic injury. Several different hypothalamic grading systems have been developed in the past (19), including recent applications of machine learning in predicting ACP invasiveness through radiomic methodologies (134). Advancements in imaging modalities, such as 7-T MRI or fMRI, significantly enhance hypothalamic structure visualization, aiding neurosurgeons in precise surgical resection. Despite recent enhancements in understanding hypothalamic syndrome, effective pharmaceutical interventions for hypothalamic obesity remain elusive, and data on treating neurocognitive deficits in childhood-onset CP are insufficient (5). Consequently, an effective remedy for hypothalamic syndrome, posing a significant challenge in childhood-onset CP treatment, remains absent. Future research should prioritize exploring the molecular mechanisms underlying CP invasion of the hypothalamus to develop strategies for preventing and treating hypothalamic syndrome.

12 Conclusion

Adamantomatous craniopharyngioma (ACP) represents a complex intracranial tumor. Despite significant strides in ACP

research and treatment over the past three decades, achieving full control of this often-termed "most challenging brain tumor" remains elusive. Recent clinical perspectives have shifted towards managing cysts and treating ACP as a chronic neurosurgical condition, emphasizing the importance of achieving a high-quality, long-term life for patients. This may open up a new potential avenue for ACP treatment. However, the long-term risks of cyst reaggregation and tumor recurrence still need to be fully evaluated. The primary objective in ACP treatment remains the amalgamation of maximal safe resection with radiation therapy, ongoing cyst decompression, and pharmacotherapy to balance long-term tumor control and quality of life. Simultaneously, owing to ACP's relative rarity and the tumor's heterogeneity, conducting clinical and foundational trials to bolster international collaboration across diverse nations will significantly enhance our comprehensive comprehension of this condition.

Author contributions

AC: Writing – original draft, Writing – review & editing, Conceptualization, Data curation. MA: Data curation. TS: Resources, Supervision.

Funding

The author(s) declare that no financial support was received for the research, authorship, and/or publication of this article.

Acknowledgments

The authors thank Hui Luo for her useful suggestions and language modification.

Conflict of interest

The authors declare that the research was conducted in the absence of any commercial or financial relationships that could be construed as a potential conflict of interest.

Publisher's note

References

1. Goldberg GM, Eshbaugh DE. Squamous cell nests of the pituitary gland as related to the origin of craniopharyngiomas. A study of their presence in the newborn and infants up to age four. *Arch Pathol* (1960) 70:293–9.

2. Karavitaki N, Cudlip S, Adams CB, Wass JA. Craniopharyngiomas. *Endocrine Rev* (2006) 27(4):371–97. doi: 10.1210/er.2006-0002

3. Johnson LN, Hepler RS, Yee RD, Frazee JG, Simons KB. Magnetic resonance imaging of craniopharyngioma. *Am J Ophthalmol* (1986) 102(2):242–4. doi: 10.1016/0002-9394(86)90152-2

4. Nielsen EH, Feldt-Rasmussen U, Poulsgaard L, Kristensen LO, Astrup J, Jørgensen JO, et al. Incidence of craniopharyngioma in Denmark (n = 189) and estimated world incidence of craniopharyngioma in children and adults. *J neuro-oncology* (2011) 104(3):755–63. doi: 10.1007/s11060-011-0540-6

5. Müller HL, Merchant TE, Warmuth-Metz M, Martinez-Barbera JP, Puget S. Craniopharyngioma. *Nat Rev Dis Primers* (2019) 5(1):75. doi: 10.1038/s41572-019-0125-9

6. Weiner HL, Wisoff JH, Rosenberg ME, Kupersmith MJ, Cohen H, Zagzag D, et al. Craniopharyngiomas: a clinicopathological analysis of factors predictive of recurrence and functional outcome. *Neurosurgery* (1994) 35(6):1001–11. doi: 10.1227/00006123-199412000-00001

7. Martinez-Barbera JP, Buslei R. Adamantinomatous craniopharyngioma: pathology, molecular genetics and mouse models. *J Pediatr Endocrinol Metab JPEM* (2015) 28(1-2):7–17. doi: 10.1515/jpem-2014-0442

8. Drapeau A, Walz PC, Eide JG, Rugino AJ, Shaikhouni A, Mohyeldin A, et al. Pediatric craniopharyngioma. *Child's nervous system* (2019) 35(11):2133–2145. doi: 10.1007/s00381-019-04300-2

9. Bi WL, Santagata S. Skull base tumors: neuropathology and clinical implications. *Neurosurgery* (2022) 90(3):243–61. doi: 10.1093/neuros/nyab209

10. Hengartner AC, Prince E, Vijmasi T, Hankinson TC. Adamantinomatous craniopharyngioma: moving toward targeted therapies. *Neurosurgical Focus* (2020) 48(1):E7. doi: 10.3171/2019.10.FOCUS19705

11. Henderson J.R. F, Schwartz TH. Update on management of craniopharyngiomas. *J neuro-oncology* (2022) 156(1):97–108. doi: 10.1007/s11060-021-03906-4

12. Pascual JM, Rosdolsky M, Prieto R, Winter E, Ulrich W. Jakob Erdheim (1874-1937): father of hypophyseal-duct tumors (craniopharyngiomas). *Virchows Archiv an Int J Pathol* (2015) 467(4):459–69. doi: 10.1007/s00428-015-1798-4

13. Li S, Wu B, Xiao Y, Wu J, Yang L, Yang C, et al. Exploring the pathological relationships between adamantinomatous craniopharyngioma and contiguous structures with tumor origin. *J neuro-oncology* (2022) 159(2):485–97. doi: 10.1007/s11060-022-04084-7

14. Campanini ML, Colli LM, Paixao BM, Cabral TP, Amaral FC, MaChado HR, et al. CTNNB1 gene mutations, pituitary transcription factors, and MicroRNA expression involvement in the pathogenesis of adamantinomatous craniopharyngiomas. *Hormones Cancer* (2010) 1(4):187–96. doi: 10.1007/s12672-010-0041-7

15. Semba S, Han SY, Ikeda H, Horii A. Frequent nuclear accumulation of beta-catenin in pituitary adenoma. *Cancer* (2001) 91(1):42–8. doi: 10.1002/1097-0142(20010101)91:1<42::aid-cncr6>3.0.co;2-7

16. Hölsken A, Buchfelder M, Fahlbusch R, Blümcke I, Buslei R. Tumour cell migration in adamantinomatous craniopharyngiomas is promoted by activated Wnt-signalling. *Acta neuropathologica* (2010) 119(5):631–9. doi: 10.1007/s00401-010-0642-9

17. Gaston-Massuet C, Andoniadou CL, Signore M, Jayakody SA, Charolidi N, Kyeyune R, et al. Increased Wingless (Wnt) signaling in pituitary progenitor/stem cells gives rise to pituitary tumors in mice and humans. *Proc Natl Acad Sci United States America* (2011) 108(28):11482–7. doi: 10.1073/pnas.1101553108

18. Andoniadou CL, Matsushima D, Mousavy Gharavy SN, Signore M, Mackintosh AI, Schaeffer M, et al. Sox2(+) stem/progenitor cells in the adult mouse pituitary support organ homeostasis and have tumor-inducing potential. *Cell Stem Cell* (2013) 13(4):433–45. doi: 10.1016/j.stem.2013.07.004

19. Apps JR, Muller HL, Hankinson TC, Yock TI, Martinez-Barbera JP. Contemporary biological insights and clinical management of craniopharyngioma. *Endocrine Rev* (2023) 44(3):518–38. doi: 10.1210/endrev/bnac035

20. Desiderio C, Rossetti DV, Castagnola M, Massimi L, Tamburrini G. Adamantinomatous craniopharyngioma: advances in proteomic research. *Child's nervous system* (2021) 37(3):789–97. doi: 10.1007/s00381-020-04750-z

21. Donson AM, Apps J, Griesinger AM, Amani V, Witt DA, Anderson RCE, et al. Advancing Treatment for Pediatric Craniopharyngioma Consortium. Molecular analyses reveal inflammatory mediators in the solid component and cyst fluid of human adamantinomatous craniopharyngioma. *J neuropathology Exp Neurol* (2017) 76(9):779–88. doi: 10.1093/jnen/nlx061

22. Bianchi F, Benato A, Massimi L. Treatment of cystic craniopharyngiomas: an update. *Adv Tech standards Neurosurg* (2022) 45:139–76. doi: 10.1007/978-3-030-99166-1_4

23. Apps JR, Carreno G, Gonzalez-Meljem JM, Haston S, Guiho R, Cooper JE, et al. Tumour compartment transcriptomics demonstrates the activation of inflammatory and odontogenic programmes in human adamantinomatous craniopharyngioma and identifies the MAPK/ERK pathway as a novel therapeutic target. *Acta neuropathologica* (2018) 135(5):757–77. doi: 10.1007/s00401-018-1830-2

24. Pettorini BL, Inzitari R, Massimi L, Tamburrini G, Caldarelli M, Fanali C, et al. The role of inflammation in the genesis of the cystic component of craniopharyngiomas. *Child's nervous system ChNS Off J Int Soc Pediatr Neurosurg* (2010) 26(12):1779–84. doi: 10.1007/s00381-010-1245-4

25. Rushing EJ, Wesseling P. Towards an integrated morphological and molecular WHO diagnosis of central nervous system tumors: a paradigm shift. *Curr Opin Neurol* (2015) 28(6):628–32. doi: 10.1097/WCO.0000000000000258

26. Okada T, Fujitsu K, Ichikawa T, Miyahara K, Tanino S, Niino H, et al. Unicystic ameloblastomatoid cystic craniopharyngioma: pathological discussion and clinical significance of cyst formation in adamantinomatous craniopharyngioma. *Pediatr Neurosurg* (2016) 51(3):158–63. doi: 10.1159/000442992

27. Burger P, Scheithauer B, Vogel F. *Surgical pathology of the nervous system and its coverings. 4th edn*. Philadelphia: Churchill Livingstone (2002).

28. Schmalisch K, Beschorner R, Psaras T, Honegger J. Postoperative intracranial seeding of craniopharyngiomas–report of three cases and review of the literature. *Acta neurochirurgica* (2010) 152(2):313–9. doi: 10.1007/s00701-009-0538-4

29. Yang Y, Shrestha D, Shi XE, Zhou Z, Qi X, Qian H. Ectopic recurrence of craniopharyngioma: Reporting three new cases. *Br J Neurosurg* (2015) 29(2):295–7. doi: 10.3109/02688697.2014.967751

30. Gabel BC, Cleary DR, Martin JR, Khan U, Snyder V, Sang U H. Unusual and rare locations for craniopharyngiomas: clinical significance and review of the literature. *World Neurosurg* (2017) 98:381–7. doi: 10.1016/j.wneu.2016.10.134

31. Renfrow JJ, Greeneway GP, Carter L, Couture DE. Intraventricular recurrence of a craniopharyngioma: case report. *J neurosurgery. Pediatr* (2018) 22(4):393–6. doi: 10.3171/2018.4.PEDS18112

32. Rachinger W, Oehlschlaegel F, Kunz M, Fuetsch M, Schichor C, Thurau S, et al. Cystic craniopharyngiomas: microsurgical or stereotactic treatment? *Neurosurgery* (2017) 80(5):733–43. doi: 10.1227/NEU.0000000000001408

33. Piloni M, Gagliardi F, Bailo M, Losa M, Boari N, Spina A, et al. Craniopharyngioma in pediatrics and adults. *Adv Exp Med Biol* (2023) 1405:299–329. doi: 10.1007/978-3-031-23705-8_11

34. Prieto R, Pascual JM, Barrios L. Optic chiasm distortions caused by craniopharyngiomas: clinical and magnetic resonance imaging correlation and influence on visual outcome. *World Neurosurg* (2015) 83(4):500–29. doi: 10.1016/j.wneu.2014.10.002

35. Hollon TC, Savastano LE, Altshuler D, Barkan AL, Sullivan SE. Ventriculoscopic surgery for cystic retrochiasmatic craniopharyngiomas: indications, surgical technique, and short-term patient outcomes. *Operative Neurosurg (Hagerstown Md.)* (2018) 15 (2):109–19. doi: 10.1093/ons/opx220

36. Takano S, Akutsu H, Mizumoto M, Yamamoto T, Tsuboi K, Matsumura A. Neuroendoscopy followed by radiotherapy in cystic craniopharyngiomas–a long-term follow-up. *World Neurosurg* (2015) 84(5):1305–15.e152. doi: 10.1016/j.wneu.2015.06.022

37. Lauretti L, Legninda Sop FY, Pallini R, Fernandez E, D'Alessandris QG. Neuroendoscopic treatment of cystic craniopharyngiomas: A case series with systematic review of the literature. *World Neurosurg* (2018) 110:e367–73. doi: 10.1016/j.wneu.2017.11.004

38. Mohd-Ilham IM, Ahmad-Kamal GR, Wan Hitam WH, Shatriah I. Visual presentation and factors affecting visual outcome in children with craniopharyngioma in east coast states of peninsular Malaysia: A five-year review. *Cureus* (2019) 11(4):e4407. doi: 10.7759/cureus.4407

39. Wan MJ, Zapotocky M, Bouffet E, Bartels U, Kulkarni AV, Drake JM. Long-term visual outcomes of craniopharyngioma in children. *J neuro-oncology* (2018) 137 (3):645–51. doi: 10.1007/s11060-018-2762-3

40. Chen C, Okera S, Davies PE, Selva D, Crompton JL. Craniopharyngioma: a review of long-term visual outcome. *Clin Exp Ophthalmol* (2003) 31(3):220–8. doi: 10.1046/j.1442-9071.2003.00648.x

41. Qiao N, Yang X, Li C, Ma G, Kang J, Liu C, et al. The predictive value of intraoperative visual evoked potential for visual outcome after extended endoscopic endonasal surgery for adult craniopharyngioma. *J Neurosurg* (2021) 135(6):1714–24. doi: 10.3171/2020.10.JNS202779

42. Zhou Z, Zhang S, Hu F. Endocrine disorder in patients with craniopharyngioma. *Front Neurol* (2021) 12:737743. doi: 10.3389/fneur.2021.737743

43. Van Effenterre R, Boch AL. Craniopharyngioma in adults and children: a study of 122 surgical cases. *J Neurosurg* (2002) 97(1):3–11. doi: 10.3171/jns.2002.97.1.0003

44. Elliott RE, Jane JAJR, Wisoff JH. Surgical management of craniopharyngiomas in children: meta-analysis and comparison of transcranial and transsphenoidal approaches. *Neurosurgery* (2011) 69(3):630–43. doi: 10.1227/NEU.0b013e31821a872d

45. Muller HL. Childhood craniopharyngioma. Recent advances in diagnosis, treatment and follow-up. *Hormone Res* (2008) 69(4):193–202. doi: 10.1159/000113019

46. Hoffman HJ, De Silva M, Humphreys RP, Drake JM, Smith ML, Blaser SI. Aggressive surgical management of craniopharyngiomas in children. *J Neurosurg* (1992) 76(1):47–52. doi: 10.3171/jns.1992.76.1.0047

47. Mende KC, Kellner T, Petersenn S, Honegger J, Evangelista-Zamora R, Droste M, et al. Clinical situation, therapy, and follow-up of adult craniopharyngioma. *J Clin Endocrinol Metab* (2020) 105(1):dgz043. doi: 10.1210/clinem/dgz043

48. Park YS, Chang JH, Park YG, Kim DS. Recurrence rates after neuroendoscopic fenestration and Gamma Knife surgery in comparison with subtotal resection and Gamma Knife surgery for the treatment of cystic craniopharyngiomas. *J Neurosurg* (2011) 114(5):1360–8. doi: 10.3171/2009.9.JNS09301

49. Eveslage M, Calaminus G, Warmuth-Metz M, Kortmann RD, Pohl F, Timmermann B, et al. The postopera tive quality of life in children and adolescents with craniopharyngioma. *Deutsches Arzteblatt Int* (2019) 116(18):321–8. doi: 10.3238/arztebl.2019.0321

50. Hetelekidis S, Barnes PD, Tao ML, Fischer EG, Schneider L, Scott RM, et al. 20-year experience in childhood craniopharyngioma. *Int J Radiat oncology biology Phys* (1993) 27(2):189–95. doi: 10.1016/0360-3016(93)90227-m

51. Sun F, Sun X, Du X, Xing H, Yang B. Factors related to endocrine changes and hormone substitution treatment during pre- and post-operation stages in craniopharyngioma. *Oncol Lett* (2017) 13(1):250–2. doi: 10.3892/ol.2016.5418

52. Chakrabarti I, Amar AP, Couldwell W, Weiss MH. Long-term neurological, visual, and endocrine outcomes following transnasal resection of craniopharyngioma. *J Neurosurg* (2005) 102(4):650–7. doi: 10.3171/jns.2005.102.4.0650

53. Marx S, Tsavdaridou I, Paul S, Steveling A, Schirmer C, Eördögh M, et al. Quality of life and olfactory function after suprasellar craniopharyngioma surgery-a single-center experience comparing transcranial and endoscopic endonasal approaches. *Neurosurgical Rev* (2021) 44(3):1569–82. doi: 10.1007/s10143-020-01343-x

54. Schreckinger M, Walker B, Knepper J, Hornyak M, Hong D, Kim JM, et al. Post-operative diabetes insipidus after endoscopic transsphenoidal surgery. *Pituitary* (2013) 16(4):445–51. doi: 10.1007/s11102-012-0453-1

55. Chen A, Zhou R, Yao X, Tong Z, Li J, Xiang R, et al. Neuroendoscopic surgery combined with Ommaya reservoir placement for cystic craniopharyngiomas: 11 years of experience in a single institution. *Br J Neurosurg* (2022), 1–7. doi: 10.1080/02688697.2022.2152776

56. Young SC, Zimmerman RA, Nowell MA, Bilaniuk LT, Hackney DB, Grossman RI, et al. Giant cystic craniopharyngiomas. *Neuroradiology* (1987) 29(5):468–73. doi: 10.1007/BF00341745

57. Chen A, Zhou R, Yao X, Ai M, Sun T. Neuroendoscopic treatment of giant cystic craniopharyngioma in the foramen magnum: report of two cases. *Child's nervous system* (2021) 37(7):2387–90. doi: 10.1007/s00381-020-04965-0

58. Kiran NA, Suri A, Kasliwal MK, Garg A, Ahmad FU, Mahapatra AK. Gross total excision of pediatric giant cystic craniopharyngioma with huge retroclival extension to the level of foramen magnum by anterior trans petrous approach: report of two cases and review of literature. *Child's nervous system* (2008) 24(3):385–91. doi: 10.1007/s00381-007-0522-3

59. Connolly J.R. ES, Winfree CJ, Carmel PW. Giant posterior fossa cystic craniopharyngiomas presenting with hearing loss. Report of three cases and review of the literature. *Surg Neurol* (1997) 47(3):291–9. doi: 10.1016/s0090-3019(96)00253-4

60. Zhao R, Deng J, Liang X, Zeng J, Chen X, Wang J. Treatment of cystic craniopharyngioma with phosphorus-32 intracavitary irradiation. *Child's nervous system* (2010) 26(5):669–74. doi: 10.1007/s00381-009-1025-1

61. Moorthy RK, Backianathan S, Rebekah G, Rajshekhar V. Utility of interval imaging during focused radiation therapy for residual cystic craniopharyngiomas. *World Neurosurg* (2020) 141:e615–24. doi: 10.1016/j.wneu.2020.05.258

62. Buhl R, Lang EW, Barth H, Mehdorn HM. Giant cystic craniopharyngiomas with extension into the posterior fossa. *Child's nervous system* (2000) 16(3):138–42. doi: 10.1007/s003810050480

63. Goyal A, Singh AK, Sinha S. Giant cystic craniopharyngioma with posterior fossa extension. *Pediatr Neurosurg* (2002) 37(1):50–1. doi: 10.1159/000065103

64. Gangemi M, Seneca V, Mariniello G, Colella G, Magro F. Combined endoscopic and microsurgical removal of a giant cystic craniopharyngioma in a six-year-old boy. *Clin Neurol Neurosurg* (2009) 111(5):472–6. doi: 10.1016/j.clineuro.2009.01.002

65. Sener RN, Kismali E, Akyar S, Selcuki M, Yalman O. Large craniopharyngioma extending to the posterior cranial fossa. *Magnetic resonance Imaging* (1997) 15 (9):1111–2. doi: 10.1016/s0730-725x(97)00137-9

66. Akinduro OO, Izzo A, Lu VM, Ricciardi L, Trifiletti D, Peterson JL, et al. Endocrine and visual outcomes following gross total resection and subtotal resection of adult craniopharyngioma: systematic review and meta-analysis. *World Neurosurg* (2019) 127:e656–68. doi: 10.1016/j.wneu.2019.03.239

67. Locatelli D, Massimi L, Rigante M, Custodi V, Paludetti G, Castelnuovo P, et al. Endoscopic endonasal transsphenoidal surgery for sellar tumors in children. *Int J Pediatr otorhinolaryngology* (2010) 74(11):1298–302. doi: 10.1016/j.ijporl.2010.08.009

68. Ceylan S, Caklili M, Emengen A, Yilmaz E, Anik Y, Selek A, et al. An endoscopic endonasal approach to craniopharyngioma via the infrachiasmatic corridor: a single center experience of 84 patients. *Acta neurochirurgica* (2021) 163(8):2253–68. doi: 10.1007/s00701-021-04832-0

69. Fong RP, Babu CS, Schwartz TH. Endoscopic endonasal approach for craniopharyngiomas. *J neurosurgical Sci* (2021) 65(2):133–9. doi: 10.23736/S0390-5616.21.05097-9

70. Cossu G, Jouanneau E, Cavallo LM, Elbabaa SK, Giammattei L, Starnoni D, et al. Surgical management of craniopharyngiomas in adult patients: a systematic review and

consensus statement on behalf of the EANS skull base section. *Acta neurochirurgica* (2020) 162(5):1159–77. doi: 10.1007/s00701-020-04265-1

71. Na MK, Jang B, Choi KS, Lim TH, Kim W, Cho Y, et al. Craniopharyngioma resection by endoscopic endonasal approach versus transcranial approach: A systematic review and meta-analysis of comparative studies. *Front Oncol* (2022) 12:1058329. doi: 10.3389/fonc.2022.1058329

72. Qiao N, Li C, Liu F, Ru S, Cai K, Jia Y, et al. Risk factors for cerebrospinal fluid leak after extended endoscopic endonasal surgery for adult patients with craniopharyngiomas: a multivariate analysis of 364 cases. *J Neurosurg* (2023), 1–12. doi: 10.3171/2023.5.JNS222791

73. Cavallo LM, Frank G, Cappabianca P, Solari D, Mazzatenta D, Villa A, et al. The endoscopic endonasal approach for the management of craniopharyngiomas: a series of 103 patients. *J Neurosurg* (2014) 121(1):100–13. doi: 10.3171/2014.3.JNS131521

74. Zhou Y, Wei J, Jin T, Hei Y, Jia P, Lin J, et al. Extended endoscopic endonasal approach for resecting anterior intrinsic third ventricular craniopharyngioma. *Front Oncol* (2022) 12:998683. doi: 10.3389/fonc.2022.998683

75. Shoubash LI, El Refaee E, Al Menabbawy A, Refaat MI, Fathalla H, Schroeder HWS. Endoscopic transcortical-transventricular approach in treating third ventricular craniopharyngiomas-case series with technical note and literature review. *Operative Neurosurg (Hagerstown Md.)* (2022) 22(4):192–200. doi: 10.1227/ONS.0000000000000114

76. Cavallo LM, Solari D, Esposito F, Cappabianca P. The endoscopic endonasal approach for the management of craniopharyngiomas involving the third ventricle. *Neurosurgical Rev* (2013) 36(1):27–38. doi: 10.1007/s10143-012-0403-4

77. Steiert C, Grauvogel J, Roelz R, Demerath T, Schnell D, Beck J, et al. Stereotactic cysto-ventricular catheters in craniopharyngiomas: an effective minimally invasive method to improve visual impairment and achieve long-term cyst volume reduction. *Neurosurgical Rev* (2021) 44(6):3411–20. doi: 10.1007/s10143-021-01510-8

78. Delitala A, Brunori A, Chiappetta F. Purely neuroendoscopic transventricular management of cystic craniopharyngiomas. *Child's nervous system* (2004) 20(11-12):858–62. doi: 10.1007/s00381-004-0943-1

79. Tirakotai W, Schulte DM, Bauer BL, Bertalanffy H, Hellwig D. Neuroendoscopic surgery of intracranial cysts in adults. *Child's nervous system* (2004) 20(11-12):842–51. doi: 10.1007/s00381-004-0941-3

80. Schubert T, Trippel M, Tacke U, van Velthoven V, Gumpp V, Bartelt S, et al. Neurosurgical treatment strategies in childhood craniopharyngiomas: is less more? *Child's nervous system* (2009) 25(11):1419–27. doi: 10.1007/s00381-009-0978-4

81. Moussa AH, Kerasha AA, Mahmoud ME. Surprising outcome of ommaya reservoir in treating cystic craniopharyngioma: a retrospective study. *Br J Neurosurg* (2013) 27(3):370–3. doi: 10.3109/02688697.2012.741732

82. Frio F, Solari D, Cavallo LM, Cappabianca P, Raverot G, Jouanneau E. Ommaya reservoir system for the treatment of cystic craniopharyngiomas: surgical results in a series of 11 adult patients and review of the literature. *World Neurosurg* (2019) 132: e869–77. doi: 10.1016/j.wneu.2019.07.217

83. Wang A, Tenner MS, Tobias ME, Mohan A, Kim D, Tandon A. A novel approach using electromagnetic neuronavigation and a flexible neuroendoscope for placement of ommaya reservoirs. *World Neurosurg* (2016) 96:195–201. doi: 10.1016/j.wneu.2016.08.127

84. Mori R, Joki T, Nonaka Y, Ikeuchi S, Abe T. Parallel insertion endoscopic technique for precise catheter placement in cystic craniopharyngiomas. *J neurological surgery. Part A Cent Eur Neurosurg* (2014) 75(6):442–6. doi: 10.1055/s-0033-1349341

85. Vitaz TW, Hushek S, Shields CB, Moriarty T. Changes in cyst volume following intraoperative MRI-guided Ommaya reservoir placement for cystic craniopharyngioma. *Pediatr Neurosurg* (2001) 35(5):230–4. doi: 10.1159/000050427

86. Liu X, Yu Q, Zhang Z, Zhang Y, Li Y, Liu D, et al. Same-day stereotactic aspiration and Gamma Knife surgery for cystic intracranial tumors. *J Neurosurg* (2012) 117 Suppl:45–8. doi: 10.3171/2012.7.GKS121019

87. Lau JC, Kosteniuk SE, Walker T, Iansavichene A, Macdonald DR, Megyesi JF. Operative complications with and without image guidance: A systematic review and meta-analysis of the ommaya reservoir literature. *World Neurosurg* (2019) 122:404–14. doi: 10.1016/j.wneu.2018.11.036

88. Pettorini BL, Tamburrini G, Massimi L, Caldarelli M, Di Rocco C. Endoscopic transventricular positioning of intracystic catheter for treatment of craniopharyngioma. *Tech note. J neurosurgery. Pediatr* (2009) 4(3):245–8. doi: 10.3171/2009.4.PEDS0978

89. Sampath R, Wadhwa R, Tawfik T, Nanda A, Guthikonda B. Stereotactic placement of ventricular catheters: does it affect proximal malfunction rates? *Stereotactic Funct Neurosurg* (2012) 90(2):97–103. doi: 10.1159/000333831

90. Wang G, Zhang X, Feng M, Guo F. Comparing survival outcomes of gross total resection and subtotal resection with radiotherapy for craniopharyngioma: a meta-analysis. *J Surg Res* (2018) 226:131–9. doi: 10.1016/j.jss.2018.01.029

91. Schoenfeld A, Pekmezci M, Barnes MJ, Tihan T, Gupta N, Lamborn KR, et al. The superiority of conservative resection and adjuvant radiation for craniopharyngiomas. *J neuro-oncology* (2012) 108(1):133–9. doi: 10.1007/s11060-012-0806-7

92. Dandurand C, Sepehry AA, Asadi Lari MH, Akagami R, Gooderham P. Adult craniopharyngioma: case series, systematic review, and meta-analysis. *Neurosurgery* (2018) 83(4):631–41. doi: 10.1093/neuros/nyx570

93. Clark AJ, Cage TA, Aranda D, Parsa AT, Sun PP, Auguste KI, et al. A systematic review of the results of surgery and radiotherapy on tumor control for pediatric craniopharyngioma. *Child's nervous system* (2013) 29(2):231–8. doi: 10.1007/s00381-012-1926-2

94. Yang I, Sughrue ME, Rutkowski MJ, Kaur R, Ivan ME, Aranda D, et al. Craniopharyngioma: a comparison of tumor control with various treatment strategies. *Neurosurgical Focus* (2010) 28(4):E5. doi: 10.3171/2010.1.FOCUS09307

95. Merchant TE, Hoehn ME, Khan RB, Sabin ND, Klimo P, Boop FA, et al. Proton therapy and limited surgery for paediatric and adolescent patients with craniopharyngioma (RT2CR): a single-arm, phase 2 study. *Lancet Oncol* (2023) 24 (5):523–34. doi: 10.1016/S1470-2045(23)00146-8

96. Bishop AJ, Greenfield B, Mahajan A, Paulino AC, Okcu MF, Allen PK, et al. Proton beam therapy versus conformal photon radiation therapy for childhood craniopharyngioma: multi-institutional analysis of outcomes, cyst dynamics, and toxicity. *Int J Radiat oncology biology Phys* (2014) 90(2):354–61. doi: 10.1016/j.ijrobp.2014.05.051

97. Winkfield KM, Linsenmeier C, Yock TI, Grant PE, Yeap BY, Butler WE, et al. Surveillance of craniopharyngioma cyst growth in children treated with proton radiotherapy. *Int J Radiat oncology biology Phys* (2009) 73(3):716–21. doi: 10.1016/j.ijrobp.2008.05.010

98. Lee CC, Yang HC, Chen CJ, Hung YC, Wu HM, Shiau CY, et al. Gamma Knife surgery for craniopharyngioma: report on a 20-year experience. *J Neurosurg* (2014) 121 Suppl:167–78. doi: 10.3171/2014.8.GKS141411

99. Chung WY, Pan DH, Shiau CY, Guo WY, Wang LW. Gamma knife radiosurgery for craniopharyngiomas. *J Neurosurg* (2000) 93 Suppl 3:47–56. doi: 10.3171/jns.2000.93.supplement

100. Julow J, Backlund EO, Lányi F, Hajda M, Bálint K, Nyáry I, et al. Long-term results and late complications after intracavitary yttrium-90 colloid irradiation of recurrent cystic craniopharyngiomas. *Neurosurgery* (2007) 61(2):288–96. doi: 10.1227/01.NEU.0000255528.68963.EF

101. Prasad D, Steiner M, Steiner L. Gamma knife surgery for craniopharyngioma. *Acta neurochirurgica* (1995) 134(3-4):167–76. doi: 10.1007/BF01417685

102. Guimarães MM, Cardeal DD, Teixeira MJ, Lucio JEDC, Sanders FH, Kuromoto RK, et al. Brachytherapy in paediatric craniopharyngiomas: a systematic review and meta-analysis of recent literature. *Child's nervous system* (2022) 38(2):253–62. doi: 10.1007/s00381-021-05378-3

103. Yu X, Christ SM, Liu R, Wang Y, Hu C, Feng B, et al. Evaluation of long-term outcomes and toxicity after stereotactic phosphorus-32-based intracavitary brachytherapy in patients with cystic craniopharyngioma. *Int J Radiat oncology biology Phys* (2021) 111(3):773–84. doi: 10.1016/j.ijrobp.2021.05.123

104. Hasegawa T, Kondziolka D, Hadjipanayis CG, Lunsford LD. Management of cystic craniopharyngiomas with phosphorus-32 intracavitary irradiation. *Neurosurgery* (2004) 54(4):813–22. doi: 10.1227/01.neu.0000114262.30035.af

105. Kickingereder P, Maarouf M, El Majdoub F, Fuetsch M, Lehrke R, Wirths J, et al. Intracavitary brachytherapy using stereotactically applied phosphorus-32 colloid for treatment of cystic craniopharyngiomas in 53 patients. *J neuro-oncology* (2012) 109 (2):365–74. doi: 10.1007/s11060-012-0902-8

106. Pollack IF, Lunsford LD, Slamovits TL, Gumerman LW, Levine G, Robinson AG. Stereotaxic intracavitary irradiation for cystic craniopharyngiomas. *J Neurosurg* (1988) 68(2):227–33. doi: 10.3171/jns.1988.68.2.0227

107. Pollock BE, Lunsford LD, Kondziolka D, Levine G, Flickinger JC. Phosphorus-32 intracavitary irradiation of cystic craniopharyngiomas: current technique and long-term results. *Int J Radiat oncology biology Phys* (1995) 33(2):437–46. doi: 10.1016/0360-3016(95)00175-X

108. Shahzadi S, Sharifi G, Andalibi R, Zali A, Ali-Asgari A. Management of cystic craniopharyngiomas with intracavitary irradiation with 32P. *Arch Iranian Med* (2008) 11(1):30–4.

109. Barriger RB, Chang A, Lo SS, Timmerman RD, DesRosiers C, Boaz JC, et al. Phosphorus-32 therapy for cystic craniopharyngiomas. *Radiotherapy Oncol* (2011) 98 (2):207–12. doi: 10.1016/j.radonc.2010.12.001

110. Yu X, Zhang J, Liu R, Wang Y, Wang H, Wang P, et al. Interstitial radiotherapy using phosphorus-32 for giant posterior fossa cystic craniopharyngiomas. *J neurosurgery. Pediatr* (2015) 15(5):510–8. doi: 10.3171/2014.10.PEDS14302

111. Maarouf M, El Majdoub F, Fuetsch M, Hoevels M, Lehrke R, Berthold F, et al. Stereotactic intracavitary brachytherapy with P-32 for cystic craniopharyngiomas in children. *Strahlentherapie und Onkologie* (2016) 192(3):157–65. doi: 10.1007/s00066-015-0910-7

112. Mottolese C, Stan H, Hermier M, Berlier P, Convert J, Frappaz D, et al. Intracystic chemotherapy with bleomycin in the treatment of craniopharyngiomas. *Child's nervous system* (2001) 17(12):724–30. doi: 10.1007/s00381-001-0524-5

113. Hukin J, Steinbok P, Lafay-Cousin L, Hendson G, Strother D, Mercier C, et al. Intracystic bleomycin therapy for craniopharyngioma in children: the Canadian experience. *Cancer* (2007) 109(10):2124–31. doi: 10.1002/cncr.22633

114. Mottolese C, Szathmari A, Berlier P, Hermier M. Craniopharyngiomas: our experience in Lyon. *Child's nervous system* (2005) 21(8-9):790–8. doi: 10.1007/s00381-005-1242-1

115. Lafay-Cousin L, Bartels U, Raybaud C, Kulkarni AV, Guger S, Huang A, et al. Neuroradiological findings of bleomycin leakage in cystic craniopharyngioma. *Rep three cases. J Neurosurg* (2007) 107(4 Suppl):318–23. doi: 10.3171/PED-07/10/318

116. Haisa T, Ueki K, Yoshida S. Toxic effects of bleomycin on the hypothalamus following its administration into a cystic craniopharyngioma. *Br J Neurosurg* (1994) 8 (6):747–50. doi: 10.3109/02688699409101192

117. Savas A, Erdem A, Tun K, Kanpolat Y. Fatal toxic effect of bleomycin on brain tissue after intracystic chemotherapy for a craniopharyngioma: case report. *Neurosurgery* (2000) 46(1):213–7. doi: 10.1097/00006123-200001000-00043

118. Liu W, Fang Y, Cai B, Xu J, You C, Zhang H. Intracystic bleomycin for cystic craniopharyngiomas in children (abridged republication of cochrane systematic review). *Neurosurgery* (2012) 71(5):909–15. doi: 10.1227/NEU.0b013e31826d5c31

119. Zhang S, Fang Y, Cai BW, Xu JG, You C. Intracystic bleomycin for cystic craniopharyngiomas in children. *Cochrane Database systematic Rev* (2016) 7(7): CD008890. doi: 10.1002/14651858.CD008890.pub4

120. Zheng J, Fang Y, Cai BW, Zhang H, Liu W, Wu B, et al. Intracystic bleomycin for cystic craniopharyngiomas in children. *Cochrane Database systematic Rev* (2014) 9): CD008890. doi: 10.1002/14651858.CD008890.pub3

121. Mrowczynski OD, Langan ST, Rizk EB. Craniopharyngiomas: A systematic review and evaluation of the current intratumoral treatment landscape. *Clin Neurol Neurosurg* (2018) 166:124–30. doi: 10.1016/j.clineuro.2018.01.039

122. Cavalheiro S, Di Rocco C, Valenzuela S, Dastoli PA, Tamburrini G, Massimi L, et al. Craniopharyngiomas: intratumoral chemotherapy with interferon-alpha: a multicenter preliminary study with 60 cases. *Neurosurgical Focus* (2010) 28(4):E12. doi: 10.3171/2010.1.FOCUS09310

123. Kilday JP, Caldarelli M, Massimi L, Chen RH, Lee YY, Liang ML, et al. Intracystic interferon-alpha in pediatric craniopharyngioma patients: an international multicenter assessment on behalf of SIOPE and ISPN. *Neuro-oncology* (2017) 19(10):1398–407. doi: 10.1093/neuonc/nox056

124. Gan HW, Morillon P, Albanese A, Aquilina K, Chandler C, Chang YC, et al. National UK guidelines for the management of paediatric craniopharyngioma. *Lancet Diabetes Endocrinol* (2023) 11(9):694–706. doi: 10.1016/S2213-8587(23)00162-6

125. Hölsken A, Gebhardt M, Buchfelder M, Fahlbusch R, Blümcke I, Buslei R. EGFR signaling regulates tumor cell migration in craniopharyngiomas. *Clin Cancer research: an Off J Am Assoc Cancer Res* (2011) 17(13):4367–77. doi: 10.1158/1078-0432.CCR-10-2811

126. Patel K, Allen J, Zagzag D, Wisoff J, Radmanesh A, Gindin T, et al. Radiologic response to MEK inhibition in a patient with a WNT-activated craniopharyngioma. *Pediatr Blood Cancer* (2021) 68(3):e28753. doi: 10.1002/pbc.28753

127. Grob S, Mirsky DM, Donson AM, Dahl N, Foreman NK, Hoffman LM, et al. Targeting IL-6 is a potential treatment for primary cystic craniopharyngioma. *Front Oncol* (2019) 9:791. doi: 10.3389/fonc.2019.00791

128. Mollá E, Martí-Bonmatí L, Revert A, Arana E, Menor F, Dosdá R, et al. Craniopharyngiomas: identification of different semiological patterns with MRI. *Eur Radiol* (2002) 12(7):1829–36. doi: 10.1007/s00330-001-1196-y

129. d'Avella E, Vitulli F, Berardinelli J, Cinalli G, Solari D, Cappabianca P, et al. Systematic review of transcranial and endoscopic endonasal approaches for craniopharyngiomas in children: is there an evolution? *J neurosurgery. Pediatr* (2023), 1–12. doi: 10.3171/2023.9.PEDS23117

130. Mazzatenta D, Zoli M, Guaraldi F, Ambrosi F, Faustini Fustini M, Pasquini E, et al. Outcome of endoscopic endonasal surgery in pediatric craniopharyngiomas. *World Neurosurg* (2020) 134:e277–88. doi: 10.1016/j.wneu.2019.10.039

131. Wu J, Pan C, Xie S, Tang B, Fu J, Wu X, et al. A propensity-adjusted comparison of endoscopic endonasal surgery versus transcranial microsurgery for pediatric craniopharyngioma: a single-center study. *J neurosurgery. Pediatr* (2021) 29 (3):325–34. doi: 10.3171/2021.10.PEDS21392

132. Sterkenburg AS, Hoffmann A, Gebhardt U, Warmuth-Metz M, Daubenbüchel AM, Müller HL. Survival, hypothalamic obesity, and neuropsychological/psychosocial status after childhood-onset craniopharyngioma: newly reported long-term outcomes. *Neuro-oncology* (2015) 17(7):1029–38. doi: 10.1093/neuonc/nov044

133. Bogusz A, Müller HL. Childhood-onset craniopharyngioma: latest insights into pathology, diagnostics, treatment, and follow-up. *Expert Rev Neurother* (2018) 18 (10):793–806. doi: 10.1080/14737175.2018.1528874

134. Ma G, Kang J, Qiao N, Zhang B, Chen X, Li G, et al. Non-invasive radiomics approach predict invasiveness of adamantinomatous craniopharyngioma before surgery. *Front Oncol* (2021) 10:599888. doi: 10.3389/fonc.2020.599888

frontiers | Frontiers in Oncology

TYPE Systematic Review
PUBLISHED 10 January 2024
DOI 10.3389/fonc.2023.1346951

OPEN ACCESS

EDITED BY
Cesare Zoia,
San Matteo Hospital Foundation (IRCCS), Italy

REVIEWED BY
Christian F. Freyschlag,
Innsbruck Medical University, Austria
Natale Quartuccio,
Azienda Ospedaliera Ospedali Riuniti Villa Sofia Cervello, Italy

*CORRESPONDENCE
Yan Chen
drchenyan@jlu.edu.cn

RECEIVED 30 November 2023
ACCEPTED 20 December 2023
PUBLISHED 10 January 2024

CITATION
Yu P, Wang Y, Su F and Chen Y (2024) Comparing [18F]FET PET and [18F]FDOPA PET for glioma recurrence diagnosis: a systematic review and meta-analysis.
Front. Oncol. 13:1346951.
doi: 10.3389/fonc.2023.1346951

Comparing [18F]FET PET and [18F]FDOPA PET for glioma recurrence diagnosis: a systematic review and meta-analysis

Pengbo Yu, Yinan Wang, Fengbo Su and Yan Chen*

Department of Neurosurgery, The Second Hospital of Jilin University, Changchun, China

Purpose: The purpose of our meta-analysis and systematic review was to evaluate and compare the diagnostic effectiveness of [18F]FET PET and [18F]FDOPA PET in detecting glioma recurrence.

Methods: Sensitivities and specificities were assessed using the DerSimonian and Laird methodology, and subsequently transformed using the Freeman-Tukey double inverse sine transformation. Confidence intervals were computed employing the Jackson method, while heterogeneity within and between groups was evaluated through the Cochrane Q and I^2 statistics. If substantial heterogeneity among the studies was observed ($P < 0.10$ or $I^2 > 50\%$), we conducted meta-regression and sensitivity analyses. Publication bias was assessed through the test of a funnel plot and the application of Egger's test. For all statistical tests, except for assessing heterogeneity ($P < 0.10$), statistical significance was determined when the two-tailed P value fell below 0.05.

Results: Initially, 579 publications were identified, and ultimately, 22 studies, involving 1514 patients(1226 patients for [18F]FET PET and 288 patients for [18F]FDOPA PET), were included in the analysis. The sensitivity and specificity of [18F]FET PET were 0.84 (95% CI, 0.75-0.90) and 0.86 (95% CI, 0.80-0.91), respectively, while for [18F]FDOPA PET, the values were 0.95 (95% CI, 0.86-1.00) for sensitivity and 0.90 (95% CI, 0.77-0.98) for specificity. A statistically significant difference in sensitivity existed between these two radiotracers (P=0.04), while no significant difference was observed in specificity (P=0.58).

Conclusion: It seems that [18F]FDOPA PET demonstrates superior sensitivity and similar specificity to [18F] FET PET. Nevertheless, it's crucial to emphasize that [18F]FDOPA PET results were obtained from studies with limited sample sizes. Further larger prospective studies, especially head-to-head comparisons, are needed in this issue.

Systematic Review Registration: identifier CRD42023463476

KEYWORDS

glioma, [18F]FET PET, [18F]FDOPA PET, recurrence, meta-analysis

1 Introduction

Glioma, a primary tumor of the central nervous system, represents a formidable challenge in the realm of oncology due to its infiltrative nature and variable biological behavior (1, 2).Nevertheless, a few months into treatment, numerous patients experience pseudoprogression or radiation necrosis, conditions frequently indistinguishable from tumor recurrence (3). Given the potential aggressiveness of glioma recurrence, early detection is paramount in facilitating interventions that can potentially extend patient survival and improve their quality of life (4).

Historically, conventional imaging modalities such as computed tomography (CT) and magnetic resonance imaging (MRI) have played a pivotal role in glioma diagnosis and monitoring (5).While these methods have provided essential insights into tumor structure and volume, they have shown limitations in distinguishing between active tumor tissue and post-treatment changes, often leading to equivocal results (6). CT scans utilize X-rays to create detailed cross-sectional images of the brain, allowing clinicians to visualize the tumor's location, size, and its impact on surrounding structures. However, CT scans are limited in their capacity to differentiate different types of brain tissue with precision. This lack of specificity can lead to difficulties in distinguishing active tumor tissue from non-cancerous changes, such as post-treatment radiation effects or edema, which can yield false-positive results. MRI, a non-invasive imaging technique, offers superior soft tissue contrast and is especially valuable in delineating tumor boundaries and identifying associated brain edema (4). However, similar to CT, MRI also faces challenges when it comes to distinguishing between recurrent tumor and radiation-induced changes (7). Glioma recurrence can present with subtle changes that may overlap with post-treatment effects, causing diagnostic ambiguity (2, 8). These limitations have spurred the exploration of advanced imaging techniques that can offer improved specificity and sensitivity in detecting glioma recurrence (9, 10).

A significant development in this pursuit is the application of positron emission tomography (PET) imaging using radiolabeled amino acids like [18F]FET (O-(2-[18F]fluoroethyl)-L-tyrosine) and [18F]FDOPA (6-[18F]fluoro-L-DOPA). These radiotracers have shown promise in glioma recurrence diagnosis by capitalizing on the increased metabolic activity of tumor cells. [18F]FET is an amino acid analog that is actively transported into tumor cells, reflecting increased amino acid metabolism associated with malignancy (11, 12), known for its minimal uptake in normal brain tissue and rapid clearance from non-tumor cells, displays a distribution pattern predominantly focused within the tumor, enhancing the contrast between malignant and healthy tissues (13). Conversely, [18F]FDOPA PET relies on the radiotracer 6-[18F]fluoro-L-DOPA, which is a precursor of dopamine and is actively transported into cells (14). Like [18F]FET PET, [18F]FDOPA PET can detect regions of heightened metabolic activity, but it does so by targeting amino acid metabolism differently. [18F]FDOPA, on the other hand, shows a somewhat different biodistribution, characterized by a higher basal level of uptake in normal brain tissue but still demonstrates a significant increase in uptake in tumor cells (15). This distinction in biodistribution between [18F]FET and [18F]FDOPA is pivotal in their application for glioma recurrence detection and forms a basis for ongoing comparative studies. Some studies suggest that [18F]FET PET may offer superior diagnostic accuracy due to its specificity for amino acid transport, while others argue that [18F]FDOPA PET's ability to probe different aspects of amino acid metabolism makes it a preferable choice (12, 14).

In light of the ongoing debate surrounding the diagnostic accuracy of [18F]FET PET and [18F]FDOPA PET in glioma recurrence, this systematic review and meta-analysis seek to provide a rigorous and evidence-based comparison of these imaging techniques. Our primary objective is to assess the diagnostic performance of [18F]FET PET and [18F]FDOPA PET in detecting glioma recurrence, including their sensitivity and specificity.

2 Materials and methods

Our review has been registered with PROSPERO, the international prospective register of systematic reviews, under the identifier CRD42023463476.

2.1 Search strategy

A comprehensive search was conducted of the PubMed and Embase databases for all available literatures through September 10, 2023 based on the following combination of terms:(1)Positron-Emission Tomography OR PET OR Positron-Emission Tomography; (2)Regeneration OR Recurrence OR pseudoprogression OR recurrent OR relapse OR Recrudescence OR radionecrosis;(3) Glioma OR Glioma OR Glial Cell Tumor OR Mixed Glioma OR Malignant Glioma;(4) fluoroethyltyrosine OR FET OR fluorodopa F-18 OR FDOPA OR fluorodopa OR 18F-dopa. Studies that were potentially related were also enclosed from the reference lists.

2.2 Inclusion and exclusion criteria

Only studies that met all of the following condition were included: (1) Articles evaluating the diagnostic efficiency of [18F]FET PET or [18F]FDOPA PET in detecting glioma recurrence; (2) Patients under suspicion of recurrent glioma, without any limitations related to age, gender, race, or geographical origin; (3) A prerequisite for inclusion is a minimum of 10 patients or lesions.; (3) The reference standard included histopathological confirmation or imaging follow-up, a requirement that should be explicitly stated in the article; (4) True positive (TP), false positive (FP), true negative (TN), false negative (FN) data could be extracted. The exclusion condition were: (1) Irrelevant topic; (2) Duplicated articles; (3) Cell or animal experiments; (4) Non-English articles; (5) Abstract, editorial comments, letters, case reports, review and meta-analyses. After reviewing the titles and abstracts of the articles based on the incorporation and exclusion criteria, we evaluated the

full-text variants of the selected articles to confirm their adherence to the inclusion criteria. Any disagreements between scholars were solved by consensus.

2.3 Quality assessment and data extraction

Using the Quality Assessment of Diagnostic Performance Studies (QUADAS-2) methodology (16), two independent researchers assessed the quality of the included studies. They evaluated each study's risk of bias and applicability, rating them as either high, low, or unclear in these aspects. In case of any disputes, a third reviewer was consulted for resolution. The analysis was conducted using RevMan (version 5.4).

Data extraction for all incorporated papers was carried out separately by two researchers(Table 1). The data that were extracted included: (1) The author, year of publication; (2) Study characteristics including country, study design, analysis, duration, reference standard; (3) Patient characteristics including variety of patients, mean/median age; (4) Technical characteristics including types of tracers, parameter, TP, FP, FN, TN. Data were manually accessed from the literature, tables, and figures when not clearly stated. If the article lacked sufficient information, we will contact the corresponding authors by email and request further data or interpretation. Any disagreements between the two researchers were consequently resolved by consensus.

2.4 Data synthesis and statistical analysis

The sensitivities and specificities were evaluated using the DerSimonian and Laird method and transformed with the Freeman-Tukey double inverse sine transformation. The confidence intervals were calculated using the Jackson method. The Cochrane Q and I^2 statistics were used to assess the heterogeneity within and between groups. If the heterogeneity between the studies differed significantly ($P < 0.10$ or $I^2 > 50\%$), meta-regression analysis and sensitivity analysis were performed by reassessing the sensitivities or specificities following the omission of articles one by one. This was done to evaluate the robustness of the overall sensitivities or specificities and to identify single studies that may contribute to heterogeneity.

Publication bias was assessed through a funnel plot and Egger's test. Except for heterogeneity ($P < 0.10$), a two-tailed p-value below 0.05 was considered statistically significant for all statistical tests. Statistical analyses were performed using the R software for statistical computing and graphics version 4.3.1.

3 Results

3.1 Literature search and study selection

The initial search yielded a total of 579 publications. After eliminating 112 duplicated studies, we identified 467 unique studies. Upon reviewing the titles and abstracts, 437 studies were excluded. Among the remaining results, 4 lacked available data, 2 had fewer than 10 patients, and 2 utilized different radiotracers. Finally, 22 studies assessing the diagnostic accuracy of glioma recurrence diagnosis, involving 1514 patients, were included in the analysis. This encompassed 17 articles specifically focusing on [18F]FET PET (11, 17–32) and an additional 5 articles centered on [18F]FDOPA PET (33–37). The PRISMA flow diagram of the study selection process was shown in Figure 1.

3.2 Study description and quality assessment study description and quality assessment

Table 1 presents the study characteristics and technical details derived from the 22 selected studies, encompassing a total of 1514 patients. Additionally, we conducted an assessment of the study quality, utilizing the Quality Assessment of Diagnostic Accuracy Studies (QUADAS-2) tool (16). The quality evaluation graph elucidated that the primary area of high-risk bias concerns was centered around patient selection (Figure 2), primarily due to the fact that many of the studies did not involve consecutive patient recruitment. In general, the risk of bias in the articles was deemed acceptable.

3.3 Diagnostic performance of [18F]FET PET and [18F]FDOPA PET for glioma recurrence

The pooled sensitivity for glioma recurrence was 0.84 (95% CI, 0.75-0.90) for [18F]FET PET and 0.95 (95% CI, 0.86-1.00) for [18F]FDOPA PET (Figure 3). Likewise, the pooled specificity for [18F]FET PET was 0.86 (95% CI, 0.80-0.91), while for [18F]FDOPA PET, it was 0.90 (95% CI, 0.77-0.98)(Figure 4). A statistically significant difference in sensitivity existed between these two radiotracers ($P=0.04$), while no significant difference was observed in specificity ($P=0.58$).

Regarding the sensitivity of [18F]FET PET and [18F]FDOPA PET for glioma recurrence, the I^2 was 82%, 75%, respectively. In terms of the specificity of [18F]FET PET and [18F]FDOPA PET, the I^2 were 57% and 63%. For [18F] FET PET, we did not find the reason for its sensitivity heterogeneity through sensitivity analysis and meta-regression analysis (Figure 5) (Table 2). This may be related to significant differences in the study duration of different studies and many of the studies did not involve consecutive patient recruitment. The meta-regression analysis showed that the reference standard ($P=0.01$ for specificity) may account for the heterogeneity (Table 2). Sensitivity analysis, excluding data from Kebir et al. (25) and Maurer et al. (24),resulted in a combined specificity of 0.83 (95% CI: 0.78-0.87) and 0.83 (95% CI: 0.81-0.92) with low heterogeneity ($I^2 = 31\%$ and $I^2 = 47\%$), respectively (Figure 6). For [18F]FDOPA PET, sensitivity analysis by excluding data from Rozenblum et al. (33) reported a combined specificity of 0.96(95% CI: 0.89-1.00), with an acceptable heterogeneity ($I^2 = 0\%$) (Figure 7). Sensitivity analysis, after the

TABLE 1 Characteristics of the included studies and patients.

Author	Year	Country	Type of tracers	Study duration	Study design	Analysis	Reference standard	Parameter	No. of patients	Mean/ Median age	TP	FP	FN	TN
Vidmar et al.	2022	Slovenia	[18F]FET PET	2019-2021	Retro	LB	Pathology and follow-up imaging	TBRmax	47	Median(range):44 (17-72)	9	7	2	24
Muller et al.	2022	Germany	[18F]FET PET	NA	Retro	LB	Pathology and follow-up imaging	TBRmean + TBRmax	151	Median(range):52 (20-78)	8	9	4	37
Puranik et al.	2021	India	[18F]FET PET	2017-2019	Retro	PB	Pathology and follow-up imaging	T/Wm	72	NA	35	6	4	27
Paprottka et al.	2021	Germany	[18F]FET PET	2017-2020	Retro	LB	Pathology and follow-up imaging	TBRmean	66	Mean+SD:54.91 ± 12.2	14	11	3	46
Werner et al.	2021	Germany	[18F]FET PET	2018-2020	Retro	PB	Pathology and follow-up imaging	TBRmean	23	Mean+SD:58 ± 9	9	1	2	11
Steidl et al.	2021	Germany	[18F]FET PET	2016-2019	Retro	PB	Pathology and follow-up imaging	Slope	104	Median(range):52 (20-78)	13	13	8	70
Lohmann et al.	2020	Germany	[18F]FET PET	NA	Pro	PB	Pathology and follow-up imaging	TBRmax	34	Mean ± SD:57 ± 12	13	6	3	12
Kebir et al.	2020	Germany	[18F]FET PET	NA	Retro	PB	follow-up imaging	TBRmean	44	Median(range):55 (34-79)	5	0	9	30
Maurer et al.	2020	Germany	[18F]FET PET	2016-2019	Retro	PB	Pathology and follow-up imaging	TBRmax	127	Mean+SD:50 ± 12	23	28	10	66
Bashir et al.	2019	Denmark	[18F]FET PET	2011-2019	Pro	LB	Pathology and follow-up imaging	TBRmax	146	Median(range):59.5 (21–80)	150	1	2	15
Kertels et al.	2018	Germany	[18F]FET PET	2010-2016	Retro	PB	Pathology and follow-up imaging	TBR80%	36	Mean+SD:54 ± 14	23	1	5	7
Pyka et al.	2018	Germany	[18F]FET PET	2015-2017	Retro	LB	Pathology and follow-up imaging	FET 30-40	47	Mean+SD:53 ± 11	40	2	10	11
Galldiks et al.	2015	Germany	[18F]FET PET	2006-2013	Retro	LB	Pathology	TBRmean/TTP	124	Mean+SD:52 ± 14	113	0	8	11
Dunkl et al.	2015	Germany	[18F]FET PET	2006-2012	Retro	LB	Pathology	18F-FET kinetic pattern	18	Median(range):13 (1–18)	10	1	3	10
Herrmann et al.	2013	Germany	[18F]FET PET	NA	Retro	PB	Pathology and follow-up imaging	visual scale	110	Mean+SD:51.7 ± 12.1	69	8	12	21
Jeong et al.	2010	Korea	[18F]FET PET	2003-2009	Retro	PB	Pathology and follow-up imaging	SUVmax	32	Mean+SD:47.3 ± 10	20	0	3	9

(Continued)

10.3389/fonc.2023.1346951

TABLE 1 Continued

Author	Year	Country	Type of tracers	Study duration	Study design	Analysis	Reference standard	Parameter	No. of patients	Mean/ Median age	TP	FP	FN	TN
Rachinger et al.	2005	Germany	[18F]FET PET	2001-2003	Retro	PB	Pathology and follow-up imaging	SUVmax	45	Mean+SD:45 ± 12	31	1	0	13
Rozenblum et al.	2022	France	[18F] FDOPA PET	2015-2020	Retro	PB	Pathology and follow-up imaging	TBRmean	106	Median:54	58	10	13	25
Pellerin et al.	2021	Germany	[18F] FDOPA PET	2015-2018	Pro	PB	Pathology and follow-up imaging	T-map and isocontour map	58	Mean+SD:53.1 ± 14.3	22	2	2	32
Li et al.	2021	China	[18F] FDOPA PET	2016-2019	Pro	PB	Pathology and follow-up imaging	L/G	43	Mean ± SD:38.5 ± 6.37	34	1	0	8
Zaragori et al.	2020	France	[18F] FDOPA PET	2012-2017	Retro	PB	follow-up imaging	TBRmax	51	Median(range):51 (21-75)	16	1	1	33
Karunanithi et al.	2014	India	[18F] FDOPA PET	2009-2010	Pro	PB	Pathology and follow-up imaging	T/C	30	NA	22	1	0	7

PB, patient-based; LB, lesion-based; Pro, prospective; Retro, retrospective; NA, not available.

exclusion of data from Rozenblum et al. (33), yielded a combined sensitivity of 0.98 (95% CI: 0.92-1.00) with minimal heterogeneity (I^2 = 33%) (Figure 8).

3.4 Publication bias

The funnel plot asymmetry test revealed a significant publication bias regarding the sensitivity of [18F]FET PET, as indicated by Egger's test (P=0.01), no significant publication bias was found in relation to the specificity of [18F]FET PET (P=0.06). No notable publication bias was observed in sensitivity and specificity for [18F]FDOPA PET (P=0.25, 0.86).

4 Discussion

The detection of recurrent signs during post-treatment follow-up for glioma patients portends an unfavorable prognosis. Several studies indicate that patients experiencing their first recurrence have a median survival time of only 9 to 10 months (38). The central question that has spurred extensive debate within the neuro-oncology community revolves around the optimal choice between [18F]FET PET and [18F]FDOPA PET for the diagnosis of glioma recurrence (14, 39–41).

It seems that [18F]FDOPA PET demonstrates superior sensitivity and similar specificity to [18F] FET PET. [18F]FET PET exhibits a pooled sensitivity of 0.84 (95% CI, 0.75-0.90) and specificity of 0.86 (95% CI, 0.80-0.91), while [18F]FDOPA PET demonstrates a pooled sensitivity of 0.95 (95% CI, 0.86-1.00) and specificity of 0.90 (95%CI, 0.77-0.98).These results underscore that both radiotracers are valuable tools in clinical practice (14). It seems that [18F]FDOPA PET demonstrates superior sensitivity in detecting glioma recurrence when contrasted with [18F]FET PET. This may be due to their slightly different mechanisms of action. [18F]FET, an amino acid analog, is transported into tumor cells via amino acid transporters. It capitalizes on the increased amino acid metabolism observed in malignant tissue (42). Conversely, [18F] FDOPA, a precursor of dopamine, is actively transported into cells and reflects increased amino acid metabolism as well. Its advantage lies in targeting different aspects of amino acid metabolism, which may contribute to its diagnostic sensitivity in distinguishing between recurrent tumor and treatment-related changes (43).

Despite numerous published studies, the selection of the ideal radiotracer for discriminating between authentic glioma recurrence and spurious progression remains undetermined. Previously, two meta-analyses regarding [18F]FET PET or [18F]FDOPA PET for glioma recurrence have been conducted and published. According to a meta-analysis by Yu et al. (14), the findings suggest that [18F] FDOPA PET exhibited superior diagnostic performance in patients with glioma recurrence. In summary, within the glioma subgroup, [18F]FDOPA PET demonstrated superior ability across all outcomes compared to [18F]FET PET: sensitivity (0.94 vs. 0.78) and specificity (0.89 vs. 0.75). However, in this article, all data pertaining to the diagnosis of glioma recurrence using [18F]FDOPA PET were sourced from a compilation of three studies (comprising

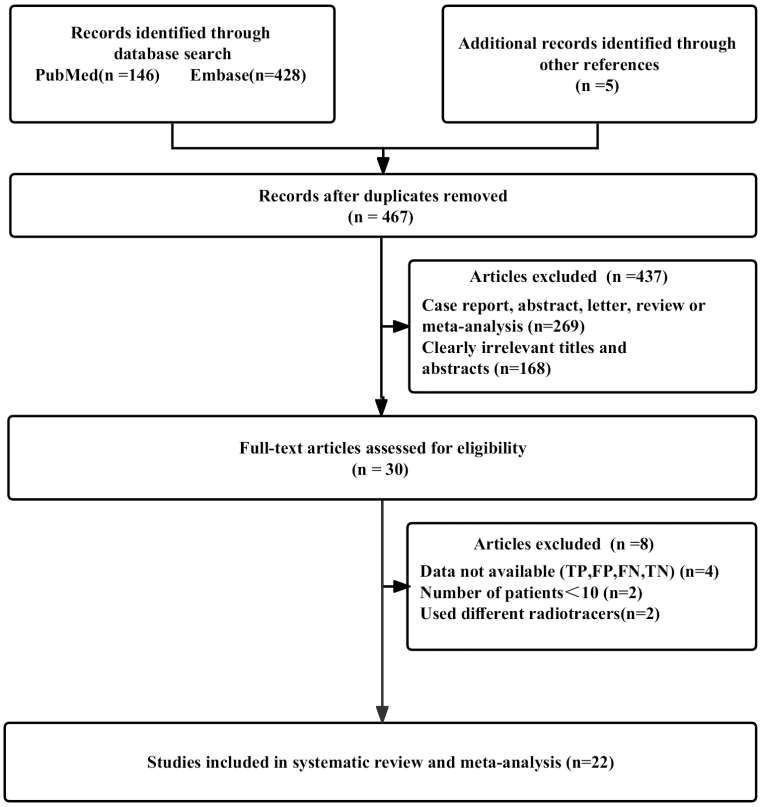

FIGURE 1
The PRISMA flow chart of investigation selection procedure.

10 studies) conducted by the same research institution and authored by Karunanithi et al. (37, 43, 44) This circumstance could potentially undermine the reliability of the research data, consequently impacting the outcomes of subgroup analysis. In 2023, Tian et al (12). conducted a systematic review and meta-analysis of the diagnostic performance of different PET imaging agents for glioma recurrence. They included 15 articles that met the inclusion criteria, and ultimately showed that [18F]FET had the highest SUCRA values (diagnostic performance) in sensitivity, specificity, positive predictive value, and accuracy, followed by 18F-FDOPA. Indicating that [18F]FET is one of the most popular imaging agents for glioma recurrence. However due to the limitations of network meta-analysis, articles that only evaluate individual [18F]FET PET or [18F]FDOPA PET were not included, resulting in many available articles being excluded, further affecting the credibility of their articles. While prior meta-analyses have explored this topic to varying degrees, several factors differentiate our study and make it a valuable addition to the existing body of literature. One of the critical strengths of our analysis is the incorporation of the most recent and up-to-date studies (9, 17–22, 33–35). This inclusion ensures that our findings are aligned with the latest research developments, providing the most relevant insights for clinical practice.

Heterogeneity is an inherent challenge in meta-analyses, and it was indeed observed in our study, there was high heterogeneity in [18F]FET PET (sensitivity and specificity) and [18F]FDOPA PET (sensitivity and specificity). In order to find out the source of the heterogeneity and improve the reliability of our research results, we have adopted several strategies such as meta-regression and sensitivity analysis. For [18F] FET PET, we were unable to

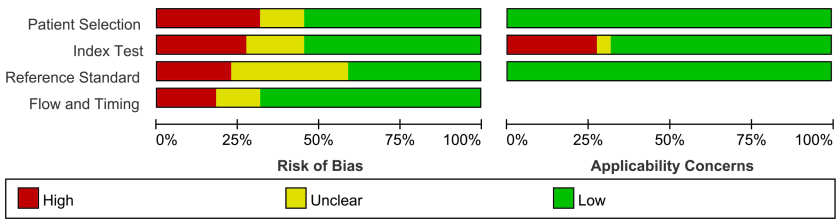

FIGURE 2
Risk of bias items presented as percentages across all articles using the QUADAS-2 tool.

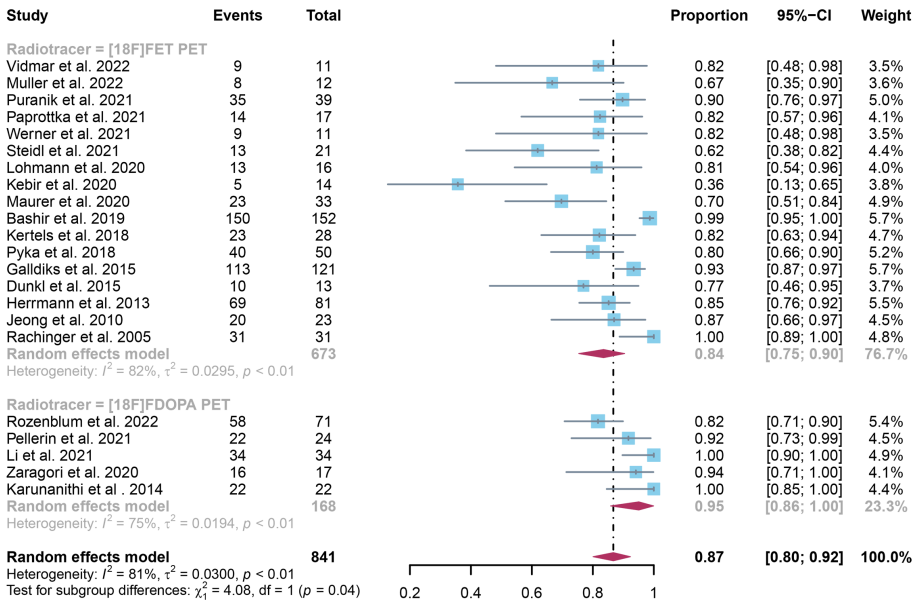

FIGURE 3
Forest plot comparing sensitivity of [18F]FET PET and [18F]FDOPA PET in glioma recurrence.

identify the cause of sensitivity heterogeneity through sensitivity analysis and meta-regression. One possible source of heterogeneity is the significant difference in research duration between included studies. Some studies encompassed longer follow-up periods, while others had relatively shorter intervals. This temporal variability can introduce heterogeneity in the assessment of glioma recurrence due to changes in disease progression and treatment response over time. Another contributing factor is the observation that many studies did not involve consecutive recruitment of patients. This non-consecutive recruitment approach can introduce selection bias, as patients with differing disease characteristics or treatment histories may be included, affecting the overall diagnostic accuracy. Meta-regression analysis showed that reference standard was the possible cause of specificity heterogeneity. Sensitivity analysis by excluding data from Kebir et al. (25) and Maurer et al. (24) demonstrated a combined specificity of 0.83 and 0.83 with low heterogeneity (I^2 = 31%, I^2 = 47%). This variance could be attributed to the distinct impact of various chemotherapy regimens on the frequency and characteristics of glioma pseudoprogression. For [18F]FDOPA PET, sensitivity analysis by excluding data from Rozenblum et al.

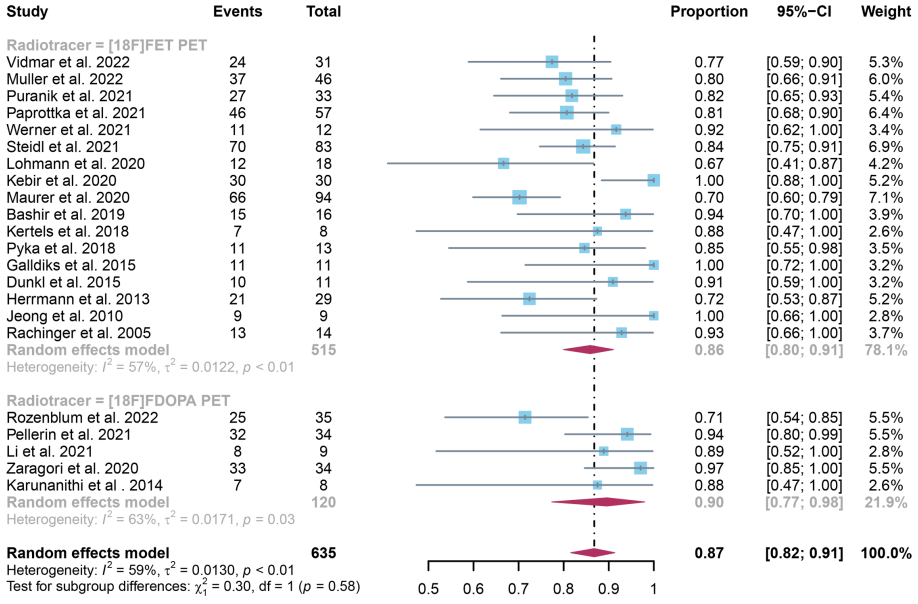

FIGURE 4
Forest plot comparing specificity of [18F]FET PET and [18F]FDOPA PET in glioma recurrence.

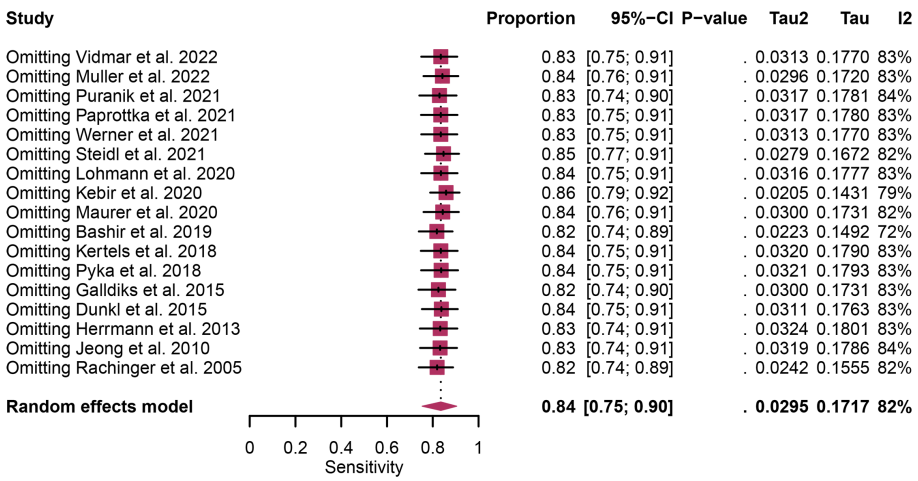

FIGURE 5
Sensitivity analysis evaluating heterogeneity in [18F]FET PET sensitivity for glioma recurrence diagnosis.

(33) showed a combined specificity of 0.96, with an satisfactory heterogeneity (I^2 = 0%), sensitivity analysis by excluding data from Rozenblum et al. (33) yielded a combined sensitivity of 0.98, with low heterogeneity (I^2 = 33%), which could be explained by different cut-off thresholds. However, difference in imaging protocols, such as radiotracer dosage, imaging timing, and scanner technology, can also contribute to heterogeneity.

When assessing the advantages and disadvantages of [18F] FET PET and [18F]FDOPA PET for glioma recurrence diagnosis, it is essential to consider not only diagnostic accuracy but also practical aspects such as cost and accessibility. [18F]FDOPA PET exhibits commendable sensitivity in detecting glioma recurrence, making it a valuable tool for identifying subtle disease progression. Its ability to probe various aspects of amino acid metabolism allows [18F]FDOPA PET to effectively differentiate between active tumor tissue and treatment-related changes, enhancing diagnostic accuracy (45). But [18F]FDOPA PET can be cost-prohibitive for some healthcare systems and may be less accessible in certain regions, limiting its widespread use. While [18F]FDOPA PET has shown promise, it is relatively newer compared to [18F]FET PET,

TABLE 2 Meta-regression analysis for [18F]FET PET in glioma recurrence.

Covariate	Studies, n	Sensitivity (95%CI)	*P*-value	Specificity (95%CI)	*P*-value
Number of patients included			0.78		0.43
>100	11	0.83(0.73-0.91)		0.88(0.80-0.94)	
≤100	6	0.84(0.68-0.95)		0.83(0.73-0.90)	
Race			0.58		0.59
White	15	0.83(0.73-0.91)		0.85(0.79-0.91)	
Yellow	2	0.89(0.79-0.96)		0.91(0.68-1.00)	
Study design			0.13		0.61
Retrospective	15	0.82(0.73-0.89)		0.86(0.80-0.92)	
Prospective	2	0.94(0.68-1.00)		0.82(0.50-1.00)	
Analysis			0.43		0.89
Patient-based	7	0.87(0.76-0.96)		0.85(0.79-0.90)	
Lesion-based	10	0.81(0.69-0.91)		0.86(0.77-0.94)	
Reference standard			0.13		0.01
Pathology and follow-up imaging	14	0.85(0.77-0.92)		0.82(0.77-0.86)	
Pathology	2	0.89(0.68-0.10)		0.89(0.68-1.00)	
Follow-up imaging	1	0.84(0.75-0.90)		1.00(0.86-1.00)	

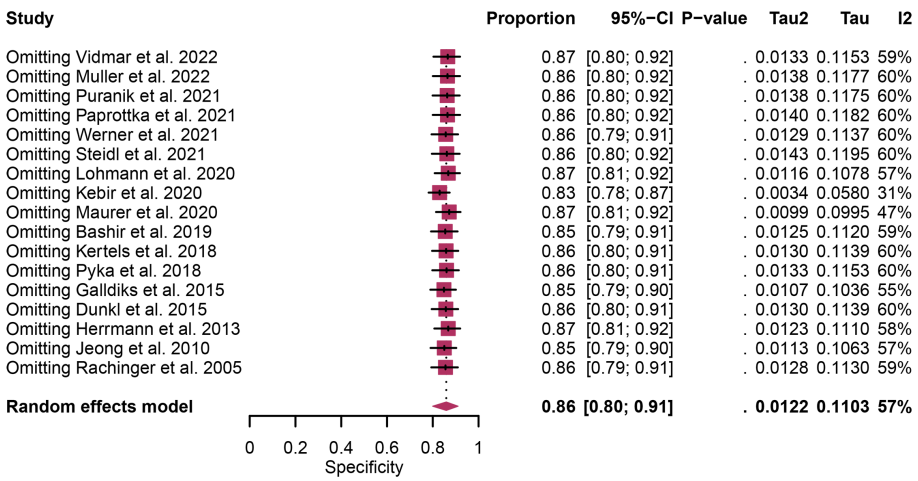

FIGURE 6
Sensitivity analysis evaluating heterogeneity in [18F]FET PET specificity for glioma recurrence diagnosis.

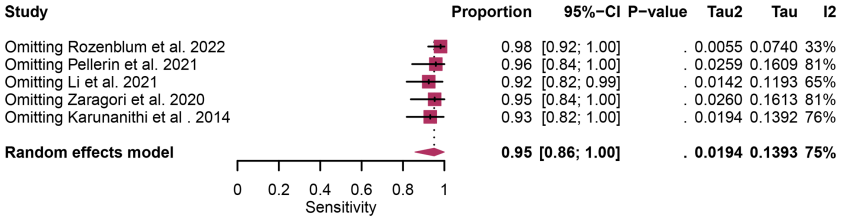

FIGURE 7
Sensitivity analysis evaluating heterogeneity in [18F]FDOPA PET sensitivity for glioma recurrence diagnosis.

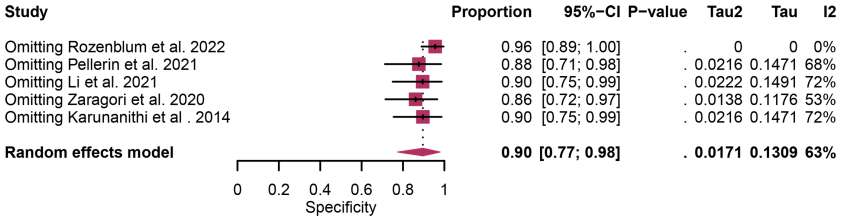

FIGURE 8
Sensitivity analysis evaluating heterogeneity in [18F]FDOPA PET specificity for glioma recurrence diagnosis.

which has a longer history in clinical practice (46, 47). [18F]FET PET, while effective, may exhibit slightly lower sensitivity compared to [18F]FDOPA PET in specific cases. Because the dependence of [18F] FET on amino acid transporters may be affected by the integrity of the blood-brain barrier, in some cases affecting its accuracy (41). However, [18F] FET PET is more widespread and cheaper than [18F] FDOPA PET, making it a practical choice for many clinical environments (46). The choice between these two imaging agents should be guided by careful consideration of patient-specific factors, clinical context, cost, and accessibility. Further larger studies that focus on cost-effective comparison were needed.

[18F] FDOPA PET and [18F] FET PET are specialized forms of positron emission tomography that utilize specific radiotracers to target and visualize brain tumors. MRI, on the other hand, uses magnetic fields and radio waves to create detailed images of the

brain (48).The effectiveness of [18F] FDOPA PET and [18F] FET PET lies in their ability to detect changes at a molecular level, often before these changes are visible on MRI. One study by Xiaoxue T et al. conducted a Bayesian network meta-analysis to evaluate the diagnostic accuracy of six different imaging modalities, including [18F] FDOPA PET and [18F] FET PET, for differentiating glioma recurrence from post-radiotherapy changes. The study revealed that [18F] FDOPA PET has the highest sensitivity (0.84) among the evaluated modalities, indicating its effectiveness in correctly identifying true positive cases of recurrent glioma. For [18F] FET PET, the sensitivity is 0.73, which is also relatively high, though slightly lower than [18F] FDOPA PET. MRI had the highest specificity (0.81), demonstrating its superior accuracy in correctly identifying non-recurrent cases (12). This suggests that in clinical practice, combining these imaging techniques could offer a more balanced and comprehensive diagnostic approach, utilizing the high sensitivity of PET tracers and the high specificity of MRI.

It is imperative to acknowledge the limitations of this systematic review and meta-analysis. First, only five studies provided adequate data to assess the diagnostic performance of [18F]FDOPA PET in glioma recurrence detection, resulting in a limited sample size (33–37). Second, the heterogeneity observed in our study remains a challenge that impacts the generalizability of our findings. While our sensitivity analysis and meta-regression provided valuable insights, some degree of unexplained heterogeneity still exist. Third, the diagnostic performance of [18F]FET PET and [18F] FDOPA PET may be influenced by various factors not accounted for in our analysis, such as the specific tracer dosage, timing of imaging, and variations in scanner technology. Standardization of these aspects in future research would contribute to a more comprehensive understanding of these imaging modalities.

5 Conclusion

In light of the findings mentioned earlier, it seems that [18F] FDOPA PET demonstrates superior sensitivity and similar specificity to [18F] FET PET. Nevertheless, it's crucial to emphasize that [18F]FDOPA PET results were obtained from studies with limited sample sizes. Further larger prospective studies, especially head-to-head comparisons, are need in this issue.

Data availability statement

The original contributions presented in the study are included in the article/Supplementary Material. Further inquiries can be directed to the corresponding author.

Author contributions

PY: Data curation, Formal Analysis, Methodology, Software, Writing – original draft. YW: Data curation, Software, Writing – original draft. FS: Formal Analysis, Methodology, Writing – original draft. YC: Conceptualization, Supervision, Validation, Visualization, Writing – review & editing.

Funding

The author(s) declare that no financial support was received for the research, authorship, and/or publication of this article.

Conflict of interest

The authors declare that the research was conducted in the absence of any commercial or financial relationships that could be construed as a potential conflict of interest.

Publisher's note

Supplementary material

The Supplementary Material for this article can be found online at: https://www.frontiersin.org/articles/10.3389/fonc.2023.1346951/full#supplementary-material

References

1. Ostrom QT, Patil N, Cioffi G, Waite K, Kruchko C, Barnholtz-Sloan JS. CBTRUS statistical report: primary brain and other central nervous system tumors diagnosed in the United States in 2013-2017. *Neuro Oncol* (2020) 22(12 Suppl 2):iv1–iv96. doi: 10.1093/neuonc/noaa200

2. Brandsma D, van den Bent MJ. Pseudoprogression and pseudoresponse in the treatment of gliomas. *Curr Opin Neurol* (2009) 22(6):633–8. doi: 10.1097/WCO.0b013e328332363e

3. Parvez K, Parvez A, Zadeh G. The diagnosis and treatment of pseudoprogression, radiation necrosis and brain tumor recurrence. *Int J Mol Sci* (2014) 15(7):11832–46. doi: 10.3390/ijms150711832

4. Verma N, Cowperthwaite MC, Burnett MG, Markey MK. Differentiating tumor recurrence from treatment necrosis: a review of neuro-oncologic imaging strategies. *Neuro Oncol* (2013) 15(5):515–34. doi: 10.1093/neuonc/nos307

5. Wu Y, Den Z, Lin Y. Accuracy of susceptibility-weighted imaging and dynamic susceptibility contrast magnetic resonance imaging for differentiating high-grade glioma from primary central nervous system lymphomas: meta-analysis. *World Neurosurg* (2018) 112:e617–e23. doi: 10.1016/j.wneu.2018.01.098

6. Chao ST, Ahluwalia MS, Barnett GH, Stevens GH, Murphy ES, Stockham AL, et al. Challenges with the diagnosis and treatment of cerebral radiation necrosis. *Int J Radiat Oncol Biol Phys* (2013) 87(3):449–57. doi: 10.1016/j.ijrobp.2013.05.015

7. Zikou A, Sioka C, Alexiou GA, Fotopoulos A, Voulgaris S, Argyropoulou MI. Radiation necrosis, pseudoprogression, pseudoresponse, and tumor recurrence: imaging challenges for the evaluation of treated gliomas. *Contrast Media Mol Imaging* (2018) 2018:6828396. doi: 10.1155/2018/6828396

8. la Fougère C, Suchorska B, Bartenstein P, Kreth FW, Tonn JC. Molecular imaging of gliomas with PET: opportunities and limitations. *Neuro Oncol* (2011) 13(8):806–19. doi: 10.1093/neuonc/nor054

9. Page MJ, McKenzie JE, Bossuyt PM, Boutron I, Hoffmann TC, Mulrow CD, et al. The PRISMA 2020 statement: an updated guideline for reporting systematic reviews. *Bmj* (2021) 372:n71. doi: 10.1136/bmj.n71

10. Zuniga RM, Torcuator R, Jain R, Anderson J, Doyle T, Ellika S, et al. Efficacy, safety and patterns of response and recurrence in patients with recurrent high-grade gliomas treated with bevacizumab plus irinotecan. *J Neurooncol* (2009) 91(3):329–36. doi: 10.1007/s11060-008-9718-y

11. Bashir A, Mathilde Jacobsen S, Mølby Henriksen O, Broholm H, Urup T, Grunnet K, et al. Recurrent glioblastoma versus late posttreatment changes: diagnostic accuracy of O-(2-[18F]fluoroethyl)-L-tyrosine positron emission tomography (18F-FET PET). *Neuro Oncol* (2019) 21(12):1595–606. doi: 10.1093/neuonc/noz166

12. Xiaoxue T, Yinzhong W, Meng Q, Lu X, Lei J. Diagnostic value of PET with different radiotracers and MRI for recurrent glioma: a Bayesian network meta-analysis. *BMJ Open* (2023) 13(3):e062555. doi: 10.1136/bmjopen-2022-062555

13. Calabria FF, Chiaravalloti A, Jaffrain-Rea ML, Zinzi M, Sannino P, Minniti G, et al. 18F-DOPA PET/CT physiological distribution and pitfalls: experience in 215 patients. *Clin Nucl Med* (2016) 41(10):753–60. doi: 10.1097/RLU.0000000000001318

14. Yu J, Zheng J, Xu W, Weng J, Gao L, Tao L, et al. Accuracy of (18)F-FDOPA positron emission tomography and (18)F-FET positron emission tomography for differentiating radiation necrosis from brain tumor recurrence. *World Neurosurg* (2018) 114:e1211–e24. doi: 10.1016/j.wneu.2018.03.179

15. Fuenfgeld B, Mächler P, Fischer DR, Esposito G, Rushing EJ, Kaufmann PA, et al. Reference values of physiological 18F-FET uptake: Implications for brain tumor discrimination. *PloS One* (2020) 15(4):e0230618. doi: 10.1371/journal.pone.0230618

16. Whiting PF, Rutjes AW, Westwood ME, Mallett S, Deeks JJ, Reitsma JB, et al. QUADAS-2: a revised tool for the quality assessment of diagnostic accuracy studies. *Ann Intern Med* (2011) 155(8):529–36. doi: 10.7326/0003-4819-155-8-201110180-00009

17. Paprottka KJ, Kleiner S, Preibisch C, Kofler F, Schmidt-Graf F, Delbridge C, et al. Fully automated analysis combining [(18)F]-FET-PET and multiparametric MRI including DSC perfusion and APTw imaging: a promising tool for objective evaluation of glioma progression. *Eur J Nucl Med Mol Imaging* (2021) 48(13):4445–55. doi: 10.1007/s00259-021-05427-8

18. Skoblar Vidmar M, Doma A, Smrdel U, Zevnik K, Studen A. The value of FET PET/CT in recurrent glioma with a different IDH mutation status: the relationship between imaging and molecular biomarkers. *Int J Mol Sci* (2022) 23(12):6787. doi: 10.3390/ijms23126787

19. Müller M, Winz O, Gutsche R, Leijenaar RTH, Kocher M, Lerche C, et al. Static FET PET radiomics for the differentiation of treatment-related changes from glioma progression. *J Neurooncol* (2022) 159(3):519–29. doi: 10.1007/s11060-022-04089-2

20. Puranik AD, Rangarajan V, Dev ID, Jain Y, Purandare NC, Sahu A, et al. Brain FET PET tumor-to-white mater ratio to differentiate recurrence from post-treatment changes in high-grade gliomas. *J Neuroimaging* (2021) 31(6):1211–8. doi: 10.1111/jon.12914

21. Steidl E, Langen KJ, Hmeidan SA, Polomac N, Filss CP, Galldiks N, et al. Sequential implementation of DSC-MR perfusion and dynamic [(18)F]FET PET allows efficient differentiation of glioma progression from treatment-related changes. *Eur J Nucl Med Mol Imaging* (2021) 48(6):1956–65. doi: 10.1007/s00259-020-05114-0

22. Werner JM, Weller J, Ceccon G, Schaub C, Tscherpel C, Lohmann P, et al. Diagnosis of pseudoprogression following lomustine-temozolomide chemoradiation in newly diagnosed glioblastoma patients using FET-PET. *Clin Cancer Res* (2021) 27 (13):3704–13. doi: 10.1158/1078-0432.CCR-21-0471

23. Lohmann P, Elahmadawy MA, Gutsche R, Werner JM, Bauer EK, Ceccon G, et al. FET PET radiomics for differentiating pseudoprogression from early tumor progression in glioma patients post-chemoradiation. *Cancers (Basel)* (2020) 12 (12):3835. doi: 10.3390/cancers12123835

24. Maurer GD, Brucker DP, Stoffels G, Filipski K, Filss CP, Mottaghy FM, et al. (18) F-FET PET imaging in differentiating glioma progression from treatment-related changes: A single-center experience. *J Nucl Med* (2020) 61(4):505–11. doi: 10.2967/jnumed.119.234757

25. Kebir S, Schmidt T, Weber M, Lazaridis L, Galldiks N, Langen KJ, et al. A preliminary study on machine learning-based evaluation of static and dynamic FET-PET for the detection of pseudoprogression in patients with IDH-wildtype glioblastoma. *Cancers (Basel)* (2020) 12(11):3080. doi: 10.3390/cancers12113080

26. Kertels O, Mihovilovic MI, Linsenmann T, Kessler AF, Tran-Gia J, Kircher M, et al. Clinical utility of different approaches for detection of late pseudoprogression in glioblastoma with O-(2-[18F]Fluoroethyl)-L-tyrosine PET. *Clin Nucl Med* (2019) 44 (9):695–701. doi: 10.1097/RLU.0000000000002652

27. Pyka T, Hiob D, Preibisch C, Gempt J, Wiestler B, Schlegel J, et al. Diagnosis of glioma recurrence using multiparametric dynamic 18F-fluoroethyl-tyrosine PET-MRI. *Eur J Radiol* (2018) 103:32–7. doi: 10.1016/j.ejrad.2018.04.003

28. Dunkl V, Cleff C, Stoffels G, Judov N, Sarikaya-Seiwert S, Law I, et al. The usefulness of dynamic O-(2-18F-fluoroethyl)-L-tyrosine PET in the clinical evaluation of brain tumors in children and adolescents. *J Nucl Med* (2015) 56(1):88–92. doi: 10.2967/jnumed.114.148734

29. Galldiks N, Dunkl V, Stoffels G, Hutterer M, Rapp M, Sabel M, et al. Diagnosis of pseudoprogression in patients with glioblastoma using O-(2-[18F]fluoroethyl)-L-tyrosine PET. *Eur J Nucl Med Mol Imaging* (2015) 42(5):685–95. doi: 10.1007/s00259-014-2959-4

30. Herrmann K, Czernin J, Cloughesy T, Lai A, Pomykala KL, Benz MR, et al. Comparison of visual and semiquantitative analysis of 18F-FDOPA-PET/CT for recurrence detection in glioblastoma patients. *Neuro Oncol* (2014) 16(4):603–9. doi: 10.1093/neuonc/not166

31. Jeong SY, Lee TH, Rhee CH, Cho AR, Il Kim B, Cheon GJ, et al. 3'-deoxy-3'-[(18)F]fluorothymidine and O-(2-[(18)F]fluoroethyl)-L-tyrosine PET in patients with suspicious recurrence of glioma after multimodal treatment: initial results of a retrospective comparative study. *Nucl Med Mol Imaging* (2010) 44(1):45–54. doi: 10.1007/s13139-009-0007-2

32. Rachinger W, Goetz C, Pöpperl G, Gildehaus FJ, Kreth FW, Holtmannspötter M, et al. Positron emission tomography with O-(2-[18F]fluoroethyl)-l-tyrosine versus magnetic resonance imaging in the diagnosis of recurrent gliomas. *Neurosurgery.* (2005) 57(3):505–11. doi: 10.1227/01.NEU.0000171642.49553.B0

33. Rozenblum L, Zaragori T, Tran S, Morales-Martinez A, Taillandier L, Blonski M, et al. Differentiating high-grade glioma progression from treatment-related changes with dynamic [(18)F]FDOPA PET: a multicentric study. *Eur Radiol* (2023) 33(4):2548–60. doi: 10.1007/s00330-022-09221-4

34. Li C, Yi C, Chen Y, Xi S, Guo C, Yang Q, et al. Identify glioma recurrence and treatment effects with triple-tracer PET/CT. *BMC Med Imaging* (2021) 21(1):92. doi: 10.1186/s12880-021-00624-1

35. Pellerin A, Khalifé M, Sanson M, Rozenblum-Beddok L, Bertaux M, Soret M, et al. Simultaneously acquired PET and ASL imaging biomarkers may be helpful in differentiating progression from pseudo-progression in treated gliomas. *Eur Radiol* (2021) 31(10):7395–405. doi: 10.1007/s00330-021-07732-0

36. Zaragori T, Ginet M, Marie PY, Roch V, Grignon R, Gauchotte G, et al. Use of static and dynamic [(18)F]-F-DOPA PET parameters for detecting patients with glioma recurrence or progression. *EJNMMI Res* (2020) 10(1):56. doi: 10.1186/s13550-020-00645-x

37. Karunanithi S, Bandopadhyaya GP, Sharma P, Kumar A, Singla S, Malhotra A, et al. Prospective comparison of (99m)Tc-GH SPECT/CT and (18)F-FDOPA PET/CT for detection of recurrent glioma: a pilot study. *Clin Nucl Med* (2014) 39(2):e121–8. doi: 10.1097/RLU.0b013e318279bcd8

38. Xu T, Chen J, Lu Y, Wolff JE. Effects of bevacizumab plus irinotecan on response and survival in patients with recurrent Malignant glioma: a systematic review and survival-gain analysis. *BMC Canc* (2010) 10:252. doi: 10.1186/1471-2407-10-252

39. Ginet M, Zaragori T, Marie PY, Roch V, Gauchotte G, Rech F, et al. Integration of dynamic parameters in the analysis of (18)F-FDopa PET imaging improves the prediction of molecular features of gliomas. *Eur J Nucl Med Mol Imaging* (2020) 47 (6):1381–90. doi: 10.1007/s00259-019-04509-y

40. Galldiks N, Niyazi M, Grosu AL, Kocher M, Langen KJ, Law I, et al. Contribution of PET imaging to radiotherapy planning and monitoring in glioma patients - a report of the PET/RANO group. *Neuro Oncol* (2021) 23(6):881–93. doi: 10.1093/neuonc/noab013

41. Evangelista L, Cuppari L, Bellu L, Bertin D, Caccese M, Reccia P, et al. Comparison between 18F-dopa and 18F-fet PET/CT in patients with suspicious recurrent high grade glioma: A literature review and our experience. *Curr Radiopharm* (2019) 12(3):220–8. doi: 10.2174/1874471012666190115124536

42. Laverman P, Boerman OC, Corstens FH, Oyen WJ. Fluorinated amino acids for tumour imaging with positron emission tomography. *Eur J Nucl Med Mol Imaging* (2002) 29(5):681–90. doi: 10.1007/s00259-001-0716-y

43. Karunanithi S, Sharma P, Kumar A, Khangembam BC, Bandopadhyaya GP, Kumar R, et al. Comparative diagnostic accuracy of contrast-enhanced MRI and (18)F-FDOPA PET-CT in recurrent glioma. *Eur Radiol* (2013) 23(9):2628–35. doi: 10.1007/s00330-013-2838-6

44. Karunanithi S, Sharma P, Kumar A, Khangembam BC, Bandopadhyaya GP, Kumar R, et al. 18F-FDOPA PET/CT for detection of recurrence in patients with glioma: prospective comparison with 18F-FDG PET/CT. *Eur J Nucl Med Mol Imaging* (2013) 40(7):1025–35. doi: 10.1007/s00259-013-2384-0

45. Galldiks N, Stoffels G, Filss C, Rapp M, Blau T, Tscherpel C, et al. The use of dynamic O-(2-18F-fluoroethyl)-l-tyrosine PET in the diagnosis of patients with progressive and recurrent glioma. *Neuro Oncol* (2015) 17(9):1293–300. doi: 10.1093/neuonc/nov088

46. Langen KJ, Heinzel A, Lohmann P, Mottaghy FM, Galldiks N. Advantages and limitations of amino acid PET for tracking therapy response in glioma patients. *Expert Rev Neurother* (2020) 20(2):137–46. doi: 10.1080/14737175.2020.1704256

47. Jager PL, Vaalburg W, Pruim J, de Vries EG, Langen KJ, Piers DA. Radiolabeled amino acids: basic aspects and clinical applications in oncology. *J Nucl Med* (2001) 42 (3):432–45.

48. Zaccagna F, Grist JT, Quartuccio N, Riemer F, Fraioli F, Caracò C, et al. Imaging and treatment of brain tumors through molecular targeting: Recent clinical advances. *Eur J Radiol* (2021) 142:109842. doi: 10.1016/j.ejrad.2021.109842

frontiers | Frontiers in Oncology

TYPE Methods
PUBLISHED 30 January 2024
DOI 10.3389/fonc.2023.1248452

OPEN ACCESS

EDITED BY
Dimitrios N. Kanakis,
University of Nicosia, Cyprus

REVIEWED BY
Melih Kuncan,
Siirt University, Türkiye
Surendiran B,
National Institute of Technology Puducherry, India

*CORRESPONDENCE
G. Dheepak
dg6154@srmist.edu.in

RECEIVED 05 July 2023
ACCEPTED 12 December 2023
PUBLISHED 30 January 2024

CITATION
Dheepak G, J. AC and Vaishali D (2024) Brain tumor classification: a novel approach integrating GLCM, LBP and composite features.
Front. Oncol. 13:1248452.
doi: 10.3389/fonc.2023.1248452

Brain tumor classification: a novel approach integrating GLCM, LBP and composite features

G. Dheepak*, Anita Christaline J. and D. Vaishali

Department of Electronics & Communication Engineering, Faculty of Engineering and Technology, SRM Institute of Science and Technology, Vadapalani Campus, Chennai, TN, India

Identifying and classifying tumors are critical in-patient care and treatment planning within the medical domain. Nevertheless, the conventional approach of manually examining tumor images is characterized by its lengthy duration and subjective nature. In response to this challenge, a novel method is proposed that integrates the capabilities of Gray-Level Co-Occurrence Matrix (GLCM) features and Local Binary Pattern (LBP) features to conduct a quantitative analysis of tumor images (Glioma, Meningioma, Pituitary Tumor). The key contribution of this study pertains to the development of interaction features, which are obtained through the outer product of the GLCM and LBP feature vectors. The utilization of this approach greatly enhances the discriminative capability of the extracted features. Furthermore, the methodology incorporates aggregated, statistical, and non-linear features in addition to the interaction features. The GLCM feature vectors are utilized to compute these values, encompassing a range of statistical characteristics and effectively modifying the feature space. The effectiveness of this methodology has been demonstrated on image datasets that include tumors. Integrating GLCM (Gray-Level Co-occurrence Matrix) and LBP (Local Binary Patterns) features offers a comprehensive representation of texture characteristics, enhancing tumor detection and classification precision. The introduced interaction features, a distinctive element of this methodology, provide enhanced discriminative capability, resulting in improved performance. Incorporating aggregated, statistical, and non-linear features enables a more precise representation of crucial tumor image characteristics. When utilized with a linear support vector machine classifier, the approach showcases a better accuracy rate of 99.84%, highlighting its efficacy and promising prospects. The proposed improvement in feature extraction techniques for brain tumor classification has the potential to enhance the precision of medical image processing significantly. The methodology exhibits substantial potential in facilitating clinicians to provide more accurate diagnoses and treatments for brain tumors in forthcoming times.

KEYWORDS

brain tumor, GLCM, LBP, texture, composite feature, aggregated feature, non-linear feature

1 Introduction

A tumor is an abnormal growth of cells which occurs in any portion of the human body. Over two hundred various kinds of cancer, such as lung, blood, breast, heart, lymphoma, etc. have been reported (1). According to World Health Organization (WHO) fact sheet 2022, cancer has been the leading cause of death with 10 million deaths reported (2). Among the various types of tumors, brain tumors have been the primary reason for death in various age and gender groups and are also challenging to treat. A tumor in the human brain is a collection of malignant cells which develops when brain tissues suddenly and abnormally extend. There are different types of brain tumors, some are non-cancerous (benign) and some are cancerous (3). The human brain acts as the body's control hub. It coordinates the actions of vast numbers of neurons and their many connections. Tumor in the brain disrupts normal brain activities and the nervous system processes. The need to overcome the disadvantages of manual tumor image analysis, which is both time-consuming and vulnerable to human subjectivity, motivated machine learning based techniques of classifying tumors.

As discussed by Abdusalomov et al. (4) Glioma, Meningioma, Pitutary seem to be the common types of brain tumors that look like non-cancerous, but may be. Hence this research intends to study these brain tumors and classify them by incorporating advanced features such as GLCM and LBP, as well as interaction features and statistical analysis. This method has the potential to significantly improve the precision of medical image processing for more precise brain tumor identification and treatment planning.

The primary contributions of this present investigation are

- This research introduces a novel methodology for comprehensive texture analysis of tumor images. The approach integrates Gray-Level Co-occurrence Matrix (GLCM) and Local Binary Pattern (LBP) features. GLCM features capture spatial pixel intensity relationships, while LBP features identify local texture patterns. Together, these features provide a detailed insight into tumor textures, facilitating improved understanding and tumor classification.
- A novel feature generation technique has been proposed, which generates interaction features by multiplying GLCM and LBP feature vectors. This technique generates a new set of features that enhance the discriminative ability of the model, thereby enhancing its capacity to differentiate between various tumor morphologies. The incorporation of these interaction features enables the acquisition of a broader spectrum of texture data, resulting in a greater comprehension of tumor characteristics.
- In addition, the methodology incorporates the computation of aggregated characteristics derived from GLCM properties. These aggregated features, which consist of the sum, mean, and median of the GLCM features, provide a more comprehensive view of the overall characteristics of tumor textures.
- For Tumor classification Support Vector Machine (SVM) is implemented with extracted features which enhances the performance of tumor classification.

The next section discusses the various research works related to tumors and their classification.

2 Related literature

In order to categorize common brain tumor types, Kaplan et al. (5) have used nLBP and αLBP feature extraction approaches. Using the K-Nearest Neighbour (Knn) model and the nLBPd = 1 method, they achieved a high 95.56% success rate of identifying tumors. Another study by Abdusalomov et al. (4) used YOLOv7 and transfer learning to improve brain tumor diagnosis in MRI scans, they report an outstanding 99.5% accuracy for identifying the most common types of brain tumors Glioma, Meningioma, Pitutary. However, they also acknowledge the need for additional research, particularly for minor tumor identification (4).

Research by Kaya et al. (6) used a novel feature extraction technique based on co-occurrence matrices from vibration data to address the problem of accurate bearing issue identification. Effective success rates were obtained by utilizing 1D-LBP and machine learning: 87.50% for dataset 1 (various speeds), 96.5% for dataset 2 (fault size in mm), and 99.30% for dataset 3 (fault type - inner ring, outer ring, ball). Study by Solani et al. (7) examines the difficulties in diagnosing brain tumors and provides information on the potential of MR imaging. They adopt statistical and machine learning techniques to detect brain tumor for a chosen dataset. Yildirim et al. (8) have studied the most accepted forms of brain tumors include gliomas, meningiomas, and pituitary. They say that the optimal course of action for treating these tumors may differ reliant on the type. Brain tumors can be challenging to classify, even for experts, due to heterogeneous imaging findings (8).

According to Shinde et al. (9), while progress has been made in classifying anomalies in medical imaging, there are still challenges to overcome. These include, but are not limited to, model selection, data description, error detection, data sufficiency, and result reliability. As a result, there is no one highest benchmark for categorizing medical images. So, it is quite problematic in computer vision and machine learning domains. The algorithms mentioned generally are developed using soft computing and model-based methodologies, and their results are reliable (9). With the help of mobile sensor inputs, work by Kuncan et al. (10) presents a unique feature extraction approach called DS-1D-LBP for human activity recognition (HAR). They have successfully classified with the Extreme Learning Machine (ELM) with a high success rate of 96.87%. Research by Shil et al. (11) rely heavily on features that have been manually constructed and then provided to a classifier, such as Support Vector Machine, Decision Tree, or k-Nearest Neighbour (KNN). Khalid et al. state that the extensive nature of the dataset can cause delays in feature engineering, thereby increasing the likelihood of errors and highlighting the significance of domain expertise (12).

Processing and analyzing MRI images of brain tumors is one of the most challenging and promising new areas of study. An MRI, which employs magnetic fields and radio waves to generate overall images of internal body structures, is essential for determining the optimal course of treatment for a tumor and its progression.

Texture features based on GLCM were first introduced by Haralick et al. (13) in 1979. In biomedical field, advantage of the textural properties of images aids in image classification.

There are numerous methods available to derive the relevant data from imaging modalities for region-based segmentation, including artificial neural network (ANN), fuzzy clustering means (FCM), support vector machine (SVM), knowledge-based techniques, and the expectation-maximization (EM) algorithm technique. Image analysis using SVM and BWT methods was suggested by Bahadure et al. (14) for detecting and classifying brain tumors using MRI. Skull stripping, in which non-brain tissues are removed, allowed for a 95% detection rate utilizing this method. Joseph et al. (15) introduced a technique for segmenting MRI brain images for tumor diagnosis that combines the K-means clustering algorithm and morphological filtering technique. Alfonse and Salem (16) suggested a method for automatically classifying MRI scans for brain tumors using a support vector machine. The researchers employed Fast Fourier Transform (FFT) to extract features to enhance the classifier's precision. Additionally, they utilized technology that exhibited minimal redundancy and maximum relevance to reduce the number of features.

In order to better segregate brain tumors, Shree et al. (17) pre-processed the images using multiple noise removal methods. Their research employed DWT and GLCM-based characteristics of brain tumors. Any residual noise after segmentation was filtered out using morphological filtering procedures. The suggested model was trained and evaluated using the probabilistic neural network classifier for pinpointing tumor locations in brain MRI scans. Yao et al. (18) provided a method that includes extracting texture characteristics using the wavelet transform and classifier as SVM with an accuracy of 83% to process and address protocols of diverse images and non-linearity of actual data to classify improved MRI images related to contrast. Principal component analysis (PCA) and a radial basis function kernel with SVM were proposed by Kumar and Vijayakumar (19) for classifying and segmenting brain tumors. They were able to achieve 94% success rate using this strategy.

Saleck et al. (20) developed a Fuzzy C-Mean (FCM) way of figuring out the size of a patient's brain tumor. They could figure out how many groups were there in the FCM by looking at the intensity of each pixel. This approach uses GLCM texture feature extraction to forecast the threshold value. The generic performance of a model is established by how sensitive, specific, and accurate it is.

Considering the research going on in this field, it seems evident that choosing appropriate features of tumor images and adopting appropriate machine learning classifiers will lead to better identification of tumors.

Based on the literature survey, this research intends to study three types of brain tumors (Glioma, Meningioma, Pituitary) and classify them by incorporating novel and advanced features such as GLCM and LBP, as well as interaction features and statistical analysis. This research work introduces novel contributions in the following aspects:

- **Interaction Features:** The extraction of interaction features involves the computation of the outer product between the Gray-Level Co-occurrence Matrix (GLCM) and Local Binary Pattern (LBP) feature vectors. The aforementioned process results in the formation of a matrix that effectively encompasses the interplay between spatial and local texture data. The matrix is subsequently converted into a unidimensional array in order to constitute the collection of interaction features.
- **Non-linear Features:** Another significant contribution is applying a logarithmic transformation to the GLCM features. This transformation generates non-linear features, allowing for the capturing of complex relationships within tumor images. By incorporating these non-linear features, the research improves the discriminative power of the feature set and enables a more sophisticated analysis and interpretation of the tumor image properties.

3 Proposed methodology

Publicly available databases Figshare Dataset (13) has been used in this study since it is one of the most common datasets used by many other researchers. This brain tumor dataset contains 3064 T1-weighted contrast enhanced images from 233 patients for three kinds of brain tumor: meningioma (708 slices), glioma (1426 slices), and pituitary tumor (930 slices) (21). The conversion to grayscale from RGB is performed to enrich the images further. The three brain tumor images used are Glioma, Meningioma, and pituitary tumor. As proposed by Demirhan et al. (22) converting the input images to grayscale gives a simplified representation is obtained that effectively captures the overall brightness information while eliminating the complexities associated with color. The parameters include boosting the signal-to-noise ratio, making MR images look better, removing the background of unwanted sections, smoothing the inner parts and keeping the essential edges intact. The proposed work is depicted in Figure 1.

4 Feature extraction

To extract significant features from brain MRI images, six types of feature extraction techniques have been implemented in this study, as listed in Table 1. Using these techniques, important aspects of the images could be identified and analyzed.

4.1 GLCM feature extraction

Texture analysis facilitates the differentiation between healthy and unhealthy tissues for visual perception and ML algorithm. In addition, it reveals differences between malignant tumors and normal tissues that might not be observable by the naked eye. By selecting efficient statistical features for early diagnosis, the accuracy can be improved. Second-order statistical texture features can be extracted using GLCM. Creating a GLCM matrix and then deriving statistical metrics from this matrix measures the frequency with

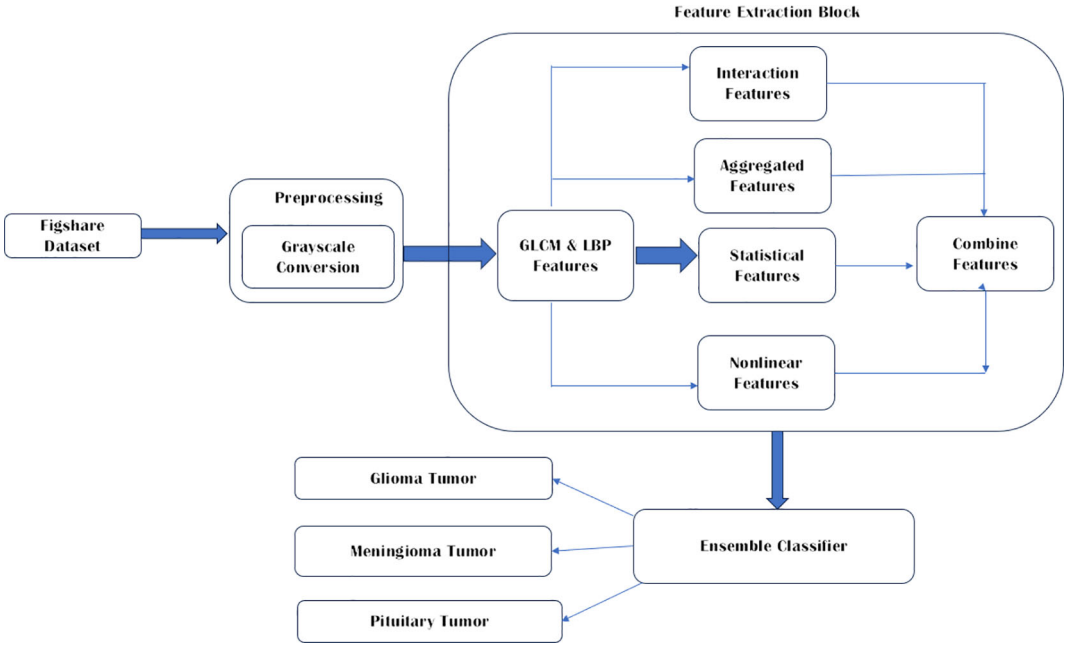

FIGURE 1
Overall proposed model architecture.

which pairs of pixels with specific values and a specific spatial relationship appear in an image. GLCM, or Gray-level spatial dependence matrix (GLSDM), has been used in this research used to extract the statistical features. GLCM was first proposed by Haralick et al. (23) for describing the geographical relationship between pixels with different levels of Gray-level.

To analyze an image's texture statistically, the GLCM counts how often pairs of pixels with the same value and the same relative position appear in the image. By determining the frequency with which pairs of pixels with a given weight and in a given spatial relationship occur in an image, the GLCM functions can characterize an image's texture through the extraction of statistical measurements. The Gray-Level Co-occurrence Matrix (GLCM) is a two-dimensional histogram where each pair of 'p' and 'q' represents the frequency with which the events 'p' and 'q' occur. As a function of distance S = 1, angle (0 degrees horizontal, 45 degrees positive diagonal, 90 degrees vertical, and 135 degrees negative diagonal), and gray scales 'p' and 'q', it determines the frequency with which a pixel of intensity 'p' occurs in proximity to a pixel of intensity 'q' at a given distance 'S' and orientation.

TABLE 1 Feature etxtraction Techniques used in this research work.

S.No	Feature Extraction Technique used
1	Grey Level Co-occurrence Matrix (GLCM) Features
2	Local Binary Patterns (LBP) Features
3	Interaction Features
4	Aggregated Features
5	Statistical Features
6	Nonlinear Features

After computing GLCM, five different statistical features are extracted from GLCM. These extracted features include,

Contrast: Determines the local variances of the grey-level co-occurrence matrix.

Homogeneity: Determines the proximity of the GLCM element distribution to the GLCM diagonal.

Dissimilarity: Quantifies the range of grayscale intensity.

Energy: It will calculate the pixel's uniformity.

Correlation: Calculates the average degree to which each pixel in the image is connected with its neighbors.

The formulas used to calculate the above characteristic features are shown in Table 2.

4.2 LBP features

The Local Binary Patterns (LBP) technique is a widely employed texture descriptor in image processing and computer vision. Local texture representation is a straightforward yet efficient method used to depict the texture characteristics of an image. This

TABLE 2 Features of GLCM.

Contrast	$\sum (i-j^2) \star (P\ i,j)$
Dissimilarity	$= \sum P_{i,j}\lvert i-j\rvert$
Homogeneity	$= \sum \frac{P(i,j)}{(1+\lvert i-j\rvert)}$
Energy	$= \sum \frac{P(i,j)}{(1+\lvert i-j\rvert)}$
Correlation	$= \sum \frac{(i-\mu i)(j-\mu J)}{(\sigma i \star \sigma j)}$

technique has been extensively applied in various domains, such as object recognition, face detection, and image segmentation. The step wise LBP Feature Extraction is, each pixel is compared with its neighboring pixels. Consider the Gray value of the center pixel as g_c, and the gray value of the neighboring pixel as g_p. Comparison is carried out with using Equation 1.

$$S(g_p, g_c) = if \quad g_p \geq = g_c \quad else \quad 0 \tag{1}$$

A circle of radius R is centered around the center pixel and the function S is applied to P evenly spaced pixels.

4.3 Interaction features

A novel approach implemented in this research is the extraction of image features for tumor classification, wherein a strategy for generating interaction features is employed with the aim of potentially improving the performance of the model. This approach entails the integration of two sets of important attributes: the GLCM attributes and LBP attributes, both of which effectively capture fundamental properties of the images being analyzed.

The GLCM features provides insights into the spatial interdependence of pixel intensities within an image, effectively capturing and representing texture details. In contrast, the features of LBP provide a quantification of the local spatial patterns of pixel luminance, thereby providing supplementary information regarding texture.

The computation of interaction features involves the outer product of the feature vectors obtained from GLCM and LBP. In mathematical terms, the outer product of the GLCM features vector (g) and the LBP features vector (l) yields a matrix (M). Each element $M_{i,j}$ of this matrix represents the product of the ith GLCM feature and the jth LBP feature. The aforementioned statement aptly describes the correlation between the respective GLCM and LBP features.

Subsequently, the interaction matrix is transformed into a one-dimensional vector, thereby generating a novel set of features that capture the interplay between the initial feature sets. The inclusion of this extended feature set, in combination with the existing GLCM and LBP features, offers a more exhaustive and refined depiction of the image. Consequently, it has the potential to improve the machine learning model's capacity to differentiate between various tumor classifications.

The steps involved in interaction features are,

Defining GLCM and LBP features vector: GLCM feature vector is defined as

$g = g_1, g_2, g_3, \ldots g_m$ and the LBP feature vectors as $l = l_1, l_2, l_3, \ldots l_n$ in which 'm' is the number of GLCM features and 'n' is number of LBP features.

Calculating the outer product: The matrix 'M' is obtained by computing the outer product of the two given vectors. The matrix is provided as follows:

$$M = g \otimes \mathrm{l} = \begin{bmatrix} g_1 l_1 & \cdots & g_1 l_n \\ \vdots & \ddots & \vdots \\ g_m l_1 & \cdots & g_m l_n \end{bmatrix} \tag{2}$$

Each element of this matrix $M_{ij} = g_i l_j$ is a new feature created which captures the interaction between i^{th} GLCM feature as well as with j^{th} LBP feature.

Combining interaction features and original features: The original GLCM and LBP features are combined with the interaction features to create the final feature vector for each image. If the GLCM feature vector 'g' has a size of m and the LBP feature vector 'l' has a size of n, then the final feature vector will have a size of $m + n + mXn$.

These procedures describe how interaction features are generated from GLCM and LBP features. This augmented feature set has the potential to provide a more comprehensive and nuanced image representation, thereby enhancing the performance of the image classification model.

Here GLCM calculates at 4 different angles such as (0, 45, 90, and 135 degrees). The GLCM algorithm proceeds by computing five distinct properties, namely 'contrast', 'dissimilarity', 'homogeneity', 'energy', and 'correlation', for each angle. These properties are then used to generate a vector of GLCM features. Assuming the vector representing the GLCM features for an image is [10, 20, 30, 40, 50]. The aforementioned values indicate that the contrast is 10, the dissimilarity is 20, the homogeneity is 30, the energy is 40, and the correlation is 50.

The LBP algorithm is employed to calculate the LBP values using 8 sampling points positioned evenly along a circle with a radius of 1. Subsequently, the histogram of these LBP patterns is computed. Suppose the Local Binary Patterns (LBP) features for a given image are represented by a histogram consisting of 256 bins. The values within this histogram range from 0.01 to 0.01, with each bin containing a distinct value.

The interaction features are generated through the computation of the outer product between the feature vectors of the Grey Level Co-occurrence Matrix (GLCM) and the Local Binary Patterns (LBP).

For the purpose of explanation, consider a simplified scenario where only first five bins of LBP features. These bins are represented by the values [0.01, 0.02, 0.03, 0.04, 0.05].

The 5x5 matrix is obtained by computing the outer product of the GLCM features [10, 20, 30, 40, 50] and the first 5 LBP features [0.01, 0.02, 0.03, 0.04, 0.05]. The value of each element in this matrix is obtained by multiplying a feature from the Grey Level Co-occurrence Matrix (GLCM) with a feature from the Local Binary Patterns (LBP) feature.

The 5x5 matrix is obtained by taking the outer product of the GLCM features [10, 20, 30, 40, 50] and the first 5 LBP features [0.01, 0.02, 0.03, 0.04, 0.05]. The value of each element in this matrix is obtained by multiplying a feature derived from GLCM with a feature derived from the LBP algorithm as represented in Equation 3.

$$\begin{bmatrix} 10*0.01 & \cdots & 10*0.05 \\ \vdots & \ddots & \vdots \\ 50*0.01 & \cdots & 50*0.05 \end{bmatrix} \quad (3)$$

The interaction features offer way to capture the potentially significant connections among various elements of an image's texture. The precise dynamics of these interactions are dependent upon the data and the attributes of the images under examination. In the context of tumor images, these interactions may potentially expose complicated patterns that are pivotal in distinguishing between various tumor types.

4.4 Aggregated features

The aggregated features represent the additional statistical features of GLCM features. The GLCM features can be consolidated into more straightforward statistical measures. The mean, median, and total of the GLCM characteristics are these statistical measurements. The steps involved in aggregated features calculation is shown in Algorithm 1.

```
Input: GLCM Features
Output: Aggregated Features
Initialize sum as 0
for each GLCM feature in the input do
    Add the GLCM feature to the sum
end for
Compute mean as sum divided by the total number of GLCM features
Sort the GLCM features in ascending order
Compute the median based on the sorted list of GLCM features
Output the sum, mean, and median as the aggregated features
```

Algorithm 1. Calculation of aggregated features.

The features extracted from aggregated features are as follows,

Sum: The total number of GLCM characteristics is determined. This gives us a single number that can be taken as a measure of the "amount" of GLCM features in the image. If the GLCM characteristics are represented by the vector g = [$g1$, $g2$,…gn] then $g\_m = g1 + g2 + \ldots + gn$ gives the total.

Mean: The average GLCM characteristics are determined. This gives us a single number that stands in for the "typical" value of the GLCM feature in the image.

$G_{Mean} = \frac{(g1+g2+\ldots gn)}{n}$ gives the mean, where 'n' defines the GLCM features total numbers.

Median: GLCM features median are computed. When the GLCM features are ordered numerically, this yields a single value that characterizes the "middle" value. The median is the midpoint if 'n' is an odd number. If 'n' is divisible by 2, then the median is the midpoint between those two values.

Following these computations, the aggregated GLCM features take the form of a vector with three elements, which are denoted by the notations [*g_sum, g_mean, and g_median*].

The aggregated features (sum, mean, and median) provide a summary of the GLCM features, capturing various aspects of their level and distribution. In addition to the GLCM features, LBP features, interaction features, statistical features, and non-linear features, these characteristics are added to the final feature vector for each image.

Pattern recognition, machine learning, and image classification employ aggregated features such as summation, average, and median. The raw features are condensed, effectively representing the central tendency and overall pattern of the data, thereby offering a simplified yet meaningful perspective of the dataset. The aforementioned properties exhibit a lower degree of variation compared to individual data points, thereby enhancing the robustness of models against the presence of noisy or outlier data. The utilization of these techniques results in a reduction of data dimensionality, thereby enhancing the efficiency of algorithms. The inclusion of aggregated features in a model has been observed to enhance its predictive performance by uncovering latent data patterns. The code provided utilizes the GLCM attributes to generate aggregated features that summarize the textural characteristics of the image. This has the potential to enhance the tumor classification model.

4.5 Statistical GLCM features

A set of statistical measures derived from GLCM of an image constitutes the statistical GLCM features. The GLCM matrix depicts the spatial relationship among image pixel pairs. Each element of the GLCM indicates the probability that two pixels with a particular grey level will occur at a particular distance apart. GLCM statistical traits are used to describe an image's texture (24). Texture is how the pixels in an image are placed in space. It can be used to tell the difference between different kinds of images, like images of nature, medical images, and images of factories, etc.

The following features are derived under statistical GLCM features,

Variance: The variance quantifies the degree to which GLCM features deviate from their mean value. When the variance of the GLCM features is high, the values they take on span a wide range, whereas when it's low, the features tend to cluster tightly around the mean. Equation 2 represent the variance formulation. Provided that GLCM feature vector $g = [g_1, g_2 \ldots g_m]$. Where 'm' is the number of GLCM features.

$$variance = \; = \frac{1}{m}\sum_{i=1}^{m}(g_i - mean)^2 \quad (4)$$

Where, average of GLCM features is mean.

Skewness: The concept of skewness pertains to the degree of asymmetry exhibited by the distribution of GLCM features in relation to their mean value. Skewness is computed as Equation 5,

$$skewness = \frac{1}{m}\sum_{i=1}^{m}\left(\frac{g_i - mean}{std}\right)^3 \quad (5)$$

Where 'std' is the standard deviation of GLCM features.

Kurtosis: Kurtosis assesses the tailedness of GLCM feature distributions. High kurtosis shows thick tails and a strong peak, indicating many outliers. Low kurtosis shows light tails and a flat peak, indicating no outliers. Mathematically Kurtosis is expressed in Equation 6.

$$kurtosis = \frac{1}{m}\sum_{i=1}^{m}\left(\frac{g_i - mean}{std}\right)^4 - 3 \quad (6)$$

From Equations 3, 4 'm' is the number of GLCM features and g_i refers to the i^{th} element of GLCM feature vector.

These statistical GLCM characteristics can shed light on how the GLCM features are typically distributed. Statistical GLCM features exhibit information on the texture's variability, asymmetry, and outliers, while GLCM features themselves capture the texture details within the image.

The incorporation of statistical GLCM features, such as variance, skewness, and kurtosis, enhances the predictive model by encompassing supplementary distributional information pertaining to the GLCM features. The statistical measures employed in this study shed light on subtle texture variations that may not be easily distinguishable solely from the raw GLCM features, as they effectively capture the spread, asymmetry, and tailedness of these features. The model's exceptional performance metrics, such as its nearly perfect accuracy, precision, recall, and F1 score, are likely enhanced by the incorporation of statistical GLCM features, although other factors may also contribute to these outcomes. The inclusion of these features enhances the diversity of the 1547-feature set, thereby augmenting the model's capacity to accurately classify the tumor images. Statistical GLCM features play a crucial role in enhancing the predictive performance of the model by providing detailed information regarding the texture characteristics of the image.

4.6 Non-linear features

Another set of novel features of this research work, in terms of non-linear features, is computed from the GLCM feature vectors by applying a logarithmic transformation. This process generates non-linear features from the GLCM feature vectors. These GLCM feature vectors, obtained from grayscale image analysis, contain numerical values representing various statistical measures. The application of the logarithmic transformation on these GLCM feature vectors gives rise to the non-linear features. These non-linear features capture intricate patterns and relationships in the data, which may enhance the performance of machine learning models.

The procedure for obtaining non-linear features from the features derived from the Grey Level Co-occurrence Matrix (GLCM) is as follows,

GLCM feature computation: The initial stage entails the computation of the Gray-Level Co-occurrence Matrix (GLCM) features, which serve to extract texture information from the image. The aforementioned features consist of contrast, dissimilarity, homogeneity, energy, and correlation. The computations pertain to the manipulation of the Grey Level Co-Occurrence Matrix (GLCM), a matrix that denotes the occurrence frequency of various combinations of pixel intensities within the image.

The GLCM features can be denoted as C(contrast), D (dissimilarity), H(homogeneity),

E (energy), and Corr(correlation).

Applying Non-linear Transformation: Once the GLCM features have been computed, a non-linear transformation is applied to these features by utilizing the natural logarithm function. The transformation is represented by,

$$nq\,.\,logq(m) = \log(m+1) \quad (7)$$

From Equation 7 where, 'm' as the scalar value or the array of the input for which the natural log is to be determined and the input array is being incremented by '1' which is referred as 'm+1' in Equation 3. Later, the modified array log function is '(m+1)' which is being computed for each element present in GLCM vector. The resultant of this log function is the non-linear features.

The computation of the non-linear features corresponding to each GLCM feature is performed in the following manner.

$$C' = \log(1 + C) \quad (8)$$

$$D' = \log(1 + D) \quad (9)$$

$$H' = \log(1 + H) \quad (10)$$

$$E' = \log(1 + E) \quad (11)$$

$$Corr' = \log(1 + Corr) \quad (12)$$

Where Equations 8-12 represent the transformed GLCM features.

In the given transformation, it is crucial to add one to the original feature value, denoted as C, before applying the natural logarithm function, represented as C' = log(1+C). The need for this adjustment arises in cases where the correlation coefficient 'C' is equal to zero, as the natural logarithm of zero is undefined. This lack of definition can result in computational challenges. The inclusion of a constant term enables the logarithmic transformation to be applicable to all conceivable values of 'C', encompassing the value of zero. This step is crucial in ensuring the integrity and precision of the feature engineering process. The identical process is employed for the remaining GLCM features, ensuring the integrity of all modified features.

The primary objective of employing the logarithmic transformation is to effectively capture and accentuate non-linear relationships and variations present within the GLCM features. Through the utilization of the logarithm function, the feature values undergo a transformation, resulting in their representation on a logarithmic scale. The utilization of this technique can facilitate the identification of patterns, intensify the differentiation between elements, and enhance the accuracy of the representation of the characteristics of the GLCM.

Non-linear transformations have the potential to effectively capture complex structures within the data, which may not be easy to identify through the original features. Consequently, the utilization of such transformations has the capacity to enhance the performance of machine learning models.

4.7 Concatenated features

Finally, the various features including GLCM, LBP, interaction, aggregated, statistical, and non-linear features are consolidated into a unified feature vector for every image. The process involves arranging all the features consecutively to create a lengthy vector. The concatenated feature vector serves as a representation of the image within the feature space, enabling its utilization in subsequent analysis or machine learning endeavours.

TABLE 3 Performance metrics formula.

Metric	Formula
Accuracy	(TP + TN)/(TP + TN + FP + FN)
Precision	TP/(TP + FP)
Recall	TP/(TP + FN)
F1-score	2 * (precision * recall)/(precision + recall)
Sensitivity	TPR
Specificity	TNR
TPR	TP/(TP + FN)
FPR	FP/(FP + TN)
FNR	FN/(TP + FN)
TNR	TN/(FP + TN)

5 Results & discussion

The brain tumor classification model was implemented in Python. Statistical and non-linear feature extraction were used in conjunction with GLCM, LBP, Interaction, and aggregation to create the model. Finally, we classified brain tumors using a support vector machine.

Proposed Composite Feature Extraction Model Performance

In this work, a set of performance metrics have been computed to evaluate the effectiveness of the proposed composite Feature Extraction model, as illustrated in Table 3.

Tables 4–8 compares the proposed Composite Feature Extraction model's sensitivity, precision, specificity, accuracy, DSC, FPR, and FNR metrics with 23 existing models.

Table 4 presents a comprehensive evaluation of performance metrics for different models, including the Composite Feature Extraction model proposed in this study. The assessed metrics include Precision, Recall (or sensitivity), F1-score, Specificity, and Accuracy.

The proposed Composite Feature Extraction model demonstrates exceptional performance in brain tumor classification, achieving approximately 99.83% across all key metrics: Precision, Recall, F1-score, Specificity, and Accuracy. The obtained result indicates the model's high reliability in accurately identifying tumors and healthy cases, effectively reducing false outcomes. The balanced F1-score shows the model's consistent performance in precision and recall. Overall, the model's robustness and superior performance signify its effectiveness in brain tumor classification, surpassing existing models.

The presented Table 5 provides a comparative analysis of the Dice Similarity Coefficient (DSC) values of different models utilized to classify three distinct types of brain tumors, namely glioma, meningioma, and pituitary tumors. The Dice similarity coefficient (DSC) is an essential metric to quantify the degree of similarity between the predicted and actual tumor regions observed in brain images. A greater DSC (Dice similarity coefficient) value indicates a higher level of accuracy in the model, particularly in accurately classifying and distinguishing glioma, meningioma, and pituitary tumors. As proposed, the Composite Feature Extraction model demonstrates exceptional performance with a Dice Similarity Coefficient (DSC) value of 99.6. This value signifies the model's superior accuracy in effectively classifying the three distinct types of brain tumors, surpassing the performance of existing models.

Table 6 illustrates the Composite Feature Extraction model's enhanced efficacy in classifying tumors. The model demonstrates superior performance compared to existing models, as evidenced by its remarkably low False Positive Rate (FPR) of 0.00625 and a False Negative Rate (FNR) of 0.0. These results highlight the model's exceptional accuracy and reliability in effectively reducing false alarms and missed detections.

Table 7 presents the categorization of Meningioma, Glioma, and Pituitary Tumours utilizing various machine-learning techniques. The combined studies used a total of 3064 samples.

TABLE 4 Comparison of performance metrics: existing models with composite feature extraction (proposed model).

Author/Name of Model	Precision	Recall or sensitivity	F1-score	Specificity	Accuracy
Gupta et al, 2019 (24)	98.84	97.25	97.21	98.12	96.28
Rasool et al (25),	98.1	98.00	–	–	98.12
Fine-tuned EfficientNetB2, 2023 (26)	98.65	98.77	–	99.34	98.86
DAWE Model, 2021 (27)	97.4	95.6	–	96.9	99.3
proposed Composite Feature Extraction Model	**99.837**	**99.836**	**99.836**	**99.836**	**99.83**

The bold letter used are highlighting the proposed model used in the manuscript.

TABLE 5 DSC comparison: composite feature extraction vs. existing models.

Name of the Model	Dice Similarity Coefficient (DSC)
HOG + LBP + deep features, 2021 (28)	96.11
RG + MKM + U-NET, 2020 (29)	90
DAWE Model, 2021 (27)	96.5
Multiscale Cascaded Multitask Network, 2023 (30)	96.21
Proposed Composite Feature Extraction Model	**99.6**

The bold letter used are highlighting the proposed model used in the manuscript.

TABLE 6 FPR and FNR comparison: composite feature extraction vs. existing models.

Model	FPR	FNR
DAE-JOA, 2020 (31)	0.46	0.04
Stacked auto-encoder, 2019 (32)	0.07	0.1
DWAE model (27)	0.0625	0.031
Proposed Composite Feature Extraction Model	**0.00625**	**0.0**

The bold letter used are highlighting the proposed model used in the manuscript.

The proposed methodologies for image classification include a Convolutional Neural Network (CNN) model achieving an accuracy of 97.3%. Additionally, a hybrid approach combining Convolutional Dictionary Learning and AlexNet achieves a 91-96% accuracy range. Another model, BrainMRNet, incorporates hypercolumns, attention modules, and residual blocks, achieving an accuracy range of 96-98%. The proposed Composite Feature Extraction model utilizing GLCM, LBP, and Composite Features achieves an accuracy of 99.83% compared with other existing models.

In this research work, SVM classifier with a linear kernel is implemented to classify different types of tumors. The input data is processed and converted into the desired format using the kernel function. The complexity of a linear Support Vector Machine (SVM) is lower than that of a non-linear SVM, resulting in faster training.

Support Vector Machines (SVMs) can effectively classify data points by projecting them onto a feature space with many dimensions, even in cases where the data points are not linearly separable. Once a separator between the categories has been identified, the data is transformed, representing the division as a hyperplane. In the present context, the performance metrics of accuracy, precision, recall, and F1 score indicate that SVM can effectively discriminate between various classes of brain tumors. Accurately classifying brain tumors is paramount in medical diagnosis and subsequent treatment planning.

The comparison of various techniques for classifying brain tumors is presented in Table 8. Several models are included in this study, such as BMRI-NET, which is a stack ensemble model. Additionally, a two-channel deep neural network (DNN) model, GoogleNet with K-nearest neighbors (KNN), VGG-16, Resnet50, and InceptionV3 models, a simple convolutional neural network (CNN), a multiscale cascaded multitask network, and the DL (ResNet50V2) model are also considered. The accuracy of the data falls within the range of 96.3% to 99.68%.

The highest accuracy of 99.83% was achieved by employing a combination of Composite Feature Extraction techniques, namely Grey Level Co-occurrence Matrix (GLCM), Local Binary Patterns (LBP), and Composite Features, in conjunction with an SVM-Linear classifier. The findings of this study indicate that the technique examined in this research is the most prominent method for classifying brain tumors when compared to other approaches, exhibiting exceptional levels of accuracy.

From Figure 2, the model's classification performance is considered exceptional based on the Area Under the Curve (AUC) values obtained from the Receiver Operating Characteristic (ROC) analysis. The model achieves a perfect Area Under the Curve (AUC) score of 1.00, indicating its ability to classify instances belonging to Class 0 and Class 2 accurately. Despite encountering challenges and exhibiting a few inaccuracies, the model's overall performance remains commendable, evidenced by its high Area Under the Curve (AUC) value of 0.92. However, it is essential to consider the comprehensive evaluation of the model's performance. It is noteworthy that the micro-average AUC achieves a near-perfect score of 0.99, indicating the model's high efficacy across all classes.

A significant amount of time, specifically 654.45 seconds, was dedicated to the analysis of image features, such as the Grey Level Co-occurrence Matrix (GLCM) and Local Binary Pattern (LBP),

TABLE 7 Comparison based on dataset: composite feature extraction vs. existing models.

Author	Brain Tumor classes	Image Dataset	Feature Extraction/selection	Accuracy
Fransisco Javier Diaz-pernas, MPDI 2021	Meningioma, Glioma, and Pituitary Tumor	3064	CNN model	97.3
XiaoqingGu, Neuroscience, 2021	Meningioma, Glioma, and Pituitary Tumor	3064	Convolutional dictionary learning+AlexNet	91-96
Mesut T, Springer 2021	Meningioma, Glioma, and Pituitary Tumor	3064	BrainMRNet, including hypercolumn technique, attention modules, and residual blocks	96-98
Proposed Composite Feature Extraction model	**Meningioma, Glioma, and Pituitary Tumor**	**3064**	**GLCM, LBP, and Composite Features**	**99.83**

The bold letter used are highlighting the proposed model used in the manuscript.

TABLE 8 Accuracy comparison: composite feature extraction vs. existing models.

Author	Technique used	Accuracy (%)
Asif et al., 2023 (33)	BMRI-NET (Stack ensemble model)	98.69
Jyostna et al., 2021 (34)	Two-channel DNN model	98.04
Deepak and Amir 2019 (35)	GoogleNet + KNN	98.00
Alshayeji et al., 2021 (36)	Concatenation of 2 CNN	97.37
Patel M 2023 (37)	VGG-16, Resnet50, InceptionV3	0.975 for VGG-16, 0.95 for Resnet50, 0. 915 for InceptionV3
Latif G (2022) (38)	CNN	96.30
Z. Sobhaninia et al. (2023) (30),	Multiscale Cascaded Multitask Network	97.98
Md.A. Talukder et al. (2023) (39),	DL (ResNet50V2)	99.68
Proposed Composite Feature Extraction model	**GLCM, LBP, and Composite Features+SVM-Linear**	**99.83**

The bold letter used are highlighting the proposed model used in the manuscript.

during the extraction process. However, the training process of the Support Vector Machine (SVM) classifier using these features was completed in a mere 0.16 seconds. The utilization of resources in this study was primarily focused on feature extraction rather than model training. With a strikingly low ratio of 0.00024389, the outstanding efficiency of computation is evident in this scenario, clearly demonstrating the high priority of computing resources.

The model attained a perfect average accuracy score of 1.0 on the training data, regardless of the varying sizes of the training sets. Nevertheless, notwithstanding the flawless score, the model exhibited commendable performance on the validation data. The predictive capabilities of the model exhibit a high level of robustness, as indicated by a mean accuracy score that falls within the range of 0.993 to 0.998. Furthermore, it is worth noting that the model consistently demonstrated strong performance across a diverse set of data folds, as indicated by the narrow range of standard deviations, which varied between 0.013 and 0.035.

6 Conclusion

Based on the obtained results, the classification model demonstrates exceptional performance, with an accuracy, precision, recall, and F1 score that are all close to 1, indicating a high success rate in classifying across all three classes of brain tumors (Glioma, Meningioma, Pitutary). The model also demonstrates a 100% True Positive Rate (no false negatives) and

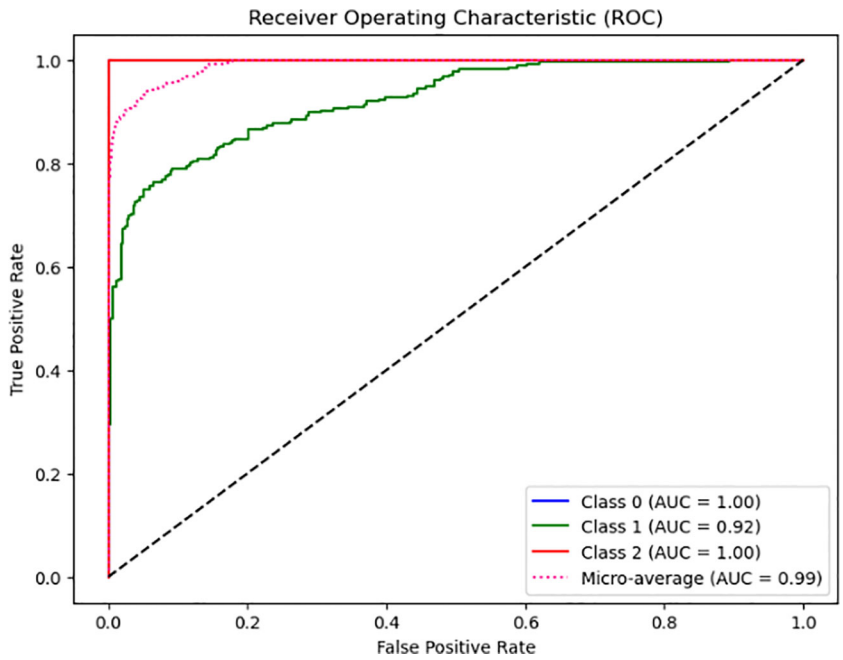

FIGURE 2
Proposed composite feature extraction model ROC plot.

a 0% False Negative Rate (no false positives), in addition to a very low False Positive Rate, indicating an excellent balance between sensitivity and specificity.

This work presents a novel methodology that offers an improved representation of tumor image textures by combining LBP and GLCM features. The addition of interaction features, which are created by taking the outer product of the GLCM and LBP vectors, greatly improves the derived features' ability to discriminate. This unique feature distinguishes the strategy from other approaches. Furthermore, an even more thorough representation of critical tumor image characteristics is obtained through the integration of aggregated, statistical, and non-linear information. Combining the approach with a linear support vector machine classifier yields 99.84% of accuracy rate. We opted to use the Figshare dataset so as to compare our classification accuracies with existing research done with same dataset. Being better than other research outcomes, this method can be applied to real time data.

As the most time-consuming phase, future research could concentrate on streamlining the extraction of features. In addition, future research may investigate the possibility of utilizing the extracted detailed features with less computational time. Another objective of future research is to analyze and classify high-grade brain tumors comprehensively utilizing high-grade brain tumors dataset to improve an understanding of complex tumors.

Data availability statement

The original contributions presented in the study are included in the article/supplementary material. Further inquiries can be directed to the corresponding author.

Ethics statement

Ethical review and approval was not required for the study on human participants in accordance with the local legislation and institutional requirements. Written informed consent from the patients/participants or patients/participants' legal guardian/next of kin was not required to participate in this study in accordance with the national legislation and the institutional requirements.

Author contributions

All authors listed have made a substantial, direct, and intellectual contribution to the work, and approved it for publication.

Funding

The author(s) declare that no financial support was received for the research, authorship, and/or publication of this article.

Acknowledgments

We would also like to thank SRM Institute of science and Technology, Vadapalani Campus for supporting us in providing good lab infrastructure to carry out our research.

Conflict of interest

The authors declare that the research was conducted in the absence of any commercial or financial relationships that could be construed as a potential conflict of interest.

Publisher's note

References

1. Davis CP. Cancer causes, types, treatment, stages and prevention. In: *Cancer: Symptoms, Causes, Treatment, Stages, Prevention (medicinenet.com)*. MedicineNet (2023).

2. Cancer. In: *Cancer (who.int)*. WHO Factsheet.

3. *Brain Tumor Brain tumor - Symptoms and causes* (2022). Mayo Clinic (Accessed August 04, 2022).

4. Abdusalomov AB, Mukhiddinov M, Whangbo TK. Brain tumor detection based on deep learning approaches and magnetic resonance imaging. *Cancers (Basel)* (2023) 15(16):4172. doi: 10.3390/cancers15164172

5. Kaplan K, Kaya Y, Kuncan M, Ertunç HM. Brain tumor classification using modified local binary patterns (LBP) feature extraction methods. *Med Hypotheses* (2020) 139:109696. doi: 10.1016/j.mehy.2020.109696

6. Kaya Y, Kuncan M, Kaplan K, MiNaz MR, Ertunç HM. A new feature extraction approach based on one dimensional gray level co-occurrence matrices for bearing fault classification. *J Exp Theor Artif Intell* (2020) 33(1):161–78. doi: 10.1080/0952813x.2020.1735530

7. Solanki S, Singh UP, Chouhan SS, Jain S. Brain tumor detection and classification using intelligence techniques: an overview. *IEEE Access* (2023) 11:12870–86. doi: 10.1109/access.2023.3242666

8. Yildirim M, Cengil E, Eroglu Y, Cinar A. Detection and classification of glioma, meningioma, pituitary tumor, and normal in brain magnetic resonance imaging using deep learning-based hybrid model. *Iran J Comput Sci* (2023) 6:455–464. doi: 10.1007/s42044-023-00139-8

9. Shinde AS, Mahendra BM, Nejakar SM, Herur S, Bhat N. Performance analysis of machine learning algorithm of detection and classification of brain tumor using computer vision. *Adv Eng Software* (2022) 173:103221. doi: 10.1016/j.advengsoft.2022.103221

10. Kuncan F, Kaya Y, Kuncan M. A novel approach for activity recognition with down-sampling 1D local binary pattern features. *Adv Electrical Comput Eng* (2019) 19 (1):35–44. doi: 10.4316/aece.2019.01005

11. Shil SK, Polly FP, Hossain MA, Ifthekhar MS, Uddin MN, Jang YM. (2017). An improved brain tumor detection and classification mechanism, in: *2017 International Conference on Information and Communication Technology Convergence (ICTC)*, Jeju, Korea (South. pp. 54–7. doi: 10.1109/ictc.2017.8190941

12. Khalid S, Khalil T, Nasreen S. (2014). A survey of feature selection and feature extraction techniques in machine learning, in: *2014 Science and Information Conference*, London, UK. pp. 372–8. doi: 10.1109/sai.2014.6918213

13. Haralick RM. Statistical and structural approaches to texture. *Proc IEEE* (1979) 67(5):786–804. doi: 10.1109/PROC.1979.11328

14. Bahadure NB, Ray AK, Thethi HP. Image analysis for MRI based brain tumor detection and feature extraction using biologically inspired BWT and SVM. *Int J Biomed Imaging* (2017) 2017:1–12. doi: 10.1155/2017/9749108

15. Joseph RP, Singh CS. Brain tumor MRI image segmentation and detection in image processing. *Int J Res Eng Technol* (2014) 03(13):1–5. doi: 10.15623/ijret.2014.0313001

16. Alfonse M, Salem M. An automatic classification of brain tumors through MRI using support vector machine. *Egypt Comput Sci J* (2016) 40:11–21.

17. Shree NV, Kumar TKS. Identification and classification of brain tumor MRI images with feature extraction using DWT and probabilistic neural network. *Brain Inf* (2018) 5(1):23–30. doi: 10.1007/s40708-017-0075-5

18. Yao J, Chen JC, Chow C. Breast tumor analysis in dynamic contrast enhanced MRI using texture features and wavelet transform. *IEEE J Selected Topics Signal Process* (2009) 3(1):94–100. doi: 10.1109/jstsp.2008.2011110

19. Kumar P, Vijayakumar B. Brain tumour mr image segmentation and classification using by PCA and RBF kernel based support vector machine. *Middle-East J Sci Res* (2015) 23(9):2106–16.

20. Saleck MM, Elmoutaouakkil A, Mouçouf M. (2017). Tumor detection in mammography images using fuzzy C-means and GLCM texture features, in: *14th International Conference on Computer Graphics, Imaging and Visualization*, . pp. 122– 5.

21. Cheng J. Brain tumor dataset. (2017). doi: 10.6084/m9.figshare.1512427.v5

22. Demirhan A, Törü M, Güler İ. Segmentation of tumor and edema along with healthy tissues of brain using wavelets and neural networks. *IEEE J Biomed Health Inf* (2015) 19(4):1451–8. doi: 10.1109/jbhi.2014.2360515

23. Haralick RM, Shanmugam K, Dinstein I. Textural features for image classification. *IEEE Trans Syst Man Cybern* (1973) 3(6):610–21. doi: 10.1109/TSMC.1973.4309314

24. Gupta N, Bhatele PR, Khanna P. Glioma detection on brain MRIs using texture and morphological features with ensemble learning. *Biomed Signal Process Control* (2019) 47:115–25. doi: 10.1016/j.bspc.2018.06.003

25. Rasool MI, Ismail NH, Boulila W, Ammar A, Samma H, Yafooz WMS, et al. A hybrid deep learning model for brain tumour classification. *Entropy* (2022) 24(6):799. doi: 10.3390/e24060799

26. Zulfiqar F, Bajwa UI, Mehmood Y. Multi-class classification of brain tumor types from MR images using EfficientNets. *Biomed Signal Process Control* (2023) 84:104777. doi: 10.1016/j.bspc.2023.104777

27. Isselmou AEK, Xu G, Shuai Z, Saminu S, Javaid I, Ahmad IS, et al. Brain tumor detection and classification on MR images by a deep wavelet auto-encoder model. *Diagnostics* (2021) 11(9):1589. doi: 10.3390/diagnostics11091589

28. Biratu ES, Schwenker F, Debelee TG, Kebede SR, Negera WG, Molla HT. Enhanced region growing for brain tumor MR image segmentation. *J Imaging* (2021) 7 (2):22. doi: 10.3390/jimaging7020022

29. Saba T, Mohamed AA, El-Affendi MA, Amin J, Sharif M. Brain tumor detection using fusion of hand crafted and deep learning features. *Cogn Syst Res* (2020) 59:221–30. doi: 10.1016/j.cogsys.2019.09.007

30. Sobhaninia Z, Karimi N, Khadivi P, Samavi S. Brain tumor segmentation by cascaded multiscale multitask learning framework based on feature aggregation. *Biomed Signal Process Control* (2023) 85:104834. doi: 10.1016/j.bspc.2023.104834

31. Raja PMS, Rani AV. Brain tumor classification using a hybrid deep autoencoder with Bayesian fuzzy clustering-based segmentation approach. *Biocybernetics Biomed Eng* (2020) 40(1):440–53. doi: 10.1016/j.bbe.2020.01.006

32. Amin J, Sharif M, Gul N, Raza M, Anjum MA, Nisar MF, et al. Brain tumor detection by using stacked autoencoders in deep learning. *J Med Syst* (2019) 44(2). doi: 10.1007/s10916-019-1483-2

33. Asif S, Zhao M, Chen X, Zhu Y. BMRI-NET: A deep stacked ensemble model for multi-class brain tumor classification from MRI images. *Interdiscip Sciences: Comput Life Sci* (2023) 15:499–514. doi: 10.1007/s12539-023-00571-1

34. Bodapati JD, Shaik NS, Naralasetti V, Mundukur NB. Joint training of two-channel deep neural network for brain tumor classification. *SIViP* (2021) 15(4):753–60. doi: 10.1007/s11760-020-01793

35. Deepak S, Ameer PM. Brain tumor classification using deep CNN features via transfer learning. *Comput Biol Med* (2019) 111:103345. doi: 10.1016/j.compbiomed.2019.103345

36. Al-Shayeji M, Al-Buloushi J, Ashkanani A, Abed S. Enhanced brain tumor classification using an optimized multi-layered convolutional neural network architecture. *Multimedia Tools Appl* (2021) 80(19):28897–917. doi: 10.1007/s11042-021-10927-8

37. Patel M. *Brain tumor detection using MRI images, MS Thesis, California State University, San Bernardino, Electronic Theses Projects, and Dissertations* (2023). Available at: https://scholarworks.lib.csusb.edu/etd/1602.

38. Latif G. DeepTumor: framework for Brain MR image classification, Segmentation and Tumor Detection. *Diagnostics* (2022) 12(11):2888. doi: 10.3390/diagnostics12112888

39. Sharma AK, Nandal A, Dhaka A, Polat K, Nour M, Alenezi F, et al. HOG transformation-based feature extraction framework in modified Resnet50 model for brain tumor detection. *Biomed Signal Process Control* (2023) 84:104737. doi: 10.1016/j.bspc.2023.104737

frontiers | Frontiers in Neurology

TYPE Methods
PUBLISHED 28 February 2024
DOI 10.3389/fneur.2024.1358531

OPEN ACCESS

EDITED BY
Dimitrios N. Kanakis,
University of Nicosia, Cyprus

REVIEWED BY
Andrea Di Cristofori,
IRCCS San Gerardo dei Tintori Foundation, Italy
Peter Lin,
Cytelligen, United States

*CORRESPONDENCE
Hannah R. Barber
✉ hannah.barber@bristol.ac.uk

RECEIVED 19 December 2023
ACCEPTED 12 February 2024
PUBLISHED 28 February 2024

CITATION
Barber HR, Perks CM and Kurian KM (2024) Evaluating circulating tumour cell enrichment techniques to establish an appropriate method for clinical application in glioblastomas.
Front. Neurol. 15:1358531.
doi: 10.3389/fneur.2024.1358531

Evaluating circulating tumour cell enrichment techniques to establish an appropriate method for clinical application in glioblastomas

Hannah R. Barber[1,2]*, Claire M. Perks[2] and Kathreena M. Kurian[1]

[1]Brain Tumor Research Centre, Bristol Medical School, Translational Health Sciences, Southmead Hospital, University of Bristol, Bristol, United Kingdom, [2]Cancer Endocrinology Group, Bristol Medical School, Translational Health Sciences, Southmead Hospital, University of Bristol, Bristol, United Kingdom

Brain tumours reduce life expectancy for an average of 20 years per patient, the highest of any cancer. A third of brain tumour patients visit their GP at least five times before diagnosis and many of those are diagnosed late through emergency departments. A possible solution to this challenge is to utilise a "liquid biopsy" blood test designed for circulating tumour cells (CTCs). Such a test could be applied at a primary healthcare centre, contributing to informed decision making for diagnostic imaging referrals. Furthermore, it could also be applied at secondary health care centres for the ongoing monitoring of disease recurrence. There is increased interest in CTC enrichment methods as a potential approach for faster diagnosis and monitoring of disease progression. The aim of this review to compare four CTC enrichment methods - OncoQuick®, Screen Cell®, pluriBead® and Cell Search® – with the objective of identifying a suitable method for application in the clinical setting for the isolation of CTCs from glioblastomas.

KEYWORDS

liquid biopsy, brain tumour, circulating tumour cells, enrichment methods, glioblastoma, blood test

1 Introduction

Globally, it was estimated that 308,102 people were diagnosed with a primary central nervous system (CNS) tumour in 2020, with incidence rates projected to rise by 6% between 2014 and 2035 (1, 2). Brain tumours cause more fatalities in children and adults under the age of 40 than any other cancer, reducing the life expectancy by an average of 20 years per patient, the highest of any cancer (3, 4).

Despite advances in surgical resection, chemotherapy and radiotherapy, around only 13.5% of adults survive brain tumours for five or more years after diagnosis (5). Data compiled by the Brain Tumour Charity found that a third of brain tumour patients had visited their GP at least five times before diagnosis (6, 7). Furthermore, over 50% are diagnosed via emergency departments rather than the GP; many of those patients presenting later in the course of the disease with large, inoperable tumours (8, 9).

Presently diagnosis and disease monitoring rely on access to imaging in secondary care, which is costly and overburdened: with 230,000 patients waiting more than a month for test results (10). Imaging can also intermittently produce false positive results due to non-malignant inflammatory changes mimicking tumour recurrence (11). Subsequent to imaging, the patient will undergo neurosurgery, during which a diagnostic tissue biopsy is taken. However, this biopsy provides static information that becomes obsolete as the cancer evolves. Different sub-clones expressing altered targetable biomarkers may emerge within the cancer during the course of the disease, highlighting the limitations of relying solely on static biopsy data (12). A better understanding of intertumoral heterogeneity is required to inform mechanisms of tumour resistance to therapies (13, 14). Consequently, there is an urgent need to utilise innovative methodology to improve patient diagnosis and overall survival.

A potential solution is to utilise a liquid biopsy assay for circulating tumour cells (CTCs) in peripheral blood samples from brain tumour patients. Not only are these simple blood tests low in cost and minimally invasive; they could be implemented in both the primary or secondary care setting (15). This has the potential to expedite diagnosis, monitor tumour genomic changes through serial samples and detect early relapse or resistance to current therapies (16, 17).

The benefits of CTC detection have been widely explored in other malignancies such as breast, colorectal, prostate, gastric, bladder, melanoma and small and non-small cell lung carcinoma cancer (18–26). In 2013, the LANSCAPE trial investigated CTC levels in breast cancer patients, with metastases to the brain, before and after treatment with lapatinib and capecitabine at 21 days, in Her2 positive tumours (27). The trial demonstrated a correlation between CNS metastasis response, outcome, and early CTC clearance under targeted treatment of Her2 positive, metastatic breast cancer (27). CTC count has also been shown to predict progression-free survival and overall survival in non-small cell lung carcinomas after multivariate analysis (23).

Using MTW9 carcinomas, (28) demonstrated that the presence of large numbers of tumour cells in the blood is not, by itself, a sufficient condition for metastatsis to occur. Multiple studies have similarly demonstrated that despite the detection of a high number of cancer cells in the blood, as few as 0.01% of CTCs develop into secondary tumours (29–31). CTC intravasation can occur through active and passive shedding (32). Bockhorn et al. (33), identified the loss of CD44 and α3 integrin in CTCs shed from renal cell carcinoma. Both CD44 and α3 integrin play a role in cell adhesion and a reduction makes it much easier for the cells to pass into the blood stream (34, 35). Blood vessels created by angiogenesis are immature, malformed and leaky with detached endothelial cells and an irregular or missing basement membrane (36, 37). Although it is not fully understood how these abnormalities affect intravasation it most likely helps with this process and could also account for non-viable cells, as well as viable cells, being leaked into the blood stream (38, 39). Proliferating cells have also been shown to compress and collapse intra-tumour blood vessels, which would enable the tumour cells to passively enter the blood stream (38, 39).

Throughout tumour progression there is active cross-talk between the tumour cells and micro-environment (30). This signalling is mediated by cell-to-cell interactions and cytokine/growth factors. Morphological changes which support metastasis are triggered by this signalling (40). Neurons, a crucial component of the glioma microenvironment, have been shown to regulate malignant growth in an activity dependent manner (41, 42). Synaptic communication is suggested to occur through AMPA (α-amino-3-hydroxy-5-methyl-4-isoxazole propionic acid) receptors, particularly the glutamate receptor (43). Glutamate, a key neurotransmitter, is considered a potential growth factor for glioma development (44).

Many studies have supported the hypothesis that neoplasms are heterogeneous and there is a distinct sub-population of tumour cells, with differing angiogenic, invasive and metastatic properties (45). This distinct subgroup can use epithelial-mesenchymal transition (EMT) to become increasingly motile, which in turn enables them to migrate to the vascular system through growth factor and nutrient gradients (46, 47). In contrast to the passive model described above these cells have been shown to actively migrate, passing either paracellularly through the endothelial cell junction or transcellularly through the endothelial cell body into the blood stream (48). These highly metastatic cells have been shown to produce matrix metalloproteinases, which actively digest the interstitial matrix and basement membrane, enabling them to pass through the tissue into the blood stream (49).

CTC arrest can be triggered by several obstacles within the bloodstream, including entrapment by capillaries; reduced diameter dimensions and biomechanical constriction forces of the capillary lumen, which have been shown to severely deform the cell cytoplasm and nucleus thus triggering cell death (50, 51). It has been suggested that capillary constriction can reduce the potential for CTCs to enter the vessels by as much as 90% (52). The role of capillary entrapment is less clear because entrapment may also be important for metastatic progression, enabling CTCs to adapt to the new environment, facilitating invasion and colonisation at the metastatic site (53, 54). In order to survive in the bloodstream CTCs must also evade hemodynamic shear forces and the immune system (55, 56). However, increasing evidence is emerging that CTCs are not as mechanically fragile as first thought and in fact can withstand fluid shear stresses encountered through circulation (57). CTCs have been shown to induce platelet activation and aggregation to protect their survival in the blood stream. Mounting evidence has also validated this interaction as a key feature of metastasis (58–61).

Originating from glial cells it is estimated that gliomas account for 75% of all primary malignant brain tumours (62). Glioblastomas (GBMs), the most aggressive and common glioma, are associated with dismal prognosis and rapid recurrence, despite multimodal therapies (62, 63). GBM cells are highly migratory and extensive infiltration of these cells into the brain parenchyma makes remedial surgical resection almost impossible (64). Systemic metastases from GBMs however are incredibly rare, 0.5% metastasise compared to 10–45% of other primary cancers that metastasise to the brain. It is thought that the brain's distinct microenvironment, containing the blood brain barrier and stem cell niches, significantly influences this rate (65).

The permeability of the blood–brain barrier is associated with GBM progression, heightened intravasation chances, and is suggested to be due to the disruption of endothelial/ astrocytic interaction and impaired vessel formation (66). Davis (67), reported the first ever case of GBM metastasis. Since then this number has increased progressively: this is thought to be due to improvements in imaging and patient survival (68). Metastatic GBM cells can spread through blood and lymphatic vessels (69). Onda et al. (70), undertook autopsies on 51 patients who had died from GBM and found that 14 of the 51 cases had dissemination by cerebral fluid.

Since 2014, there has been substantial progression in CTC isolation and characterisation from high grade glioma patients

(Table 1). Sullivan et al. (71), found isolated CTCs had elevated markers, which are associated with the more aggressive mesenchymal subtype. GBMs can be divided into 4 subtypes: proneural, neural, classical and mesenchymal (82). The mesenchymal subtype, characterized by higher migratory capabilities, is associated with worse prognosis and is strongly linked to GBM metastases and recurrences (83, 84). Microglia have been shown to induce mesenchymal status through the tumour necrosis factor alpha (TNF-α)/nuclear factor kappa-light-chain-enhancer of activated B cells (NF-κB) pathway. Additionally, hypoxia has been shown to induce transition and increase stem cell markers in GBM cells (84, 85). Multiple subtypes coexist within the same tumour, and mesenchymal transition is thought to occur late in GBMs, resulting in a more aggressive, invasive and recurrent tumour (86, 87).

A study by (72), determined that genomic abnormalities not only correlate between isolated CTCs and the tumour of origin, but also revealed the maintenance of epidermal growth factor receptor (EGFR) amplification in CTCs, indicating sustained growth potential. EGFR also promotes stemness in GBM cells (88). Although cohort numbers were small, results suggest that CTC detection could be used to identify GBM patients with a large tumour or those at risk of recurrence (72). In another study, utilising sensitive immunocytochemical detection, with glial fibrillary acidic protein (GFAP) as a marker for CTCs in peripheral blood cytospin preparations, putative CTC cells were detected in 29 out 141 GBM patients (73). Furthermore, these reputed CTCs were more frequently detected in patients with EGFR gene amplification in the corresponding tumour tissues (73).

In 2016 (74), detected 7 different glioma subtypes in peripheral blood samples using an integrated cellular and molecular approach. Clinical data revealed that CTC detection was superior to MRI in monitoring treatment response and differentiating radionecrosis (74). This study identified nonhematogenic aneuploid circulating aneupolid cells in seven diverse subtypes of brain glioma and reported their significance. This has been further supported by Li et al. (89), who detected and characterised aneuploud circulating rare cells in glioma patients and demonstrated their unique clinical significance.

Malara et al. (75), captured CTCs in a 67-year-old GBM patient pre- and 2 months post-surgery. Interestingly, the post-surgery sample showed a higher number of CTCs. Unfortunately, the patient experienced tumour recurrence 9 months after the sample, and succumbed to the disease 5 months later (75).

Zhang et al. (76), found that the positive rate of CTCs in gliomas increased progressively with the advancing stage of glioma. They utilised cell surface marker independent technology based on telomerase specific, replication-selective oncolytic herpes-simplex-virus-1, which identifies viable CTCs from a wide range of malignancies. The first evidence of CTC clusters was confirmed by (77), who noted them in 53.8% of progressive GBM patients. Bang-Christensen et al. (78), successfully isolated CTCs in every blood sample processed with magnetic beads coated with VAR2CSA malarial protein (rVAR2), which detected CTCs through the protein oncofetal chondroitin sulfate. Spiral microfluidic technology was used by (79), to successfully isolate CTCs from GBM patients. The study also demonstrated that patients with CTC counts equal to 0 after surgery had significantly longer recurrence free survival.

A sized based separation protocol with MetaCell® tubes was used by (80), to detect more mutations in CTC samples compared with the paired primary tumour. Qi et al. (81), used biocompatible parylene polymer membranes, with a pore diameter of 8 μm under a high flow rate, to enrich CTCs without requiring tumour cell-specific capture. Qi et al. (81), found CTC numbers to be higher in astrocytoma samples compared to oligodendroglioma samples. A number of CTC-white blood cell clusters, which could be used to monitor recurrence, were also detected in the study. Qi et al. (81), noted no difference in glioma subtype but in contrast found that resection could promote CTCs. It was also found that the level of CTCs was related to p53 mutation, isocitrate dehydrogenase 1 (IDH1) status and poor outcome (81).

CTC isolation techniques can be divided into 2 broad groups: physical and biological (90). Physical properties include separation by size, elasticity and surface charge (91). Methods used include density gradient centrifugation, microfiltration, microfluidics and dielectrophoresis (92). Antibodies with conjugated magnetic or non-magnetic beads are used to separate the CTCs through their biological properties. This can be either through positive selection, CTCs targeted directly, or negative selection, blood cells for example, are targeted and removed through this method (93).

The aim of this review is to assess and compare four commercially available methods for CTC enrichment: OncoQuick®, Screen Cell®, pluriBead® and Cell Search®. By analysing performance metrics and clinical adaptability, the objective of this study is to provide guidance in selecting a suitable method for potential translational application in the clinical setting, with a primary focus on the isolation of CTCs from GBMs. Commercially available methods were intentionally selected in this study to facilitate easier implementation in the clinical setting.

Each method applies a distinct enrichment technique. The Cell Search® system uses anti-epithelial cell adhesion molecule (EpCAM) conjugated with magnetic beads to isolate CTCs. This system is among the most widely used CTC enrichment techniques, as it is the only CTC detection system approved by the Food and Drug Administration in the United States for the enumeration of CTCs in metastatic colorectal, prostate, and breast cancers (94). Pierga et al. (27), used the Cell Search system to demonstrate that CTCs can be used as early predictive markers for poor overall survival and progression free survival in metastatic breast cancer patients. The study also demonstrated the use of CTCs in monitoring treatment benefit. The downside to this system is that it solely relies on EpCAM for detection. Therefore alternative methods have been developed.

The OncoQuick® method, which uses density gradient centrifugation has been shown to yield higher relative tumour enrichment when compared to standard to the standard density gradient centrifugation system Ficoll (95). In addition to CTC detection in gliomas, the OncoQuick® method has successfully isolated CTCs in studies involving colorectal cancer, melanoma and breast cancer patients (18, 96, 97). The isolation of CTCs through pluriBead® involves the use of non-magnetic beads coupled with monoclonal antibodies specific to the CTC surface antigens. Pierzchalski et al. (98), successfully validated this system for simultaneous separation of CD4+ and CD8+ cells from human EDTA-blood samples. The ScreenCell® method, which captures CTCs through size isolation, determined CTCs in patients with a less favourable stage III laryngeal squamous cell carcinoma (99). The ScreenCell® method has also isolated CTCs from urinary bladder, metastatic prostate and colorectal cancer (100–102).

10.3389/fneur.2024.1358531

TABLE 1 Summary of publications and the methods used to isolate and characterize circulating tumour cells (CTCs) in high grade glioma patients.

Publication	CTC isolation method	CTC characterisation	Results *n* = number of patients with CTCs	Limitations
Publications positively identifying CTCs in glioma patients				
(71)	Enriched from GBM patients. Blood processed through a CTC-iChip® (magnetically tagged CD45 and CD16). Immunofluorescence guided single cell micromanipulation used to isolate CTCs (EGFR, c-MET and CDH11).	IHC glioma marker panel (SOX2, Tubulin, beta-3, EGFR, A2B5, and c-MET). FISH used to determine EGFR gene amplification in CTCs from known amplified cases.	*n* = 28/87 RNA-ISH demonstrated an enrichment for mesenchymal transcripts and a reduction of neural differentiation markers.	Relies on immunostaining for CTC characterisation, may be missed due to CTC heterogeneity. Could not determine whether surgical or radiation induced disruption of BBB enhances CTC dissemination.
(72)	Enriched from high grade glioma patients. Blood samples centrifuged in OncoQuick® tubes.	Incubated with telomerase-responsive adenoviral probe (via GFP expression). Secondary IF (Nestin and EGFR).	*n* = 8/11 pre-radiotherapy *n* = 1/8 post- radiotherapy EGFR amplification in CTCs correlates with solid tumours.	Limited pilot data. Need more serial measurements throughout the treatment and disease for each patient. Telomerase is elevated in other tumour histologies.
(73)	Enriched from GBM patients. MNC isolated by ficoll density gradient centrifugation. Cytospins prepared from MNC. GFAP positive single cells isolated by micromanipulation.	Chromogenic and fluorescent IHC (GFAP, CD45 and EGFR). Further characterisation of CTC and associated tumour: comparative genomic hybridization, sequence analysis and FISH.	*n* = 29/141 Observed association between EGFR amplification and release of CTCs. Common genomic abnormalities in CTCs and GBM tumours.	Low detection rates. GFAP can be detected in other cell types.
(74)	Enriched from glioma patients (7 subtypes). Subtraction enrichment for removal of white and red blood cells.	Interphase FISH for detection of chromosome 8 polyploidy.	*n* = 24/31 CTCs could be detected in 7 subtypes of glioma. No difference between low and high grade. CTCs could be used to distinguish tumour from necrosis. CTCs could be used to predict tumour recurrence.	Limited pilot data.
(75)	Enriched from patients with focal intracranial lesions – GBM and Diffuse Large B-Cell Lymphoma. Density gradient centrifugation followed by short-time culture on chamber-slides.	IF for Vimentin. Fixed with Cytofix aerosol preparation, stained with Hematoxylin and Eosin for pathological analysis.	*n* = 2/2 No obvious pathological difference between excisional and liquid biopsy in diagnostic evaluation of space-occupying brain lesions. Early detection of tumour recurrence.	Limited dataset.
(76)	Enriched from glioma patients (grade II-IV). Transduced with HSV1-hTERT-GFP.	Flow cytometry (CD45-/GFP+) >3 CTCs per 4 mL blood	>3 CTCs per 4 ml blood *n* = 11/23 grade II *n* = 9/13 grade III *n* = 12/15 grade IV The positive rate of CTCs in gliomas rose progressively with advancing stage of disease.	Small sample size. Enrichment and characterisation process is lengthy.
(77)	Enriched from recurrent or progressive GBM patients. Parsortix microfluidic cassette technology (label free physical capture) to detect single and clustered CTCs in an antigen independent manner.	Captured cells stained with a cocktail of antibodies (EGFR, Ki67, EB1 and CD45 to exclude WBCs).	*n* = 7/13 First evidence that circulating GBM can overcome the blood brain barrier and reach peripheral circulation.	Limited pilot data. Relies on immunostaining for CTC characterisation, may be missed due to CTC heterogeneity.

(Continued)

TABLE 1 (Continued)

Publication	CTC isolation method	CTC characterisation	Results *n* = number of patients with CTCs	Limitations
(78)	Enriched from glioma patients (grade II-IV). Magnetic beads coated with VAR2CSA malarial protein (rVAR2) to capture CTCs through the protein oncofetal chrondroitin sulfate.	Fluorophore-conjugated rVAR2, CD45 and CD66b was used for microscopic detection of the captured cells. CTCs classified as rVAR2+/CD45-/CD66b- Targeted whole exome sequencing identified gene with cancer indicative mutations (RB1, TP53/EPM2AIP1, and TP53/ALK).	10/10 No correlation between the number of CTCs and WHO grade.	Limited dataset.
(79)	Enriched from glioblastoma patients. Spiral microfluidic technology.	Characterisation with immunofluorescence for GFAP and cell surface vimentin. CD45 was used to differentiate white blood cells. DNA FISH was used for the detection of EGFR amplification.	13/20 patients (9/20 before surgery and 11/19 after surgery). Patients with CTC counts equal to 0 after surgery had significantly longer recurrence free survival.	Limited cohort. Lack of specific markers for the characterisation of CTCs.
(80)	Enriched from GBM, astrocytoma and low grade glioma patients. Sized based separation protocol and MetaCell® tubes.	Vital fluorescent staining microscopy with defined characteristics (nuclear size and contour, visible cytoplasm, prominent nucleoli, high nuclear-cytoplasmic ratio, fatty cytoplasm, and mitochondrial network presence) ($n = 18$). Next,-generation sequencing ($n = 8$).	$n = 18/18$ CTCs successfully cultured. More mutations detected in CTC samples compared with paired primary tumour. Highlights potential for CTCs to be used for glioma diagnosis, patient monitoring and recurrence.	Limited dataset.
(81)	Primary diffused glioma patients. Biocompatible parylene polymer membrane with a pore diameter of 8 µm under a high flow rate, enriching CTCs without requiring tumour cell-specific capture.	Characterisation using antibody cocktail, SOX2, Tubulin, beta-3, EGFR, A2B5 and c-MET, with a series of criteria of malignant features.	Recurred glioma = 7/8 36/42 had detectable CTC. CTCs higher in astrocytomas compared to oligodendrogliomas. Large number of CTC-WBC clusters detected and could help monitor. Recurrence. No difference noted in glioma subtype. CTC level related to P53 mutation, IDH1 status and poor outcome. Resection may promote CTCs in gliomas.	Limited cohort.

GBM, glioblastoma; EGFR, epidermal growth factor receptor; c-Met, mesenchymal-epithelial transition factor; CDH11, Cadherin 11; IHC, immunohistochemistry; SOX2, sex determining region Y-box transcription factor 2; FISH, fluorescence *in situ* hybridization; RNA-ISH, ribonucleic acid *in situ* hybridization; BBB, blood brain barrier; GFP, green fluorescent protein; IF, immunofluorescence; MNC, mononuclear cells; GFAP, glial fibrillary acidic protein; HSV1, Herpes Simplex Virus Type 1; hTERT, human telomerase reverse transcriptase; EB1, end binding protein 1; WBCs, white blood cells; RB1, Retinoblastoma 1; ALK, anaplastic lymphoma kinase; WHO, World Health Organisation; IDH1, isocitrate dehydrogenase 1.

2 Methods (including materials and equipment)

2.1 Cell culture

To evaluate the four enrichment techniques OncoQuick®, Screen Cell®, Cell Search® and pluriBead®, the human GBM cell line U251 MG, obtained from Sigma Aldrich (Irvine, North Ayrshire, UK), was spiked at various densities in healthy donor ethylenediaminetetraacetic acid (EDTA)-anticoagulated whole blood samples. Normal whole blood was collected using the standard venepuncture technique.

Table 2 provides information on the human cell lines used in this review, including the corresponding culture media used, and the enrichment technique undertaken. All cells were cultured in a humidified environment at 37°C with 95% air and 5% carbon dioxide.

2.2 CTC enrichment techniques

2.2.1 OncoQuick® (Greiner Bio-One, Gloucestershire, UK)

The OncoQuick® technique isolates CTCs through density gradient centrifugation (Figure 1). In 2014 (72), successfully isolated CTCs from

TABLE 2 Human cell lines used for this review and the corresponding culture media.

Cell line	Origin	Media	Enrichment Technique
U251 MG (Sigma Aldrich)	Glioblastoma	Eagle's Minimum Essential Medium containing Earle's Balanced Salt Solution (EMEM(EBSS)) (Sigma-Aldrich), supplemented with 2 mM L-glutamine (Sigma-Aldrich), 1% non-essential amino acids (NEAA) (Sigma-Aldrich), 1 mM sodium pyruvate (Sigma-Aldrich) and 10% fetal bovine serum (FBS) (Gibco, Paisley, UK).	OncoQuick®, Screen Cell®, pluriBead® and Cell Search®
PNT2 (Sigma-Aldrich)	Normal prostate	Roswell Park Memorial Institute (RPMI) 1,640 Medium (Sigma), 2 mM glutamine and 10% FBS	Cell Search®
VCaP (ATCC)	Prostate carcinoma	Dulbecco's Modified Eagle Medium (DMEM) (ATCC 30–2002) plus 10% FBS;	Cell Search®
LNCaP (ATCC)	Prostate adenocarcinoma	Kaighn's Modification of Ham's F-12 Medium (ATCC 30–2004) plus 10% FBS.	Cell Search®
PC-3 (ATCC)	Prostate adenocarcinoma	Kaighn's Modification of Ham's F-12 Medium (ATCC 30–2004) plus 10% FBS.	Cell Search®
T24 (ATCC)	Urinary bladder transitional carcinoma	Modified McCoy's 5a Medium (ATCC, 30–2007) plus 10% FBS.	Cell Search®
RT4 (ATCC)	Urinary bladder transitional carcinoma	Modified McCoy's 5a Medium (ATCC, 30–2007) plus 10% FBS.	Cell Search®
TCCSUP (ATCC).	Bladder transitional-cell carcinoma	EMEM(EBSS), supplemented with NEAA plus 10% FBS.	Cell Search®
MCF10A (Sigma-Aldrich)	Normal breast	MEGM™ (Mammary Epithelial Cell Growth Medium) BulletKit™ (Lonza). The gentamycin-amphotericin B mix, provided with this kit was replaced with 100 ng/ml cholera toxin (Sigma).	Cell Search®
MCF7 (ATCC)	Breast adenocarcinoma	Modified EMEM (EBSS) (ATCC 30-2003) plus 10% FBS.	Cell Search®
Hs578T (ATCC)	Breast carcinoma	DMEM (ATCC 30–2002) plus 0.01 mg/mL human insulin (Gibco) plus 10% FBS.	Cell Search®
T47D (ATCC)	Breast carcinoma	Modified RPMI-1640 Medium (ATCC 30–2001) plus 10% FBS.	Cell Search®

All cells were cultured in a humidified environment at 37°C with 95% air and 5% carbon dioxide.

high grade glioma patients using this method. To validate this method 15 ml of normal EDTA-anticoagulated whole blood was spiked with U251 MG cell densities: 1×10^4 and 1.5×10^2. Before starting the enrichment process the OncoQuick® tubes and normal whole blood samples were pre-cooled on ice for 10–15 min. The blood sample was then added carefully to the upper compartment of the OncoQuick® tube ensuring that the separation medium under the porous barrier was not disturbed. The OncoQuick® tube was then spun at 1,600 *g* for 20 min at 4°C, with a slow acceleration and no brake. Following centrifugation any captured tumour cells resided between the lower separation medium (blue) and the upper plasma (yellow). The liquid above the porous barrier was collected with a sterile serological pipette and transferred to a fresh sterile centrifuge tube. Walls of the OncoQuick® tube were carefully rinsed with 5 ml OncoQuick® wash buffer to collect any remaining tumour cells. This was then transferred to the centrifuge tube. Total volume in the new centrifuge tube was made up to 50 ml with wash buffer and the tube was inverted 5 times to mix the sample. Any cells present were pelleted by spinning the sample at 200 g for 10 min. The supernatant was removed leaving a pellet in 5 ml wash buffer. The pellet was re-suspended by carefully tapping the tube. This step was then repeated by adding another 45 ml of wash buffer. The supernatant was carefully aspirated without disturbing the cell pellet. The pellet was then re-suspended in growth media and transferred to a 24 well cell culture plate. Cells were then maintained in a humidified atmosphere at 37°C in 5% carbon dioxide.

2.2.2 Screen Cell® (Sarcelles, France)

The Screen Cell® method captures CTCs through size isolation (Figure 2). As the blood sample travels through the filter, unlike the blood cells, the CTCs are too large to pass so are captured on the surface of the filter. To test this procedure, 3 ml of normal whole blood was spiked with U251 MG cell densities: 3×10^3 and 2×10^1. This was the most rapid method that was evaluated taking only 3 min to process the sample. Two different Screen Cell® kits were tested. Screen Cell®-Live Cell Detachment (LCD) kit is used to culture captured CTCs. Following filtration, the filter is released into a 24 well tissue culture plate and media is added. Cytological studies can be performed on the filter once the cells have adhered. Screen Cell®-Molecular Biology (MB) Kit is used for molecular biology examinations. Each pack includes a single DNAse and RNAse free filtration device, specialised buffer, and a collection tube. This unit enables DNA/RNA to be extracted directly from cells captured on the capsule's filter or the cells can be cultured and subsequently analysed. Both kits followed the same procedure. The blood sample was transferred into a 15 ml sterile conical tube and 1 mL of Screen Cell® LC buffer was added to the sample. The tube was inverted 5 times and left to incubate for 3 min. For Screen Cell®-LCD samples only, 1.6 ml of growth media was added before the tube was inverted to homogenize. Before the blood samples were added to the device the protective membrane was removed, and a blood collection tube was placed underneath to create a vacuum. Following filtration, the device was carefully separated, and the filter was released into a 24 well plate. The plates were then maintained in a humidified atmosphere at 37°C in 5% carbon dioxide.

2.2.3 Cell Search® System (Janssen Diagnostics, South Raritan, USA)

The Cell Search® system uses an immuno-magnetic separation procedure to separate target cells (Figure 3). The cells are then stained with fluorescence-labelled monoclonal antibodies.

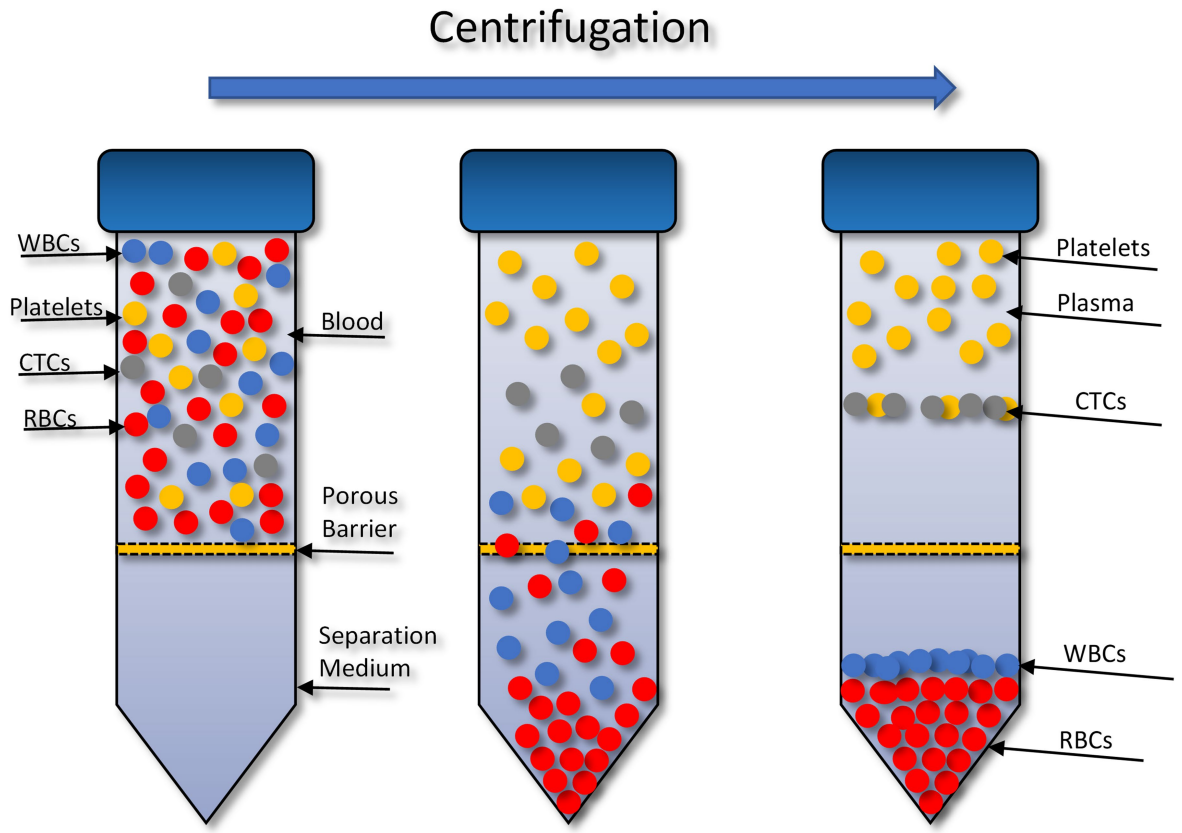

FIGURE 1
Circulating tumour cell (CTC) enrichment using the OncoQuick® technique. This method uses density centrifugation combined with a porous barrier to isolate CTCs. RBCs, red blood cells; WBCs, white blood cells. Figure created with PowerPoint.

To validate this method 7.5 ml of normal whole blood was spiked with 1×10^4 U251 MG cells. This is the minimum amount of blood required by the Cell Search® System. A CellSave Preservative Tube was used for blood collection, following which the tube was inverted 8 times to mix the sample with the anticoagulant and preservatives. The blood sample was then spiked with the U251 MG cells. Prior to processing, the spiked blood sample was transferred to a CellTracks® AutoPrep® System tube. The dilution buffer (6.5 ml) was added to the blood sample and the tube was inverted 5 times to mix. The samples were then centrifuged at 800 *g* for 10 min with no brake. During the run the system adds ferrofluid to the sample. Ferrofluid contains particles which have a magnetic core and are coated in monoclonal antibodies to bind to target cell antigens. The system adds a strong magnetic field to pull the labelled cells to the side and aspirates the blood. The magnetic field is then removed, and the cells are re-suspended in sample buffer. Another magnetic field is applied to separate the target cells from the wash buffer. Fluorescence-labelled antibodies are applied to bind to the target cell antigens and the cells are once more separated using a magnetic field. Finally, a cell fixative is applied, and the cells are transferred to a cartridge inside a specialised cell presentation fixture (MagNest®), through its strong magnetic field. The MagNest® is then loaded onto CellTracks Analyser II®, which identifies target cells through its fluorescent staining patterns.

2.2.4 pluriBead® (pluriSelect, Lepzig, Germany)

The pluriBead® method captures CTCs using non-magnetic beads coupled with monoclonal antibodies specific to CTC surface antigens (Figure 4). Six S-pluriBead® suspensions were developed specifically for this project. Antibodies selected were anti-EGFR, anti-mesenchymal-epithelial transition factor (c-MET) and anti-cadherin 11 (CDH11). Sullivan et al. (71), had previously isolated GBM CTCs by targeting these cell surface antigens. Six antibody clones were selected to maximise the chances of successfully capturing the cells: OB-Cadherin – clone N-12 (sc-30314, Santa Cruz Biotechnology, Heidelberg, Germany), OB-Cadherin – clone 16G5(ab151446, abcam, Cambridge UK), EGFR – clone 528(sc-120, Santa Cruz Biotechnology), EGFR – clone MGR1(ALX-804-572-C100, Enzo, Exeter, UK), EGFR – clone ICR10(ab231, abcam) and c-MET – clone EP1454Y (ab51067, abcam).

As recommended by the manufacturer the beads were initially tested with cells suspended in 3 mL growth media before spiking whole blood. The density of U251 MG cells used to test each bead was 3×10^3. To validate each S-pluriBead® suspension, buffer A (150 µl) was added to 3 ml growth media, spiked with U251 MG cells. The S-pluriBead® suspension was vortexed and 120 µl were added to the sample, which was then left to mix for 30 min using a horizontal roller mixer. Following incubation, the S-pluriStrainer was placed on top of a sterile 50 ml centrifuge

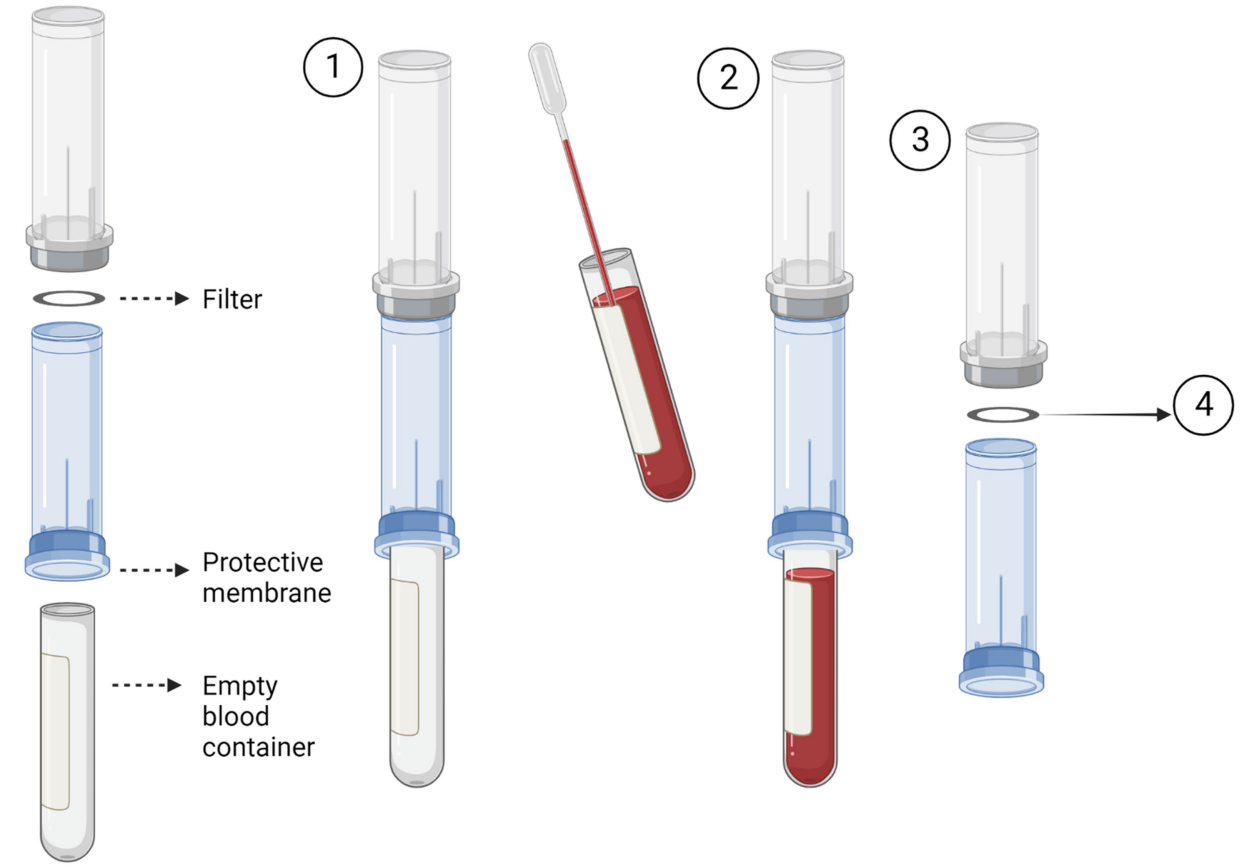

FIGURE 2
Circulating tumour cell (CTC) enrichment using Screen Cell®. This method captures the CTCs through size isolation on the surface of a membrane filter. A blood tube is inserted into the bottom of the device to create a vacuum (1). The pre-prepared blood sample is then added to the device. The blood then passes through the filter and is collected in the inserted blood tube (2). After the blood has fully passed through the filter, the device is separated (3). The filter is then removed and used for the desired test i.e., cell culture or molecular biology. Figure created with Biorender.

tube and equilibrated by adding 1 ml of wash buffer. The sample was then poured carefully onto the pluriStrainer to capture the beads with potential tumour cells attached. The beads were washed with 20 mL of wash buffer in 2 ml steps. The inner and outer surfaces of the strainer were washed to avoid target contamination. A connector was then attached to a fresh centrifuge tube and the luer-lock was closed. The strainer containing the beads was then attached to the connector, making sure the fit was tight. The beads were re-suspended in 1 ml of wash buffer and 10 µl of the suspension were placed in a 24 well plate to check whether any target cells were bound to the beads under a microscope. Activated buffer D was then added along the wall of the strainer and left to incubate for 10 min. Following incubation, 1 ml of wash buffer was added and the suspension was mixed 10 times with a pipette, making sure the mesh filter was not touched. The luer-lock was then opened, and the beads were washed with 10 ml of wash buffer. The connector and strainer were removed, and the cells were spun for 10 min at 300 g. The supernatant was carefully aspirated to leave 0.5 ml, making sure any potential pellet was not disturbed. Finally, 1 ml growth media was added to the potential pellet which was then re-suspended using a pipette and transferred to a 24 well plate. Cells were then maintained in a humidified atmosphere at 37°C in 5% carbon dioxide.

2.3 Cell characterisation

2.3.1 Immunofluorescence

Before staining, the isolated U251 MG cells were grown on a µ-Chamber 8 well (Ibidi, Glasgow, UK) for 24 h at a density of 300 µl of 5×10^4 cells/ml per well. Following this the cells were fixed in 3% paraformaldehyde (Alfa Aesar, Heysham, UK)/phosphate buffered saline (PBS) solution for 20 min and then permeabilised with 0.1% Triton-X100 (Thermo Fisher Scientific, Loughborough, UK)/PBS (150 µl/well) for 15 min, washing with PBS between each step. The cells were then blocked with 3% bovine serum albumin [BSA/PBS for 1 h and then incubated with the primary antibody, EGFR (EP38Y, abcam) diluted in 3% BSA at a ratio of 1:100 at room temperature for 1 h]. 3% BSA/PBS was used as a negative control. The cells were then washed in PBS before the secondary antibody, Alexa Flour 488 goat anti-mouse (Invitrogen, Thermo Fisher Scientific) diluted in 3% BSA/PBS at a ratio of 1:500, was applied for 1 h. The cells were

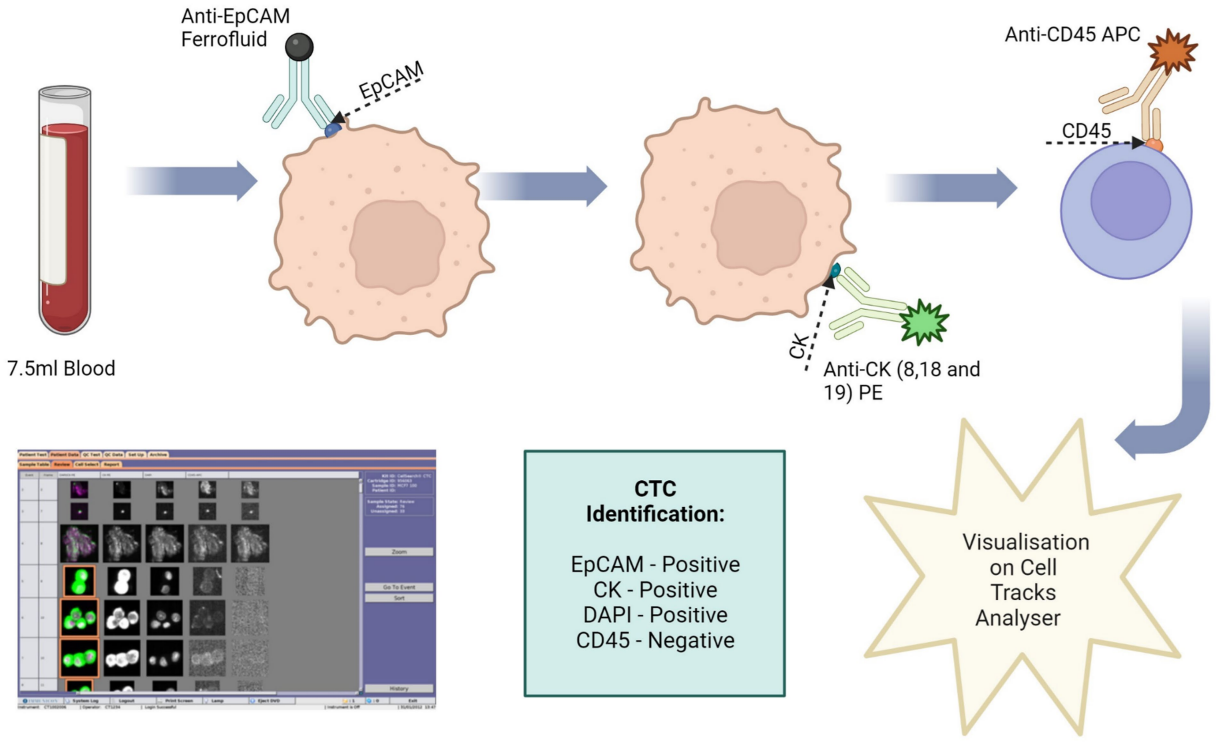

FIGURE 3
Circulating tumour cell (CTC) enrichment using the Cell Search® System. This system uses anti-epithelial cell adhesion molecule (EpCAM) conjugated with magnetic beads to isolate CTCs. The cells are then stained with fluorescence-labelled monoclonal antibodies, which target cytokeratin (CK) 8, 18 and 19. CTCs are identified as epithelial cell adhesion molecule (EpCAM) positive, CK positive, 4′,6-diamidino-2-phenylindole (DAPI) positive and CD45 negative. Image made with Biorender.

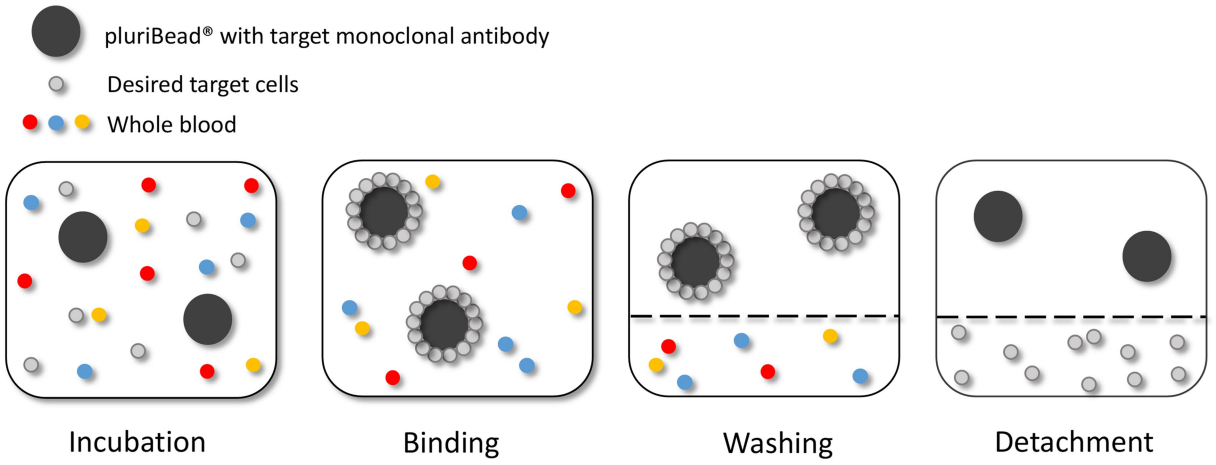

FIGURE 4
Circulating tumour cell (CTC) enrichment using the pluriBead® technique. This method captures the CTCs using non-magnetic beads coupled with monoclonal antibodies specific to CTC surface antigens. Figure created with PowerPoint.

then washed in PBS and one drop of mounting medium with 4′,6-diamidino-2-phenylindole (DAPI) (Vector Laboratories, Peterborough, UK) was applied to each chamber. The cells were then viewed using a fluorescent microscope at x40 and x100 magnification.

2.3.2 Trypan blue exclusion

Total viable cell numbers were determined using the trypan blue exclusion assay. Following trypsinisation, resulting cell suspensions were mixed 1:1 with trypan blue dye and counted using a haemocytometer (Neubauer chamber). Trypan blue is excluded by

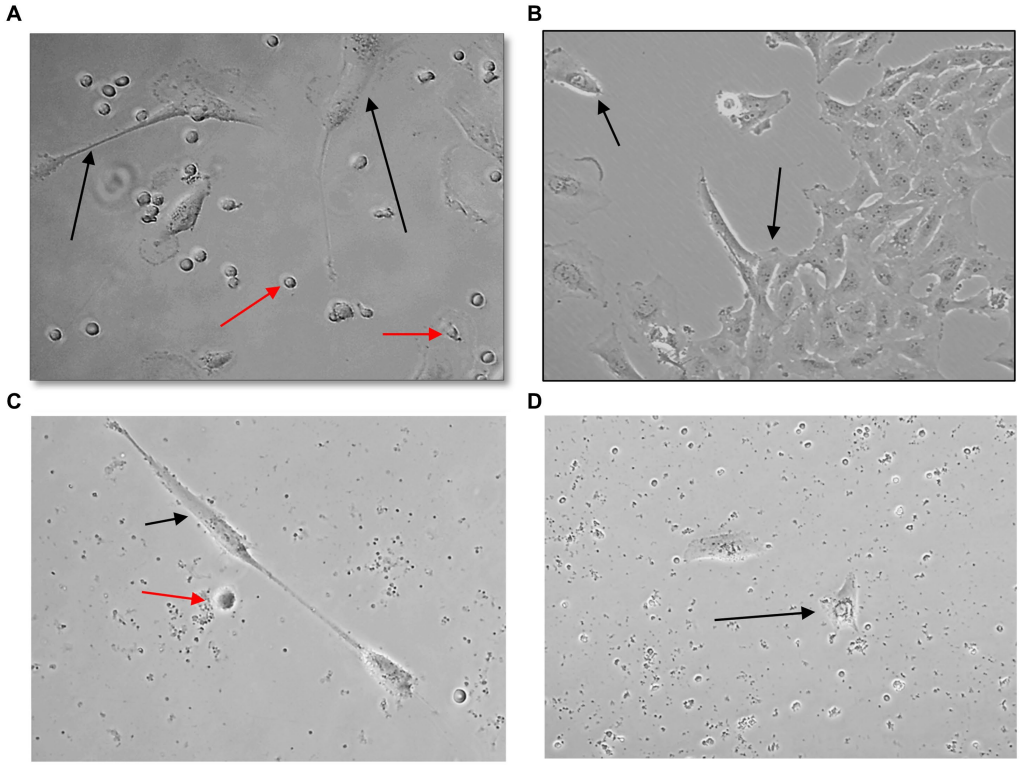

FIGURE 5
Captured U251 MG cells following OncoQuick® processing of spiked whole blood. Images taken two **(A,C)** and seven **(B,D)** days after $1x10^4$ **(A,B)** and $1.5x10^2$ **(C,D)** U251 MG cells were spiked in 15ml of normal whole blood and processed with the OncoQuick® method. U251 MG cells (black arrows) were successfully seeded and cultured on 24 well plates. The red arrows highlight red blood cells which were also captured. x40 and x80 magnification.

viable cells, conversely cells that have undergone cell death have compromised cell membranes and therefore take up the trypan blue dye.

2.3.3 Protein extraction and western immunoblotting

Total protein was extracted from cells using lysis buffer [10 mM tris hydrochloride (HCL) (Sigma), 50 mM sodium chloride (NaCl, Sigma), 5 mM EDTA (Sigma), 1% (v/v) triton X-100 (Sigma), 15 mM tetrasodium pyrophosphate (Sigma), 50 mM sodium fluoride (Sigma), 100 uM sodium orthovanadate (Sigma), phosphatase (Sigma, P5726), and protease (Sigma, P8340) inhibitors (10 ul/1 mL lysis buffer)].

Protein quantification was completed using a Pierce™ BCA (Bicinchoninic acid) Assay kit (ThermoFisher Scientific, 23227), iMark™ Microplate Reader (Bio-Rad, UK) and accompanying Microplate Manager® Software. 30ug of whole cell lysate were diluted 1:1 with laemmli x 2 sample buffer concentrate and 10% 2-mercaptoethanol (Sigma). Samples were then heated at 95°C for 5 min in an AccuBlock™ digital dry bath (Labnet International). After sodium dodecyl sulfate–polyacrylamide gel electrophoresis (SDS-PAGE), the separated proteins were transferred to a nitrocellulose membrane (Bio-rad, 1620094). Non-specific binding sites were blocked with 5% BSA in tris-buffered saline TWEEN®20 (TBS-T) for 60 min at room temperature. The membrane was then probed with EpCAM (ab32392, abcam) at a dilution of 1:2500 in 5% BSA overnight at 4°C before being washed in TBS-T and then incubated with anti-rabbit secondary (Sigma, A0545) at a dilution of 1:2000 in 5% BSA for 60 min at room temperature. Proteins were visualised by clarity enhanced-chemiluminescence (ECL) substrate (BioRad, 1,705,061) using BioRad Chemidoc XRS + system and analysed using Image Lab software (BioRad).

3 Results

3.1 OncoQuick®

U251 MG cells were successfully isolated and cultured, when OncoQuick® processed 1×10^4 and 1.5×10^2 cells spiked in 15 ml of normal whole blood (Figure 5). The captured U251 MG cells were labelled using EGFR and DAPI immunofluorescence (Figure 6), suggesting that immunofluorescence could be used as an effective tool for CTC cell characterisation.

3.2 Screen Cell®

A high number of U251 MG cells were captured on the filter using the Screen Cell®- LCD kit and the cells were successfully cultured for 7 days (Figures 7A,B). To evaluate the sensitivity of Screen Cell®-CC the procedure was repeated with just 2×10^1 cells in 3 ml of normal whole blood. In this case the procedure was successfully able to capture the U251 MG cells, which were then cultured (Figure 7). The Screen Cell®-MB kit was also used to

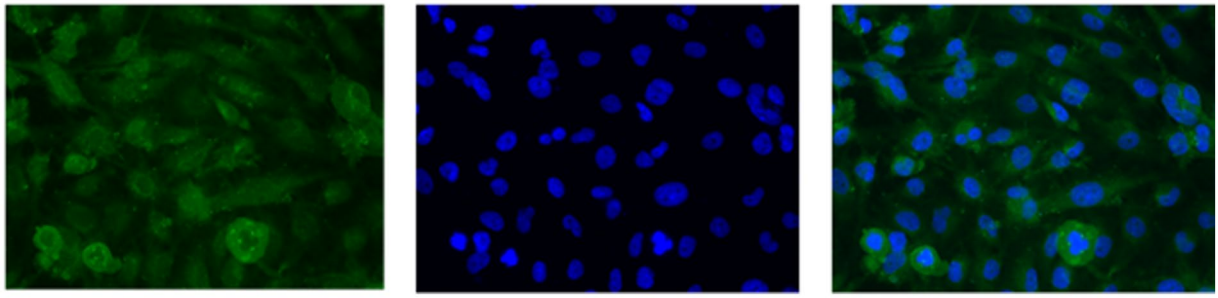

FIGURE 6
U251 MG cells captured with the OncoQuick® technique, from spiked normal whole blood, were stained with immunofluorescence using the markers epidermal growth factor receptor EGFR (green, transmembrane protein) and 4′,6-diamidino-2-phenylindole (DAPI) (blue, nuclear marker). x40 magnification.

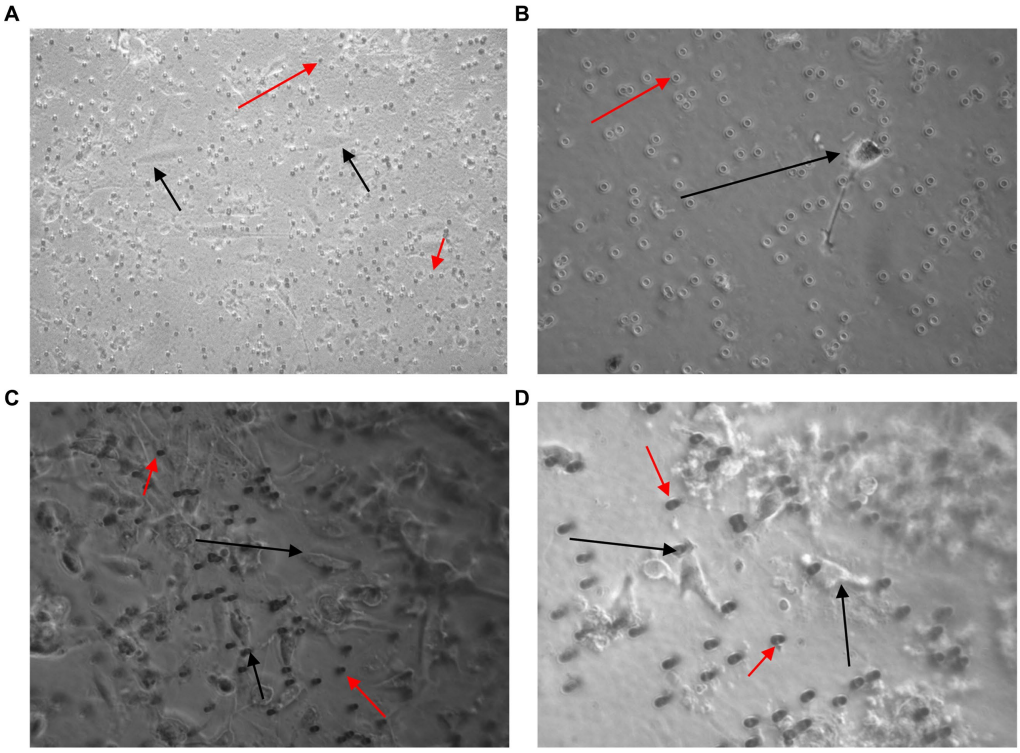

FIGURE 7
Images taken 7 days after 3×10^3 **(A,C)** and 2×10^1 **(B,D)** U251 MG cells were spiked in 3 ml of normal whole blood and processed using the Screen Cell®-LCD **(A,B)** and Screen Cell®-MB kit **(C,D)**. U251 MG cells (black arrow) were successfully seeded and cultured on the 24 well plate. The red arrow indicates blood cells, which were also captured. x40 and x100 magnification.

successfully isolate, and culture 3×10^3 and 3×10^2 U251 MG cells spiked in 3 mL of normal whole blood (Figures 7C,D).

3.3 Cell Search®

The Cell Search® System uses EpCAM to detect and enumerate CTCs. Although EpCAM is absent in the healthy brain tissue, a study by Chen et al., identified that not only was there an overexpression of EpCAM in gliomas, but it also correlated significantly with malignancy (103). To determine whether EpCAM was present in U251 MG cells SDS-PAGE electrophoresis and western blotting was conducted (Figure 8A).

In contrast to cell lysates from T47D (human breast carcinoma), RT4 (human bladder transitional-cell carcinoma) and MCF7 (human breast adenocarcinoma) cells, analysed alongside the U251 MG cells, no EpCAM was detected in the U251 MG cell lysate or in the T24 (human urinary bladder transitional carcinoma) cell line.

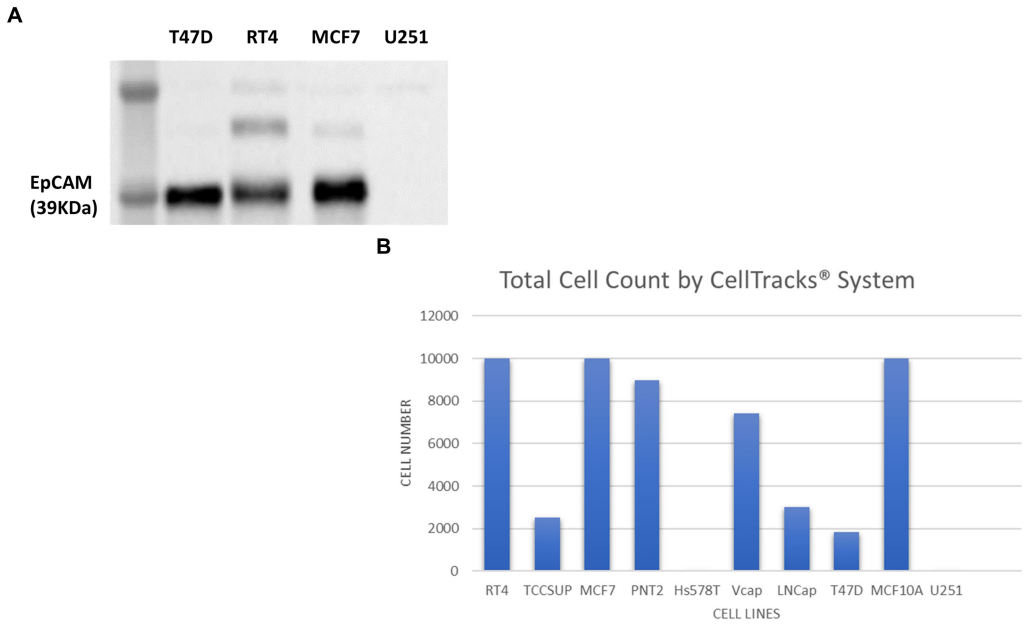

FIGURE 8
Immunoblot analysis of EpCAM protein expression in T47D (human breast carcinoma), RT4 (human bladder transitional-cell carcinoma), T24 (human urinary bladder transitional carcinoma), MCF7 (human breast adenocarcinoma) and U251 MG (human glioblastoma) cell lines **(A)**. The number of cells identified by the Cell Search® System when 1×10^4 cells, from RT4, MCF7, T47D, TCCSUP (human bladder transitional-cell carcinoma), PNT2 (normal human prostate), Hs578T (human breast carcinoma, ATCC), VCaP (human prostate carcinoma, ATCC), LNCaP (human prostate adenocarcinoma) and MCF10A (normal human breast) were spiked into 7.5 ml normal blood samples **(B)**.

To confirm these findings using the Cell Search® System, U251 MG cells were run alongside the following cells lines RT4, MCF7, T47D, TCCSUP (human bladder transitional-cell carcinoma), PNT2 (normal human prostate), Hs578T (human breast carcinoma), VCaP (human prostate carcinoma), LNCaP (human prostate adenocarcinoma), MCF10A (normal human breast). Each sample contained 7.5 ml of normal whole blood spiked with 1×10^4 cells. Figure 8B demonstrates the number of EpCAM positive cells detected for each cell line. As anticipated no U251 MG cells were detected by this system compared to the MCF7 cells, for example, which had demonstrated EpCAM positivity in the western blot.

3.4 pluriBead®

The pluriBead® method was first analysed with 3×10^3 U251 MG cells suspended in growth media. Each set of beads, with a separate clone of antibody adhered to it, was tested. Prior to detachment, 10 µl of each solution was taken and pipetted onto a 24 well plate so that it could be checked under a microscope to see if any U251 MG cells had adhered to the beads. No U251 MG cells could be detected at this stage with any of the antibody clones. Following processing the cell pellet was re-suspended in growth media and seeded onto a 24 well plate. The plate was then examined 48 h later to see if any U251 MG cells had been successfully captured (Figure 9). An average of only 2U251 MG cells ($n = 3$) were detected with each antibody clone, except EGFR (clone 528) despite the media initially being spiked with 3×10^3 U251 MG cells.

To further determine the effectiveness of the pluriBead® method the technique was repeated with an alternative cell line PC3 (prostate adenocarcinoma, Sigma-Aldrich). On completion of this technique a much higher yield of PC3 cells had been captured for each antibody. A trypan blue exclusion assay was undertaken to determine the number of viable cells successfully isolated by each monoclonal antibody (Figure 10).

The pluriBead® used were designed specifically for this study. The markers, EGFR, c-Met and CDH11, which have previously been used successfully to capture GBM CTCs, were selected to isolate the cells (71). When viewing the beads, prior to the detachment stage, it appeared that no U251 MG cells had been successfully captured despite processing 3×10^3 cells. A very small number of cells (≈2 cells) were noted growing 48 h later, however this could be due to contamination rather than successful capture by the beads.

4 Discussion

The Cell Search® System was unable to detect U251 MG cells spiked in normal whole blood due to the lack of EpCAM on the surface of these cells. Modifications could be made to the system to include additional markers, but at present only EpCAM positive cells are detected by this system.

Other studies have shown the failure of the Cell Search® System to detect rare CTCs and also detect CTCs in patients with a widely metastatic disease, despite those patients have high

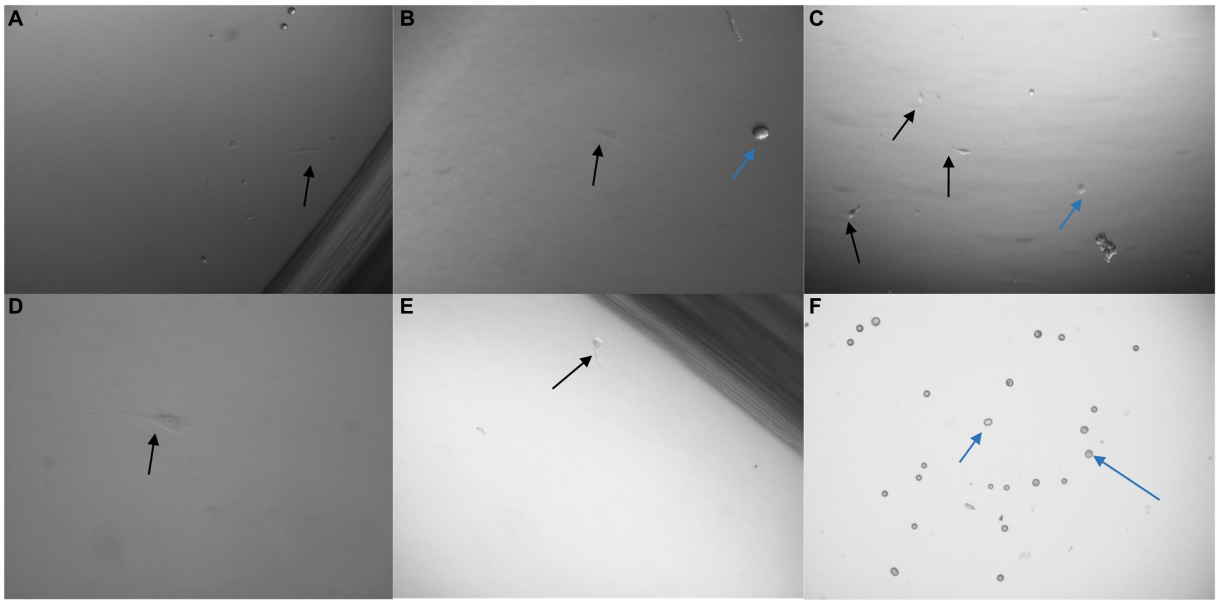

FIGURE 9
Images taken 48h after 3x10^{3}U251 MG cells were processed with a non-magnetic bead suspension each coupled with a different monoclonal antibody: EGFR clone ICR10 **(A)**, OB-Cadherin clone N-12 **(B)**, c-Met clone EP1454Y **(C)**, EGFR clone MGR1 **(D)**, OB-Cadherin clone 16G5 **(E)** and EGFR clone 528 **(F)**. On completion of the pluriBead® technique the cell suspensions were seeded on a 24 well plate in cell media and cultured at 37°C and 5% carbon dioxide. An average of only 2U251 MG cells (black arrow), (*n*=3), were detected with each antibody clone, except EGFR (clone 528) despite the media initially being spiked with 3x10^{3}U251 MG cells. The blue arrows indicate beads which were also noted. x40 magnification.

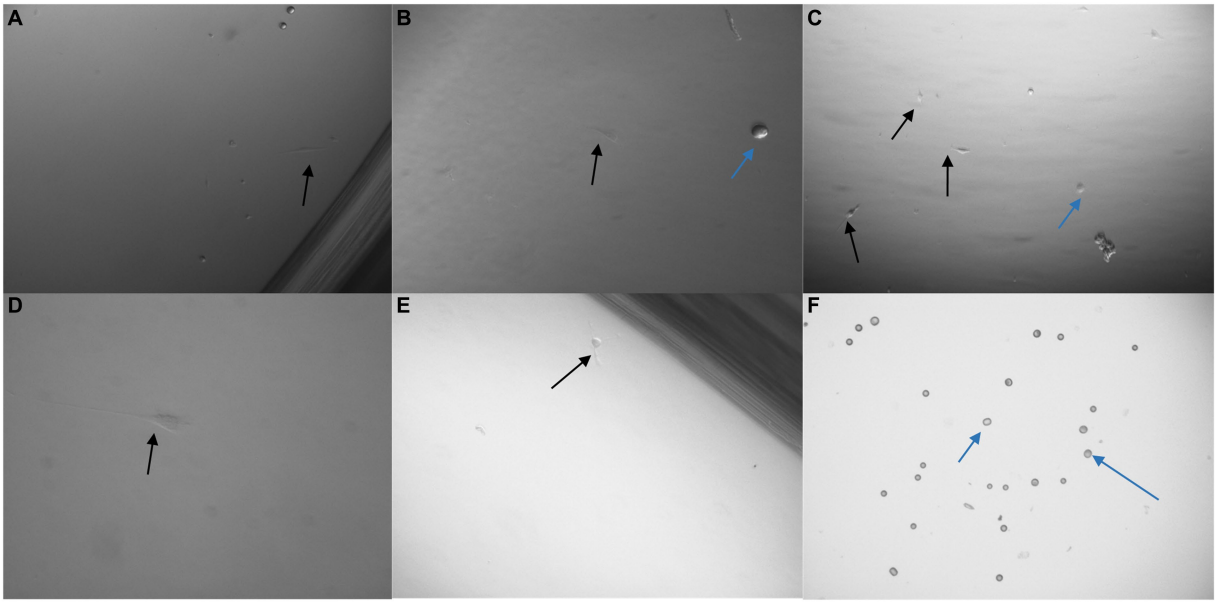

FIGURE 10
3 x 10^3 PC3 cells were processed with a non-magnetic bead suspension coupled with six separate monoclonal antibodies EGFR clone 528 **(A,B)**, OB-Cadherin clone N-12 **(C,E)**, EGFR clone ICR10 **(D)**, OB-Cadherin clone 16G5, EGFR clone MGR1 and c-Met clone EP1454Y **(F)**. **(A–C)** Taken prior to detachment phase of the pluriBead® technique. **(D–F)** Taken 72 h after pluriBead® cell suspensions were cultured in cell media at 37°C and 5% carbon dioxide. x40 and x100 magnification. Black arrows depict PC3 cells and the blue arrows indicate beads observed. PC3 cell counts were undertaken using trypan blue dye exclusion assay 72 h after pluriBead® technique.

numbers of CTCs identified through alternative methods (94, 104, 105).

Tumour progression is associated with a loss of epithelial features and a transition towards a mesenchymal phenotype, a process known as EMT. Tumour cells are known to undergo EMT as a means of entering circulation (106). A loss in epithelial markers, such as EpCAM, would prevent the CTCs from being detected by the Cell Search® System. Konigsberg et al. (107), determined, in metastaic breast cancer patients, that the density gradient centrifugation method OncoQuick® appeared advantageous for CTC isolation compared to MACS HEA MicroBeads® (MACS), which also relied on EpCAM immunomagmetic enrichment technology. This technology also requires the costly purchase of the Cell Search® System, which could prevent many clinical settings from using this system.

The U251 MG cells were successfully enriched using the OncoQuick® method, which correlates with the findings from (72), who successfully isolated CTCs from high grade glioma patients using this method. Although the method was successful, many steps were required to perform the analysis, which is time consuming. This is an important factor to consider when reviewing this technique for clinical application. Numerous steps would also increase the chances of losing 'rare' CTCs, particularly when transferring the solution between centrifuge tubes. The manufacturer recommends that the plasma fraction is discarded when platelet contamination is seen following centrifugation. Removing the plasma fraction could result in loss of CTCs due to unwanted contamination of this fraction. Alternatively, CTCs could form non-specific aggregates, which could cause them to move to the bottom gradient, again leading to false negative results. CTCs have been shown to bind with platelets, fibroblasts, and leukocytes to evade blood stream hazards (108, 109). If CTCs are present in these clusters, they could also move to the bottom gradient and subsequently be missed through the OncoQuick® method.

GBMs have a high degree of intratumoral heterogeneity (110). CTC profiles can change during tumour cell dissemination (111–113). Before entering the blood CTCs undergo varying degrees of EMT, which leads to variability in cell markers (114). Although the selected markers for the pluriBead® technique are associated with tumorigenesis and cell migration in GBMs, c-Met acting as an independent predictor for GBMs, they are heterogenous (115–117). The successful capture of PC3 cells compared to U251 MG isolation, suggests that the selected markers were not present on the surface of the U251 MG cells. This also highlights the potential difficulty of attempting to capture CTCs in a clinical setting using the pluriBead® technique.

To isolate GBM CTCs using purely biological properties rather than their physical properties increases the chances of CTCs being missed. Multiple clones of the same primary antibody were selected for the pluriBead® technique. One clone typically binds to just one target molecule presenting a single epitiope. The epitopes present could vary greatly in each CTC, even from the same parent tumour, which would minimise the successful chances of capturing CTCs with pluriBead®. To increase the possibility of capturing CTCs, the pluriBead® technique could be repeated overall several rounds with beads conjugated to different antibodies. This however also increases the chances of losing CTCs, particularly when there could just be one CTC present in the blood sample. This would also increase the time required for the completion of this technique.

Both Screen Cell®- LCD and Screen Cell®-MB kits were able to isolate U251 MG cells, which were then successfully cultured. The Screen Cell® method was easy to use and rapid, taking only 3 min to perform the process. The technique is also sensitive, capturing cells from a blood sample, which had been spiked with just 2×10^1 U251 MG cells. Another benefit of the method is the single enrichment step, consisting of blood passing directly through a filter, which may reduce the chance for CTCs to be lost. Both kits offer the advantage of supporting further analysis of markers. The Screen Cell®-MB kit has a particular advantage that the cells can be analysed directly for DNA/RNA, or they can be cultured first and then analysed for DNA/RNA. This quick and cheap method could be undertaken at the patient's bedside with no requirement for pre-processing. Fast enrichment also minimises disruption to the CTCs, which preserves the cell phenotype.

Cell counts used for the validation of the enrichment techniques used in this study were as recommended by the manufacturers. A clear limitation of this study is that the cell counts are much higher than those expected when if clinical samples were tested with the selected method. Nonetheless this has provided us with a good opportunity to assess the limitations of each method, even with a higher cell count. Bang-Christensen et al. (78), reported enriching between 0.5 and 42 CTCs in 3 ml blood. Therefore 3 mL of normal whole blood spiked with 2×10^1 U251 MG cells was used to test the sensitivity of the ScreenCell® technique. The ScreenCell® method was successfully able to isolate the U251 MG cells at this concentration. Another limitation of this study is that commercial cultures rather than patient derived cultures have been used. Additionally, the techniques were not validated on patient plasma samples.

In comparison to the other enrichment methods compared in this study, Screen Cell® appears most favourable to use in a healthcare setting as it is simple, cheap and quick to use (Table 3). Only one step is required before the CTCs are captured on the membrane filter, through size isolation, thus, maximising the chances of CTC capture. This method could be easily introduced into a busy clinical setting, where reliable and quick results are required. This system offers an option for simple cytomorpholical diagnosis after routine staining of CTCs. It also supports a number of other potential characterisation techniques and could enable captured CTCs to be successfully cultured.

By contrast, isolation methods which rely on single CTC biomarkers such as pluriBead® and the Cell Search® System could lead to higher false negative results, due to CTC heterogeneity. EGFR for example, which was used to characterise isolated U251 MG cells, demonstrates heterogeneous expression in GBMs (115). A multi-step process such as the OncoQuick technique could also lead to CTCs being missed, due to them being lost during one of the processing stages.

The potential benefit of using GBM CTCs diagnostically in the healthcare setting is threefold: it could enable earlier diagnosis, disease monitoring and potential reassurance of the worried well. Out of the four commercially available CTC enrichment methods – OncoQuick®, Screen Cell®, pluriBead® and Cell Search®- we found that the Screen Cell® method offered the most potential for translational application in the clinical setting. Alongside being simple, cheap and quick, this CTC enrichment method was not

TABLE 3 Advantages and disadvantages of the OncoQuick®, ScreenCell®, Cell Search® and pluriBead® enrichment techniques.

Enrichment Technique	Rationale	Advantages	Disadvantages
OncoQuick®	Enumeration by combined density-based centrifugation and filtration. Integration of a porous barrier above the separation media captures CTCs and enables smaller white and red blood cells to pass through.	Label-free technique, which captures modified and viable cells. Cost effective. Successfully captured U251 MG cells. Captured cells were successfully cultured and characterized using immunofluorescence. Cultured cells could be used for xenografting in immunocompromised mice. Able to process 15 mL of whole blood using this method, which may increase chances of capturing CTCs.	Multi-step process, cells can be lost and time consuming (difficult in a busy clinical setting). Contamination with blood cells noted. CTCs could be lost in supernatant.
ScreenCell®	Enrichment using a membrane microfilter	Simple, convenient, cost effective. No mechanical damage to cells. Successfully captured U251 MG cells. Cells maintain viability so can be cultured subsequent to processing. Captures cells based on size separation using a single step process, therefore less chance for CTCs to be missed. Technique suitable for a busy clinical setting. Method enables CTC cells to be cultured after enrichment and captured cells can be used for molecular typing, genetic profiling and xenografting.	Contamination with blood cells noted. Manufacturer recommends using a 3 mL blood sample, which may decrease chances of capturing CTCS.
Cell Search®	Immunomagnetic enrichment with ferrofluid nanoparticles that target EpCAM. Characterisation with cytokeratin (8, 18+, and 19+) monoclonal antibodies. CD45 antibody used to differentiate white blood cells from CTCs.	Automatic technique. Simple, convenient and easy to operate. No pre-treatment required. Highly sensitive and reproducible. First and only clinically validated, FDA approved, blood test for enumerating CTCs.	Costly, need to purchase instrument as well as Cell Search® components. Did not capture U251 MG cells, – only enriches CTCs with cell surface EpCAM. CTCs are widely heterogenous. Relying on cell surface markers for enrichment could lead to false negative results.
pluriBead®	Enumeration by antibody coated beads, which target CTC surface antigens. The pluriBeads® are bound to CTCs are then sieved to isolate cells from whole blood. CTCs can then be removed from beads for characterisation.	Method is sensitive and quick. High purity of CTCs. CTCs can be cultured following enrichment. A variety of characterisation techniques can be under taken on the isolated CTCs including molecular typing and genetic profiling.	Relies on cell surface markers to isolate CTCs. CTCs are heterogenous so a higher chance of missing the CTCs. Multi-step process so cells could be easily lost. To date no universal CTC antigens have been identified. Only a very small number (≈ 2) of U251 MG cells captured through this method. This could be potentially due to contamination rather than the beads successfully capturing the cells. Manufacturer recommends using a 3 mL blood sample, which may decrease chances of capturing CTCS.

CTCs, circulating tumour cells; EpCAM, epithelial cell adhesion molecule.

limited to isolating CTCs through one characteristic. It also supports a wide range of downstream analysis options. Further validation of the ScreenCell® technique is now required, which will be completed on GBM patient blood samples in a clinically relevant setting.

Data availability statement

The original contributions presented in the study are included in the article/supplementary material, further inquiries can be directed to the corresponding author.

Ethics statement

The studies involving humans were approved by The Brain Tumour Bank South West and Brain UK Ethics 15/006. The studies were conducted in accordance with the local legislation and institutional requirements. The participants provided their written informed consent to participate in this study.

Author contributions

HB: Conceptualization, Data curation, Formal analysis, Investigation, Methodology, Project administration, Validation, Visualization, Writing – original draft, Writing – review & editing, Funding acquisition. CP: Supervision, Writing – original draft, Writing – review & editing. KK: Supervision, Writing – original draft, Writing – review & editing, Conceptualization, Funding acquisition.

Funding

The author(s) declare financial support was received for the research, authorship, and/or publication of this article. This study was funded through the June Henry Memorial Fund and David Telling Grant.

Acknowledgments

We would like to acknowledge Bristol Philanthropy, the June Henry Memorial Fund and David Telling Charitable Trust for their support with this study.

Conflict of interest

The authors declare that the research was conducted in the absence of any commercial or financial relationships that could be construed as a potential conflict of interest.

Publisher's note

References

1. Cancer.Net. (2023). Brain tumour: statistics. Available at: https://www.cancer.net/cancer-types/brain-tumor/statistics (Accessed 24 November 2023).

2. Smittenaar CR, Petersen KA, Stewart K, Moitt N. Cancer incidence and mortality projections in the UK until 2035. *Br J Cancer*. (2016) 115:1147–55. doi: 10.1038/bjc.2016.304

3. Brain Tumour Research. (2023). Stark facts. Available at: https://braintumourresearch.org/blogs/campaigning/stark-facts (Accessed 24 November 2023).

4. Burnet NG, Jefferies SJ, Benson RJ, Hunt DP, Treasure FP. Years of life lost (YLL) from cancer is an important measure of population burden--and should be considered when allocating research funds. *Br J Cancer*. (2005) 92:241–5. doi: 10.1038/sj.bjc.6602321

5. Cancer Research UK. (2020). Brain, other CNS and intracranial tumours statistics. Available at: https://www.cancerresearchuk.org/health-professional/cancer-statistics/statistics-by-cancer-type/brain-other-cns-and-intracranial-tumours#heading-Zero (Accessed 24 November 2023)

6. Lyratzopoulos G, Abel GA, Mcphail S, Neal RD, Rubin GP. Measures of promptness of cancer diagnosis in primary care: secondary analysis of national audit data on patients with 18 common and rarer cancers. *Br J Cancer*. (2013) 108:686–90. doi: 10.1038/bjc.2013.1

7. The Brain Tumour Charity. (2016). How long does it take to get diagnosed?. Available at: https://www.thebraintumourcharity.org/news/blog-post/diagnosis-times/ (Accessed 24 November 2023).

8. Elliss-Brookes L, Mcphail S, Ives A, Greenslade M, Shelton J, Hiom S, et al. Routes to diagnosis for cancer - determining the patient journey using multiple routine data sets. *Br J Cancer*. (2012) 107:1220–6. doi: 10.1038/bjc.2012.408

9. Public Health England. (2015). National Cancer Intelligence Network Short Report - Routes to diagnosis 2015 update: brain tumours.

10. Burki TK. Long waiting times for the test results for NHS patients. *Lancet Oncol*. (2016) 17:e274. doi: 10.1016/S1470-2045(16)30209-1

11. Strauss SB, Meng A, Ebani EJ, Chiang GC. Imaging glioblastoma posttreatment: progression, pseudoprogression, pseudoresponse, radiation necrosis. *Radiol Clin North Am*. (2019) 57:1199–216. doi: 10.1016/j.rcl.2019.07.003

12. Swanton C. Intratumor heterogeneity: evolution through space and time. *Cancer Res*. (2012) 72:4875–82. doi: 10.1158/0008-5472.CAN-12-2217

13. Ramón YCS, Sesé M, Capdevila C, Aasen T, De Mattos-Arruda L, Diaz-Cano SJ, et al. Clinical implications of intratumor heterogeneity: challenges and opportunities. *J Mol Med (Berl)*. (2020) 98:161–77. doi: 10.1007/s00109-020-01874-2

14. Yong E. Cancer biomarkers: written in blood. *Nature*. (2014) 511:524–6. doi: 10.1038/511524a

15. Liskova A, Samec M, Koklesova L, Giordano FA, Kubatka P, Golubnitschaja O. Liquid biopsy is instrumental for 3PM dimensional solutions in Cancer management. *J Clin Med*. (2020) 9:2749. doi: 10.3390/jcm9092749

16. Mitra A, Mishra L, Li S. EMT, CTCs and CSCs in tumor relapse and drug-resistance. *Oncotarget*. (2015) 6:10697–711. doi: 10.18632/oncotarget.4037

17. Pawlikowska P, Faugeroux V, Oulhen M, Aberlenc A, Tayoun T, Pailler E, et al. Circulating tumor cells (CTCs) for the noninvasive monitoring and personalization of non-small cell lung cancer (NSCLC) therapies. *J Thorac Dis*. (2019) 11:S45–56. doi: 10.21037/jtd.2018.12.80

18. Clawson GA, Kimchi E, Patrick SD, Xin P, Harouaka R, Zheng S, et al. Circulating tumor cells in melanoma patients. *PLoS One*. (2012) 7:e41052. doi: 10.1371/journal.pone.0041052

19. De Bono JS, Scher HI, Montgomery RB, Parker C, Miller MC, Tissing H, et al. Circulating tumor cells predict survival benefit from treatment in metastatic castration-resistant prostate cancer. *Clin Cancer Res*. (2008) 14:6302–9. doi: 10.1158/1078-0432.CCR-08-0872

20. Gazzaniga P, De Berardinis E, Raimondi C, Gradilone A, Busetto GM, De Falco E, et al. Circulating tumor cells detection has independent prognostic impact in high-risk non-muscle invasive bladder cancer. *Int J Cancer*. (2014) 135:1978–82. doi: 10.1002/ijc.28830

21. Hiltermann TJN, Pore MM, Van Den Berg A, Timens W, Boezen HM, Liesker JJW, et al. Circulating tumor cells in small-cell lung cancer: a predictive and prognostic factor. *Ann Oncol*. (2012) 23:2937–42. doi: 10.1093/annonc/mds138

22. Huang X, Gao P, Song Y, Sun J, Chen X, Zhao J, et al. Relationship between circulating tumor cells and tumor response in colorectal cancer patients treated with chemotherapy: a meta-analysis. *BMC Cancer*. (2014) 14:976. doi: 10.1186/1471-2407-14-976

23. Krebs MG, Sloane R, Priest L, Lancashire L, Hou JM, Greystoke A, et al. Evaluation and prognostic significance of circulating tumor cells in patients with non-small-cell lung cancer. *J Clin Oncol*. (2011) 29:1556–63. doi: 10.1200/JCO.2010.28.7045

24. Lucci A, Hall CS, Lodhi AK, Bhattacharyya A, Anderson AE, Xiao L, et al. Circulating tumour cells in non-metastatic breast cancer: a prospective study. *Lancet Oncol*. (2012) 13:688–95. doi: 10.1016/S1470-2045(12)70209-7

25. Matsusaka S, Chìn K, Ogura M, Suenaga M, Shinozaki E, Mishima Y, et al. Circulating tumor cells as a surrogate marker for determining response to chemotherapy

in patients with advanced gastric cancer. *Cancer Sci*. (2010) 101:1067–71. doi: 10.1111/j.1349-7006.2010.01492.x

26. Racila E, Euhus D, Weiss AJ, Rao C, Mcconnell J, Terstappen LW, et al. Detection and characterization of carcinoma cells in the blood. *Proc Natl Acad Sci U S A*. (1998) 95:4589–94. doi: 10.1073/pnas.95.8.4589

27. Pierga JY, Bidard FC, Cropet C, Tresca P, Dalenc F, Romieu G, et al. Circulating tumor cells and brain metastasis outcome in patients with HER2-positive breast cancer: the LANDSCAPE trial. *Ann Oncol*. (2013) 24:2999–3004. doi: 10.1093/annonc/mdt348

28. Butler TP, Gullino PM. Quantitation of cell shedding into efferent blood of mammary adenocarcinoma. *Cancer Res*. (1975) 35:512–6.

29. Chambers AF, Groom AC, Macdonald IC. Dissemination and growth of cancer cells in metastatic sites. *Nat Rev Cancer*. (2002) 2:563–72. doi: 10.1038/nrc865

30. Fidler IJ. Metastasis: quantitative analysis of distribution and fate of tumor emboli labeled with 125 I-5-iodo-2′-deoxyuridine. *J Natl Cancer Inst*. (1970) 45:773–82.

31. Yoshida K, Fujikawa T, Tanabe A, Sakurai K. Quantitative analysis of distribution and fate of human lung cancer emboli labeled with 125I-5-iodo-2′-deoxyuridine in nude mice. *Surg Today*. (1993) 23:979–83. doi: 10.1007/BF00308973

32. Micalizzi DS, Maheswaran S, Haber DA. A conduit to metastasis: circulating tumor cell biology. *Genes Dev*. (2017) 31:1827–40. doi: 10.1101/gad.305805.117

33. Bockhorn M, Roberge S, Sousa C, Jain RK, Munn LL. Differential gene expression in metastasizing cells shed from kidney tumors. *Cancer Res*. (2004) 64:2469–73. doi: 10.1158/0008-5472.CAN-03-0256

34. Chang YS, Di Tomaso E, Mcdonald DM, Jones R, Jain RK, Munn LL. Mosaic blood vessels in tumors: frequency of cancer cells in contact with flowing blood. *Proc Natl Acad Sci U S A*. (2000) 97:14608–13. doi: 10.1073/pnas.97.26.14608

35. Zheng G, Zhang J, Zhao H, Wang H, Pang M, Qiao X, et al. α3 integrin of cell-cell contact mediates kidney fibrosis by integrin-linked kinase in proximal tubular E-cadherin deficient mice. *Am J Pathol*. (2016) 186:1847–60. doi: 10.1016/j.ajpath.2016.03.015

36. Jain RK. Molecular regulation of vessel maturation. *Nat Med*. (2003) 9:685–93. doi: 10.1038/nm0603-685

37. Tong RT, Boucher Y, Kozin SV, Winkler F, Hicklin DJ, Jain RK. Vascular normalization by vascular endothelial growth factor receptor 2 blockade induces a pressure gradient across the vasculature and improves drug penetration in tumors. *Cancer Res*. (2004) 64:3731–6. doi: 10.1158/0008-5472.CAN-04-0074

38. Cavallaro U, Christofori G. Cell adhesion in tumor invasion and metastasis: loss of the glue is not enough. *Biochim Biophys Acta*. (2001) 1552:39–45. doi: 10.1016/s0304-419x(01)00038-5

39. Padera TP, Stoll BR, Tooredman JB, Capen D, Di Tomaso E, Jain RK. Pathology: cancer cells compress intratumour vessels. *Nature*. (2004) 427:695. doi: 10.1038/427695a

40. Pernot S, Evrard S, Khatib AM. The give-and-take interaction between the tumor microenvironment and immune cells regulating tumor progression and repression. *Front Immunol*. (2022) 13:850856. doi: 10.3389/fimmu.2022.850856

41. Venkatesh HS, Tam LT, Woo PJ, Lennon J, Nagaraja S, Gillespie SM, et al. Targeting neuronal activity-regulated neuroligin-3 dependency in high-grade glioma. *Nature*. (2017) 549:533–7. doi: 10.1038/nature24014

42. Venkatesh HS, Johung T, Caretti V, Noll A, Tang Y, Nagaraja S, et al. Neuronal activity promotes glioma growth through Neuroligin-3 secretion. *Cell*. (2015) 161:803–16. doi: 10.1016/j.cell.2015.04.012

43. Venkatesh HS, Morishita W, Geraghty AC, Silverbush D, Gillespie SM, Arzt M, et al. Electrical and synaptic integration of glioma into neural circuits. *Nature*. (2019) 573:539–45. doi: 10.1038/s41586-019-1563-y

44. Sontheimer H. A role for glutamate in growth and invasion of primary brain tumors. *J Neurochem*. (2008) 105:287–95. doi: 10.1111/j.1471-4159.2008.05301.x

45. Ibrahim-Hashim A, Robertson-Tessi M, Enriquez-Navas PM, Damaghi M, Balagurunathan Y, Wojtkowiak JW, et al. Defining Cancer subpopulations by adaptive strategies rather than molecular properties provides novel insights into intratumoral evolution. *Cancer Res*. (2017) 77:2242–54. doi: 10.1158/0008-5472.CAN-16-2844

46. Genna A, Vanwynsberghe AM, Villard AV, Pottier C, Ancel J, Polette M, et al. EMT-associated heterogeneity in circulating tumor cells: sticky friends on the road to metastasis. *Cancers (Basel)*. (2020) 12:1632. doi: 10.3390/cancers12061632

47. Tashireva LA, Savelieva OE, Grigoryeva ES, Nikitin YV, Denisov EV, Vtorushin SV, et al. Heterogeneous manifestations of epithelial-mesenchymal plasticity of circulating tumor cells in breast Cancer patients. *Int J Mol Sci*. (2021) 22:2504. doi: 10.3390/ijms22052504

48. Herman H, Fazakas C, Haskó J, Molnár K, Mészáros Á, Nyúl-Tóth Á, et al. Paracellular and transcellular migration of metastatic cells through the cerebral endothelium. *J Cell Mol Med*. (2019) 23:2619–31. doi: 10.1111/jcmm.14156

49. Shiomi T, Lemaître V, D'armiento J, Okada Y. Matrix metalloproteinases, a disintegrin and metalloproteinases, and a disintegrin and metalloproteinases with thrombospondin motifs in non-neoplastic diseases. *Pathol Int*. (2010) 60:477–96. doi: 10.1111/j.1440-1827.2010.02547.x

50. Yamamoto N, Jiang P, Yang M, Xu M, Yamauchi K, Tsuchiya H, et al. Cellular dynamics visualized in live cells in vitro and in vivo by differential dual-color nuclear-cytoplasmic fluorescent-protein expression. *Cancer Res*. (2004) 64:4251–6. doi: 10.1158/0008-5472.CAN-04-0643

51. Yamauchi K, Yang M, Jiang P, Yamamoto N, Xu M, Amoh Y, et al. Real-time in vivo dual-color imaging of intracapillary cancer cell and nucleus deformation and migration. *Cancer Res*. (2005) 65:4246–52. doi: 10.1158/0008-5472.CAN-05-0069

52. Weiss L, Nannmark U, Johansson BR, Bagge U. Lethal deformation of cancer cells in the microcirculation: a potential rate regulator of hematogenous metastasis. *Int J Cancer*. (1992) 50:103–7. doi: 10.1002/ijc.2910500121

53. Follain G, Herrmann D, Harlepp S, Hyenne V, Osmani N, Warren SC, et al. Fluids and their mechanics in tumour transit: shaping metastasis. *Nat Rev Cancer*. (2020) 20:107–24. doi: 10.1038/s41568-019-0221-x

54. Kienast Y, Von Baumgarten L, Fuhrmann M, Klinkert WE, Goldbrunner R, Herms J, et al. Real-time imaging reveals the single steps of brain metastasis formation. *Nat Med*. (2010) 16:116–22. doi: 10.1038/nm.2072

55. Leone K, Poggiana C, Zamarchi R. The interplay between circulating tumor cells and the immune system: from immune escape to cancer immunotherapy. *Diagnostics (Basel)*. (2018) 8:59. doi: 10.3390/diagnostics8030059

56. Regmi S, Fu A, Luo KQ. High shear stresses under exercise condition destroy circulating tumor cells in a microfluidic system. *Sci Rep*. (2017) 7:39975. doi: 10.1038/srep39975

57. Krog BL, Henry MD. Biomechanics of the circulating tumor cell microenvironment. *Adv Exp Med Biol*. (2018) 1092:209–33. doi: 10.1007/978-3-319-95294-9_11

58. Anvari S, Osei E, Maftoon N. Interactions of platelets with circulating tumor cells contribute to cancer metastasis. *Sci Rep*. (2021) 11:15477. doi: 10.1038/s41598-021-94735-y

59. Lim M, Park S, Jeong HO, Park SH, Kumar S, Jang A, et al. Circulating tumor cell clusters are cloaked with platelets and correlate with poor prognosis in Unresectable pancreatic Cancer. *Cancers (Basel)*. (2021) 13:5272. doi: 10.3390/cancers13215272

60. Liu Y, Zhang Y, Ding Y, Zhuang R. Platelet-mediated tumor metastasis mechanism and the role of cell adhesion molecules. *Crit Rev Oncol Hematol*. (2021) 167:103502. doi: 10.1016/j.critrevonc.2021.103502

61. Lou XL, Sun J, Gong SQ, Yu XF, Gong R, Deng H. Interaction between circulating cancer cells and platelets: clinical implication. *Chin J Cancer Res*. (2015) 27:450–60. doi: 10.3978/j.issn.1000-9604.2015.04.10

62. Lv K, Cao X, Wang R, Du P, Fu J, Geng D, et al. Neuroplasticity of glioma patients: brain structure and topological network. *Front Neurol*. (2022) 13:871613. doi: 10.3389/fneur.2022.871613

63. Tamimi AF, Juweid M. Epidemiology and outcome of glioblastoma In: S De Vleeschouwer, editor. *Glioblastoma*. Brisbane (AU): Codon Publications (2017)

64. So JS, Kim H, Han KS. Mechanisms of invasion in glioblastoma: extracellular matrix, ca(2+) signaling, and glutamate. *Front Cell Neurosci*. (2021) 15:663092. doi: 10.3389/fncel.2021.663092

65. Lah TT, Novak M, Breznik B. Brain malignancies: glioblastoma and brain metastases. *Semin Cancer Biol*. (2020) 60:262–73. doi: 10.1016/j.semcancer.2019.10.010

66. Luo H, Shusta EV. Blood-brain barrier modulation to improve glioma drug delivery. *Pharmaceutics*. (2020) 12:1085. doi: 10.3390/pharmaceutics12111085

67. Davis L. Spongioblastoma multiforme of the brain. *Ann Surg*. (1928) 87:8–14.

68. Undabeitia J, Castle M, Arrazola M, Pendleton C, Ruiz I, Úrculo E. Multiple extraneural metastasis of glioblastoma multiforme. *An Sist Sanit Navar*. (2015) 38:157–61. doi: 10.4321/S1137-66272015000100022

69. Frank S, Kuhn SA, Brodhun M, Mueller U, Romeike B, Kosmehl H, et al. Metastatic glioblastoma cells use common pathways via blood and lymphatic vessels. *Neurol Neurochir Pol*. (2009) 43:183–90.

70. Onda K, Tanaka R, Takahashi H, Takeda N, Ikuta F. Cerebral glioblastoma with cerebrospinal fluid dissemination: a clinicopathological study of 14 cases examined by complete autopsy. *Neurosurgery*. (1989) 25:533–40. doi: 10.1227/00006123-198910000-00005

71. Sullivan JP, Nahed BV, Madden MW, Oliveira SM, Springer S, Bhere D, et al. Brain tumor cells in circulation are enriched for mesenchymal gene expression. *Cancer Discov*. (2014) 4:1299–309. doi: 10.1158/2159-8290.CD-14-0471

72. Macarthur KM, Kao GD, Chandrasekaran S, Alonso-Basanta M, Chapman C, Lustig RA, et al. Detection of brain tumor cells in the peripheral blood by a telomerase promoter-based assay. *Cancer Res*. (2014) 74:2152–9. doi: 10.1158/0008-5472.CAN-13-0813

73. Müller C, Holtschmidt J, Auer M, Heitzer E, Lamszus K, Schulte A, et al. Hematogenous dissemination of glioblastoma multiforme. *Sci Transl Med*. (2014) 6:247ra101. doi: 10.1126/scitranslmed.3009095

74. Gao F, Cui Y, Jiang H, Sui D, Wang Y, Jiang Z, et al. Circulating tumor cell is a common property of brain glioma and promotes the monitoring system. *Oncotarget*. (2016) 7:71330–40. doi: 10.18632/oncotarget.11114

75. Malara N, Guzzi G, Mignogna C, Trunzo V, Camastra C, Della Torre A, et al. Non-invasive real-time biopsy of intracranial lesions using short time expanded circulating tumor cells on glass slide: report of two cases. *BMC Neurol*. (2016) 16:127. doi: 10.1186/s12883-016-0652-x

76. Zhang W, Bao L, Yang S, Qian Z, Dong M, Yin L, et al. Tumor-selective replication herpes simplex virus-based technology significantly improves clinical detection and prognostication of viable circulating tumor cells. *Oncotarget*. (2016) 7:39768–83. doi: 10.18632/oncotarget.9465

77. Krol I, Castro-Giner F, Maurer M, Gkountela S, Szczerba BM, Scherrer R, et al. Detection of circulating tumour cell clusters in human glioblastoma. *Br J Cancer*. (2018) 119:487–91. doi: 10.1038/s41416-018-0186-7

78. Bang-Christensen SR, Pedersen RS, Pereira MA, Clausen TM, Løppke C, Sand NT, et al. Capture and detection of circulating glioma cells using the recombinant VAR2CSA malaria protein. *Cell*. (2019) 8:998. doi: 10.3390/cells8090998

79. Müller Bark J, Kulasinghe A, Hartel G, Leo P, Warkiani ME, Jeffree RL, et al. Isolation of circulating tumour cells in patients with glioblastoma using spiral microfluidic technology - a pilot study. *Front Oncol*. (2021) 11:681130. doi: 10.3389/fonc.2021.681130

80. Kolostova K, Pospisilova E, Pavlickova V, Bartos R, Sames M, Pawlak I, et al. Next generation sequencing of glioblastoma circulating tumor cells: non-invasive solution for disease monitoring. *Am J Transl Res*. (2021) 13:4489–99.

81. Qi Y, Sun Q, Deng G, Zhang H, Xu Y, Li Y, et al. Identifying circulating glioma cells and their clusters as diagnostic markers by a novel detection platform. *Clin Transl Med*. (2021) 11:e318. doi: 10.1002/ctm2.318

82. Verhaak RG, Hoadley KA, Purdom E, Wang V, Qi Y, Wilkerson MD, et al. Integrated genomic analysis identifies clinically relevant subtypes of glioblastoma characterized by abnormalities in PDGFRA, IDH1, EGFR, and NF1. *Cancer Cell*. (2010) 17:98–110. doi: 10.1016/j.ccr.2009.12.020

83. Balbous A, Cortes U, Guilloteau K, Villalva C, Flamant S, Gaillard A, et al. A mesenchymal glioma stem cell profile is related to clinical outcome. *Oncogenesis*. (2014) 3:e91. doi: 10.1038/oncsis.2014.5

84. Bhat KPL, Balasubramaniyan V, Vaillant B, Ezhilarasan R, Hummelink K, Hollingsworth F, et al. Mesenchymal differentiation mediated by NF-κB promotes radiation resistance in glioblastoma. *Cancer Cell*. (2013) 24:331–46. doi: 10.1016/j.ccr.2013.08.001

85. Bar EE, Lin A, Mahairaki V, Matsui W, Eberhart CG. Hypoxia increases the expression of stem-cell markers and promotes clonogenicity in glioblastoma neurospheres. *Am J Pathol*. (2010) 177:1491–502. doi: 10.2353/ajpath.2010.091021

86. Ozawa T, Riester M, Cheng YK, Huse JT, Squatrito M, Helmy K, et al. Most human non-GCIMP glioblastoma subtypes evolve from a common proneural-like precursor glioma. *Cancer Cell*. (2014) 26:288–300. doi: 10.1016/j.ccr.2014.06.005

87. Sottoriva A, Spiteri I, Piccirillo SG, Touloumis A, Collins VP, Marioni JC, et al. Intratumor heterogeneity in human glioblastoma reflects cancer evolutionary dynamics. *Proc Natl Acad Sci U S A*. (2013) 110:4009–14. doi: 10.1073/pnas.1219747110

88. Jin X, Yin J, Kim SH, Sohn YW, Beck S, Lim YC, et al. EGFR-AKT-Smad signaling promotes formation of glioma stem-like cells and tumor angiogenesis by ID3-driven cytokine induction. *Cancer Res*. (2011) 71:7125–34. doi: 10.1158/0008-5472.CAN-11-1330

89. Li M, Gao F, Ren X, Dong G, Chen H, Lin AY, et al. Nonhematogenic circulating aneuploid cells confer inferior prognosis and therapeutic resistance in gliomas. *Cancer Sci*. (2022) 113:3535–3546. doi: 10.1111/cas.15516

90. Chauhan A, Kaur R, Ghoshal S, Pal A. Exploration of circulating tumour cell (CTC) biology: a paradigm shift in liquid biopsy. *Indian J Clin Biochem*. (2021) 36:131–42. doi: 10.1007/s12291-020-00923-4

91. Sharma S, Zhuang R, Long M, Pavlovic M, Kang Y, Ilyas A, et al. Circulating tumor cell isolation, culture, and downstream molecular analysis. *Biotechnol Adv*. (2018) 36:1063–78. doi: 10.1016/j.biotechadv.2018.03.007

92. Harouaka RA, Nisic M, Zheng SY. Circulating tumor cell enrichment based on physical properties. *J Lab Autom*. (2013) 18:455–68. doi: 10.1177/2211068213494391

93. Ferreira MM, Ramani VC, Jeffrey SS. Circulating tumor cell technologies. *Mol Oncol*. (2016) 10:374–94. doi: 10.1016/j.molonc.2016.01.007

94. Kaifi JT, Kunkel M, Das A, Harouaka RA, Dicker DT, Li G, et al. Circulating tumor cell isolation during resection of colorectal cancer lung and liver metastases: a prospective trial with different detection techniques. *Cancer Biol Ther*. (2015) 16:699–708. doi: 10.1080/15384047.2015.1030556

95. Gertler R, Rosenberg R, Fuehrer K, Dahm M, Nekarda H, Siewert JR. Detection of circulating tumor cells in blood using an optimized density gradient centrifugation. Recent results in cancer research. Fortschritte der Krebsforschung. *Progres Dans Les Recherches Cancer*. (2003) 162:149–55. doi: 10.1007/978-3-642-59349-9_13

96. Nomura M, Yokoyama Y, Yoshimura D, Minagawa Y, Yamamoto A, Tanaka Y, et al. Simple detection and culture of circulating tumor cells from colorectal Cancer patients using poly(2-Methoxyethyl acrylate)-coated plates. *Int J Mol Sci*. (2023) 24:3949. doi: 10.3390/ijms24043949

97. Rossi T, Gallerani G, Angeli D, Cocchi C, Bandini E, Fici P, et al. Single-cell NGS-based analysis of copy number alterations reveals new insights in circulating tumor cells persistence in early-stage breast Cancer. *Cancers*. (2020) 12:2490. doi: 10.3390/cancers12092490

98. Pierzchalski A, Mittag A, Bocsi J, Tarnok A. An innovative cascade system for simultaneous separation of multiple cell types. *PloS one* (2013) 8:e74745. doi: 10.1371/journal.pone.0074745

99. Rizzo MI, Ralli M, Nicolazzo C, Gradilone A, Carletti R, Di Gioia C, et al. Detection of circulating tumor cells in patients with laryngeal cancer using ScreenCell: comparative pre- and post-operative analysis and association with prognosis. *Oncol Lett*. (2020) 19:4183–8. doi: 10.3892/ol.2020.11528

100. Hendricks A, Brandt B, Geisen R, Dall K, Röder C, Schafmayer C, et al. Isolation and enumeration of CTC in colorectal Cancer patients: introduction of a novel cell imaging approach and comparison to cellular and molecular detection techniques. *Cancers*. (2020) 12:2643. doi: 10.3390/cancers12092643

101. Jahan M, Mittal A, Rao S, Kishore S, Singh A, Jadli M, et al. Cytomorphologic visualization of circulating tumor cells in urinary bladder cancer patients using ScreenCell™ technology: potential as a simple cytology test. *Diagn Cytopathol*. (2023) 51:E219–23. doi: 10.1002/dc.25141

102. Theil G, Bialek J, Weiß C, Lindner F, Fornara P. Strategies for isolating and propagating circulating tumor cells in men with metastatic prostate Cancer. *Diagnostics*. (2022) 12:497. doi: 10.3390/diagnostics12020497

103. Chen X, Ma WY, Xu SC, Liang Y, Fu YB, Pang B, et al. The overexpression of epithelial cell adhesion molecule (EpCAM) in glioma. *J Neuro-Oncol*. (2014) 119:39–47. doi: 10.1007/s11060-014-1459-5

104. Andree KC, van Dalum G, Terstappen LW. Challenges in circulating tumor cell detection by the CellSearch system. *Mol Oncol*. (2016) 10:395–407. doi: 10.1016/j.molonc.2015.12.002

105. Joosse SA, Pantel K. Biologic challenges in the detection of circulating tumor cells. *Cancer Res*. (2013) 73:8–11. doi: 10.1158/0008-5472.CAN-12-3422

106. Hyun KA, Koo GB, Han H, Sohn J, Choi W, Kim SI, et al. Epithelial-to-mesenchymal transition leads to loss of EpCAM and different physical properties in circulating tumor cells from metastatic breast cancer. *Oncotarget*. (2016) 7:24677–87. doi: 10.18632/oncotarget.8250

107. Königsberg R, Obermayr E, Bises G, Pfeiler G, Gneist M, Wrba F, et al. Detection of EpCAM positive and negative circulating tumor cells in metastatic breast cancer patients. *Acta Oncol*. (2011) 50:700–10. doi: 10.3109/0284186X.2010.549151

108. Nash GF, Turner LF, Scully MF, Kakkar AK. Platelets and cancer. *Lancet Oncol*. (2002) 3:425–30. doi: 10.1016/S1470-2045(02)00789-1

109. Palumbo JS, Talmage KE, Massari JV, La Jeunesse CM, Flick MJ, Kombrinck KW, et al. Tumor cell-associated tissue factor and circulating hemostatic factors cooperate to increase metastatic potential through natural killer cell-dependent and-independent mechanisms. *Blood*. (2007) 110:133–41. doi: 10.1182/blood-2007-01-065995

110. Becker AP, Sells BE, Haque SJ, Chakravarti A. Tumor heterogeneity in glioblastomas: from light microscopy to molecular pathology. *Cancers (Basel)*. (2021) 13:761. doi: 10.3390/cancers13040761

111. Hou JM, Krebs M, Ward T, Sloane R, Priest L, Hughes A, et al. Circulating tumor cells as a window on metastasis biology in lung cancer. *Am J Pathol*. (2011) 178:989–96. doi: 10.1016/j.ajpath.2010.12.003

112. Kallergi G, Papadaki MA, Politaki E, Mavroudis D, Georgoulias V, Agelaki S. Epithelial to mesenchymal transition markers expressed in circulating tumour cells of early and metastatic breast cancer patients. *Breast Cancer Res*. (2011) 13:R59. doi: 10.1186/bcr2896

113. Mego M, Mani SA, Lee BN, Li C, Evans KW, Cohen EN, et al. Expression of epithelial-mesenchymal transition-inducing transcription factors in primary breast cancer: the effect of neoadjuvant therapy. *Int J Cancer*. (2012) 130:808–16. doi: 10.1002/ijc.26037

114. Gorges TM, Tinhofer I, Drosch M, Röse L, Zollner TM, Krahn T, et al. Circulating tumour cells escape from EpCAM-based detection due to epithelial-to-mesenchymal transition. *BMC Cancer*. (2012) 12:178. doi: 10.1186/1471-2407-12-178

115. Eskilsson E, Røsland GV, Solecki G, Wang Q, Harter PN, Graziani G, et al. EGFR heterogeneity and implications for therapeutic intervention in glioblastoma. *Neuro-Oncology*. (2018) 20:743–52. doi: 10.1093/neuonc/nox191

116. Olmez OF, Cubukcu E, Evrensel T, Kurt M, Avci N, Tolunay S, et al. The immunohistochemical expression of c-met is an independent predictor of survival in patients with glioblastoma multiforme. *Clin Transl Oncol*. (2014) 16:173–7. doi: 10.1007/s12094-013-1059-4

117. Schulte JD, Srikanth M, Das S, Zhang J, Lathia JD, Yin L, et al. Cadherin-11 regulates motility in normal cortical neural precursors and glioblastoma. *PLoS One*. (2013) 8:e70962. doi: 10.1371/journal.pone.0070962

frontiers | Frontiers in Oncology

TYPE Case Report
PUBLISHED 13 March 2024
DOI 10.3389/fonc.2024.1279897

OPEN ACCESS

EDITED BY
Dimitrios N. Kanakis,
University of Nicosia, Cyprus

REVIEWED BY
Vuong Trieu,
Oncotelic, Inc., United States
Raees Tonse,
Baptist Hospital of Miami, United States

*CORRESPONDENCE
Maninder Kaur
kmaninder@llu.edu

RECEIVED 18 August 2023
ACCEPTED 21 February 2024
PUBLISHED 13 March 2024

CITATION
Edelbach B, Gospodarev V, Lopez-Gonzalez M, Deisch J and Kaur M (2024) Unusual presentation of glioblastoma in the brainstem: a case report of a diffuse pontine glioblastoma multiforme and surgical management. *Front. Oncol.* 14:1279897. doi: 10.3389/fonc.2024.1279897

Unusual presentation of glioblastoma in the brainstem: a case report of a diffuse pontine glioblastoma multiforme and surgical management

Brandon Edelbach[1], Vadim Gospodarev[2], Miguel Lopez-Gonzalez[2], Jeremy Deisch[3] and Maninder Kaur[2*]

[1]School of Medicine, Loma Linda University, Loma Linda, CA, United States, [2]Department of Neurosurgery, Loma Linda University Medical Center, Loma Linda, CA, United States, [3]Department of Pathology, Loma Linda University Medical Center, Loma Linda, CA, United States

Diffuse pontine glioblastoma multiforme is a rare subtype of glioblastoma associated with a poor prognosis. In this case report, we present a unique case of diffuse primary pontine glioblastoma multiforme in a patient without any supratentorial lesions. We review the symptoms, treatment options, and case management of patients with infratentorial glioblastoma multiforme and compare these with our patient. Our patient presented with symptoms including progressive diplopia, gait disturbance, and lower extremity weakness. Magnetic resonance imaging revealed a diffuse lesion involving the pons and biopsy revealed only mildly-atypical glial infiltrates. Consequentially, diagnosis was driven by genetic analysis. Due to the location of the tumor, surgery was not considered a viable option. Instead, the patient received radiation therapy along with concomitant and adjuvant temozolomide chemotherapy which has resulted in improvement of symptoms. This case highlights the challenges of managing diffuse primary pontine glioblastoma multiforme and the need for more effective treatment options for this rare subtype of glioblastoma. Despite aggressive treatment, the prognosis for patients with infratentorial glioblastoma multiforme remains poor, with a median survival time of less than a year. Further research is needed to improve our understanding of the biology and optimal management of this disease.

KEYWORDS

glioblastoma multiforme, pons, radiation therapy, temozolomide therapy, infratentorial glioblastoma multiforme, molecular subtyping, STUPP regimen

1 Introduction

One of the most common malignancies of the central nervous system (CNS) are glioblastomas representing 14.3% of all CNS tumors and 49.1% of all malignant CNS tumors. Glioblastoma multiforme (GBM) are WHO grade IV tumors which are characteristically highly vascularized and possess a significant propensity to disperse throughout the brain parenchyma (1). These tumors are most commonly located in the frontal lobe of the supratentorial compartment (2). GBM has an increased incidence among men ages 70-85 years; furthermore, these tumors are approximately two times more prevalent among Caucasians than African-American patients (3). GBM had one of the lowest survival rate of 8 months with only 6.8% of patients surviving beyond 5 years (3). Additionally, older patients diagnosed with GBM often have worse prognosis (4). GBM often presents non-specifically with headaches, seizures, paresthesia, vision changes and personality changes.

The genetic morphology of GBM is crucial from not only a therapeutic perspective but also prognostically. GBMs appear to be derived from neural progenitors (5). These tumors arise from either neural stem cells or differentiated astrocytes, however there is still some debate over the origin of GBMs (6). Several common GBM biomarkers include O-6-methylguanine DNA methyltransferase (MGMT) and DNA wide methylation (marked by CpG island methylation) which were both associated better prognosis, while amplification of the epidermal growth factor receptor (EGFR) and the IDH wild type which is associated with telomerase reverse transcriptase (TERT) promoter methylation were both associated with decreased survival times (3). Mutations of the TERT gene occurred at a high frequency (seen in 70% of glioblastomas) (7, 8). Additionally the EGFR mutations were present in 57% of patients (9).

In order to improve diagnosis and treatment of these genetically heterogeneous tumors, a subclassification scheme was proposed by Philips et al. which divided GBMs into proneural, proliferative, and mesenchymal subclasses. Tumor subdivision was based on biomarker expression. The Mesenchymal and proliferative subclasses had an astrocytic morphology, often presenting in patients over 50 years old, and were associated with Akt activation, PTEN loss and gain of chromosome 7 and loss of chromosome 10. The mesenchymal subclass was characterized by the VEGF and CD44 markers while the proliferative subclass was associated with PCNA and TOP2A markers. The proneural subclass was found to develop in significantly younger patients, averaging 40 years old, and was associated with the longest survival time of the three subclasses and was associated with markers DLL3, BCAN, and Olig2 and was found to have PTEN intact, EGFR normal and Notch activation (10). These subclasses were proposed to exist along a spectrum with proneural and proliferative subclasses progressing to mesenchymal subclass (11). The prognostic capabilities of these tumor markers were found to be good (12). Since this initial subclassification, a fourth subclass was added as the classical group which was associated with EGFR mutations and a lack of TP53 mutations as well as mutations of the RB pathway. This subdivision was found to improve treatment and prognosis of patients with GBM of this specific genetic morphology (13).

While the traditional therapy for GBM resided in a surgical approach, the improved classification of GBM according to genetic morphology has increased the therapeutic capabilities of medicinal approach. The chemotherapy regimens focus exploitation of these tumor genetics. Patients found to have GBM with epigenetic silencing of MGMT DNA repair gene have significantly improved prognosis when treated with an alkylating agent such as temozolomide (TMZ) (14). When coupled with radiation (25 Gy), this therapy, known as Stupps regimen, is known to induce DNA double strand breaks and significantly improve patient prognosis. Additionally, it has been found that the addition of O-6-benzylguanine further enhances therapeutic effects of Stupps regimen (15). In addition to TMZ, carmustine and fotemustine have also been reported to have some therapeutic effect and are often used in combination with surgery. EGFR may also be targeted with bevacizumab which is a monoclonal antibody designed as an anti-angiogenic agent which has been found to significantly improve the prognosis of the classical subclass of GBM (16).

GBM is also associated with several cancer syndromes due to germline gene mutations including Li-Fraumeni syndrome (associated with P53), Neurofibromatosis 1/2 (NF-1 and NF-2 genes respectively), Turcots syndrome and BRCA syndrome. Additionally, these syndromes may be accelerated by predisposing events, however this has not been clearly established in the literature (17).

2 Case report

A 69 year old male patient with a past medical history of hypertension, and right eye blindness for 11-12 years due to retinal vein thrombosis was referred to us for subdural hemorrhage. The patient had been taken to an outside hospital and had a CT taken showing a left temporal subdural hemorrhage (5mm x 7cm x 4 cm) and a lumbar puncture. The patient was then transferred to our ED and an additional CT was taken confirming the subdural hemorrhage, which was felt to be stable. The patient reported he had fallen and hit his head. The patient denied dizziness, chest palpitations, seizures or unilateral weakness and stated that he did not lose consciousness during the incident. Furthermore, the patient had similar events several times over the past 7 to 8 months along with symptoms of progressive worsening gait and headaches which he had been seen by outside institutions. Upon questioning the patient revealed a history of symptoms including difficulty ambulating, bilateral tongue and facial numbness and dysarthria. Subsequently, further imaging was completed and MRI revealed a diffuse hypodensity of the pons and cerebellum which had extension into the left internal capsule and left corona radiata. (Figures 1, 2)

As no biopsy had been previously conducted, we felt that it was necessary to perform a biopsy for tissue diagnosis. A right sided retrosigmoid skull-base craniectomy approach for microsurgical right sided cerebellopontine angle approach was planned with the intention of conducting cerebellar and lateral pons biopsies. These

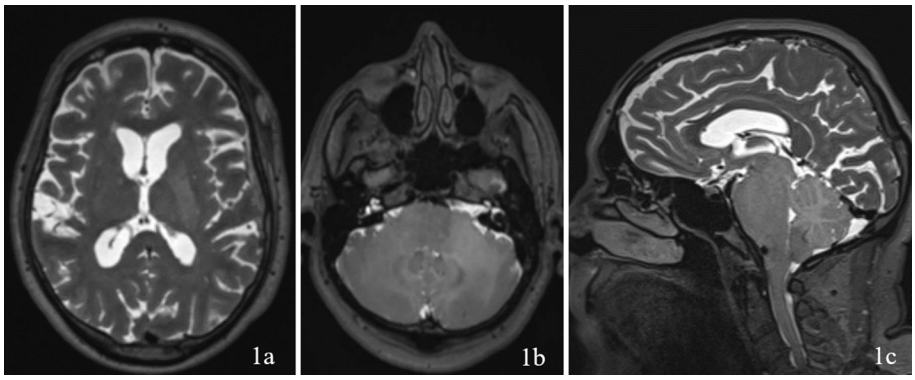

FIGURE 1
Imaging with T2WI sequence on 1a (axial through internal capsule/corona radiata), 1b (axial through pons/cerebellum), and 1c (sagittal) demonstrating diffuse hypodensity of the left internal capsule and left corona radiata.

biopsies were to be at the inferolateral aspect of the trigeminal nerve root entry zone.

The patient was brought into the operating room (OR) and was adequately prepped and positioned to exposed the right retrosigmoid area. The incision was planned with reference to the transverse sinus. The incision was made in a "C" fashion and then dissection revealed the suboccipital bone and mastoid. A single bur hole was placed and then enlarged to expose the inferior aspect of the transverse sinus and posterior portion of the sigmoid sinus. After this, we reached the signmoid transverse junction and via microscopy dissected the dura in a T-fashion. After encountering the cerebellum, the biopsy was planned with the Stealth navigation equipment after which we continued further to the pons and took an additional biopsy using the same technique. These were sent to pathology who reported that the cerebellum was in fact normal tissue; while the pons was nondiagnostic. Consequentially, additional permanent samples of the pons were taken at the inferolateral area of the trigeminal nerve root entry one. The patient was then closed appropriately and extubated without additional complications.

Upon reviewing the second set of permanent tissue samples, pathology identified a somewhat atypical glial infiltrate (Figure 3) with the majority of the astroglia nuclei labeling Ki-67 (Figure 4). Coupled with the radiology data (Figures 1, 2), these results were only somewhat suggestive of an infiltrating astroglia neoplasm. To obtain enhanced characterization of the lesion, IDH1/R132H, ATRX, H3K27me3, and p53 immunohistochemical studies were conducted. However, these studies revealed no molecular signatures typical of astroglia neoplasia. Subsequentially, additional genetic studies were performed at Mayo Clinic Laboratory. These results indicated a mutant TERT gene promoter and PIK3R1 mutant as well as wild type for IDH1/2, ATRX, and TP53. These genetic results were suggestive as a glioblastoma WHO grade 4 tumor. Furthermore, the negative result for H3K27 was used to rule out the possibility of a diffuse midline glioma.

The final diagnosis of the patient according to molecular subtyping was a TERT promoter mutation which supported an integrated diagnosis of glioblastoma. Furthermore, the lack of IDH, ATRX, or TP53 mutations was suggestive of an aggressive glial neoplasm. The whole point of this challenging pathologic diagnosis is that it is primarily based on the molecular findings identified on NGS testing of the very limited biopsy sampling. This diagnosis thus falls under the category of "molecular glioblastoma", and that it is not possible to establish a morphologic diagnosis of glioblastoma

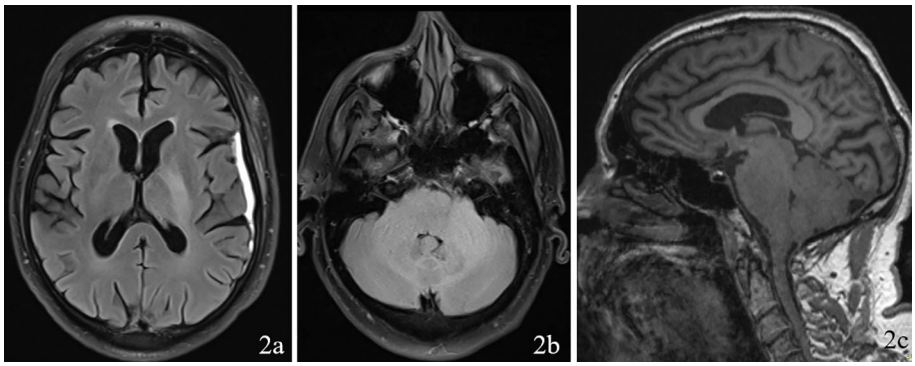

FIGURE 2
Imaging with FLAIR sequence on 2a (axial through internal capsule/corona radiata), 2b (axial through pons/cerebellum), and 2c (sagittal) demonstrating diffuse hypodensity of the left the pons and cerebellum.

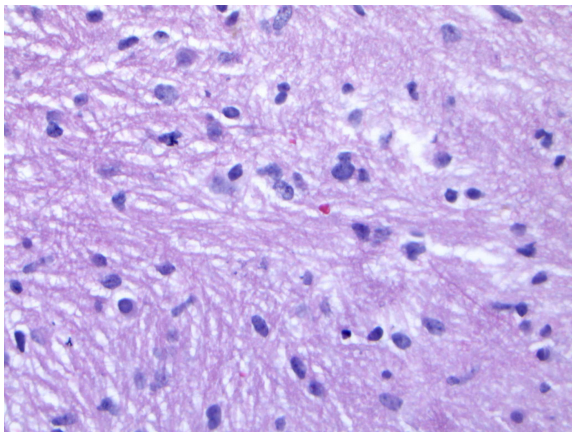

FIGURE 3
Hematoxylin and eosin (H&E) staining of tumor biopsy. Distinct features of atypical glial infiltrate are not definitively demonstrated and it is not feasible to establish a morphologic diagnosis of glioblastoma given the pontine location, as a biopsy sufficient to establish such a diagnosis would likely kill the patient.

given the pontine location, as a biopsy sufficient to establish such a diagnosis would likely kill the patient. As such, figures providing histologic proof of glioblastoma identity do not exist.

In accordance with the molecular subtype of our patients GBM, we treated the patient with the traditional STUPP regimen (radiotherapy (4848.0 Gy administered in 21 fractions) plus concomitant temozolomide). After completion of this initial therapy, MRI revealed no new tumor progression. The patient was then maintained via STUPP protocol which was scheduled for twelve cycles of temozolomide (dosing 150 mg/m2) on a 28-day cycle. Due to side effects related to the chemotherapy treatment the patient requested a break from treatment at the sixth iteration. Thus, upon completing the fifth iteration, maintenance treatment was temporarily discontinued. However, upon follow-up MRI the patient demonstrated showed two areas of focal enhancement, one at the right middle cerebellar peduncle and the second at the left parietal subependymal region along the posterior aspect of the body of the left lateral ventricle. Maintenance therapy was reinitiated at this point and focal radiation was considered.

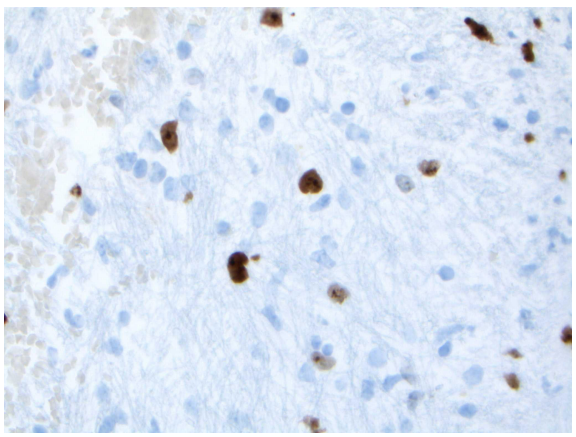

FIGURE 4
Nuclei labeling Ki-67 highlighting scattered atypical cells.

One month after re-initiation of treatment (13 months after initial start of chemotherapy), MRI demonstrated mild increase in size of the right cerebellar peduncle rim enhancing lesion (9mm x 6mm x 11mm as compared to 7mm x 5mm x 8mm). The lesion along the left parietal lobe subependymal region was stable at this point. At this point it was decided to administer focal proton therapy (30 Gy in 10 fractions) at the right cerebellar peduncle rim enhancing lesion along with continuation of maintenance temozolomide therapy.

At last follow-up the patient had demonstrated limited symptomatic improvement. Oral sensation has improved and the patient handling of oral secretions has improved. Although the patient still reports some numbness of the lower lip. Additionally, articulation of speech is much improved and coughing is reduced. Furthermore, the patient can maintain eye contact and demonstrates improved cognitive awareness.

3 Discussion

While supratentorial glioblastomas are among the most common type of glioblastomas, infratentorial glioblastomas are exceedingly rare tumors with an incidence rate of approximately 1.2% (18). In a recent multicenter retrospective study conducted by Weber et al., the median age of cerebellar GBM was reported to be 50.3 years, and 20% of the patients had brainstem invasion. The survival rate for these patients was found to be 14.7%, and brainstem invasion was identified as a poor prognostic factor (19). The clinical presentation of infratentorial GBM is similar to that of supratentorial GBM, with symptoms such as ataxia, dysmetria, tinnitus, dysarthria, and hemiparesis reported in both cases (18). However, in the presented case, the patient had no remarkable supratentorial spread of GBM contributing to the longstanding symptomatic progression prior to diagnosis (7-8 months). Reports of purely infratentorial GBM are rare. Magoha et al. described a homogenously hypointense ring enhancing lesion in the right brain stem in a young female patient presenting with right sided headache, hemiparesis, and tremor. Histologic examination was suggestive of GBM. Magoha et al. also reported temozolamide therapy with adjuvant radiotherapy was found to be useful in treating the malignancy (20). Additionally, Newton et al. described a 13 year old male with a pontine GBM which metastasized to the peritoneal cavity (which was attributed to a ventriculoperitoneal shunt) (21). Salas et al. reported an infratentorial GBM in a newborn which had a similar genetic profile to the tumor in this case report, mainly that it had no mutations in association with the TP53 gene (22). Lastly, Stark et al. reported only seven cases of infratentorial GBM out of 577 patients with GBM, with two patients presenting with GBM of the brainstem (18). Stark et al. concluded that the Ki67 and GFAP expression of supratentorial GBM bore no differences from infratentorial GBM. Lastly, Stark et al. also found temozolomide to be an effect therapeutic intervention for patients with infratentorial GBM (18).

Diagnosing infratentorial GBM can be challenging, as these tumors often have non-specific radiologic features (23). Of the

patients presented by Stark et al., the first patient presented with symptoms of right hemiparesis, and the second patient had symptoms of vertigo, facial palsy, and dysphagia, with a survival time of 52 and 40 weeks, respectively (18). The second patient presented with left oculomotor palsy and hydrocephalus. These symptoms reminisce our patients' symptoms. Furthermore, within infratentorial GBM in general the most frequently reported symptoms were ataxia, dysmetria, dysarthria, hemiparesis, and vertigo (18, 20–22).

It is hypothesized that infratentorial GBM may represent metastatic processes from supratentorial GBM dispersing through the cerebrospinal fluid (24). Our patient did not present with any imaging suggestive of a supratentorial GBM, suggesting that our patient presented with a primary GBM of the pons. The tumor described by Salas et al. was in a newborn which was used as evidence to support the claim that primary infratentorial GBM may represent a developmental pathology (22). However, the occurrence of the genetically similar primary infratentorial GBM in this case report occurring in an older man suggests that this process is not necessarily limited to developmental anomalies. Lastly, it is important to note that the two previously reported cases of brainstem GBM presented much younger than our patient and had shorter associated survival times.

4 Conclusion

In conclusion, we presented a case of a unique diffuse primary pontine glioblastoma multiforme, which was managed with radiotherapy plus concomitant and adjuvant temozolomide. Our treatment approach was based on the molecular subtype of the patient's GBM, and was in accordance with the standard treatment for supratentorial GBMs. Despite aggressive treatment, the prognosis for patients with infratentorial glioblastoma multiforme remains poor. Further studies are needed to improve our understanding of the biology of this rare subtype of glioblastoma and develop more effective treatment strategies. Nevertheless, our case highlights the importance of personalized medicine and the use of molecular profiling to guide treatment decisions in patients with glioblastoma multiforme. We hope that this report will contribute to the growing body of knowledge on diffuse pontine glioblastoma multiforme and help clinicians make more informed treatment decisions for their patients.

Data availability statement

The original contributions presented in the study are included in the article/supplementary material. Further inquiries can be directed to the corresponding author.

Ethics statement

Written informed consent was obtained from the individual for the publication of any potentially identifiable images or data included in this article.

Author contributions

BE: Writing – original draft, Writing – review & editing. VG: Writing – review & editing. ML-g: Writing – review & editing. JD: Writing – review & editing. MK: Writing – review & editing.

Funding

The author(s) declare that financial support was received for the research, authorship, and/or publication of this article. This research received no external funding.

Conflict of interest

The authors declare that the research was conducted in the absence of any commercial or financial relationships that could be construed as a potential conflict of interest.

Publisher's note

References

1. D'Alessio A, Proietti G, Sica G, Scicchitano BM. Pathological and molecular features of glioblastoma and its peritumoral tissue. *Cancers (Basel)*. (2019) 11:469. doi: 10.3390/cancers11040469

2. Lam S, Lin Y, Zinn P, Su J, Pan IW. Patient and treatment factors associated with survival among pediatric glioblastoma patients: A Surveillance, Epidemiology, and End Results study. *J Clin Neurosci*. (2018) 47. doi: 10.1016/j.jocn.2017.10.041

3. Ostrom QT, Cioffi G, Waite K, Kruchko C, Barnholtz-Sloan JS. CBTRUS statistical report: primary brain and other central nervous system tumors diagnosed in the United States in 2014-2018. *Neuro-oncology*. (2021) 23:1-105. doi: 10.1093/neuonc/noab200

4. Chen L, Ma J, Zou Z, Liu H, Liu C, Gong S, et al. Clinical characteristics and prognosis of patients with glioblastoma: A review of survival analysis of 1674 patients based on SEER database. *Med (Baltimore)*. (2022) 101:e32042. doi: 10.1097/MD.0000000000032042

5. Holland EC, Celestino J, Dai C, Schaefer L, Sawaya RE, Fuller GN. Combined activation of Ras and Akt in neural progenitors induces glioblastoma formation in mice. *Nat Genet*. (2000) 25:55–7. doi: 10.1038/75596

6. Bachoo RM, Maher EA, Ligon KL, Sharpless NE, Chan SS, You MJ, et al. Epidermal growth factor receptor and Ink4a/Arf: convergent mechanisms governing terminal differentiation and transformation along the neural stem cell to astrocyte axis. *Cancer Cell*. (2002) 1:269–77. doi: 10.1016/S1535-6108(02)00046-6

7. Arita H, Narita Y, Fukushima S, Tateishi K, Matsushita Y, Yoshida A, et al. Upregulating mutations in the TERT promoter commonly occur in adult Malignant gliomas and are strongly associated with total 1p19q loss. *Acta Neuropathol*. (2013) 126:267–76. doi: 10.1007/s00401-013-1141-6

8. Eckel-Passow JE, Lachance DH, Molinaro AM, Walsh KM, Decker PA, Sicotte H, et al. Glioma groups based on 1p/19q, IDH, and TERT promoter mutations in tumors. *N Engl J Med*. (2015) 372:2499–508. doi: 10.1056/NEJMoa1407279

9. Maire CL, Ligon KL. Molecular pathologic diagnosis of epidermal growth factor receptor. *Neuro Oncol*. (2014) 16 Suppl 8:viii1–6. doi: 10.1093/neuonc/nou294

10. Phillips HS, Kharbanda S, Chen R, Forrest WF, Soriano RH, Wu TD, et al. Molecular subclasses of high-grade glioma predict prognosis, delineate a pattern of disease progression, and resemble stages in neurogenesis. *Cancer Cell*. (2006) 9:157–73. doi: 10.1016/j.ccr.2006.02.019

11. Ohgaki H, Kleihues P. The definition of primary and secondary glioblastoma. *Clin Cancer Res*. (2013) 19:764–72. doi: 10.1158/1078-0432.CCR-12-3002

12. Li H, Wang Z, Sun C, Li S. Establishment of a cell senescence related prognostic model for predicting prognosis in glioblastoma. *Front Pharmacol*. (2022) 13:1034794. doi: 10.3389/fphar.2022.1034794

13. Verhaak RGW, Hoadley KA, Purdom E, Wang V, Qi Y, Wilkerson MD, et al. An integrated genomic analysis identifies clinically relevant subtypes of glioblastoma characterized by abnormalities in PDGFRA, IDH1, EGFR and NF1. *Cancer Cell*. (2010) 17:98. doi: 10.1016/j.ccr.2009.12.020

14. Hegi ME, Diserens AC, Gorlia T, Hamou MF, de Tribolet N, Weller M, et al. MGMT gene silencing and benefit from temozolomide in glioblastoma. *N Engl J Med*. (2005) 352:997–1003. doi: 10.1056/NEJMoa043331

15. Chakravarti A, Erkkinen MG, Nestler U, Stupp R, Mehta M, Aldape K, et al. Temozolomide-mediated radiation enhancement in glioblastoma: a report on underlying mechanisms. *Clin Cancer Res*. (2006) 12:4738–46. doi: 10.1158/1078-0432.CCR-06-0596

16. Wu W, Klockow JL, Zhang M, Lafortune F, Chang E, Jin L, et al. Glioblastoma Multiforme (GBM): An overview of current therapies and mechanisms of resistance. *Pharmacol Res*. (2021) 171:105780. doi: 10.1016/j.phrs.2021.105780

17. Kyritsis AP, Bondy ML, Rao JS, Sioka C. Inherited predisposition to glioma. *Neuro Oncol*. (2010) 12:104–13. doi: 10.1093/neuonc/nop011

18. Stark AM, Maslehaty H, Hugo HH, Mahvash M, Mehdorn HM. Glioblastoma of the cerebellum and brainstem. *J Clin Neurosci*. (2010) 17:1248–51. doi: 10.1016/j.jocn.2010.02.015

19. Weber DC, Miller RC, Villà S, Hanssens P, Baumert BG, Castadot P, et al. Outcome and prognostic factors in cerebellar glioblastoma multiforme in adults: a retrospective study from the Rare Cancer Network. *Int J Radiat Oncol Biol Phys*. (2006) 66:179–86. doi: 10.1016/j.ijrobp.2006.04.035

20. Magoha M a. A, Rowland TL, Musau CK, Omar MA. Infratentorial glioblastoma multiforme: case report and review of literature. *East Afr Med J*. (2017) 94:398–404.

21. Newton HB, Rosenblum MK, Walker RW. Extraneural metastases of infratentorial glioblastoma multiforme to the peritoneal cavity. *Cancer*. (1992) 69:2149–53. doi: 10.1002/(ISSN)1097-0142

22. Salas S, Agut T, Rovira C, Canizo D, Lavarino C, Garcia-Alix A. Infratentorial congenital glioblastoma multiforme. A rare tumour with a still unknown biology. *Rev Neurol*. (2016) 63:411–4. doi: 10.33588/rn.6309.2016208

23. Kikuchi K, Hiratsuka Y, Kohno S, Ohue S, Miki H, Mochizuki T. Radiological features of cerebellar glioblastoma. *J Neuroradiol*. (2016) 43:260–5. doi: 10.1016/j.neurad.2015.10.006

24. Hamilton MG, Tranmer BI, Hagen NA. Supratentorial glioblastoma with spinal cord intramedullary metastasis. *Can J Neurol Sci*. (1993) 20:65–8. doi: 10.1017/S0317167100047454

frontiers | Frontiers in Oncology

TYPE Original Research
PUBLISHED 07 May 2024
DOI 10.3389/fonc.2024.1357789

OPEN ACCESS

EDITED BY
Cesare Zoia,
San Matteo Hospital Foundation (IRCCS), Italy

REVIEWED BY
Suojun Zhang,
Huazhong University of Science and Technology, China
Xingchen Peng,
Sichuan University, China

*CORRESPONDENCE
Mohammadreza Saghafi
imansaghafi86@gmail.com
Hamidreza Saghafi
hamidrezasaghafi.md@gmail.com

†These authors have contributed equally to this work

RECEIVED 18 December 2023
ACCEPTED 17 April 2024
PUBLISHED 07 May 2024

CITATION
Anvari K, Seilanian Toussi M, Saghafi M, Javadinia SA, Saghafi H and Welsh JS (2024) Extended dosing (12 cycles) vs conventional dosing
(6 cycles) of adjuvant temozolomide in adults with newly diagnosed high-grade gliomas: a randomized, single-blind, two-arm, parallel-group controlled trial. *Front. Oncol.* 14:1357789. doi: 10.3389/fonc.2024.1357789

Extended dosing (12 cycles) vs conventional dosing (6 cycles) of adjuvant temozolomide in adults with newly diagnosed high-grade gliomas: a randomized, single-blind, two-arm, parallel-group controlled trial

Kazem Anvari [1†], Mehdi Seilanian Toussi [2†], Mohammadreza Saghafi [3*], Seyed Alireza Javadinia [4†], Hamidreza Saghafi [5*] and James S. Welsh [6]

[1]Cancer Research Center, Faculty of Medicine, Mashhad University of Medical Sciences, Mashhad, Iran, [2]Department of Urology, Roswell Park Comprehensive Cancer Center, Buffalo, NY, United States, [3]Qazvin University of Medical Sciences, Qazvin, Qazvin, Iran, [4]Non-Communicable Diseases Research Center, Sabzevar University of Medical Sciences, Sabzevar, Iran, [5]Faculty of Medicine, Tehran Medical Branch of Islamic Azad University, Tehran, Iran, [6]Department of Radiation Oncology, Loyola University Chicago Stritch School of Medicine, Edward Hines Jr., VA Hospital, Maywood, IL, United States

Purpose: Maximum safe surgical resection followed by adjuvant chemoradiation and temozolomide chemotherapy is the current standard of care in the management of newly diagnosed high grade glioma. However, there are controversies about the optimal number of adjuvant temozolomide cycles. This study aimed to compare the survival benefits of 12 cycles against 6 cycles of adjuvant temozolomide adults with newly diagnosed high grade gliomas.

Methods: Adult patients with newly diagnosed high grade gliomas, and a Karnofsky performance status>60%, were randomized to receive either 6 cycles or 12 cycles of adjuvant temozolomide. Patients were followed-up for assessment of overall survival (OS) and progression-free survival (PFS) by brain MRI every 3 months within the first year after treatment and then every six months.

Results: A total of 100 patients (6 cycles, 50; 12 cycles, 50) were entered. The rate of treatment completion in 6 cycles and 12 cycles groups were 91.3% and 55.1%, respectively. With a median follow-up of 26 months, the 12-, 24-, 36-, and 48-month OS rates in 6 cycles and 12 cycles groups were 81.3% vs 78.8%, 58.3% vs 49.8%, 47.6% vs 34.1%, and 47.6% vs 31.5%, respectively (p-value=.19). Median OS of 6 cycles and 12 cycles groups were 35 months (95% confidence interval (CI), 11.0 to 58.9) and 23 months (95%CI, 16.9 to 29.0). The 12-, 24-, 36-, and 48-month PFS rates in 6 cycles and 12 cycles groups were 70.8% vs 56.9%, 39.5% and 32.7%, 27.1% vs 28.8%, and 21.1% vs 28.8%, respectively (p=.88). The Median PFS of 6 cycles and 12 cycles groups was 18 months (95% CI, 14.8 to 21.1) and 16 (95% CI, 11.0 to 20.9) months.

Conclusion: Patients with newly diagnosed high grade gliomas treated with adjuvant temozolomide after maximum safe surgical resection and adjuvant chemoradiation do not benefit from extended adjuvant temozolomide beyond 6 cycles.

Trial registration: Prospectively registered with the Iranian Registry of Clinical Trials: IRCT20160706028815N3. Date registered: 18/03/14.

KEYWORDS

high grade gliomas, adjuvant temozolomide, survival, extended chemotherapy, randomized controlled trial, glioblastoma multiforme

1 Introduction

Glioblastoma is the most common and most aggressive tumor primary brain tumor originating from astrocytes. With a 3-year survival of approximately 10 percent, the dire prognosis of this tumor has not improved significantly in recent years (1). Complete resection of this tumor is almost impossible due to the invasive nature of the tumor and involvement of eloquent parts of the brain. Adjuvant post-surgical treatment is required to prevent or delay recurrence.

The current standard of care for newly diagnosed patients with appropriate performance status is maximum safe surgical resection, post-operative radiation concomitant with daily oral temozolomide and adjuvant chemotherapy with temozolomide (2). This recommendation is based on a randomized trial that recorded a significant benefit of the combined temozolomide and radiotherapy protocol over the radiotherapy alone arm (overall survival at 2 years, 27.2% versus 10.9%) (3). In this standard protocol (sometimes called the Stupp regimen), 3-dimentional radiotherapy of 60 Gy in 30 fractions is administered concomitant with temozolomide (75 mg/m^2, 7 days per week). Then, after 4 weeks from radiation termination, patients receive up to six courses of adjuvant temozolomide (150-200 mg/m^2 for 5 days every 28 days). A cohort retrospective cohort study using linked population bases from a cancer registry in Australia, revealed that patients treated in 2010-2012 (which corresponds to the era of temozolomide use), had better median survival than those treated in the pre-temozolomide period of 2001-2003 (10.6 months vs. 7.4 months) (4). However, these figures confirm that the prognosis of patients with glioblastoma has remained dismal. To date, the trials on using other treatment modalities like stereotactic radiosurgery, heavy charged particles, interstitial brachytherapy, tumor treating fields (TT-Fields), antiangiogenic therapy, immunotherapy, and gene therapy have shown inconsistent or disappointing results (5). In an attempt to improve survival, adjuvant dose dense adjuvant temozolomide (75 mg/m^2 on days 1 to 21 every 28 days) has been compared against standard adjuvant protocol with no encouraging result (6, 7).

Considering lack of effective salvage treatment in case of recurrence, it has been a usual practice in many centers to extend the adjuvant temozolomide beyond 6 courses up to 12, especially in patients who tolerate well the treatment well with no evidence of progression (8–11). The results of retrospective and randomized trials on the benefit of such extended adjuvant treatment have not been consistent. Extended treatment may increase the toxicity of treatment and it worsens the economic burden of treatment (12). Furthermore, there are reports that continued treatment may induce resistance to the ongoing alkylating agents and alters response to salvage therapy (13, 14).

In this prospective randomized trial, we aimed to assess the feasibility of extended adjuvant temozolomide (12 courses) and compare it against standard treatment (6 courses) in eligible patients with glioblastoma.

2 Methods

2.1 Participants

The study was conducted at three main tertiary referral Cancer Treatment Centers of Mashhad, Iran including the Oncology Clinics of Imam Reza and Omid Educational Hospitals both affiliated with Mashhad University of Medical Sciences as well as Reza Radiotherapy Oncology Center between April 2018 and October 2020.We enrolled newly diagnosed patients with pathologically confirmed glioblastoma multiforme or anaplastic astrocytoma who had undergone tumor resection, had a Karnofsky performance status of >60%, normal kidney and liver functions tests, and adequate bone marrow capacity. Patients were excluded in cases with a previous history of malignancy, previous treatment with chemotherapy and/or radiotherapy, and if they selected strictly palliative treatment (receiving radiation therapy alone or altered fractionated radiotherapy).

2.2 Study design

In this randomized, single-blind, parallel-group trial, we assigned the eligible patients at the commencement of chemoradiation to

receive either 6 cycles or 12 cycles of adjuvant temozolomide by block randomization [2:2]. In this context, the letter A or letter B was allocated to the 6 cycles or 12 cycles groups, drawing four potential combinations (i.e., AABB, BBAA, ABAB, and BABA). The envelope randomization method was used to assign patients to each group.

Before starting the treatment, all patients underwent brain MRI to assess the residual tumor. We performed staging work-up according to the last version of the National Comprehensive Cancer Network (NCCN) guidelines for Central Nervous System Cancers (15, 16). Brain CT scan with contrast with a slice separation of 5 mm was obtained for 3D conformal radiotherapy planning. Treatment planning was performed using Radiation Therapy Oncology Group (RTOG) two phase or European Organization for Research and Treatment of Cancer (EORTC) single phase recommendations for target definition (1). All patients received focal external beam irradiation of 60 Gy in 30 fractions. The patients received concurrent temozolomide (75 mg/m^2, daily) based on Stupp's protocol (2). Adjuvant chemotherapy with single agent oral temozolomide (150-200 mg/m^2, the first to fifth day, every 28 days) was started four weeks after the completion of chemoradiation.Adjuvant temozolomide was initiated at a dose of 150 mg/m^2 and the doses was increased to 200 mg/m^2 and continued at this dose if there was an absence of any grade 2-4 hematologic toxicities. The patients received ondansetron (4 mg every 8 hours) as antiemetic prophylaxis during the concurrent chemoradiation, and the adjuvant chemotherapy. Before each course of chemotherapy, patients were inquired about their signs and symptoms, underwent physical examination and Complete Blood Count (CBC) to assess the treatment toxicity, as well as signs and symptoms of the disease progression/recurrence. Moreover, a brain MRI with gadolinium contrast was obtained every 3 months within the first year after treatment termination, then every six months to detect possible local disease progression/recurrence.

2.3 Variables

2.3.1 Survival analysis

The time interval in months between the first pathologic diagnosis and the first evidence of disease recurrence (presence of newly enhancive tumoral lesion within or outside of radiotherapy field) or disease progression (an increase in enhancive lesion size by 25 percent) was considered as the progression-free survival (PFS) (3). The overall survival (OS) was defined as the time interval in months between the initial pathologic diagnosis and death/last visit.

2.3.2 Treatment toxicity

The Eastern Cooperative Oncology Group Common Toxicity Criteria V 5.0 (ECOG-CTC) was used to assess chemotherapy-induced neutropenia, thrombocytopenia, anemia, constipation, diarrhea, nausea, vomiting, and alopecia using a 4-grade scoring system (through mildest to most severe; grade 0 to grade 4).

2.4 Ethics

This trial was registered in the Iranian Registration of clinical trials (IRCT20160706028815N3), prospectively. The study protocol was approved by the Ethics Committee of Mashhad University of Medical Sciences (approval code: IR.MUMS.fm.REC.1396.449) and was conducted according to the Declaration of Helsinki. Undersigned informed consent forms were obtained from all patients prior to the enrollment.

2.5 Statistical analyses and sample size

2.5.1 Sample size

Considering the 12-month survival rate of 82.9% and 100% in patients with high-grade glioma receiving 6 or more than 6- cycles of adjuvant temozolomide respectively in a previous study (4), with a type I error rate of.05 and statistical power of 80%, the sample size was calculated to be 31 patients in each group ($n = \frac{(Z_{1-\frac{\alpha}{2}}+Z_{1-\beta})^2(P_1(1-P_1)+P_2(1-P_2))}{(d)^2}$). However, due to potential loss to follow-up, we designed the trial to enroll at least 50 patients in each group.

2.5.2 Statistical analyses

The normality of data was assessed by Shapiro–Wilk test using the Statistical Package for Social Science version 22 (SPSS Inc., Chicago, Illinois). All data had a normal distribution. Therefore, categorical data and quantitative data were analyzed using Chi square (Fisher's exact test) and t test, respectively. Intention-to-treat analysis was adopted to perform statistical analysis. The survival data were presented by Kaplan-Meier curves and were analyzed by univariate log-rank (5). A p-value <0.05 was considered statistically significant. Moreover, Multivariate Cox regression analysis was used to detect the contributing factors to overall survival of patients with high-grade glioma.

3 Results

3.1 Patients

From April 2018 until October 2020, 100 patients from 3 institutions in Mashhad, Iran were randomly assigned to receive 6 cycles (50 patients) or 12 cycles of adjuvant temozolomide (50 patients). In 6-cycle group, three patients died after the completion of chemoradiation and the chemotherapy regimen of one patient was changed to bevacizumab-based chemotherapy due to disease progression before the first course of adjuvant temozolomide. In 12-cycle group, only one patient did not receive allocation since he died after the completion of chemoradiation (Figure 1).

Both groups were similar in term of age, performance status, focal neurological signs, tumor resection, and histology. Male gender was more frequent in the 6-cycle group than the 12-cycle group. Table 1 reveals the demographic and clinical characteristics of the two groups.

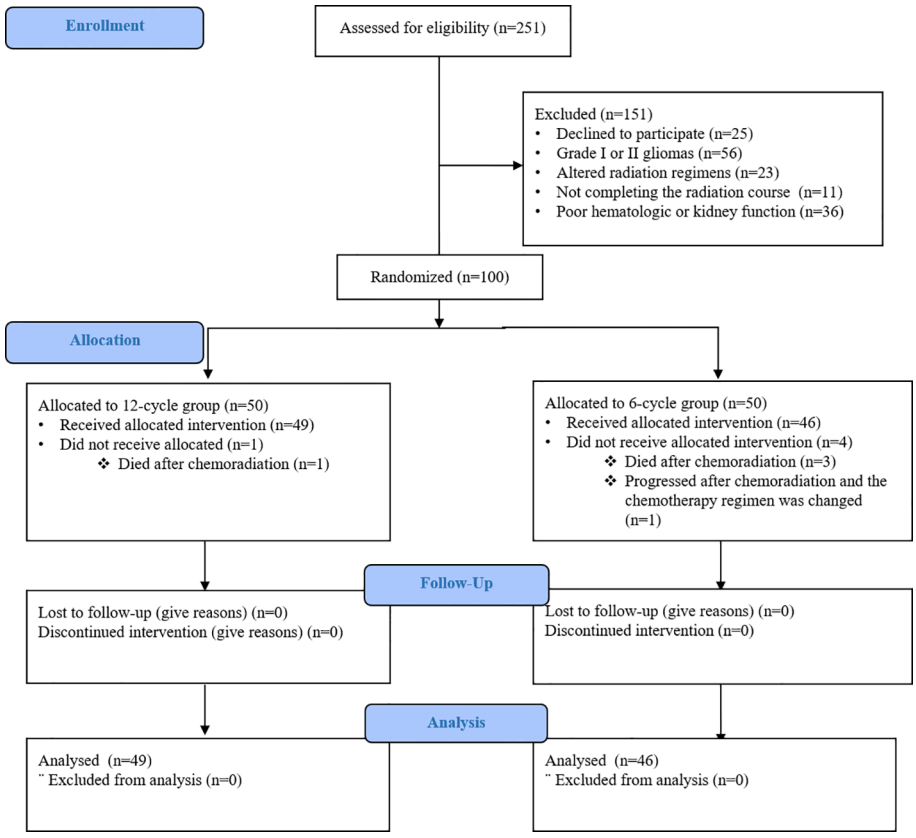

FIGURE 1
Consort flow diagram.

3.2 The delivery of treatment

The median number of chemotherapy courses in the 6-cycle and 12-cycle groups were 5 (range: 1 to 6) and 10 (range: 2-12) respectively. Overall, 77/95 patients (81%) completed 6 courses of chemotherapy without progression. Table 2 shows events that caused adjuvant treatment cessation (progression and/or death) before each cycle for both groups.

3.3 Survival and progression

With a median follow-up of 26 months, the 12-, 24-, 36-, and 48- month OS rates in 6-cycle and 12-cycle groups were 81.3% vs 78.8%, 58.3% vs 49.8%, 47.6% vs 34.1%, and 47.6% vs 31.5%, respectively (p=.19). Median OS of 6 cycles and 12 cycles groups were 35 months (95% confidence interval (CI), 11.0 to 58.9) and 23 months (95%CI, 16.9 to 29.0). The 12-, 24-, 36-, and 48- month PFS rates in 6 cycles and 12 cycles groups were 70.8% vs 56.9%, 39.5% and 32.7%, 27.1% vs 28.8%, and 21.1% vs 28.8%, respectively (p=.88). Median PFS of 6 cycles and 12 cycles groups were 18 months (95% CI, 14.8 to 21.1) and 16 (95% CI, 11.0 to 20.9) months (Figure 2).

TABLE 1 The characteristics of the patients at baseline.

Characteristics	Entire group: 95 patients		
	TMZ 6-cycle, 46 patients n (%)	TMZ 12-cycle, 49 patients n (%)	P value
Male Gender	37(80.4)	28 (57.1)	0.015
Age > 45	22 (47.8)	25 (51)	0.75
Karnofsky Performance Status ≥ 80%	32 (69.5)	31 (63.2)	0.43
Focal neurological deficits	16 (34.8)	18 (36.7)	0.83
Tumor resection: Gross total Subtotal Biopsy only	 8 (17.4) 28 (60.9) 10 (21.7)	 9 (18.4) 24 (49) 16 (32.7)	0.43
Histology: Glioblastoma Anaplastic astrocytoma	 37 (80.4) 9 (19.6)	 40 (81.6) 9 (18.4)	0.82

YMZ: temozolomide.

TABLE 2 The discontinuation rate of temozolomide per courses during the adjuvant treatment.

	6-cycle group n (%)	Cause of discontinuation	12-cycle group n (%)	Cause of discontinuation
Cycle 1	1 (2.2)	Death	0	–
Cycle 2	1 (2.2)	Death	2 (4.1)	Death (1)/Disease progression (1)
Cycle 3	0	–	5 (10.2)	Death (4)/Disease progression (1)
Cycle 4	0	–	2 (4.1)	Death (1)/Disease progression (1)
Cycle 5	2 (4.3)	Death	2 (4.1)	Death (2)
Cycle 6	0	–	3 (6.1)	Death (1)/Disease progression (2)
Cycle 7	–	–	2 (4.1)	Death (2)
Cycle 8	–	–	3 (6.1)	Death (1)/Disease progression (2)
Cycle 9	–	–	2 (4.1)	Disease progression (2)
Cycle 10	–	–	0	–
Cycle 11	–	–	1 (2)	Disease progression
Cycle 12	–	–	0	–

Univariant regression analysis showed that male gender (hazard ratio (HR) 2.5, p=.03), age below 45-year-old (HR.39, p=.01), performance status (HR.95, p=.003), and histology of glioblastoma multiform (HR 4.5, p=.03) are the main predictors of survival. However, in multivariant regression analysis, performance status remained a significant predictor of survival survival (HR.9, p=.02) (Table 3).

3.4 Safety

The most serious toxicity was grade 3 neutropenia, which was observed in 2 patients of the 6-cycles group and grades 3 and 4 thrombocytopenia, which were observed in 2 and 1 patients respectively in the 6-cycles group. Other toxicities were illustrated in Table 4. As shown in the table, only mild adverse events were relatively more frequent in 12-cycle group.

4 Discussion

This randomized study in glioblastoma patients who had undergone maximum safe surgical resection and who had completed adjuvant chemoradiation, did not show benefit from extended adjuvant temozolomide compared to the standard adjuvant course of temozolomide in terms of overall survival or progression free survival. We designed the randomization on an intent-to-treat basis to avoid selection bias. Therefore, patients who failed to complete adjuvant chemotherapy for any reason were not excluded from analysis.

In a retrospective study, Seiz et al. evaluated a group of 114 newly diagnosed glioblastoma patients treated by maximum safe surgical resection, temozolomide based chemo-irradiation and adjuvant temozolomide (TMZ). The adjuvant chemotherapy continued until tumor progression or appearance of intolerance. They found a significant correlation between median time to progression (TTP) as well as overall survival (OS) and the number of chemotherapy cycles (17). However, given the retrospective nature of the study, a selection bias might be a limiting factor, as long survivors had more chance to receive more extended cycles of chemotherapy. In another retrospective cohort study by Skardelly et al. (14), 107 patients with glioblastoma were divided into three groups of receiving less than 6 cycles (Group A), exactly 6 cycles (group B), and more than 6 cycles (group C). The decision to continue or stop adjuvant temozolomide was based on physician's discretion. The 12.7 month overall in group A was significantly lower than group B (25.2 months) and C (28.6 months). Patients in group C were younger than group B (age less than 50, 57.7% vs. 18.7%). Multivariate Cox regression did not prove an overall survival advantage for group C against group B. At the time of first progression, the response rate to TMZ/lomustine rechallenge was higher in group B than group C (47% versus 13%). The lower survival rate in group A can be attributed to unresponsive tumors causing early progression and/or unfavorable individual prognostic factors.

There are retrospective studies that analyzed glioblastoma patients who remained progression free at the end of 6 cycles of adjuvant TMZ therapy. In an analysis of a German Glioma Network cohort, Gramatzki et al. identified 142 patients who were progression free at 6 cycles of adjuvant TMZ, among whom 61 continued the treatment to at least 7 maintenance cycles (median 11, range 7-20). After adjusting for age, extent of resection, Karnofsky performance status, and presence of residual tumor and O^6-methylguanine DNA methyltransferase *(MGMT)* promoter methylation status, no significant difference in OS (HR = 1.6, 95% CI: 0.8-3.3; P = .22) and PFS (HR = 0.8, 95% CI: 0.4-1.6; P = .56) was detected between two groups (18). Roldán Urgoiti et al. (19) identified a cohort of 273 glioblastoma patients by Alberta Cancer Registry among whom 52 (19%) underwent surgery, chemoradiation and were progression free at 6 cycles of adjuvant therapy. They found that patients who received more than 6 cycles (median 11, range 7-13) had significantly more favorable median

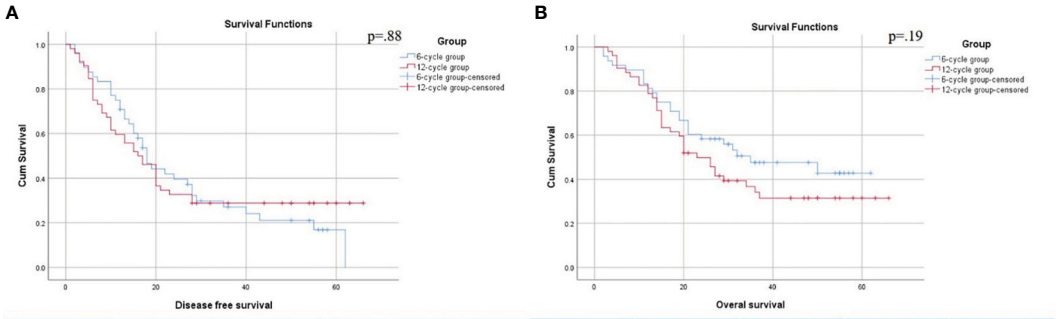

Time	12 months	24 month	36 month	48 month
6 cycle	70.8%	39.5%	27.1%	21.1%
12 cycle	56.9%	32.7%	28.8%	28.8%

Time	12 months	24 month	36 month	48 month
6 cycle	81.3%	58.3%	47.6%	47.6%
12 cycle	78.8%	49.8%	34.1%	31.5%

FIGURE 2
PFS **(A)** and OS **(B)** of patients with HGG based on the treatment groups.

survival than those receiving 6 cycle according to the Stupp protocol (3) (24.6 versus 16.5 months respectively, p=0.031). According to the authors, their institution amended their policy to allow physician to extend adjuvant chemotherapy up to 12 cycles provided patients had no progression and minimal toxicity. Therefore, physician's discretion played a role in selecting patients for extended treatment probably those with more favorable general condition at the end of 6 cycles.

In several studies, patients who completed 6 cycles of adjuvant TMZ without progression were divided into two groups of continued versus no further treatment and prospectively analyzed. Blumenthal et al. performed a retrospective meta-analysis of 4 prospective clinical trials for newly diagnosed patients with glioblastoma who were progression free at least 28 days after cycle 6 of adjuvant temozolomide (20). Patients receiving 6 cycles were compared with those who continued treatment beyond 6 cycles. The decision to continue treatment was based on physician's discretion. Among 624 patients eligible for analysis, 291 continued the treatment up to progression or 12 cycles. Patients who treated more than 6 cycles had significantly more favorable progression-free survival (hazard ratio 0.8, [0.65-0.98] p=0.03), but no significant difference in overall survival was detected (hazard ratio 0.92 [0.71-1.19], p=0.52). The physicians' discretion for continuing treatment can cause a selection bias in favor of the group receiving beyond 6 cycles. In a multicentric randomized trial in Spain by Balana et al. (21), Patients who were progression free at cycle 6 of adjuvant therapy were randomly assigned to stop group (79 patients) and extended group (80 patients). The chemotherapy in the extended treatment group continued until 12 courses or progression. Extended treatment was not associated with a significant benefit in terms of 6-months survival rate (61.3% vs 55.7%). Hematological toxicity, albeit being mild, was more frequent in the extended arm.

Some studies randomized newly diagnosed patients at diagnosis or at the chemoradiation termination into two groups of 6-cycle and more than 6 cycles of adjuvant TMZ therapy with intention to treat (ITT) basis. In a study in India, Bhandari et al. randomized 40 patients after chemo-irradiation into 6-cycle and 12-cycle groups. The median number of adjuvant chemotherapy in 6-cycle and 12-cycle groups was 6 (range, 3-6) and 12 (3-12) respectively. Patients

TABLE 3 regression analysis of contributing factors to overall survival of patients with high-grade glioma.

	Univariant analysis			Multivariant analysis		
	HR	95% CI	P value	HR	95% CI	P value
Group of study (6-cycle)	.989	.48-2	.97			
Gender (male)	2.5	.96-6.6	.03	2.5	.9-6.5	.06
Age (<45 years old)	.39	.18-.84	.01	.5	.2-1.1	.08
Performance status (%)	.95	.91-.98	.003	.9	.92-.99	.02
Preoperative tumor size (cm)	1	.88-1.2	.658			
Peritumoral edema (negative)	.39	.13-1.1	.08			
Midline shift (negative)	.5	.21-1.1	.1			
Histology (GBM)	4.8	1.1-20.4	.03	3.5	.8-15.3	.08
Type of surgery (biopsy and STR)	1.5	.5-4.4	.4			
CTV (cm3)	1	.9-1	.5			

10.3389/fonc.2024.1357789

TABLE 4 Treatment toxicity in patients treated with 6 or 12 cycles of temozolomide.

Adverse event	6-cycle group 45 patients N (%)				12-Cycle group 49 patients N (%)			
	Grade 1	Grade 2	Grade 3	Grade 4	Grade 1	Grade 2	Grade 3	Grade 4
Neutropenia	39 (84.8)	5 (10.9)	2 (4.3)	0	46 (95.8)	2 (4.2)	0	0
Thrombocytopenia	39 (84.8)	4 (8.7)	2 (4.3)	1	44 (91.7)	4 (8.3)	0	0
Anemia	44 (95.7)	2 (4.3)	0	0	47 (97.9)	1 (2.1)	0	0
Nausea/vomiting	36 (87.2)	3 (6.6)	0	0	45 (95.7)	2 (4.2)	0	0

in the 12-cycle group showed more favorable PFS (12.6 vs 16.8 months, P=0.069) and OS (15.4 vs 23.8 months, P=0.044). However, in a meta-analysis, Gupta et al. (22) considered four randomized clinical trials that recruited newly diagnosed patients with glioblastoma following concurrent chemoradiation and found different results. 358 eligible patients were randomly assigned to 6 cycles or > 6 cycles. The two groups (> 6 cycles vs 6 cycles) had no significant difference in terms of risk of progression (HR=0.82, 95% CI:0.61-1.1 P=0.18) or death (HR=0.87, 95% CI: 0.6-1.27, p=0.12). Overall, the authors concluded that their data did not suggest benefits from extending treatment, especially when considering possible increased toxicity to patients, and enhanced cost for the health system. In another meta-analysis by Attarian et al. (23) of four randomized studies consisting of 882 glioblastoma patients in total, no significant difference in PFS [(12.0 months (95% CI 9.0 to 15.0) vs. 10.0 months (95% CI 7.0 to 12.0), P = 0.270] and OS [23.0 months (95% CI 19.0 to 27.0) vs 24.0 months (95% CI 20.0 to 28.0), P = 0.73] was found between patients assigned to 6-cycle or extended adjuvant treatment.

Previous studies have demonstrated that the methylation of the *MGMT* gene promoter is a significant predictor of survival in patients receiving concurrent and adjuvant temozolomide therapy (3, 24). The result of the meta-analytic study by Blumenthal et al. (20) suggested that patients with methylated *MGMT* promoter status may particularly benefit from extended treatment in terms of progression-free survival (HR 0.65 [0.50–0.85], *P* <.01); however, overall survival was not affected by *MGMT* promoter methylation. There is no randomized trial to assess if extended treatment is particularly beneficial in patients whose tumors exhibit methylated MGMT promoters. The lack of information regarding methylation status of tumors is one of the limitations of our study. However, there is no recommendation for selecting patients for the current standard treatment based on methylation status. Pseudo-progression, which occurs in 20% to 30% of patients with glioblastoma following the Stupp regimen, may present a clinical conundrum (25) and affect progression-free survival (PFS) analysis. However, randomization of patients mitigates the effect of pseudo-progression on comparing groups analysis. Moreover, overall survival (OS) is a more robust endpoint.

Main limitation of present study is not assessing IDH mutation and MGMT status. In fact, a median OS of 35 months in patients undergoing to 6 cycles of TMZ might be influenced by IDH mutation since none of the patients are reported to undergo to tumor treating fields; while a median OS of 23 months may be related with a high prevalence of MGMT methylated patients, for example. About MGMT status, it is worth mentioning that patients with MGMT hypermethylation might benefit from extended TMZ schedule; but in this study there are no stratifications about MGMT status. This is important since mixing up all HHG patients receiving TMZ may led to an erroneous interpretation of the results. In fact, it may be found that MGMT hypermethylated patients may benefit from an extended TMZ schedule (or maybe not). The reason behind it is that the study was conducted between 2018 and 2020 when HGG patients were evaluated based on WHO 2016 Classification of CNS Tumours Diffuse astrocytic and oligodendroglial tumours and the has been reported two years later to observe enough events. Therefore, measurement of genes/molecular profile alterations were not mandatory. On the other hand, number of patients who underwent gross total resection was substantially lower from other trials and it may limit the extrapolation of our study.

Overall, consistent with the results of our study, most high-quality randomized trials and meta-analytic studies do not support a significant benefit for the extended adjuvant therapy, especially when considering higher toxicity (albeit mild) and economic burden on the patients, society and health system. The survival gains from the extended therapy, if any, has been small, which significantly reduces the cost-benefit of the continued treatment. Moreover, the extended treatment may reduce response to salvage treatment, which may explain the lack of OS benefit for extended therapy despite having a small PFS superiority in some studies. However, a subgroup of patients with special molecular characteristics (26–28) might still benefit significantly from the extended treatment and or novel treatment modalities; this hypothesis warrants further investigation.

Data availability statement

The raw data supporting the conclusions of this article will be made available by the authors, without undue reservation.

Ethics statement

The studies involving humans were approved by the Ethics Committee of Mashhad University of Medical Sciences. The studies were conducted in accordance with the local legislation and institutional requirements. The participants provided their written informed consent to participate in this study.

Author contributions

KA: Data curation, Funding acquisition, Investigation, Methodology, Project administration, Supervision, Validation, Writing – original draft, Writing – review & editing. MT: Conceptualization, Formal analysis, Funding acquisition, Investigation, Methodology, Project administration, Supervision, Validation, Visualization, Writing – original draft, Writing – review & editing. MS: Data curation, Investigation, Methodology, Writing – original draft, Writing – review & editing. SJ: Conceptualization, Investigation, Methodology, Writing – original draft, Writing – review & editing. HS: Investigation, Methodology, Writing – original draft, Writing – review & editing. JW: Supervision, Validation, Writing – original draft, Writing – review & editing.

Funding

The author(s) declare financial support was received for the research, authorship, and/or publication of this article. The present work is part of M.D. thesis which was approved by School of Medicine, Mashhad University of Medical Sciences (NO T5251; residency program of Radio-Oncology, MS). This study was fully funded by the Mashhad University of Medical Sciences (961130 to MT).

Acknowledgments

We would like to thank the study participants for their desirable cooperation and useful advices.

Conflict of interest

The authors declare that the research was conducted in the absence of any commercial or financial relationships that could be construed as a potential conflict of interest.

Publisher's note

References

1. Ostrom QT, Gittleman H, Liao P, Vecchione-Koval T, Wolinsky Y, Kruchko C, et al. CBTRUS statistical report: primary brain and other central nervous system tumors diagnosed in the United States in 2009–2013. *Neuro-oncology*. (2016) 18:v1–v75. doi: 10.1093/neuonc/now207

2. Sulman EP, Ismaila N, Chang SM. Radiation therapy for glioblastoma: American Society of Clinical Oncology clinical practice guideline endorsement of the American Society for Radiation Oncology guideline. *J Oncol Pract*. (2017) 13:123–7. doi: 10.1200/JOP.2016.018937

3. Stupp R, Hegi ME, Mason WP, van den Bent MJ, Taphoorn MJ, Janzer RC, et al. Effects of radiotherapy with concomitant and adjuvant temozolomide versus radiotherapy alone on survival in glioblastoma in a randomised phase III study: 5-year analysis of the EORTC-NCIC trial. *Lancet Oncol*. (2009) 10:459–66. doi: 10.1016/S1470-2045(09)70025-7

4. Johnston A, Creighton N, Parkinson J, Koh ES, Wheeler H, Hovey E, et al. Ongoing improvements in postoperative survival of glioblastoma in the temozolomide era: a population-based data linkage study. *Neuro-oncol Pract*. (2020) 7:22–30. doi: 10.1093/nop/npz021

5. Zhang H, Wang R, Yu Y, Liu J, Luo T, Fan F. Glioblastoma treatment modalities besides surgery. *J Cancer*. (2019) 10:4793. doi: 10.7150/jca.32475

6. Gilbert MR, Wang M, Aldape KD, Stupp R, Hegi ME, Jaeckle KA, et al. Dose-dense temozolomide for newly diagnosed glioblastoma: a randomized phase III clinical trial. *J Clin Oncol*. (2013) 31:4085. doi: 10.1200/JCO.2013.49.6968

7. Armstrong TS, Wefel JS, Wang M, Gilbert MR, Won M, Bottomley A, et al. Net clinical benefit analysis of radiation therapy oncology group 0525: a phase III trial comparing conventional adjuvant temozolomide with dose-intensive temozolomide in patients with newly diagnosed glioblastoma. *J Clin Oncol*. (2013) 31:4076. doi: 10.1200/JCO.2013.49.6067

8. Easaw JC, Mason WP, Perry J, Laperrière N, Eisenstat DD, Del Maestro R, et al. Canadian recommendations for the treatment of glioblastoma multiforme. *Curr Oncol*. (2007) 14:110–7. doi: 10.3747/co.2007.119

9. Barbagallo GM, Paratore S, Caltabiano R, Palmucci S, Parra HS, Privitera G, et al. Long-term therapy with temozolomide is a feasible option for newly diagnosed glioblastoma: a single-institution experience with as many as 101 temozolomide cycles. *Neurosurg Focus*. (2014) 37:E4. doi: 10.3171/2014.9.FOCUS14502

10. Malkoun N, Chargari C, Forest F, Fotso MJ, Cartier L, Auberdiac P, et al. Prolonged temozolomide for treatment of glioblastoma: preliminary clinical results and prognostic value of p53 overexpression. *J neuro-oncol*. (2012) 106:127–33. doi: 10.1007/s11060-011-0643-0

11. Nabors LB, Portnow J, Ammirati M, Baehring J, Brem H, Brown P, et al. Central nervous system cancers, version 1.2015. *J Natl Compr Cancer Netw*. (2015) 13:1191–202. doi: 10.6004/jnccn.2015.0148

12. Dixit S, Baker L, Walmsley V, Hingorani M. Temozolomide-related idiosyncratic and other uncommon toxicities: a systematic review. *Anti-cancer Drugs*. (2012) 23:1099–106. doi: 10.1097/CAD.0b013e328356f5b0

13. Happold C, Roth P, Wick W, Schmidt N, Florea AM, Silginer M, et al. Distinct molecular mechanisms of acquired resistance to temozolomide in glioblastoma cells. *J neurochem*. (2012) 122:444–55. doi: 10.1111/j.1471-4159.2012.07781.x

14. Skardelly M, Dangel E, Gohde J, Noell S, Behling F, Lepski G, et al. Prolonged temozolomide maintenance therapy in newly diagnosed glioblastoma. *oncol*. (2017) 22:570–5. doi: 10.1634/theoncologist.2016-0347

15. Nabors LB, Portnow J, Ammirati M, Baehring J, Brem H, Butowski N, et al. NCCN guidelines insights: central nervous system cancers, version 1.2017. *J Natl Compr Cancer Netw*. (2017) 15:1331–45. doi: 10.6004/jnccn.2017.0166

16. Horbinski C, Nabors LB, Portnow J, Baehring J, Bhatia A, Bloch O, et al. NCCN guidelines® Insights: central nervous system cancers, version 2.2022. *J Natl Compr Canc Netw*. (2023) 21:12–20. doi: 10.6004/jnccn.2023.0002

17. Seiz M, Krafft U, Freyschlag CF, Weiss C, Schmieder K, Lohr F, et al. Long-term adjuvant administration of temozolomide in patients with glioblastoma multiforme: experience of a single institution. *J Cancer Res Clin Oncol*. (2010) 136:1691–5. doi: 10.1007/s00432-010-0827-6

18. Gramatzki D, Kickingereder P, Hentschel B, Felsberg J, Herrlinger U, Schackert G, et al. Limited role for extended maintenance temozolomide for newly diagnosed glioblastoma. *Neurology*. (2017) 88:1422–30. doi: 10.1212/WNL.0000000000003809

19. Roldán Urgoiti GB, Singh AD, Easaw JC. Extended adjuvant temozolomide for treatment of newly diagnosed glioblastoma multiforme. *J neuro-oncol*. (2012) 108:173–7. doi: 10.1007/s11060-012-0826-3

20. Blumenthal DT, Gorlia T, Gilbert MR, Kim MM, Burt Nabors L, Mason WP, et al. Is more better? The impact of extended adjuvant temozolomide in newly diagnosed glioblastoma: a secondary analysis of EORTC and NRG Oncology/RTOG. *Neuro-oncology*. (2017) 19:1119–26. doi: 10.1093/neuonc/nox025

21. Balana C, Vaz MA, Manuel Sepúlveda J, Mesia C, Del Barco S, Pineda E, et al. A phase II randomized, multicenter, open-label trial of continuing adjuvant temozolomide beyond 6 cycles in patients with glioblastoma (GEINO 14-01). *Neuro-oncology*. (2020) 22:1851–61. doi: 10.1093/neuonc/noaa107

22. Gupta T, Talukdar R, Kannan S, Dasgupta A, Chatterjee A, Patil V. Efficacy and safety of extended adjuvant temozolomide compared to standard adjuvant temozolomide in glioblastoma: updated systematic review and meta-analysis. *Neuro-oncol Pract*. (2022) 9:354–63. doi: 10.1093/nop/npac036

23. Attarian F, Taghizadeh-Hesary F, Fanipakdel A, Javadinia SA, Porouhan P, PeyroShabany B, et al. A systematic review and meta-analysis on the number of adjuvant temozolomide cycles in newly diagnosed glioblastoma. *Front Oncol*. (2021) 4839. doi: 10.3389/fonc.2021.779491

24. Hegi ME, Diserens AC, Gorlia T, Hamou MF, de Tribolet N, Weller M, et al. MGMT gene silencing and benefit from temozolomide in glioblastoma. *New Engl J Med*. (2005) 352:997–1003. doi: 10.1056/NEJMoa043331

25. Brandes AA, Tosoni A, Spagnolli F, Frezza G, Leonardi M, Calbucci F, et al. Disease progression or pseudoprogression after concomitant radiochemotherapy treatment: pitfalls in neurooncology. *Neuro-oncology*. (2008) 10:361–7. doi: 10.1215/15228517-2008-008

26. Aum DJ, Kim DH, Beaumont TL, Leuthardt EC, Dunn GP, Kim AH. Molecular and cellular heterogeneity: the hallmark of glioblastoma. *Neurosurg Focus*. (2014) 37:E11. doi: 10.3171/2014.9.FOCUS14521

27. Parker NR, Khong P, Parkinson JF, Howell VM, Wheeler HR. Molecular heterogeneity in glioblastoma: potential clinical implications. *Front Oncol*. (2015) 5:55. doi: 10.3389/fonc.2015.00055

28. Cloughesy TF, Cavenee WK, Mischel PS. Glioblastoma: from molecular pathology to targeted treatment. *Annu Rev Pathol: Mech Dis*. (2014) 9:1–25. doi: 10.1146/annurev-pathol-011110-130324

frontiers | Frontiers in Neurology

TYPE Review
PUBLISHED 15 May 2024
DOI 10.3389/fneur.2024.1387986

OPEN ACCESS

EDITED BY
Cesare Zoia,
San Matteo Hospital Foundation (IRCCS), Italy

REVIEWED BY
Felix Stengel,
Cantonal Hospital St.Gallen, Switzerland
Yan Zou,
Henan University, China

*CORRESPONDENCE
Melike Mut
✉ mm2ee@uvahealth.org

RECEIVED 19 February 2024
ACCEPTED 01 May 2024
PUBLISHED 15 May 2024

CITATION
Nwafor DC, Obiri-Yeboah D, Fazad F, Blanks W and Mut M (2024) Focused ultrasound as a treatment modality for gliomas.
Front. Neurol. 15:1387986.
doi: 10.3389/fneur.2024.1387986

Focused ultrasound as a treatment modality for gliomas

Divine C. Nwafor[1], Derrick Obiri-Yeboah[2], Faraz Fazad[1], William Blanks[3] and Melike Mut[1]*

[1]Department of Neurosurgery, University of Virginia, Charlottesville, VA, United States, [2]Department of Neurological Surgery, Cleveland Clinic Lerner College of Medicine of Case Western Reserve University, Cleveland, OH, United States, [3]Department of Neurosurgery, Rockefeller Neuroscience Institute, West Virginia University, Morgantown, WV, United States

Ultrasound waves were initially used as a diagnostic tool that provided critical insights into several pathological conditions (e.g., gallstones, ascites, pneumothorax, etc.) at the bedside. Over the past decade, advancements in technology have led to the use of ultrasound waves in treating many neurological conditions, such as essential tremor and Parkinson's disease, with high specificity. The convergence of ultrasound waves at a specific region of interest/target while avoiding surrounding tissue has led to the coined term "focused ultrasound (FUS)." In tumor research, ultrasound technology was initially used as an intraoperative guidance tool for tumor resection. However, in recent years, there has been growing interest in utilizing FUS as a therapeutic tool in the management of brain tumors such as gliomas. This mini-review highlights the current knowledge surrounding using FUS as a treatment modality for gliomas. Furthermore, we discuss the utility of FUS in enhanced drug delivery to the central nervous system (CNS) and highlight promising clinical trials that utilize FUS as a treatment modality for gliomas.

KEYWORDS

focused ultrasound, glioma, glioblastoma, clinical trials, HIFUS, LIFUS, blood–brain barrier

1 Introduction

Central nervous system (CNS) tumors are diverse tumors with distinct and variable intrinsic characteristics. Of this broad category, roughly 28.8% are comprised of tumors with neuroepithelial origin, with an incidence rate of 5.56 per 100,000 persons. Glioblastoma, the most common and one of the most aggressive primary glial tumors has an incidence rate of 2.52 per 100,000 persons (1). In other words, there are over 10,000 new glioblastoma diagnoses in the United States annually. Notably, these tumors are not homogenously distributed among the population; they have higher incidences in specific ethnicity subgroups (2).

Over the past decades, much research has been conducted on the epidemiology of primary CNS tumors, including glial tumors; however, advancement has yet to be made in novel treatment modalities that significantly extend the duration and quality of life in patients suffering from these tumors. Epidemiology and early detection strategies are essential to studying any malignant process; however, due to the aggressive nature of certain subsets of these tumors, including glioblastoma, their clinical impact is limited (3). The current mainstay treatment of glioblastoma includes resection, radiation therapy, and chemotherapy (4, 5). Even with gross total resection and maximal radiation therapy and chemotherapy, survival rates are less than 2 years for most patients. New surgical tools, such as 5-aminolevulinic acid (5-ALA)

and volumetric MRI evaluation, can help maximize the extent of surgical resection; however, they still offer relatively low survival benefits (6).

Ultrasound technology has been studied for its ablative effects on the brain since the 1950s. Still, significant limitations, such as the need for a craniotomy window and difficulty with targeting precision, prevented it from gaining mainstream attention until decades later. Elias et al. conducted the first pilot study of focused ultrasound thalamotomy for essential tremors, showing that this was a safe and effective treatment (7). Thereafter, the indications for FUS have continued to grow, including treating Parkinsonian tremors/rigidity or managing many neuropsychiatric conditions (8). New indications for FUS beyond functional neurodegenerative disease conditions remain under study; however, data from several neurosurgical laboratories have begun to provide new evidence that supports the use of FUS in treating CNS glioma.

Additionally, the effect of novel drugs, such as immune checkpoint inhibitors, is significantly dampened secondary to the difficulty of such inhibitors permeating the intact blood–brain barrier. To address this difficulty, blood–brain barrier opening utilizing FUS provides a novel solution that allows novel chemo/immunotherapy to reach their desired targets and more effectively treat CNS tumors. This mini-review article discusses focused ultrasound and its novel applications in treating gliomas. Finally, we highlight promising clinical trials utilizing FUS as a glioma treatment modality.

2 Types and mechanisms of FUS

"Ultrasound" refers to a wave possessing a frequency beyond human hearing, typically $f > 20$ kHz (9). Ultrasound imaging has been employed for decades to visualize anatomic structures in the medical field—for example, prenatal or transthoracic echocardiogram. However, recent research focuses on the applications of ultrasound for therapeutic purposes. Ultrasound imaging converts electrical energy into mechanical energy by transmitting acoustic waves through a transducer (10). These waves penetrate tissues –such as skin and muscle–to reach molecules within deeper structures. Thereafter, the waves can either be absorbed, scattered, or reflected. When a molecule with a suitable frequency encounters the ultrasound waveform, energy transfer occurs; this concept is known as resonance (11).

Interventional ultrasound for ablative and non-ablative purposes utilizes the same principles governing ultrasound imaging. The waves produced can interfere constructively or destructively. These unique properties underlie the use of ultrasound waves as a diagnostic and therapeutic tool by controlling the interference of ultrasound waves (12). Constructive interference occurs when two or more waves meet, and their peaks or troughs overlap. The resultant wave in constructive interference results in a final wave with a greater amplitude than each individual wave. Conversely, destructive interference occurs when the consequent wave from two or more waves results in an overall final waveform with a smaller amplitude due to waves canceling out (13). In general, FUS aims to allow in-phase waves to converge at the therapeutic target location (12, 14).

FUS is an ultrasound modality that utilizes a concave transducer to converge ultrasound waves into a focused beam. FUS can be categorized as higher-frequency (HIFUS) and low-frequency (LIFUS). HIFUS is often used to ablate specific targets, whereas LIFUS is often used to improve drug delivery to specific targets (14). HIFUS beam intensities are typically between 100–10,000 with the objective of the thermal ablation of tissue, while LIFUS ranges from 0.125–3 W/cm^2 (14). The applications of HIFUS for functional neurosurgery have been vast, ranging from ablating the globus pallidus internus in Parkinson's disease to ablating an epileptic hippocampal focus (15, 16). Delivery of FUS waves is affected by skull fat and bone. FUS wave delivery can be enhanced by applying gasless water between the ultrasound transducer and the scalp. Concurrently, this also minimizes thermal damage. Magnetic resonance-guided imaging (MRgFUS) is critical in identifying/planning the target area and monitoring ablation size. If the target area is heated beyond 56°C for a few seconds, thermo-ablation occurs via protein denaturation and coagulative necrosis. MRgFUS allows monitored and controlled real-time thermometry, which enables immediate evaluation of treatment response (17).

Wave energy is created by passing an electrical current through a transducer to achieve thermoablation with HIFUS. Continuous high-pressure waves are then directed at a small target point, resulting in tissue destruction via a thermal effect. LIFUS ultrasound utilizes injected exogenous microbubbles to open the blood–brain barrier (BBB) by applying ultrasound non-thermal waves that promote microbubble size change/expansion – this is referred to as "stable cavitation." The perturbations in the size of the microbubbles promote BBB opening (18). Recent studies suggest BBB closure occurs within 48 h after LIFUS without causing injury or harm to the patient (19). Figure 1 demonstrates the proposed mechanisms and application of HIFUS and LIFUS in treating CNS tumors.

3 FUS in the management of glioma

The BBB is a selective dynamic barrier composed of endothelial cells with tight junction proteins, astrocytic end-feet processes, surrounding pericytes, and basal lamina that plays a critical role as a semi-permeable interface between the systemic circulation and brain parenchyma. In health, the BBB is important as it protects the brain from harmful toxins/molecules and inflammatory immune cells - and ultimately maintains cerebral homeostasis by regulating nutrients via modulation of proteins and enzymes found in several cell types of the BBB (20). However, in many disease states, such as CNS tumors, the selectivity of the BBB presents a challenge for therapeutic drugs to reach desired targets. Traditionally, neurosurgeons have mitigated this problem by increasing the dose of the drug – which worsens the adverse effect. Another option is intraventricular or intrathecal drug delivery. Though the effects of these two drug delivery methods strategies are pronounced compared to intra-arterial drug delivery, they do not effectively address the lesion of interest. Furthermore, specificity is significantly reduced (21).

In the early stages of glioma growth, tumor cells initially resemble the BBB, and as they continue to proliferate and progress, they form a new barrier known as the blood–brain tumor barrier (BBTB). The BBTB is distinct from the BBB in that it is characterized by an aberrant distribution of healthy BBB cell types (e.g., pericytes), astrocytic end-feet loss, neuronal dysfunction, increased expression of proteins that encourage drug transport efflux, and a heterogenous permeability between the tumor core and periphery (22–24). The BBB and BBTB limit the entry of chemotherapies and immunotherapies to reach CNS

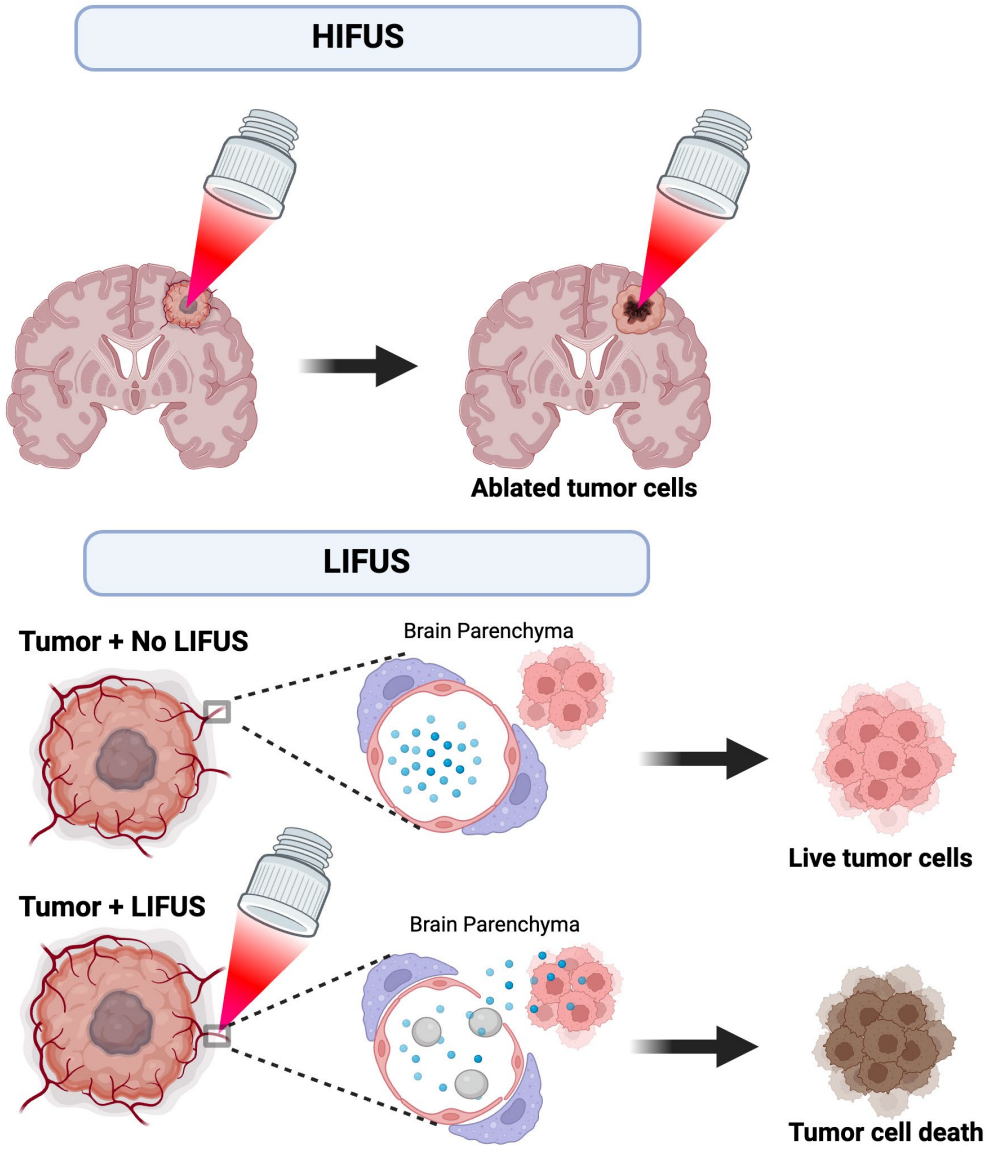

FIGURE 1
Proposed mechanism and application of HIFUS and LIFUS. HIFUS utilizes non-invasive, high-energy focused ultrasound waves to thermally ablate tumors. Alternatively, LIFUS utilizes lower ultrasound wave energy and microbubbles (grey) to disrupt the blood–brain barrier (BBB) and transiently allow chemotherapy/immunotherapy (blue) to permeate into the brain parenchyma. Ultimately, these treatments reach the tumor cell targets and promote cell death.

tumor targets (25). Traditionally, hyperosmotic agents such as mannitol have increased BBTB permeability to therapeutic agents when managing glioma and other CNS tumors (26, 27). Though mannitol has provided some success, it has many drawbacks that include limited BBTB opening (15 min), non-selective BBTB opening that can also affect healthy BBB, limited permeability to larger molecules, and systemic effects such as electrolyte abnormalities, injury to kidneys, and worsening of heart failure (28). Numerous strategies, including the use of prodrug formulations, chemical barrier disruption, intraarterial injection, surgical circumvention, thermotherapy, etc., have all been investigated as ways to circumvent the BBB and BBTB but have had limited success (25).

FUS is a safe thermotherapy modality shown to ablate CNS tumors directly or enhance drug delivery across BBB/BBTB for tumor treatment. Other forms of thermotherapies include radiofrequency microwaves, laser-interstitial thermotherapy (LITT), and magnetic disruption (25, 29). These modalities work via induction of intracranial hyperthermia, which causes potentiation of radiotherapy and chemotherapy. Additionally, the resulting hyperthermia demonstrates preferential glioma cell cytotoxicity and increases BBB permeability and tumor cell death through heat-shock protein-mediated cytotoxicity (25, 29, 30). FUS holds the most promise of the various thermotherapy modalities due to its noninvasive nature, efficacy, and ease of performing. Experiments in rat models have demonstrated a higher (38.6%) CSF-to-plasma ratio for temozolomide transferred with focused ultrasound relative to 22% observed in control modalities (25, 31). Like other modalities in this treatment class, FUS thermos-mechanically disrupts the BBB; however, a combination of LIFUS with intravenous injection of albumin-coated octafluropropane

microbubbles has been shown to produce only a transient opening of the BBB, thereby significantly decreasing permanent tissue damage (25, 32, 33).

FUS–mediated BBB disruption has been used successfully to deliver numerous agents in animal models including doxorubicin (34, 35), trastuzumab (36), temozolomide (31), interleukin-12 (37), anti-programmed cell death-ligand-1 antibody (38), poly (ethylene glycol) - poly (lactic acid) nanoparticles (39), adeno-associated virus (40), and AP-1 lipoplatin (41). Recent studies have quantified 2000kD as the upper particle size limit for successful FUS-mediated BBB transfer – a size limit encompassing numerous therapeutic agents (25, 42, 43). Beyond the mechanical opening of the BBB/BBTB to allow for enhanced drug delivery, FUS has also been shown to decrease the expression of efflux transporters, reduce junctional proteins, and modify the dispersion of nanoparticles in the extracellular space (44–47). There is growing translational research evidence for successful BBB disruption using FUS, as discussed above, which has led to numerous clinical trials further to assess the role of FUS in glioma treatment, as detailed in Table 1.

In conjunction with BBB/BBTB opening, FUS use in managing CNS tumors has allowed for better sampling of tumor-specific biomarkers secreted into systemic circulation during FUS-associated BBB/BBTB opening. This process is referred to as liquid biopsy (48). Analyses of these biomarkers may enable early detection, predict recurrence, and assess treatment response. Alternatively, FUS can be used to achieve CNS tumor ablation via hyperthermia. McDannold et al. and Coluccia et al. and others have demonstrated the successful utility of HIFUS ablation in managing CNS tumors (49, 50). Yet, the definitive role of HIFUS ablation in the management of glioma remains to be clinically validated, though preclinical studies have demonstrated success in glioma treatment (14). Interestingly, preclinical data also suggest that the hyperthermia from HIFUS ablation may sensitize glioma cells to radiation therapy (51).

4 Adjuncts to FUS in the treatment of glioma

4.1 Sonodynamic therapy (SDT)

Sonodynamic therapy (SDT), a treatment modality similar in mechanism to photodynamic therapy (PDT), is a promising alternative treatment being investigated for glioma treatment. In PDT, a light-activated photosensitizer generates reactive oxygen species (ROS), facilitating cytotoxic effects on neoplastic cells. While effective, PDT is limited to superficial lesions because of the limited penetration of laser light into brain tissue (52, 53). This challenge is overcome in SDT, which employs a low-intensity ultrasound, offering superior tissue penetrance (54). SDT combines focused ultrasound with sonosensitizers, which sensitize cells to sound-induced destruction, minimizing adverse events and maximizing target responses (48, 55). Examples of sonosensitizers include 5-ALA, ATX-70, and Hypocrellin (56–58). The efficacy of SDT has been shown in studies by Sheehan et al., which demonstrated SDT's efficacy in rat C6 and human U87 glioma cells by showing FUS and 5-ALA-induced cell death through ROS generation (59). These findings were further validated in other experiments demonstrating that focused ultrasound combined with systemic 5-ALA effectively treated gliomas in rodent models (60–63).

Overcoming the blood–brain barrier (BBB) remains a critical challenge in SDT, as most sonosensitizers cannot cross it. As a result, other studies have investigated the possibility of combining LIFUS with BBB modifiers, such as microbubbles, to increase the permeability of the BBB and improve SDT efficacy (64–66). Sonosensitizers used in Sonodynamic Therapy (SDT) comprise benign molecules that induce cytotoxic effects under an acoustic field (56). Several of these molecules are similar to those used in photodynamic therapy and are usually porphyrin-based or related compounds such as protoporphyrin IX and hematoporphyrin, among others. Emerging evidence suggests these molecules generate ROS upon exposure to ultrasound waves (67). *In vitro* investigations by Shen et al. demonstrated the efficacy of sinoporphyrin sodium, derived from photofrin II, as a sonosensitizer, showcasing significant antitumor effects on human glioblastoma cell lines (67) Particularly noteworthy was this sonosensitizer's ability to infiltrate cancer cells and accumulate within mitochondria, thus instigating cytotoxicity via ROS production (67).

It is crucial to highlight that despite their preferential uptake by tumors, these agents exhibit considerable hydrophobicity, which results in ubiquitous distribution (68). However, as postulated by Raspagliesi et al., for cytotoxic effects to manifest in any tissue, three concurrent events must occur: (1) ultrasound administration, (2) sonosensitizer administration, and (3) the presence of a lesion where the latter attains significant concentration. Consequently, our current acceptance of SDT's non-invasiveness towards normal brain tissue resulted from this concept, which suggests that the accumulation of sonosensitizer in healthy tissue without the other two concurrent events will render it inconsequential in the healthy tissue (69). Thus, the ideal sonosensitizer selection is crucial in SDT and should demonstrate high tumor cell affinity, prolonged neoplasm retention, and minimal impact on healthy brain parenchyma (70–72).

4.2 Histotripsy

Histotripsy is a non-thermal HIFUS technique that presents a promising avenue for mechanical ablation of brain tissue and tumors with precise localization, devoid of thermal effects (73). This technique employs short-duration, high-amplitude ultrasound pulses to induce acoustic cavitation within tissues, which results in inward erosion at tissue-liquid interfaces and liquefaction in dense tissue (74–76). The liquefaction process forms acellular debris, which is then gradually resorbed by the body over several months (77). Histotripsy differs from earlier thermal techniques like shockwave therapy and HIFUS because it produces more precise ablations with well-defined margins, minimizing damage to surrounding healthy tissue (14, 78).

The short duration of histotripsy ultrasound pulses restricts cavitation to the focal zone of interest, preventing extraneous tissue damage and allowing for precisely targeted ablations (79–81). This is achieved by forming dense cavitation "bubble clouds" at the focal point, which generates mechanical shearing forces and stress in the target tissue, causing cell disintegration and extracellular matrix fragmentation within those target tissues (74, 82). Cavitation migration is notably hindered outside the focal region due to insufficient amplitude to sustain dense bubble cloud formation in the off-target sites (83). The ability of histotripsy to produce clear margin lesions with minimal complications in cortical tissue has been

TABLE 1 Summary of findings for completed and ongoing clinical trials utilizing fus to treat glioma/glioblastoma.

Trial name	Phase	Status	Summary	Treatment	Trial identifier	Publications
Non-Invasive Focused Ultrasound (FUS) with Oral Panobinostat in Children with Progressive Diffuse Midline Glioma (DMG)	1	Ongoing	Children with progressive diffuse midline gliomas (DMG) treated with oral Panobinostat using FUS with microbubbles and neuro-navigator-controlled sonication.	FUS + Chemotherapy	NCT04804709	N/A
FUS Etoposide for DMG - A Feasibility Study	1	Ongoing	Children with progressive DMG treated with oral etoposide using focused ultrasound with microbubbles.	FUS + Chemotherapy	NCT05762419	N/A
A Phase 2 Study of Sonodynamic Therapy (SDT) Using SONALA-001 and ExAblate 4,000 Type 2.0 in Patients with Diffuse Intrinsic Pontine Glioma (DIPG)	2	Ongoing	Sonodynamic therapy (SDT) using SONALA-001 and ExAblate Type 2.0 device and to determine the maximum tolerated dose (MTD) or recommended phase 2 dose (RP2D) of MR-Guided Focused Ultrasound (MRgFUS) energy in combination with SONALA-001.	FUS	NCT05123534	N/A
Study of SDT Therapy in Participants with Recurrent High-Grade Glioma (HGG)	0	Ongoing	Ascending energy doses of SDT utilizing the MRgFUS combined with IV aminolevulinic acid (ALA) to assess safety and efficacy in participants with recurrent HGG. Participants who are scheduled for resection will be administered IV ALA approximately six to seven (6–7) hours prior to receiving SDT.	FUS	NCT04559685	N/A
Assessment of Safety and Feasibility of ExAblate BBB Disruption in Gliobastoma(GBM) Patients	N/A	Completed	Evaluate the safety of the ExAblate Model 4,000 Type 2.0 used as a tool to disrupt the BBB in patients with high grade glioma undergoing standard of care therapy. Findings demonstrated that MRgFUS can safely open BBB in GBM patients.	FUS	NCT04998864	N/A
Assessment of Safety and Feasibility of ExAblate Blood–Brain Barrier (BBB) Disruption	N/A	Ongoing	Evaluate the safety of the ExAblate Model 4,000 Type 2 used as a tool to disrupt the BBB in patients with high grade glioma undergoing standard of care therapy.	FUS	NCT03551249	N/A
ExAblate Treatment of Brain Tumors	N/A	Completed; results not published	A Study to Evaluate the Safety and Feasibility of Transcranial MRI-Guided Focused Ultrasound Surgery in the Treatment of Brain Tumors	FUS	NCT01473485	N/A
Assessment of Safety and Feasibility of ExAblate BBB Disruption for Treatment of Glioma	N/A	Completed	First proof of concept study demonstrating that MRgFUS enriches systemic circulating brain-derived biomarkers via a process known as liquid biopsy.	FUS	NCT03616860	PMID: 33693781
BBB Disruption Using ExAblate Focused Ultrasound with Doxorubicin for Treatment of Pediatric diffuse intrinsic pontine glioma (DIPG)	Phase 1	Ongoing	Evaluate the safety and efficacy of targeted BBB disruption with ExAblate Model 4,000 Type2.0/2.1 in combination with Doxorubicin therapy for the treatment of DIPG in pediatric patients	FUS + Chemotherapy	NCT05630209	N/A
BBB Disruption for Liquid Biopsy in Subjects with GBM	N/A	Ongoing	Evaluate the safety and efficacy of targeted BBB disruption with ExAblate Model 4,000 Type 2.0/2.1 for liquid biopsy in subjects with suspected GBM	FUS	NCT05383872	N/A
Efficacy and Safety of NaviFUS System add-on Bevacizumab in Recurrent GBM Patients	N/A	Completed	To investigate the efficacy and safety of FUS add-on bevacizumab in recurrent GBM patients. Findings demonstrated that MRgFUS can safely open BBB and enhances bevacizumab delivery which significantly decreased tumor growth and increased median survival.	FUS + Chemotherapy	NCT04446416	PMID: 27192459
SDT in Patients with Recurrent GBM	Phase 1	Ongoing	Evaluate the safety and feasibility of combining an investigational drug called 5-ALA with neuronavigation-guided low-intensity focused ultrasound (LIFUS) for patients who have recurrent GBM. SDT will take place prior to surgery for recurrent GBM.	FUS	NCT06039709	N/A
Safety of BBB Disruption Using NaviFUS System in Recurrent GBM Patients	N/A	Completed; results not published	Evaluate the safety and find the tolerated ultrasound dose of transient opening of the BBB by using the NaviFUS System in recurrent GBM patients.	FUS	NCT03626896	N/A

ALA, Aminolevulinic acid; BBB, Blood–Brain Barrier; DIPG, Pediatric diffuse intrinsic pontine glioma; DMG, Diffuse Midline Glioma; FUS, Focused Ultrasound; GBM, Gliobastoma; HGG, High-Grade Glioma; LIFUS, low-intensity focused ultrasound; MRgFUS, MR-Guided Focused Ultrasound; SDT, Sonodynamic Therapy; TMZ, Temozolomide.

10.3389/fneur.2024.1387986

demonstrated in detail in porcine models, suggesting its potential in brain tumor treatment (73).

Recent studies have highlighted that the acellular debris resulting from histotripsy-induced liquefaction contains tumor antigens, damage-associated molecular patterns, and heat shock proteins, potentially stimulating a tumor-specific cytotoxic T-cell response (84). Additionally, histotripsy may elicit inflammatory responses involving macrophages and B-cell lymphocytes, as evidenced in melanoma and hepatocellular carcinoma preclinical studies (74). Qu et al. showed that histotripsy in mice with melanoma or hepatocellular carcinoma not only stimulated local tumor infiltration by immune cells but also stimulated inflammation at other tumor sites not targeted by histotripsy (14, 85). While these results are promising, it is important to highlight that this study was not conducted in gliomas. Thus, whether a similar inflammatory response will be replicated in glioma remains to be determined. Further work is needed to delineate the role of histotripsy in glioma treatment.

5 Challenges associated with FUS

The evolving landscape of FUS holds promise for improving therapeutic outcomes through thermal ablation and novel treatment modalities, including focal BBB disruption for drug delivery enhancement. Yet, substantial challenges persist in achieving consistent and clinically meaningful outcomes. Historically, inadequate visual monitoring, thermometric control, and precise focal point determination were predominant challenges faced with FUS utility in managing CNS conditions. Advances in the utility of stereotactic skull frames, MRI-guided imaging, and thermometric monitoring have helped address these challenges (49). Though MRI-guided FUS is advantageous over Ultrasound-guided FUS because it provides a superior resolution, it should be noted that thermal ablation may interfere with MRI resolution. MRI-based acoustic radiation is a novel tool that may be useful in limiting the effects of thermal ablation (86, 87).

Further technical difficulties have been reported with FUS use, such as skull and scalp heterogeneities. These may attenuate US propagation to the target location, impeding the desired temperature for an ablative effect. Utilization of lower frequencies aids in addressing this issue; however, lowering the frequency may also induce tissue damage by cavitation. Furthermore, the translation of findings from animal studies to human clinical trials must be carefully analyzed, mainly since the human skull is thicker and harder than that of rodents. Hence, US wave attenuation is expected to be more significant in humans (87).

While FUS is a promising tool, a recent study investigating the risk of bias in animal studies and non-randomized clinical brain tumor trials showed a high risk of bias, methodological inconsistencies, and significant ethical limitations in animal and human brain tumor studies (88). Given the increasing popularity of FUS use in treating several CNS clinical conditions, it is paramount that a global initiative is established to standardize research methodologies and uphold stringent ethical norms.

6 Conclusion

Glioma/glioblastoma is a life-altering diagnosis for the patient. Significant advancements in developing new therapeutics to treat glioma and glioblastoma have flourished. However, these advancements have been halted by the inability of a vast number of these therapies to cross the BBB/BBTB. FUS serves as an emerging non-invasive treatment modality that could address enhanced drug delivery across BBTB and/or be used in conjunction with radiosurgery or surgical resection to improve outcomes in patients diagnosed with glioma/glioblastoma. While several ongoing clinical trials are exploring the role of FUS in brain tumors (i.e., enhanced drug delivery and tumor ablation), data on FUS use in treating spinal cord tumors is lacking. Further investigation is required to address microbubbles' type and administration route and the FUS's short- and long-term impact on the host immune response profile.

Author contributions

DN: Writing – original draft, Writing – review & editing. DO-Y: Writing – original draft, Writing – review & editing. FF: Writing – original draft, Writing – review & editing. WB: Writing – original draft, Writing – review & editing. MM: Writing – original draft, Writing – review & editing.

Funding

The author(s) declare that no financial support was received for the research, authorship, and/or publication of this article.

Conflict of interest

The authors declare that the research was conducted in the absence of any commercial or financial relationships that could be construed as a potential conflict of interest.

Publisher's note

References

1. Ostrom QT, Gittleman H, Liao P, Vecchione-Koval T, Wolinsky Y, Kruchko C, et al. CBTRUS statistical report: primary brain and other central nervous system tumors diagnosed in the United States in 2010-2014. *Neuro-Oncology*. (2017) 19:v1–v88. doi: 10.1093/neuonc/nox158

2. Dubrow R, Darefsky AS. Demographic variation in incidence of adult glioma by subtype, United States, 1992-2007. *BMC Cancer*. (2011) 11:325. doi: 10.1186/1471-2407-11-325

3. Omuro A, DeAngelis LM. Glioblastoma and other malignant gliomas: a clinical review. *JAMA*. (2013) 310:1842–50. doi: 10.1001/jama.2013.280319

4. Kanderi T, Gupta V. Glioblastoma Multiforme In *StatPearls*. Stefaan De Smedt editor. (Netherlands: StatPearls Publishing) (2024)

5. Stummer W, Reulen HJ, Meinel T, Pichlmeier U, Schumacher W, Tonn JC, et al. Extent of resection and survival in glioblastoma multiforme: identification of and adjustment for bias. *Neurosurgery*. (2008) 62:564–76. doi: 10.1227/01.neu.0000317304.31579.17

6. Aiudi D, Iacoangeli A, Dobran M, Polonara G, Chiapponi M, Mattioli A, et al. The prognostic role of volumetric MRI evaluation in the surgical treatment of glioblastoma. *J Clin Med*. (2024) 13:849. doi: 10.3390/jcm13030849

7. Elias WJ, Huss D, Voss T, Loomba J, Khaled M, Zadicario E, et al. A pilot study of focused ultrasound thalamotomy for essential tremor. *N Engl J Med*. (2013) 369:640–8. doi: 10.1056/NEJMoa1300962

8. Baek H, Lockwood D, Mason EJ, Obusez E, Poturalski M, Rammo R, et al. Clinical intervention using focused ultrasound (FUS) stimulation of the brain in diverse neurological disorders. *Front Neurol*. (2022) 13:880814. doi: 10.3389/fneur.2022.880814

9. Darmani G, Bergmann TO, Butts Pauly K, Caskey CF, de Lecea L, Fomenko A, et al. Non-invasive transcranial ultrasound stimulation for neuromodulation. *Clin Neurophysiol*. (2022) 135:51–73. doi: 10.1016/j.clinph.2021.12.010

10. Siedek F, Yeo SY, Heijman E, Grinstein O, Bratke G, Heneweer C, et al. Magnetic resonance-guided high-intensity focused ultrasound (MR-HIFU): technical background and overview of current clinical applications (part 1). *Rofo*. (2019) 191:522–30. doi: 10.1055/a-0817-5645

11. Johns LD. Nonthermal effects of therapeutic ultrasound: the frequency resonance hypothesis. *J Athl Train*. (2002) 37:293–9.

12. Darrow DP. Focused ultrasound for neuromodulation. *Neurotherapeutics*. (2019) 16:88–99. doi: 10.1007/s13311-018-00691-3

13. Canney MS, Bailey MR, Crum LA, Khokhlova VA, Sapozhnikov OA. Acoustic characterization of high intensity focused ultrasound fields: a combined measurement and modeling approach. *J Acoust Soc Am*. (2008) 124:2406–20. doi: 10.1121/1.2967836

14. Hersh AM, Bhimreddy M, Weber-Levine C, Jiang K, Alomari S, Theodore N, et al. Applications of focused ultrasound for the treatment of glioblastoma: a new frontier. *Cancers (Basel)*. (2022) 14:4920. doi: 10.3390/cancers14194920

15. Lescrauwaet E, Vonck K, Sprengers M, Raedt R, Klooster D, Carrette E, et al. Recent advances in the use of focused ultrasound as a treatment for epilepsy. *Front Neurosci*. (2022) 16:886584. doi: 10.3389/fnins.2022.886584

16. Moosa S, Martínez-Fernández R, Elias WJ, Del Alamo M, Eisenberg HM, Fishman PS. The role of high-intensity focused ultrasound as a symptomatic treatment for Parkinson's disease. *Mov Disord*. (2019) 34:1243–51. doi: 10.1002/mds.27779

17. Jolesz FA. MRI-guided focused ultrasound surgery. *Annu Rev Med*. (2009) 60:417–30. doi: 10.1146/annurev.med.60.041707.170303

18. Zhong YX, Liao JC, Liu X, Tian H, Deng LR, Long L. Low intensity focused ultrasound: a new prospect for the treatment of Parkinson's disease. *Ann Med*. (2023) 55:2251145. doi: 10.1080/07853890.2023.2251145

19. Rezai AR, Ranjan M, Haut MW, Carpenter J, D'Haese PF, Mehta RI, et al. Focused ultrasound-mediated blood-brain barrier opening in Alzheimer's disease: long-term safety, imaging, and cognitive outcomes. *J Neurosurg*. (2023) 139:275–83. doi: 10.3171/2022.9.Jns221565

20. Nwafor DC, Brichacek AL, Mohammad AS, Griffith J, Lucke-Wold BP, Benkovic SA, et al. Targeting the blood-brain barrier to prevent Sepsis-associated cognitive impairment. *J Cent Nerv Syst Dis*. (2019) 11:1179573519840652. doi: 10.1177/1179573519840652

21. Wu D, Chen Q, Chen X, Han F, Chen Z, Wang Y. The blood-brain barrier: structure, regulation, and drug delivery. *Signal Transduct Target Ther*. (2023) 8:217. doi: 10.1038/s41392-023-01481-w

22. Abbott NJ, Patabendige AA, Dolman DE, Yusof SR, Begley DJ. Structure and function of the blood-brain barrier. *Neurobiol Dis*. (2010) 37:13–25. doi: 10.1016/j.nbd.2009.07.030

23. van Tellingen O, Yetkin-Arik B, de Gooijer MC, Wesseling P, Wurdinger T, de Vries HE. Overcoming the blood-brain tumor barrier for effective glioblastoma treatment. *Drug Resist Updat*. (2015) 19:1–12. doi: 10.1016/j.drup.2015.02.002

24. Wu T, Dai Y. Tumor microenvironment and therapeutic response. *Cancer Lett*. (2017) 387:61–8. doi: 10.1016/j.canlet.2016.01.043

25. Hendricks BK, Cohen-Gadol AA, Miller JC. Novel delivery methods bypassing the blood-brain and blood-tumor barriers. *Neurosurg Focus*. (2015) 38:E10. doi: 10.3171/2015.1.Focus14767

26. Iwadate Y, Namba H, Saegusa T, Sueyoshi K. Intra-arterial mannitol infusion in the chemotherapy for malignant brain tumors. *J Neuro-Oncol*. (1993) 15:185–93. doi: 10.1007/bf01053940

27. Siegal T, Rubinstein R, Bokstein F, Schwartz A, Lossos A, Shalom E, et al. In vivo assessment of the window of barrier opening after osmotic blood-brain barrier disruption in humans. *J Neurosurg*. (2000) 92:599–605. doi: 10.3171/jns.2000.92.4.0599

28. Doolittle ND, Muldoon LL, Culp AY, Neuwelt EA. Delivery of chemotherapeutics across the blood-brain barrier: challenges and advances. *Adv Pharmacol*. (2014) 71:203–43. doi: 10.1016/bs.apha.2014.06.002

29. Lee Titsworth W, Murad GJ, Hoh BL, Rahman M. Fighting fire with fire: the revival of thermotherapy for gliomas. *Anticancer Res*. (2014) 34:565–74.

30. Watanabe M, Tanaka R, Hondo H, Kuroki M. Effects of antineoplastic agents and hyperthermia on cytotoxicity toward chronically hypoxic glioma cells. *Int J Hyperth*. (1992) 8:131–8. doi: 10.3109/02656739209052885

31. Wei KC, Chu PC, Wang HY, Huang CY, Chen PY, Tsai HC, et al. Focused ultrasound-induced blood-brain barrier opening to enhance temozolomide delivery for glioblastoma treatment: a preclinical study. *PLoS One*. (2013) 8:e58995. doi: 10.1371/journal.pone.0058995

32. Hynynen K, McDannold N, Vykhodtseva N, Jolesz FA. Noninvasive MR imaging-guided focal opening of the blood-brain barrier in rabbits. *Radiology*. (2001) 220:640–6. doi: 10.1148/radiol.2202001804

33. Konofagou EE. Optimization of the ultrasound-induced blood-brain barrier opening. *Theranostics*. (2012) 2:1223–37. doi: 10.7150/thno.5576

34. Kovacs Z, Werner B, Rassi A, Sass JO, Martin-Fiori E, Bernasconi M. Prolonged survival upon ultrasound-enhanced doxorubicin delivery in two syngenic glioblastoma mouse models. *J Control Release*. (2014) 187:74–82. doi: 10.1016/j.jconrel.2014.05.033

35. Treat LH, McDannold N, Vykhodtseva N, Zhang Y, Tam K, Hynynen K. Targeted delivery of doxorubicin to the rat brain at therapeutic levels using MRI-guided focused ultrasound. *Int J Cancer*. (2007) 121:901–7. doi: 10.1002/ijc.22732

36. Kinoshita M, McDannold N, Jolesz FA, Hynynen K. Noninvasive localized delivery of Herceptin to the mouse brain by MRI-guided focused ultrasound-induced blood-brain barrier disruption. *Proc Natl Acad Sci USA*. (2006) 103:11719–23. doi: 10.1073/pnas.0604318103

37. Chen PY, Hsieh HY, Huang CY, Lin CY, Wei KC, Liu HL. Focused ultrasound-induced blood-brain barrier opening to enhance interleukin-12 delivery for brain tumor immunotherapy: a preclinical feasibility study. *J Transl Med*. (2015) 13:93. doi: 10.1186/s12967-015-0451-y

38. Ye D, Yuan J, Yue Y, Rubin JB, Chen H. Focused ultrasound-enhanced delivery of Intranasally administered anti-programmed cell death-ligand 1 antibody to an intracranial murine glioma model. *Pharmaceutics*. (2021) 13:190. doi: 10.3390/pharmaceutics13020190

39. Yao L, Song Q, Bai W, Zhang J, Miao D, Jiang M, et al. Facilitated brain delivery of poly (ethylene glycol)-poly (lactic acid) nanoparticles by microbubble-enhanced unfocused ultrasound. *Biomaterials*. (2014) 35:3384–95. doi: 10.1016/j.biomaterials.2013.12.043

40. Thévenot E, Jordão JF, O'Reilly MA, Markham K, Weng YQ, Foust KD, et al. Targeted delivery of self-complementary adeno-associated virus serotype 9 to the brain, using magnetic resonance imaging-guided focused ultrasound. *Hum Gene Ther*. (2012) 23:1144–55. doi: 10.1089/hum.2012.013

41. Yang FY, Horng SC. Chemotherapy of glioblastoma by targeted liposomal platinum compounds with focused ultrasound. *Annu Int Conf IEEE Eng Med Biol Soc*. (2013) 2013:6289–92. doi: 10.1109/embc.2013.6610991

42. Chen H, Konofagou EE. The size of blood-brain barrier opening induced by focused ultrasound is dictated by the acoustic pressure. *J Cereb Blood Flow Metab*. (2014) 34:1197–204. doi: 10.1038/jcbfm.2014.71

43. Choi JJ, Wang S, Tung YS, Morrison B 3rd, Konofagou EE. Molecules of various pharmacologically-relevant sizes can cross the ultrasound-induced blood-brain barrier opening in vivo. *Ultrasound Med Biol*. (2010) 36:58–67. doi: 10.1016/j.ultrasmedbio.2009.08.006

44. Bunevicius A, McDannold NJ, Golby AJ. Focused ultrasound strategies for brain tumor therapy. *Oper Neurosurg (Hagerstown)*. (2020) 19:9–18. doi: 10.1093/ons/opz374

45. Hersh DS, Anastasiadis P, Mohammadabadi A, Nguyen BA, Guo S, Winkles JA, et al. MR-guided transcranial focused ultrasound safely enhances interstitial dispersion of large polymeric nanoparticles in the living brain. *PLoS One*. (2018) 13:e0192240. doi: 10.1371/journal.pone.0192240

46. Hersh DS, Nguyen BA, Dancy JG, Adapa AR, Winkles JA, Woodworth GF, et al. Pulsed ultrasound expands the extracellular and perivascular spaces of the brain. *Brain Res*. (2016) 1646:543–50. doi: 10.1016/j.brainres.2016.06.040

47. Jalali S, Huang Y, Dumont DJ, Hynynen K. Focused ultrasound-mediated bbb disruption is associated with an increase in activation of AKT: experimental study in rats. *BMC Neurol*. (2010) 10:114. doi: 10.1186/1471-2377-10-114

48. Roberts JW, Powlovich L, Sheybani N, LeBlang S. Focused ultrasound for the treatment of glioblastoma. *J Neuro-Oncol*. (2022) 157:237–47. doi: 10.1007/s11060-022-03974-0

49. Coluccia D, Fandino J, Schwyzer L, O'Gorman R, Remonda L, Anon J, et al. First noninvasive thermal ablation of a brain tumor with MR-guided focused ultrasound. *J Ther Ultrasound*. (2014) 2:17. doi: 10.1186/2050-5736-2-17

50. MacDonell J, Patel N, Rubino S, Ghoshal G, Fischer G, Burdette EC, et al. Magnetic resonance-guided interstitial high-intensity focused ultrasound for brain tumor ablation. *Neurosurg Focus*. (2018) 44:E11. doi: 10.3171/2017.11.Focus17613

51. Man J, Shoemake JD, Ma T, Rizzo AE, Godley AR, Wu Q, et al. Hyperthermia sensitizes glioma stem-like cells to radiation by inhibiting AKT signaling. *Cancer Res*. (2015) 75:1760–9. doi: 10.1158/0008-5472.Can-14-3621

52. Gong Z, Dai Z. Design and challenges of Sonodynamic therapy system for Cancer Theranostics: from equipment to sensitizers. *Adv Sci (Weinh)*. (2021) 8:2002178. doi: 10.1002/advs.202002178

53. Yoshida M, Kobayashi H, Terasaka S, Endo S, Yamaguchi S, Motegi H, et al. Sonodynamic therapy for malignant glioma using 220-kHz transcranial magnetic resonance imaging-guided focused ultrasound and 5-Aminolevulinic acid. *Ultrasound Med Biol*. (2019) 45:526–38. doi: 10.1016/j.ultrasmedbio.2018.10.016

54. McHale AP, Callan JF, Nomikou N, Fowley C, Callan B. Sonodynamic therapy: concept, mechanism and application to Cancer treatment. *Adv Exp Med Biol*. (2016) 880:429–50. doi: 10.1007/978-3-319-22536-4_22

55. Pan X, Wang H, Wang S, Sun X, Wang L, Wang W, et al. Sonodynamic therapy (SDT): a novel strategy for cancer nanotheranostics. *Sci China Life Sci*. (2018) 61:415–26. doi: 10.1007/s11427-017-9262-x

56. Bonosi L, Marino S, Benigno UE, Musso S, Buscemi F, Giardina K, et al. Sonodynamic therapy and magnetic resonance-guided focused ultrasound: new therapeutic strategy in glioblastoma. *J Neuro-Oncol*. (2023) 163:219–38. doi: 10.1007/s11060-023-04333-3

57. Wu SK, Santos MA, Marcus SL, Hynynen K. MR-guided focused ultrasound facilitates Sonodynamic therapy with 5-Aminolevulinic acid in a rat glioma model. *Sci Rep*. (2019) 9:10465. doi: 10.1038/s41598-019-46832-2

58. Zhang C, Wu J, Liu W, Zheng X, Zhang W, Lee CS, et al. A novel hypocrellin-based assembly for sonodynamic therapy against glioblastoma. *J Mater Chem B*. (2021) 10:57–63. doi: 10.1039/d1tb01886h

59. Sheehan K, Sheehan D, Sulaiman M, Padilla F, Moore D, Sheehan J, et al. Investigation of the tumoricidal effects of sonodynamic therapy in malignant glioblastoma brain tumors. *J Neuro-Oncol*. (2020) 148:9–16. doi: 10.1007/s11060-020-03504-w

60. Anttinen H, Terho EO, Myllyla R, Savolainen ER. Two serum markers of collagen biosynthesis as possible indicators of irreversible pulmonary impairment in farmer's lung. *Am Rev Respir Dis*. (1986) 133:88–93. doi: 10.1164/arrd.1986.133.1.88

61. Jeong EJ, Seo SJ, Ahn YJ, Choi KH, Kim KH, Kim JK. Sonodynamically induced antitumor effects of 5-aminolevulinic acid and fractionated ultrasound irradiation in an orthotopic rat glioma model. *Ultrasound Med Biol*. (2012) 38:2143–50. doi: 10.1016/j.ultrasmedbio.2012.07.026

62. Ohmura T, Fukushima T, Shibaguchi H, Yoshizawa S, Inoue T, Kuroki M, et al. Sonodynamic therapy with 5-aminolevulinic acid and focused ultrasound for deep-seated intracranial glioma in rat. *Anticancer Res*. (2011) 31:2527–33.

63. Song D, Yue W, Li Z, Li J, Zhao J, Zhang N. Study of the mechanism of sonodynamic therapy in a rat glioma model. *Onco Targets Ther*. (2014) 7:1801–10. doi: 10.2147/ott.S52426

64. Arvanitis CD, Vykhodtseva N, Jolesz F, Livingstone M, McDannold N. Cavitation-enhanced nonthermal ablation in deep brain targets: feasibility in a large animal model. *J Neurosurg*. (2016) 124:1450–9. doi: 10.3171/2015.4.Jns142862

65. Jones RM, McMahon D, Hynynen K. Ultrafast three-dimensional microbubble imaging in vivo predicts tissue damage volume distributions during nonthermal brain ablation. *Theranostics*. (2020) 10:7211–30. doi: 10.7150/thno.47281

66. McDannold N, Clement GT, Black P, Jolesz F, Hynynen K. Transcranial magnetic resonance imaging- guided focused ultrasound surgery of brain tumors: initial findings in 3 patients. *Neurosurgery*. (2010) 66:323–32; discussion 332. doi: 10.1227/01.Neu.0000360379.95800.2f

67. Shen Y, Chen Y, Huang Y, Zeng X, Huang L, Diao X, et al. An in vitro study on the antitumor effect of sonodynamic therapy using sinoporphyrin sodium on human glioblastoma cells. *Ultrasonics*. (2021) 110:106272. doi: 10.1016/j.ultras.2020.106272

68. Liu Q, Wang X, Wang P, Xiao L, Hao Q. Comparison between sonodynamic effect with protoporphyrin IX and hematoporphyrin on sarcoma 180. *Cancer Chemother Pharmacol*. (2007) 60:671–80. doi: 10.1007/s00280-006-0413-4

69. Raspagliesi L, D'Ammando A, Gionso M, Sheybani ND, Lopes MB, Moore D, et al. Intracranial Sonodynamic therapy with 5-Aminolevulinic acid and sodium fluorescein: safety study in a porcine model. *Front Oncol*. (2021) 11:679989. doi: 10.3389/fonc.2021.679989

70. Nomikou N, Li YS, McHale AP. Ultrasound-enhanced drug dispersion through solid tumours and its possible role in aiding ultrasound-targeted cancer chemotherapy. *Cancer Lett*. (2010) 288:94–8. doi: 10.1016/j.canlet.2009.06.028

71. Son S, Kim JH, Wang X, Zhang C, Yoon SA, Shin J, et al. Multifunctional sonosensitizers in sonodynamic cancer therapy. *Chem Soc Rev*. (2020) 49:3244–61. doi: 10.1039/c9cs00648f

72. Wang C, Tian Y, Wu B, Cheng W. Recent Progress toward imaging application of multifunction Sonosensitizers in Sonodynamic therapy. *Int J Nanomedicine*. (2022) 17:3511–29. doi: 10.2147/ijn.S370767

73. Sukovich JR, Cain CA, Pandey AS, Chaudhary N, Camelo-Piragua S, Allen SP, et al. In vivo histotripsy brain treatment. *J Neurosurg*. (2018) 131:1331–8. doi: 10.3171/2018.4.Jns172652

74. Khokhlova VA, Fowlkes JB, Roberts WW, Schade GR, Xu Z, Khokhlova TD, et al. Histotripsy methods in mechanical disintegration of tissue: towards clinical applications. *Int J Hyperth*. (2015) 31:145–62. doi: 10.3109/02656736.2015.1007538

75. Xu Z, Ludomirsky A, Eun LY, Hall TL, Tran BC, Fowlkes JB, et al. Controlled ultrasound tissue erosion. *IEEE Trans Ultrason Ferroelectr Freq Control*. (2004) 51:726–36. doi: 10.1109/tuffc.2004.1308731

76. Xu Z, Owens G, Gordon D, Cain C, Ludomirsky A. Noninvasive creation of an atrial septal defect by histotripsy in a canine model. *Circulation*. (2010) 121:742–9. doi: 10.1161/circulationaha.109.889071

77. Xu Z, Hall TL, Vlaisavljevich E, Lee FT Jr. Histotripsy: the first noninvasive, non-ionizing, non-thermal ablation technique based on ultrasound. *Int J Hyperth*. (2021) 38:561–75. doi: 10.1080/02656736.2021.1905189

78. Gambihler S, Delius M, Brendel W. Biological effects of shock waves: cell disruption, viability, and proliferation of L1210 cells exposed to shock waves in vitro. *Ultrasound Med Biol*. (1990) 16:587–94. doi: 10.1016/0301-5629(90)90024-7

79. Giorgio A, Tarantino L, de Stefano G, Coppola C, Ferraioli G. Complications after percutaneous saline-enhanced radiofrequency ablation of liver tumors: 3-year experience with 336 patients at a single center. *AJR Am J Roentgenol*. (2005) 184:207–11. doi: 10.2214/ajr.184.1.01840207

80. Vlaisavljevich E, Kim Y, Owens G, Roberts W, Cain C, Xu Z. Effects of tissue mechanical properties on susceptibility to histotripsy-induced tissue damage. *Phys Med Biol*. (2014) 59:253–70. doi: 10.1088/0031-9155/59/2/253

81. Vlaisavljevich E, Maxwell A, Warnez M, Johnsen E, Cain CA, Xu Z. Histotripsy-induced cavitation cloud initiation thresholds in tissues of different mechanical properties. *IEEE Trans Ultrason Ferroelectr Freq Control*. (2014) 61:341–52. doi: 10.1109/TUFFC.2014.6722618

82. Edsall C, Khan ZM, Mancia L, Hall S, Mustafa W, Johnsen E, et al. Bubble cloud behavior and ablation capacity for histotripsy generated from intrinsic or artificial cavitation nuclei. *Ultrasound Med Biol*. (2021) 47:620–39. doi: 10.1016/j.ultrasmedbio.2020.10.020

83. Parsons JE, Cain CA, Abrams GD, Fowlkes JB. Pulsed cavitational ultrasound therapy for controlled tissue homogenization. *Ultrasound Med Biol*. (2006) 32:115–29. doi: 10.1016/j.ultrasmedbio.2005.09.005

84. Roberts WW. Development and translation of histotripsy: current status and future directions. *Curr Opin Urol*. (2014) 24:104–10. doi: 10.1097/mou.0000000000000001

85. Qu S, Worlikar T, Felsted AE, Ganguly A, Beems MV, Hubbard R, et al. Non-thermal histotripsy tumor ablation promotes abscopal immune responses that enhance cancer immunotherapy. *J Immunother Cancer*. (2020) 8:e000200. doi: 10.1136/jitc-2019-000200

86. Ghanouni P, Pauly KB, Elias WJ, Henderson J, Sheehan J, Monteith S, et al. Transcranial MRI-guided focused ultrasound: a review of the technologic and neurologic applications. *AJR Am J Roentgenol*. (2015) 205:150–9. doi: 10.2214/AJR.14.13632

87. Perez-Neri I, Gonzalez-Aguilar A, Sandoval H, Pineda C, Rios C. Potential goals, challenges, and safety of focused ultrasound application for central nervous system disorders. *Curr Neuropharmacol*. (2022) 20:1807–10. doi: 10.2174/1570159X20666220201092908

88. Thavarajasingam SG, Kilgallon JL, Ramsay DSC, Aval LM, Tewarie IA, Kramer A, et al. Methodological and ethical challenges in the use of focused ultrasound for blood-brain barrier disruption in neuro-oncology. *Acta Neurochir*. (2023) 165:4259–77. doi: 10.1007/s00701-023-05782-5

frontiers | Frontiers in Oncology

TYPE Original Research
PUBLISHED 17 May 2024
DOI 10.3389/fonc.2024.1362990

OPEN ACCESS

EDITED BY
John Bianco,
Princess Maxima Center for Pediatric Oncology, Netherlands

REVIEWED BY
Haidy G. Nasief,
Medical College of Wisconsin, United States
Paola Feraco,
Santa Chiara Hospital, Italy

*CORRESPONDENCE
Ying Hu
yinghu@wchscu.cn

RECEIVED 29 December 2023
ACCEPTED 02 May 2024
PUBLISHED 17 May 2024

CITATION
Hu Y and Zhang K (2024) Noninvasive assessment of Ki-67 labeling index in glioma patients based on multi-parameters derived from advanced MR imaging.
Front. Oncol. 14:1362990.
doi: 10.3389/fonc.2024.1362990

Noninvasive assessment of Ki-67 labeling index in glioma patients based on multi-parameters derived from advanced MR imaging

Ying Hu[1,2]* and Kai Zhang[1]

[1]Department of Radiology, West China Hospital, Sichuan University, Chengdu, China, [2]West China Biomedical Big Data Center, West China Hospital, Sichuan University, Chengdu, China

Purpose: To investigate the predictive value of multi-parameters derived from advanced MR imaging for Ki-67 labeling index (LI) in glioma patients.

Materials and Methods: One hundred and nine patients with histologically confirmed gliomas were evaluated retrospectively. These patients underwent advanced MR imaging, including dynamic susceptibility-weighted contrast enhanced MR imaging (DSC), MR spectroscopy imaging (MRS), diffusion-weighted imaging (DWI) and diffusion-tensor imaging (DTI), before treatment. Twenty-one parameters were extracted, including the maximum, minimum and mean values of relative cerebral blood flow (rCBF), relative cerebral blood volume (rCBV), relative mean transit time (rMTT), relative apparent diffusion coefficient (rADC), relative fractional anisotropy (rFA) and relative mean diffusivity (rMD) respectively, and ration of choline (Cho)/creatine (Cr), Cho/N-acetylaspartate (NAA) and NAA/Cr. Stepwise multivariate regression was performed to build multivariate models to predict Ki-67 LI. Pearson correlation analysis was used to investigate the correlation between imaging parameters and the grade of glioma. One-way analysis of variance (ANOVA) was used to explore the differences of the imaging parameters among the gliomas of grade II, III, and IV.

Results: The multivariate regression showed that the model of five parameters, including $rCBV_{max}$ (RC=0.282), $rCBF_{max}$ (RC=0.151), $rADC_{min}$ (RC= -0.14), rFA_{max} (RC=0.325) and Cho/Cr ratio (RC=0.157) predicted the Ki-67 LI with a root mean square (RMS) error of 0. 0679 (R^2 = 0.8025).The regression check of this model showed that there were no multicollinearity problem (variance inflation factor: $rCBV_{max}$, 3.22; $rCBF_{max}$, 3.14; $rADC_{min}$, 1.96; rFA_{max}, 2.51; Cho/Cr ratio, 1.64), and the functional form of this model was appropriate (F test: p=0.682). The results of Pearson correlation analysis showed that the $rCBV_{max}$, $rCBF_{max}$, rFA_{max}, the ratio of Cho/Cr and Cho/NAA were positively correlated with Ki-67 LI and the grade of glioma, while the $rADC_{min}$ and rMD_{min} were negatively correlated with Ki-67 LI and the grade of glioma.

Conclusion: Combining multiple parameters derived from DSC, DTI, DWI and MRS can precisely predict the Ki-67 LI in glioma patients.

KEYWORDS

magnetic resonance imaging, diffusion tensor imaging, diffusion weighted imaging, perfusion imaging, magnetic resonance spectroscopy, glioma, Ki-67 labeling index

Introduction

Glioma is the most common neuroepithelial tumor of the cerebral nervous system (1). Ki-67 labeling index (LI) is a nuclear antigen expressed only by proliferating cells (2). Previous studies showed that Ki-67 LI was one of the vital biological behavior biomarkers in glioma and correlated with glioma grading and prognosis (3, 4).Therefore, accurate measurement of the Ki-67 LI is important for grading and synthesizing prognosis information in glioma.

Advanced MR imaging, such as dynamic susceptibility-weighted contrast enhanced imaging (DSC), diffusion-weighted imaging (DWI), diffusion tensor imaging (DTI) and magnetic resonance spectroscopic imaging (MRS), provide important information for evaluating tumors preoperatively. DSC magnetic resonance (MR) imaging is the most commonly used MR perfusion technique in clinical practice and is well established for evaluating relative cerebral blood volume (rCBV) and relative cerebral blood flow (rCBF) in brain tumors (5). Many studies have shown that the rCBV and the rCBF correlate with tumor grade and tumor vascularity (6, 7). Diffusion tensor imaging (DTI) can provide two quantitative parameters, namely mean diffusivity (MD) which is inversely correlated with tumor cellularity and grading in glioma (8) and fractional anisotropy (FA) (9). Recent studies demonstrated that the FA derived from DTI may correlate with tumor cellularity (10). Diffusion-weighted imaging (DWI) can noninvasively provide insight into the microscopic properties of tissues through evaluating Brownian movement of water, and the apparent diffusion coefficient (ADC) value can quantitatively reflect cellularity of the lesions (11, 12). MRS is a noninvasive tool which estimates the concentration of metabolites (13). Previous studies showed that choline (Cho)-containing compounds in tumors were considered to be markers for cell proliferation (14). Shimizu H and colleagues found a direct correlation between Ki-67 LI and Cho, Cho/Cr and Cho/NAA ratio (14).

To date, most of studies explored the correlation between individual parameters and Ki-67 LI. Few studies have combined multiple parameters to predict Ki-67 LI. Although there have been some efforts to combine advanced MR imaging in characterizing gliomas (15, 16). However, most of these studies focused on the grading of gliomas (17, 18) and few focused on cell proliferation or Ki-67 LI.

Therefore, the aim of this work was to investigate whether the multi-parameters derived from DSC, MRS, DWI and DTI technique can predict Ki-67 LI in glioma patients using stepwise multivariate regression.

Abbreviations: ADC, Apparent diffusion coefficient; AIC, Akaike information criterion; BIC, Bayesian information criterion; CBV, Cerebral blood volume; Cho, Choline; Cr, Creatine; DTI, Diffusion tensor imaging; DSC, Dynamic susceptibility-weighted contrast enhanced imaging; DWI, Diffusion-weighted imaging; FA, fractional anisotropy; MD, mean diffusivity; MRS, Magnetic resonance spectroscopy imaging; NAA, N-acetylaspartate; ROI, Region of interest; RMSE, Root mean square error;VOI, Volume of interest.

Materials and methods

Participants

The institutional review board approved this retrospective study and waived the informed consent requirement. We retrospectively reviewed our institution's database and identified 710 patients who underwent MR imaging for brain tumor evaluation from September 2018 to December 2023. Among these patients, 109 patients were finally enrolled for analysis according to the following inclusion criteria: a) patients were confirmed to have gliomas by pathologic analysis (excluded 357 subjects); b) The samples of pathologic analysis were from surgical resection (excluded 29 subjects); c) the reports of pathologic analysis included Ki-67 LI (excluded 39 subjects); d) The MR imaging were performed before any treatment (excluded 156 subjects); e) Their MR imaging had adequate image acquisition and without motion or susceptibility artifact (excluded 20 subjects). Therefore, 109 patients (61 men and 48 women, aged 4–80 years; mean age, 41.63 years) were finally evaluated.

MR acquisition

MR acquisition were performed with a 3-T MR imaging system (Magnetom Skyra, Siemens Healthineers) with a twenty channel head and neck combined coil. All patients underwent conventional MR imaging and DTI, DWI, MRS and DSC imaging. The precontrast DTI protocol included TR/TE, 6000/93 ms; FOV, 230mm × 230mm; Matrix, 128 × 128; section thickness, 3 mm; voxel size, 1.8×1.8×3mm; number of section, 44; diffusion gradient encoding in 30 directions; b value, 1000 s/mm2.DWI scan parameters were as follows: TR/TE = 8200/102 ms; FOV, 230mm × 230mm; Matrix, 128 × 128; section

thickness, 5 mm; b values = 0 and 1000 s/mm^2. Multivoxel 2D MR spectroscopy was performed before the administration of contrast agent. The detailed imaging parameters for the MRS study were as follows: TR/TE, 1700/135 ms; flip angle 90°; section thickness, 10mm; FOV, 160mm×160mm; voxel size,10×10×10mm; coding phase, 16 ×16; Averages, 1. DSC MR perfusion imaging was performed by using a gradient-echo echo-planar sequence during the administration of 0.2 mmol/kg of gadoterate meglumine delivered with a power injector at a rate of 2ml/s followed by a 20ml bolus of saline administered at the same rate. Scan parameters were as follows: TR/TE, 1640 ms/30 ms; flip angle 90°; Averages, 1; FOV, 220 mm×220 mm; matrix 128 ×128; section thickness, 5mm; voxel size, 1.7×1.7×5mm; number of section, 21.

Image processing and analysis

All imaging data were transferred from the scanner to a MMWP workstation (Siemens Healthcare, Erlangen, Germany) for postprocessing. For quantitative analysis, CBV maps, CBF maps, MTT maps, ADC maps, FA maps and MD maps were independently evaluated by two experienced neuro-radiologists who were blinded to the clinical and pathological information and any disagreements were resolved by consensus. The multi-parameters were calculated according to the method described in the previous studies (8, 19). The specific steps were as follows: a) Five circular regions of interest (ROIs) of 25mm^2 to 30mm^2 were carefully placed within the regions with the highest signal strength in the contrast-enhanced T1-weighted images to ensure the ROIs were placed in the solid component of a tumor and the normal tissue, the cystic, large necrotic, or hemorrhagic components of the tumor were avoided. These locations were then copied to the CBV maps, CBF maps, MTT maps, ADC maps, FA maps and MD maps; b) Five circular ROIs of same size from a) were placed in contralateral normal-appearing white matter. The mean value of these five ROIs was calculated as reference value; c) The highest, lowest, and mean CBV, CBF, MTT, ADC, FA and MD among the five ROIs acquired from a) were divided by the reference value to compute $rCBV_{max}$, $rCBV_{min}$, $rCBV_{mean}$, $rCBF_{max}$, $rCBF_{min}$, $rCBF_{mean}$, $rMTT_{max}$, $rMTT_{min}$, $rMTT_{mean}$, $rADC_{max}$, $rADC_{min}$, $rADC_{mean}$, rFA_{max}, rFA_{min}, rFA_{mean}, rMD_{max}, rMD_{min}, rMD_{mean}. An example of ROI placement was shown in Figure 1.

The spectra were automatically analyzed for the relative signal intensity (area under the fitted peaks in the time domain) of the

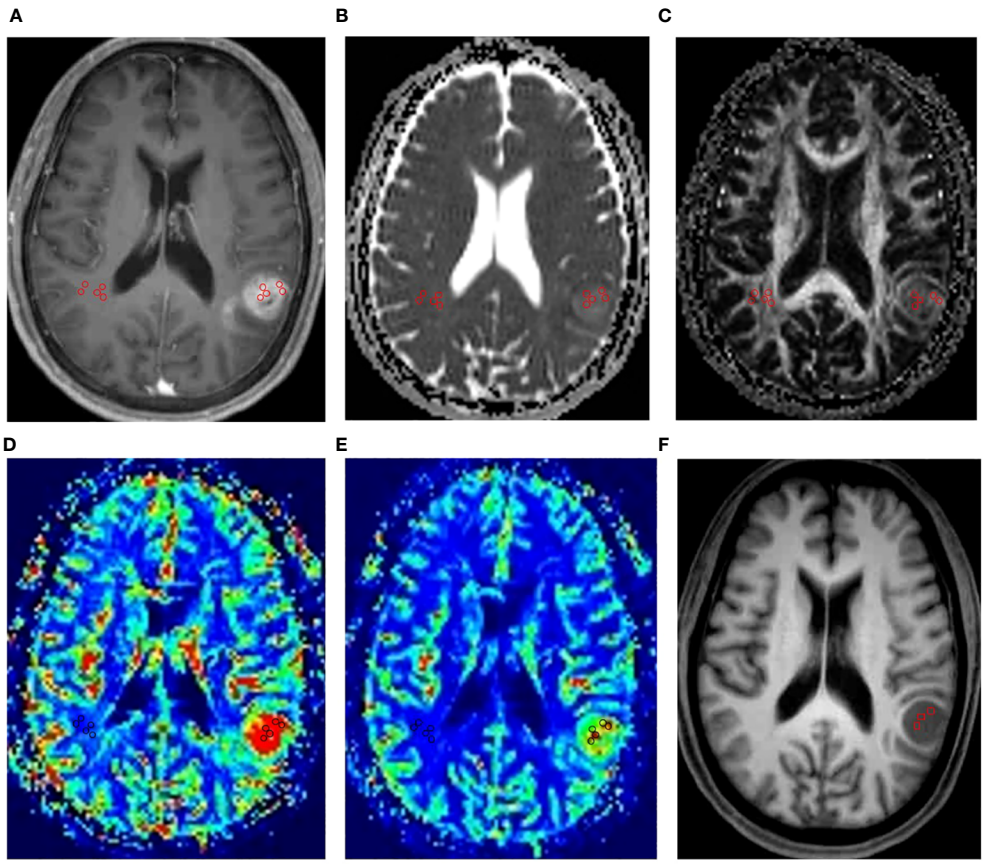

FIGURE 1
An example of ROI placement. This figure showed the ROI placement for a 62-year-old male patient with IDH1 wild-type grade IV glioma in the left temporal lobe. Firstly, we placed five circular regions of interest (ROIs) of 25mm^2 to 30mm^2 within the regions with the highest signal strength in the contrast-enhanced T1-weighted images **(A)**. Then, we copied the ROIs to the ADC maps **(B)**, FA maps **(C)**, CBV maps **(D)**, CBF maps **(E)**. Finally, five circular ROIs of same size from the above maps were placed in contralateral normal-appearing white matter. In MRS, the VOIs were placed in the structural MR imaging **(F)** within the solid portion of the tumor to avoid contamination from normal tissue or areas of necrosis, cysts or hemorrhage.

following metabolites: Cho, Cr, NAA. The metabolite peaks were assigned at the following frequencies: choline (Cho) at 3.22 ppm, creatine (Cr) at 3.02 ppm, N-acetylaspartate (NAA) at 2.02 ppm. We selected one to three Volumes of interest (VOIs) (250mm^3 to 300mm^3) within the solid portion of the tumor to avoid contamination from normal tissue or areas of necrosis, cysts or hemorrhage based on conventional MR imaging as much as possible. The measured metabolites in these VOIs were averaged to represent the tumor. The ratios of Cho/Cr, Cho/NAA and NAA/Cr were finally calculated.

Pathology

The histopathologic diagnosis was performed by pathologists and based on the WHO 2016 classification (20). The specimens were obtained from continuous sections after surgical resection. Surgical specimens were fixed in formalin and embedded in paraffin. The hematoxylin and eosin-stained specimens were checked to make the primary histopathological tissue diagnoses. The Ki-67 LI was obtained using the technique described in previous study (10, 21). Briefly, Ki-67 immunohistochemical staining was performed on paraffin embedded sections using the MIB-1 anti-human Ki-67 LI mouse monoclonal antibody (Dako, Carpinteria CA) at dilution of 1/600 and the EnvisionTM FLEX Targeted Retrieval System at high pH (Dako). Diaminobenzidine (DAB) was used as the chromogen. The Ki-67 LI was determined by calculating the percentage of MIB-1–positive tumor cell nuclei in a microscopic field containing approximately 400 to 500 tumor cells.

In each case, areas with the highest number of positive-staining tumor nuclei were selected for calculating the Ki-67 LI.

Statistical analyses

Interobserver and intraobserver reliability coefficient of MRI parameters was assessed using intraclass correlation coefficients (ICC) with 95% confidence intervals (SPSS, version 20.0, IBM). All other statistical analyses were performed using stata (version,15.0). Firstly, the Pearson correlation was used to analyze the correlation between each parameter and Ki-67 LI respectively. Through correlation analysis, we screened out the imaging indicators that had the greatest correlation with Ki-67 LI among the maximum, minimum and mean values of CBF, CBV, MTT, ADC, FA and MD respectively. Using these indicators with high correlation with Ki-67 LI to represent tumors can reduce the possible mismatch between the location of pathological sampling and the placement of ROI or VOI. Therefore, these screened indicators and those obtained in MRS were used for subsequent statistical analysis.

Jones (22) pointed out that it is most appropriate to use multivariate linear regression to explore the predictive relationship between multiple parameters. In this study, Ki-67 LI was dependent variable, the image indicators were independent variables, age and sex were control variables.

The following was the mathematical formula and statistical process of the regression model of this study:

$$\text{Regressionequation}: Y_{ik} = \alpha + \beta_{ik}X_{ik} + \varepsilon_{ik}(i = 1 \ldots \ldots 79; k = 1 \ldots \ldots n)$$

Where i is the sample size and k is the number of model's independent variables. Yik is the predicted value of the dependent variable (Ki-67 LI) and Xik is the column vectors, which represents the independent variables. βik is the regression coefficient of the kth variable (ie, the prediction effect), and εik is the regression residual term, α is the intercept term of the regression equation. The above selected image indicators were gradually added into the model as independent variables according to the order of correlation with Ki-67 LI to form the predictive model of Ki-67 LI. We used the R2, RMSE, AIC and BIC to assess model quality.

We used the Ki-67 LI prediction model constructed above in the validation sample set to estimate the Ki-67 LI index for these subjects, and t test was used to compare whether there were differences between these predicted Ki-67 LI and the actual Ki-67 LI.

In addition, we analyzed the correlation between imaging indicators and the grade of glioma using the Pearson correlation analysis. We compared the differences of imaging indicators among the gliomas of grade II, III, and IV using one-way analysis of variance (ANOVA). *Post-hoc* tests using Bonferroni correction for multiple comparisons. Since there were only two subjects with glioma of grade I in this study, gliomas with tumor grade I were not included in the group comparison.

Results

Among the 109 subjects included in this study, 79 subjects (age, 40.63 ± 16.82 years; age range, 4–80 years; female, 49; male, 30) were used as a dataset to construct the predictive model of Ki 67 LI, and 30 subjects (age, 43.16 ± 15.71 years; age range, 9–76 years; female, 12; male, 18) were used as a validation set for the predictive model. The information for the samples used to construct the Ki-67 LI prediction model was shown in Table 1. The average size of the ROIs which were placed within the solid component of the tumor were 26.3 ± 11.9mm^2 for the neuroradiologist A and 28.75 ± 15.10 mm^2 for the neuroradiologist B, respectively. There was no difference in the size of ROIs by the two neuroradiologists. The detailed size of ROIs placed by two neuroradiologists in each MRI maps were listed in Table 2. Intra-observer and inter-observer agreements for MRI parameters were good to excellent with ICCs ranging from 0.836 to 0.964 (Table 3).

The results of the correlation analysis between each imaging indicators and Ki-67 LI showed that the $rCBV_{max}$ (r=0.815, p<0.001), $rCBF_{max}$ (r=0.782, p<0.001), $rADC_{min}$ (r= -0.657, p<0.001), rFA_{max} (r=0.8, p<0.001), rMD_{min} (r=-0.682, p<0.001) had relatively high correlation with Ki-67 LI (Table 3). Therefore, the above indicators and ratios of Cho/Cr and Cho/NAA were included in subsequent stepwise regression analysis and group comparison. The ratio of NAA/Cr was not correlated with Ki-67 LI, so it was excluded from stepwise regression analysis.

The regression coefficients listed in our study were all non-standardized coefficients unless otherwise stated. The results of the

TABLE 1 Patient demographic data characteristics.

Grade/ Histology	IDH (Mut/ WT)	Sex (Male/ Female)	Age (Mean ± SD)	Ki-67 (Mean ± SD)
Grade I (n=2)	0/2	1/1	14 ± 9.899	0.045 ± 0.007
Pilocytic astrocytoma (n=2)	0/2	1/1	14 ± 9.899	0.045 ± 0.007
Grade II (n=30)	18/12	18/12	38.567 ± 16.425	0.071 ± 0.053
Diffuse astrocytoma (n=17)	7/10	11/6	35.688 ± 17.296	0.059 ± 0.040
Oligodendro-glioma (n=11)	11/0	7/4	41.09 ± 13.042	0.09 ± 0.068
Pleomorphic xanthoastrocytoma (n=2)	0/2	0/2	37 ± 31.113	0.055 ± 0.064
Grade III (n=15)	6/9	7/8	46.4 ± 9.326	0.189 ± 0.085
Anaplastic astrocytoma (n=8)	1/7	4/4	47.5 ± 10.085	0.169 ± 0.059
Anaplastic oligodendro-glioma (n=7)	5/2	3/4	45.143 ± 8.989	0.211 ± 0.108
Grade IV (n=32)	2/30	23/9	41.531 ± 18.719	0.301 ± 0.146
Glioblastoma (n=25)	1/24	18/7	46.8 ± 15.885	0.33 ± 0.141
Diffuse midline glioma (n=7)	1/6	5/2	21.875 ± 15.459	0.183 ± 0.12
Sum (n=79)	26/53	49/30	40.633 ± 16.822	0.186 ± 0.148

SD, standard deviation; IDH, Isocitrate dehydrogenase; Mut, IDH-mutant; WT, IDH-wild-type.

TABLE 2 The size of the ROIs or VOIs.

Parameter	Mean ± SD*	Mean ± SD*	P value
	Radiologists A	Radiologists B	
$rCBV_{min}$	26.164 ± 2.012 (mm^2)	27.149 ± 2.378 (mm^2)	0.056
$rCBV_{mean}$	27.235 ± 1.954 (mm^2)	26.150 ± 2.320 (mm^2)	0.061
$rCBV_{max}$	26.567 ± 2.177 (mm^2)	25.852 ± 2.543 (mm^2)	0.053
$rCBF_{min}$	27.419 ± 2.124 (mm^2)	26.234 ± 2.491 (mm^2)	0.066
$rCBF_{mean}$	26.320 ± 2.066 (mm^2)	26.535 ± 2.433 (mm^2)	0.134
$rCBF_{max}$	26.512 ± 2.289 (mm^2)	27.112 ± 2.656 (mm^2)	0.078
$rMTT_{min}$	26.282 ± 2.138 (mm^2)	26.876 ± 2.505 (mm^2)	0.271
$rMTT_{mean}$	26.183 ± 2.080 (mm^2)	26.497 ± 2.447 (mm^2)	0.186
$rMTT_{max}$	27.315 ± 2.303 (mm^2)	26.329 ± 2.570 (mm^2)	0.053
$rADC_{min}$	26.667 ± 2.251 (mm^2)	26.818 ± 2.617 (mm^2)	0.357
$rADC_{mean}$	26.568 ± 2.193 (mm^2)	27.213 ± 2.559 (mm^2)	0.089
$rADC_{max}$	26.137 ± 2.416 (mm^2)	26.715 ± 1.782 (mm^2)	0.092
rFA_{min}	26.289 ± 1.993 (mm^2)	26.165 ± 2.359 (mm^2)	0.371
rFA_{mean}	27.151 ± 1.935 (mm^2)	26.166 ± 2.301 (mm^2)	0.061
rFA_{max}	26.583 ± 2.158 (mm^2)	26.198 ± 2.524 (mm^2)	0.376
rMD_{min}	27.354 ± 2.105 (mm^2)	26.550 ± 2.471 (mm^2)	0.082
rMD_{mean}	26.536 ± 2.047 (mm^2)	26.551 ± 2.413 (mm^2)	0.467
rMD_{max}	27.568 ± 2.270 (mm^2)	26.583 ± 2.636 (mm^2)	0.079
Cho/Cr	272.18 ± 20.99 (mm^3)	268.44 ± 2.014 (mm^3)	0.183
Cho/NAA	264.01 ± 22.41 (mm^3)	270.45 ± 25.83 (mm^3)	0.299
NAA/Cr	274.33 ± 23.64 (mm^3)	270.77 ± 28.06 (mm^3)	0.357

*The values listed in this column were the size of the ROIs. #The values listed in this column were the p-values of the T-test between the two neuro radiologists. The subscript "min" indicated the minimum value. The subscript "mean" indicated the mean value. The subscript "max" indicated the maximum value. rCBV, relative cerebral blood volume; rCBF, relative cerebral blood flow; rMTT, relative mean transit time; rADC, relative apparent diffusion coefficient; rFA, relative fractional anisotropy; rMD, relative mean diffusivity; Cho/Cr, choline/creatine; Cho/NAA, choline/N-acetylaspartate; NAA/Cr, N-acetylaspartate/creatine; SD, standard deviation.

stepwise regression analyses were as follows (Table 4): The model 1 showed that the regression coefficient of $rCBV_{max}$ was 0.03 (P<0.001). In this model, the regression coefficients of age and sex were not statistically significant. Therefore, we excluded age and sex in the subsequent model construction. When the rFA_{max} was added, the model had higher R^2 and lower RMSE, AIC and BIC, which means model 2 had better explanatory power for Ki-67 LI. In addition, the regression coefficient of $rCBV_{max}$ was 0.03 (P<0.01). Thus, the model 1 overestimated the regression coefficient of $rCBV_{max}$. We found that the model 3 had higher R^2 and lower RMSE, AIC and BIC compared to model 2. The model 4 had higher increased R^2 and lower RMSE, AIC and BIC compared to model 3. Therefore, model 3 was better than model 2, and model 4 was better than model 3. In model 4, the regression coefficient of rMD_{min} was not statistically significant. Therefore, we excluded rMD_{min} in the subsequent model construction. The model 5 had higher increased R^2 and lower RMSE, AIC and BIC compared to model 4. The model 6 had higher increased R^2 and lower RMSE, AIC and BIC compared to model 5. Therefore, model 5 was better than model 4, and model 6 was better than model 5. In addition, the value of regression coefficient of $rCBV_{max}$, rFA_{max}, $rCBF_{max}$ were gradually decreased from model 1 to model 6 (Table 4), which means that the regression coefficients were overestimated in model 1 to model 5. The R^2 in model 7 were similar with model 6. However, the RMSE, AIC and BIC were increased in model 7 compared to model 6 (Table 4). That is to say, the explanatory power of model 7 did not increase, but the simplicity of the model was affected compared to model 6.

We could conclude that model 6 ($Ki67 = 0.0199 + 0.0108rCBV_{max} + 0.219rFA_{max} + 0.00677rCBF_{max} + 0.0115Cho/Cr - 0.0443rADC_{min}$) may be the best model among these seven models. The standardized regression coefficients of each imaging indicator in this model were as follows: $rCBV_{max}$ (RC= 0.282), rFA_{max} (RC=0.325), $rCBF_{max}$ (RC=0.151), $rADC_{min}$ (RC= -0.14), Cho/Cr (RC=0.157).

Then, we did regression check on model 6 and the results showed that there were no multicollinearity problem (Variance inflation factors of all independent variables were less than five: rCBVmax, 3.22; rCBFmax, 3.14; rADCmin, 1.96; rFAmax, 2.51;

TABLE 3 The results of correlation analysis and intra-class correlation coefficients.

Parameter	Mean ± SD*	r (P)#	ICC (95%CI)##	
			Inter-observer	Intra-observer
$rCBV_{min}$	3.879 ± 3.054	0.357 (0.001)	0.931 (0.905–0.951)	0.964 (0.943–0.972)
$rCBV_{mean}$	4.703 ± 2.686	0.755(<0.001)	0.925 (0.914–0.963)	0.958 (0.933–0.975)
$rCBV_{max}$	6.023 ± 3.877	0.815 (<0.001)	0.942 (0.900–0.978)	0.953 (0.929–0.968)
$rCBF_{min}$	3.495 ± 2.568	0.502 (<0.001)	0.946 (0.931–0.959)	0.949 (0.931–0.960)
$rCBF_{mean}$	4.700 ± 2.641	0.755(<0.001)	0.920 (0.892–0.928)	0.923 (0.898–0.940)
$rCBF_{max}$	5.866 ± 3.290	0.782 (<0.001)	0.909 (0.882–0.919)	0.918 (0.894–0.933)
$rMTT_{min}$	1.044 ± 0.187	-0.184 (0.105)	0.897 (0.687–0.921)	0.911 (0.882–0.936)
$rMTT_{mean}$	1.104 ± 0.627	-0.053 (0.64)	0.857 (0.633–0.914)	0.905 (0.892–0.943)
$rMTT_{max}$	1.486 ± 0.200	-0.150 (0.188)	0.869 (0.662–0.932)	0.921 (0.878–0.956)
$rADC_{min}$	1.400 ± 0.460	-0.657 (<0.001)	0.961 (0.943–0.972)	0.962 (0.944–0.973)
$rADC_{mean}$	1.496 ± 0.510	-0.367 (<0.001)	0.933 (0.904–0.941)	0.936 (0.911–0.953)
$rADC_{max}$	1.851 ± 0.808	-0.422 (<0.001)	0.922 (0.894–0.932)	0.931 (0.907–0.946)
rFA_{min}	0.3 ± 0.145	0.787 (<0.001)	0.876 (0.666–0.900)	0.890 (0.861–0.915)
rFA_{mean}	0.35 ± 0.183	0.778 (<0.001)	0.836 (0.612–0.893)	0.884 (0.871–0.922)
rFA_{max}	0.414 ± 0.219	0.8 (<0.001)	0.848 (0.641–0.911)	0.901 (0.857–0.935)
rMD_{min}	1.826 ± 0.142	-0.682 (<0.001)	0.940 (0.922–0.951)	0.941 (0.923–0.952)
rMD_{mean}	1.998 ± 0.087	-0.533 (<0.001)	0.912 (0.883–0.920)	0.915 (0.890–0.932)
rMD_{max}	2.188 ± 0.088	-0.548 (<0.001)	0.901 (0.873–0.911)	0.910 (0.886–0.925)
Cho/Cr	2.784 ± 2.014	0.627 (<0.001)	0.884 (0.675–0.908)	0.898 (0.869–0.923)
Cho/NAA	2.030 ± 1.271	0.402 (<0.001)	0.844 (0.621–0.901)	0.892 (0.879–0.930)
NAA/Cr	1.560 ± 1.183	0.086 (0.454)	0.856 (0.650–0.919)	0.908 (0.865–0.943)

*The values listed in this column were the measurements of Multi-parameters derived from MR Imaging. #The values listed in this column were the results of correlation analysis between each parameter and ki-67 respectively. Data in parentheses were P values. ##Data in parentheses are the 95% confidence interval. The subscript "min" indicated the minimum value. The subscript "mean" indicated the mean value. The subscript "max" indicated the maximum value. rCBV, relative cerebral blood volume; rCBF, relative cerebral blood flow; rMTT, relative mean transit time; rADC, relative apparent diffusion coefficient; rFA, relative fractional anisotropy; rMD, relative mean diffusivity; Cho/Cr, choline/creatine; Cho/NAA, choline/N-acetylaspartate; NAA/Cr, N-acetylaspartate/creatine; SD, standard deviation; ICC, intraclass correlation coefficient; CI, confidence interval.

Cho/Cr ration, 1.64), which means that the model had no redundant information. In addition, the regression check demonstrated that the residuals were normally distributed (Shapiro-Wilk W normality test: z, 2.140; p, 0.016), which means that the model did not miss important variables. Finally, there was an appropriate functional form (Test for appropriate functional form: F, 0.502; p, 0.682). The scatterplot matrix showed that Ki-67 LI was positively linearly distributed with rCBVmax, rCBFmax, rFAmax and ratio of Cho/Cr respectively, while it was negatively linearly distributed with rADCmin (Figure 2). We used the Ki-67 LI prediction model obtained above to estimate the Ki-67 LI of the validation sample. There was no difference (P=0.087 for t test) between the estimation of Ki-67 LI (0.177 ± 0.126) estimate and the actual value of Ki-67 LI (0.186 ± 0.147) in the validation sample.

In addition, the analysis of the correlation between imaging indicators and the grade of glioma showed that the rCBVmax, rCBFmax, rFAmax, the ratio of Cho/Cr and Cho/NAA were positively correlated with the grade of glioma, while the rADCmin and rMDmin were negatively correlated with the grade of glioma (Table 5). The results of ANOVA showed that the rCBVmax, rCBFmax, rADCmin, rFAmax, rMDmin, the ration of Cho/Cr and Cho/NAA were different among grade II, III, and IV (Table 5). The *Post-hoc* tests showed that the rCBVmax, rCBFmax, rADCmin and rFAmax were different between grade II and grade III, the rCBVmax, rCBFmax, rADCmin, rFAmax, rMDmin, the ration of Cho/Cr and Cho/NAA were different between grade II and grade IV, and the rFAmax, rMDmin and the ration of Cho/Cr were different between grade III and grade IV (Table 5). The box blots of rCBVmax, the rCBFmax, the rADCmin, the rFAmax, the rMDmin, the ration of Cho/Cr, the Cho/NAA and the NAA/Cr in grade II, grade III and grade IV gliomas were showed in Figure 3.

Discussion

This study estimated Ki-67 LI in glioma patients based on multi-parameters derived from DSC, DWI, DTI and MR spectroscopy imaging using multivariate regression and

TABLE 4 The results of stepwise multivariable regression.

Variables	Model 1	Model 2	Model 3	Model 4	Model 5	Model 6	Model 7
$rCBV_{max}$	0.0300***	0.0189***	0.0140**	0.0133**	0.0125**	0.0108**	0.0108**
rFA_{max}		0.299***	0.247**	0.245**	0.224**	0.219**	0.220**
$rCBF_{max}$			0.0106**	0.00812	0.00926*	0.00677**	0.00680
rMD_{min}				-0.101			
$rADC_{min}$					-0.0427**	-0.0443**	-0.0444**
Cho/Cr						0.0115*	0.0117*
Cho/NAA							-0.000748
Age	0.00108						
Sex	-0.0219						
Constant	-0.0253	-0.0518***	-0.0636***	0.1411	0.0225	0.0199	0.0208
R_{adj}^2	0.6815	0.7584	0.7781	0.782	0.7875	0.8025	0.8025
RMSE	0.08511	0.07364	0.07103	0.07089	0.06999	0.06793	0.06839
AIC	-161.1932	-185.0233	-189.7623	-189.1394	-191.16	-194.9535	-192.966
BIC	-151.7154	-177.9149	-180.2845	-177.2921	-179.3128	-180.7368	-176.3799

The data listed in the table were non-standardized coefficients. rCBVmax, maximum relative cerebral blood volume; rCBFmax, maximum relative cerebral blood flow; rADCmin, minimum relative apparent diffusion coefficient; rFAmax, maximum relative fractional anisotropy; rMDmin, minimum relative mean diffusivity; Cho/Cr, the ration of choline and creatine; Cho/NAA, the ration of choline and N-acetylaspartate; NAA/Cr, the ration of N-acetylaspartate and creatine; RMSE, root mean square error; AIC, Akaike information criterion; BIC, Bayesian information criterion. "-" indicated that the variables in the column were not included in the row correspondence model.
***p<0.01, **p<0.05, *p<0.1

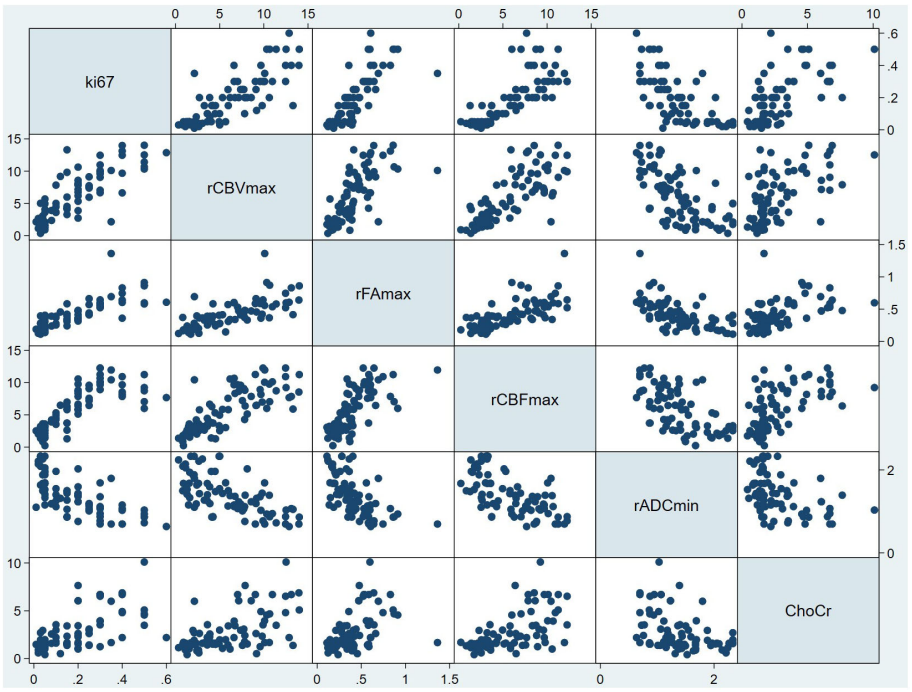

FIGURE 2
Scatterplot matrix of all variables in model 6. In each plot, the variable to the side of the graph was used as the Y variable, and the variable above and below the graph was used as the X variable. For example, in all the plots in the first column, the horizontal coordinate was Ki-67 LI, and the vertical coordinate from top to bottom was rCBVmax, the rFAmax, the rCBFmax, the rADCmin and Cho/Cr respectively. In addition, in all the plots in the first row, the vertical coordinate was Ki-67 LI, and the horizontal coordinate from left to right was rCBVmax, the rFAmax, the rCBFmax, the rADCmin and Cho/Cr respectively. From this figure, it can be seen that Ki-67 LI may have a positive correlation with rCBVmax, rFAmax, rCBFmax,Cho/Cr ration, while Ki-67 LI may have a negative correlation with rADCmin. ChoCr, Cho/Cr ration; rCBVmax, maximum relative cerebral blood volume; rCBF, relative cerebral blood flow; $rADC_{min}$, minimum relative apparent diffusion coefficient; rFA_{max}, maximum relative fractional anisotropy.

TABLE 5 The results of correlation analysis between each parameter and grade and the results of group comparison.

Parameter	Mean ± SD			r (P)*	ANOVA#	Grade II vs Grade III #	Grade II vs Grade IV #	Grade III vs Grade IV #
	Grade II	Grade III	Grade IV					
$rCBV_{max}$	3.055 ± 2.48	6.498 ± 3.193	8.738 ± 3.287	0.649 (<0.001)	<0.001	0.002	<0.001	0.062
$rCBF_{max}$	3.416 ± 2.198	6.348 ± 2.700	8.159 ± 2.685	0.663 (<0.001)	<0.001	0.002	<0.001	0.076
$rADC_{min}$	1.684 ± 0.366	1.303 ± 0.409	1.134 ± 0.377	-0.586 (<0.001)	<0.001	0.009	<0.001	0.367
rFA_{max}	0.252 ± 0.095	0.401 ± 0.126	0.574 ± 0.23	0.630 (<0.001)	<0.001	0.026	<0.001	0.007
rMD_{min}	1.913 ± 0.083	1.889 ± 0.113	1.702 ± 0.103	-0.704 (<0.001)	<0.001	0.737	<0.001	<0.001
Cho/Cr	1.549 ± 0.7	2.702 ± 1.832	4.055 ± 2.236	0.554 (<0.001)	<0.001	0.110	<0.001	0.047
Cho/NAA	1.323 ± 0.432	2.203 ± 1.406	2.473 ± 1.407	0.283 (0.012)	<0.001	0.054	0.001	0.748
NAA/Cr	1.32 ± 0.782	1.384 ± 0.903	1.715 ± 1.308	0.022 (0.849)	0.314	0.982	0.347	0.608

*The values listed in this column were the results of correlation analysis between each parameter and grade of glioma respectively. The P values were listed in parentheses. #The values listed in these column were the P values of ANOVA and Post-hoc tests. rCBVmax, maximum relative cerebral blood volume; rCBFmax, maximum relative cerebral blood flow; rADCmin, minimum relative apparent diffusion coefficient; rFAmax, maximum relative fractional anisotropy; rMDmin, minimum relative mean diffusivity; Cho/Cr, the ration of choline and creatine; Cho/NAA, the ration of choline and N-acetylaspartate; NAA/Cr, the ration of N-acetylaspartate and creatine; SD, standard deviation.

demonstrated that combining multiple parameters can precisely predict the Ki-67 LI. The model in our study with five dominant variables ($rCBV_{max}$, $rCBV_{max}$, $rADC_{min}$, rFA_{max} and Cho/Cr ratio) could predict Ki-67 LI with an R^2 of 0. 8025 and a root mean square (RMS) error of 0.0679.

In addition, we found that $rCBV_{max}$, $rCBF_{max}$, rFA_{max}, the ratio of Cho/Cr and Cho/NAA were positively correlated with Ki-67 LI and the grade of glioma, while the $rADC_{min}$ and rMD_{min} were negatively correlated with Ki-67 LI and the grade of glioma.

The results about the correlation between various imaging indicator and Ki-67 LI and the grade of glioma in our study were generally agree with previous studies. Many studies reported a significant inverse correlation between ADC values or ADC ratio (lesion-to-normal) and Ki-67 LI (21, 22). Yan et al. (23) demonstrated that ADC was a reliable biomarker in predicting the proliferation level. This may be due to the level of ADC signal correlated with cell density in gliomas (23). MD measures the average motion of water molecules, independent of tissue directionality (24); it is considered a synonym of the coefficient of diffusion in different space guidelines (25). Therefore, our study also found that the rMD_{min} were negatively correlated with Ki-67 LI and the grade of glioma. Fractional anisotropy (FA) provides a quantitative estimation of diffusion anisotropy, and positive correlation was observed between the FA and Ki-67 LI in many studies (26, 27). George A. Alexiou and colleagues found significant negative correlation between the ADC ratio (lesion-to-normal ration) and the Ki-67 LI (rho = −0.545, p = 0.0087) and significant positive correlation between the FA ratio and the Ki-67 LI (rho = 0.489, p =0.02) (26). DSC imaging has been widely used to estimate CBV and CBF. Many studies reported a positive

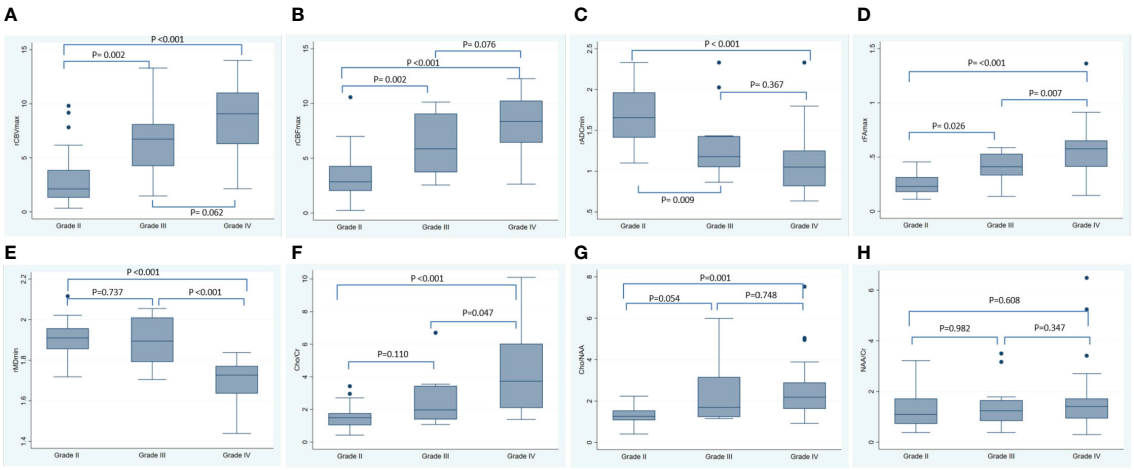

FIGURE 3
The box blots of various MRI metrics in different tumor grade. This figure showed the box plots for the rCBVmax **(A)**, the rCBFmax **(B)**, the rADCmin **(C)**, the rFAmax **(D)**, the rMDmin **(E)**, the Cho/Cr **(F)**, the Cho/NAA **(G)** and the NAA/Cr **(H)** in grade II, grade III and grade IV gliomas. The P-values listed in the picture were the results of *Post-hoc* tests using Bonferroni correction for multiple comparisons. rCBF, relative cerebral blood flow; rCBV, relative cerebral blood volume; rADC, relative apparent diffusion coefficient; rFA, relative fractional anisotropy; rMD, relative mean diffusivity; Cho/Cr, choline/creatine; Cho/NAA, choline/N-acetylaspartate; NAA/Cr, N-acetylaspartate/creatine; SD, standard deviation.

correlation between absolute or relative CBV and CBF values and cell density (28, 29). George A. Alexiou (26) and Anastasia K. Zikou (27) found strong correlation between rCBV and the Ki-67 LI in glioma (rho = 0.853, $p < 0.0001$) and in glioblastomas (r = 0.628, p = 0.07). Higher Cho metabolites at MR spectroscopy indicate increased membrane turnover and increased cellular density (30). However, Hiroaki Shimizu and colleagues showed that the Cho value tends to be underestimated in heterogeneous tumors resulting from intratumoral cyst, necrosis, hematoma, and indicate that the Cho value may no longer be reliable (14). Hiroaki Shimizu and colleagues demonstrated a linear relationship between the Ki-67 LI and Cho/Cr ratio (r =0.58, p = 0.02) and the Cho/NAA ratio (r= 0.60, p=0.02) (16). The regression coefficients between Ki-67 LI and $rCBV_{max}$, $rADC_{min}$, rFA_{max} and Cho/Cr ration in our study were relatively lower in our study compared with previous studies. The inconsistency may be due to the differences in statistical analyses. They performed univariate linear regression analysis which may lead to miscalculation of regression coefficients resulting from missing important variables. The above showed that diffusion, perfusion and spectroscopy imaging can be used to assess vascularity, metabolic activity, biochemical concentration and cellularity. These may be the reasons for the correlation between the parameters obtained in advanced MRI and the Ki-67 LI and the grade of glioma in this study.

We are not aware of previous work presenting Ki-67 predictive models based on multi-parameters derived from MR imaging using stepwise multivariate regression. Recently, Evan D. H. Gates and colleagues estimated Ki-67 maps using multi-parameters and reported the random forest algorithm best modeled Ki-67 with 4 imaging inputs (T2-weighted, fractional anisotropy, cerebral blood flow, Ktrans) and with a RMSE of 0.035 (R^2 = 0.75) (4). In our study, the model with also 5 variables ($rCBV_{max}$, $rCBF_{max}$, $rADC_{min}$, rFA_{max} and Cho/Cr ration) predicted Ki-67 LI with a RMSE of 0.0679 (R^2 = 0.8025). The RMSE in our research was slightly larger, the reason maybe the MR sequences and statistical analyses were different between our and their study which may lead to some differences in results. However, our model was tested by regression diagnosis which showed there was an appropriate functional form and the model did not miss important variables. In addition, we also tested in the validation set that there was no statistical difference between the Ki-67 LI evaluated by the predictive model constructed in this study and the actual Ki-67 LI. Therefore, our model also had important clinical value in noninvasively predicting the Ki-67 LI.

Ki-67 LI, a tumor cell proliferation index, is a widely recognized biomarker for quantitative evaluation of glioma growth and prognosis of patients (31). The Ki-67 LI prediction model constructed in this study will lead to more accurate characterization of tumors and allows us to distinguish between high-proliferating and low-proliferating gliomas. Such features afford additional presurgical information to the conventional morphological images. In clinical application, we suggest that advanced magnetic resonance examination, especially DTI, DWI, DSC and MRS imaging, be performed before surgery in glioma patients, and combine the model in our study to predict Ki-67 LI before surgery to noninvasive evaluation of pathological features of glioma.

This study has several limitations. Firstly, this was a retrospective research and only DSC, DWI, DTI and MR spectroscopy imaging were analyzed. In the future, more advanced MR imaging techniques need to be included to verify the results of this study. Second, the relation between the ROIs placement on the parameter maps of MR imaging and the histologic sampling used for the proliferation analysis remains unclear, although Ki-67 LI was determined in the highest density of stained areas. Another limitation was the heterogeneity of Ki-67 LI in glioma. The Ki-67 LI of the same lesion in the same patient in different areas was very different, although we try to enroll the maximum of Ki-67 LI in the section in this study, and select the ROI representing the most serious lesions in the image, so as to achieve the match between MR image and pathology as much as possible. The third limitation is that all MRI scans were performed on a single machine, which can avoid errors due to different machines, but it is also impossible to know whether the models constructed in this study will be applicable on other MRI machines. In the future, it is necessary to include more patients scanned on different MRI machines to verify whether the model obtained in this study is applicable to other machines, or to build a standardized model that can be applied to different MRI machines. The fourth limitation is that due to the limited sample size, the prediction model of glioma histological type was not constructed in this study, and the prediction model of glioma Ki-67 LI was not constructed according to the histological types. It may be possible to get a more accurate predictive model by building models based on histological types. Therefore, a larger sample size including various histological types will be needed in the future to complete this work. Finally, there are many new methods for feature extraction of magnetic resonance data, such as texture analysis. It is unknown whether the magnetic resonance parameters obtained by these new methods can build a more reliable prediction model for Ki-67 LI. Although the magnetic resonance parameters obtained in this study are more convenient compared with texture analysis, it is of great value to use more new magnetic resonance parameters to construct the Ki-67 LI model, and compare the differences between the model obtained in this study and the model obtained by the new method, or standardize the model between the parameters obtained by the traditional method and the parameters obtained by the new method.

In conclusion, we found that $rCBV_{max}$, $rCBF_{max}$, $rADC_{min}$, rFA_{max} and Cho/Cr ratio are correlated to Ki-67 LI in glioma patients. At the same time, combining multiple parameters derived from DSC, DWI, DTI and MRS can precisely predict the Ki-67 LI in glioma patients. This will allow us to noninvasively evaluate the pathological features and predict the prognosis of patients with glioma before surgery, and provide some information for the selection of clinical treatment.

Data availability statement

The raw data supporting the conclusions of this article will be made available by the authors, without undue reservation.

Ethics statement

The studies involving humans were approved by West China hospital of Sichuan University. The studies were conducted in accordance with the local legislation and institutional requirements. The participants provided their written informed consent to participate in this study.

Author contributions

YH: Writing – review & editing, Writing – original draft, Visualization, Validation, Supervision, Software, Resources, Project administration, Methodology, Investigation, Funding acquisition, Formal analysis, Data curation, Conceptualization. KZ: Writing – review & editing, Visualization, Software, Resources, Project administration, Methodology, Investigation, Formal analysis, Data curation.

Funding

The author(s) declare that no financial support was received for the research, authorship, and/or publication of this article.

Conflict of interest

The authors declare that the research was conducted in the absence of any commercial or financial relationships that could be construed as a potential conflict of interest.

Publisher's note

References

1. Su C, Jiang J, Zhang S, Shi J, Xu K, Shen N, et al. Radiomics based on multicontrast MRI can precisely differentiate among glioma subtypes and predict tumor-proliferative behavior. *Eur Radiol*. (2019) 29:1986–96. doi: 10.1007/s00330-018-5704-8

2. Burger PC, Shibata T, Kleihues P. The use of the monoclonal antibody Ki-67 in the identification of proliferating cells: application to surgical neuropathology. *Am J Surg Pathol*. (1986) 10:611–7. doi: 10.1097/00000478-198609000-00003

3. Torp SH. Diagnostic and prognostic role of Ki-67 immunostaining in human astrocytomas using four different antibodies. *Clin Neuropathol*. (2002) 21:252–7.

4. Gates EDH, Lin JS, Weinberg JS, Hamilton J, Prabhu SS, Hazle JD, et al. Guiding the first biopsy in glioma patients using estimated Ki-67 maps derived from MRI: conventional versus advanced imaging. *Neuro-oncology*. (2019) 21:527–36. doi: 10.1093/neuonc/noz004

5. Cha S, Knopp EA, Johnson G, Wetzel SG, Litt AW, Zagzag D. Intracranial mass lesions: dynamic contrast enhanced susceptibility-weighted echo-planar perfusion MR imaging. *Radiology*. (2002) 223:11–29. doi: 10.1148/radiol.2231010594

6. Sugahara T, Korogi Y, Kochi M, Ikushima I, Hirai T, Okuda T, et al. Correlation of MR imaging determined cerebral blood volume maps with histologic and angiographic determination of vascularity of gliomas. *AJR Am J Roentgenol*. (1998) 171:1479–86. doi: 10.2214/ajr.171.6.9843274

7. Aronen HJ, Gazit IE, Louis DN, Buchbinder BR, Pardo FS, Weisskoff RM, et al. Cerebral blood volume maps of gliomas: comparison with tumor grade and histologic findings. *Radiology*. (1994) 191:41–51. doi: 10.1148/radiology.191.1.8134596

8. Higano S, Yun X, Kumabe T, Watanabe M, Mugikura S, Umetsu A, et al. Malignant astrocytic tumors: clinical importance of apparent diffusion coefficient in prediction of grade and prognosis. *Radiology*. (2006) 241:839 – 46. doi: 10.1148/radiol.2413051276

9. Liu X, Tian W, Kolar B, Yeaney GA, Qiu X, Johnson MD. MR diffusion tensor and perfusion-weighted imaging in preoperative grading of supratentorial non enhancing gliomas. *Neuro-oncology*. (2011) 13:447–55. doi: 10.1093/neuonc/noq197

10. Kinoshita M, Hashimoto N, Goto T, Kagawa N, Kishima H, Izumoto S, et al. Fractional anisotropy and tumor cell density of the tumor core show positive correlation in diffusion tensor magnetic resonance imaging of Malignant brain tumors. *Neuroimage*. (2008) 43:29–35. doi: 10.1016/j.neuroimage.2008.06.041

11. Zeng Q, Dong F, Shi F, Ling C, Jiang B, Zhang J. Apparent diffusion coefficient maps obtained from high b value diffusion-weighted imaging in the preoperative evaluation of gliomas at 3T: comparison with standard b value diffusion-weighted imaging. *Eur Radiol*. (2017) 27:5309–15. doi: 10.1007/s00330-017-4910-0

12. Yang X, Hu C, Xing Z, Lin Y, Su Y, Wang X. Prediction of Ki-67 labeling index, ATRX mutation, and MGMT promoter methylation status in IDH-mutant astrocytoma by morphological MRI, SWI, DWI, and DSC-PWI. *Eur Radiol*. (2023) 33:7003–14. doi: 10.1007/s00330-023-09695-w

13. Nelson SJ, Kadambi AK, Park I, Li Y, Crane J, Olson M, et al. Association of early changes in 1H MRSI parameters with survival for patients with newly diagnosed glioblastoma receiving a multimodality treatment regimen. *Neuro-oncology*. (2016) 19:430–9. doi: 10.1093/neuonc/now159

14. Shimizu H, Kumabe T, Shirane R, Yoshimoto T. Correlation between choline level measured by proton MR spectroscopy and Ki-67 labeling index in gliomas. *AJNR Am J Neuroradiol*. (2000) 21:659–65.

15. Law M, Cha S, Knopp EA, Johnson G, Arnett J, Litt AW. High-grade gliomas and solitary metastases: differentiation by using perfusion and proton spectroscopic imaging. *Radiology*. (2002) 222:715–21. doi: 10.1148/radiol.2223010558

16. Law M, Yang S, Wang H, Babb JS, Johnson G, Cha S, et al. Glioma grading: sensitivity, specificity, and predictive values of perfusion MR imaging and proton MR spectroscopic imaging compared with conventional MR imaging. *Am J Neuroradiol*. (2003) 24:1989–98.

17. Vamvakas A, Williams SC, Theodorou K, Kapsalaki E, Fountas K, Kappas C, et al. Imaging biomarker analysis of advanced multiparametric MRI for glioma grading. *Physica Med*. (2019) 60:188–98. doi: 10.1016/j.ejmp.2019.03.014

18. Wang Q, Li Q, Mi R, Ye H, Zhang H, Chen B, et al. Radiomics nomogram building from multiparametric MRI to predict grade in patients with glioma: A cohort study. *J Magnetic Resonance Imaging*. (2019) 49:825–33. doi: 10.1002/jmri.26265

19. Calvar JA, Meli FJ, Romero C, Calcagno ML, Yánez P, Martinez AR, et al. Characterization of brain tumors by MRS, DWI and Ki-67 labeling index. *J Neurooncol*. (2005) 72:273–80. doi: 10.1007/s11060-004-3342-2

20. Louis DN, Perry A, Reifenberger G, von Deimling A, Figarella-Branger D, Cavenee WK, et al. The 2016 World Health Organization classification of tumors of the central nervous system: a summary. *Acta neuropathologica*. (2016) 131:803–20. doi: 10.1007/s00401-016-1545-1

21. Saksena S, Jain R, Narang J, Scarpace L, Schultz LR, Lehman NL, et al. Predicting survival in glioblastomas using diffusion tensor imaging metrics. *J Magn Reson Imaging*. (2010) 32:788–95. doi: 10.1002/jmri.22304

22. Jones AM. Health econometrics[M]. *Elsevier*. (2000) 1:265–344. doi: 10.1016/S1574-0064(00)80165-1

23. Yan R, Haopeng P, Xiaoyuan F, Jinsong W, Jiawen Z, Chengjun Y, et al. Non-Gaussian diffusion MR imaging of glioma: comparisons of multiple diffusion parameters and correlation with histologic grade and MIB-1 (Ki-67 labeling) index. *Neuroradiology*. (2016) 58:121–32. doi: 10.1007/s00234-015-1606-5

24. Pierpaoli C, Basser PJ. Toward a quantitative assessment of diffusion anisotropy. *Magn Reson Med*. (1996) 36:893–906. doi: 10.1002/mrm.1910360612

25. Mori S, Barker PB. Diffusion magnetic resonance imaging: its principle and applications. *Anat Rec*. (1999) 257:102–9. doi: 10.1002/(ISSN)1097-0185

26. Alexiou GA, Zikou A, Tsiouris S, et al. Correlation of diffusion tensor, dynamic susceptibility contrast MRI and 99mTc-Tetrofosmin brain SPECT with tumor grade and Ki-67 immunohistochemistry in glioma. *Clin Neurol Neurosurg*. (2014) 116:41–5. doi: 10.1016/j.clineuro.2013.11.003

27. Zikou AK, Alexiou GA, Kosta P, Goussia A, Astrakas L, Tsekeris P, et al. Diffusion tensor and dynamic susceptibility contrast MRI in glioblastoma. *Clin Neurol Neurosurg*. (2012) 114:607–12. doi: 10.1016/j.clineuro.2011.12.022

28. Sadeghi N, Salmon I, Decaestecker C, Levivier M, Metens T, Wikler D, et al. Stereotactic comparison among cerebral blood volume, methionine uptake, and histopathology in brain glioma. *Am J Neuroradiol*. (2007) 28:455–61.

29. Sadeghi N, D'Haene N, Decaestecker C, Levivier M, Metens T, Maris C, et al. Apparent diffusion coefficient and cerebral blood volume in brain gliomas: relation to tumor cell density and tumor microvessel density based on stereotactic biopsies. *Am J Neuroradiol*. (2008) 29:476–82. doi: 10.3174/ajnr.A0851

30. Tamiya T, Kinoshita K, Ono Y, Matsumoto K, Furuta T, Ohmoto T. Proton magnetic resonance spectroscopy reflects cellular proliferative activity in astrocytomas. *Neuroradiology*. (2000) 42:333–38. doi: 10.1007/s002340050894

31. Jiang JS, Hua Y, Zhou XJ, Shen DD, Shi JL, Ge M, et al. Quantitative assessment of tumor cell proliferation in brain gliomas with dynamic contrast-enhanced MRI. *Acad Radiol*. (2019) 26:1215–21. doi: 10.1016/j.acra.2018.10.012

frontiers | Frontiers in Oncology

TYPE Original Research
PUBLISHED 21 May 2024
DOI 10.3389/fonc.2024.1335401

OPEN ACCESS

EDITED BY
Dimitrios N. Kanakis,
University of Nicosia, Cyprus

REVIEWED BY
Debanjan Bhattacharya,
University of Cincinnati, United States
Zheng He,
Qilu Hospital of Shandong University, Qingdao, China
Guillermo Alberto Gomez,
University of South Australia, Australia

*CORRESPONDENCE
Falko Lange
falko.lange@uni-rostock.de

RECEIVED 08 November 2023
ACCEPTED 16 April 2024
PUBLISHED 21 May 2024

CITATION
Lange F, Gade R, Einsle A, Porath K, Reichart G, Maletzki C, Schneider B, Henker C, Dubinski D, Linnebacher M, Köhling R, Freiman TM and Kirschstein T (2024) A glutamatergic biomarker panel enables differentiating Grade 4 gliomas/astrocytomas from brain metastases. *Front. Oncol.* 14:1335401. doi: 10.3389/fonc.2024.1335401

A glutamatergic biomarker panel enables differentiating Grade 4 gliomas/astrocytomas from brain metastases

Falko Lange[1,2]*, Richard Gade[1], Anne Einsle[1], Katrin Porath[1], Gesine Reichart[1], Claudia Maletzki[3], Björn Schneider[4], Christian Henker[5], Daniel Dubinski[5], Michael Linnebacher[6], Rüdiger Köhling[1,2], Thomas M. Freiman[5] and Timo Kirschstein[1,2]

[1]Oscar-Langendorff-Institute of Physiology, University Medical Center Rostock, Rostock, Germany, [2]Center for Transdisciplinary Neurosciences Rostock, University of Rostock, Rostock, Germany, [3]Hematology, Oncology, Palliative Medicine, University Medical Center Rostock, Rostock, Germany, [4]Institute of Pathology, University Medical Center Rostock, Rostock, Germany, [5]Department of Neurosurgery, University Medical Center Rostock, Rostock, Germany, [6]Molecular Oncology and Immunotherapy, Clinic of General Surgery, University Medical Center Rostock, Rostock, Germany

Background: The differentiation of high-grade glioma and brain tumors of an extracranial origin is eminent for the decision on subsequent treatment regimens. While in high-grade glioma, a surgical resection of the tumor mass is a fundamental part of current standard regimens, in brain metastasis, the burden of the primary tumor must be considered. However, without a cancer history, the differentiation remains challenging in the imaging. Hence, biopsies are common that may help to identify the tumor origin. An additional tool to support the differentiation may be of great help. For this purpose, we aimed to identify a biomarker panel based on the expression analysis of a small sample of tissue to support the pathological analysis of surgery resection specimens. Given that an aberrant glutamate signaling was identified to drive glioblastoma progression, we focused on glutamate receptors and key players of glutamate homeostasis.

Methods: Based on surgically resected samples from 55 brain tumors, the expression of ionotropic and metabotropic glutamate receptors and key players of glutamate homeostasis were analyzed by RT-PCR. Subsequently, a receiver operating characteristic (ROC) analysis was performed to identify genes whose expression levels may be associated with either glioblastoma or brain metastasis.

Results: Out of a total of 29 glutamatergic genes analyzed, nine genes presented a significantly different expression level between high-grade gliomas and brain metastases. Of those, seven were identified as potential biomarker candidates including genes encoding for AMPA receptors *GRIA1*, *GRIA2*, kainate receptors *GRIK1* and *GRIK4*, metabotropic receptor *GRM3*, transaminase *BCAT1* and the glutamine synthetase (encoded by *GLUL*). Overall, the biomarker panel achieved an accuracy of 88% (95% CI: 87.1, 90.8) in predicting the tumor entity. Gene expression data, however, could not discriminate between patients with seizures from those without.

Conclusion: We have identified a panel of seven genes whose expression may serve as a biomarker panel to discriminate glioblastomas and brain metastases at the molecular level. After further validation, our biomarker signatures could be of great use in the decision making on subsequent treatment regimens after diagnosis.

KEYWORDS

glioblastoma, brain metastasis, glutamate, glutamate receptors, biomarker, epilepsy

1 Introduction

High grade glioma (CNS WHO grade 4) and brain metastases represent the most frequent tumors in the CNS (1, 2). Yet, the therapies of both diseases differ fundamentally. In case of a glioblastoma, treatment aims to total bulk resection in combination with subsequent radio-chemotherapy (3), whereas in the case of brain metastases, the primary tumor must be taken into account (4). Differentiating both tumor entities in the radiological imaging may be challenging (5). Once a primary extracranial malignancy is known, a tumor bulk in the MRI is more likely to be a brain metastasis. A multifocal appearance is also indicative of an extracranial origin of the tumor. In the case of single bulk, however, diagnosis may be ambiguous. Several MRI-based studies presented approaches to address this demand, that may in the future possibly become useful as additional tools to predict the tumor entity (6–8). Currently, the gold standard is still a histopathologic assessment. Tissue biopsies are common when MRI does not lead to an unequivocal diagnosis. Hence, additional biomarkers easy to obtain would be of great interest to distinguish glioblastoma from metastasis.

In glioblastoma, various pathophysiological processes were identified that drive the progression of the disease (9), including aberrant glutamatergic mechanisms (10–12). In patients suffering from glioma, the extracellular glutamate levels surrounding the tumor mass were identified as elevated (13, 14). High levels of glutamate contribute to hyperexcitability of tumor-surrounding neurons, epileptic seizures, and in the end, may favor tumor bulk expansion by excitotoxicity (15, 16). Since survival of patients suffering from glioblastoma is limited to approximately 15 months, maintaining the quality of life by preventing seizures is one of the main goals. To achieve seizure-free conditions, anticonvulsants targeting glutamate signaling are frequently in use (17, 18). On the molecular level, glutamate is released from the tumor cells in exchange for cystine via solute carrier family 7 member 11 (SLC7A11; xCT), an antiporter that was found to be upregulated in glioma (19). Cystine is an essential precursor for glutathione synthesis to address oxidative stress. Furthermore, the Na^+-dependent uptake of glutamate via solute carrier family 1 member 2 (SLC1A2; EAAT2) is impaired by downregulation or mislocalization of the transporter (20–22). In isocitrate dehydrogenase 1 (IDH1) wildtype glioblastoma, branched chain amino acid transaminase 1 (BCAT1) is also often upregulated and may contribute to a glutamatergic phenotype (23, 24). In addition to glutamate shuttling and metabolism of glioma cells, ionotropic and metabotropic glutamate receptors were identified to contribute to the tumor progression (11). The glioblastoma cells express α-amino-3-hydroxy-5-methyl-4-isoxazolepropionic acid (AMPA) receptors to a varying extent (25, 26), and exposure to AMPA receptors inhibitor perampanel resulted in antitumoral effects (27, 28). In neuro-gliomal synapses, transmission via AMPA receptors favored the glioma progression (29–31). With respect to metabotropic glutamate receptors, group II receptors (mGluR2 and mGluR3) in particular contributed to cancer growth (32–34).

The impact of an aberrant glutamate signaling in non-neuronal cancers is highly variable and less well studied (summarized in Ref (35). and Ref (36).). While glutamate receptors and transporters were found to be altered in most malignancies such as lung carcinoma (37–39) and pancreatic adenocarcinoma (40, 41), the overall glutamatergic phenotypes are less pronounced than in tumors of neural or glial origin. Therefore, aiming for identifying a mechanistically driven biomarker panel to distinguish glioblastoma and brain metastasis at the pathomolecular level, we investigated the expression of glutamate receptors and key players of glutamate homeostasis in human tumor tissue samples. Since aberrant glutamate signaling may contribute to tumor-associated epilepsy, we further asked whether gene expression patterns might differ between glioblastoma patients suffering from seizures and those without reported epilepsy.

2 Materials and methods

2.1 Patients and tumor samples

Tumor tissue samples were obtained from patients treated at the Department of Neurosurgery of the Rostock University Medical Center, Germany from 2011 to 2023. Inclusion criteria were diagnosed CNS WHO Grade 4 glioma (IDH1-wildtype) and CNS WHO grade 4 astrocytoma (IDH1-mutant) or brain tumors with

extracranial origin (42). In this study, IDH1-wildtype and IDH1-mutant were merged in one high-grade primary brain tumor group (referred to as high-grade glioma or HGG). In our study, tissues from a total of 55 individuals (29 male and 26 female), with informed written patient consent (ethics registration IDs: A45-2007, A2018-0167, A2019-0187) were included. All procedures involving patients were approved by local Ethics Committee (University Medical Center Rostock). Patients that were initially diagnosed as glioblastoma prior surgical resection, but in the subsequent histopathological assessment rated as low-grade glioma, were excluded from the study. The clinical data were obtained from the Department of Neurosurgery, the Department of Neurology, and the Institute of Pathology. An overview of the two patient cohorts (including data on sex, age, tumor localization, origin of the primary tumor for MET and information on molecular status (IDH mutation, MGMT promoter methylation) for HGG) is presented in Supplementary Table 1 and Supplementary Table 2 respectively. Process of diagnosis of the tumor entity was conducted as described in the German guidelines on glioma, that is based on WHO classification and suggestions of the ciMPACT-NOW consortium (42). The presence of epileptic seizures was clinically documented via patient history and/or was diagnosed by additional EEG analysis.

2.2 RNA isolation and cDNA synthesis

To extract RNA from snap-frozen surgical samples, tissues of the size of approx. 3x3x3 mm^3 were pestled employing a vibration mill (MM 400 Mixer Mill, Retsch, Haan, Germany) and subjected to TRIzol reagent (Invitrogen, Carlsbad, CA, USA). RNA isolation was performed according to the manufacturer's instructions. Afterwards, any traces of genomic DNA were removed employing DNA-free™ DNA Removal Kit (Invitrogen). For cDNA synthesis, all reagents were from Promega Corporation (Madison, WI, USA). For a total volume of 25 µl, 1 µg RNA was reverse-transcribed into cDNA by means of Moloney Murine Leukemia Virus Reverse Transcriptase, RNase H Minus, Point Mutant (200 U) and RNasin Plus RNase inhibitor (25 U) in the presence of random hexamers (0.25 µg) and dNTP Mix (0.4 mM each). Initially, the random hexamers and the RNA were incubated for 5 min at 70°C. The following sequence was 10 min at 20°C, 50 min at 40°C followed by 15 min at 70°C. All synthesized cDNAs were quantified and stored at -80°C until further usage.

2.3 Quantitative RT-PCR

Relative quantification of target cDNA levels by real-time PCR was performed in a qTOWER^3 detection system (Analytik Jena AG, Jena, Germany). Therefore, AceQ qPCR SYBR Green Master Mix (Absource Diagnostics, Munich, Germany) and human gene-specific primers (TIB Molbiol, Berlin, Germany; Supplementary Table 3) were used. *GAPDH* (glyceraldehyde-3-phosphate dehydrogenase) and *TBP* (TATA-box binding protein) served as house-keeping gene controls. All data were analyzed for both housekeeping genes. In the current manuscript, the data based on *TBP* are presented, since TBP expression was found to be more robust in glioblastoma (43). Primer sequences (see Supplementary Table 3) for ionotropic and metabotropic glutamate receptors were obtained from Ref (25). and genes associated with glutamate homeostasis were from Lange et al., 2019 (27). PCR conditions were 95°C for 5 min, followed by 40 cycles of 10 s at 95°C/30 s at 60°C. To further address the quality of the primers used in our study, melting curves at the end of each RT-PCR were recorded (15 s; 0.1°C-steps; see Supplementary Figure 1 and Supplementary 2 for sample melting curves for each gene). Real-time PCR products were subjected to gel electrophoresis (2% agarose). Here, for each set of primers only one PCR product was determined (Supplementary Figure 3). For each biological sample the relative expression of each mRNA (based on technical duplicates) compared to the housekeeping gene *TBP* was calculated according to the equation $\Delta Ct = Ct_{target} - Ct_{TBP}$. The relative amount of target mRNA was expressed as $10^3 \times 2^{-\Delta Ct}$.

2.4 Immunohistochemistry

Analysis of glutamate receptor expression on the protein level was performed on paraffin-embedded tumor tissues. For this purpose, 5-µm-sections were prepared and deparaffinization was done by a standard protocol. For the immunohistochemistry of GluA1 (encoded by GRIA1) and GluA2 (encoded by GRIA2) heat-induced antigen retrieval (10 min cooking time, 0.05% Tween-20 in 10 mM citrate buffer, pH 6.0) was carried out to enhance the immunofluorescent signal. After cooling down for 20 min and 3×10 min washing in PBS, sections were first incubated for 20 min with 0.1% triton-X (in PBS), washed with PBS (2×10 min), and afterwards incubated for 60 min with 10% normal goat serum (NGS; Thermo Fisher Scientific, Waltham, MA, USA). Next, tissue sections were incubated with the primary antibody for anti-GluA1 antibody (Abcam; ab183797; diluted 1:100), anti-GluA2 antibody (Abcam; ab20629; diluted 1:100) or anti-mGluR3 antibody (Thermo Fisher Scientific; MA5-31749; diluted 1:200) respectively at 4°C overnight. Next day, slices were washed 3x10 min with PBS and were exposed to secondary antibodies (Alexa Fluor 488 goat anti-rabbit (Thermo Fisher Scientific; A-11034; diluted 1:400 in PBS/1% NGS) or Cyanine5 (Cy5) goat anti-mouse (Thermo Fisher Scientific; A10524, diluted 1:200 in PBS/1% NGS). Afterwards, the slices were counterstained and mounted with ProLong Gold Antifade Reagent containing 4',6-diamidino-2-phenylindole (DAPI, Thermo Fisher Scientific, P36931). Fluorescence analysis was performed by using a laser-scanning microscope (Leica DMI 6000, Wetzlar, Germany) and Leica Application Suite (v. 2.0.0.13332) software. At 100x magnification, regions of interest in the tumor sections were placed and mean fluorescent signals of Alexa Fluor 488, Cy5 and DAPI were estimated. The ratio of the secondary antibody signal and DAPI was calculated to estimate the relative glutamate receptor expressions. Protein expressions were compared with relative mRNA expression by calculating the Pearson correlation coefficients.

2.5 Statistical analysis

Statistical analyses were performed with IBM SPSS Statistics (Version 27, IBM, Ehningen, Germany). The expression data are presented as box-and-whisker plots. The box represents 25th and 75th percentiles separated by the median, while whiskers show 10th and 90th percentiles. Outliers are marked as circles. The arithmetic mean is illustrated as a red line. Group differences were tested for significance using the nonparametric Mann-Whitney U test. In the main body of the text, the gene expressions were compared as fold difference of the means between high-grade glioma and metastasis. A receiver operating characteristic (ROC) analysis was used to identify genes with high area under the curve (AUC) values (>0.8) that may serve as potential biomarker candidates. To estimate the optimal cut-points, Youden indices were calculated as sum of sensitivity and selectivity. A t-test was used to compare receptor expression in immunochemical experiments. Pearson correlation coefficients were calculated to estimate the effects of age or sex on the occurrence of epilepsy in Grade 4 glioma/astrocytoma and to compare the expression of selected candidates on protein and mRNA level. A significance level of $p<0.05$ was considered statistically significant.

3 Results

3.1 Expression of glutamate receptors and genes associated with glutamate homeostasis in brain tumors

The aim of this study was to identify candidate genes whose expression highly differs between high-grade glioma/astrocytoma (henceforth abbreviated as high-grade glioma or "HGG") and brain tumors with extracranial origin (brain metastasis or "MET"). In our study, we included a total of 55 patients of whom 35 were diagnosed with HGG (40% female) and 20 suffered from brain metastasis (60% female; Table 1). The median age at diagnosis was rather comparable between both cohorts; patients with HGG showed a median age of 68 years (29-91 years) and those with MET a median of 58 years (42-75 years). In the study, 33/35 CNS WHO 4 brain cancers were diagnosed as glioblastoma (IDH1-wildtype) and two were classified as IDH1-mutant astrocytoma (Supplementary Table 1). As summarized in Supplementary Table 2, metastases derived from lung cancer (n=11), breast cancer (n=3), colorectal/rectal cancer (n=3) or were of renal carcinoma, melanoma, and cervical cancer origin (one patient in each case).

TABLE 1 Overview of Grade 4 glioma/astrocytoma and brain metastasis cohorts.

	HGG (n=35)	MET (n=20)
sex	f:14 | m:21	f:12 | m:8
age (y)	68 (29–91)	58 (42–75)
occur. of epilepsy	51.4%	20%

Based on real-time PCR analysis, no significant differences between HGG and MET in the relative expression of N-methyl-D-aspartate (NMDA) receptors were determined (Figure 1A; Mann-Whitney U test). In marked contrast, AMPA receptor subunits *GRIA1* (~20-fold difference; $p<0.001$) and *GRIA2* (~90-fold difference; $p<0.001$) were found to be higher expressed in HGG than in the MET cohort (Figure 1B). Interestingly, the *GRIA3* expression was found to be lower in HGG than in MET (~2.4-fold difference; $p=0.01$). With respect to kainate receptors, the subunits *GRIK1* (~46-fold difference; $p<0.001$) and *GRIK4* (~1.8-fold difference; $p<0.001$) were also higher expressed in HGG than in MET (Figure 1C). As shown in Figure 2A, *GRM3* is the only metabotropic glutamate receptor gene that showed a differential expression (~11-fold higher expression in HGG; $p<0.001$) between both patient cohorts (Figure 2A).

The last group analyzed were genes that are associated with glutamate shuttling and metabolism. Our analysis revealed that *GLUL* (~17.2-fold difference; $p<0.001$) a gene encoding for glutamine synthetase, branched chain amino acid transaminase 1 (*BCAT1*; ~4.7-fold difference; $p<0.001$), and *SLC7A11* (~1.1-fold difference; $p= 0.005$), encoding the xCT cystine/glutamate transporter, were higher expressed in HGG (Figure 2B). Remarkably, no difference in the expression of *EAAT2* (encoded by *SLC1A2*), a Na^+/glutamate co-transporter previously reported to be downregulated in glioma (21, 22), was determined. Exclusion of astrocytoma samples from the statistical analysis had no impact on the results with respect to significant differences between both cohorts.

Three of the differentially expressed glutamate receptors (*GRIA1*, *GRIA2*, *GRM3*) were selected for immunohistological verification of the mRNA expression (Figure 3). In a subset of 10 patients (5 samples per tumor cohort), no significant difference was found in the expression of GluA2 between both tumor entities (Figure 3A; $p=0.227$, Student's t-test). However, in congruence with the gene expression, protein expressions of GluA1 ($p=0.038$) and mGluR3 ($p=0.045$) were found to be significantly higher in HGG than in MET. Altogether, correlation between those three candidates on the RNA and protein level failed to reach the significance level (n=10 patients; Pearson correlation coefficient was 0.31; $p=0.0951$).

3.2 No association between the prevalence of seizures and glutamate receptor expression

Next, we asked whether glutamate receptor expression in the tumor tissue was associated with an epileptic phenotype in patients suffering from HGG, as pathophysiological glutamate signaling may contribute to tumor-associated seizures (11, 44). In our study, 51% (n=18) of the patients exhibited an epileptic phenotype (Table 1).

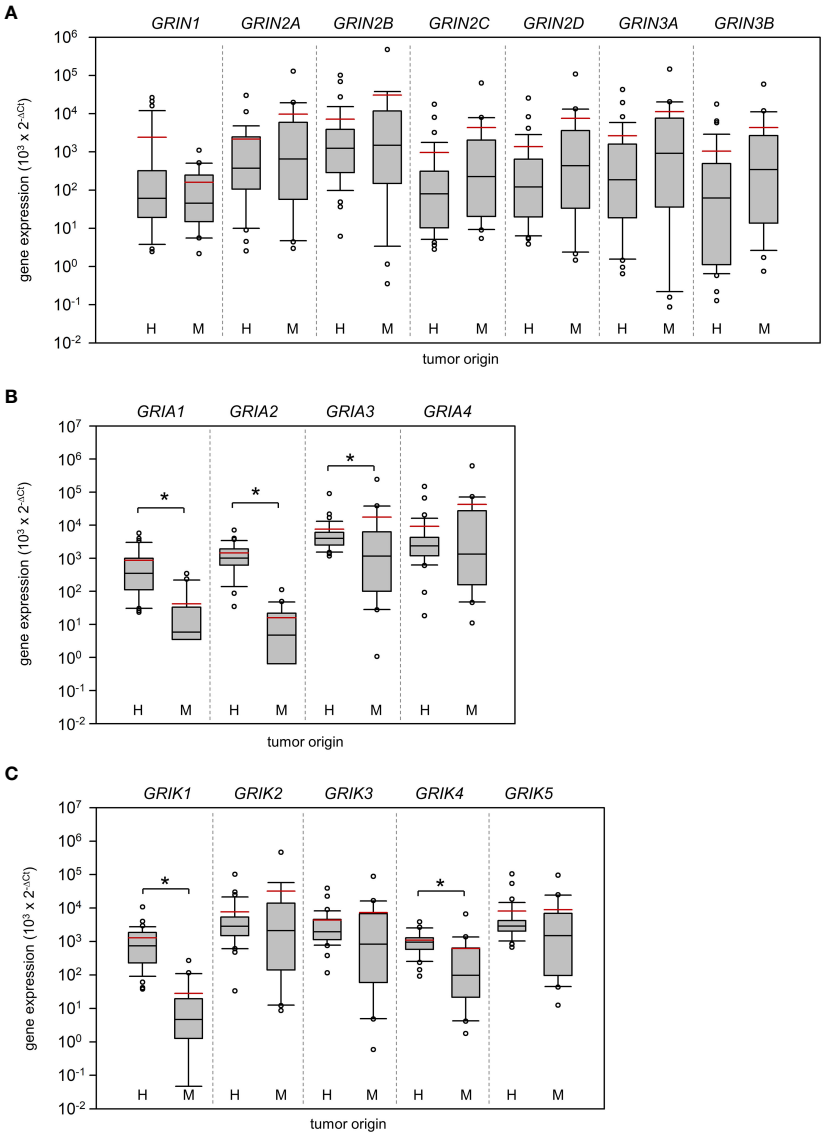

FIGURE 1
Expression of ionotropic glutamate receptors in Grade 4 gliomas/astrocytomas and brain metastases. RNA was isolated from grade 4 glioma/astrocytoma (H, n=35) and brain metastasis samples (M, n=20), and reverse-transcribed in cDNA as described in the material and methods section. Subsequently, the mRNA expression of **(A)** NMDA receptors, **(B)** AMPA receptors, **(C)** KA receptors and house-keeping control TATA-box binding protein (*TBP*) was assessed by real-time PCR. The box-and-whisker plots represent relative amounts ($10^3 \times 2^{-\Delta Ct}$) of target mRNA. Median is shown as a black-coloured line and the mean is red; *p<0.05 (Mann-Whitney U test).

However, no significant differences in all investigated genes between both HGG cohorts were detected (Supplementary Figure 4 and Supplementary Figure 5). Interestingly, an inverse correlation between the occurrence of seizures and age was determined (n=34 patients; Pearson correlation coefficient was -0.408; p=0.0165). The cohort suffering from epilepsy had a median age of 52 years (29-91 years) and those patients without seizures were 72 years-old (39-80 years). As shown in previous studies (45, 46), sex did not correlate with diagnosed epilepsy (n=34 patients; Pearson correlation coefficient was 0.228; p=0.194).

3.3 A ROC analysis elucidated a set of genes to potentially distinguish Grade 4 glioma/astrocytoma and brain metastasis

To further investigate the expression pattern of glutamatergic genes that may help to differentiate HGG and MET on the molecular level, a ROC analysis (sensitivity vs. 1–specificity) was performed. It was hypothesized that among the statistically significant identified nine genes (Figure 1 and Figure 2), potential biomarker candidates could be evaluated. In the ROC analysis, an

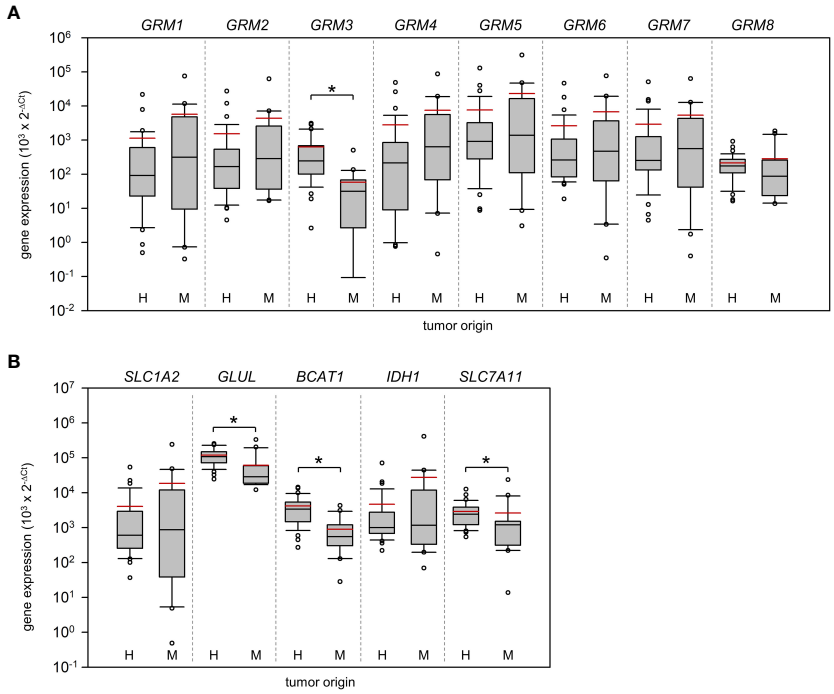

FIGURE 2
Expression of metabotropic glutamate receptors and key players of glutamate homeostasis in Grade 4 gliomas/astrocytomas and brain metastases. RNA was isolated from grade 4 glioma/astrocytoma (H, n=35) and brain metastasis samples (M, n=20) and reverse-transcribed in cDNA. Subsequently, the mRNA expression of **(A)** metabotropic receptors (*GRM1-8*) and **(B)** key players of glutamate shuttling (*SLC1A2* and *SLC7A11* coding for EAAT2 and xCT antiporter respectively) and metabolism (*IDH1, BCAT1, GLUL*), and house-keeping control *TBP* was quantified by real-time PCR. The box-and-whisker plots represent relative amounts ($10^3 \times 2^{-\Delta Ct}$) of target mRNA. Median is shown as a black-coloured line and the mean is red; *p<0.05 (Mann-Whitney U test).

area under the curve (AUC) with >0.8 was assumed as robust value to distinguish both tumor cohorts.

In seven of nine genes, an AUC >0.8 was found (Figure 4). This included *GRIA1*, *GRIA2*, and *GRIK1* with AUCs even >0.9, and *GRIK4*, *GRM3*, *GLUL* and *BCAT1* with AUC >0.8, while *GRIA3* and *SLC7A11* presented AUCs of 0.712 and 0.729 respectively (Figure 4B). All the remaining gene expression patterns presented AUCs <0.7 (Supplementary Figure 6 and Supplementary Figure 7) and were excluded as biomarker candidates.

To estimate the optimal cut-point, Youden indices were calculated for each AUC of the target genes with an AUC >0.8 (Table 2). Additionally, the ΔCt values of these cut-points were calculated (Table 2). Furthermore, for each biological sample it was determined whether the ΔCt of the Youden indices could be used as a predictor of the tumor entity. On average for all genes, an accuracy of 88% (95% CI: 87.1, 90.8) to predict the correct tumor entity was found (Table 2). Hence, a panel of genes was needed to ensure that the correct disease was predicted. In 30 out of 55 tissue samples, the ΔCt values of all seven genes could be used to decide on the correct tumor entity (true positive or true negative). In 14 surgical samples, six of seven were correct. Of the remaining eleven samples, 5/7 (n=4), 4/7 (n=4) and 3/7(n=3) ΔCt values in our model were found to be true positives or true negatives, respectively.

4 Discussion

After determination of a neoplastic mass in the brain, a rapid diagnosis of the tumor entity is crucial for the decision on subsequent treatment regimens. With a history of extracranial malignancy, a brain cancer is often appropriately classified as a metastasis. However, without a cancer history, differentiating high-grade glioma from metastasis remains challenging in the imaging. At least two predictive biomarkers were established in high-grade glioma. Both, *MGMT* promoter methylation and *IDH1* mutations are associated with a better overall survival of patients with primary brain cancers (47). After diagnosis, patients exhibiting a high rate of *MGMT* promoter methylation had a 50% longer median survival when treated with temozolomide (48). However, no molecular fingerprints were proposed to distinguish brain metastasis and glioblastoma. Especially in tumor samples that may be insufficient for precise histopathological examination like biopsy specimens, a set of biomarkers requiring only a small amount of tissue could be a supportive tool.

Our major finding was the identification of a panel of seven genes that may support a differentiation at the pathomolecular level. This set of genes includes all subgroups of receptors and key players of glutamate homeostasis. First, two ionotropic AMPA receptors, GRIA1 and GRIA2 were found to be higher expressed in primary

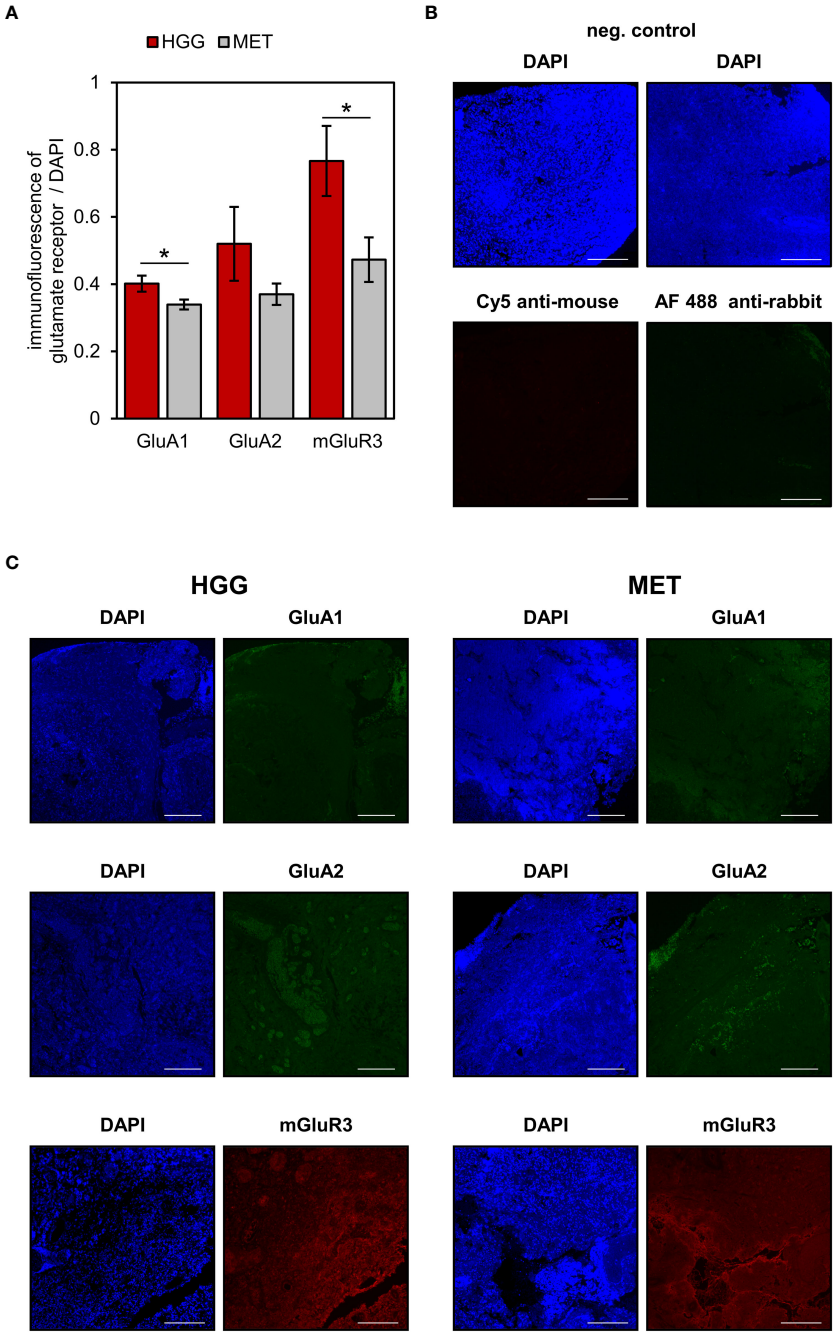

FIGURE 3
Glutamate receptors expression in human brain tumour slices. AMPA receptor subunits GluA1 and GluA2 (shown in green) and metabotropic receptor mGluR3 (red) were determined in the tumour area. Additionally, nuclei were counterstained with DAPI (blue). **(A)** The fluorescence levels of glutamate receptors and DAPI were used to quantify receptor expression in glioblastoma (n=5) and metastasis (n=5) tissues as described in detail in the material & methods section. Data are presented as mean ± SEM; *p<0.05 (Student's t-test). **(B)** Negative controls of Alexa Fluor 488 and Cy5-conjugated secondary antibodies. **(C)** Representative images are based on microscopic photographs that were taken at 100× magnification. Bars represent 200 µm.

brain tumors. AMPA receptors contributed to migration and survival of glioma cells (49, 50). Currently, AMPA receptors were found to be enriched at the tumor rim in neuro-gliomal synapsis and mediated fast excitatory postsynaptic currents (29, 31). An inhibition of AMPA receptors by perampanel affected proliferation and survival of glioblastoma cells under *in vitro* conditions (27, 51, 52). However, *in vivo* experiments could not confirm the antitumoral effects (53). In accordance with our study, Brocke et al., 2010 found the AMPA receptor subunit GRIA4 to be highly expressed (25). But no difference between metastasis and primary brain cancers were detected for this AMPA receptor subunit. A second group of ionotropic glutamate receptors with potential biomarker candidates are kainate (KA) receptors. The KA receptor subunits encoded by *GRIK1* and *GRIK4* presented a highly differential expression. So far, KA receptor functions in glioblastoma were scarcely investigated. In agreement with our data, juvenile glioblastoma expressed all five

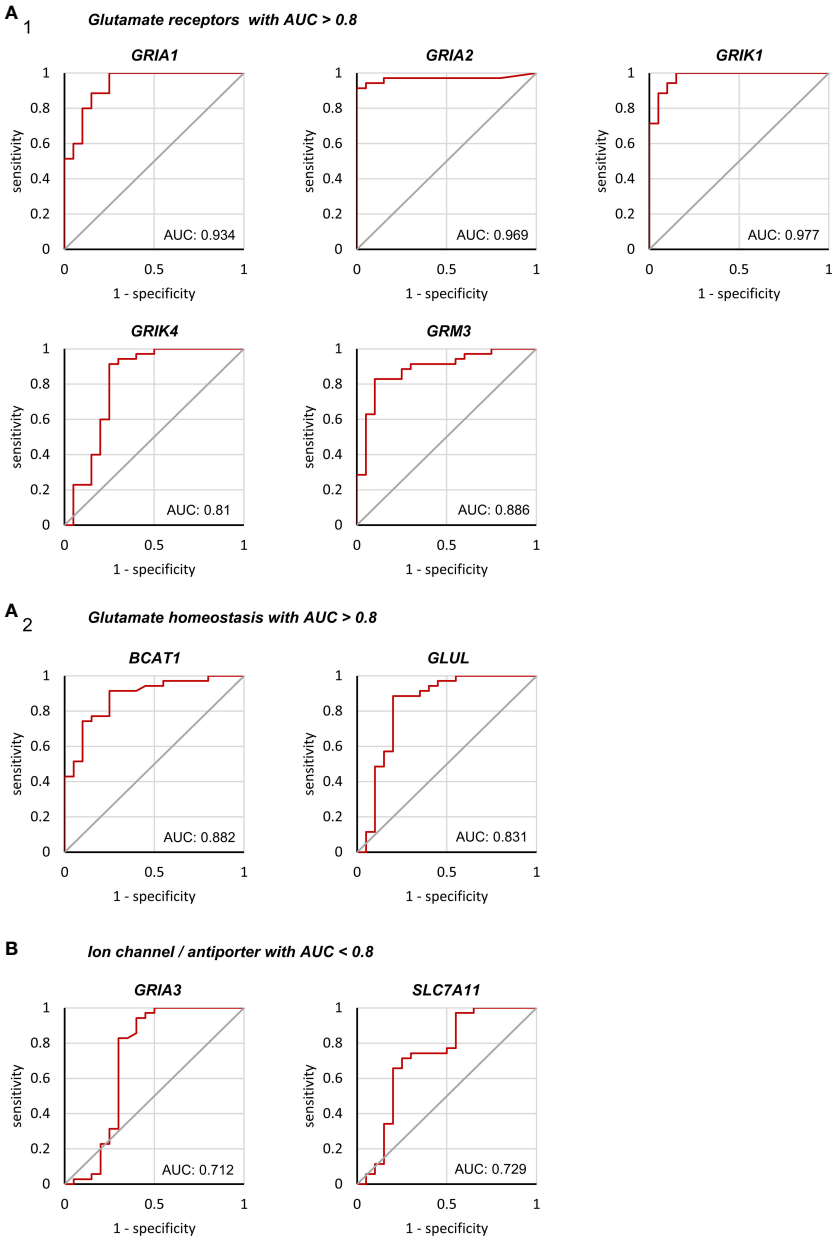

FIGURE 4
Binary classification of Grade 4 glioma/astrocytoma and brain metastasis by receiver operating characteristic analyses. ROC analyses were performed on a total of 55 tissue samples obtained from surgery (n=35 grade 4 glioma/astrocytoma, n=20 brain metastases). Only genes with an AUC>0.8 are presented in **(A_1)** encoding for glutamate receptors and **(A_2)** glutamate homeostasis. **(B)** Both, *GRIA3* and *SLC7A11* failed to reach an AUC>0.8 and were excluded as biomarker candidates (see supplementary 6 and 7 for the remaining genes with AUC<0.8).

subunits of KA receptors (25). KA receptors are primarily expressed in CNS in pre- and post-synaptic membranes, but may also fulfil non-synaptic functions (54). So far, KA receptors were also reported in permanent cell lines including glioblastoma, lung cancer, breast cancer and colon carcinoma (26), but cellular functions remained elusive. Interestingly, NMDA receptors presented no differential expression between both tumor cohorts. Recently, NMDA receptors were identified to be involved in chemoresistance to temozolomide (55) and radiosensitivity (56).

In the group of metabotropic glutamate receptors, mGluR3 (encoded by *GRM3*) was the only receptor subtype with a differential expression, that also was present in a varying protein expression in a subset of the samples. Since, mGluR3 was higher expressed in glioblastoma than most other tumor entities (incl. lung, colon, and breast cancer), it is not an unexpected candidate (57). Our data indicate that the distinction is not primarily due to an overexpression of mGluR3 with respect to other metabotropic glutamate receptors in glioblastoma, but primarily due to a low expression in metastases. In glioblastoma, the expression of mGluR3 is inversely correlated with the survival of patients (57, 58). In preclinical models, an inhibition of mGluR3 *in vitro* revealed antitumoral effects, but failed to prolong survival *in vivo* (57). However, a low expression profile or inhibition of mGluR3 may increase susceptibility to temozolomide (58, 59). In lung cancer, representing the primary origin of more than half of the

10.3389/fonc.2024.1335401

TABLE 2 Youden indices of target gene expressions.

			HGG		MET		HGG+MET
gene	Youden index	ΔCt	correct prediction	% of cohort	correct prediction	% of cohort	accuracy (%)
GRIA1	0.736	4.52	31/35	88.6	17/20	85	87.3
GRIA2	0.914	2.81	32/35	91.4	20/20	100	94.5
GRIK1	0.836	2.85	31/35	88.6	19/20	95	90.9
GRIK4	0.664	1.91	32/35	91.4	15/20	75	85.5
GRM3	0.729	3.55	29/35	82.9	18/20	90	85.5
GLUL	0.686	5.93	31/35	88.6	16/20	80	85.5
BCAT1	0.664	0.13	32/35	91.4	15/20	75	85.5
						total accuracy: ~88%	

metastases in our study, mGluR3 was reported to be absent (26) and for this reason may highly affect the overall expression pattern of the metastases cohort.

In the group of glutamate shuttling and metabolism genes, only *BCAT1* and *GLUL* presented an AUC >0.8. The glutamate-synthesizing aminotransferase BCAT1 (produces glutamate from α-ketoglutarate) may overproduce glutamate in tumors and an upregulation of *BCAT1*, that may in part be driven by hypoxic conditions of fast-growing glioblastoma (60), was associated with poor patient survival (61, 62). As a partner in crime, the glutamine synthetase (GS; encoded by *GLUL*) may be upregulated in high-grade glioma (63), whereas other malignancies presented mixed results (64). Glutamine represents a major component in various metabolic cascades of the tumor cells to address energy consumption and demand of newly synthesized nucleotides (65). Furthermore, a high expression of the enzyme is correlated with the prevalence of seizures and in addition a reduced survival (66). Interestingly, we found only a relatively high but not excellent correlation between xCT expression and tumor origin (AUC=0.729). One reason could be the overexpression of xCT in lung carcinoma (38) and colon carcinoma (67) that could have been preserved in the metastases. In marked contrast, Na^+/glutamate co-transporter EAAT2 described as often downregulated in glioblastoma (22), showed no association between tumor entity and expression at all.

The Youden indices were used as cut-points and ΔCt values were calculated. Since TATA-binding protein (TBP) was used as housekeeping gene, ΔCt values may vary from the proposed values employing different housekeeping genes or adapted real-time PCR conditions. In our analysis, the gene panel was used to predict the correct tumor entity in 88% of the cases. A reduction of genes may reduce the power of prediction. Quite the opposite, including one or more genes away from glutamate signaling may further strengthen the approach. To sum up the functions of our biomarker candidates, the pathophysiological interactions are illustrated in Figure 5. One may speculate that in the long-term our biomarker panel could be integrated after initial imaging of the brain, to help on the decision for a subsequent surgical resection of a high-grade glioma or whether a more conservative therapy should be pursued in case of a brain metastasis.

Tumor-associated epilepsy presents not only a serious impact on the quality of life, but with respect to a status epilepticus, it is a neurological emergency associated with a high mortality. Hence, administration of anticonvulsants for seizure-control is often indicated (68). Anticonvulsants are administered prior to surgery to prevent seizures while excising the tumor mass. Since glutamate-mediated signaling was identified to contribute to both, glioma progression and tumor-associated seizures, targeting glutamate receptors like AMPAR may kill two birds with one stone (10, 11). Remarkably, in our study, no differences of the expression pattern within the glioblastoma cohort with respect to the prevalence of

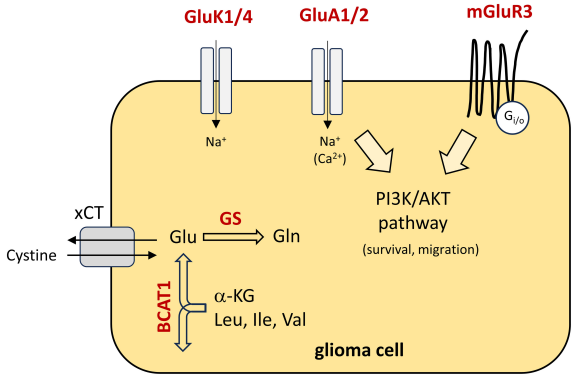

FIGURE 5
Schematic presentation of the pathophysiological function of the biomarker panel in glioma cells. Biomarker candidates are highlighted in red colour and their functions are illustrated. Briefly, in the cytoplasm, glutamate (Glu) is synthesised from α-ketoglutarate (α-KG) and branched-chain essential amino acids by BCAT1. In glioblastoma, glutamate is primarily released via cystine/glutamate antiporter solute carrier family 7 member 11 (xCT). Cystine is an essential precursor for glutathione synthesis, to counteract oxidative stress in fast-growing tumours. In addition, glutamate is catalysed to glutamine (Gln) by glutamine synthetase (GS). With respect to glutamate receptors, the metabotropic receptor mGluR3 is coupled to downstream signalling pathways like the PI3K/AKT pathway and contribute to migration and survival of the tumour cells. In part, AMPA receptors (GluA1/2) may also contribute to an activation of downstream signalling pathways due to calcium influx. Little is known on the function of kainate receptors (GluK1/4). Leu, Leucine; Ile, isoleucine; Val, Valine.

epileptic seizures were found. Epilepsy was less frequent in older patients, which is in line with a previous study by Iuchi et al. (69), though other studies reported no significant difference in age (45, 46). Yuen et al., 2012 reported a correlation of intracellular glutamate levels and seizures (16), but based on our dataset we could not confirm an association of receptor/transporter expression and an epileptic phenotype as previously suggested (16, 70). Since glutamate-mediated signaling was identified to be crucial in tumor growth and invasion (71, 72), glutamate receptor-mediated signaling of tumor-surrounding neurons and astrocytes may be altered.

Why could our expression pattern not distinguish between patients suffering from seizures and those without epilepsy? There could be at least three possibilities. First, the sample size of our study could be underpowered to identify genes associated with seizures. Second, functional pathologies like the disruption of the blood-brain barrier or perturbations of GABAergic neurotransmission may contribute to generation of seizures independent of gene expression (73). Furthermore, an increase in intracranial pressure due to bulk expansion and incidence of brain oedema may also provoke tumor-associated seizures. Those mechanisms may have masked our findings with respect to differential gene expression patterns.

One limitation in our study is the overall sample size. While brain metastases overall are not infrequently diagnosed, the treatment of the primary tumor is often clinically more urgent. As a result, the cranial tumor bulk is closely monitored but only in some cases excised. Obviously, access to a large database of metastases is limited. As we aimed for a feasible approach suitable for everyday use to differentiate high-grade glioma and brain metastasis, our analysis is based on tumor tissue samples expression, but not on single-cells data. Therefore, various cells other than cancer cells such as endothelial cells could also be subjected to expression analysis. One may speculate that single-cell analysis would reveal even more differences in the glutamatergic gene expression pattern.

5 Conclusion

To sum up, we identified seven genes (*GRIA1*, *GRIA2*, *GRIK1*, *GRIK4*, *GRM3*, *GLUL*, *BCAT1*) whose mRNA expression may serve as potential molecular biomarker candidates to distinguish glioblastoma and brain metastases tissue derived from surgical resections. The expression pattern could be of use to support the pathological assessment of the material taken from surgery without further resection volumes. Since a potential limitation of our study is the overall sample size, we encourage other groups to test these candidates to evaluate our proposed panel of genes. Especially, with respect to the xCT expression (*SLC7A11*), further investigations may reveal a higher correlation of the gene expression with glioblastoma.

Data availability statement

The data presented in this study are available on reasonable request from the corresponding author.

Ethics statement

The studies involving humans were approved by Ethics committee of the University Medical Center Rostock St.-Georg-Str. 108 18055 Rostock. The studies were conducted in accordance with the local legislation and institutional requirements. The participants provided their written informed consent to participate in this study.

Author contributions

FL: Data curation, Writing – original draft, Conceptualization, Formal analysis, Visualization. RG: Data curation, Investigation, Visualization, Writing – review & editing. AE: Investigation, Writing – review & editing. KP: Investigation, Writing – review & editing. GR: Data curation, Visualization, Writing – review & editing. CM: Resources, Writing – review & editing. BS: Resources, Writing – review & editing. CH: Resources, Writing – review & editing. DD: Resources, Writing – review & editing. ML: Resources, Writing – review & editing. RK: Writing – review & editing. TF: Resources, Writing – review & editing. TK: Conceptualization, Writing – review & editing.

Funding

The author(s) declare that no financial support was received for the research, authorship, and/or publication of this article.

Acknowledgments

The authors wish to thank Simone Rackow for excellent technical assistance.

Conflict of interest

The authors declare that the research was conducted in the absence of any commercial or financial relationships that could be construed as a potential conflict of interest.

Publisher's note

All claims expressed in this article are solely those of the authors and do not necessarily represent those of their affiliated organizations, or those of the publisher, the editors and the reviewers. Any product that may be evaluated in this article, or claim that may be made by its manufacturer, is not guaranteed or endorsed by the publisher.

Supplementary material

The Supplementary Material for this article can be found online at: https://www.frontiersin.org/articles/10.3389/fonc.2024.1335401/full#supplementary-material

References

1. Barnholtz-Sloan JS, Sloan AE, Davis FG, Vigneau FD, Lai P, Sawaya RE. Incidence proportions of brain metastases in patients diagnosed (1973 to 2001) in the Metropolitan Detroit Cancer Surveillance System. *J Clin Oncol*. (2004) 22:2865–72. doi: 10.1200/JCO.2004.12.149

2. Schaff LR, Mellinghoff IK. Glioblastoma and other primary brain Malignancies in adults: A review. *JAMA*. (2023) 329:574–87. doi: 10.1001/jama.2023.0023

3. Wen PY, Weller M, Lee EQ, Alexander BM, Barnholtz-Sloan JS, Barthel FP, et al. Glioblastoma in adults: a Society for Neuro-Oncology (SNO) and European Society of Neuro-Oncology (EANO) consensus review on current management and future directions. *Neuro-oncology*. (2020) 22:1073–113. doi: 10.1093/neuonc/noaa106

4. Valiente M, Ahluwalia MS, Boire A, Brastianos PK, Goldberg SB, Lee EQ, et al. The evolving landscape of brain metastasis. *Trends Cancer*. (2018) 4:176–96. doi: 10.1016/j.trecan.2018.01.003

5. Fordham AJ, Hacherl CC, Patel N, Jones K, Myers B, Abraham M, et al. Differentiating glioblastomas from solitary brain metastases: an update on the current literature of advanced imaging modalities. *Cancers (Basel)*. (2021) 13:2960. doi: 10.3390/cancers13122960

6. Sunwoo L, Yun TJ, You SH, Yoo RE, Kang KM, Choi SH, et al. Differentiation of glioblastoma from brain metastasis: qualitative and quantitative analysis using arterial spin labeling MR imaging. *PloS One*. (2016) 11:e0166662. doi: 10.1371/journal.pone.0166662

7. Kamimura K, Kamimura Y, Nakano T, Hasegawa T, Nakajo M, Yamada C, et al. Differentiating brain metastasis from glioblastoma by time-dependent diffusion MRI. *Cancer Imaging*. (2023) 23:75. doi: 10.1186/s40644-023-00595-2

8. Romano A, Moltoni G, Guarnera A, Pasquini L, Di Napoli A, Napolitano A, et al. Single brain metastasis versus glioblastoma multiforme: a VOI-based multiparametric analysis for differential diagnosis. *Radiol Med*. (2022) 127:490–7. doi: 10.1007/s11547-022-01480-x

9. Nørøxe DS, Poulsen HS, Lassen U. Hallmarks of glioblastoma: a systematic review. *ESMO Open*. (2016) 1:e000144. doi: 10.1136/esmoopen-2016-000144

10. Huberfeld G, Vecht CJ. Seizures and gliomas–towards a single therapeutic approach. *Nat Rev Neurol*. (2016) 12:204–16. doi: 10.1038/nrneurol.2016.26

11. Lange F, Hörnschemeyer J, Kirschstein T. Glutamatergic mechanisms in glioblastoma and tumor-associated epilepsy. *Cells*. (2021) 10:1226. doi: 10.3390/cells10051226

12. Corsi L, Mescola A, Alessandrini A. Glutamate receptors and glioblastoma multiforme: an old "Route" for new perspectives. *Int J Mol Sci*. (2019) 20(7):1796. doi: 10.3390/ijms20071796

13. Marcus HJ, Carpenter KLH, Price SJ, Hutchinson PJ. *In vivo* assessment of high-grade glioma biochemistry using microdialysis: a study of energy-related molecules, growth factors and cytokines. *J Neurooncol*. (2010) 97:11–23. doi: 10.1007/s11060-009-9990-5

14. Roslin M, Henriksson R, Bergström P, Ungerstedt U, Bergenheim AT. Baseline levels of glucose metabolites, glutamate and glycerol in Malignant glioma assessed by stereotactic microdialysis. *J Neurooncol*. (2003) 61:151–60. doi: 10.1023/a:1022106910017

15. Buckingham SC, Campbell SL, Haas BR, Montana V, Robel S, Ogunrinu T, et al. Glutamate release by primary brain tumors induces epileptic activity. *Nat Med*. (2011) 17:1269–74. doi: 10.1038/nm.2453

16. Yuen TI, Morokoff AP, Bjorksten A, D'Abaco G, Paradiso L, Finch S, et al. Glutamate is associated with a higher risk of seizures in patients with gliomas. *Neurology*. (2012) 79:883–9. doi: 10.1212/WNL.0b013e318266fa89

17. de Bruin ME, van der Meer PB, Dirven L, Taphoorn MJB, Koekkoek JAF. Efficacy of antiepileptic drugs in glioma patients with epilepsy: a systematic review. *Neurooncol Pract*. (2021) 8:501–17. doi: 10.1093/nop/npab030

18. Tabaee Damavandi P, Pasini F, Fanella G, Cereda GS, Mainini G, DiFrancesco JC, et al. Perampanel in brain tumor-related epilepsy: A systematic review. *Brain Sci*. (2023) 13:326. doi: 10.3390/brainsci13020326

19. Chung WJ, Lyons SA, Nelson GM, Hamza H, Gladson CL, Gillespie GY, et al. Inhibition of cystine uptake disrupts the growth of primary brain tumors. *J Neurosci*. (2005) 25:7101–10. doi: 10.1523/JNEUROSCI.5258-04.2005

20. Ye ZC, Rothstein JD, Sontheimer H. Compromised glutamate transport in human glioma cells: reduction-mislocalization of sodium-dependent glutamate transporters and enhanced activity of cystine-glutamate exchange. *J Neurosci*. (1999) 19:10767–77. doi: 10.1523/JNEUROSCI.19-24-10767.1999

21. de Groot JF, Liu TJ, Fuller G, Yung WKA. The excitatory amino acid transporter-2 induces apoptosis and decreases glioma growth in *vitro* and in *vivo*. *Cancer Res*. (2005) 65:1934–40. doi: 10.1158/0008-5472.CAN-04-3626

22. Buccoliero AM, Caporalini C, Scagnet M, Mussa F, Giordano F, Sardi I, et al. Angiocentric glioma-associated seizures: The possible role of EATT2, pyruvate carboxylase and glutamine synthetase. *Seizure*. (2021) 86:152–4. doi: 10.1016/j.seizure.2021.02.014

23. Tönjes M, Barbus S, Park YJ, Wang W, Schlotter M, Lindroth AM, et al. BCAT1 promotes cell proliferation through amino acid catabolism in gliomas carrying wild-type IDH1. *Nat Med*. (2013) 19:901–8. doi: 10.1038/nm.3217

24. McBrayer SK, Mayers JR, DiNatale GJ, Shi DD, Khanal J, Chakraborty AA, et al. Transaminase inhibition by 2-hydroxyglutarate impairs glutamate biosynthesis and redox homeostasis in glioma. *Cell*. (2018) 175:101–116.e25. doi: 10.1016/j.cell.2018.08.038

25. Brocke KS, Staufner C, Luksch H, Geiger KD, Stepulak A, Marzahn J, et al. Glutamate receptors in pediatric tumors of the central nervous system. *Cancer Biol Ther*. (2010) 9:455–68. doi: 10.4161/cbt.9.6.10898

26. Stepulak A, Luksch H, Gebhardt C, Uckermann O, Marzahn J, Sifringer M, et al. Expression of glutamate receptor subunits in human cancers. *Histochem Cell Biol*. (2009) 132:435–45. doi: 10.1007/s00418-009-0613-1

27. Lange F, Weßlau K, Porath K, Hörnschemeyer J, Bergner C, Krause BJ, et al. AMPA receptor antagonist perampanel affects glioblastoma cell growth and glutamate release in vitro. *PloS One*. (2019) 14:e0211644. doi: 10.1371/journal.pone.0211644

28. Salmaggi A, Corno C, Maschio M, Donzelli S, D'Urso A, Perego P, et al. Synergistic effect of perampanel and temozolomide in human glioma cell lines. *J Personalized Med*. (2021) 11:390. doi: 10.3390/jpm11050390

29. Venkatesh HS, Morishita W, Geraghty AC, Silverbush D, Gillespie SM, Arzt M, et al. Electrical and synaptic integration of glioma into neural circuits. *Nature*. (2019) 573:539–45. doi: 10.1038/s41586-019-1563-y

30. Venkataramani V, Tanev DI, Strahle C, Studier-Fischer A, Fankhauser L, Kessler T, et al. Glutamatergic synaptic input to glioma cells drives brain tumour progression. *Nature*. (2019) 573:532–8. doi: 10.1038/s41586-019-1564-x

31. Venkataramani V, Yang Y, Schubert MC, Reyhan E, Tetzlaff SK, Wißmann N, et al. Glioblastoma hijacks neuronal mechanisms for brain invasion. *Cell*. (2022) 185:2899–2917.e31. doi: 10.1016/j.cell.2022.06.054

32. D'Onofrio M, Arcella A, Bruno V, Ngomba RT, Battaglia G, Lombari V, et al. Pharmacological blockade of mGlu2/3 metabotropic glutamate receptors reduces cell proliferation in cultured human glioma cells. *J Neurochem*. (2003) 84:1288–95. doi: 10.1046/j.1471-4159.2003.01633.x

33. Arcella A, Carpinelli G, Battaglia G, D'Onofrio M, Santoro F, Ngomba RT, et al. Pharmacological blockade of group II metabotropic glutamate receptors reduces the growth of glioma cells in *vivo*. *Neuro Oncol*. (2005) 7:236–45. doi: 10.1215/S1152851704000961

34. Ciceroni C, Arcella A, Mosillo P, Battaglia G, Mastrantoni E, Oliva MA, et al. Type-3 metabotropic glutamate receptors negatively modulate bone morphogenetic protein receptor signaling and support the tumourigenic potential of glioma-initiating cells. *Neuropharmacology*. (2008) 55:568–76. doi: 10.1016/j.neuropharm.2008.06.064

35. García-Gaytán AC, Hernández-Abrego A, Díaz-Muñoz M, Méndez I. Glutamatergic system components as potential biomarkers and therapeutic targets in cancer in non-neural organs. *Front Endocrinol*. (2022) 13:1029210. doi: 10.3389/fendo.2022.1029210

36. Rao R, Shah S, Bhattacharya D, Toukam DK, Cáceres R, Pomeranz Krummel DA, et al. Ligand-gated ion channels as targets for treatment and management of cancers. *Front Physiol*. (2022) 13:839437. doi: 10.3389/fphys.2022.839437

37. North WG, Gao G, Jensen A, Memoli VA, Du J. NMDA receptors are expressed by small-cell lung cancer and are potential targets for effective treatment. *CPAA*. (2010) 2:31–40. doi: 10.2147/CPAA

38. Ji X, Qian J, Rahman SMJ, Siska PJ, Zou Y, Harris BK, et al. xCT (SLC7A11)-mediated metabolic reprogramming promotes non-small cell lung cancer progression. *Oncogene*. (2018) 37:5007–19. doi: 10.1038/s41388-018-0307-z

39. Lim JKM, Delaidelli A, Minaker SW, Zhang HF, Colovic M, Yang H, et al. Cystine/glutamate antiporter xCT (SLC7A11) facilitates oncogenic RAS transformation by preserving intracellular redox balance. *PNAS*. (2019) 116:9433–42. doi: 10.1073/pnas.1821323116

40. Herner A, Sauliunaite D, Michalski CW, Erkan M, Oliveira TD, Abiatari I, et al. Glutamate increases pancreatic cancer cell invasion and migration via AMPA receptor activation and Kras-MAPK signaling. *Int J Cancer*. (2011) 129:2349–59. doi: 10.1002/ijc.25898

41. North WG, Liu F, Lin LZ, Tian R, Akerman B. NMDA receptors are important regulators of pancreatic cancer and are potential targets for treatment. *CPAA*. (2017) 9:79–86. doi: 10.2147/CPAA

42. Louis DN, Perry A, Wesseling P, Brat DJ, Cree IA, Figarella-Branger D, et al. The 2021 WHO classification of tumors of the central nervous system: a summary. *Neuro-Oncology*. (2021) 23:1231–51. doi: 10.1093/neuonc/noab106

43. Valente V, Teixeira SA, Neder L, Okamoto OK, Oba-Shinjo SM, Marie SKN, et al. Selection of suitable housekeeping genes for expression analysis in glioblastoma using quantitative RT-PCR. *BMC Mol Biol*. (2009) 10:17. doi: 10.1186/1471-2199-10-17

44. Aronica E, Ciusani E, Coppola A, Costa C, Russo E, Salmaggi A, et al. Epilepsy and brain tumors: Two sides of the same coin. *J Neurol Sci*. (2023) 446:120584. doi: 10.1016/j.jns.2023.120584

45. Berendsen S, Varkila M, Kroonen J, Seute T, Snijders TJ, Kauw F, et al. Prognostic relevance of epilepsy at presentation in glioblastoma patients. *Neuro Oncol*. (2016) 18:700–6. doi: 10.1093/neuonc/nov238

46. Dührsen L, Sauvigny T, Ricklefs FL, Mende KC, Schaper M, Matschke J, et al. Seizures as presenting symptom in patients with glioblastoma. *Epilepsia*. (2019) 60:149–54. doi: 10.1111/epi.14615

47. Sareen H, Ma Y, Becker TM, Roberts TL, de Souza P, Powter B. Molecular biomarkers in glioblastoma: A systematic review and meta-analysis. *Int J Mol Sci*. (2022) 23:8835. doi: 10.3390/ijms23168835

48. Hegi ME, Diserens AC, Gorlia T, Hamou MF, de Tribolet N, Weller M, et al. MGMT gene silencing and benefit from temozolomide in glioblastoma. *New Engl J Med*. (2005) 352:997–1003. doi: 10.1056/NEJMoa043331

49. Ishiuchi S, Tsuzuki K, Yoshida Y, Yamada N, Hagimura N, Okado H, et al. Blockage of Ca(2+)-permeable AMPA receptors suppresses migration and induces apoptosis in human glioblastoma cells. *Nat Med*. (2002) 8:971–8. doi: 10.1038/nm746

50. Ishiuchi S, Yoshida Y, Sugawara K, Aihara M, Ohtani T, Watanabe T, et al. Ca2+-permeable AMPA receptors regulate growth of human glioblastoma via Akt activation. *J Neurosci*. (2007) 27:7987–8001. doi: 10.1523/JNEUROSCI.2180-07.2007

51. Yagi C, Tatsuoka J, Sano E, Hanashima Y, Ozawa Y, Yoshimura S, et al. Anti–tumor effects of anti–epileptic drugs in Malignant glioma cells. *Oncol Rep*. (2022) 48:1–12. doi: 10.3892/or

52. Tatsuoka J, Sano E, Hanashima Y, Yagi C, Yamamuro S, Sumi K, et al. Anti-tumor effects of perampanel in Malignant glioma cells. *Oncol Lett*. (2022) 24:421. doi: 10.3892/ol

53. Lange F, Hartung J, Liebelt C, Boisserée J, Resch T, Porath K, et al. Perampanel add-on to standard radiochemotherapy in *vivo* promotes neuroprotection in a rodent F98 glioma model. *Front Neurosci*. (2020) 14:598266. doi: 10.3389/fnins.2020.598266

54. Contractor A, Mulle C, Swanson GT. Kainate receptors coming of age: milestones of two decades of research. *Trends Neurosciences*. (2011) 34:154–63. doi: 10.1016/j.tins.2010.12.002

55. Tsuji S, Nakamura S, Shoda K, Yamada T, Shimazawa M, Nakayama N, et al. NMDA receptor signaling induces the chemoresistance of temozolomide via upregulation of MGMT expression in glioblastoma cells. *J Neurooncol*. (2022) 160:375–88. doi: 10.1007/s11060-022-04154-w

56. Müller-Längle A, Lutz H, Hehlgans S, Rödel F, Rau K, Laube B. NMDA receptor-mediated signaling pathways enhance radiation resistance, survival and migration in glioblastoma cells-A potential target for adjuvant radiotherapy. *Cancers (Basel)*. (2019) 11:503. doi: 10.3390/cancers11040503

57. Wirsching HG, Silginer M, Ventura E, Macnair W, Burghardt I, Claassen M, et al. Negative allosteric modulators of metabotropic glutamate receptor 3 target the stem-like phenotype of glioblastoma. *Mol Ther - Oncolytics*. (2021) 20:166–74. doi: 10.1016/j.omto.2020.12.009

58. Ciceroni C, Bonelli M, Mastrantoni E, Niccolini C, Laurenza M, Larocca LM, et al. Type-3 metabotropic glutamate receptors regulate chemoresistance in glioma stem cells, and their levels are inversely related to survival in patients with Malignant gliomas. *Cell Death Differ*. (2013) 20:396–407. doi: 10.1038/cdd.2012.150

59. Maier JP, Ravi VM, Kueckelhaus J, Behringer SP, Garrelfs N, Will P, et al. Inhibition of metabotropic glutamate receptor III facilitates sensitization to alkylating chemotherapeutics in glioblastoma. *Cell Death Dis*. (2021) 12:723. doi: 10.1038/s41419-021-03937-9

60. Zhang B, Chen Y, Shi X, Zhou M, Bao L, Hatanpaa KJ, et al. Regulation of branched-chain amino acid metabolism by hypoxia-inducible factor in glioblastoma. *Cell Mol Life Sci*. (2021) 78:195–206. doi: 10.1007/s00018-020-03483-1

61. Yi L, Fan X, Li J, Yuan F, Zhao J, Nistér M, et al. Enrichment of branched chain amino acid transaminase 1 correlates with multiple biological processes and contributes to poor survival of IDH1 wild-type gliomas. *Aging (Albany NY)*. (2021) 13:3645–60. doi: 10.18632/aging.v13i3

62. Cho HR, Jeon H, Park CK, Park SH, Kang KM, Choi SH. BCAT1 is a new MR imaging-related biomarker for prognosis prediction in IDH1-wildtype glioblastoma patients. *Sci Rep*. (2017) 7:17740. doi: 10.1038/s41598-017-17062-1

63. Tardito S, Oudin A, Ahmed SU, Fack F, Keunen O, Zheng L, et al. Glutamine synthetase activity fuels nucleotide biosynthesis and supports growth of glutamine-restricted glioblastoma. *Nat Cell Biol*. (2015) 17:1556–68. doi: 10.1038/ncb3272

64. Castegna A, Menga A. Glutamine synthetase: localization dictates outcome. *Genes (Basel)*. (2018) 9:108. doi: 10.3390/genes9020108

65. Natarajan SK, Venneti S. Glutamine metabolism in brain tumors. *Cancers*. (2019) 11:1628. doi: 10.3390/cancers11111628

66. Rosati A, Poliani PL, Todeschini A, Cominelli M, Medicina D, Cenzato M, et al. Glutamine synthetase expression as a valuable marker of epilepsy and longer survival in newly diagnosed glioblastoma multiforme. *Neuro Oncol*. (2013) 15:618–25. doi: 10.1093/neuonc/nos338

67. Tang B, Zhu J, Liu F, Ding J, Wang Y, Fang S, et al. xCT contributes to colorectal cancer tumorigenesis through upregulation of the MELK oncogene and activation of the AKT/mTOR cascade. *Cell Death Dis*. (2022) 13:1–15. doi: 10.1038/s41419-022-04827-4

68. Sánchez-Villalobos JM, Aledo-Serrano Á, Villegas-Martínez I, Shaikh MF, Alcaraz M. Epilepsy treatment in neuro-oncology: A rationale for drug choice in common clinical scenarios. *Front Pharmacol*. (2022) 13:991244. doi: 10.3389/fphar.2022.991244

69. Iuchi T, Hasegawa Y, Kawasaki K, Sakaida T. Epilepsy in patients with gliomas: incidence and control of seizures. *J Clin Neurosci*. (2015) 22:87–91. doi: 10.1016/j.jocn.2014.05.036

70. Robert SM, Buckingham SC, Campbell SL, Robel S, Holt KT, Ogunrinu-Babarinde T, et al. SLC7A11 expression is associated with seizures and predicts poor survival in patients with Malignant glioma. *Sci Transl Med*. (2015) 7:289ra86. doi: 10.1126/scitranslmed.aaa8103

71. Takano T, Lin JH, Arcuino G, Gao Q, Yang J, Nedergaard M. Glutamate release promotes growth of Malignant gliomas. *Nat Med*. (2001) 7:1010–5. doi: 10.1038/nm0901-1010

72. Lyons SA, Chung WJ, Weaver AK, Ogunrinu T, Sontheimer H. Autocrine glutamate signaling promotes glioma cell invasion. *Cancer Res*. (2007) 67:9463–71. doi: 10.1158/0008-5472.CAN-07-2034

73. Hills KE, Kostarelos K, Wykes RC. Converging mechanisms of epileptogenesis and their insight in glioblastoma. *Front Mol Neurosci*. (2022) 15:903115. doi: 10.3389/fnmol.2022.903115

frontiers | Frontiers in Neurology

TYPE Hypothesis and Theory
PUBLISHED 07 June 2024
DOI 10.3389/fneur.2024.1387958

OPEN ACCESS

EDITED BY
Cesare Zoia,
San Matteo Hospital Foundation (IRCCS), Italy

REVIEWED BY
Andrea Bianconi,
University Hospital of the City of Health and Science of Turin, Italy
Giorgio Carrabba,
University of Milano-Bicocca, Italy

*CORRESPONDENCE
Melike Mut
✉ mm2ee@virginia.edu

RECEIVED 19 February 2024
ACCEPTED 28 May 2024
PUBLISHED 07 June 2024

CITATION
Mut M, Zhang M, Gupta I, Fletcher PT, Farzad F and Nwafor D (2024) Augmented surgical decision-making for glioblastoma: integrating AI tools into education and practice.
Front. Neurol. 15:1387958.
doi: 10.3389/fneur.2024.1387958

Augmented surgical decision-making for glioblastoma: integrating AI tools into education and practice

Melike Mut[1]*, Miaomiao Zhang[2], Ishita Gupta[2], P. Thomas Fletcher[2], Faraz Farzad[1] and Divine Nwafor[1]

[1]Department of Neurosurgery, University of Virginia, Charlottesville, VA, United States, [2]Department of Electrical and Computer Engineering, Department of Computer Science, University of Virginia, Charlottesville, VA, United States

Surgical decision-making for glioblastoma poses significant challenges due to its complexity and variability. This study investigates the potential of artificial intelligence (AI) tools in improving "decision-making processes" for glioblastoma surgery. A systematic review of literature identified 10 relevant studies, primarily focused on predicting resectability and surgery-related neurological outcomes. AI tools, especially rooted in radiomics and connectomics, exhibited promise in predicting resection extent through precise tumor segmentation and tumor-network relationships. However, they demonstrated limited effectiveness in predicting postoperative neurological due to dynamic and less quantifiable nature of patient-related factors. Recognizing these challenges, including limited datasets and the interpretability requirement in medical applications, underscores the need for standardization, algorithm optimization, and addressing variability in model performance and then further validation in clinical settings. While AI holds potential, it currently does not possess the capacity to emulate the nuanced decision-making process utilized by experienced neurosurgeons in the comprehensive approach to glioblastoma surgery.

KEYWORDS

glioblastoma, artificial intelligence, machine learning, deep learning, surgical decision making, connectomics, resection

Introduction

High-grade gliomas (HGG) stand as the most prevalent and deadly primary malignant brain tumors in adults. Among these, glioblastoma (GBM) is the most frequent malignant brain tumor, constituting 14.2% of all tumors and 50.9% of all malignant tumor. In the United States, its incidence is reported at 3.27 per 100,000 population. Typically affecting individuals with a median age of 65 years, GBM exhibits a remarkably poor overall survival, despite the implementation of combined radio-chemotherapy. Survival durations typically range between 15 and 17 months, with a median survival of only 8 months (1).

The decision-making process for surgical interventions in patients with GBM is inherently challenging, suffering from a lack of clear guidelines, particularly regarding the choice between biopsy and resection. Surgeons are confronted with the intricate task of assessing resectability, carefully balancing the advantages of decompression and cytoreduction against the potential neurological consequences. Navigating the diverse clinical landscape characterized by varied

glioma molecular subtypes, tumor locations, sizes, eloquent area involvement, and co-existing medical complexities poses a formidable challenge (2).

Moreover, while individual surgeons manifest considerable variability in their clinical judgment regarding surgical resectability, aggregated responses from a large number of surgeons prove to be more consistent and predictive. Sonabend et al. (3) demonstrated a robust correlation between surgical resectability in GBM patients and defined GBM resectability through the wisdom of the crowd. Their study, derived from the pooled responses of 13 surgeons and the percentage of contrast-enhancing tumors, revealed a significant correlation. Despite notable variability in individual surgical goals among neurosurgeons, the resectability index, derived from the pooled responses of surgeons, exhibited a strong correlation with the percentage of contrast-enhancing residual tumor.

Recognizing cognitive biases and understanding decision-making processes are pivotal in enhancing patient care, especially in neurosurgery where errors carry significant consequences. The Dual Process Theory (DPT) illuminates two cognitive processes – analytical and rapid, unconscious and biased implicit processes. Despite the prevalent belief in analytical decision-making, much of daily clinical decisions are influenced by the rapid and unconscious implicit system, leading to inherent human biases (4). The growing adoption of AI, machine learning (ML), and deep learning (DL), particularly with the analysis of extensive datasets, presents a compelling foundation for developing an AI-based prediction and probably decision-making systems.

AI encompasses the use of computers and technology to mimic intelligent behavior and critical thinking, similar to humans. Within AI, ML is a subset that employs methods capable of automatically identifying patterns in data for predicting future data or making decisions under uncertainty. The learning process in ML can take the form of supervised or unsupervised learning. Supervised learning establishes a pattern connecting inputs to outputs using a labeled set of input–output pairs, for tasks like classification and regression. In contrast, unsupervised learning extracts patterns or structures from input data without relying on labeled data or predefined outcomes. Such learning algorithms extract patterns from input data without predefined outcomes, revealing insights that may not be immediately apparent, for example, personalized treatment strategies and hidden disease patterns. ML/AI techniques have become increasingly important in healthcare applications, providing innovative solutions to various challenges in clinical settings (Table 1). For example, supervised learning methods, such as classification and regression, are often developed for disease diagnostics and prediction, as well as stratifying individuals based on risk factors. Notably, ML algorithms have been shown to analyze medical imaging data using Convolutional Neural Networks (CNNs)-based networks, enabling accurate and efficient detection of anomalies in radiology or pathology images (11, 12). The integration of DL, ensemble methods, and reinforcement learning further improves the capabilities of ML applications in healthcare, paving the way for more precise diagnostics, optimized treatment strategies, and improved patient outcomes. As these techniques continue to evolve, they hold the potential to transform healthcare delivery, making it more personalized, efficient, and data driven.

In recent years, AI applications in medicine, spanning various medical specialties, have experienced significant growth. A notable advancement in radiology involves the transformation of biomedical images, such as magnetic resonance imaging (MRI), into mineable data, coupled with their analysis using AI techniques—commonly referred to as "radiomics" (13). Radiomics aims to extract quantitative and reproducible information from diagnostic images, focusing on the analysis of complex patterns that may be challenging for the human eye to discern or quantify. This approach entails capturing properties of tissues and lesions, including shape and heterogeneity. In the realm of brain tumors, radiomic research is dedicated to identifying features that describe the tumor and its microenvironment. The overarching objective is to construct predictive models for various tumor variables and patient outcomes. Notably, these radiomic models surpass their clinical counterparts in performance, offering predictions for outcomes in GBM, such as overall survival (OS), progression-free survival, molecular subtypes, and genetic alterations (13). The literature is increasingly featuring AI tools designed to predict the resectability of GBM. Table 1 summarizes some of the methodologies, evaluation techniques, and outcomes for AI/ML models in glioma imaging and prediction.

The main goal of this study is to conduct a thorough literature review, concentrating on current AI tools. The objective is to analyze a wide range of predictive factors, both tumoral and non-tumoral, along with their potential interactions. This review explores the use of AI tools in the context of surgical decision-making for GBM patients, with a specific focus on predicting resectability and surgery related early postoperative neurological outcomes.

Methods

The literature search for the study involved the use of three bibliographic databases (Pubmed, Web of Science, Google Scholar, and Scopus) from their respective inception date to January 2024. The search term constructs used in all three databases were "connectomics" or "radiomics" and "AI" or "deep learning" or "machine learning" and "glioblastoma" and "surgical" or "decision making." This search string generated a total of 117 articles. Two investigators (AMM and FF) independently screened the titles, abstracts, and full texts retrieved from all three databases to determine the eligibility of the studies. Publications outside the scope of neurosurgery, preclinical studies, non-peer reviewed, duplicates, and GBM/HGG studies focused on AI or ML at the molecular level were excluded from the study. The study's inclusion criteria involved the application of an AI model developed by the researchers to patients with GBM. The focus was on using the AI model for surgical decision-making, specifically assessing resectability and estimating surgery-related neurological outcomes and complications. Out of the 117 studies generated, only 10 studies were included in this study.

Results

Studies utilizing AI tools in surgical decision-making are grouped under 2 headings: predicting resectability and predicting postoperative complications and neurological outcome. The studies are listed in Table 2.

TABLE 1 Examples of AI tools for glioma imaging and prediction.

Focus of the Study	Methodology	Evaluation Technique	Outcome/Performance	Remarks
Predicting surgical resectability (5)	Artificial NN	Receiver Operator Characteristic (ROC) curves; Area Under Curve (AUC) and accuracy calculations	AUC of 0.87–0.92; Accuracy of 83–87%	Compared against logistic regression and a standard grading system
Differentiation between non-enhancing tumor and vasogenic edema (6)	Support Vector Machine (SVM) Classifier	ROC analysis	Misclassification error reduced to 2.4% with post-processing	Utilized T1 perfusion MRI parameters
Prediction of tumor recurrence or necrosis (7)	Convolutional NN combined with Long Short-Term Memory (CNN-LSTM)	AUC, AUPRC, F1-score	AUC of 0.83; AUPRC of 0.87; F1-score of 0.74	Combined MRI data and clinical features
Differentiating vasogenic edema from non-enhancing tumor (8)	DL with multimodal MRI	Accuracy, sensitivity, specificity	Accuracy up to 90.3%; sensitivity and specificity significantly better than neurosurgeons	Histology examination of the resected tissue for validation
Differentiation between pseudo-progression and true progression (9)	DL model	ROC analysis; Leave-one-out cross-validation	AUC up to 0.92; Accuracy up to 87% for predicting PsP	Utilized preoperative and intraoperative MRI data
Predicting regions of local recurrence in GBM (10)	ML with voxel-based radiomic features	AUC, Accuracy, Precision, Recall, F1 Score, Cohen's Kappa	AUC of 0.81 ± 0.09, Accuracy of 0.84 ± 0.06, Precision of 0.48 ± 0.24, Recall of 0.76 ± 0.22, F1 Score of 0.53 ± 0.17, Cohen's Kappa of 0.45 ± 0.18	Utilized postoperative MRI data

NN, Neural network; DL, Deep learning; ML, Machine Learning; MRI, Magnetic resonance imaging.

Predicting resectability

Numerous prior studies conducting volumetric assessments and assessing resection extent have concentrated on the percentage of the removed tumor volume. A classification system that integrates both relative tumor reduction and absolute residual tumor volume has been suggested. However, there is a presumption that the absolute residual volume might carry more significance as a prognostic factor than the relative reduction of tumor volume. In 2022, the Response Assessment in Neuro-Oncology (RANO) Resect Group introduced a revised classification system, which, in contrast to the earlier systems, incorporates only absolute residual tumor volumes. Upon application of the resulting extent of resection (EOR) classification system, distinct survival outcomes were observed among the respective categories. Patients stratified into "supramaximal contrast enhancing (CE) resection" demonstrated superior outcomes compared to those with "maximal CE resection," with the latter group being superior to patients with "submaximal CE resection." Patients designated as "biopsy" exhibited the least favorable progression-free survival (14). The findings of this study offer a basis for developing an AI-powered prediction system to evaluate the extent of resection in gliomas.

Segmentation proves valuable not only for evaluating tumor borders but also for AI tools to efficiently segment and quantify the volume of both CE and non-CE areas of GBMs. An integral aspect of image processing in GBM, characterized by heterogeneity, is the precise segmentation of distinct tumor components, including viable tumor, edema, and necrosis. Fathi Kazerooni et al. (15) utilized a semi-automatic multi-parametric approach, integrating anatomical magnetic resonance imaging (MRI) with physiological modalities like diffusion-weighted imaging (DWI) and perfusion-weighted imaging (PWI). Thirteen GBM patients underwent T2-weighted imaging, PWI, and DWI. The spatial fuzzy C-means algorithm combined with region growing enhanced the delineation of pathogenic regions. The multi-parametric approach, coupled with semi-automatic segmentation, demonstrated a sensitivity, specificity, and dice score exceeding 80%, showcasing its potential for precise tumor characterization and efficient pre-surgical treatment planning.

Marcus et al. (16) developed a grading system based on preoperative MRI features to predict surgical resectability in gliomas. The study utilized an artificial neural network (NN) for improved prediction compared to traditional methods. The grading system incorporated anatomical features from pre-operative MRI, including the contrast-enhancing tumor was within 10 mm of the ventricles; bilateral location if the contrast-enhancing tumor extended into the corpus callosum; eloquent location if the tumor extended into motor or sensory cortex, language cortex, insula, or basal ganglia; large size if the diameter exceeded 40 mm; and associated edema if hypointensity extended more than 10 mm from the contrast-enhancing tumor. Each feature was equally weighted, and lesions were categorized based on the sum of points; as low (0–1 points), moderate (2–3 points), or high complexity (4–5 points). The study demonstrated varying rates of complete removal of CE tumors, ranging from 3.4% in high complexity lesions to 50.0% in low complexity lesions. Despite study limitations, including a small dataset and retrospective design, the authors believe the ANN can aid surgical decision-making and contribute to more meaningful comparisons in future research.

Kommers et al. (17) proposed a Standardized Glioblastoma Surgery Imaging Reporting and Data System (GSI-RADS) based on an automated method of tumor segmentation to provide standardized reports on tumor features relevant for GBM surgery. Tumor parts were segmented using both a human rater and an automated algorithm, and the extracted tumor features were compared. The study

TABLE 2 Studies utilizing AI tools in surgical decision-making.

Author, Year	Data	AI model description
Fathi-Kazerooni, 2015	MRI	DL for segmentation, using advanced NN to delineate tumor boundaries
Marcus, 2020	MRI	Artificial NN to recognize complex patterns in imaging data
Kommers, 2021	MRI	Deep NN for enhanced segmentation, along with sophisticated algorithms for tumor and tissue differentiation
Zanier, 2023	*Multimodal Brain Tumor Segmentation Challenge (BraTS)*	ML for tumor segmentation
Yeung, 2021	Connectome	ML with a connectome-based approach, analyzing brain network connectivity to assess tumor impact
Osipowicz, 2023	Connectome	Connectomics software [for analyzing T1 MRI, DWI and resting-state fMRI data and Hollow-tree Super (HoTS) method for mapping and analyzing abnormal brain connectivity]
Morell, 2022	Connectome	Connectomics platform, a ML tool for comprehensive brain network mapping and analysis to make surgical decisions
Luckett, 2023	Resting State fMRI	3D convolutional NN for fMRI data, extracting features from brain activity patterns to predict surgical outcomes
Caverzasi, 2016	Residual bootstrap q-ball fiber tracking	ML for DTI analysis for surgical planning
Ille, 2022	nTMS, Connectome	Integrated ML for non-invasive mapping with nTMS and connectome data to enhance surgical accuracy

ML, Machine learning; DL, Deep Learning; NN, Neural network; MRI, Magnetic resonance imaging; DWI, diffusion weighted imaging; DTI, Diffusion tensor imaging; fMRI, Functional Magnetic resonance imaging; nTMS, Navigated transcranial magnetic stimulation.

demonstrated agreement between automated and manual segmentations in various tumor features, including laterality, contralateral infiltration, tumor volumes, multifocality, location profiles, residual tumor volumes, resectability indices, and tumor probability maps via an open access software.

Zanier et al. (18) developed and validated a ML model for segmentation on MRI scans, enabling the assessment of percentage-wise tumor reduction post-intracranial surgery for gliomas. The preoperative segmentation model (U-Net) utilized MRI scans from 1,053 patients from the Multimodal Brain Tumor Segmentation Challenge (BraTS) 2021 and those who underwent surgery at the University Hospital in Zurich. Evaluation was conducted on a holdout set of 285 images from the same sources. The postoperative model was created with 72 scans and validated on 45 scans from the BraTS 2015 and Zurich dataset. The algorithm determined the extent of resection in 44.1% of the cases.

The conventional strategy in surgical neuro-oncology aims to preserve function in eloquent areas, primarily within the left dominant hemisphere to prevent aphasia. In non-eloquent regions, particularly outside the left perisylvian areas, surgery is often performed in asleep patients, potentially utilizing motor-evoked potentials to prevent hemiplegia in cases involving or near the central area. Surgical selection and planning traditionally focus on the local topography of the glioma, with limited considerations for the entire brain circuitry. However, the emerging field of mapping macro-scale neural connectivity has led to a reevaluation of classical cognitive models. This paradigm shift advocates moving from a localized understanding of brain processing to adopting a meta-networking theory of cerebral functions (19). Adopting the perspective of dynamic interactions characterized by fluctuations between segregation and integration in functional connectivity, contemporary surgical neuro-oncology is oriented toward achieving a connectome-based resection (20). This entails removing the diffuse neoplasm until real-time detection of critical cortico-subcortical circuits that underlie various functions such as movement execution, somatosensory feedback, visual function, visuospatial cognition, language (including articulatory, phonological, verbal semantic, and syntactic processing), and higher cognitive functions like executive functions (notably working memory and mental flexibility), multimodal semantics, and mentalizing. A notable insight is the substantial variability observed at the cortical level, contrasting with minimal variability at the subcortical level. A two-level model of inter-individual variability proposed by Duffau is characterized by high cortical variation and low subcortical variation suggests careful assessment of connectomics for surgical planning (21).

Many researchers performed AI tools to predict the resectability based on connectomics to better assess the postoperative neurological outcome. Connectomics, the investigation of the brain's entire neural connections, known as the 'connectome,' is centered around the complex white matter pathways responsible for transmitting information between cortical and subcortical structures. The initiation of the Human Connectome Project (HCP) in 2010 has been a driving force behind the surge in interest in connectomics within both cognitive neuroscience and neurosurgery, serving as a watershed moment, instigating extensive exploration into the realm of functional brain connectivity. The persistent effort to unravel the intricate functional networks and connections within the nervous system remains an area of compelling potential for glioma surgery (22).

The definition of eloquence in neurosurgery has evolved, with the primary objective of brain tumor surgery being the optimal balance between oncologic treatment and preserving neurological function (23). While maximizing tumor resection enhances survival, the occurrence of new postoperative neurological deficits diminishes quality of life and overall survival (24–26). Traditional preoperative mapping methods focus on eloquent areas such as language, visual, and sensorimotor networks. However, these techniques, including diffusion tensor imaging (DTI), navigated transcranial magnetic stimulation (rTMS), and functional MRI, present logistical challenges and require specialized personnel (27). Beyond traditional eloquent areas, non-traditional regions affecting personality,

executive function, visuospatial abilities, metacognition, semantic memory, and other cognitive functions also impact patients' quality of life. Understanding and preserving these non-traditional eloquent areas, encompassing salience, default mode, limbic, central executive, and dorsal attention networks, is crucial. Moving beyond a localizationist paradigm, the modern brain mapping approach recognizes function within large-scale brain networks and sub-networks, rather than fixed anatomical areas. To minimize the risk of neurologic deficits, it is imperative to develop mapping tools capable of identifying both traditional and non-traditional eloquent areas. Quicktome™, a novel cloud-based platform utilizing machine-learning and reparcellation techniques, addresses the limitations of existing technologies by accurately mapping brain networks in anomalous anatomy, such as brains with tumors. Quicktome™ was developed through the integration of machine-learning techniques to produce reliable visualizations of crucial brain networks. These visualizations can be utilized in conjunction with standard neuronavigation, aiming to reduce the occurrence of deficits (28, 29).

The potential of Quicktome™ appears promising for evaluating the influence of brain tumors on large-scale networks, including both traditional and non-traditional eloquent areas, during preoperative planning. Morrell et al. (30) used this machine-learning platform to evaluate eloquent brain regions in patients undergoing brain tumor resection, employing a thorough analysis of large-scale brain networks. Of the 100 participants, the central executive network exhibited the highest incidence of alteration (49%), followed by the default mode (43%) and dorsal attention networks (32%). Notably, patients with preoperative deficits demonstrated a significantly higher number of affected networks compared to those without deficits (average 3.42 vs. 2.19, $p < 0.001$). Moreover, individuals without neurologic deficits manifested 2.19 affected and 1.51 at-risk networks, predominantly associated with non-traditional eloquent areas ($p < 0.001$). Even in patients lacking evident deficits on standard neurologic exams, non-traditional eloquent areas were frequently affected. Integrating machine-learning techniques for non-invasive brain mapping into clinical practice holds promise for preserving higher-order cognitive functions linked to these affected networks in neuro-oncology patients.

Luckett et al. (31) introduced a 3D Convolutional Neural Network (3DCNN) designed for mapping language and motor resting-state networks using minimal resting-state functional MRI (RS-fMRI) data. The 3DCNN, trained on diverse datasets, demonstrated a robust 96% out-of-sample validation accuracy. Control data comparisons revealed an impressive 97.9% similarity in mappings with 50 or 200 RS-fMRI time points. In patients with GBM multiforme, the 3DCNN accurately mapped language and motor networks, showcasing its effectiveness in presurgical planning. The study revealed the AI potential of the 3DCNN in revolutionizing preoperative planning for GBM multiforme resection, emphasizing the significant reduction in scan time and improved surgical outcomes.

Cepeda et al. (10) assessed a predictive model for identifying future recurrence areas in GBM using voxel-based radiomics analysis of MRI data. Conducted across multiple institutions, the retrospective analysis included GBM patients who underwent complete resection of enhancing tumors, with 55 meeting the study criteria. The cohort was divided into training ($N = 40$) and testing ($N = 15$) sets. Follow-up MRI provided ground truth for defining recurrence, while postoperative multiparametric MRI enabled extraction of voxel-based radiomic features. Deformable co-registration aligned MRI sequences, facilitating segmentation of the peritumoral and enhancing tumor regions. Voxels overlapping between these areas were labeled as recurrence, others as nonrecurrence. Four machine learning classifiers were trained, with the Categorical Boosting (CatBoost) model achieving the best performance on the test set (AUC = 0.81 ± 0.09, accuracy = 0.84 ± 0.06) using region-based evaluation. The study demonstrated accurate prediction of future recurrence regions, suggesting potential benefits for optimizing surgical and radiotherapy strategies to enhance patient survival in glioblastoma.

Predicting postoperative complications and neurological outcome

Although complete resection is linked to improved survival, it poses risks of neurological deficits, occurring in approximately 1 in 10 patients (32). A crucial determinant of survival outcomes is the development of new postoperative neurological impairments, especially among patients aged over 60, those experiencing at least one new impairment exhibited the poorest survival outcome (median of 11.6 months), whereas those without new impairments achieved the best outcome (median of 28.4 months) after the complete resection of contrast enhancing tumor (24). The repercussions of these deficits can be profound, impacting both the quality of life and, ultimately, the survival of individuals affected by GBM. Choosing a universally applicable surgical modality stands as the first crucial step in the treatment of gliomas.

Predicting the outcome of a surgical procedure is a multifaceted and intricate decision-making process that takes into consideration various parameters. This encompasses factors specific to the tumor, individual patient characteristics, elements related to the health system, and considerations tied to the surgeon's expertise. These considerations encompass the accessibility of surgical tools, the patient's frailty, neurological condition, existing comorbidities, and even psychological aspects. Additional factors such as geographical location, ethical and social considerations, healthcare and malpractice systems, and the availability of post-operative management and care by the neuro-oncology team add layers of complexity to this prediction. Surgeon-related factors also play a crucial role in this comprehensive assessment. The surgeon's experience and their approach to the functional neurooncology concept are pivotal elements in this convoluted assessment. Gerritsen et al. (2) conducted a survey with 224 responses from neurosurgeons across 41 countries, predominantly male (90.2%) and with diverse practice settings. The study revealed significant differences in decision-making processes among neurosurgeons, particularly between academic and non-academic/private practice respondents and European vs. US neurosurgeons. Key factors influencing treatment choice for GBM patients included tumor location, preoperative patient functioning, and neurological morbidity. While most agreed on resection followed by adjuvant therapy as the best choice, nearly a quarter favored biopsy in older patients, citing a perceived risk of morbidity outweighing survival benefits. Perioperative factors influencing an aggressive or defensive approach varied based on surgeon experience, practice setting, and

geographical location. Tumor location and eloquence were deemed crucial factors, with differences observed in responses related to the location of tumors in or near eloquent areas. The study emphasized the impact of multidisciplinary neuro-oncology tumor boards and highlighted varying perspectives on age-related considerations in GBM surgery.

Efforts to formulate the decision-making process have been made in the literature. Ferroli et al. (33) devised the Milan Complexity Scale as a result of a study that evaluated consecutive elective tumor resection surgeries. This scale aims to predict neurological clinical deterioration post-surgery, incorporating factors such as tumor size, cranial nerve manipulation, brain vessel manipulation, posterior fossa location, and involvement of eloquent areas. The retrospective study, involving 746 patients with meningiomas and GBMs, produced a grading scale ranging from 0 to 8, where higher scores suggest a potential worse clinical outcome. No AI-based system has utilized this score to predict postoperative outcomes, and its applicability may be further challenged by the evolving definition of "eloquence."

Our search revealed only two studies to predict postoperative complication or surgical outcome by AI tools.

Caverzasi et al. (34) used a residual bootstrap q-ball fiber tracking to map language pathways and rated tract injury impact on language function after glioma resection. Residual bootstrap q-ball fiber tracking was used to segment eight language pathways in 35 glioma patients. The rating scale for pathway damage significantly correlated with language performance. Preservation of the left arcuate fasciculus and superior longitudinal fasciculus correlated with no long-term deficits, while damage ensured deficits. The authors predict long-term language deficits post-surgery based on white matter tract integrity.

Ille et al. (27) enrolled 60 non-aphasic patients with left hemispheric perisylvian gliomas to investigate the prediction of surgery-related aphasia (SRA) based on function-specific connectome network properties under different fractional anisotropy thresholds combining navigated transcranial magnetic stimulation. Preoperative connectome analysis helped predict SRA development with an accuracy of 73.3% and sensitivity of 78.3%. This study provided a new perspective of function-specific connectome analysis to investigate language function in neurooncological patients. A preoperative connectome analysis seems promising to perform risk assessments predicting the development of postoperative neurological deficit.

Discussion

The optimal surgical approaches for GBM remain a subject of ongoing debate among surgeons due to the intricate heterogeneity of gliomas, including factors such as location, grade, and patient-specific considerations. The AI tools have emerged as transformative elements in addressing these challenges, enhancing resectability and outcome prediction by capturing intricate relationships among variables. Real-time decision support, integrating automated segmentation systems with immediate feedback during preoperative and intraoperative evaluations, is a groundbreaking concept empowering neurosurgeons to make informed decisions based on imaging data.

The advancement and deployment of advanced AI algorithms are pivotal in enhancing imaging capabilities for GBM surgery. These algorithms excel in precisely delineating tumors and continuously refining their performance through learning from diverse datasets. The utilization of DL techniques becomes essential for managing the intricate patterns and variability inherent in GBM imaging. Integration of multimodal imaging, incorporating data from functional MRI, diffusion tensor imaging (DTI), and positron emission tomography (PET), offers a comprehensive perspective of tumors and surrounding structures, thereby enhancing diagnostic precision and treatment strategies. Bianconi et al. (35) demonstrated the effectiveness of an automated U-Net algorithm for GBM segmentation in clinical MRI datasets, both before and after surgery. Their validated approach addresses challenges such as low-quality imaging and improves the reliability of postoperative assessments, crucial for advancing surgical planning and prognostic predictions in neuro-oncology.

While preoperative connectome analysis holds promise for predicting the risk of neurological deficits before surgery, the challenge lies in developing an AI system to evaluate postoperative complications and neurological outcomes. Creating such a system would provide neurosurgeons with access to an evidence-based therapeutic blueprint tailored to the diverse needs of individual patients. Future AI models in intracranial tumor surgery may draw insights from existing literature based on surgeons' predictions for surgery related neurological outcomes and postoperative complications. The dependence on surgeons' predictions, whether through AI tools or other methods, presents a fundamental flaw. Currently, there is a lack of studies, including those involving AI tools, specifically focused on developing a tool for predicting postoperative deterioration or surgical outcomes. Surgeons typically make treatment decisions based on factors such as tumor location, size, and interaction with surrounding structures. In a prospective study involving 299 patients undergoing intracranial tumor surgery, neurosurgeons displayed a consistent tendency to overestimate postoperative functional levels, especially regarding the ability to perform normal activities at 30 days. The assessment, using the Karnofsky Performance Scale, revealed that neurosurgeons underestimated in 15% of cases, accurately estimated in 23%, and overestimated in 62% (36). Future AI models in intracranial tumor surgery may draw from existing literature based on surgeons' predictions for surgical outcomes and postoperative complications. However, it is noted that despite the significance of functional status, surgeons tend to exhibit an overly optimistic bias when predicting postoperative functional levels. The challenge lies in developing an AI system based on predictions with limited accuracy and value. Since surgeons often exhibit an overly optimistic bias when predicting postoperative functional levels, shared decision-making, involving patients in complex treatment choices, is considered a viable approach. Nevertheless, accurately predicting the impact and trajectory of deficits, along with their implications for the quality of life, remains a challenging endeavor (37–42). Designing an AI system to assess postoperative complications and neurological outcomes, granting neurosurgeons access to an evidence-based therapeutic blueprint for a diverse range of individual patients, presents a challenging task.

Utilizing AI tools in the education and training of residents raises additional concerns. A proactive approach is crucial to mitigate biases and enhance decision-making quality, beginning with acknowledging inherent biases in thought processes. Many clinicians, particularly during their early training years, lack formal education

on the cognitive aspects of medical decision-making and bias recognition. Therefore, the introduction of training programs, especially in graduate medical education, becomes essential. These programs should empower physicians to identify cognitive biases, understand decision-making processes, and reflect on past errors. Integrating AI into such programs could further enhance bias recognition and decision-making by providing data-driven insights, potentially transforming the way physicians navigate cognitive challenges throughout their careers (4).

Limitations and challenges

The application of AI in neurosurgery introduces both promise and challenges. To effectively leverage AI in this field, several key considerations and hurdles must be addressed.

- Dataset Challenges:
  - Extensive datasets are essential for AI training, but often lack verification in clinical settings.
  - Variability in model performances and controversial findings add complexity.
- Radiomic Workflow Optimization:
  - Optimizing parameters in radiomic workflows, covering tumor segmentation, feature extraction, and model training, is crucial.
  - Comparing multiple ML algorithms within the same population is vital for understanding performance impacts.
- Focus on Resectability Prediction:
  - Current studies predominantly focus on developing AI tools for predicting resectability.
  - Surgeons base treatment decisions on factors such as tumor location, size, and interaction with surrounding structures.
- Challenges in Predicting Neurological Outcomes:
  - AI faces hurdles in predicting postoperative neurological outcomes.
  - Data quality and quantity are critical, emphasizing the need for interpretability in medical applications.
- Surgeon Bias and Shared Decision-Making:
  - Surgeons tend to exhibit an optimistic bias in predicting postoperative functional levels.
  - Shared decision-making, involving patients in complex treatment choices, is considered viable.
- Clinical Validation for Generalizability:
  - Clinical validation is a rigorous requirement to ensure the reliability and generalizability of AI models.
  - Testing models on independent datasets and diverse patient populations is necessary.
- Collaboration and Continuous Feedback:
  - Collaboration with research institutions and participation in clinical trials are imperative.
  - Establishing a continuous feedback loop in AI systems is pivotal for ongoing improvements and knowledge incorporation, in accuracy, and reliability.
- Ethical and Regulatory Considerations:
  - Patient privacy, transparent decision-making, and adherence to regulatory standards are critical ethical and regulatory considerations.
  - Responsible integration of AI in neurosurgery is essential for patient safety and trust.
- AI in Education and Training:
  - Using AI tools in the education and training of residents raises concerns without establishing formal education based on established curriculum.
  - A proactive approach is crucial, starting with acknowledging inherent biases in thought processes.
  - Introducing training programs, particularly in graduate medical education, becomes essential, with the potential integration of AI to enhance bias recognition and decision-making.

Addressing these challenges and considerations is essential for the successful integration of AI in neurosurgery. This involves not only technical advancements but also ethical, regulatory, and educational initiatives to ensure the responsible and effective use of AI in improving patient outcomes.

Future directions

AI relies significantly on high-quality and annotated data for accurate and trustworthy predictions. Particularly, the fields of radiomics and connectomics are advancing, incorporating enhanced imaging technologies. Collaboration with research institutions and participation in clinical trial initiatives remains imperative for integrating automated segmentation systems into ongoing studies. This collaborative effort contributes valuable data to research endeavors focused on understanding GBM heterogeneity, treatment responses, and patient outcomes. Establishing a continuous feedback loop in AI systems, wherein the system learns from new patient data and outcomes, is pivotal. This iterative process leads to ongoing improvements in accuracy, reliability, and the incorporation of emerging knowledge in GBM research. Looking ahead, the goal is to enhance automated GBM segmentation and reporting systems, ultimately improving patient care and contributing to a deeper understanding of GBM radiomics and connectomics. While navigating through these challenges and considerations, the integration of AI tools in GBM management has immense potential for advancing patient care, refining treatment strategies, and contributing to the broader comprehension of surgical decision making.

Conclusion

The primary aim is to contribute to comprehensive effectiveness research and offer valuable insights for well-informed decision-making in surgeries for GBM. An innovative AI system should seamlessly integrate imaging, radiomics, RANO criteria, resectability studies, and connectomics, along with surgery related neurological outcomes, to enhance assessment and contribute to education and training. Despite challenges, these approaches are transforming medicine, and healthcare providers should prepare for the era of AI. However, it is crucial to acknowledge that despite these advancements, the technology remains distant from replicating the nuanced and educated decision-making of an experienced neurosurgeon.

Data availability statement

The raw data supporting the conclusions of this article will be made available by the authors, without undue reservation.

Author contributions

MM: Conceptualization, Data curation, Formal analysis, Investigation, Methodology, Supervision, Visualization, Writing – original draft, Writing – review & editing. MZ: Data curation, Investigation, Supervision, Writing – review & editing. IG: Investigation, Writing – review & editing. PF: Supervision, Writing – review & editing. FF: Investigation, Writing – review & editing. DN: Investigation, Writing – review & editing.

Funding

The author(s) declare that no financial support was received for the research, authorship, and/or publication of this article.

Conflict of interest

The authors declare that the research was conducted in the absence of any commercial or financial relationships that could be construed as a potential conflict of interest.

Publisher's note

All claims expressed in this article are solely those of the authors and do not necessarily represent those of their affiliated organizations, or those of the publisher, the editors and the reviewers. Any product that may be evaluated in this article, or claim that may be made by its manufacturer, is not guaranteed or endorsed by the publisher.

References

1. Ostrom QT, Price M, Neff C, Cioffi G, Waite KA, Kruchko C, et al. CBTRUS statistical report: primary brain and other central nervous system Tumors diagnosed in the United States in 2016-2020. *Neuro-Oncology*. (2023) 25:149. doi: 10.1093/neuonc/noad149

2. Gerritsen JKW, Broekman MLD, De Vleeschouwer S, Schucht P, Jungk C, Krieg SM, et al. Decision making and surgical modality selection in glioblastoma patients: an international multicenter survey. *J Neuro-Oncol*. (2022) 156:465–82. doi: 10.1007/s11060-021-03894-5

3. Sonabend AM, Zacharia BE, Cloney MB, Sonabend A, Showers C, Ebiana V, et al. Defining glioblastoma Resectability through the wisdom of the crowd: a proof-of-principle study. *Neurosurgery*. (2017) 80:590–601. doi: 10.1227/NEU.0000000000001374

4. Fargen KM, Friedman WA. The science of medical decision making: neurosurgery, errors, and personal cognitive strategies for improving quality of care. *World Neurosurg*. (2014) 82:e21–9. doi: 10.1016/j.wneu.2014.03.030

5. Moawad A. W., Janas A., Baid U., Ramakrishnan D., Jekel L., Krantchev K. (2023). The Brain Tumor Segmentation (BraTS-METS) Challenge 2023: Brain Metastasis Segmentation on Pre-treatment MRI. ArXiv [Preprint].

6. Sengupta A, Agarwal S, Gupta PK, Ahlawat S, Patir R, Gupta RK, et al. On differentiation between vasogenic edema and non-enhancing tumor in high-grade glioma patients using a support vector machine classifier based upon pre and post-surgery MRI images. *Eur J Radiol*. (2018) 106:199–208. doi: 10.1016/j.ejrad.2018.07.018

7. Jang BS, Jeon SH, Kim IH, Kim IA. Prediction of Pseudoprogression versus progression using machine learning algorithm in glioblastoma. *Sci Rep*. (2018) 8:12516. doi: 10.1038/s41598-018-31007-2

8. Gao Y, Xiao X, Han B, Li G, Ning X, Wang D, et al. Deep learning methodology for differentiating glioma recurrence from radiation necrosis using multimodal magnetic resonance imaging: algorithm development and validation. *JMIR Med Inform*. (2020) 8:e19805. doi: 10.2196/19805

9. Akbari H, Rathore S, Bakas S, Nasrallah MP, Shukla G, Mamourian E, et al. Histopathology-validated machine learning radiographic biomarker for noninvasive discrimination between true progression and pseudo-progression in glioblastoma. *Cancer*. (2020) 126:2625–36. doi: 10.1002/cncr.32790

10. Cepeda S, Luppino LT, Pérez-Núñez A, Solheim O, García-García S, Velasco-Casares M, et al. Predicting regions of local recurrence in glioblastomas using voxel-based Radiomic features of multiparametric postoperative MRI. *Cancers*. (2023) 15:1894. doi: 10.3390/cancers15061894

11. Noorbakhsh-Sabet N, Zand R, Zhang Y, Abedi V. Artificial intelligence transforms the future of health care. *Am J Med*. (2019) 132:795–801. doi: 10.1016/j.amjmed.2019.01.017

12. Zhang S, Bamakan SMH, Qu Q, Li S. Learning for personalized medicine: a comprehensive review from a deep learning perspective. *IEEE Rev Biomed Eng*. (2019) 12:194–208. doi: 10.1109/RBME.2018.2864254

13. Mayerhoefer ME, Materka A, Langs G, Häggström I, Szczypiński P, Gibbs P, et al. Introduction to Radiomics. *J Nucl Med*. (2020) 61:488–95. doi: 10.2967/jnumed.118.222893

14. Karschnia P, Young JS, Dono A, Häni L, Sciortino T, Bruno F, et al. Prognostic validation of a new classification system for extent of resection in glioblastoma: a report of the RANO resect group. *Neuro-Oncology*. (2023) 25:940–54. doi: 10.1093/neuonc/noac193

15. Fathi Kazerooni A, Mohseni M, Rezaei S, Bakhshandehpour G, Saligheh Rad H. Multi-parametric (ADC/PWI/T2-w) image fusion approach for accurate semi-automatic segmentation of tumorous regions in glioblastoma multiforme. *MAGMA*. (2015) 28:13–22. doi: 10.1007/s10334-014-0442-7

16. Marcus AP, Marcus HJ, Camp SJ, Nandi D, Kitchen N, Thorne L. Improved prediction of surgical Resectability in patients with glioblastoma using an artificial neural network. *Sci Rep*. (2020) 10:5143. doi: 10.1038/s41598-020-62160-2

17. Kommers I, Bouget D, Pedersen A, Eijgelaar RS, Ardon H, Barkhof F, et al. Glioblastoma surgery imaging-reporting and data system: standardized reporting of tumor volume, location, and Resectability based on automated segmentations. *Cancers*. (2021) 13:854. doi: 10.3390/cancers13122854

18. Zanier O, Da Mutten R, Vieli M, Regli L, Serra C, Staartjes VE. Deep EOR: automated perioperative volumetric assessment of variable grade gliomas using deep learning. *Acta Neurochir*. (2023) 165:555–66. doi: 10.1007/s00701-022-05446-w

19. Duffau H. Brain connectomics applied to oncological neuroscience: from a traditional surgical strategy focusing on glioma topography to a meta-network approach. *Acta Neurochir*. (2021a) 163:905–17. doi: 10.1007/s00701-021-04752-z

20. Herbet G, Duffau H. Revisiting the functional anatomy of the human brain: toward a meta-networking theory of cerebral functions. *Physiol Rev*. (2020) 100:1181–228. doi: 10.1152/physrev.00033.2019

21. Duffau H. A two-level model of interindividual anatomo-functional variability of the brain and its implications for neurosurgery. *Cortex*. (2017) 86:303–13. doi: 10.1016/j.cortex.2015.12.009

22. Shah HA, Mehta NH, Saleem MI, D'Amico RS. Connecting the connectome: a bibliometric investigation of the 50 most cited articles. *Clin Neurol Neurosurg*. (2022) 223:107481. doi: 10.1016/j.clineuro.2022.107481

23. Duffau H. The death of localizationism: the concepts of functional connectome and neuroplasticity deciphered by awake mapping, and their implications for best care of brain-damaged patients. *Rev Neurol*. (2021b) 177:1093–103. doi: 10.1016/j.neurol.2021.07.016

24. Aabedi AA, Young JS, Zhang Y, Ammanuel S, Morshed RA, Dalle Ore C, et al. Association of Neurological Impairment on the relative benefit of maximal extent of resection in Chemoradiation-treated newly diagnosed Isocitrate dehydrogenase wild-type glioblastoma. *Neurosurgery*. (2022) 90:124–30. doi: 10.1227/NEU.0000000000001753

25. Eyupoglu IY, Buchfelder M, Savaskan NE. Surgical resection of malignant gliomas-role in optimizing patient outcome. *Nat Rev Neurol*. (2013) 9:141–51. doi: 10.1038/nrneurol.2012.279

26. McGirt MJ, Mukherjee D, Chaichana KL, Than KD, Weingart JD, Quinones-Hinojosa A. Association of surgically acquired motor and language deficits on overall survival after resection of glioblastoma multiforme. *Neurosurgery*. (2009) 65:463–9. doi: 10.1227/01.NEU.0000349763.42238.E9

27. Ille S, Zhang H, Sogerer L, Schwendner M, Schöder A, Meyer B, et al. Preoperative function-specific connectome analysis predicts surgery-related aphasia after glioma resection. *Hum Brain Mapp*. (2022) 43:5408–20. doi: 10.1002/hbm.26014

28. Osipowicz K, Profyris C, Mackenzie A, Nicholas P, Rudder P, Taylor HM, et al. Real world demonstration of hand motor mapping using the structural connectivity atlas. *Clin Neurol Neurosurg*. (2023) 228:107679. doi: 10.1016/j.clineuro.2023.107679

29. Yeung JT, Taylor HM, Nicholas PJ, Young IM, Jiang I, Doyen S, et al. Using Quicktome for intracerebral surgery: early retrospective study and proof of concept. *World Neurosurg*. (2021) 154:e734–42. doi: 10.1016/j.wneu.2021.07.127

30. Morell AA, Eichberg DG, Shah AH, Luther E, Lu VM, Kader M, et al. Using machine learning to evaluate large-scale brain networks in patients with brain tumors: traditional and non-traditional eloquent areas. *Neurooncol Adv*. (2022) 4:vdac142. doi: 10.1093/noajnl/vdac142

31. Luckett PH, Park KY, Lee JJ, Lenze EJ, Wetherell JL, Eyler LT, et al. Data-efficient resting-state functional magnetic resonance imaging brain mapping with deep learning. *J Neurosurg*. (2023) 139:1258–69. doi: 10.3171/2023.3.JNS2314

32. Taylor MD, Bernstein M. Awake craniotomy with brain mapping as the routine surgical approach to treating patients with supratentorial intraaxial tumors: a prospective trial of 200 cases. *J Neurosurg*. (1999) 90:35–41. doi: 10.3171/jns.1999.90.1.0035

33. Ferroli P, Broggi M, Schiavolin S, Acerbi F, Bettamio V, Caldiroli D, et al. Predicting functional impairment in brain tumor surgery: the big five and the Milan complexity scale. *Neurosurg Focus*. (2015) 39:E14. doi: 10.3171/2015.9.FOCUS15339

34. Caverzasi E, Hervey-Jumper SL, Jordan KM, Lobach IV, Li J, Panara V, et al. Identifying preoperative language tracts and predicting postoperative functional recovery using HARDI q-ball fiber tractography in patients with gliomas. *J Neurosurg*. (2016) 125:33–45. doi: 10.3171/2015.6.JNS142203

35. Bianconi A, Rossi LF, Bonada M, Zeppa P, Nico E, De Marco R, et al. Deep learning-based algorithm for postoperative glioblastoma MRI segmentation: a promising new tool for tumor burden assessment. *Brain Inform*. (2023) 10:26. doi: 10.1186/s40708-023-00207-6

36. Sagberg LM, Drewes C, Jakola AS, Solheim O. Accuracy of operating neurosurgeons' prediction of functional levels after intracranial tumor surgery. *J Neurosurg*. (2017) 126:1173–80. doi: 10.3171/2016.3.JNS152927

37. Barry MJ, Edgman-Levitan S. Shared decision making--pinnacle of patient-centered care. *N Engl J Med*. (2012) 366:780–1. doi: 10.1056/NEJMp1109283

38. Brennum J, Maier CM, Almdal K, Engelmann CM, Gjerris M. Primo non nocere or maximum survival in grade 2 gliomas? A medical ethical question. *Acta Neurochir*. (2015) 157:155–64. doi: 10.1007/s00701-014-2304-5

39. Godolphin W. The role of risk communication in shared decision making. *BMJ*. (2003) 327:692–3. doi: 10.1136/bmj.327.7417.692

40. Leu S, Cahill J, Grundy PL. A prospective study of shared decision-making in brain tumor surgery. *Acta Neurochir*. (2023) 165:15–25. doi: 10.1007/s00701-022-05451-z

41. Sorensen von Essen H, Piil K, Dahl Steffensen K, Rom Poulsen F. Shared decision making in high-grade glioma patients-a systematic review. *Neurooncol Pract*. (2020) 7:589–98. doi: 10.1093/nop/npaa042

42. Sorensen von Essen H, Stacey D, Dahl Steffensen K, Guldager R, Rom Poulsen F, Piil K. Decisional needs of patients with recurrent high-grade glioma and their families. *Neurooncol Pract*. (2022) 9:402–10. doi: 10.1093/nop/npac046

frontiers | Frontiers in Oncology

TYPE Case Report
PUBLISHED 11 June 2024
DOI 10.3389/fonc.2024.1308497

OPEN ACCESS

EDITED BY
John Bianco,
Princess Maxima Center for Pediatric Oncology, Netherlands

REVIEWED BY
Prerana Jha,
Karkinos Healthcare Private Limited, India
Wade Mueller,
Medical College of Wisconsin, United States
Randall Treffy,
Medical College of Wisconsin, in collaboration with reviewer WM

*CORRESPONDENCE
Zhanxiang Wang
wangzx@xmu.edu.cn

RECEIVED 06 October 2023
ACCEPTED 29 May 2024
PUBLISHED 11 June 2024

CITATION
Jia F, Kang Y and Wang Z (2024) Case report: A 53-year-old woman with synchronous WHO classification II and IV gliomas. *Front. Oncol.* 14:1308497. doi: 10.3389/fonc.2024.1308497

Case report: A 53-year-old woman with synchronous WHO classification II and IV gliomas

Fang Jia, Yin Kang and Zhanxiang Wang*

Department of Neurosurgery, Xiamen Key Laboratory of Brain Center, the First Affiliated Hospital of Xiamen University, School of Medicine, Xiamen University, Xiamen, China

Introduction: Glioma is the most common primary intracranial neoplasm with a relatively poor prognosis.

Case presentation: Here, we present a unique case of a 53-year-old woman with two histopathologically distinct gliomas at the initial diagnosis. She presented with headaches and left limb weakness before admission, and magnetic resonance imaging (MRI) showed right frontal and basal ganglia area involvement combined with hemorrhage. The patient underwent a navigation-guided craniotomy for tumor removal. Pathological examination revealed the right frontal lobe lesion as a WHO grade II IDH-NOS astrocytoma, but the right parietal lobe lesion was a WHO grade IV IDH-mutant diffuse astrocytoma. Molecular detection of the parietal lesion revealed a point mutation at the R132 locus of the *IDH1* gene, no mutation in the *TERT* promoter, amplification of the epidermal growth factor receptor, and a non-homozygous *CDKN2A/B* deletion.

Discussion: In-depth epigenomic analysis and molecular examination revealed that one patient had two different brain tumors, underscoring the importance of performing a comprehensive brain tumor workup.

Conclusion: This unique case confirms that adjacent astrocytomas may have different molecular pathogenesis and provides novel insights into the development of gliomas.

KEYWORDS

glioblastoma, astrocytoma, IDH, WHO grade, synchronous, case report

Abbreviations: WHO, World Health Organization; IDH, Isocitrate Dehydrogenase; NOS, Not otherwise specified; PCRR, polymerase chain reaction fluorescent.

Introduction

In 2021, the World Health Organization (WHO) released the fifth edition of the Classification of Tumors of the Central Nervous System (1). In this updated edition, IDH-mutant glioblastoma, formerly known as "secondary glioblastoma", is now described as IDH-mutant, grade IV astrocytoma. Additionally, astrocytoma with IDH-mutant grade III and synonymous *CDKN2B* and/or *CDKN2A* deletions were also characterized as astrocytoma, IDH mutations, grade IV, albeit with a relatively low histopathologic grade (1, 2). The detailed interaction mechanism between IDH1/2 and CDKN2A/B remains unclear at the biomolecular level. Current research has focused more on the discrepancies between grade 4, IDH-mutant astrocytoma, and glioblastoma (3–6). Few clinical studies have been conducted specifically on this phenotype, and current knowledge remains limited (5).

The simultaneous presence of multiple foci, remarkably homologous foci with different histopathologic compositions, is rare in all types of gliomas (7). Based on radiologic and/or pathologic features, complicating lesions can be divided into multifocal and multicentric categories (8). Multicentric gliomas fail to differentiate due to genetic defects in stem cells, resulting in defective, highly proliferative cell populations that form tumor centers (9). Multifocal gliomas, on the other hand, represent the presence of multiple tumor foci that are differentially associated and have consistent genetic variants (8). Due to this rarity, the underlying molecular relationships of synchronous lesions are poorly understood. Thus far, despite the worse prognosis of multifocal/multicentric gliomas, their treatment is roughly the same as for single lesions (9).

The co-occurrence of astrocytoma of different molecular and histologic classifications at initial diagnosis in a single individual has never been previously described in the literature. We emphasized the importance of integrated genetic and pathology analysis for synchronous gliomas.

Case presentation

The patient, a previously healthy 53-year-old woman, attended a local clinic with a progressive headache accompanied by nonprojectile vomiting. Later, the patient's symptoms worsened, and she developed weakness in the left limb. She underwent an MRI scan, which showed occupational hemorrhage in the right frontal lobe and basal ganglia region and blood accumulation in the knee of the corpus callosum with subcerebral falciform herniation. The larger lesion was located in the right parietal lobe, showing signs of isometric T1-weighted images (T1WIs) and T2WIs and contrast enhancement with peri-lesion edema and midline shift, size approximately 5.1*4.2*3.7 cm^3 (Figures 1A, B). The other lesion was a saccular mass located in the right frontal lobe (Figures 1C). Several nodular, clustered bands of edema with hyperintensity on fluid-attenuated inversion recovery (FLAIR) images and diffusion-weighted imaging (DWI) were seen (Figures 1D–G). She subsequently underwent a navigation-guided trans-frontal craniotomy using electrophysiology to detect functional brain areas. A sub-total resection (STR) was performed to avoid causing dysfunction in the basal ganglia region. Intraoperative ultrasound was used to assess tumor resection. Postoperatively, the patient's left-sided muscle strength recovered from grade II to grade IV, and MRI revealed minimal contrast enhancement of residual lesions (Figure 1H).

Histopathological analysis of the parietal lesion demonstrated a WHO grade IV IDH-mutant diffuse astrocytoma with mesenchymal vascular, endothelial cell proliferation, and palisading necrosis. Microscopically, the cells were dense, tightly arranged, and of variable size, coarse chromatin, visible nucleoli, and nuclear schizophrenia was atypical (Figures 2A, B). The cells were positive for *GFAP*, *IDH1*, *Olig-2*, *NeuN*, *Nestin*, *NF*, *S100*, *CD34*, *SYN*, *EMN*, and Vimentin, but negative for ATRX by immunohistochemistry. The Ki-67 proliferation index was significantly increased, labeling up to approximately 55% of tumor cells. Most cells showed strong *p53* staining (80%), and immunofluorescence of *EGFR* was positive. Detection of *CDKN2A/B* by fluorescence *in situ* hybridization (FISH) suggested non-purifying deletions (Figures 2C, D). PCRR-Fluorescent with QIAamp FFPE Tissue Kit confirmed the presence of *IDH1* R132 mutation and revealed no *TERT* promoter mutations (Table 1, Supplementary Figure S1). Pathological diagnosis of the frontal lesion was a WHO grade II IDH-NOS (Isocitrate Dehydrogenase-Not otherwise specified) diffuse astrocytoma without necrosis and microvascular proliferation (Figures 2E, F). The Ki-67 proliferation index was slightly increased, marking approximately 2% of tumor cells. The cells were positive for p53, and ATRX staining was not observed (Supplementary Figure S2). The patient tolerated the operation well, continued to improve clinically, and achieved a Karnofsky Performance Scale (KPS) score of 80 at discharge. The patient will then be treated one month later with concurrent temozolomide (TMZ) and radiation, the standard Stupp regimen. Based on follow-up MRI, the patient is currently in a tolerable disease state (Supplementary Figure S3).

Discussion

In this study, we describe the first case of a patient with two adjacent but histologically distinct primary gliomas at initial treatment. The most notable finding was a WHO grade IV diffuse astrocytoma with the IDH1 R132 mutation in the right parietal basal ganglia region pathology, which differed from the WHO grade II astrocytoma, IDH-NOS found in the right frontal lobe lesion.

This discovery raises two possible pathogenic mechanisms. One speculation is that the right parietal lesion is a secondary lesion derived from the frontal tumor. The different IDH mutations may suggest an evolved trajectory resulting in more invasive clones able to metastasize transmission (8, 10). In this case, glioma cells in the parietal lesion probably possess a more remarkable ability to metastasize through cerebrospinal fluid or cortical tract fibers. Another speculation is the existence of two separate and synchronously evolving multicentric tumors. Higher proportions of IDH1 mutations have been reported in low-grade astrocytomas compared with those in primary glioblastomas and

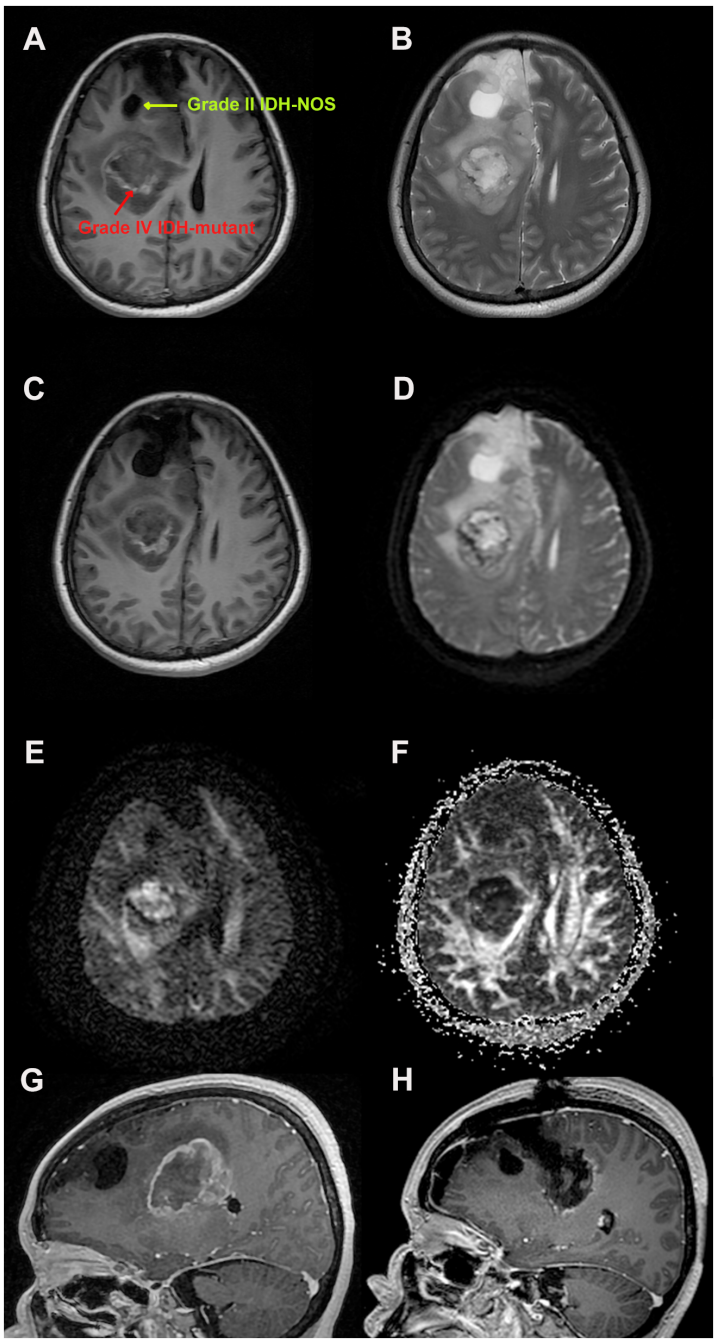

FIGURE 1
Magnetic resonance imaging findings during the patients' treatment. **(A)** Axial post-enhancement T1 weighted images showing a right-sided contrast lesion in the parietal and basal ganglia area, measuring 5.1*4.2*3.7 cm^3, and a right frontal lobe cystic mass. **(B)** Axial post-enhancement T2 weighted Propeller images to avoid artifacts. **(C)** Heterogenous, T1 weighted isometric lesion in the basal ganglia area, with midline shift and sub-calcaneal hernia. **(D)** Axial T1-FLAIR-weighted images showing parietal lesions as heterogeneous lesions with high contrast frontal cystic masses. Diffusion tensor imaging **(E)** showing the cerebral neurofibril trajectory and factional anisotropy **(F)**. **(G)** Preoperative sagittal T1-weighted images reveal two heterogeneous lesions with peripheral edema zone. **(H)** Postoperative sagittal T1-weighted images showing sub-total tumor resection with partial contrast (to avoid neurological deficits).

oligodendrogliomas (11–13). Considering this may be an early clonal mutation, different IDH1 mutations may indicate the simultaneous progression of two separate low-grade gliomas (14). In 1996, Watanabe et al. reported the presence of distinct genetic alterations in what were previously called primary and secondary glioblastomas (15). EGFR alterations are prevalent in primary glioblastoma but infrequent in secondary glioblastoma. P53 mutations are much more common in secondary glioblastoma but rare in primary glioblastoma. Interestingly, both p53 (80% positive) and EGFR alterations were detected in the right parietal lesion. But we do not suggest that these two lesions are bi-primary or completely separate tumors since they share the same P53 and

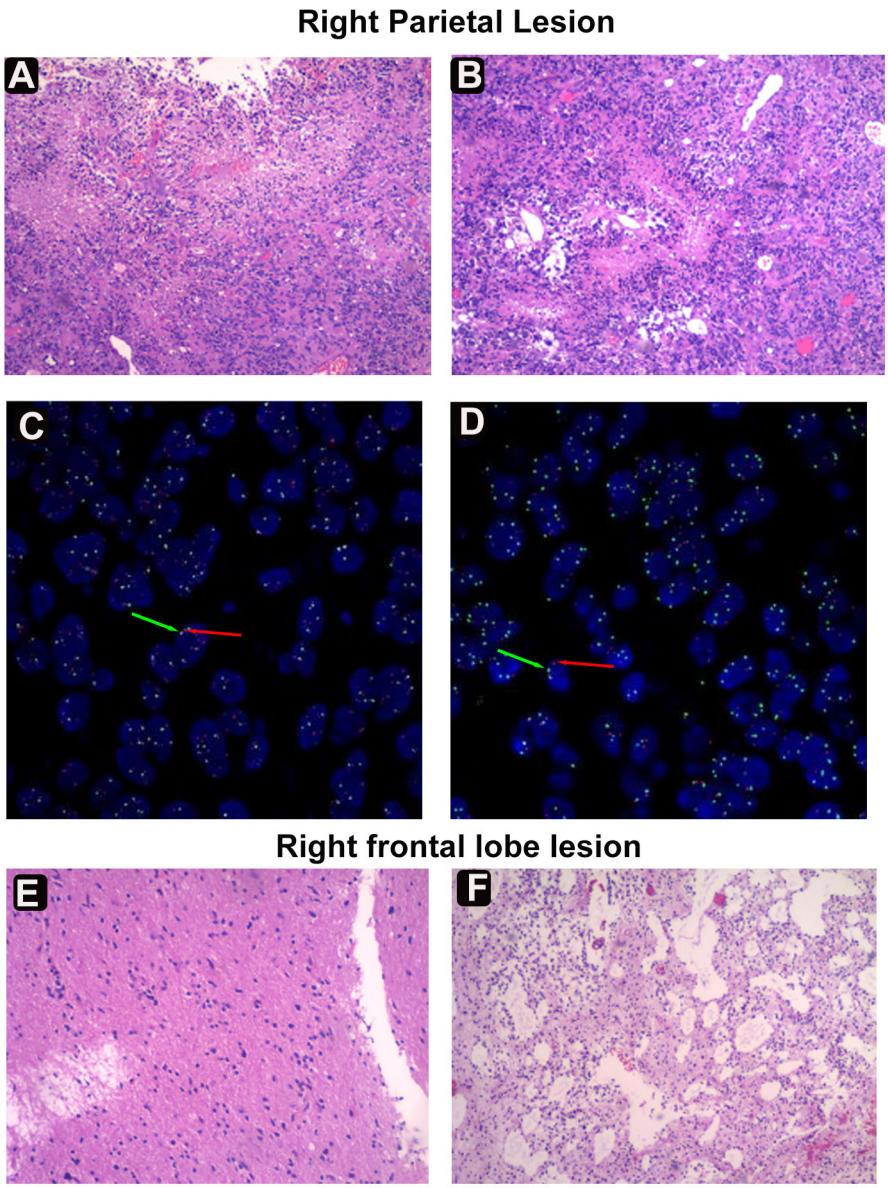

FIGURE 2
Histological and fluorescence *in situ* hybridization (FISH) examinations. **(A)** Diffuse infiltrating growth of tumor cells seen microscopically. **(B)** Tumor cells of variable size, with coarse chromatin, nucleoli, and nuclear fission. Dense growth of tumorigenic astrocyte-like cells in the Virchow-Robin interstitial. **(C)** FISH assay revealing the EGFR amplification. The red arrow represents the gene EGFR, a total of 207; The green arrow denotes the GSP-17 chromosome, a total of 75. **(D)** FISH assay suggesting *CDKN2A/B* nonpure deletion. Green arrow (G) for/CSP9, red arrow (R) for CDKN2A. **(E)** Tumor cells are infiltrated in sheets of nests, cells are ovoid/short pike with mild cell morphology. **(F)** Lower cell density and microcyst formation in the frontal area.

TABLE 1 Comparison of the immunohistochemistry and genetic findings between the right frontal and parietal lobe lesions.

Parietal lobe lesion	Frontal lobe lesion
WHO-grade IV, IDH 1 R132 mutation	WHO-grade II, IDH-NOS
Ki67 (55%+), p53 (80% +)	Ki67 (2%+), p53 (+)
TERT-promoter, wildtype	TERT-promoter, wildtype
ATRX (-) by IHC	ATRX (-) by IHC
EGFR-positive, CDKN2A-negative by FISH	

ATRX mutations and are anatomically adjacent. The discoveries suggest that ATRX and P53 mutations may first appeared in glial precursor cells. Afterwards, these cells acquired EGRF mutations and became grade IV diffuse astrocytoma. The remaining cells turned into IDH-NOS grade II astrocytoma. This case suggests that IDH mutations could subsequently occur after other genetic changes. In 2020, Yoon et al. made a similar point (16). In their case, the new lesion was diagnosed as glioblastoma six years after a surgical of IDH-mutant diffuse astrocytoma. In recent years, exosomes have been found to perform an important role in intercellular communication, and exosomes secreted by cancer

cells have a powerful ability to alter the distant and local microenvironment (17). We speculate that glioma cells in the frontal and parietal lesions may communicate via nanoscale vesicles in neurons and glial cells.

A literature search identified only two published cases of oligodendrogliomas WHO grade-2 and astrocytomas WHO grade-2 (18). Singha et al. described two similar patients with seizure who suffered from oligodendrogliomas of the left parietal lobe and astrocytomas of the right frontal lobe (18). At 6-month follow-up, the patients' imaging and clinical status remained stable. However, they only performed routine pathological examinations and immunohistochemical tests and did not provide molecular profiling to demonstrate the different biological backgrounds of the two gliomas reported.

Another critical point is the impact of the novel WHO classification in 2021 on clinical care compared to the WHO classification in 2016 (1, 19). Before this update, the patient's right parietal tumor was classified as an IDH-mutant glioblastoma and, therefore, should receive a gross tumor resection and adjuvant chemotherapy and radiotherapy (20). Based on the latest 2021 WHO classification, the tumor is currently classified as a WHO grade IV IDH-mutant diffuse astrocytoma. Considering her health condition, we performed a sub-total tumor resection.

Conclusion

We report here a rare case of adjacent multifocal diffuse astrocytoma with distinct WHO grades, IDH mutations, and biological background. A combination of molecular and histologic parameters uncovered distinct clonal origins of the two lesions. We also highlighted the differences between the 2016 WHO classification and the updated 2021 version regarding glioma classifications.

Data availability statement

The original contributions presented in the study are included in the article/Supplementary Material. Further inquiries can be directed to the corresponding author.

Ethics statement

The participants provided their written informed consent for the publication of their potentially-identifying data and/or images.

Author contributions

FJ: Writing – original draft, Writing – review & editing. YK: Conceptualization, Investigation, Software, Writing – review & editing. ZW: Data curation, Methodology, Supervision, Writing – original draft.

Funding

The author(s) declare that no financial support was received for the research, authorship, and/or publication of this article.

Conflict of interest

The authors declare that the research was conducted in the absence of any commercial or financial relationships that could be construed as a potential conflict of interest.

Publisher's note

Supplementary material

The Supplementary Material for this article can be found online at: https://www.frontiersin.org/articles/10.3389/fonc.2024.1308497/full#supplementary-material

SUPPLEMENTARY FIGURE 1
Detection of TERT, IDH1/2 mutations in tumor individualized therapy-related genes in the parietal lesion.

SUPPLEMENTARY FIGURE 2
The whole diagnostic histopathology report for this patient.

SUPPLEMENTARY FIGURE 3
Magnetic resonance images two months after discharge. **(A)** Axial post-enhancement FLAIR images. **(B, C)**. Axial T2-weighted propeller images after enhancement to avoid artifacts. **(D)**. Axial T1-FLAIR weighted images. Diffusion tensor images revealing nerve fiber trajectories **(E)** and anisotropy **(F)** in the brain. Sagittal **(G)** and coronal **(H)** T1-weighted images.

References

1. Louis DN, Perry A, Wesseling P, Brat DJ, Cree IA, Figarella-Branger D, et al. The 2021 WHO classification of tumors of the central nervous system: a summary. *Neuro Oncol.* (2021) 23:1231–51. doi: 10.1093/neuonc/noab106

2. Brat DJ, Aldape K, Colman H, Figrarella-Branger D, Fuller GN, Giannini C, et al. cIMPACT-NOW update 5: recommended grading criteria and terminologies for IDH-mutant astrocytomas. *Acta Neuropathol.* (2020) 139:603–8. doi: 10.1007/s00401-020-02127-9

3. Stewart J, Sahgal A, Chan AKM, Soliman H, Tseng CL, Detsky J, et al. Pattern of recurrence of glioblastoma versus grade 4 IDH-mutant astrocytoma following chemoradiation: A retrospective matched-cohort analysis. *Technol Cancer Res Treat.* (2022) 21:15330338221109650. doi: 10.1177/15330338221109650

4. Sohn B, An C, Kim D, Ahn SS, Han K, Kim SH, et al. Radiomics-based prediction of multiple gene alteration incorporating mutual genetic information in glioblastoma

and grade 4 astrocytoma, IDH-mutant. *J Neurooncol*. (2021) 155:267–76. doi: 10.1007/s11060-021-03870-z

5. Wong QH, Li KK, Wang WW, Malta TM, Noushmehr H, Grabovska Y, et al. Molecular landscape of IDH-mutant primary astrocytoma Grade IV/glioblastomas. *Mod Pathol*. (2021) 34:1245–60. doi: 10.1038/s41379-021-00778-x

6. Ensign SPF, Jenkins RB, Giannini C, Sarkaria JN, Galanis E, Kizilbash SH. Translational significance of CDKN2A/B homozygous deletion in isocitrate dehydrogenase-mutant astrocytoma. *Neuro-Oncology*. (2023) 25:28–36. doi: 10.1093/neuonc/noac205

7. Terakawa Y, Yordanova YN, Tate MC, Duffau H. Surgical management of multicentric diffuse low-grade gliomas: functional and oncological outcomes: clinical article. *J Neurosurg*. (2013) 118:1169–75. doi: 10.3171/2013.2.JNS121747

8. Agopyan-Miu A, Banu MA, Miller ML, Troy C, Hargus G, Canoll P, et al. Synchronous supratentorial and infratentorial oligodendrogliomas with incongruous IDH1 mutations, a case report. *Acta Neuropathol Commun*. (2021) 9:160. doi: 10.1186/s40478-021-01265-9

9. Patil CG, Eboli P, Hu J. Management of multifocal and multicentric gliomas. *Neurosurg Clin N Am*. (2012) 23:343–50. doi: 10.1016/j.nec.2012.01.012

10. Sun Z, Zhao Y, Wei Y, Ding X, Tan C, Wang C. Identification and validation of an anoikis-associated gene signature to predict clinical character, stemness, IDH mutation, and immune filtration in glioblastoma. *Front Immunol*. (2022) 13:939523. doi: 10.3389/fimmu.2022.939523

11. Appay R, Dehais C, Maurage C-A, Alentorn A, Carpentier C, Colin C, et al. CDKN2A homozygous deletion is a strong adverse prognosis factor in diffuse Malignant IDH-mutant gliomas. *Neuro-Oncology*. (2019) 21:1519–28. doi: 10.1093/neuonc/noz124

12. Macaulay RJ. Impending impact of molecular pathology on classifying adult diffuse gliomas. *Cancer Control*. (2015) 22:200–5. doi: 10.1177/107327481502200211

13. Theeler BJ, Ellezam B, Melguizo-Gavilanes I, de Groot JF, Mahajan A, Aldape KD, et al. Adult brainstem gliomas: Correlation of clinical and molecular features. *J Neurol Sci*. (2015) 353:92–7. doi: 10.1016/j.jns.2015.04.014

14. Visani M, Acquaviva G, Marucci G, Paccapelo A, Mura A, Franceschi E, et al. Non-canonical IDH1 and IDH2 mutations: a clonal and relevant event in an Italian cohort of gliomas classified according to the 2016 World Health Organization (WHO) criteria. *J Neuro-Oncol*. (2017) 135:245–54. doi: 10.1007/s11060-017-2571-0

15. Watanabe K, Tachibana O, Sata K, Yonekawa Y, Kleihues P, Ohgaki H. Overexpression of the EGF receptor and p53 mutations are mutually exclusive in the evolution of primary and secondary glioblastomas. *Brain Pathol*. (1996) 6:217–23. doi: 10.1111/j.1750-3639.1996.tb00848.x

16. Yoon BH, Park JS, Kang S, Kwon NJ, Lee KS, Kim CY, et al. IDH-wildtype secondary glioblastoma arising in IDH-mutant diffuse astrocytoma: a case report. *Br J Neurosurg*. (2023) 37:1233–6. doi: 10.1080/02688697.2020.1837733

17. Zhang L, Yu D. Exosomes in cancer development, metastasis, and immunity. *Biochim Biophys Acta Rev Cancer*. (2019) 1871:455–68. doi: 10.1016/j.bbcan.2019.04.004

18. Singhal I, Coss D, Mueller W, Straza M, Krucoff MO, Santos-Pinheiro F. Case report: Two unique cases of co-existing primary brain tumors of glial origin in opposite hemispheres. *Front Oncol*. (2022) 12:1018840. doi: 10.3389/fonc.2022.1018840

19. Louis DN, Perry A, Reifenberger G, von Deimling A, Figarella-Branger D, Cavenee WK, et al. The 2016 world health organization classification of tumors of the central nervous system: a summary. *Acta Neuropathol*. (2016) 131:803–20. doi: 10.1007/s00401-016-1545-1

20. Melhem JM, Detsky J, Lim-Fat MJ, Perry JR. Updates in IDH-wildtype glioblastoma. *Neurotherapeutics*. (2022) 19:1705–23. doi: 10.1007/s13311-022-01251-6

frontiers | Frontiers in Neurology

TYPE Review
PUBLISHED 03 July 2024
DOI 10.3389/fneur.2024.1393572

OPEN ACCESS

EDITED BY
Kalpana K. Shrivastava,
Defence Institute of Physiology and Allied Sciences (DRDO), India

REVIEWED BY
Olga Makarova,
Russian National Research Center of Surgery named after B.V. Petrovsky, Russia
Haroon Ahmad,
University of Maryland School of Medicine, United States

*CORRESPONDENCE
E. D. Namiot
enamiot@gmail.com

RECEIVED 29 February 2024
ACCEPTED 31 May 2024
PUBLISHED 03 July 2024

CITATION
Namiot ED, Zembatov GM and Tregub PP (2024) Insights into brain tumor diagnosis: exploring *in situ* hybridization techniques.
Front. Neurol. 15:1393572.
doi: 10.3389/fneur.2024.1393572

Insights into brain tumor diagnosis: exploring *in situ* hybridization techniques

E. D. Namiot[1]*, G. M. Zembatov[1] and P. P. Tregub[1,2,3]

[1]Department of Pathophysiology, First Moscow State Medical University (Sechenov University), Moscow, Russia, [2]Brain Research Department, Federal State Scientific Center of Neurology, Moscow, Russia, [3]Scientific and Educational Resource Center, Innovative Technologies of Immunophenotyping, Digital Spatial Profiling and Ultrastructural Analysis, Peoples' Friendship University of Russia (RUDN University), Moscow, Russia

Objectives: Diagnosing brain tumors is critical due to their complex nature. This review explores the potential of *in situ* hybridization for diagnosing brain neoplasms, examining their attributes and applications in neurology and oncology.

Methods: The review surveys literature and cross-references findings with the OMIM database, examining 513 records. It pinpoints mutations suitable for *in situ* hybridization and identifies common chromosomal and gene anomalies in brain tumors. Emphasis is placed on mutations' clinical implications, including prognosis and drug sensitivity.

Results: Amplifications in EGFR, MDM2, and MDM4, along with Y chromosome loss, chromosome 7 polysomy, and deletions of PTEN, CDKN2/p16, TP53, and DMBT1, correlate with poor prognosis in glioma patients. Protective genetic changes in glioma include increased expression of ADGRB3/1, IL12B, DYRKA1, VEGFC, LRRC4, and BMP4. Elevated MMP24 expression worsens prognosis in glioma, oligodendroglioma, and meningioma patients. Meningioma exhibits common chromosomal anomalies like loss of chromosomes 1, 9, 17, and 22, with specific genes implicated in their development. Main occurrences in medulloblastoma include the formation of isochromosome 17q and SHH signaling pathway disruption. Increased expression of BARHL1 is associated with prolonged survival. Adenomas mutations were reviewed with a focus on adenoma-carcinoma transition and different subtypes, with MMP9 identified as the main metalloprotease implicated in tumor progression.

Discussion: Molecular-genetic diagnostics for common brain tumors involve diverse genetic anomalies. *In situ* hybridization shows promise for diagnosing and prognosticating tumors. Detecting tumor-specific alterations is vital for prognosis and treatment. However, many mutations require other methods, hindering *in situ* hybridization from becoming the primary diagnostic method.

KEYWORDS

***in situ* hybridization, FISH, glioblastoma, oligodendroglioma, meningioma, ependymoma, medulloblastoma, pituitary adenoma**

Introduction

The importance of diagnosing brain tumors is underscored by the severity of their clinical presentations and the complexities involved in treating neoplasms within this region (1). It's crucial to note the continued absence of effective therapeutic strategies for the most prevalent types of brain tumors (2, 3). Early diagnosis and molecular-genetic

profiling of tumors are emerging as promising avenues for developing treatment modalities (4, 5).

The evolution of molecular-genetic techniques has significantly bolstered our capacity to prognosticate tumor outcomes and evaluate the propensity for tumor development (6–9). Within this domain, *in situ* hybridization methods, encompassing both fluorescent and chromogenic variants, play a pivotal role in tumor interrogation (10). These methodologies diverge primarily in signal detection mechanisms and sensitivity, with fluorescent hybridization being particularly salient in brain tumor diagnosis (11, 12). In the realm of neurobiology, the emergence of probes targeting mutations in key genes such as c-myc, EGFR, and topoisomerase IIa offers profound insights into brain tumor pathogenesis (13–16). These advancements hold promise for improving both diagnostic accuracy and treatment strategies for brain tumors.

The principle of *in situ* hybridization (ISH) relies on the interaction between labeled nucleotide probes and target RNA/DNA sequences (17–19). Generally, the process involves several steps: preparing the tissue or cells (such as cell pellets or paraffin-embedded tissues), preparing specific probes (often commercially available for routine diagnostics), and finally, the hybridization and visualization steps (18). Each of these steps has its own limitations. For example, fluorescent probes used in FISH (fluorescence *in situ* hybridization) analysis can only detect deletions up to 200 kb, leaving smaller genomic changes undetected (18, 20). Commercial probes typically come with detailed information, including the target gene, probe localization, and the specific protocol to be followed (18). Probe design is an area of ongoing research, with recent advancements such as improved detection of amyloid-β peptides in Alzheimer's disease (21, 22). The duration of ISH analysis can vary significantly, with hybridization alone taking place overnight (18). Consequently, the entire analysis process can take several days.

In the field of genetic diagnostics, *in situ* hybridization techniques are indispensable for probing genetic material within cells without compromising tissue integrity (17). Widely embraced in medical practice, they offer precise detection of genetic variations (23). Fluorescence *In Situ* Hybridization (FISH) analysis is one of many possible options, enabling targeted hybridization during cellular division (24). Additionally, the advent of two-color chromogenic hybridization has further broadened the scope of genetic analysis (14, 25). These techniques utilize probes with complementary sequences and fluorescent tags for visualization, facilitating concurrent examination of multiple genetic targets (26–29). While *in situ* hybridization typically targets cells in the resting phase, its application to dividing cells occasionally enhances result clarity (30–32). Presently, gene-or location-specific probes are favored for their precision and can be tailored using DNA libraries (33, 34). These advancements hold promise for deepening our understanding of cellular genetics.

It's worth highlighting that visualizing *in situ* hybridization results enables the application of diverse microscopic techniques for 3D signal visualization within tissues (35). Modern technologies such as FISHQuant, coupled with optimizations in analysis steps utilizing novel buffering systems to enhance tissue sample stability, are gaining widespread adoption (36). The stability of probes is contingent on various factors; for instance, DNA probes are generally deemed more resilient than mRNA, whereas microRNA exhibits remarkable stability (26).

Hybridization techniques provide insight not only into DNA but also RNA sequences simultaneously (13). When examining mRNA, chromogenic hybridization is a common choice, utilizing dioxigenin as a marker detectable through specific peroxidases (37–39). However, this method lacks the precision required for chromosomal analysis, essential for diagnosing chromosomal mutations—a prevalent cause of brain tumors. In neurogenetics, *in situ* hybridization can uncover anomalies such as microdeletions (indicating the absence of signal on one chromosome copy), translocations (evidenced by signals from a gene on one chromosome to another), and aneuploidies (revealing changes in chromosome) (16, 18). These genetic aberrations play a critical role in diagnosing various types of brain tumors (40).

Despite the promising potential of *in situ* hybridization techniques in tumor diagnosis, their application to brain tumors is hampered by the lack of comprehensive mutation data characterizing the molecular-genetic profile of these tumors. Thus, our review aimed to scrutinize literature sources delineating diagnostic features identified through *in situ* hybridization for profiling the most prevalent brain tumors. We then cross-referenced these findings with the Online Mendelian Inheritance in Man (OMIM) database, examining 513 records to pinpoint mutations suitable for *in situ* hybridization methods. Our analysis focused on mutations in genes with well-established molecular bases, excluding those associated with syndromes featuring multiple tumors, such as MSH6 and MLH1. Therefore, we included only the genes marked with an asterisk (*) and a plus sign (+) on the OMIM website, as all other entries (e.g., those with # and % symbols) refer solely to phenotype descriptions and do not represent specific loci.

Astrocytomas and oligodendrogliomas

Glioblastomas, classified as Grade IV malignancies, exhibit the poorest prognosis among central nervous system tumors, with a median survival of only 15 months (40, 41). These tumors can be stratified into two distinct subgroups. The first subgroup, predominant in individuals over 60, is characterized by EGFR amplification, suggesting an unfavorable prognosis. Conversely, the second subgroup, more prevalent in younger patients, presents with a protracted disease course and is associated with mutations in the p53 transcription factor, a critical regulator of the cell cycle (42, 43). Notably, literature indicates that FISH hybridization does not confer significant advantages in detecting mutations within this gene during mitotic recombination (44). However, remarkable advancements have been made in the analysis of EGFR gene amplification, offering promising diagnostic avenues for anaplastic oligodendrogliomas and small cell glioblastomas. This advancement is particularly noteworthy considering the challenges posed by distinguishing these tumors solely through traditional histological methods. Furthermore, an intriguing aspect lies in the co-deletion of 1p/19q, playing a pivotal role in diagnosing anaplastic oligodendrogliomas and exhibiting notable sensitivity to chemotherapy (24).

Given the significant mortality rate attributed to glioblastoma, there is a particular interest in identifying genes associated with the risk of the most unfavorable prognosis. Using the FISH method, researchers have identified monosomies of chromosome 10q, frequently accompanied by trisomies of chromosome 7 (45). These genetic alterations, along with mutations or loss of the PTEN gene, are

TABLE 1 Mutations identified in glioblastoma cells using the FISH method.

Gene / chromosome	Prognosis	Additional information	References
Amplifications			
PDGFR	Does not affect prognosis.	Primary glioblastoma.*	(49)
EGFR	Poor (older than 60 years)**	Primary glioblastoma.	(27)
MDM2	Poor prognosis.	Resistance to EGFR-TKIs.	(47)
MDM4	Poor prognosis.	Resistance to EGFR-TKIs.	(47)
KDR	Does not affect prognosis.	More often with PDGFRA.	(50)
CDK4	Less resistance to bevacizumab.	Infiltration by immunosuppressive macrophages.	(51, 52)
KIT	Does not affect prognosis.	More common in individuals younger than 60 years old.	(49, 50)
VEGFR2	Does not affect prognosis.	Primary glioblastoma.*	(49)
Monosomies / chromosome losses			
Y chromosome	Poor prognosis.	Does not differentiate between primary and secondary glioblastomas.	(41, 53)
Chromosome 10	Does not affect prognosis.	Precedes trisomy of chromosome 7.	(41)
Polysomies			
X chromosome	Does not affect prognosis.	Inactivation in healthy women increases the risk of glioblastoma.	(41, 54)
Chromosome 7	Poor prognosis.	It can be used for diagnosis.***	(55)
Deletions			
PTEN	Poor prognosis.	When pTERT mutation occurs, it is often accompanied by EGFR amplification.	(41, 56)
CDKN2/p16	Poor prognosis.	Increased sensitivity to antimetabolites.	(39)
TP53	Poor prognosis.	Most commonly missense mutations.	(18)
1p/19q	For anaplastic gliomas, the prognosis is favorable, while for glioblastomas, the significance remains unclear.	The preferred treatment includes procarbazine, lomustine, and vincristine.	(55, 57)
DMBT1	Poor prognosis.	The preferred method is PCR/qPCR.	(45)

*These were also detected in secondary glioblastomas.
**The prognosis was better for individuals under 60 years old.
***Alongside EGFR amplification, monosomy of chromosome 10, mutations in pTERT, in the absence of typical histological features.

strongly linked to extremely low survival rates. However, despite this correlation, the method fails to distinguish between primary and secondary subgroups of glioblastomas (46). In a notable study, researchers observed that the transition from astrocytomas to glioblastomas is associated with sequential occurrences of trisomy of chromosome 7 and monosomy of chromosome 10. However, individually, these genetic aberrations lack diagnostic significance. Similar trends were observed for sex chromosomes, with the FISH method revealing a disomy of the X chromosome, often coupled with the absence of the Y chromosome, detected in 71% of primary glioblastoma samples (47).

Mutations in genes such as PTEN, DMBT1, CDK4, and the deletion of the tumor suppressor gene p16 have been identified in glioblastomas (48–53). In a study conducted by Koshiyama et al. (48), which involved 40 glioblastoma patients, FISH analysis revealed monosomy of chromosome 10 in 52.5% of cases, polysomy of chromosome 7 in 50%, and PTEN gene deletion in 35% of cases, all of which were associated with an unfavorable prognosis. Loss of p16 expression has been proposed as a prognostic factor in glioblastoma patients, especially when combined with IDH mutations (49). While glioblastomas with wild-type IDH lack prognostic value, other studies suggest a correlation between p16 deletion and increased chemotherapy sensitivity (49, 50).

Mutations in the DMBT1 gene, situated on chromosome 10, have also been associated with a poorer prognosis. Notably, most studies rely on PCR/qPCR techniques to detect mutations in this gene (51). Furthermore, while the FISH method is capable of detecting only monosomies for chromosome 10 mutations commonly observed in glioblastomas, microsatellite analysis proves more effective in identifying other variants (51). Another limitation of FISH is its inability to assess methylation status, crucial in genes like MGMT, which correlates with a more favorable chemotherapy outcome (54). For further insights, Table 1 offers an overview of the target genes analyzed in glioblastoma cells using the FISH technique.

Despite its significance, FISH analysis encounters certain limitations, particularly in diagnosing pilocytic astrocytomas. This is due to their frequent association with neurofibromatosis type 1, characterized by the loss of NF1 gene expression (58). Detecting this deletion using fluorescent hybridization becomes practically impossible (59, 60). However, it's worth noting that this limitation does not preclude the possibility of sporadic forms of astrocytomas, which can be examined using the FISH method provided there are

relevant mutations (61). Thus, despite its limitations, FISH remains a valuable tool in diagnostics, offering insights into the molecular-genetic profile of tumors.

Using the OMIM database, we examined 265 records containing "glioblastoma/+glioblastoma" fragments and selected mutations suitable for detection through hybridization methods (Figure 1). Throughout the database analysis, we identified mutations/changes with positive prognostic implications, as well as those linked to glioblastoma development or bearing a negative prognosis. Notably, a substantial portion of changes associated with a favorable prognosis involved immune response activation in response to tumor growth. For instance, heightened ectopic expression of VEGF-C facilitated the binding of CD8+ receptors on T-lymphocytes to tumor cells (OMIM 601528). However, the glioblastoma microenvironment, alongside tumor cells themselves, often exhibits immunosuppressive effects, which can be counteracted by elevated IL-12 cytokine expression (OMIM 161561). Furthermore, decreased ICAM-1 receptor expression correlated with reduced tumor sensitivity to cytotoxic lymphocytes (OMIM 147840). Conversely, elevated LRRC4 and BMP4 expression correlated with smaller tumor sizes and slower growth rates (OMIM 610486; OMIM 112262). It's worth noting that while most researchers employ PCR for expression analysis, the possibility of utilizing *in situ* hybridization methods for the same purposes remains open.

One of the crucial steps in the pathogenesis of glioblastoma is the mutation of the EGFR receptor, which can occur concurrently with the formation of hybrid genes (e.g., EGFR/SEPT14 and EGFR/TACC) (OMIM 131550; OMIM 612140). In other cases, a mutant variant known as EGFRvIII emerges, leading to heightened SVAT3 expression through phosphorylation (OMIM 601743). Consequently, elevated SVAT3 expression correlates with active glioblastoma progression, as does the formation of the SVAT3/OSMR coreceptor complex (OMIM 601743). The predominant mutations in the EGFR gene involve deletions of exons 2–7 and amplification (OMIM 131550), which can be detected using *in situ* hybridization. Another gene of practical

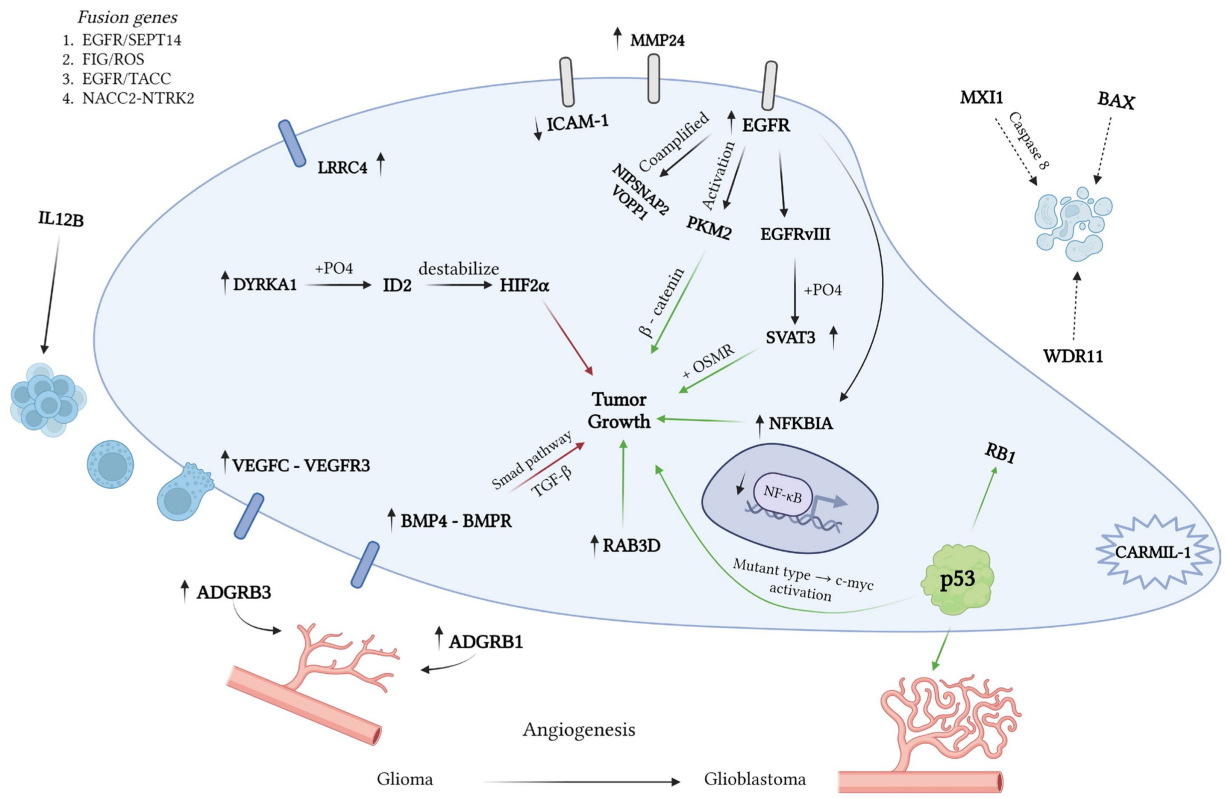

FIGURE 1
Various mutations influence the pathogenesis of glioblastoma, with green arrows denoting a positive effect and red arrows indicating a negative one. Using the OMIM database, we identified 265 records containing "glioblastoma" and "+glioblastoma." Our analysis unveiled mutations with a positive prognosis linked to immune response activation. For instance, VEGFC expression enhances prognosis by fostering the binding of CD8 T cells to tumor cells (OMIM 601528). However, the glioblastoma microenvironment suppresses the immune response via high IL12 expression (OMIM 161561). LRRC4 and BMP4 expression correlate with smaller tumor size and slower growth (OMIM 610486; OMIM 112262). EGFR mutations, including hybrid genes EGFR/SEPT14 and EGFR/TACC (OMIM 131550; OMIM 612140), play a pivotal role in glioblastoma development. The formation of the mutant EGFRvIII variant results in increased SVAT3 expression and active progression (OMIM 601743). The SVAT3/OSMR complex portends a negative prognosis. Deletions in EGFR exons 2–7 and amplification in the EGFR gene are also critical (OMIM 131550). RAB3D is associated with low survival rates. Glioblastoma's uncontrolled division stems from tyrosine kinase activation. The hybrid FIG/ROS gene and mutations in FGFR1 are linked to tyrosine kinase activation. Deletions in NFKBIA, NF1, and TRIM8, along with loss of heterozygosity in growth-suppressor genes (WDR11, BAX, MXI1), are associated with low survival rates. Co-amplification of NIPSNAP2 and VOPP1 accelerates tumor growth and worsens prognosis (OMIM 603004; OMIM 611915). Angiogenesis plays a crucial role in tumor growth, often stimulated by p53 gene mutation in high-grade gliomas. In benign tumors, neo-vascularization is inhibited by ADGRB1 expression (OMIM 602682).

significance is RAB3D, associated with decreased survival rates (OMIM 604350).

Overall, glioblastoma, like many other CNS tumors, is characterized by uncontrolled growth driven by aberrant activation of tyrosine kinases (61). Notably, glioblastoma samples have shown the presence of hybrid FIG/ROS genes, associated with constitutive tyrosine kinase activation, akin to FGFR1 gene mutation (OMIM 165020; OMIM 136350). Deletions in NFKBIA, NF1, and TRIM8 genes have also been linked to poor survival rates (OMIM 164008; OMIM 613113; OMIM 606125). Loss of heterozygosity or complete inactivation is more common in tumor suppressor genes, including WDR11, BAX, and MXI1 (OMIM 606417; OMIM 600040; OMIM 600020). Additionally, co-amplification of NIPSNAP2 and VOPP1 has been shown to accelerate tumor growth and worsen prognosis (OMIM 603004; OMIM 611915). Angiogenesis plays a crucial role in tumor growth, which, in the case of high-grade gliomas, can be stimulated by mutations in the p53 gene (OMIM 191170). In benign tumors, neo-vascularization is inhibited by the expression of ADGRB1 (OMIM 602682).

Fragments containing "oligodendroglioma/+oligodendroglioma" were discovered in 31 sources within the OMIM database. However, the majority of genes harbor mutations that are challenging to assess using *in situ* hybridization. For instance, mutations in PIK3CA have been linked to anaplastic oligodendroglioma (OMIM 171834). Oligodendrogliomas are characterized by elevated expression of OLIG1/2, which is specific to this tumor type (OMIM 606385; OMIM 606386). Similarly to glioblastoma, increased expression of the metalloproteinase MMP24 is associated with a poor prognosis (OMIM 604871). While the loss of tumor suppressor gene expression is not unique to oligodendroglioma, specific losses of DMBT1 and NKX6-2 are notable (OMIM 601969; OMIM 605955). Detection of TRIM8 is common in both glioblastomas and anaplastic oligodendrogliomas (OMIM 606125). Lastly, heightened expression of ATP8A1 and ATAD2B is observed, with the latter also detectable in glioblastoma cells (OMIM 609542; OMIM 615347).

Meningiomas

Meningiomas are predominantly benign, comprising about 85% of cases classified as Grade I according to the WHO classification. They typically have a favorable prognosis, with a low recurrence risk not exceeding 5% (62, 63). However, it's important to note the existence of malignant variants and instances of aggressive progression characterized by rapid growth and pronounced clinical symptoms (64).

The FISH analysis offers a distinct advantage in identifying mutations that signal a negative prognosis, even in cases lacking clear histological indicators. Among the earliest mutations often detected through FISH analysis are those occurring in the NF2 gene, present in nearly half of all meningioma cases (65). These early mutations typically include monosomy of chromosome 22, where the NF2 gene is located, as well as loss of the DAL-1 gene (66). Further malignant progression of meningiomas is associated with deletions in chromosomes 1p or 14q (67). Notably, the prognosis is considered particularly poor in cases of co-deletion of 1p/14q, even in the absence of histological signs of malignancy (64, 68, 69).

In addition to the aforementioned mutations, some researchers have identified an association between anaplastic meningioma and the amplification of the 17q23 region and PS6K, both of which are linked to tumor progression (27). A recent study revealed that grade I meningiomas recurring after resection were often associated with the deletion of the p36 region of the 1st chromosome (70). Through quantitative FISH analysis, it was found that meningiomas with a higher degree of malignancy (WHO grade III) exhibit shorter telomeres (71). Additionally, FISH analysis has indicated that deletions in the 17q region may serve as early markers of tumor progression (72). Thus, fluorescence *in situ* hybridization can be considered one of the primary approaches for molecular-genetic profiling of meningiomas.

During the analysis of 64 entries from the OMIM database using the queries "meningioma/+meningioma," additional mutations available for detection by *in situ* hybridization methods were identified (Figure 2). The primary mutation leading to meningioma development is often the loss of chromosome 22, resulting in the loss of the NF2 gene, which inhibits tumor formation (OMIM 607379). formation (OMIM 607379). Besides mutations in this gene, other regions of chromosome 22 associated with meningiomas were also identified. It is believed that in the presence of an intact chromosome 22, the loss of the first chromosome is necessary for the development of a more aggressive anaplastic variant of meningioma (73). Independent deletions of the ALPL and CDKN2C genes, located on the first chromosome, were detected in patients with meningiomas (74, 75). Regarding the involvement of p73 in meningioma development, available information does not indicate correlations between clinical outcomes and expression (76). However, some studies suggest an increase in p73 expression with tumor grade (77). Another early event considered is the deletion of DAL1, which acts as a tumor suppressor under physiological conditions (OMIM 605331).

It's worth highlighting the deletion of the PDGFB gene located on chromosome 1, which is associated with early tumor onset (OMIM 190040). Another notable marker specific to spinal meningiomas is the region on chromosome 17, SMARCE1 (OMIM 603111). Chromosome 17 abnormalities, such as deletions and amplifications, are often observed in meningiomas, unlike chromosome 9, which is almost always lost in meningioma cells (78). The deletion of chromosome 9 is linked to the loss of important genes CDKN2B, p14, and CDKN2A, which normally suppress tumor development (74, 79). Mutations in the IGFBP7 signaling pathway, also disrupted in various carcinomas, are identified in meningiomas (OMIM 602867). Like other central nervous system tumors, meningiomas can develop as part of tumors with multiple localizations. For example, this occurs with the loss of heterozygosity of the BAP-1 gene (OMIM 603089). Additionally, there's an intriguing increase in the expression of the TNKS2 gene in meningioma cells, potentially associated with the immune response to tumor development (OMIM 607128).

Additionally, in the analysis of mutations in meningioma cells, heightened expression of metalloproteinase MMP24 was observed, a feature also present in oligodendrogliomas (OMIM 604871). Furthermore, the presence of overexpressed MMP25 suggests the likelihood of the tumor being an astrocytoma or glioblastoma (OMIM 608482). High levels of cholinesterase BCHE were also detected, a characteristic shared with glioblastomas and neuroblastomas (OMIM 177400). Lastly, elevated expression levels of connexin GJB2 on chromosome 13 and GJA1 on chromosome 6 were identified (OMIM 121011; OMIM 121014).

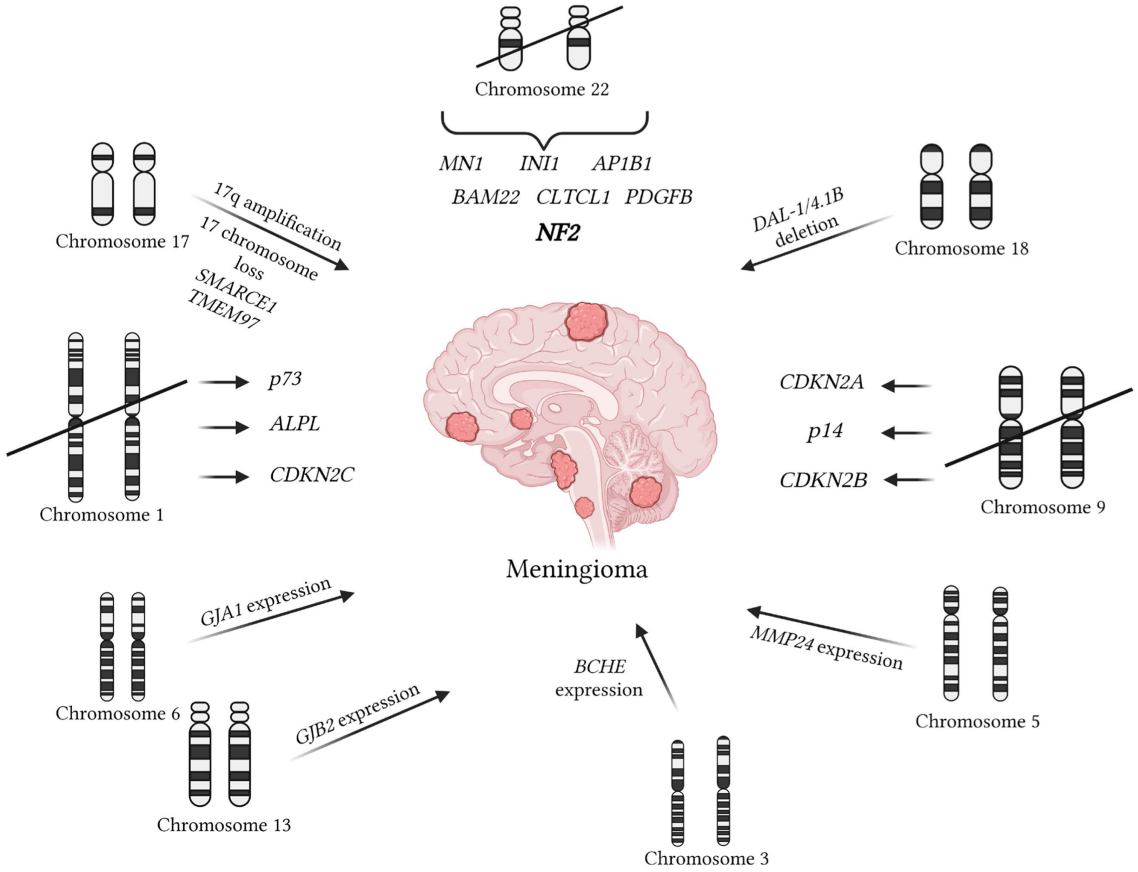

FIGURE 2
Mutations contributing to meningioma development are documented in the OMIM database. The primary mutation initiating meningioma formation is associated with the loss of chromosome 22, resulting in the absence of the NF2 gene (OMIM 607379). More aggressive forms of meningioma are linked to the loss of chromosome 1 (67). Deletions affecting the ALPL and CDKN2C genes on chromosome 1 are also associated with meningiomas (68, 69). An early event is the deletion of DAL1, which typically functions as a tumor suppressor (OMIM 605331). Additionally, the deletion of the PDGFB gene on chromosome 1, associated with early tumor development, has been noted (OMIM 190040). The SMARCE1 marker on chromosome 17 is characteristic of spinal meningiomas (OMIM 603111). Abnormalities in chromosome 17 are common, unlike chromosome 9, which plays a crucial role in tumor-suppressing genes such as CDKN2B, p14, and CDKN2A (68, 73). Furthermore, increased expression of the metalloproteinase MMP24, also present in oligodendrogliomas, has been detected (OMIM 604871). High levels of butyrylcholinesterase (BCHE), similarly found in glioblastomas and neuroblastomas, have also been identified (OMIM 177400). Elevated levels of connexins GJB2 on chromosome 13 and GJA1 on chromosome 6 have been observed (OMIM 121011; OMIM 121014). The presence of MMP25 indicates that the tumor is not a meningioma but rather an astrocytoma or glioblastoma (OMIM 608482). It is important to note that MMP25 was not present in normal brain tissue.

Ependymomas

Ependymoma, more frequently encountered in young individuals and children, is associated with neurofibromatosis type II (80). Therefore, primary investigations, including FISH analysis, are focused on the q12 region of chromosome 22, where the NF2 gene is localized (80). Many researchers note that histological classification alone is insufficient for accurate disease prognosis, and ependymoma itself carries a poor prognosis (81). It has become evident that relying solely on FISH analysis is inadequate for identifying potential disease prognosis markers (82). However, research findings using this method have identified amplification of chromosome 1, which correlates with a high degree of tumor malignancy. For instance, amplification of regions 1q21.1–32.1 has been associated with tumor recurrence, while amplification of 1q25 serves as an independent prognostic marker for patient survival (76). Recently, a specific gene translocation involving RELA and C11orf95 has been discovered, leading to the formation of a new oncogene (77).

The search using the keywords "ependymoma/+ependymoma" revealed 21 results in the OMIM database. The predominant mutation found in most ependymomas involves the formation of the oncogene C11ORF95-RELA. This fusion gene can migrate into the nucleus, activating NF-κB and promoting tumor growth (OMIM 615699). Additionally, ependymomas exhibit amplification of EPHB2 and high expression of CIZ1 (OMIM 600997; OMIM 611420). Furthermore, noteworthy is the expression of the H2-delta haplotype of the PDGFRA gene, which is also present in many embryonal tumors (OMIM 173490).

Medulloblastoma and embryonal tumors

Previously, medulloblastomas were classified into subgroups based on ErbB2 expression levels measured via immunohistochemistry (83). Elevated ErbB2 expression has been associated with the loss of the short arm of chromosome 17 and amplification of the long arm (84). Rare

chromosomal anomalies, such as amplification of the myc oncogene (occurring in 6% of cases), have been linked to unfavorable prognoses (85). Despite the low frequency of oncogene amplification across different medulloblastoma subtypes, recent studies highlight the prognostic significance of detecting C-myc/N-myc amplification at the single-cell level using FISH analysis (86). Deletions on chromosomes 10q, 16q, and 8p, as well as amplifications of chromosomes 2, 7, and 17, have also been identified in medulloblastomas (87). Notably, p53 gene mutations associated with medulloblastoma recurrences are detected in almost all central nervous system tumors (88). Molecular genetic methods have allowed the classification of medulloblastomas into four groups (89). The group with WNT gene mutations is characterized by a favorable prognosis, unlike groups 3 and 4. The presence of isochromosome 17q serves as an important prognostic marker, determined in part using fluorescence *in situ* hybridization (85).

Medulloblastomas exhibit histological similarities to embryonal tumors, particularly primitive neuroectodermal tumors (90). One key criterion for distinguishing medulloblastoma is the detection of isochromosome 17q and the presence of chromosomes 14q and 19q, whose deletion is characteristic of primitive neuroectodermal tumors (91, 92). Rhabdoid tumors (highly malignant embryonal tumors) are characterized by monosomy of chromosome 22 or a mutation in the hSNF5/INI1 gene located on the same chromosome (93, 94).

The analysis of 107 entries in the OMIM database using the keywords "medulloblastoma/+medulloblastoma" (Figure 3) revealed pivotal stages in pathogenesis, notably the disruption of the SHH signaling pathway (OMIM 600725). Mutations in the SUFU gene are recognized as one of the factors contributing to pathway hyperactivation and are occasionally associated with meningioma development (OMIM 607035). Alterations in the SHH gene are frequently linked to the desmoplastic subtype of medulloblastoma (OMIM 600725). Conversely, deletions in the ATOH1 gene inhibit the SHH signaling pathway, thwarting medulloblastoma development (OMIM 601461). Anomalies in this pathway can also induce other changes, such as increased expression of YAP1 (OMIM 606608).

Under normal circumstances, the expression of the KCTD11 gene on the 17th chromosome can inhibit SHH, and this gene is frequently subject to deletion in cases of medulloblastoma (OMIM 609848). Additionally, deletions of KCTD21 and KCTD6 may occur (OMIM 618790; OMIM 618791). As observed in many other tumors, deletion of the DMBT1 gene is also noted (OMIM 601969) in medulloblastoma. Furthermore, medulloblastoma entails a frameshift mutation in the GPR161 gene, which encodes one of the types of G protein-coupled receptors (OMIM 612250). Employing *in situ* hybridization methods during the investigation of medulloblastoma can prove valuable in conducting NGS, facilitating a more precise selection of specific DNA regions, and enabling the comparison of mutation sites with the wild type.

There are medulloblastoma variants characterized by amplification of the 17q chromosome, resulting in heightened expression of the LASP1 gene (OMIM 602920). Research indicates that suppressing this gene significantly reduces cell proliferation in medulloblastoma (OMIM 602920). Loss of the 9q chromosome segment is linked to additional loss of function in the ELP1 gene, potentially predisposing individuals to medulloblastoma development (OMIM 603722). Moreover, medulloblastoma exhibits increased expression of genes such as MYO18B (often absent in other tumors), ERBB2, ERBB4, BMI1, and KLHDC8A (OMIM 607295; OMIM 164831; OMIM 614503; OMIM 155255; OMIM 164870; OMIM 600543). Notably, the detection of ERBB2, ERBB4, and PDGFRB expression, which correlates with an unfavorable prognosis and metastasis, does not always indicate tumor progression (OMIM 155255; OMIM 173410). Conversely, overexpression of BARHL1 and NTRK3 has been associated with longer remission intervals and a more favorable prognosis (OMIM 60524; OMIM 191316).

Craniopharyngioma

This tumor type often displays aggressive behavior, impacting adjacent brain structures (95, 96). The adamantinomatous subtype occurs uniformly across age groups and is marked by specific mutations in the CTNNB1 gene, responsible for encoding beta-catenin (97). These mutations trigger the accumulation of mutated beta-catenin, thereby activating the Wnt signaling pathway, pivotal in tumor development. Conversely, the papillary subtype, more prevalent in adults, is defined by the BRAF V600E mutation (98, 99). Due to the rarity of this tumor variant and the focus on more aggressive processes, research efforts often remain constrained to observational accounts of these mutations. A study in 2022 utilized FISH analysis to reveal heightened expression of SERPINE1+ and SERPINEG1+ in macrophages surrounding adamantinomatous tumors (100). In another investigation, increased expression of the tyrosine kinase TrkA was identified. However, this analysis employed a combination of methods including immunohistochemistry, PCR, and FISH, with the latter specifically targeting NTRK1 fusions (101).

The OMIM database contains only 3 entries containing the keywords "craniopharyngioma/+craniopharyngioma." Among them, the ACVR1 gene was identified, which is highly impractical to detect using *in situ* hybridization due to the specificity of the mutation, characterized by the replacement of arginine with histidine at codon 20 (OMIM 102576).

Adenomas and adenocarcinomas

Adenomas and adenocarcinomas of the pituitary gland encompass a wide spectrum of tumors, classified into functional (often microadenomas) and non-functional (typically macroadenomas) categories (102). Notably, among the various adenoma types, some exhibit high invasiveness, such as non-functional corticotropin and thyrotropin adenomas (103, 104). Tumors with high invasiveness, based on molecular-genetic characteristics, often mimic carcinomas, adding significant interest for research purposes (104–106). Many researchers advocate for combining FISH analysis with cytogenetic studies in comparative genomic hybridization, presenting a promising avenue for investigation (107). Additionally, the majority of identified genetic alterations in adenoma development have been elucidated using immunohistochemical methods (107, 108).

A method proposed some time ago assesses the percentage of positively stained nuclei in tumor samples using the Ki-67 marker, where a level exceeding 3% indicates potential tumor invasiveness (109). It's worth noting that diminished expression of the tumor suppressor p27 is linked to invasive forms of pituitary adenomas and carcinomas (110). Comparative genomic hybridization has unveiled a significant number of chromosomal anomalies, most frequently

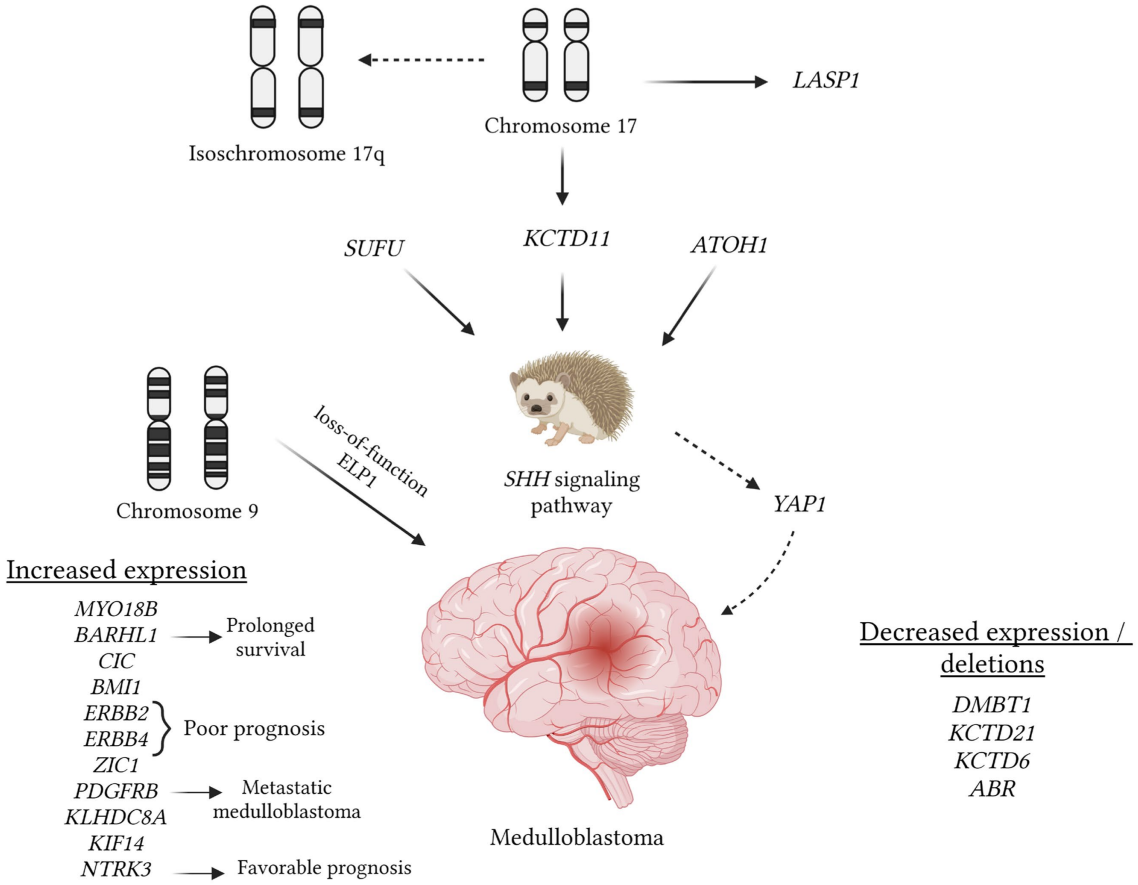

FIGURE 3
Understanding the role of various mutations in medulloblastoma pathogenesis, which can be identified using *in situ* hybridization methods, is crucial. The figure provides an overview of mutations cataloged in the OMIM database that are linked to medulloblastomas. In this tumor type, a pivotal event involves the hyperactivation of the SHH pathway, potentially due to mutations in the SUFU gene, loss of the 17th chromosome (resulting in the loss of the KCTD11 potassium channel gene), and the expression of the ATOH1 gene. The latter inhibits neuronal differentiation, thereby promoting medulloblastoma progression (OMIM 609848; OMIM 618790; OMIM 601461). Isochromosome 17q is a commonly observed aberration visualized through hybridization techniques. Conversely, amplification of the 17q region may lead to increased expression of LASP1, thereby stimulating tumor cell proliferation (OMIM 602920). Loss of the 9q chromosome segment is associated with additional loss of function in the ELP1 gene, potentially predisposing individuals to medulloblastoma development (OMIM 603722). Enhanced expression of ERBB2, ERBB4, and PDGFRB correlates with an unfavorable prognosis and tumor metastasis (OMIM 164870; OMIM 600543; OMIM 173410). In contrast, the expression of BARHL1 and NTRK3 is associated with a favorable prognosis and longer intervals without tumor progression (OMIM 60524; OMIM 191316). Besides KCTD11, deletions involving KCTD21 and KCTD6 may also occur (OMIM 618790; OMIM 618791). Similarly to many other tumors, the deletion of the DMBT1 gene is noted (OMIM 601969).

encountered in tumors producing prolactin and growth hormone. Examples of such anomalies include monosomy of chromosome 11, trisomies of chromosomes 8 and 12 (111).

The OMIM database contains 53 entries with the keywords "pituitary adenoma," but most of the gene mutations are challenging to verify using hybridization methods (Figure 4). Mutations that can be visualized using fluorescent or comparative hybridization include increased expression of CRHR1 or the C-RET gene, primarily among GH and ACTH-secreting adenomas (OMIM 122561; OMIM 164761). GDNF expression is more characteristic of GH and corticotroph adenomas, while GFRA1 expression is associated with corticotroph and somatotroph tumors (OMIM 600837; OMIM 601496). Co-expression of ESR1 and ESR2 mRNA was observed in prolactinomas as well as somatotroph and gonadotroph tumors (OMIM 601663; OMIM 133430). Interestingly, MMP9 and FGF2 expression was characteristic of invasive adenomas and pituitary carcinomas (OMIM 120361) (112). Moreover, higher expression of FGF2 relative to GFG was associated with more aggressive tumor behavior (113). The presence of BRINP3 expression was linked to gonadotroph adenomas, with this gene believed to induce proliferation, migration, and further invasion of the tumor (OMIM 618390).

In adenomas, there is a notable decrease in the expression of several genes, including JNK, Clusterin, NFKBIA, ANKA1, and PITX1 [OMIM 602149; (113)]. Loss of heterozygosity at the GRL locus may contribute to tumor resistance to negative feedback, while the expression of N-cadherin and reduced levels of caveolins I/II are associated with metastasis (113). It has been determined that the MEG3 gene acts as a suppressor of adenoma development and is exclusively present in normal pituitary tissue (OMIM 605636), whereas the PROP1 gene is detected in adenomas (OMIM 601538). Expression of ESRB is distinctive in gonadotroph and null-cell adenomas, while genes ESR1 and ESR2 are co-expressed in prolactinomas, somatotropinomas, and prolactinomas (113–115).

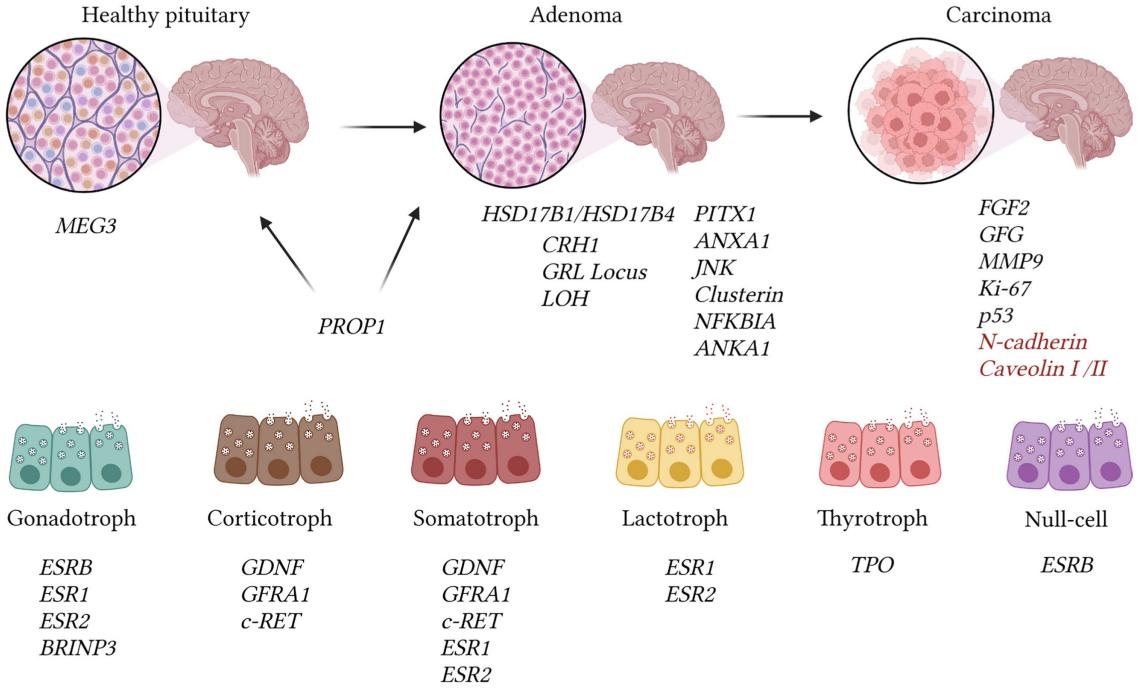

FIGURE 4
The illustration presents genetic changes identified in pituitary adenomas, drawing on data from the OMIM database and other reputable sources. Adenomas exhibit a reduction in the expression of several genes, including JNK, Clusterin, NFKBIA, ANKA1, and PITX1 [OMIM 602149; (107)]. The transition to pituitary carcinomas correlates with increased invasiveness, as reflected in alterations in MMP9 expression (OMIM 120361). Pituitary carcinomas demonstrate heightened expression of FGF2 and diminished GFG mRNA levels. Assessment of malignancy encompasses Ki-67 index (>10%) and p53 expression intensity. The expression of N-cadherin and decreased caveolins I/II levels are linked to metastasis. Nevertheless, such changes may also manifest in ordinary adenomas, according to recent research findings, hence we highlighted them in red (107). The MEG3 gene functions as a suppressor of adenoma development and is exclusively present in normal pituitary tissue (OMIM 605636). The PROP1 gene is identifiable in adenomas (OMIM 601538). Expression of ESRB is distinctive in gonadotroph and null-cell adenomas, whereas ESR1 and ESR2 mRNAs are concurrently expressed in prolactinomas, somatotropinomas, and prolactinomas (107–110). GDNF, GFRA1, and c-RET are detected in corticotroph and somatotroph tumors. Gonadotrophic tumors are characterized by BRINP3 gene expression, which is associated with tumor proliferation and invasion [OMIM 618390; (107–109)].

There is particular interest in examining the expression of various genes in hormone-producing adenomas. For example, genes HSD17B1 and HSD17B4 were found to be expressed across all types of adenomas (OMIM 109684; OMIM 601860). HSD17B3 expression was ubiquitous except in corticotroph adenomas, while HSD17B2 was present in all types except prolactinomas (OMIM 605573; OMIM 109685). Additionally, the growth suppressor MEG3 was identified, exhibiting exclusive expression in non-tumorous gonadotrophs (OMIM 605636). PPAR-gamma expression was observed in ACTH-producing tumors, and the estrogen receptor isoform ESRB was characteristic of null-cell and gonadotroph adenomas (116).

Currently, mutations in the PTTG gene have been identified, which are characteristic of functional pituitary adenomas, alongside mutations in the BRAF and MEN1A genes, potentially responsible for sporadic occurrences of these adenomas (117, 118). New mechanisms of pituitary adenoma pathogenesis have been proposed, including the amplification of HMGA2 (118). This process likely occurs through acetylation, enhancing the activity of E2F1 (119). Recently, telomeres in pituitary tumors were assessed at the single-cell level using FISH analysis (120). The findings revealed that telomere shortening and alternative lengthening (independent of telomerase) were associated with invasive carcinomas. The data indicated that 59.4% of samples exhibited shortened telomeres, while the presence of alternative telomere lengthening correlated with tumor recurrence.

Finally, we have synthesized chromosomal anomalies and specific mutations uncovered through literature scrutiny, independent of the OMIM database. These findings are depicted in Figure 5, excluding glioblastomas and oligodendrogliomas, which receive more comprehensive treatment in the table and Figure 1 (123–130). It's apparent that each tumor showcases distinct genetic and chromosomal irregularities detected within cells. The sole common thread linking ependymomas and meningiomas (occasionally, medulloblastomas) is the presence of monosomy 22 chromosome, alongside mutations in the NF2 gene located on this chromosome. Thus, the enumerated tumors may manifest within the spectrum of neurofibromatosis type 2. While some identified anomalies play a direct role in the tumor's pathogenesis, others function as prognostic indicators.

Conclusion

Molecular-genetic diagnostics of the most common and malignant brain tumors encompasses a wide range of genetic and chromosomal anomalies. The application of *in situ* hybridization methods, including their combination with PCR, sequencing, and cytogenetics, holds significant potential in diagnosing and prognosticating tumors such as glioblastomas, oligodendrogliomas, meningiomas, ependymomas, medulloblastomas, pituitary adenomas, and adenocarcinomas.

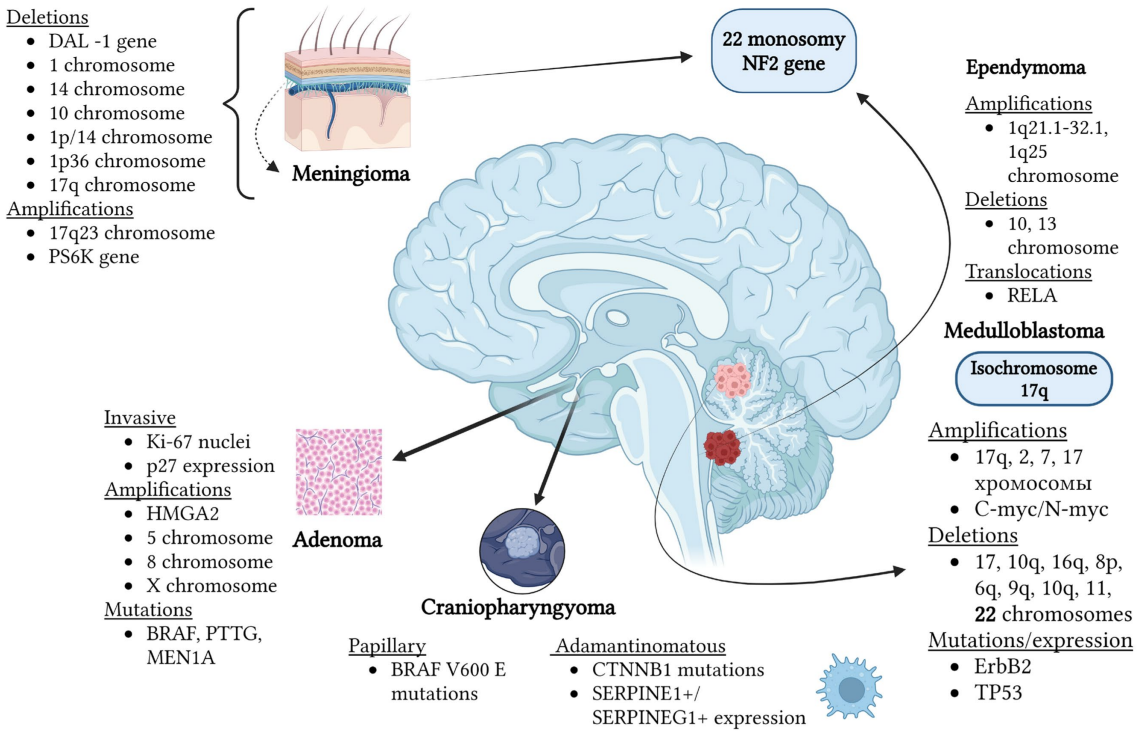

FIGURE 5
Mutations and chromosomal anomalies are detected in various types of brain tumors through FISH hybridization. As depicted in the figure, each tumor exhibits distinct genetic and chromosomal anomalies occurring within cells. The commonality between ependymomas and meningiomas (rarely for medulloblastomas) is monosomy of chromosome 22, alongside NF2 gene mutations located on this chromosome. Hence, the listed tumors may manifest within the spectrum of neurofibromatosis type 2. While some identified anomalies directly contribute to tumor development, others serve as prognostic markers. For instance, the development of pituitary adenomas has been associated with E2F1 acetylation and subsequent HMGA2 gene amplification. Overall, adenomas display extremely high heterogeneity depending, for example, on the hormone they produce. Prolactin-producing tumors are characterized by monosomy of chromosome 11 and trisomies of chromosomes 8 and 12. Amplification of chromosomes 5, 8, and X is typical for pituitary adenomas. Meningiomas with the presence of 17q23, PS6K amplifications, and 1p/14 co-deletions indicate the worst prognosis, while 1p36 deletion suggests a high likelihood of recurrence. In ependymomas, a survival marker can be the amplification of the 1q25 chromosome region. Additionally, in some cases, monosomies of chromosomes 10 and 13 are observed. Notably, the presence of isochromosome 17q in medulloblastomas allows differentiation from other embryonal tumors also developing in the cerebellum. The mutations listed in the figure can be identified through hybridization methods but do not represent a comprehensive list of all gene anomalies characteristic of different types of brain tumors (62–64, 74–77, 80–82, 103, 104, 107, 111, 112, 121, 122).

Currently, the FISH hybridization method is primary in this field, but there are modifications that can improve outcomes. While some chromosomal changes (e.g., chromosomes 1, 10, 17, and 22) and genetic mutations (e.g., MMP25, MMP9, NFKBIA, and DMBT1) are characteristic of several types of brain tumors, detecting changes specific to certain tumors (e.g., the formation of isochromosome 17q in medulloblastoma) is crucial for prognosis and therapy effectiveness. However, despite the significance of *in situ* hybridization, most mutations identified in the OMIM database require PCR or sequencing for identification, which currently does not allow *in situ* hybridization to be recognized as the primary method for diagnosing brain tumors.

Author contributions

EN: Conceptualization, Data curation, Writing – original draft, Writing – review & editing. GZ: Conceptualization, Data curation, Visualization, Writing – original draft, Writing – review & editing. PT: Conceptualization, Data curation, Supervision, Writing – original draft, Writing – review & editing.

Funding

The author(s) declare that no financial support was received for the research, authorship, and/or publication of this article.

Conflict of interest

The authors declare that the research was conducted in the absence of any commercial or financial relationships that could be construed as a potential conflict of interest.

Publisher's note

All claims expressed in this article are solely those of the authors and do not necessarily represent those of their affiliated organizations, or those of the publisher, the editors and the reviewers. Any product that may be evaluated in this article, or claim that may be made by its manufacturer, is not guaranteed or endorsed by the publisher.

References

1. Abd-Ellah MK, Awad AI, Khalaf AAM, Hamed HFA. A review on brain tumor diagnosis from MRI images: practical implications, key achievements, and lessons learned. *Magn Reson Imaging*. (2019) 61:300–18. doi: 10.1016/j.mri.2019.05.028

2. Butowski N. Epidemiology and diagnosis of brain Tumors. *Continuum*. (2015) 21:301–13. doi: 10.1212/01.CON.0000464171.50638.fa

3. Silantyev A, Falzone L, Libra M, Gurina OI, Kardashova KS, Nikolouzakis TK, et al. Current and future trends on diagnosis and prognosis of glioblastoma: from molecular biology to proteomics. *Cells*. (2019) 8:863. doi: 10.3390/cells8080863

4. Johns DA, Williams RJ, Smith CM, Nadaminti PP, Samarasinghe RM. Novel insights on genetics and epigenetics as clinical targets for paediatric astrocytoma. *Clin Transl Med*. (2024) 14:e1560. doi: 10.1002/ctm2.1560

5. Shikalov A, Koman I, Kogan NM. Targeted glioma therapy—clinical trials and future directions. *Pharmaceutics*. (2024) 16:100. doi: 10.3390/pharmaceutics16010100

6. Purow B, Schiff D. Advances in the genetics of glioblastoma: are we reaching critical mass? *Nat Rev Neurol*. (2009) 5:419–26. doi: 10.1038/nrneurol.2009.96

7. Brat DJ. Glioblastoma: biology, genetics, and behavior. *Am Soc Clin Oncol Educ Book*. (2012) 32:102–7. doi: 10.14694/edbook_am.2012.32.48

8. Lee B, Hwang S, Bae H, Choi KH, Suh YL. Diagnostic utility of genetic alterations in distinguishing IDH-wildtype glioblastoma from lower-grade gliomas: insight from next-generation sequencing analysis of 479 cases. *Brain Pathol*. (2024):e13234. doi: 10.1111/bpa.13234e13234

9. Nikolova E, Laleva L, Milev M, Spiriev T, Stoyanov S, Ferdinandov D, et al. miRNAs and related genetic biomarkers according to the WHO glioma classification: From diagnosis to future therapeutic targets. *Non-coding RNA Res*. (2023) 9:141–52. doi: 10.1016/j.ncrna.2023.10.003

10. Jensen EC. Technical review: in situ hybridization. *Anat Rec*. (2014) 297:1349–53. doi: 10.1002/ar.22944

11. Wagner F, Streubel A, Roth A, Stephan-Falkenau S, Mairinger T. Chromogenic in situ hybridisation (CISH) is a powerful method to detect ALK-positive non-small cell lung carcinomas. *J Clin Pathol*. (2013) 67:403–7. doi: 10.1136/jclinpath-2013-201974

12. Palma S, Collins N, Faulkes C, Ping B, Ferns GA, Haagsma B, et al. Chromogenic in situ hybridisation (CISH) should be an accepted method in the routine diagnostic evaluation of HER2 status in breast cancer. *J Clin Pathol*. (2006) 60:1067–8. doi: 10.1136/jcp.2006.043356

13. Todorović-Raković N. Chromogenic in situ hybridization (CISH) as a method for detection of C-Myc amplification in formalin-fixed paraffin-embedded tumor tissue: an update In: The Myc gene: Methods and protocols. Springer US: New York, NY (2021). 313–20.

14. Hagen J, Oliver A, Kalyuzhny AE. In situ hybridization (ISH) combined with immunocytochemistry (ICC) co-detection of phosphorylated EGFR in A431 cultured cells In: *Signal transduction immunohistochemistry: Methods and protocols*. Springer US: New York, NY (2022). 213–20.

15. Loay I, Badawy OM, Tarek EB, Hafez NH, El-Bolkainya N. Assessment of the concordance between fluorescence in-situ hybridization and immunohistochemistry in evaluating topoisomerase IIα in breast carcinoma. *Egypt J Pathol*. (2019) 39:43. doi: 10.4103/egjp.egjp_7_19

16. Chrzanowska NM, Kowalewski J, Lewandowska MA. Use of fluorescence in situ hybridization (FISH) in diagnosis and tailored therapies in solid tumors. *Molecules*. (2020) 25:1864. doi: 10.3390/molecules25081864

17. Levsky JM, Singer RH. Fluorescence in situ hybridization: past, present and future. *J Cell Sci*. (2003) 116:2833–8. doi: 10.1242/jcs.00633

18. Veselinyová D, Mašlanková J, Kalinová K, Mičková H, Mareková M, Rabajdová M. Selected in situ hybridization methods: principles and application. *Molecules*. (2021) 26:3874. doi: 10.3390/molecules26133874

19. Jin L, Lloyd RV. In situ hybridization: methods and applications. *J Clin Lab Anal*. (1997) 11:2–9. doi: 10.1002/(SICI)1098-2825(1997)11:1<2::AID-JCLA2>3.0.CO;2-F

20. Gozzetti A, Le Beau MM. Fluorescence in situ hybridization: Uses and limitations. *Semin Hematol*. (2000) 37:320–33. doi: 10.1016/s0037-1963(00)90013-1

21. Zhang Y, Ding C, Li C, Wang X. Advances in fluorescent probes for detection and imaging of amyloid-β peptides in Alzheimer's disease. *Adv Clin Chem*. (2021) 103:135–90. doi: 10.1016/bs.acc.2020.08.008

22. Ding C, Li C, Meng Q, Qian C, Zhang C, Yang L, et al. A label-free fluorescent probe for dynamic in situ visualization of amyloid-β peptides aggregation. *Sensors Actuators B Chem*. (2021) 347:130607:130607. doi: 10.1016/j.snb.2021.130607

23. Sampaio KB, Nascimento DDS, Garcia EF, De Souza EL. An outlook on fluorescent in situ hybridization coupled to flow cytometry as a versatile technique to evaluate the effects of foods and dietary interventions on gut microbiota. *Arch Microbiol*. (2022) 204:469. doi: 10.1007/s00203-022-03090-7

24. Fuller C, Perry A. Fluorescence in situ hybridization (FISH) in diagnostic and investigative neuropathology. *Brain Pathol*. (2002) 12:67–86. doi: 10.1111/j.1750-3639.2002.tb00424.x

25. Gajaria PK, Tambe S, Pai T, Patil A, Desai SB, Shet TM. Dual-color dual-hapten in situ hybridization (D-DISH)–comparison with fluorescence in situ hybridization (FISH) for HER2/neu testing in breast cancer. *Indian J Pathol Microbiol*. (2020) 63:194–9. doi: 10.4103/IJPM.IJPM_861_19

26. Warford A. In situ hybridisation: technologies and their application to understanding disease. *Prog Histochem Cytochem*. (2016) 50:37–48. doi: 10.1016/j.proghi.2015.12.001

27. Anderson RM. Multiplex Fluorescence in situ Hybridization (M-FISH). *Methods Mol Biol*. (2010) 659:83–97. doi: 10.1007/978-1-60761-789-1_6

28. Mota A, Schweitzer M, Wernersson E, Crosetto N, Bienko M. Simultaneous visualization of DNA loci in single cells by combinatorial multi-color iFISH. *Scientific Data*. (2022) 9:47. doi: 10.1038/s41597-022-01139-2

29. Hanna W, Kwok KW. Chromogenic in-situ hybridization: a viable alternative to fluorescence in-situ hybridization in the HER2 testing algorithm. *Mod Pathol*. (2006) 19:481–7. doi: 10.1038/modpathol.3800555

30. Nietzel A, Rocchi M, Starke H, Heller A, Fiedler W, Włodarska I, et al. A new multicolor-FISH approach for the characterization of marker chromosomes: centromere-specific multicolor-FISH (cenM-FISH). *Hum Genet*. (2001) 108:199–204. doi: 10.1007/s004390100459

31. Lengauer C, Speicher MR, Popp S, Jauch A, Taniwaki M, Nagaraja R, et al. Chromosomal bar codes produced by multicolor fluorescence in situ hybridization with multiple YAC clones and whole chromosome painting probes. *Hum Mol Genet*. (1993) 2:505–12. doi: 10.1093/hmg/2.5.505

32. Eckel H, Stumm M, Wieacker P, Kleinstein J. Fluorescence in situ hybridization analysis of unfertilized human oocytes using locus-specific DNA probes. *Reprod Technol*. (2000) 10:142. doi: 10.1093/humrep/14.suppl_3.235-a

33. Huber D, Von Voithenberg LV, Kaigala GV. Fluorescence in situ hybridization (FISH): history, limitations and what to expect from micro-scale FISH? *Micro Nano Eng*. (2018) 1:15–24. doi: 10.1016/j.mne.2018.10.006

34. Laß U, Hartmann C, Capper D, Herold-Mende C, Von Deimling A, Meiboom M, et al. Chromogenicin situ hybridization is a reliable alternative to Fluorescencein situ hybridization for diagnostic testing of 1p and 19q loss in paraffin-embedded gliomas. *Brain Pathol*. (2012) 23:311–8. doi: 10.1111/bpa.12003

35. Chea V, Pleiner V, Schweizer V, Herzog B, Bode B, Tinguely M. Optimized workflow for digitalized FISH analysis in pathology. *Diagn Pathol*. (2021) 16:42. doi: 10.1186/s13000-021-01103-5

36. Weremowicz S, Schofield DE. Preparation of cells from formalin-fixed, paraffin-embedded tissue for use in fluorescence in situ hybridization (FISH) experiments. *Curr Protoc Hum Genet*. (2007) 52:8.8.1–8. doi: 10.1002/0471142905.hg0808s52

37. Hossain MS, Hanna MG, Uraoka N, Nakamura T, Edelweiss M, Brogi E, et al. Automatic quantification of HER2 gene amplification in invasive breast cancer from chromogenic in situ hybridization whole slide images. *J Med Imaging*. (2019) 6:047501–1. doi: 10.1117/1.JMI.6.4.047501

38. Tanner M, Gancberg D, Di Leo A, Larsimont D, Rouas G, Piccart MJ, et al. Chromogenic in situ hybridization: a practical alternative for fluorescence in situ hybridization to detect HER-2/neu oncogene amplification in archival breast cancer samples. *Am J Pathol*. (2000) 157:1467–72. doi: 10.1016/S0002-9440(10)64785-2

39. AL-Temimi SM, AL-Rekabi AM. Dual color-chromogenic in situ hybridization approaches to evaluate HER2/Neu gene amplification in breast carcinomas. *Syst Rev Pharm*. (2020) 11:114. doi: 10.31838/srp.2020.10.19

40. Massaad E, Tabbarah A, Barmada M, Rbeiz J, Nasser S, Farra C. FISH analyses for 1p and 19q status on gliomas: reporting an 8 years' experience from a tertiary care center in the Middle East. *Ann Diagn Pathol*. (2022) 57:151899. doi: 10.1016/j.anndiagpath.2022.151899

41. Davis ME. Glioblastoma: overview of disease and treatment. *Clin J Oncol Nurs*. (2016) 20:S2. doi: 10.1188/16.CJON.S1.2-8

42. Hovinga KE, McCrea HJ, Brennan C, Huse J, Zheng J, Esquenazi Y, et al. EGFR amplification and classical subtype are associated with a poor response to bevacizumab in recurrent glioblastoma. *J Neuro-Oncol*. (2019) 142:337–45. doi: 10.1007/s11060-019-03102-5

43. Zhang Y, Dube C, Gibert M Jr, Cruickshanks N, Wang B, Coughlan M, et al. The p 53 pathway in glioblastoma. *Cancers*. (2018) 10:297. doi: 10.3390/cancers10090297

44. Omuro A, DeAngelis L, Wann A, Tully P, Barnes E, Montemurro N, et al. Glioblastoma multiforme and genetic mutations: the issue is not over yet. An overview of the current literature. *J Neurol Surg A Cent Eur Neurosurg*. (2020) 81:64–70. doi: 10.1055/s-0039-1688911

45. Lee D, Riestenberg RA, Haskell-Mendoza A, Bloch O. Diffuse astrocytic glioma, IDH-Wildtype, with molecular features of glioblastoma, WHO grade IV: a single-institution case series and review. *J Neuro-Oncol*. (2021) 152:89–98. doi: 10.1007/s11060-020-03677-4

46. Burger PC, Pearl DK, Aldape K, Yates AJ, Scheithauer BW, Passe SM, et al. Small cell architecture—a histological equivalent of EGFR amplification in glioblastoma

multiforme? *J Neuropathol Exp Neurol*. (2001) 60:1099–104. doi: 10.1093/jnen/60.11.1099

47. Amalfitano G, Chatel M, Paquis P, Michiels JF. Fluorescence in situ hybridization study of aneuploidy of chromosomes 7, 10, X, and Y in primary and secondary glioblastomas. *Cancer Genet Cytogenet*. (2000) 116:6–9. doi: 10.1016/S0165-4608(99)00089-8

48. Koshiyama DB, Trevisan P, Graziadio C, Rosa RF, Cunegatto B, Scholl J, et al. Frequency and clinical significance of chromosome 7 and 10 aneuploidies, amplification of the EGFR gene, deletion of PTEN and TP53 genes, and 1p/19q deficiency in a sample of adult patients diagnosed with glioblastoma from southern Brazil. *J Neuro-Oncol*. (2017) 135:465–72. doi: 10.1007/s11060-017-2606-6

49. Park JW, Kang J, Lim KY, Kim H, Kim SI, Won JK, et al. The prognostic significance of p16 expression pattern in diffuse gliomas. *J Pathol Transl Med*. (2021) 55:102–11. doi: 10.4132/jptm.2020.10.22

50. Iwadate Y, Mochizuki S, Fujimoto S, Namba H, Sakiyama S, Tagawa M, et al. Alteration of CDKN2/p16 in human astrocytic tumors is related with increased susceptibility to antimetabolite anticancer agents. *Int J Oncol*. (2000) 17:501–6. doi: 10.3892/ijo.17.3.501

51. Wessels PH, Twijnstra A, Kubat B, Ummelen MI, Claessen SM, Sciot R, et al. 10q25. 3 (DMBT1) copy number changes in astrocytoma grades II and IV. *Genes Chromosom Cancer*. (2004) 39:22–8. doi: 10.1002/gcc.10288

52. Goldhoff P, Clarke J, Smirnov I, Berger MS, Prados MD, James CD, et al. Clinical stratification of glioblastoma based on alterations in retinoblastoma tumor suppressor protein (RB1) and association with the proneural subtype. *J Neuropathol Exp Neurol*. (2012) 71:83–9. doi: 10.1097/NEN.0b013e31823fe8f1

53. Furgason JM, Koncar RF, Michelhaugh SK, Sarkar FH, Mittal S, Sloan AE, et al. Whole genome sequence analysis links chromothripsis to EGFR, MDM2, MDM4, and CDK4 amplification in glioblastoma. *Oncoscience*. (2015) 2:618. doi: 10.18632/oncoscience.178

54. Binabaj MM, Bahrami A, Shahid Sales S, Joodi M, Joudi Mashhad M, Hassanian SM, et al. The prognostic value of MGMT promoter methylation in glioblastoma: a meta-analysis of clinical trials. *J Cell Physiol*. (2018) 233:378–86. doi: 10.1002/jcp.25896

55. Joensuu H, Puputti M, Sihto H, Tynninen O, Nupponen NN. Amplification of genes encoding KIT, PDGFRα and VEGFR2 receptor tyrosine kinases is frequent in glioblastoma multiforme. *J Pathol*. (2005) 207:224–31. doi: 10.1002/path.1823

56. Nobusawa S, Stawski R, Kim YH, Nakazato Y, Ohgaki H. Amplification of the PDGFRA, KIT and KDR genes in glioblastoma: a population-based study. *Neuropathology*. (2011) 31:583–8. doi: 10.1111/j.1440-1789.2011.01204.x

57. Walentynowicz KA, Engelhardt D, Cristea S, Yadav S, Onubogu U, Salatino R, et al. Single-cell heterogeneity of EGFR and CDK4 co-amplification is linked to immune infiltration in glioblastoma. *Cell Rep*. (2023) 42:112235. doi: 10.1016/j.celrep.2023.112235

58. Li J, Perry A, James CD, Gutmann DH. Cancer-related gene expression profiles in NF1-associated pilocytic astrocytomas. *Neurology*. (2001) 56:885–90. doi: 10.1212/WNL.56.7.885

59. Caneus J, Granic A, Chial HJ, Potter H. Using fluorescence in situ hybridization (FISH) analysis to measure chromosome instability and mosaic aneuploidy in neurodegenerative diseases. In: Frade, J., Gage, F. editors *Genomic mosaicism in neurons and other cell types*. New York, NY: Neuromethods, Humana Press. (2017). 131:329–59. doi: 10.1007/978-1-4939-7280-7_16

60. Jacob K, Quang-Khuong DA, Jones DT, Witt H, Lambert S, Albrecht S, et al. Genetic aberrations leading to MAPK pathway activation mediate oncogene-induced senescence in sporadic pilocytic astrocytomas. *Clin Cancer Res*. (2011) 17:4650–60. doi: 10.1158/1078-0432.CCR-11-0127

61. Currie S, Fatania K, Frood R, Whitehead R, Start J, Lee MT, et al. Imaging Spectrum of the developing glioblastoma: a cross-sectional observation study. *Curr Oncol*. (2023) 30:6682–98. doi: 10.3390/curroncol30070490

62. Buerki RA, Horbinski CM, Kruser T, Horowitz PM, James CD, Lukas RV. An overview of meningiomas. *Future Oncol*. (2018) 14:2161–77. doi: 10.2217/fon-2018-0006

63. Konstantinos V, Vasileios K, Pavlos S. The recurrence rate in meningiomas: analysis of tumor location, histological grading, and extent of resection. *Open J Modern Neurosurg*. (2011) 2:6–10. doi: 10.4236/ojmn.2012.21002

64. Cai DX, Banerjee R, Scheithauer BW, Lohse CM, Kleinschmidt-Demasters BK, Perry A. Chromosome 1p and 14q FISH analysis in clinicopathologic subsets of meningioma: diagnostic and prognostic implications. *J Neuropathol Exp Neurol*. (2001) 60:628–36. doi: 10.1093/jnen/60.6.628

65. Yuzawa S, Nishihara H, Tanaka S. Genetic landscape of meningioma. *Brain Tumor Pathol*. (2016) 33:237–47. doi: 10.1007/s10014-016-0271-7

66. Gutmann DH, Donahoe J, Perry A, Lemke N, Gorse K, Kittiniyom K, et al. Loss of DAL-1, a protein 4.1-related tumor suppressor, is an important early event in the pathogenesis of meningiomas. *Hum Mol Genet*. (2000) 9:1495–500. doi: 10.1093/hmg/9.10.1495

67. Ishino S, Hashimoto N, Fushiki S, Date K, Mori T, Fujimoto M, et al. Loss of material from chromosome arm 1p during malignant progression of meningioma revealed by fluorescent in situ hybridization. *Cancer*. (1998) 83:360–6. doi: 10.1002/(SICI)1097-0142(19980715)83:2<360::AID-CNCR21>3.0.CO;2-Q

68. Linsler S, Kraemer D, Driess C, Oertel J, Kammers K, Rahnenführer J, et al. Molecular biological determinations of meningioma progression and recurrence. *PLoS One*. (2014) 9:e94987. doi: 10.1371/journal.pone.0094987

69. Al-Mefty O, Kadri PA, Pravdenkova S, Sawyer JR, Stangeby C, Husain M. Malignant progression in meningioma: documentation of a series and analysis of cytogenetic findings. *J Neurosurg*. (2004) 101:210–8. doi: 10.3171/jns.2004.101.2.0210

70. Damen PJ, Bulthius VJ, Hanssens PE, Lie ST, Fleischeuer R, Melotte V, et al. WHO grade I meningiomas that show regrowth after gamma knife radiosurgery often show 1p36 loss. *Sci Rep*. (2021) 11:16432. doi: 10.1038/s41598-021-95956-x

71. Yamakawa K, Mukai Y, Ye J, Muto-Ishizuka M, Ito M, Tanimoto M, et al. Telomere length was associated with grade and pathological features of meningioma. *Sci Rep*. (2022) 12:6143. doi: 10.1038/s41598-022-10157-4

72. Hemmer S, Urbschat S, Oertel J, Ketter R. Deletions in the 17q chromosomal region and their influence on the clonal cytogenetic evolution of recurrent meningiomas. *Mol Cytogenet*. (2019) 12:1–8. doi: 10.1186/s13039-019-0434-4

73. Weber RG, Boström J, Wolter M, Baudis M, Collins VP, Reifenberger G, et al. Analysis of genomic alterations in benign, atypical, and anaplastic meningiomas: toward a genetic model of meningioma progression. *Proc Natl Acad Sci*. (1997) 94:14719–24. doi: 10.1073/pnas.94.26.14719

74. Boström J, Meyer-Puttlitz B, Wolter M, Blaschke B, Weber RG, Lichter P, et al. Alterations of the tumor suppressor genes CDKN2A (p16INK4a), p14ARF, CDKN2B (p15INK4b), and CDKN2C (p18INK4c) in atypical and anaplastic meningiomas. *Am J Pathol*. (2001) 159:661–9. doi: 10.1016/S0002-9440(10)61737-3

75. Liu F, Qian J, Ma C. MPscore: a novel predictive and prognostic scoring for progressive meningioma. *Cancers*. (2021) 13:1113. doi: 10.3390/cancers13051113

76. Korshunov A, Shishkina L, Golanov A. Immunohistochemical analysis of p16INK4a, p14ARF, p18INK4c, p21CIP1, p27KIP1 and p73 expression in 271 meningiomas correlation with tumor grade and clinical outcome. *Int J Cancer*. (2003) 104:728–34. doi: 10.1002/ijc.11013

77. Nozaki M, Tada M, Kashiwazaki H, Hamou MF, Diserens AC, Shinohe Y, et al. p73 is not mutated in meningiomas as determined with a functional yeast assay but p73 expression increases with tumor grade. *Brain Pathol*. (2001) 11:296–305. doi: 10.1111/j.1750-3639.2001.tb00400.x

78. Perry A, Banerjee R, Lohse CM, Kleinschmidt-DeMasters BK, Scheithauer BW. A role for chromosome 9p21 deletions in the malignant progression of meningiomas and the prognosis of anaplastic meningiomas. *Brain Pathol*. (2002) 12:183–90. doi: 10.1111/j.1750-3639.2002.tb00433.x

79. Martínez-Glez V, Alvarez L, Franco-Hernández C, Torres-Martin M, de Campos JM, Isla A, et al. Genomic deletions at 1p and 14q are associated with an abnormal cDNA microarray gene expression pattern in meningiomas but not in schwannomas. *Cancer Genet Cytogenet*. (2010) 196:1–6. doi: 10.1016/j.cancergencyto.2009.08.003

80. Kresbach C, Dorostkar MM, Suwala AK, Wefers AK, Schweizer L, Engertsberger L, et al. Neurofibromatosis type 2 predisposes to ependymomas of various localization, histology, and molecular subtype. *Acta Neuropathol*. (2021) 141:971–4. doi: 10.1007/s00401-021-02304-4

81. Marinoff AE, Ma C, Guo D, Snuderl M, Wright KD, Manley PE, et al. Rethinking childhood ependymoma: a retrospective, multi-center analysis reveals poor long-term overall survival. *J Neuro-Oncol*. (2017) 135:201–11. doi: 10.1007/s11060-017-2568-8

82. Mendrzyk F, Korshunov A, Benner A, Toedt G, Pfister S, Radlwimmer B, et al. Identification of gains on 1q and epidermal growth factor receptor overexpression as independent prognostic markers in intracranial ependymoma. *Clin Cancer Res*. (2006) 12:2070–9. doi: 10.1158/1078-0432.CCR-05-2363

83. Das P, Puri T, Suri V, Sharma MC, Sharma BS, Sarkar C. Medulloblastomas: a correlative study of MIB-1 proliferation index along with expression of c-Myc, ERBB2, and anti-apoptotic proteins along with histological typing and clinical outcome. *Childs Nerv Syst*. (2009) 25:825–35. doi: 10.1007/s00381-009-0884-9

84. Ellison D. Classifying the medulloblastoma: insights from morphology and molecular genetics. *Neuropathol Appl Neurobiol*. (2002) 28:257–82. doi: 10.1046/j.1365-2990.2002.00419.x

85. Ramaswamy V, Northcott PA, Taylor MD. FISH and chips: the recipe for improved prognostication and outcomes for children with medulloblastoma. *Cancer Genet*. (2011) 204:577–88. doi: 10.1016/j.cancergen.2011.11.001

86. Minasi S, Gianno F, Bargiacchi L, Barresi V, Miele E, Antonelli M, et al. Case report of a pediatric medulloblastoma with concurrent MYC and MYCN subclonal amplification in distinct populations of neoplastic cells. *Virchows Arch*. (2023):1–6. doi: 10.1007/s00428-023-03560-3

87. Gilbertson R, Wickramasinghe C, Hernan R, Balaji V, Hunt D, Jones-Wallace D, et al. Clinical and molecular stratification of disease risk in medulloblastoma. *Br J Cancer*. (2001) 85:705–12. doi: 10.1054/bjoc.2001.1987

88. Okonechnikov K, Federico A, Schrimpf D, Sievers P, Sahm F, Koster J, et al. Comparison of transcriptome profiles between medulloblastoma primary and recurrent tumors uncovers novel variance effects in relapses. *Acta Neuropathol Commun*. (2023) 11:1–12. doi: 10.1186/s40478-023-01504-1

89. Taylor MD, Northcott PA, Korshunov A, Remke M, Cho YJ, Clifford SC, et al. Molecular subgroups of medulloblastoma: the current consensus. *Acta Neuropathol*. (2012) 123:465–72. doi: 10.1007/s00401-011-0922-z

90. Packer RJ, Macdonald T, Vezina G, Keating R, Santi M. Medulloblastoma and primitive neuroectodermal tumors. *Handb Clin Neurol*. (2012) 105:529–48. doi: 10.1016/b978-0-444-53502-3.00007-0

91. Burnett ME, White EC, Sih S, von Haken MS, Cogen PH. Chromosome arm 17p deletion analysis reveals molecular genetic heterogeneity in supratentorial and infratentorial primitive neuroectodermal tumors of the central nervous system. *Cancer Genet Cytogenet*. (1997) 97:25–31. doi: 10.1016/S0165-4608(96)00319-6

92. Russo C, Pellarin M, Tingby O, Bollen AW, Lamborn KR, Mohapatra G, et al. Comparative genomic hybridization in patients with supratentorial and infratentorial primitive neuroectodermal tumors. *Cancer*. (1999) 86:331–9. doi: 10.1002/(SICI)1097-0142(19990715)86:2<331::AID-CNCR18>3.0.CO;2-#

93. Biegel JA, Allen CS, Kawasaki K, Shimizu N, Budarf ML, Bell CJ. Narrowing the critical region for a rhabdoid tumor locus in 22q11. *Genes Chromosom Cancer*. (1996) 16:94–105. doi: 10.1002/(SICI)1098-2264(199606)16:2<94::AID-GCC3>3.0.CO;2-Y

94. Biegel JA, Fogelgren B, Wainwright LM, Zhou JY, Bevan H, Rorke LB. Germline INI1 mutation in a patient with a central nervous system atypical teratoid tumor and renal rhabdoid tumor. *Genes Chromosom Cancer*. (2000) 28:31–7. doi: 10.1002/(SICI)1098-2264(200005)28:1<31::AID-GCC4>3.0.CO;2-Y

95. Müller HL, Merchant TE, Warmuth-Metz M, Martinez-Barbera JP, Puget S. Craniopharyngioma. *Nat Rev Dis Prim*. (2019) 5:75. doi: 10.1038/s41572-019-0125-9

96. Apps JR, Martinez-Barbera JP. Pathophysiology and genetics in craniopharyngioma In: Honegger J, Reincke M, Petersenn S, (editors). *Pituitary tumors*. Headquarters, Cambridge, Massachusetts: Academic Press (2021). 53–66.

97. Palmer JD, Song A, Shi W. Craniopharyngioma In: E Chang, P Brown, S Lo, A Sahgal and J Suh, editors. Adult CNS radiation oncology: principles and practice. Cham: Springer (2018). 37–50.

98. Sekine S, Shibata T, Kokubu A, Morishita Y, Noguchi M, Nakanishi Y, et al. Craniopharyngiomas of adamantinomatous type harbor β-catenin gene mutations. *Am J Pathol*. (2002) 161:1997–2001. doi: 10.1016/S0002-9440(10)64477-X

99. Goschzik T, Gessi M, Dreschmann V, Gebhardt U, Wang L, Yamaguchi S, et al. Genomic alterations of adamantinomatous and papillary craniopharyngioma. *J Neuropathol Exp Neurol*. (2017) 76:126–34. doi: 10.1093/jnen/nlw116

100. Jia Y., Wang G., Ye Y., Kang E., Wu J., He X., et al. (2022). Exploration of inflammation-prognosis correlation and potential regulatory molecules in adamantinomatous craniopharyngioma, Research square preprint.

101. Xu C, Ge S, Cheng J, Gao H, Zhang F, Han A. Pathological and prognostic characterization of craniopharyngioma based on the expression of TrkA, β-catenin, cell cycle markers, and BRAF V600E mutation. *Front Endocrinol*. (2022) 13:859381. doi: 10.3389/fendo.2022.1036625

102. Melmed S, Kaiser UB, Lopes MB, Bertherat J, Syro LV, Raverot G, et al. Clinical biology of the pituitary adenoma. *Endocr Rev*. (2022) 43:1003–37. doi: 10.1210/endrev/bnac010

103. Yokoyama S, Hirano H, Moroki K, Goto M, Imamura S, Kuratsu JI. Are nonfunctioning pituitary adenomas extending into the cavernous sinus aggressive and/or invasive? *Neurosurgery*. (2001) 49:857–63. doi: 10.1227/00006123-200110000-00014

104. Kontogeorgos G. Predictive markers of pituitary adenoma behavior. *Neuroendocrinology*. (2006) 83:179–88. doi: 10.1159/000095526

105. Pernicone PJ, Scheithauer BW. Invasive pituitary adenoma and pituitary carcinoma In: *Diagnosis and management of pituitary tumors*. Totowa, NJ: Humana Press (2001). 369–85.

106. Barry S, Korbonits M. Update on the genetics of pituitary tumors. *Endocrinol Metab Clin*. (2020) 49:433–52. doi: 10.1016/j.ecl.2020.05.005

107. Kontogeorgos G. Molecular cytogenetics of pituitary adenomas, assessed by FISH technique In: *Molecular pathology of the pituitary, vol. 32*. George Kontogeorgos: Karger Publishers (2004). 205–16.

108. Magaki S., Hojat S. A., Wei B., So A., Yong W. H. (2019). An introduction to the performance of immunohistochemistry. Biobanking: Methods and Protocols, 289–298.

109. Thapar K, Kovacs K, Scheithauer BW, Stefaneanu L, Horvath E, Pernicone PJ, et al. Proliferative activity and invasiveness among pituitary adenomas and carcinomas: an analysis using the MIB-1 antibody. *Neurosurgery*. (1996) 38:99–107. doi: 10.1097/00006123-199601000-00024

110. Nakabayashi H, Sunada I, Hara M. Immunohistochemical analyses of cell cycle-related proteins, apoptosis, and proliferation in pituitary adenomas. *J Histochem Cytochem*. (2001) 49:1193–4. doi: 10.1177/002215540104900916

111. Finelli P, Giardino D, Rizzi N, Buiatiotis S, Virduci T, Franzin A, et al. Non-random trisomies of chromosomes 5, 8 and 12 in the prolactinoma sub-type of pituitary adenomas: conventional cytogenetics and interphase FISH study. *Int J Cancer*. (2000) 86:344–50. doi: 10.1002/(SICI)1097-0215(20000501)86:3<344::AID-IJC7>3.0.CO;2-8

112. Ezzat S. The role of hormones, growth factors and their receptors in pituitary tumorigenesis. *Brain Pathol*. (2001) 11:356–70. doi: 10.1111/j.1750-3639.2001.tb00405.x

113. Wattel S, Mircescu H, Venet D, Burniat A, Franc B, Frank S, et al. Gene expression in thyroid autonomous adenomas provides insight into their physiopathology. *Oncogene*. (2005) 24:6902–16. doi: 10.1038/sj.onc.1208849

114. Burman P, Casar-Borota O, Perez-Rivas LG, Dekkers OM. Aggressive pituitary tumors and pituitary carcinomas: from pathology to treatment. *J Clin Endocrinol Metabol*. (2023) 108:1585–601. doi: 10.1210/clinem/dgad098

115. Kontogeorgos G, Thodou E, Osamura RY, Lloyd RV. High-risk pituitary adenomas and strategies for predicting response to treatment. *Hormones*. (2022) 21:1–14. doi: 10.1007/s42000-021-00333-y

116. Manoranjan B, Salehi F, Scheithauer BW, Rotondo F, Kovacs K, Cusimano MD. Estrogen receptors α and β immunohistochemical expression: Clinicopathological correlations in pituitary adenomas. *Anticancer Res*. (2010) 30:2897–904. doi: 10.1096/fasebj.23.1_supplement.925.10

117. Tatsi C, Stratakis CA. The genetics of pituitary adenomas. *J Clin Med*. (2019) 9:30. doi: 10.3390/jcm9010030

118. Cohen-Cohen S, Brown DA, Himes BT, Wheeler LP, Ruff MW, Major BT, et al. Pituitary adenomas in the setting of multiple endocrine neoplasia type 1: a single-institution experience. *J Neurosurg*. (2020) 1:1–7. doi: 10.3171/2020.1.jns193538

119. Fedele M, Pierantoni GM, Visone R, Fusco A. Critical role of the HMGA2 gene in pituitary adenomas. *Cell Cycle*. (2006) 5:2045–8. doi: 10.4161/cc.5.18.3211

120. Heaphy CM, Bi WL, Coy S, Davis C, Gallia GL, Santagata S, et al. Telomere length alterations and ATRX/DAXX loss in pituitary adenomas. *Mod Pathol*. (2020) 33:1475–81. doi: 10.1038/s41379-020-0523-2

121. Fujimoto K, Arita H, Satomi K, Yamasaki K, Matsushita Y, Nakamura T, et al. TERT promoter mutation status is necessary and sufficient to diagnose IDH-wildtype diffuse astrocytic glioma with molecular features of glioblastoma. *Acta Neuropathol*. (2021) 142:323–38. doi: 10.1007/s00401-021-02337-9

122. Lau N, Feldkamp MM, Roncari L, Loehr AH, Shannon P, Gutmann DH, et al. Loss of neurofibromin is associated with activation of RAS/MAPK and PI3-K/AKT signaling in a neurofibromatosis 1 astrocytoma. *J Neuropathol Exp Neurol*. (2000) 59:759–67. doi: 10.1093/jnen/59.9.759

123. Jørgensen S, Baker A, Møller S, Nielsen BS. Robust one-day in situ hybridization protocol for detection of microRNAs in paraffin samples using LNA probes. *Methods*. (2010) 52:375–81. doi: 10.1016/j.ymeth.2010.07.002

124. Villano J L, Morgan R M, Zhang S, Kolesar J, Xiu J, Seifert H, et al. (2023). Association of CDK4 amplification with duration of response to bevacizumab in glioblastoma.

125. Łysiak M, Smits A, Roodakker KR, Sandberg E, Dimberg A, Mudaisi M, et al. Deletions on chromosome Y and downregulation of the SRY gene in tumor tissue are associated with worse survival of glioblastoma patients. *Cancers*. (2021) 13:1619. doi: 10.3390/cancers13071619

126. Li G, Zhang Z, Jin T, Liang H, Tu Y, Gong L, et al. High frequency of the X-chromosome inactivation in young female patients with high-grade glioma. *Diagn Pathol*. (2013) 8:1–9. doi: 10.1186/1746-1596-8-101

127. Weller M, Stupp R, Hegi ME, Van Den Bent M, Tonn JC, Sanson M, et al. Personalized care in neuro-oncology coming of age: why we need MGMT and 1p/19q testing for malignant glioma patients in clinical practice. *Neuro-Oncology*. (2012) 14:iv100–8. doi: 10.1093/neuonc/nos206

128. Tilak M, Holborn J, New LA, Lalonde J, Jones N. Receptor tyrosine kinase signaling and targeting in glioblastoma multiforme. *Int J Mol Sci*. (2021) 22:1831. doi: 10.3390/ijms22041831

129. Kim JH, Lee SH, Rhee CH, Park SY, Lee JH. Loss of heterozygosity on chromosome 22q and 17p correlates with aggressiveness of meningiomas. *J Neuro-Oncol*. (1998) 40:101–6. doi: 10.1023/A:1006110812240

130. Pagès M, Pajtler KW, Puget S, Castel D, Boddaert N, Tauziède-Espariat A, et al. Diagnostics of pediatric supratentorial RELA ependymomas: integration of information from histopathology, genetics, DNA methylation and imaging. *Brain Pathol*. (2019) 29:325–35. doi: 10.1111/bpa.12664

frontiers | Frontiers in Oncology

TYPE Brief Research Report
PUBLISHED 10 July 2024
DOI 10.3389/fonc.2024.1401761

OPEN ACCESS

EDITED BY
John Bianco,
Princess Maxima Center for Pediatric Oncology, Netherlands

REVIEWED BY
Emmanuel Jouanneau,
Hospices Civils de Lyon, France
Hermann Lothar Mueller,
Klinikum Oldenburg, Germany

*CORRESPONDENCE
Johannes Gojo
johannes.gojo@meduniwien.ac.at
Ute Bartels
ute.bartels@sickkids.ca

†These authors share first authorship

‡These authors share senior authorship

RECEIVED 15 March 2024
ACCEPTED 17 June 2024
PUBLISHED 10 July 2024

CITATION
Hedrich C, Patel P, Haider L, Taylor T, Lau E, Hook R, Dorfer C, Roessler K, Stepien N, Lippolis MA, Schned H, Koeller C, Mayr L, Azizi AA, Peyrl A, Lopez BR, Lassaletta A, Bennett J, Gojo J and Bartels U (2024) Feasibility, tolerability, and first experience of intracystic treatment with peginterferon alfa-2a in patients with cystic craniopharyngioma. *Front. Oncol.* 14:1401761. doi: 10.3389/fonc.2024.1401761

Feasibility, tolerability, and first experience of intracystic treatment with peginterferon alfa-2a in patients with cystic craniopharyngioma

Cora Hedrich[1†], Priya Patel[2†], Lukas Haider[3,4], Tracey Taylor[2], Elaine Lau[2], Roxanne Hook[2], Christian Dorfer[5], Karl Roessler[5], Natalia Stepien[1], Maria Aliotti Lippolis[1], Hannah Schned[1], Clara Koeller[1], Lisa Mayr[1], Amedeo A. Azizi[1], Andreas Peyrl[1], Bienvenido Ros Lopez[6], Alvaro Lassaletta[7,8], Julie Bennett[9,10], Johannes Gojo[1*‡] and Ute Bartels[9*‡]

[1]Department of Pediatrics and Adolescent Medicine, Comprehensive Center for Pediatrics and Comprehensive Cancer Center, Medical University of Vienna, Vienna, Austria, [2]Department of Pharmacy, The Hospital for Sick Children, Toronto, ON, Canada, [3]Department of Biomedical Imaging and Image-Guided Therapy, Medical University of Vienna, Vienna, Austria, [4]NMR Research Unit, Queen Square Multiple Sclerosis Centre, Queen Square Institute of Neurology, University College London, London, United Kingdom, [5]Department of Neurosurgery, Medical University of Vienna, Vienna, Austria, [6]Department of Neurosurgery, Hospital Materno Infantil de Málaga, Málaga, Spain, [7]Department of Pediatric Hematology-Oncology, Pediatric Neuro-Oncology Unit, Hospital Infantil Universitario Niño Jesús, Madrid, Spain, [8]Department of Radiation Oncology, Clinica Universidad de Navarra, Madrid, Spain, [9]Division of Paediatric Haematology and Oncology, Paediatric Brain Tumour Program, The Hospital for Sick Children, Toronto, ON, Canada, [10]Division of Medical Oncology and Hematology, Princess Margaret Cancer Centre, Toronto, ON, Canada

Background: Children with craniopharyngiomas (CPs) typically suffer from a life-long chronic disease. The younger the child, the more vulnerable the maturing brain is to invasive therapies such as surgery or radiotherapy. Therefore, treatment modalities facilitating avoidance or delay of invasive therapies are beneficial for these patients. In the last decade, intracystic injection of interferon alfa-2a or alfa-2b evolved as a treatment of choice based on efficacy and minor toxicity. However, the drug is no longer available internationally. After an extensive pharmacological review, peginterferon alfa-2a was identified as the agent with closest similarity.

Methods: A retrospective case series is described, including five patients treated with intracystic peginterferon alfa-2a for cystic CP according to an innovative care protocol. After initial CP cyst aspiration, peginterferon alfa-2a was injected once per week via an Ommaya reservoir for 6 weeks followed by response assessment with MRI.

Results: Patients' age ranged from 4 to 54 years (four patients <12 years, one adult patient). Intracystic therapy with peginterferon alfa-2a was tolerated well by all five individuals without any major toxicities and resulted in cyst shrinkage in all of the five patients. The importance of a permeability study prior to commencing intracystic therapy became apparent in one patient who suffered from cyst leakage.

Conclusions: Intracystic treatment with peginterferon alfa-2a was found to be a tolerable and efficacious treatment modality in patients with cystic CP. This experience warrants further research with a larger number of patients with measurement of long-term efficacy and safety outcomes.

KEYWORDS

craniopharyngioma, intracystic treatment, peginterferon alfa-2a, pediatric neurooncology, pediatric neurosurgery

Introduction

Adamantinomatous craniopharyngioma (CP) accounts for approximately 5%–10% of pediatric brain tumors. Histologically, they are characterized as benign tumors (1). Gross total resection would represent a cure, but due to spatial proximity or invasion of the tumor to vital anatomical structures, such as the pituitary gland, the optic pathway, the circle of Willis, and the hypothalamus, radical resection could cause serious harm to these structures and, thus, is not generally considered of clinical benefit (2–8). Typical sequelae of surgery include visual impairment, stroke, loss of endocrine function with life-long dependency on hormonal substitution, and life-threatening situations including adrenal crisis or complex electrolyte imbalances and hypothalamic dysfunction, which can result in morbid obesity (3, 4, 8, 9). Another effective method of craniopharyngioma treatment is the use of radiotherapy with good response rates across previous studies (10–13). However, the proximity to the vital structures listed above may cause the same irreversible complications as surgery along with the characteristic long-term complications of radiotherapy, namely, decreased cognitive function, vasculopathies, e.g., Moya Moya, and increased risk of secondary neoplasms (14–20).

Craniopharyngiomas typically consist of solid, calcified, and cystic components (21). Cysts occur in more than 90% of the tumors, often encompassing a major part of the tumor bulk, causing impairment of important structures such as the optic chiasm or obstruction of cerebrospinal fluid circulation (22, 23). This feature is the basis for intracystic therapy, where the neurosurgeon inserts a catheter into the cyst and attaches it to a subgaleal Ommaya reservoir. Via Ommaya reservoir access, drugs can be directly administered into the cyst. In the last decade, interferon alfa-2a and alfa-2b evolved as the treatment of choice due to persuasive efficacy and minor toxicity (22, 24–28).

Interferon alfa-2a and alfa-2b was introduced in the 1950s as an antiviral therapy and has been found to have anti-proliferative activity through inhibition of the JAK/STAT/MAPK pathways and apoptosis through the FAS pathway (29–32).

Typical internationally accepted standard of care schemes such as the São Paulo series or the Toronto protocol consist of the administration of 3 million IU interferon alfa-2a or alfa-2b three times a week (Monday, Wednesday, and Friday) for 4 weeks that were designed as a cycle (24, 33).

Two different forms of interferon alfa, namely, interferon alfa-2a (Roferon®-A) and interferon alfa-2b (Intron® A), were previously available but discontinued due to availability of pegylated forms of interferon alfa for the licensed indications. Consequently, the drugs are no longer available.

Being used to the drawbacks of treating rare but very severe diseases with orphan therapies, we set out to find an alternative drug for intracystic therapy to treat children with craniopharyngioma appropriately.

Material and methods

Development of an adapted treatment protocol

In brief, a prefilled syringe of 180 mcg (1 ml) peginterferon alfa-2a is injected once weekly via an intracystically placed Ommaya reservoir for 6 weeks (one treatment cycle). At the start of treatment course (day 1), the maximum possible amount of cystic fluid (as patient tolerates) was slowly removed. At the following administrations, the maximal possible amount of fluid (at least 1.5–2 ml) was aspirated. More cycles can be added to obtain a maximal response.

Depending on the availability of MRI slots in the institution and the need of sedation, fast MRI sequences (see below) every 3 weeks can be performed as optional diagnostic follow-up (Figure 1).

Response assessment

A complete MRI examination (34) for the evaluation of solid tumor components and surrounding key structures was performed at least every 3 months. Notably, a contrast-enhanced MRI is necessary at initial diagnosis or if a solid component progressed, whereas for the evaluation of cyst size, the contrast agent can be dismissed.

The optional fast MRI sequences for response assessment were performed according to the recommendations of the Response

Assessment in Pediatric Neuro-Oncology (RAPNO) Working Group and consist of at least three orthogonal T2-weighted sequences and conceivably additional sequences at the radiologist's discretion for optimal assessment (35). Whenever applicable, cyst size was evaluated by the local radiologist by measurement of cyst size in three dimensions.

Regular neurological exams, vision exams, testing for the pituitary function, and anthropometric measures were performed at least every 3 months for comprehensive evaluation of response assessment.

Patient data

Five patients from four different institutions (Medical University of Vienna, The Hospital for Sick Children, Princess Margaret Cancer Centre, and Hospital Infantil Universitario Niño Jesús) treated with intracystic peginterferon alfa-2a are included in this report. Data including patient demographics, symptoms at diagnosis or progression, side effects, MRI findings, and response to treatment were collected as standard of care.

In three of the five patients (patient 1, patient 3, and patient 5), the diagnosis of craniopharyngioma was confirmed by histopathology. The other two patients met classical radiological criteria, and the cyst aspiration demonstrated pathognomonic engine oil-like fluid.

Ethics

Based on thorough reviews of each patients' case within respective institutional interdisciplinary tumor boards, a suggestion of intracystic treatment was made, and informed consent was given by patient or patient's legal guardian prior to commencing treatment with peginterferon alfa-2a.

Results

Establishment of an alternative for interferon alfa-2a or alfa-2b

A literature search was conducted in October 2020 in Ovid MEDLINE and Embase to determine if there was any published literature with intracystic administration of other interferon products for the treatment of craniopharyngioma. Search terms included interferon and craniopharyngioma, and studies published from 1980 and onwards were included in the search. In addition, a review of all available interferon products was undertaken to better understand the pharmaceutical differences and to make a recommendation for off-label intracystic administration. Based on this review, it was determined that the closest interferon product marketed in Canada to interferon-alfa2 was pegylated interferon (peginterferon)-alfa2a (Pegasys®). It was important to note that peginterferon alfa-2a and peginterferon alfa-2b were not interchangeable products as the polyethylene glycol (PEG) chain and bond to the interferon-alfa molecule differed (36). PEGylation is the process of attachment of PEG polymer chains to a molecule and therefore increasing its molecular weight and improving pharmaceutical properties such as the extension of therapy effect. The systemic clearance of peginterferon alfa-2a is approximately 100-fold lower in comparison to interferon alfa-2a. The terminal half-life of peginterferon is approximately 60–80 h after intravenous and 160 h in subcutaneous administration. The dosing that was suggested for peginterferon-alpha2a for craniopharyngioma (one treatment course encompasses once weekly cystic aspirations followed by injection of 180 mcg peginterferon alfa-2a via an Ommaya reservoir for 6 weeks) was extrapolated based on the conversion of subcutaneous hepatitis C dosing of non-pegylated interferon-alfa2a to peginterferon-alpha2a (i.e., peginterferon alfa2a 180 mcg/dose once weekly = interferon alfa2a 3 million units/dose three times per week). The pharmacy team also reviewed the formulation for compatibility with intracystic administration. Typically, formulations administered via an Ommaya reservoir or intrathecally are preservative-free and isotonic. The osmolality of peginterferon alpha-2a is 375–415 mOsmol/kg (slightly hypertonic) (personal communication with Roche, February 2021), and the product also contains benzyl alcohol (37) (preservative), which can cause transient paraplegia or neurotoxicity and polysorbate 80 (38) (solubilizing agent), which can cause allergic reactions. These ingredients would not typically make for an ideal formulation for intracystic administration. However, both of these ingredients are also found in interferon-alfa2a (39), which has been used intracystically across multiple patient series. Thus, we decided to offer intracystic administration with the peginterferon-alfa-2a product disclosing the potential risks to the patient and family. First experiences in five patients treated in exact accordance to the innovative care protocol at four different institutions are presented in this article.

First clinical case series

Within an international collaboration, we compiled the first five cases treated with peginterferon alfa-2a (Table 1; Figures 2, 3) according to the same innovative care protocol for treatment guidance (Supplementary Material 1).

Patient 1 was a 7-year old boy with a CP who was previously treated with intracystic bleomycin consisting of two cycles in an interval of 6 months. Subsequently, a VP-shunt insertion and a pterional partial resection took place. Due to further cystic progression only 2 months later, he received intracystic peginterferon alfa-2a, which he tolerated well without any side effects. As a response to treatment, the central multiloculated cyst collapsed, but some small peripheral isolated cysts progressed.

Patient 2 was a 4-year-old patient who was newly diagnosed with a monocystic craniopharyngioma. A catheter was inserted to allow for aspiration of cyst fluid without the instillation of medication. This therapeutic effect was only short-lived, as the cyst returned to its original size after a month. In addition, visual acuity decreased during this interval (Table 1). At that time, no cyst fluid could be aspirated, leading to a catheter revision.

10.3389/fonc.2024.1401761

TABLE 1 * 0= stable disease or mixed response, 1= cyst shrinkage, 2= progression during therapy; **collapse of central multiloculated cyst but growth of small peripheral isolated cysts; ***0= no relevant side effects, Common Terminology Criteria for Adverse Events (CTCAE) Grade.

	Age (years)	Sex	Prior therapy	Type	Number of PEG-IFN applications	Response*	Cyst volume before/after PEG-IFN treatment	Clinical benefit	Side effects***
Patient 1[1]	7	m	2 cycles bleomycine	Multicystic	6	0	5.8 ml/collapse**	Improvement of headaches during treatment	0
Patient 2[2]	4	f	1x Cyst drainage	Monocystic	9	1	8.71 ml/0.33 ml	Minimal improvement of vision	0
Patient 3[3]	54	m	3x resection Radiation therapy	Multicystic	6	1	9.10 ml/2.10 ml	improvement of headaches, vision, and neurocognition	0
Patient 4[4]	5	f	1x Cyst drainage	Multicystic	6	1	4 ml/0.5 ml	Improvement of headaches, preservation of vision	CTCAE grade 1 (fatigue)
Patient 5[2]	12	m	1x resection	Multicystic	1	1	N/A	Preservation of vision	CTCAE grade 3 hypersensitivity reaction (hospitalization)

1: Regional University Hospital, Malaga, Spain;
2: Medical University of Vienna, Austria;
3: Princess Margaret Hospital, Toronto, Canada,
4: Hospital for Sick Children, Toronto, Canada.

Subsequently, treatment with intracystic peginterferon alfa-2a was given. The patient tolerated the therapy well, and only reported local skin pain in the area of the Ommaya reservoir and headache during the aspiration of the cyst. The residual cyst volume continuously decreased during treatment and shrunk to such a low volume, that we considered the therapy successfully completed after 9 injections (Figure 1). Four weeks after the first administration of peginterferon alfa-2a, the vision improved to a

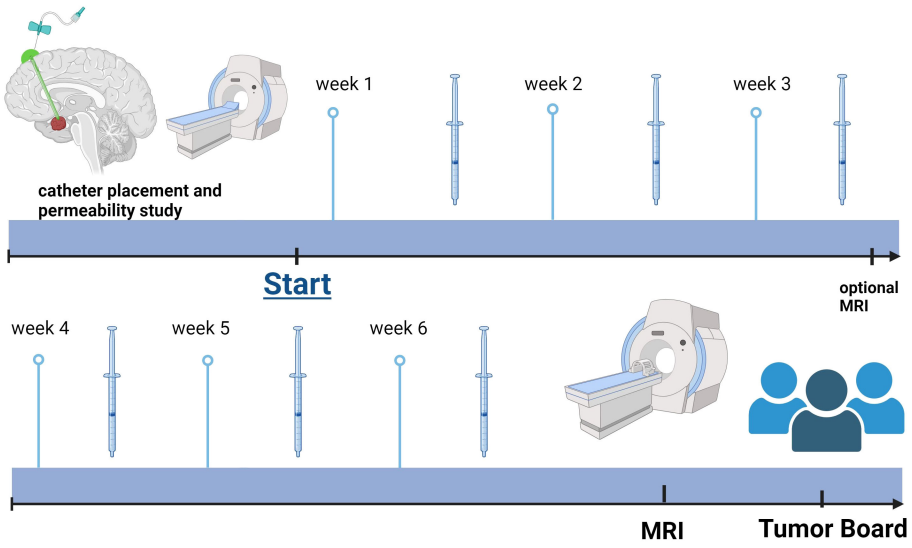

FIGURE 1
Schematic discription of the treatment protocol.

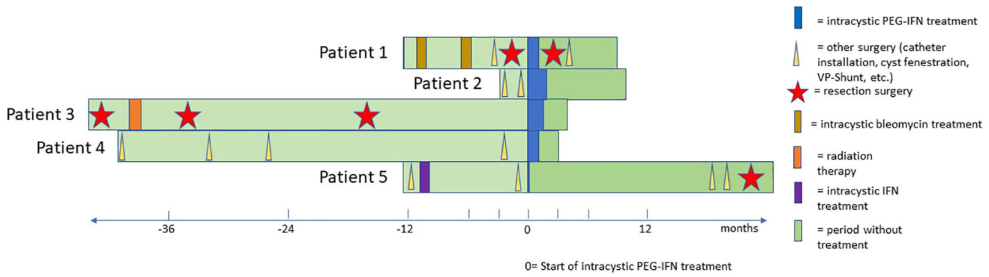

FIGURE 2
Swimmer's plot that shows the individual treatment course of each patient from the initial diagnosis until the preparation of the manuscript. The vertical purple line represents the start of cystic Peg Interferon alfa treatment in each patient.

small extent and remained stable at last follow-up. The CP cyst remained stable in size for 41 weeks after the completion of the peginteferon alfa-2a therapy (Figure 3).

Patient 3 is a 54-year-old man who was histologically diagnosed with adamantinomatous CP. Initially, he underwent a tumor resection followed by 54 Gy in 30 fractions radiation therapy. He suffered from a local recurrence twice and received debulking surgery at 1 and 3 years after the initial diagnosis. The patient suffered a stroke after the third surgery, which led to right-sided paralysis, and he experienced another cystic progression within the same year. Despite cyst aspirations, the patient had nightly headaches and visual disturbance and demonstrated difficulties with memory and slow speech due to fast refilling of the cyst. Hence, a course of intracystic peginteferon alfa-2a was suggested. After the second injection, he experienced nausea. There were no further toxicities, and he tolerated all the other procedures well. Due to a vacation, he interrupted the therapy for 2 weeks during the 6-week cycle. He subjectively noted an improvement of the headaches and the vision. Neuropsychological testing showed amelioration of memory and speech function. The assessment at the treating institution reported a decrease in the cyst volume from 9.1 ml to 2.1 ml (total shrinkage of 77%). One month after completion of treatment, the MRI scan showed a re-accumulation of fluid in the cyst. The ophthalmic examination showed a significant worsening of the vision (right eye, 20/25; left eye, 20/200). He had temporary relief of symptoms with a cyst aspiration, and another course of intracystic peginterferon alfa-2a therapy has been initiated for this patient. In this patient, some clinical improvement may be attributed to the cyst aspirations alone. However, the interval between the interventions and relapse increased after peginterferon application.

Patient 4 is a 5-year-old girl who was treated with cyst drainage and later catheter insertion and catheter revision at the first months of diagnosis of her multicystic craniopharyngioma. When a new posterior cyst showed a progression after 3 years, a new catheter was inserted medial to the pre-existing frontal one. The patient started treatment with peginterferon alfa-2a 3 years after the initial diagnosis and received one cycle. Prior to treatment, the patient reported multiple severe episodes of headaches daily. In the course of the treatment, they improved significantly and decreased in frequency to only one to two times per week. During the treatment, the patient had some flu-like symptoms and fatigue. Noteworthy, the patient did not take her prescribed hydrocortisone substitution for several days due to the taste of the pill, which may have contributed to her fatigue.

Patient 5 was a 12-year-old boy who had previously received treatment with intracystic Interferon alfa-2a at initial diagnosis (three times per week for 4 weeks) with good response. One year later, the patient suffered cystic progression, and due to catheter dysfunction, an operative revision was performed to facilitate intracystic treatment. Two days after the first administration of peginteferon alfa-2a, the patient experienced a distinct systemic reaction with general skin rash and edema. The patient was immediately admitted to his local hospital where he was treated with corticosteroids and antihistamines and showed fast remission within hours. The intracystic therapy was discontinued in this patient. Retrospectively, the catheter was dislocated outside of the cyst due to intraoperative collapse resulting in the administration of the substance in the adjacent tissue inducing a systemic reaction. Subsequently, the CP remained stable for 19 months before a new cyst emerged again, necessitating surgical treatment and placement of a new catheter. This time, a permeability study was performed, indicating leakage of contrast media. Consequently, no intracystic treatment was administered, and a partial resection followed by proton beam therapy was performed.

Discussion

Intracystic therapy with interferon alfa-2a has been used as an established modality in several institutions in the therapy of children with CP. Analysis of previous retrospective studies demonstrated an advantage in effectiveness and tolerability for intracystic interferon compared to other established therapies (22, 24–26, 31, 33). The largest trial on intratumoral interferon alfa-2a was published by the São Paulo team, who are also the pioneers in the development of intratumoral Interferon alfa-2a treatment (24). Clinical and radiological improvement was achieved in 76% of the 60 patients included (25). However, this review has no sufficient long-term follow-up data yet to inform on the duration of the cyst reduction and the time to subsequent progression.

A global, multicenter assessment on behalf of SIOPE and ISPN represents another broad clinical experience on intracystic therapy with

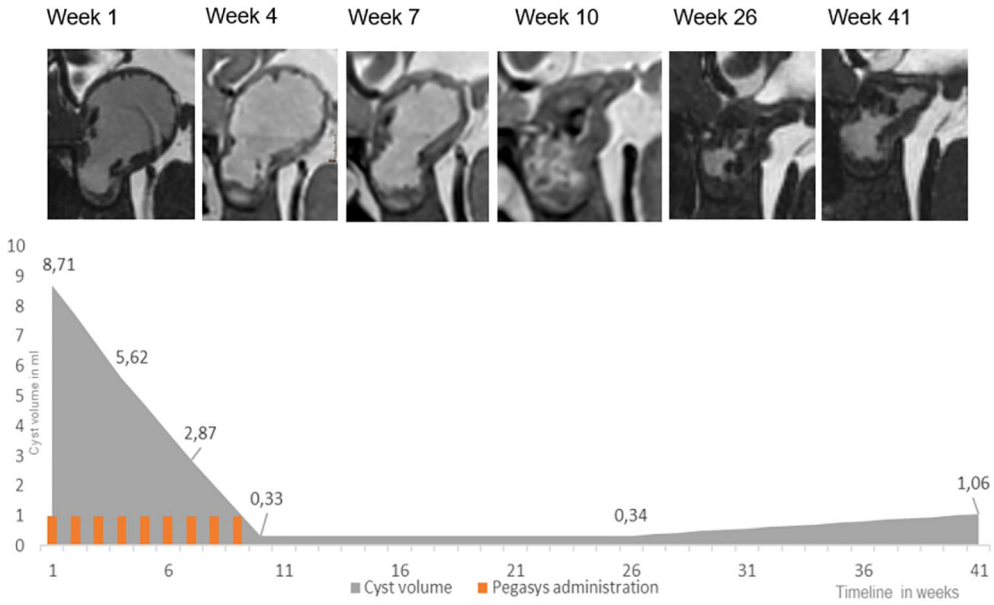

FIGURE 3
Peginterferon alfa-2a treatment in patient 2: high resolution, isotropic, strongly T2-weighted sequences, with 0.7 mm voxel size were acquired at 1.5 T using a Siemens Aera (CISS) and Philips Ingenia (BTFE). The lower panel indicates development of the cyst volume and treatment.

Interferon-alfa including 56 children in this retrospective study (26). While treatment with the previously used (unpegylated) intracystic interferon had shown to delay the need for surgical resection or radiotherapy for a median time of 5.8 years, it is important to note that the long-term efficacy of treatment with intracystic peginterferon still needs to be proven within future clinical trials. The authors proposed a global, prospective randomized clinical trial of intracystic interferon in childhood CP, but the randomized trial concept was considered too expensive and prone to fail in this rare disease by funding resources. Hence, this case series fills an important gap and demonstrates the feasibility of an intracystic peginterferon alfa-2a regimen. It is relevant to address several limitations inherent in this study. First, the series includes only five patients. However, since craniopharyngioma is a rare disease and not all craniopharyngioma patients are suitable for intracystic treatment, we consider our experience of high importance to the neuro-oncology community. Second, the data exhibit a certain heterogeneity such as differences in the decision process on the indication for the treatment, the selection of suitable patients, the previous treatments of the patients, and the follow-up due to the nature of a retrospective study. Additionally, this report does not inform on the neurosurgical aspects to fulfill the requirement of a functional intracystic catheter, which may also limit applicability of intracystic treatment. Case 5 demonstrated the importance of pursuing a permeability study at least 2 weeks postoperatively and prior to the start of intracystic treatment to rule out leakage, most likely the cause of patient's systemic toxicities (40). One case report of a 13-year-old patient treated with intracystic plus concomitantly subcutaneous pegylated interferon alfa-2b (41) described irreversible visual field loss and confirmed leakage from the intracystic catheter via computed tomographic imaging as the cause.

Herein, we present the first series of five patients treated with intracystic peginterferon alfa-2a. All patients showed prior progressive disease according to the new consensus guidelines of the Response Assessment in Pediatric Neuro-Oncology (RAPNO) committee indicated by change of cyst size and deterioration of a clinical parameter such as a new functional impairment or the need of surgical intervention (35). In general, intracystic treatment is considered particularly effective in monocystic CP. In multicystic CP, peripherical cysts may not communicate with the drained main cyst and are therefore not accessible to the intracystic treatment. This was demonstrated in patient 1 in whom the central multiloculated cyst collapsed, but a growth of small peripherical cysts was noted at the end of the treatment. A proactive approach towards intracystic therapy may postpone morbidities associated with surgical resection and irradiation as the insertion of a catheter is a low-risk operation (9), and there is a certain risk that newly developed functional impairments are not reversible once they occur. There is no doubt that delaying more aggressive surgical interventions and/or radiotherapy will be of significant benefit to young children and their maturing brains. This is in line with the main goal in treatment of CP as a chronic disease with a paradigm to maintain good quality of life (QoL) with minimally invasive intervention given the potential for substantial morbidity in the long-term outcomes of CP patients (21, 42–44).

While our findings prove the feasibility of intracystic peginterferon alfa-2a, no definite conclusions on the future significance can be made. To address these gaps, collaborative efforts across a large number of brain tumor centers must be made to design clinical trials with adherence to well-defined entry criteria, standardized treatment protocols, and interpretation of results by a reference center. With the recent advances in precision medicine,

some potential targets such as IL-6, PD1/PD-L1, MEK, IDO-1, and others have been identified for the treatment of craniopharyngioma (45–47). For example, the CONNECT 1905 phase 2 study analyzes the effects in craniopharyngioma patients treated with systemic Tocilizumab, an IL-6 receptor antagonist that is approved for the treatment of arthritis. Additionally, bevacizumab has been shown to effectively reduce cyst size in selected cases (48). The local installation of medication as with intracystic peginteferon alfa-2a appears as an attractive alternative to avoid systemic, potentially persisting side effects, in young children.

An important advantage of the pegylated formula is the possibility of a weekly administration, which represents less applications compared to the previous non-pegylated interferon therapy. This factor represents an essential benefit for the child and its caregivers, as fewer procedures are required. The administration can be done in an outpatient setting. As a consequence, the child has fewer hospital visits and less interruptions in everyday life for a whole family. Lastly, if response is present but insufficient, additional cycles can be added as needed.

Conclusion

In this case series experience using peginterferon alfa-2a for intracystic treatment, its feasibility, tolerability, and response measured in cyst shrinkage were demonstrated. The results of this case series are encouraging that peginterferon could replace previous interferon formulations with the added benefit of less frequent administrations.

Data availability statement

The raw data supporting the conclusions of this article will be made available by the authors, without undue reservation.

Ethics statement

Local ethical approval and informed consent was available at the respective institutions in accordance with the local legislation and institutional requirements. Written informed consent was obtained from the individual(s), and minor(s)' legal guardian/next of kin, for the publication of any potentially identifiable images or data included in this article.

Author contributions

CH: Conceptualization, Data curation, Formal analysis, Investigation, Methodology, Project administration, Software, Validation, Visualization, Writing – original draft, Writing – review & editing. PP: Conceptualization, Investigation, Writing – original draft, Writing – review & editing. LH: Writing – original draft, Writing – review & editing, Conceptualization, Data curation, Formal analysis, Investigation, Methodology, Project administration, Resources, Software, Validation, Visualization. TT: Conceptualization, Investigation, Writing – review & editing. EL: Conceptualization, Investigation, Validation, Writing – review & editing. RH: Conceptualization, Investigation, Writing – review & editing. CD: Conceptualization, Formal analysis, Methodology, Validation, Writing – review & editing. KR: Validation, Writing – review & editing. NS: Data curation, Investigation, Software, Validation, Visualization, Writing – review & editing. ML: Data curation, Investigation, Visualization, Writing – review & editing. HS: Data curation, Investigation, Project administration, Writing – review & editing. CK: Data curation, Investigation, Writing – review & editing. LM: Data curation, Investigation, Methodology, Software, Validation, Visualization, Writing – review & editing. AA: Data curation, Investigation, Methodology, Validation, Writing – review & editing. AP: Data curation, Investigation, Methodology, Validation, Writing – review & editing. BR: Data curation, Investigation, Writing – review & editing. AL: Data curation, Investigation, Writing – review & editing. JB: Data curation, Investigation, Writing – review & editing. JG: Writing – original draft, Writing – review & editing, Conceptualization, Data curation, Formal analysis, Funding acquisition, Investigation, Methodology, Project administration, Resources, Software, Supervision, Validation, Visualization. UB: Conceptualization, Data curation, Formal analysis, Investigation, Methodology, Project administration, Resources, Supervision, Validation, Writing – original draft, Writing – review & editing.

Funding

The author(s) declare financial support was received for the research, authorship, and/or publication of this article. The study was supported by the "Verein unser_kind" (JG) and the "Forschungsgesellschaft für Cerebrale Tumore".

Conflict of interest

The authors declare that the research was conducted in the absence of any commercial or financial relationships that could be construed as a potential conflict of interest.

Publisher's note

Supplementary material

The Supplementary Material for this article can be found online at: https://www.frontiersin.org/articles/10.3389/fonc.2024.1401761/full#supplementary-material

References

1. Magill ST, Jane JA, Prevedello DM. Editorial. Craniopharyngioma classification. *J Neurosurg*. (2021) 135:1293–5. doi: 10.3171/2020.8.JNS202666

2. Caldarelli M, Massimi L, Tamburrini G, Cappa M, Di Rocco C. Long-term results of the surgical treatment of craniopharyngioma: the experience at the Policlinico Gemelli, Catholic University, Rome. *Childs Nerv Syst*. (2005) 21:747–57. doi: 10.1007/s00381-005-1186-5

3. Cheng J, Shao Q, Pan Z, You J. Analysis and long-term follow-up of the surgical treatment of children with craniopharyngioma. *J Craniofac Surg*. (2016) 27:e763–6. doi: 10.1097/SCS.0000000000003176

4. Di Rocco C, Caldarelli M, Tamburrini G, Massimi L. Surgical management of craniopharyngiomas–experience with a pediatric series. *J Pediatr Endocrinol Metab*. (2006) 19 Suppl 1:355–66.

5. Komotar RJ, Roguski M, Bruce JN. Surgical management of craniopharyngiomas. *J Neurooncol*. (2009) 92:283–96. doi: 10.1007/s11060-009-9841-4

6. Müller HL. Childhood craniopharyngioma: current controversies on management in diagnostics, treatment and follow-up. *Expert Rev Neurother*. (2010) 10:515–24. doi: 10.1586/ern.10.15

7. Prieto R, Rosdolsky M, Hofecker V, Barrios L, Pascual JM. Craniopharyngioma treatment: an updated summary of important clinicopathological concepts. *Expert Rev Endocrinol Metab*. (2020) 15:261–82. doi: 10.1080/17446651.2020.1770081

8. Webb KL, Pruter WW, Hinkle ML, Walsh MT. Comparing surgical approaches for craniopharyngioma resection among adults and children: a meta-analysis and systematic review. *World Neurosurg*. (2023) 175:e876-e896. doi: 10.1016/j.wneu.2023.04.037

9. Lohkamp LN, Kulkarni AV, Drake JM, Rutka JT, Dirks PB, Taylor M, et al. Preservation of endocrine function after Ommaya reservoir insertion in children with cystic craniopharyngioma. *J Neurooncol*. (2022) 159:597–607. doi: 10.1007/s11060-022-04099-0

10. Clark AJ, Cage TA, Aranda D, Parsa AT, Sun PP, Auguste KI, et al. A systematic review of the results of surgery and radiotherapy on tumor control for pediatric craniopharyngioma. *Childs Nerv Syst*. (2013) 29:231–8. doi: 10.1007/s00381-012-1926-2

11. Lo AC, Howard AF, Nichol A, Sidhu K, Abdulsatar F, Hasan H, et al. Long-term outcomes and complications in patients with craniopharyngioma: the British Columbia Cancer Agency experience. *Int J Radiat Oncol Biol Phys*. (2014) 88:1011–8. doi: 10.1016/j.ijrobp.2014.01.019

12. Minniti G, Esposito V, Amichetti M, Enrici RM. The role of fractionated radiotherapy and radiosurgery in the management of patients with craniopharyngioma. *Neurosurg Rev*. (2009) 32:125–32. doi: 10.1007/s10143-009-0186-4

13. Schoenfeld A, Pekmezci M, Barnes MJ, Tihan T, Gupta N, Lamborn KR, et al. The superiority of conservative resection and adjuvant radiation for craniopharyngiomas. *J Neurooncol*. (2012) 108:133–9. doi: 10.1007/s11060-012-0806-7

14. Hess CB, Thompson HM, Benedict SH, Seibert JA, Wong K, Vaughan AT, et al. Exposure risks among children undergoing radiation therapy: considerations in the era of image guided radiation therapy. *Int J Radiat Oncol Biol Phys*. (2016) 94:978–92. doi: 10.1016/j.ijrobp.2015.12.372

15. Karapinar E, Varkal MA, Saka N. LONG-TERM THYROID DISORDERS IN CHILDREN RECEIVING ONCOLOGIC TREATMENT AND RADIOTHERAPY. *Acta Endocrinol (Buchar)*. (2022) 18:429–35. doi: 10.4183/aeb.2022.429

16. Lassaletta Á, Morales JS, Valenzuela PL, Esteso B, Kahalley LS, Mabbott DJ, et al. Neurocognitive outcomes in pediatric brain tumors after treatment with proton versus photon radiation: a systematic review and meta-analysis. *World J Pediatr*. (2023) 19:727–40. doi: 10.1007/s12519-023-00726-6

17. Leary JB, Anderson-Mellies A, Green AL. Population-based analysis of radiation-induced gliomas after cranial radiotherapy for childhood cancers. *Neurooncol Adv*. (2022) 4:vdac159. doi: 10.1093/noajnl/vdac159

18. Merchant TE, Hoehn ME, Khan RB, Sabin ND, Klimo P, Boop FA, et al. Proton therapy and limited surgery for paediatric and adolescent patients with craniopharyngioma (RT2CR): a single-arm, phase 2 study. *Lancet Oncol*. (2023) 24:523–34. doi: 10.1016/S1470-2045(23)00146-8

19. Steinbok P. Craniopharyngioma in children: long-term outcomes. *Neurol Med Chir (Tokyo)*. (2015) 55:722–6. doi: 10.2176/nmc.ra.2015-0099

20. Visser J, Hukin J, Sargent M, Steinbok P, Goddard K, Fryer C. Late mortality in pediatric patients with craniopharyngioma. *J Neurooncol*. (2010) 100:105–11. doi: 10.1007/s11060-010-0145-5

21. Otte A, Müller HL. Childhood-onset craniopharyngioma. *J Clin Endocrinol Metab*. (2021) 106:e3820–36. doi: 10.1210/clinem/dgab397

22. Steinbok P, Hukin J. Intracystic treatments for craniopharyngioma. *Neurosurg Focus*. (2010) 28:E13. doi: 10.3171/2010.1.FOCUS09315

23. Backlund EO. Treatment of craniopharyngiomas: the multimodality approach. *Pediatr Neurosurg*. (1994) 21 Suppl 1:82–9. doi: 10.1159/000120867

24. Cavalheiro S, Dastoli PA, Silva NS, Toledo S, Lederman H, da Silva MC. Use of interferon alpha in intratumoral chemotherapy for cystic craniopharyngioma. *Childs Nerv Syst*. (2005) 21:719–24. doi: 10.1007/s00381-005-1226-1

25. Cavalheiro S, Di Rocco C, Valenzuela S, Dastoli PA, Tamburrini G, Massimi L, et al. Craniopharyngiomas: intratumoral chemotherapy with interferon-alpha: a multicenter preliminary study with 60 cases. *Neurosurg Focus*. (2010) 28:E12. doi: 10.3171/2010.1.FOCUS09310

26. Kilday JP, Caldarelli M, Massimi L, Chen RHH, Lee YY, Liang ML, et al. Intracystic interferon-alpha in pediatric craniopharyngioma patients: an international multicenter assessment on behalf of SIOPE and ISPN. *Neuro Oncol*. (2017) 19:1398–407. doi: 10.1093/neuonc/nox056

27. Lohkamp LN, Kasper EM, Pousa AE, Bartels UK. An update on multimodal management of craniopharyngioma in children. *Front Oncol*. (2023) 13:1149428. doi: 10.3389/fonc.2023.1149428

28. Pancucci G, Massimi L, Caldarelli M, D'Angelo L, Sturiale C, Tamburrini G, et al. [Pediatric craniopharyngioma: long-term results in 61 cases]. *Minerva Pediatr*. (2007) 59:219–31.

29. Asmana Ningrum R. Human interferon alpha-2b: A therapeutic protein for cancer treatment. *Scientifica*. (2014) 2014:e970315. doi: 10.1155/2014/970315

30. Ierardi DF, Fernandes MJS, Silva IR, Thomazini-Gouveia J, Silva NS, Dastoli P, et al. Apoptosis in alpha interferon (IFN-α) intratumoral chemotherapy for cystic craniopharyngiomas. *Childs Nerv Syst*. (2007) 23:1041–6. doi: 10.1007/s00381-007-0409-3

31. Mrowczynski OD, Langan ST, Rizk EB. Craniopharyngiomas: A systematic review and evaluation of the current intratumoral treatment landscape. *Clin Neurol Neurosurg*. (2018) 166:124–30. doi: 10.1016/j.clineuro.2018.01.039

32. Pettorini BL, Inzitari R, Massimi L, Tamburrini G, Caldarelli M, Fanali C, et al. The role of inflammation in the genesis of the cystic component of craniopharyngiomas. *Childs Nerv Syst*. (2010) 26:1779–84. doi: 10.1007/s00381-010-1245-4

33. Bartels U. Intracystic therapies for cystic craniopharyngioma in childhood. *Front Endocrinol*. (2012) 3:39. doi: 10.3389/fendo.2012.00039

34. Avula S, Peet A, Morana G, Morgan P, Warmuth-Metz M, Jaspan T, et al. European Society for Paediatric Oncology (SIOPE) MRI guidelines for imaging patients with central nervous system tumours. *Childs Nerv Syst*. (2021) 37:2497–508. doi: 10.1007/s00381-021-05199-4

35. Hoffman LM, Jaimes C, Mankad K, Mirsky DM, Tamrazi B, Tinkle CL, et al. Response assessment in pediatric craniopharyngioma: recommendations from the Response Assessment in Pediatric Neuro-Oncology (RAPNO) Working Group. *Neuro Oncol*. (2023) 25:224–33. doi: 10.1093/neuonc/noac221

36. Foster GR. Review article: pegylated interferons: chemical and clinical differences. *Aliment Pharmacol Ther*. (2004) 20:825–30. doi: 10.1111/j.1365-2036.2004.02170.x

37. Felix J. *PRODUCT MONOGRAPH*. Pegasys®. Health Canada Product Monograph. Hoffmann-La Roche Limited. Date of Revision: November 18 2015. Accessed January 10 2021.

38. Roche | Pegasys (peginterferon α) (2023). Available online at: https://www.roche.com/solutions/pharma/productid-692190d1-d5ba-4400-9b42-ae76668123ca.

39. Drugs.com (2023). Available online at: https://www.drugs.com/pro/roferon-a.html.

40. Sharma J, Bonfield CM, Singhal A, Hukin J, Steinbok P. Intracystic interferon-α treatment leads to neurotoxicity in craniopharyngioma: case report. *J Neurosurg: Pediatr*. (2015) 16:301–4. doi: 10.3171/2015.2.PEDS14656

41. Tiedemann LM, Manley P, Smith ER, Dagi LR. Visual field loss in a case of recurrent cystic craniopharyngioma during concomitant treatment with pegylated interferon α-2b. *J Pediatr Hematology/Oncol*. (2016) 38:e26. doi: 10.1097/MPH.0000000000000468

42. Heinks K, Boekhoff S, Hoffmann A, Warmuth-Metz M, Eveslage M, Peng J, et al. Quality of life and growth after childhood craniopharyngioma: results of the multinational trial KRANIOPHARYNGEOM 2007. *Endocrine*. (2018) 59:364–72. doi: 10.1007/s12020-017-1489-9

43. Klages KL, Berlin KS, Cook JL, Merchant TE, Wise MS, Mandrell BN, et al. Health-related quality of life, obesity, fragmented sleep, fatigue, and psychosocial problems among youth with craniopharyngioma. *Psychooncology*. (2022) 31:779–87. doi: 10.1002/pon.5862

44. Laffond C, Dellatolas G, Alapetite C, Puget S, Grill J, Habrand JL, et al. Quality-of-life, mood and executive functioning after childhood craniopharyngioma treated with surgery and proton beam therapy. *Brain Inj*. (2012) 26:270–81. doi: 10.3109/02699052.2011.648709

45. Grob S, Mirsky DM, Donson AM, Dahl N, Foreman NK, Hoffman LM, et al. Targeting IL-6 is a potential treatment for primary cystic craniopharyngioma. *Front Oncol*. (2019) 9:791. doi: 10.3389/fonc.2019.00791

46. Whelan R, Hengartner A, Folzenlogen Z, Prince E, Hankinson TC. Adamantinomatous craniopharyngioma in the molecular age and the potential of targeted therapies: a review. *Childs Nerv Syst*. (2020) 36:1635–42. doi: 10.1007/s00381-020-04677-5

47. *Study Details | Nivolumab and Tovorafenib for Treatment of Craniopharyngioma in Children and Young Adults*. ClinicalTrials.gov (202). Available at: https://www.clinicaltrials.gov/study/NCT05465174?cond=Craniopharyngioma&rank=1#locations.

48. De Rosa A, Calvanese F, Ducray F, Vasiljevic A, Manet R, Raverot G, et al. First evidence of anti-VEGF efficacy in an adult case of adamantinomatous craniopharyngioma: Case report and illustrative review. *Ann Endocrinol (Paris)*. (2023) 84:727–33. doi: 10.1016/j.ando.2023.10.003

frontiers | Frontiers in Pediatrics

TYPE Case Report
PUBLISHED 23 July 2024
DOI 10.3389/fped.2024.1378608

OPEN ACCESS

EDITED BY
John Bianco,
Princess Maxima Center for Pediatric Oncology, Netherlands

REVIEWED BY
Gianluca Piccolo,
Giannina Gaslini Institute (IRCCS), Italy
Christine Fuller,
Upstate Medical University, United States

*CORRESPONDENCE
Sharon Y. Y. Low
gmslyys@nus.edu.sg

RECEIVED 29 January 2024
ACCEPTED 02 July 2024
PUBLISHED 23 July 2024

CITATION
Wu Y, Aw SJ, Jain S, Ooi LY, Tan EEK, Chang KTE, Teo HJ, Seow WT and Low SYY (2024) Pleomorphic xanthoastrocytoma with NTRK fusion presenting as spontaneous intracranial hemorrhage—case report and literature review.
Front. Pediatr. 12:1378608.
doi: 10.3389/fped.2024.1378608

Pleomorphic xanthoastrocytoma with NTRK fusion presenting as spontaneous intracranial hemorrhage—case report and literature review

Yilong Wu[1], Sze Jet Aw[2], Swati Jain[3], Li Yin Ooi[4], Enrica E. K. Tan[5], Kenneth T. E. Chang[2], Harvey J. Teo[6], Wan Tew Seow[1,7,8] and Sharon Y. Y. Low[1,7,8,9]*

[1]Neurosurgical Service, KK Women's and Children's Hospital, Singapore, Singapore, [2]Department of Pathology and Laboratory Medicine, KK Women's and Children's Hospital, Singapore, Singapore, [3]Division of Neurosurgery, University Surgical Cluster, National University Health System, Singapore, Singapore, [4]Department of Pathology, National University Hospital, National University Health System, Singapore, Singapore, [5]Paediatric Haematology/Oncology Service, KK Women's and Children's Hospital, Singapore, Singapore, [6]Department of Diagnostic and Interventional Imaging, KK Women's and Children's Hospital, Singapore, Singapore, [7]Department of Neurosurgery, National Neuroscience Institute, Singapore, Singapore, [8]SingHealth Duke-NUS Neuroscience Academic Clinical Program, Singapore, Singapore, [9]SingHealth Duke-NUS Paediatrics Academic Clinical Program, Singapore, Singapore

Background: Pleomorphic xanthoastrocytoma (PXA) is a rare brain tumor that accounts for <1% of all gliomas. An in-depth understanding of PXA's molecular makeup remains a work in progress due to its limited numbers globally. Separately, spontaneous intracranial hemorrhage (pICH) is an uncommon but potentially devastating emergency in young children, often caused by vascular malformations or underlying hematological conditions. We describe an interesting case of a toddler who presented with pICH, later found to have a PXA as the underlying cause of hemorrhage. Further molecular interrogation of the tumor revealed a neurotrophic tyrosine receptor kinase (NTRK) gene fusion and CDKN2A deletion more commonly seen in infantile high-grade gliomas. The unusual clinicopathological features of this case are discussed in corroboration with published literature.

Case presentation: A previously well 2-year-old male presented with acute drowsiness and symptoms of increased intracranial pressure secondary to a large right frontoparietal intracerebral hematoma. He underwent an emergency craniotomy and partial evacuation of the hematoma for lifesaving measures. Follow-up neuroimaging reported a likely right intra-axial tumor with hemorrhagic components. Histology confirmed the tumor to be a PXA (WHO 2). Additional molecular investigations showed it was negative for BRAFV600E mutation but was positive for CDKN2A homozygous deletion and a unique neurotrophic tyrosine receptor kinase (NTRK) gene fusion. The patient subsequently underwent second-stage surgery to proceed with maximal safe resection of the remnant tumor, followed by the commencement of adjuvant chemotherapy.

Conclusion: To date, there are very few pediatric cases of PXA that present with spontaneous pICH and whose tumors have undergone thorough molecular testing. Our patient's journey highlights the role of a dedicated multidisciplinary neuro-oncology team to guide optimal treatment.

KEYWORDS

pleomorphic xanthoastrocytoma, pediatric brain tumor, spontaneous intracranial hemorrhage, gene fusion, infantile glioma

Introduction

Gliomas are the most common primary central nervous system (CNS) tumors in children. Challenges to their management are often due to their broad spectrum of clinical behavior (1). In this group, pleomorphic xanthoastrocytoma (PXA) is a rare brain tumor accounting for <1% of all glial neoplasms (2). Affected patients are often adolescent or young adults who present with seizures (3). The latest World Health Organization (WHO) designates the grading of PXA as a WHO CNS Grade 2 neoplasm as it has a relatively favorable prognosis but a higher tendency to recur than other pediatric low-grade gliomas (LGG). Furthermore, up to one-third of them show features of anaplasia (WHO CNS Grade 3), characterized by increased mitotic activity and at times necrosis, which is associated with decreased overall survival (3–5). To date, an in-depth understanding of PXA's molecular makeup remains a work in progress due to its limited numbers globally (6). Separately, spontaneous intracranial hemorrhage (pICH) is an uncommon but potentially devastating emergency in the pediatric population. Specifically in young children, such cases often present with clinical and diagnostic challenges (7). Broadly speaking, pICH is predominantly associated with intracranial vascular anomalies (8). Other etiologies, such as hematological, systemic, and cardiac causes, brain tumors, and intracranial infections are comparatively less common (7). We describe an interesting case of a 2-year-old male who presented with life-threatening pICH that was eventually found to have a PXA as its underlying cause of hemorrhage. Further molecular interrogation of the tumor revealed it was negative for BRAFV600E mutation and positive for CDKN2A homozygous deletion. In addition, the tumor was found to have a neurotrophic tyrosine receptor kinase (NTRK) gene fusion more commonly seen in infantile high-grade gliomas (HGG) (9). The unusual clinicopathological features of this case are discussed in corroboration with published literature.

Case presentation

A previously well 2-year-old male presented with a 1-day onset of vomiting, drowsiness, and anisocoria. Prior to his presentation, there was no history of trauma, recent infection, or family history that could account for his clinical presentation. An urgent computed tomographic (CT) brain scan demonstrated a large, predominantly acute pICH in the right frontoparietal region with intraventricular extension, early hydrocephalus, and right uncal herniation. An emergency craniotomy with partial clot evacuation was performed for lifesaving measures. Due to the unusual diagnosis, the evacuated hematoma was sent for histopathology testing. Subsequent blood investigations to exclude underlying hematological, infective, and systemic causes were unremarkable. After the patient was medically stable, a follow-up magnetic resonance imaging (MRI) of his neuroaxis was arranged. This reported an ill-defined lesion in the right frontoparietal region that was intermixed with blood products and surrounding perilesional edema. No obvious intracranial vascular anomaly was noted. Additional diffusion tensor imaging (DTI) sequences showed that the remnant lesion had infiltrated into the right corticospinal tract. There was no radiological evidence of spinal metastases (Figure 1).

As part of our institution's integrated diagnostic workflow, each tumor's initial histopathological details are perused with the patient's clinical and radiological results. Next, the choice of molecular tests is selected based on these findings. In our case, histopathology of the evacuated hematoma reported an intrinsic glial neoplasm with a well-delineated border. Mitotic figures were present at 1 mitotic figure/mm^2, and the Ki-67 index was up to 5%. Of note, immunohistochemistry staining for BRAF (v-raf murine sarcoma viral oncogene homolog B1) V600E was negative. Other illustrative details of the findings are described in Figures 2 and 3. Cumulative features at this juncture resulted in the preliminary diagnosis of a WHO CNS Grade 2 PXA. Due to noticeable positivity for both ALK and pan-TRK (i.e., Figures 2E, F) during the workup, additional testing via the Archer FusionPlex Pan-Solid Tumour V2 (Invitae, San Francisco, CA, USA) was performed. This is a commercially available high-throughput next-generation sequencing (NGS) panel that identifies gene translocations and internal tandem duplications across solid tumors and sarcomas in 137 genes. This investigation demonstrated the presence of an ETV6::NTRK gene fusion (Figure 3A). The tumor was then further interrogated by the Ampliseq Childhood Cancer Panel (Illumina, San Diego, CA, USA), another NGS-based targeted gene panel, which also confirmed the presence of the ETV6::NTRK fusion. In addition, the results showed the absence of reportable single-nucleotide variants (in particular, BRAFV600E) or copy number variants. Interestingly, we noted that no sequence alteration or fusion was detected in the ALK gene for both NGS techniques. In this setting, the decision was made to concur with the NGS findings. However, a homozygous deletion of cyclin-dependent kinase inhibitor 2A (CDKN2A) was simultaneously detected. In view of this latter finding, a fluorescence *in situ* hybridization (FISH) test for the CDKN2A gene was ordered, which established its deletion in the tumor. Put together, the eventual diagnosis of a "WHO CNS Grade 2 PXA with an ETV6::NTRK fusion" was made. The patient underwent a second-stage resection to remove the remnant hemorrhagic tumor approximately 2 weeks after his initial surgery. Intraoperatively, the decision was made to leave a small sliver of tumor that infiltrated into the corticospinal tract to avoid neurological injury. Otherwise, he recovered well to a full Glasgow Coma Scale with no residual neurological deficit. The tumor specimen submitted from the second surgery was histopathologically similar to the patient's initial surgery.

The case was presented at a neuro-oncology multidisciplinary tumor (MDT) board. The MDT consisted of specialists from pediatric oncology, neuroradiology, pathology, neurosurgery, radiation oncology, and allied health teams. Specifically for this patient, the following were discussed: firstly, there was still a remnant tumor in an eloquent region of the brain; next, the Ki-67 index was 5%; and lastly, the molecular findings of an NTRK

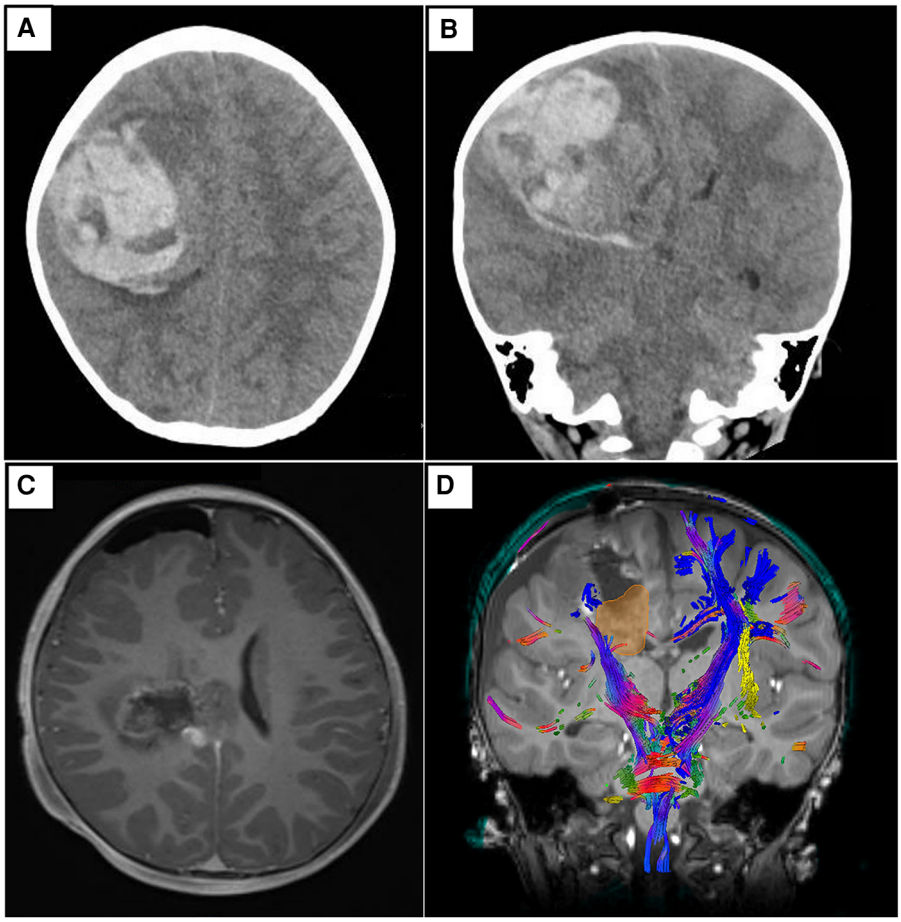

FIGURE 1
Representative non-contrast CT brain images in axial (**A**) and coronal (**B**) views. Both depict a predominantly acute intraparenchymal hematoma (6.8 × 6.4 × 5.6 cm) in the right frontoparietal region, with associated cerebral edema and mass effect. There is intraventricular extension of hemorrhage with early hydrocephalus. Subfalcine and mild right uncal herniation is seen. (**C**) Representative T1-weighted post-contrast MRI brain images in axial view. There is an irregular, ill-defined lesion with a heterogeneous signal, intermixed with blood products centered in the right frontoparietal region. The previous leftward midline shift has improved. Of note, there are foci of nodular enhancement in the periphery of the lesion that likely represent residual tumor. (**D**) Representative screenshot of relevant tractography (main corticospinal fibers in blue) in relation to the tumor (yellow-gold) from Modus Plan (Synaptive Medical, Toronto, Canada). This is a neurosurgical planning software that uses preoperative diffusion MRI data to segment out the patient's white matter tracts.

gene fusion included the lack of BRAFV600E mutation and CDKN2A homozygous deletion. The consensus was to manage the diagnosis as per an infantile HGG. A referral to the cancer genetics team was arranged. Despite much discussion during the consultation, the patient's parents declined to pursue the recommended germline testing for the patient. Subsequently, the patient was commenced on a carboplatin-based regimen of chemotherapy (10), with the option of an NTRK inhibitor in the event of relapse. In view of his young age, the role of proton beam therapy was to be held off as long as possible. Concurrently, a referral to the cancer genetics team was made for the patient to discuss the role of germline testing. However, his parents declined to proceed after the consultation. At approximately 10 months after his initial presentation, the patient remains clinically well without radiological evidence of tumor recurrence. To date, he is noted to be active and has no neurological deficit or significant developmental delay.

Discussion

Pleomorphic xanthoastrocytoma: current understanding

PXA was first described in 1979 as a distinct type of glioma that is postulated to have originated from subpial astrocytes (11). Presently, Kepes et al's (11) original description of a supratentorial astrocytoma that has a superficial cortical location and unique histological features, such as marked cellular pleomorphism, rich reticulin network, and prominent lipid-laden glial cells, is still relevant. PXA tends to be found in the supratentorial region, particularly in the temporal lobe. At times, both the leptomeninges and superficial regions of the cerebrum are anatomically involved (4). Occasionally, infratentorial cases have been described in the literature (4, 12). On neuroimaging, PXA is usually peripherally located and frequently cystic,

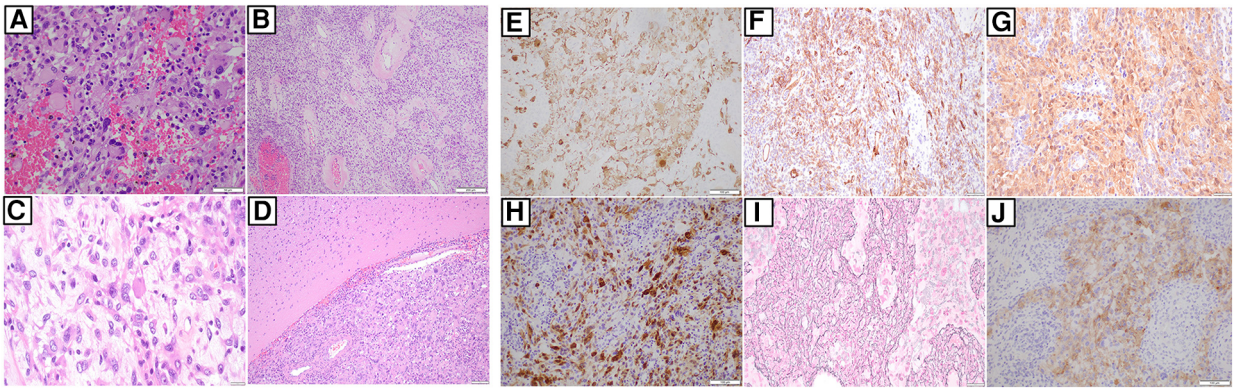

FIGURE 2
(A) Hematoxylin and eosin slide of tumor and it comprises of epithelioid to spindle cells, several of which feature large pleomorphic nuclei. Occasional cells show xanthomatous change. There is also intervening hemorrhage between the pleomorphic and xanthomatous cells. (40×) (B) Hematoxylin and eosin slide showing blood vessels with perivascular hyalinization in some areas. (10×) (C) This is a slide that shows the presence of eosinophilic bodies amongst the tumor cells. (40×) (D) Hematoxylin and eosin slide showing a well-demarcated border between the tumour and adjacent brain, without obvious infiltration. (×10). Next, immunohistochemical staining shows areas of that confirms GFAP (E), CD34 (F), S100 (G), and NeuN (H) positivity, respectively. (I) This is a slide that shows staining for reticulin deposited in several areas. (J) There is notable cytoplasmic positivity for ALK on IHC. However, follow-up molecular investigations via NGS techniques are negative for ALK (as mentioned in the main text). (All slides depicted here are 20× magnification, unless otherwise stated).

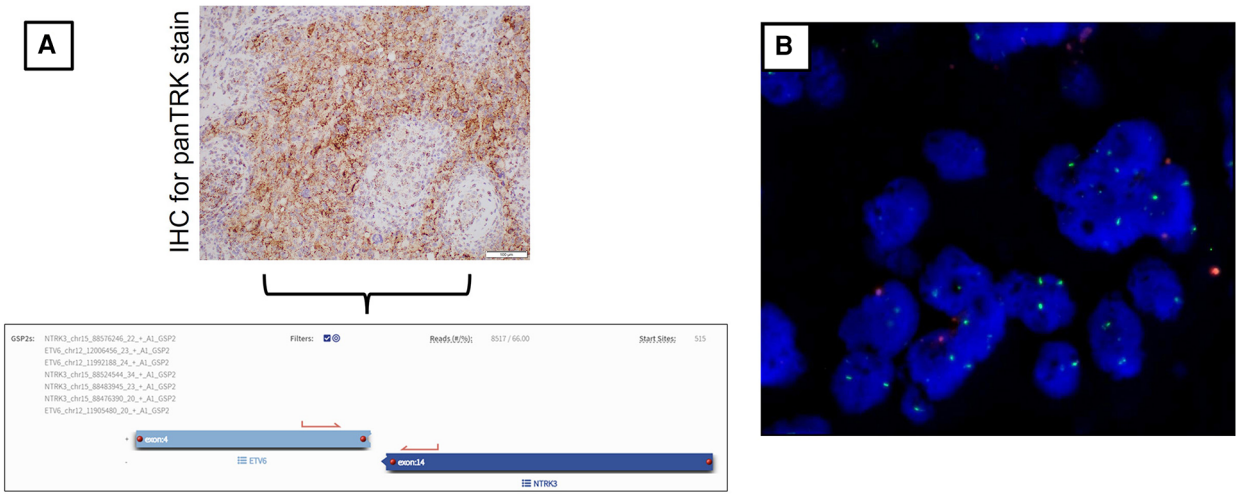

FIGURE 3
(A) Immunohistochemical stain for pan-TRK shows dot-like cytoplasmic positivity. (20×). This finding was followed up with the Archer FusionPlex Pan-Solid Tumour V2 (Invitae, San Francisco, CA, USA) for the patient's tumor whereby the results of the ETV6::NTRK3 fusion were found. The diagram also includes a screenshot analysis of the anchored multiplex PCR result. Here, an ETV6::NTRK3 fusion transcript with a percentage of unique reads (66%) spanning the breakpoint and supporting the event is identified. (B) Representative FISH image result of patient's tumor tissue. This shows the ratio of 9p21/CEP9 is 0.35, with 56% of tumor nuclei enumerated. There is no 9p21 signal, and 18% show only one copy of 9p21. Overall, these findings concur with the tumor being positive for CDKN2A deletion.

involving the cerebral cortex and overlying leptomeninges (3). Demographically, there are conflicting reports on gender predilection with some papers reporting equal occurrence in both sexes and others claiming a slight male preponderance (13). Studies report that PXA is commonly diagnosed in the second decade of life (13–15). Prevalence in the infantile HGG group (here, referring to children younger than 3–5 years old) is infrequent (16). Regarding clinical presentation, affected patients tend to present with seizures (3, 17). Neurosurgical intervention, especially total excision of the tumor has been proven to be associated with good survival outcomes (18). Although PXA is reputed to have a relatively favorable prognosis, it has an increased risk of recurrence in comparison to other pediatric LGGs. This slightly more aggressive behavior has led to its designation as either a WHO Grade 2 or 3 CNS neoplasm (3). Existing literature shows that up to one-third of PXA tumors

demonstrate anaplastic characteristics such as higher mitotic activity and necrosis, whereby both are associated with decreased overall survival (4–6). This particular subgroup is termed PXA WHO Grade 3. These tumors are more aggressive and have been reported to spread via cerebrospinal fluid (CSF), often in the setting of disease recurrence or malignant transformation (19, 20). For the PXA WHO Grade 2 tumors, the Ki-67 labeling index is generally <1%, whereas up to 15% has been reported in their WHO Grade 3 counterparts (3, 13, 21).

Clinical relevance of molecular information and gene fusions

The advent of technological advancements has provided valuable insights into the molecular profiles of pediatric gliomas. We are now aware that a significant proportion of PXA cases harbor a BRAF V600E gene mutation and or CDKN2A gene alterations (4, 22, 23). In addition, an in-depth study by Mistry et al. (23), which focused on the subset of pediatric LGG that transformed into secondary HGG, demonstrates that BRAFV600E mutations and CDKN2A deletions constitute a clinically distinct subtype of secondary HGG. Essentially, they report that BRAF and CDKN2A gene alterations are less common in the pediatric LGG cohort that do not show malignant transformation and patients with BRAF mutations had longer latency to secondary HGG (23). Next, it is noteworthy to mention the presence of CDKN2A deletion in our patient's tumor. CDKN2A is a tumor suppressor gene that encodes the p16INK4a protein and serves as an inhibitor of cell cycle progression. Molecular insights have revealed that it is a major target of mutation in many human cancers (24). Previous studies have shown that the CDKN2A homozygous deletion is an important prognostic factor for survival outcomes of IDH-mutant glioma patients regardless of histology grading (25). For instance, homozygous deletion involving the CDKN2A locus found in adult WHO Grade 3 oligodendrogliomas has been linked to lower survival, regardless of microvascular proliferation with or without necrosis (3, 26). Furthermore, in histologically lower-grade adult gliomas, CDKN2A homozygous deletion is associated with a more aggressive clinical course and is a molecular marker of Grade 4 status in the latest WHO classification (3, 27). Interestingly, a recent study of 67 PXA tumors reports up to 94% of them have pre-existing CDKN2A/B deletions. However, further analyses demonstrate this genomic alteration is not associated with overall survival (5). Instead, WHO grading for PXA is a stronger predictor of survival in the study cohort (5). Overall, molecular information for tumors is important due to paradigm shifts toward targeted therapies for challenging cancers, especially brain tumors (28). For example, the preliminary evidence for BRAF inhibitors for disease control obtained by BRAF inhibitors in tumors harboring the BRAF V600E mutation has been optimistic (29, 30). Similarly, the identification of cyclin-dependent kinase inhibitor (CDK) gene alterations has paved the way for the development of CDK-related therapeutics against various malignancies, including gliomas (31–33).

Following that, the remaining PXA cases without BRAFV600E (including our patient) have been reported to harbor RTK (receptor tyrosine kinase) gene fusions rather than MAPK(mitogen-activated protein kinase) alterations (34). At the time of this writing, there is only one other pediatric PXA case in the literature that reports an NTRK fusion (35). Broadly speaking, gene fusions are pathognomonic mutations resulting from a hybrid of two or more coding regulatory DNA sequences between genes due to genomic rearrangements from translocations, deletions, duplications, or inversions (36–38). Gene fusions are clinically relevant because they provide important information on tumorigenesis that pave the way for the development of targeted therapies for patients with specific fusions (39). In recent years, transcriptomic analyses have uncovered a subset of glioma patients carrying gene fusions (39). For affected patients, it has been reported that gene fusions can occur up to 30%–50% in high-grade gliomas (36, 37, 40). To date, collaborative genomic studies have demonstrated that infantile HGGs comprise molecularly distinct subgroups that are characterized by gene fusions (9, 41). Examples include the NTRK fusions that have been described as oncogenic drivers in several human tumors, including pediatric gliomas (42). The NTRK family comprises NTRK1, NTRK2, and NTRK3 that encode the neurotrophin receptors tropomyosin-related kinase (TRK) groups such as TrkA, TrkB, and TrkC. Gene fusions involving the NTRK family are one of the most common mechanisms of oncogenic TRK activation (43). This is clinically relevant because NTRK fusions represent a pharmacologically targetable genomic alteration (35). Therefore, potential NTRK-targeted treatment offers hope for very young brain tumor patients with limited treatment options. To date, NTRK inhibitors are currently being offered in clinical trials for primary CNS tumors with promising results (44). Here, the option of an NTRK inhibitor for our patient is feasible if conventional treatment methods fail.

Put together, a summary of our patient's pertinent molecular findings includes the following: the lack of BRAFV600E mutation, the presence of CDKN2A homozygous deletion, and an ETV6::NTRK gene fusion. Based on the current disease understanding of this rare brain tumor, it may be difficult to draw definitive conclusions in regard to the molecular results' prognostic impact on our patient. However, we are aware that PXA tumors frequently recur and are associated with decreased survival compared with other LGGs in children and young adults (3). Furthermore, malignant progression is known to be more common in PXA in comparison to other RAS/MAPK-driven LGGs (3, 45).

Neoplasm-related intracranial hemorrhage in children: an overview

In view of our patient's unusual clinical presentation, an overview of non-traumatic intracranial hemorrhagic in children is included in the following discussion. Non-

TABLE 1 Summary of pediatric cases of PXA presenting as intracranial hemorrhage.

Case number/ reference	Age (years)/ gender	Tumor location	Staged surgery (yes/ no)	Extent of resection	Histology/Ki-67 or MIB-1	Presence of BRAFv600e mutation (yes/no)	Additional molecular investigations
1 (Wind, 2009)	5/female	Left temporal	Yes	GTR	PXA (Ki-67, 2–3%)	Unknown	NIL
2 (Takamine, 2019)	11/female	Right temporal	No	GTR	PXA (Ki-67, 2%)	No	NIL
3 (Pehlivan, 2020)	6/male	Left frontoparietal	No	GTR	PXA ("low")	No	Yes, NGS panel
4. Our case	2/male	Right parietal	Yes	NTR	PXA (Ki-67, 5%)	No	Yes, NGS panel and FISH

traumatic pediatric intracranial hemorrhage (pICH) is defined as a brain parenchymal bleed with or without intraventricular extension occurring between 29 days and 18 years of age (46, 47). Typically, the incidence of pICH is cited to be extremely low in children. The exact incidence is unclear owing to current evidence relying on mostly case reports and small case series (35, 47, 48). Despite its rarity, pICH is an important cause of death and irreversible neurological injury (8). Delayed diagnosis is common because very young children have difficulties in accurately communicating complaints, and the hemorrhage can be manifested by non-specific symptoms such as irritability, somnolence, or headache. In addition, lateralizing neurological symptoms are reported less frequently in the pediatric population as compared to their adult counterparts (7, 49). Regardless, management should be prompt and thorough diagnostic workup to guide optimal clinical treatment (46, 47).

Of note, the pICH etiological spectrum differs from the adult population and is largely dominated by cerebral vascular lesions, hematological disorders, neoplasia, and systemic diseases. In addition, the literature shows that pICH can be secondary to various tumor types, including benign to malignant neoplasms (47). Erosion of cortical artery by the tumor, thin-walled tumor vessel, or unknown microvascular anomaly within the tumor have been postulated to be contributing factors for the bleeding episode (18, 50, 51). Specific to PXA, there have been only 3 other pediatric cases presenting as intracranial bleeds in the literature (Table 1).

Conclusion

The unique features of this case highlight challenges faced by various specialist teams and emphasize the importance of an integrated multidisciplinary approach to patient care. Although vascular anomalies constitute most of the underlying causes of pICH, clinicians need to be mindful to include as a differential diagnosis of brain tumors during an acute presentation. From the tumor diagnosis perspective, the role of additional molecular studies has enabled valuable information to guide adjuvant treatment. This case report adds to the limited pool of medical literature for this rare primary brain tumor. Moving forward, we advocate collaborative clinical and in-depth molecular studies at an international level.

Data availability statement

The original contributions presented in the study are included in the article/Supplementary Material; further inquiries can be directed to the corresponding author.

Ethics statement

The studies involving humans were approved by SingHealth CIRB Ref: 2014/2079. The studies were conducted in accordance with the local legislation and institutional requirements. Written informed consent for participation in this study was provided by the participants' legal guardians/next of kin. Written informed consent was obtained from the minor(s)' legal guardian/next of kin for the publication of any potentially identifiable images or data included in this article.

Author contributions

YW: Data curation, Investigation, Methodology, Resources, Writing – original draft. SA: Conceptualization, Data curation, Formal Analysis, Investigation, Software, Validation, Visualization, Writing – original draft, Writing – review & editing. SJ: Data curation, Writing – original draft. LO: Investigation, Validation, Writing – original draft. ET: Data curation, Investigation, Methodology, Resources, Writing – original draft. KC: Formal Analysis, Investigation, Methodology, Resources, Software, Writing – original draft. HT: Investigation, Resources, Writing – original draft. WS: Investigation, Methodology, Resources, Writing – original draft. SL: Conceptualization, Data curation, Formal Analysis, Project administration, Software, Validation, Visualization, Writing – original draft, Writing – review & editing.

Funding

The authors declare that financial support was received for the authorship, writing, and/or publication of this article. This project is supported by the VIVA-KKH Paediatric Brain and Solid Tumours Programme. This is a philanthropic grant that was

awarded to the institution (KK Women's and Children's Hospital) where the study was conducted.

Conflict of interest

The authors declare that the research was conducted in the absence of any commercial or financial relationships that could be construed as a potential conflict of interest.

Publisher's note

References

1. Sturm D, Pfister SM, Jones DTW. Pediatric gliomas: current concepts on diagnosis, biology, and clinical management. *J Clin Oncol*. (2017) 35:2370–7. doi: 10.1200/JCO.2017.73.0242

2. Ostrom QT, Cioffi G, Gittleman H, Patil N, Waite K, Kruchko C, et al. CBTRUS statistical report: primary brain and other central nervous system tumors diagnosed in the United States in 2012–2016. *Neuro Oncol*. (2019) 21:v1–v100. doi: 10.1093/neuonc/noz150

3. WHO Classification of Tumours. *Central Nervous System Tumours International Agency for Research on Cancer*. 5th edn France: Lyon (2021).

4. Ida CM, Rodriguez FJ, Burger PC, Caron AA, Jenkins SM, Spears GM, et al. Pleomorphic xanthoastrocytoma: natural history and long-term follow-up. *Brain Pathol*. (2015) 25:575–86. doi: 10.1111/bpa.12217

5. Vaubel R, Zschernack V, Tran QT, Jenkins S, Caron A, Milosevic D, et al. Biology and grading of pleomorphic xanthoastrocytoma-what have we learned about it? *Brain Pathol*. (2021) 31:20–32. doi: 10.1111/bpa.12874

6. Mahajan S, Dandapath I, Garg A, Sharma MC, Suri V, Sarkar C. The evolution of pleomorphic xanthoastrocytoma: from genesis to molecular alterations and mimics. *Lab Invest*. (2022) 102:670–81. doi: 10.1038/s41374-021-00708-0

7. Ciochon UM, Bindslev JBB, Hoei-Hansen CE, Truelsen TC, Larsen VA, Nielsen MB, et al. Causes and risk factors of pediatric spontaneous intracranial hemorrhage—a systematic review. *Diagnostics (Basel)*. (2022) 12(6):1459. doi: 10.3390/diagnostics12061459

8. Lo WD, Lee J, Rusin J, Perkins E, Roach ES. Intracranial hemorrhage in children: an evolving spectrum. *Arch Neurol*. (2008) 65(12):1629–33. doi: 10.1001/archneurol.2008.502

9. Chiang J, Bagchi A, Li X, Dhanda SK, Huang J, Pinto SN, et al. High-grade glioma in infants and young children is histologically, molecularly, and clinically diverse: Results from the SJYC07 trial and institutional experience. *Neuro Oncol*. (2024) 26(1):178–90. doi: 10.1093/neuonc/noad130

10. Fouladi M, Gururangan S, Moghrabi A, Phillips P, Gronewold L, Wallace D, et al. Carboplatin-based primary chemotherapy for infants and young children with CNS tumors. *Cancer*. (2009) 115:3243–53. doi: 10.1002/cncr.24362

11. Kepes JJ, Rubinstein LJ, Eng LF. Pleomorphic xanthoastrocytoma: a distinctive meningocerebral glioma of young subjects with relatively favorable prognosis. A study of 12 cases. *Cancer*. (1979) 44:1839–52. doi: 10.1002/1097-0142(197911)44:5<1839::AID-CNCR2820440543>3.0.CO;2-0

12. Mallick S, Benson R, Melgandi W, Giridhar P, Rath GK. Grade II pleomorphic xanthoastrocytoma; a meta-analysis of data from previously reported 167 cases. *J Clin Neurosci*. (2018) 54:57–62. doi: 10.1016/j.jocn.2018.05.003

13. Giannini C, Scheithauer BW, Burger PC, Brat DJ, Wollan PC, Lach B, et al. Pleomorphic xanthoastrocytoma: what do we really know about it? *Cancer*. (1999) 85:2033–45. doi: 10.1002/(SICI)1097-0142(19990501)85:9<2033::AID-CNCR22>3.0.CO;2-Z

14. Davies KG, Maxwell RE, Seljeskog E, Sung JH. Pleomorphic xanthoastrocytoma–report of four cases, with MRI scan appearances and literature review. *Br J Neurosurg*. (1994) 8:681–9. doi: 10.3109/02688699409101181

15. Lipper MH, Eberhard DA, Phillips CD, Vezina LG, Cail WS. Pleomorphic xanthoastrocytoma, a distinctive astroglial tumor: neuroradiologic and pathologic features. *AJNR Am J Neuroradiol*. (1993) 14(6):1397–404.

16. Duffner PK, Horowitz ME, Krischer JP, Burger PC, Cohen ME, Sanford RA, et al. The treatment of malignant brain tumors in infants and very young children: an update of the pediatric oncology group experience. *Neuro Oncol*. (1999) 1:152–61. doi: 10.1093/neuonc/1.2.152

17. Oladiran O, Nwosu I, Obanor S, Ogbonna-Nwosu C, Le B. Anaplastic pleomorphic xanthoastrocytoma presenting with musical hallucination. *Case Rep Neurol Med*. (2018) 2018:6428492. doi: 10.1155/2018/6428492

18. Lee DK, Cho KT, Im SH, Hong SK. Pleomorphic xanthoastrocytoma with an intracystic hemorrhage: a case report and literature review. *J Korean Neurosurg Soc*. (2007) 42:410–2. doi: 10.3340/jkns.2007.42.5.410

19. Okazaki T, Kageji T, Matsuzaki K, Horiguchi H, Hirose T, Watanabe H, et al. Primary anaplastic pleomorphic xanthoastrocytoma with widespread neuroaxis dissemination at diagnosis–a pediatric case report and review of the literature. *J Neurooncol*. (2009) 94:431–7. doi: 10.1007/s11060-009-9876-6

20. Kahramancetin N, Tihan T. Aggressive behavior and anaplasia in pleomorphic xanthoastrocytoma: a plea for a revision of the current WHO classification. *CNS Oncol*. (2013) 2:523–30. doi: 10.2217/cns.13.56

21. Phillips JJ, Gong H, Chen K, Joseph NM, van Ziffle J, Bastian BC, et al. The genetic landscape of anaplastic pleomorphic xanthoastrocytoma. *Brain Pathol*. (2019) 29:85–96. doi: 10.1111/bpa.12639

22. Zhang H, Ma XJ, Xiang XP, Wang QY, Tang JL, Yu XY, et al. Clinical, morphological, and molecular study on grade 2 and 3 pleomorphic xanthoastrocytoma. *Curr Oncol*. (2023) 30:2405–16. doi: 10.3390/curroncol30020183

23. Mistry M, Zhukova N, Merico D, Rakopoulos P, Krishnatry R, Shago M, et al. BRAF mutation and CDKN2A deletion define a clinically distinct subgroup of childhood secondary high-grade glioma. *J Clin Oncol*. (2015) 33:1015–22. doi: 10.1200/JCO.2014.58.3922

24. Purkait S, Jha P, Sharma MC, Suri V, Sharma M, Kale SS, et al. CDKN2A deletion in pediatric versus adult glioblastomas and predictive value of p16 immunohistochemistry. *Neuropathology*. (2013) 33:405–12. doi: 10.1111/neup.12014

25. Lu VM, O'Connor KP, Shah AH, Eichberg DG, Luther EM, Komotar RJ, et al. The prognostic significance of CDKN2A homozygous deletion in IDH-mutant lower-grade glioma and glioblastoma: a systematic review of the contemporary literature. *J Neurooncol*. (2020) 148:221–9. doi: 10.1007/s11060-020-03528-2

26. Appay R, Dehais C, Maurage CA, Alentorn A, Carpentier C, Colin C, et al. CDKN2A homozygous deletion is a strong adverse prognosis factor in diffuse malignant IDH-mutant gliomas. *Neuro Oncol*. (2019) 21:1519–28. doi: 10.1093/neuonc/noz126.000

27. Vij M, Cho BB, Yokoda RT, Rashidipour O, Umphlett M, Richardson TE, et al. P16 immunohistochemistry is a sensitive and specific surrogate marker for CDKN2A homozygous deletion in gliomas. *Acta Neuropathol Commun*. (2023) 11:73. doi: 10.1186/s40478-023-01573-2

28. Di Nunno V, Gatto L, Tosoni A, Bartolini S, Franceschi E. Implications of BRAF V600E mutation in gliomas: molecular considerations, prognostic value and treatment evolution. *Front Oncol*. (2022) 12:1067252. doi: 10.3389/fonc.2022.1067252

29. Kowalewski A, Durślewicz J, Zdrenka M, Grzanka D, Szylberg Ł. Clinical relevance of BRAF V600E mutation status in brain tumors with a focus on a novel management algorithm. *Target Oncol*. (2020) 15:531–40. doi: 10.1007/s11523-020-00735-9

30. Kieran MW. Targeting BRAF in pediatric brain tumors. *Am Soc Clin Oncol Educ Book*. (2014) 34:e436–40. doi: 10.14694/EdBook_AM.2014.34.e436

31. Kreuger IZM, Slieker RC, van Groningen T, van Doorn R. Therapeutic strategies for targeting CDKN2A loss in melanoma. *J Invest Dermatol*. (2023) 143:18–25.e1. doi: 10.1016/j.jid.2022.07.016

32. Baghdadi TA, Halabi S, Garrett-Mayer E, Mangat PK, Ahn ER, Sahai V, et al. Palbociclib in patients with pancreatic and biliary cancer with CDKN2A alterations: results from the targeted agent and profiling utilization registry study. *JCO Precis Oncol*. (2019) 3:1–8. doi: 10.1200/PO.19.00124

33. Yang K, Wu Z, Zhang H, Zhang N, Wu W, Wang Z, et al. Glioma targeted therapy: insight into future of molecular approaches. *Mol Cancer*. (2022) 21:39. doi: 10.1186/s12943-022-01513-z

34. Lucas CG, Abdullaev Z, Bruggers CS, Mirchia K, Whipple NS, Alashari MM, et al. Activating NTRK2 and ALK receptor tyrosine kinase fusions extend the molecular spectrum of pleomorphic xanthoastrocytomas of early childhood: a diagnostic overlap with infant-type hemispheric glioma. *Acta Neuropathol*. (2022) 143:283–6. doi: 10.1007/s00401-021-02396-y

35. Pehlivan KC, Malicki DM, Levy ML, Crawford JR. TPM3-NTRK1 fusion in a pleomorphic xanthoastrocytoma presenting with haemorrhage in a child. *BMJ Case Rep*. (2020) 13(3):e234347. doi: 10.1136/bcr-2020-234347

36. Zheng S, Fu J, Vegesna R, Mao Y, Heathcock LE, Torres-Garcia W, et al. A survey of intragenic breakpoints in glioblastoma identifies a distinct subset associated with poor survival. *Genes Dev*. (2013) 27:1462–72. doi: 10.1101/gad.213686.113

37. Frattini V, Trifonov V, Chan JM, Castano A, Lia M, Abate F, et al. The integrated landscape of driver genomic alterations in glioblastoma. *Nat Genet*. (2013) 45:1141–9. doi: 10.1038/ng.2734

38. Amatu A, Sartore-Bianchi A, Siena S. NTRK Gene fusions as novel targets of cancer therapy across multiple tumour types. *ESMO Open*. (2016) 1:e000023. doi: 10.1136/esmoopen-2015-000023

39. Yoshihara K, Wang Q, Torres-Garcia W, Zheng S, Vegesna R, Kim H, et al. The landscape and therapeutic relevance of cancer-associated transcript fusions. *Oncogene*. (2015) 34:4845–54. doi: 10.1038/onc.2014.406

40. Xu T, Wang H, Huang X, Li W, Huang Q, Yan Y, et al. Gene fusion in malignant glioma: an emerging target for next-generation personalized treatment. *Transl Oncol*. (2018) 11:609–18. doi: 10.1016/j.tranon.2018.02.020

41. Clarke M, Mackay A, Ismer B, Pickles JC, Tatevossian RG, Newman S, et al. Infant high-grade gliomas comprise multiple subgroups characterized by novel targetable gene fusions and favorable outcomes. *Cancer Discov*. (2020) 10:942–63. doi: 10.1158/2159-8290.CD-19-1030

42. Zhao X, Kotch C, Fox E, Surrey LF, Wertheim GB, Baloch ZW, et al. NTRK fusions identified in pediatric tumors: the frequency, fusion partners, and clinical outcome. *JCO Precis Oncol*. (2021) 1:PO.20.00250. doi: 10.1200/PO.20.00250

43. Vaishnavi A, Le AT, Doebele RC. TRKing down an old oncogene in a new era of targeted therapy. *Cancer Discov*. (2015) 5:25–34. doi: 10.1158/2159-8290.CD-14-0765

44. Doz F, van Tilburg CM, Geoerger B, Højgaard M, Øra I, Boni V, et al. Efficacy and safety of larotrectinib in TRK fusion-positive primary central nervous system tumors. *Neuro Oncol*. (2022) 24:997–1007. doi: 10.1093/neuonc/noab274

45. Ryall S, Tabori U, Hawkins C. Pediatric low-grade glioma in the era of molecular diagnostics. *Acta Neuropathol Commun*. (2020) 8:30. doi: 10.1186/s40478-020-00902-z

46. Beslow LA, Licht DJ, Smith SE, Storm PB, Heuer GG, Zimmerman RA, et al. Predictors of outcome in childhood intracerebral hemorrhage: a prospective consecutive cohort study. *Stroke*. (2010) 41:313–8. doi: 10.1161/STROKEAHA.109.568071

47. Boulouis G, Blauwblomme T, Hak JF, Benichi S, Kirton A, Meyer P, et al. Nontraumatic pediatric intracerebral hemorrhage. *Stroke*. (2019) 50:3654–61. doi: 10.1161/STROKEAHA.119.025783

48. Takamine Y, Yamamuro S, Sumi K, Ohta T, Shijo K, Nakanishi Y, et al. A case of pleomorphic xanthoastrocytoma with intracranial hemorrhage in a child. *NMC Case Rep J*. (2019) 6:39–42. doi: 10.2176/nmccrj.cr.2018-0174

49. Gerstl L, Badura K, Heinen F, Weinberger R, Peraud A, Dorn F, et al. Childhood haemorrhagic stroke: a 7-year single-centre experience. *Arch Dis Child*. (2019) 104:1198–202. doi: 10.1136/archdischild-2018-316749

50. Levy RA, Allen R, McKeever P. Pleomorphic xanthoastrocytoma presenting with massive intracranial hemorrhage. *Am J Neuroradiol*. (1996) 17(1):154–6.

51. Yoshida D, Kogiku M, Noha M, Takahashi H, Teramoto A. A case of pleomorphic xanthoastrocytoma presenting with massive tumoral hemorrhage. *J Neurooncol*. (2005) 71:169–71. doi: 10.1007/s11060-004-0915-z

frontiers | Frontiers in Neurology

TYPE Systematic Review
PUBLISHED 10 September 2024
DOI 10.3389/fneur.2024.1408716

OPEN ACCESS

EDITED BY
Majaz Moonis,
UMass Memorial Medical Center,
United States

REVIEWED BY
Jakob Nemir,
University Hospital Centre Zagreb, Croatia
Damodara Naidu Kommi,
University of Virginia, United States

*CORRESPONDENCE
Haihong Ma
✉ 1727359370@qq.com

†These authors have contributed equally to this work

RECEIVED 28 March 2024
ACCEPTED 26 August 2024
PUBLISHED 10 September 2024

CITATION
Abudueryimu A, Shoukeer K and Ma H (2024) Analysis of the current status and hot topics in spinal schwannoma imaging research based on bibliometrics.
Front. Neurol. 15:1408716.
doi: 10.3389/fneur.2024.1408716

Analysis of the current status and hot topics in spinal schwannoma imaging research based on bibliometrics

Abudunaibi Abudueryimu[1†], Kutiluke Shoukeer[2†] and Haihong Ma[1*]

[1]Kashi Prefecture Second People's Hospital, Kashi, China, [2]Department of Orthopedics, Sixth Affiliated Hospital of Xinjiang Medical University, Ürümqi, China

Objective: This study aims to explore the current hot topics and future research trends in spinal schwannoma imaging research, providing a reference for related studies and promoting the development of spinal schwannoma imaging.

Methods: We conducted a literature search in the Web of Science database using the search terms (((TS = (Spinal schwannoma)) AND TS = (Imaging)) OR TS = (Spinal schwannoma)) AND TS = (image) to retrieve relevant articles. The collected data, including authors, keywords, journals, countries, institutions, and references, were subjected to visual analysis using the visualization software CiteSpace 6.4.2R and VOSviewer 1.6.19.

Results: A total of 310 relevant articles were identified. After further screening based on time limits, inclusion, and exclusion criteria, 179 articles were included in the study, consisting of 132 original articles and 42 reviews. These articles were authored by 1,034 authors from 35 countries and 324 institutions and were published in 82 different journals. The included articles cited a total of 6,583 references from 1,314 journals.

Conclusion: Although the field of spinal schwannoma imaging research is not a popular research area in the medical community, there has been an increasing international interest in this field in recent years. While China ranks high in terms of the number of published articles, there is still a gap in terms of the quality and research level compared to developed countries in Europe and America. MRI, as the gold standard for diagnosing spinal schwannomas, is expected to be a research hotspot in terms of feature analysis, enhancement characteristics, and quantitative analysis. It is also hoped that China can increase its investment in research and contribute to the field by publishing high-quality articles in the future.

KEYWORDS

spinal schwannoma, imaging, bibliometrics, visual analysis, MRI

1 Introduction

Intraspinal schwannomas are one of the most common intradural extramedullary tumors, originating from the nerve sheath cells within the spinal canal. They typically present as axial pain and neurological symptoms caused by progressive compression of the spinal cord (1, 2). With the continuous development and advancement of medical imaging

technology, imaging plays a crucial role in the diagnosis, localization, and evaluation of intramedullary spinal cord tumors (3, 4). Various imaging techniques, such as magnetic resonance imaging (MRI) and computed tomography (CT) (5), provide detailed information about the tumor, including its size, shape, boundaries, internal structure, and relationship with surrounding tissues (6). Imaging studies of intramedullary spinal cord tumors not only aid in accurate diagnosis and differential diagnosis but also provide important evidence for treatment planning and surgical intervention (7). As imaging technology continues to innovate and progress, research on the imaging of intramedullary spinal cord tumors also continues to evolve (8, 9). Researchers are dedicated to exploring new imaging features, quantitative analysis methods, and the application of deep learning techniques to improve the accuracy of diagnosis and treatment outcomes for intramedullary spinal cord tumors (10, 11). Furthermore, international collaboration and communication provide a broader platform for the imaging research of intramedullary spinal cord tumors, facilitating further advancements in this field. However, despite the abundance of literature on imaging studies of intramedullary spinal cord tumors, there is currently no systematic review of the research directions and trends. Therefore, this study selected literature published in the Web of Science database to conduct an in-depth analysis of the current status and development trends in the field of imaging research on intramedullary spinal cord tumors using bibliometric methods. We aim to explore, analyze, and construct the core structure, developmental history, cutting-edge areas, and overall knowledge framework of this field, visualizing the correlations between them. It is hoped that this article will provide valuable information and insights to the medical community, promoting further progress in the imaging research and clinical applications of intramedullary spinal cord tumors.

2 Data and methods

2.1 Data collection database time limit

2.1.1 Retrieval

2.1.1.1 Search strategy

Open the advanced retrieval in the Web of Science (WoS) page, select the Web of Science core collection, and the retrieval strategy is shown in Table 1. Select keywords ((TS = (Spinal schwannoma)) AND TS = (Imaging)) ORTS = (Spinal schwannoma) AND TS = (image) to search the target literature.

2.2 Inclusion and exclusion criteria

2.2.1 Inclusion criteria

① Literature on imaging studies of intraspinal schwannoma published from 2014 to 2023; ②, review; ③ in English.

2.2.2 Exclusion criteria

① No relevance in this study; ② duplicate papers; ③ non-English language literature; ④ conference papers, abstract, translation, dissertation, dissertation, newspaper, lecture, news, etc.

TABLE 1 Search strategy for the Web of Science database.

	Retrieval type
#1	Subject words: Spinal schwannoma
#2	Subject words: Imaging
#3	Subject words: image
#4	#1 AND #2
#5	#1 AND #3
#6	#4 OR #5

2.3 Analysis of the data

Bibliometrics is a method used to analyze the production and status of publications in a specific research field from both quantitative and qualitative perspectives (12, 13). By utilizing bibliometric software like CiteSpace 6.4.2R and VOSviewer 1.6.19, we can visually analyze collected data, including authors, keywords, journals, countries, institutions, and references. VOSviewer 1.6.19 (Visualizing Scientific Landscapes) is a bibliometric analysis software commonly employed to construct collaboration, citation, and co-occurrence networks by extracting key information from numerous publications (14). In the maps generated by VOSviewer, the size and color of nodes represent the quantity and category of these items, while the thickness of the links reflects the strength of collaboration or association between items. CiteSpace 6.4.2R, developed by Professor Chaomei Chen, is another software used for bibliometric analysis and visualization. In this study, we utilized these two software tools to create visual maps and analyze the current hotspots and future trends in the field of intramedullary spinal cord tumor imaging research, taking into account factors such as publication volume, countries, institutions, journals, authors, keywords, and burst terms (15, 16).

3 Results

There are a total of 310 relevant articles in the Web of Science database. Further screening was conducted based on time limits, inclusion, and exclusion criteria (see Figure 1), resulting in a final inclusion of 179 articles, including 132 original research papers and 42 review articles. These publications were authored by 1,034 authors from 35 countries and 324 institutions, and they were published in 82 different journals. The articles cited a total of 6,583 references from 1,314 journals.

3.1 Global research status in the field of imaging studies for intraspinal schwannoma

According to the data shown in Figure 2, we can observe that the publication volume of intramedullary spinal cord tumor imaging research articles has exhibited some fluctuations over the past decade. There were relatively high publication volumes during the periods of 2015–2016 and 2020–2022, while in other years, the publication

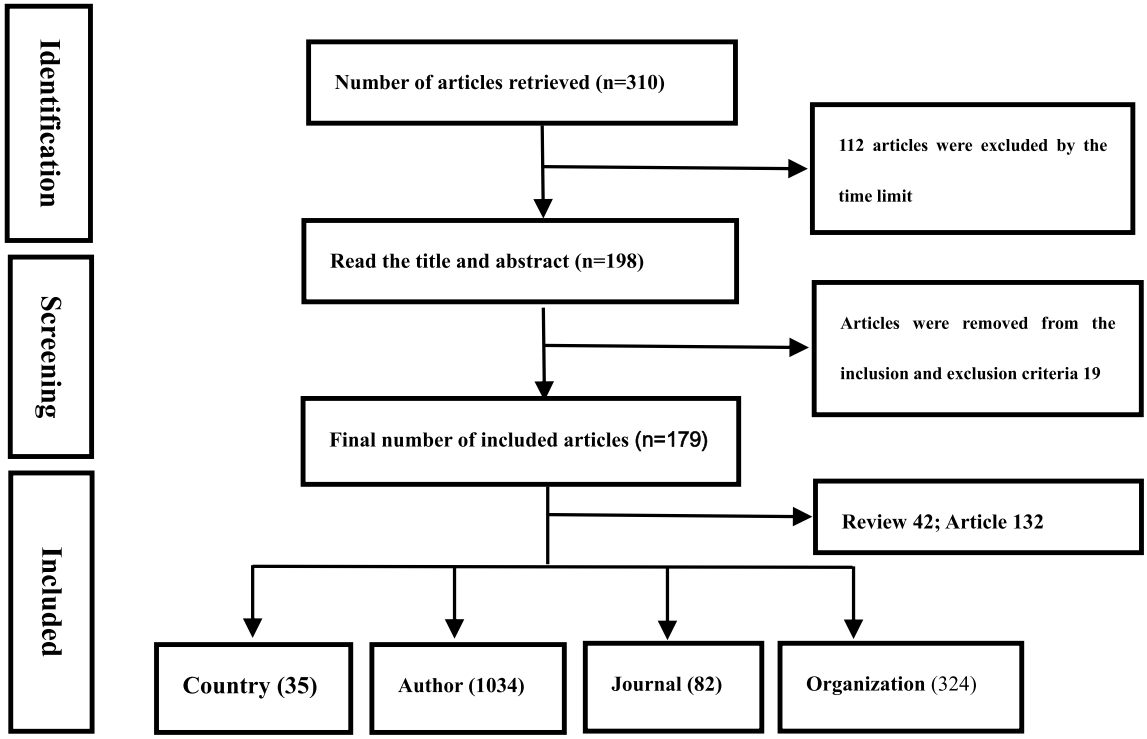

FIGURE 1
Flow chart of literature search and screening.

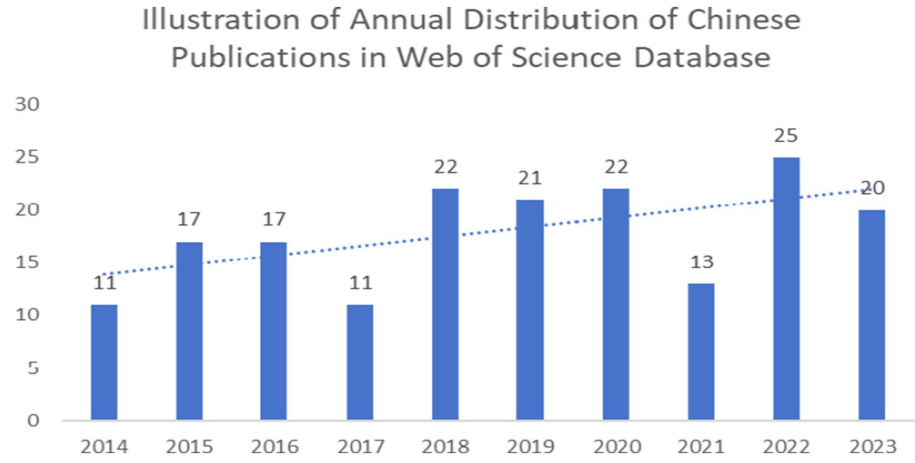

FIGURE 2
Imaging of spinal schwannoma was published in the literature.

volume remained relatively stable or slightly decreased. Specifically, from 2014 to 2017, the publication volume initially increased from 11 articles to 17 articles and then dropped back to 11 articles. However, in 2018, the publication volume significantly increased to 22 articles, representing a 100% growth compared to 2017. In 2022, there was another significant increase, reaching a peak of 25 articles, the highest value in the past decade. Overall, although the publication volume fluctuated each year, there is a general increasing trend, which may reflect the growing importance and activity in research within this field.

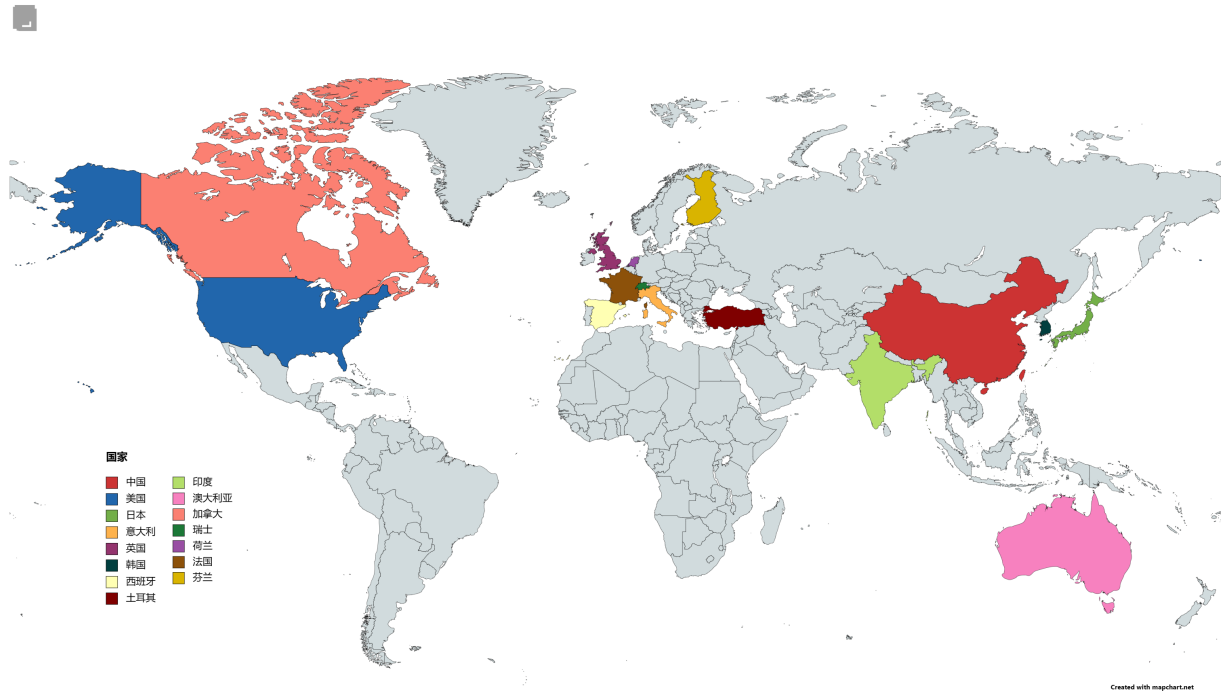

FIGURE 3
National map of the field of imaging of spinal schwannoma.

3.2 National analysis of the imaging field of intraspinal schwannoma

From the perspective of country distribution, Figure 3 displays the distribution of published countries in global intramedullary spinal cord tumor imaging research literature. Observing the chart, it can be noted that developed countries dominate the publication of related literature, particularly with a significant number of countries in the European region compared to other continents. This is associated with the presence of numerous developed countries in Europe. Table 2 lists the top 10 countries with the highest number of published literature globally. China has the highest publication volume in the field of intramedullary spinal cord tumor imaging research, with a total of 58 publications, ranking first. The United States and Japan rank second and third, with 30 and 29 publications, respectively. In terms of citation count, the United States has the highest citation count, reaching 340, ranking first. The United Kingdom and Japan rank second and third, with citation counts of 134 and 175, respectively. In terms of average citations per article, the United Kingdom performs remarkably well, with an average of 13.4 citations per article, ranking first. The United States and Spain rank second and third, with average citations per article of 11.3 and 11.2, respectively.

TABLE 2 Top 10 countries in the field of imaging of spinal schwannoma.

No.	Countries	Articles	Citation	Average citations
1	China	58	248	4.3
2	USA	30	340	11.3
3	Japan	29	175	6.03
4	Italy	12	56	4.6
5	U.K.	10	134	13.4
6	Korea	10	57	5.7
7	Germany	7	63	9.0
8	Spain	6	67	11.2
9	Turkey	6	6	1.0
10	India	5	12	2.4

3.3 National network analysis

The country collaboration network analysis graph (Figure 4) generated by VOSviewer 1.6.19 illustrates the collaboration network in the field of intramedullary spinal cord tumor imaging research, involving 35 countries. In this network, China, the United States, and Japan are considered the three major powerhouses in this field, with link strengths of 1,835, 2,703, and 1,164, respectively. The collaboration network between China and Asian countries such as Japan and South Korea is relatively close, while the United States collaborates more frequently with English-speaking countries like the United Kingdom, Canada, and Australia. It is worth noting that the collaboration among European countries is relatively even and close. This indicates that Europe has a well-developed research collaboration network in this field, with countries collectively driving scientific progress.

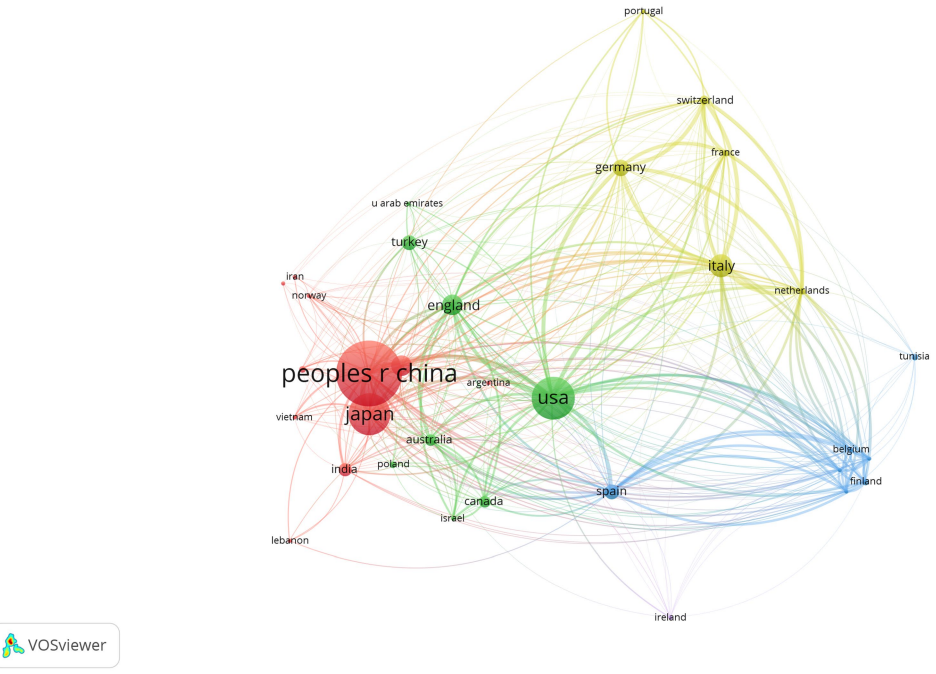

FIGURE 4
National network analysis map of the imaging field of spinal schwannoma.

TABLE 3 Top 5 authors in the field of imaging of spinal schwannoma.

No.	Author	Articles	Citations	Average citations
1	Shiro Imagama	4	23	5.7
2	Kei Ando	3	23	7.6
3	Naoki Ishiguro	3	23	7.6
4	Kazuyoshi Kobayashi	3	23	7.6
5	Satoshi Tanaka	3	16	5.3

3.4 Study authors and institutions of intraspinal schwannoma imaging

Analyzing the author and institution data (Table 3), it is found that the top five authors in terms of publication volume are all from Japan. Shiro Imagama ranks first with 4 publications, while Kei Ando, Naoki Ishiguro, and Kazuyoshi Kobayashi have 3 publications each. Their average citations per article are all 7.6, which is the highest. In terms of institutions (Table 4), Mayo Clinic and Capital Medical University both have 7 publications. However, Mayo Clinic has a higher citation count (83) and average citations per article (11.8) compared to Capital Medical University (49 citations and 7.0 average citations per article). This indicates that the Mayo Clinic has a greater research influence in this field. Jilin University ranks third with 6 publications, but its average citations per article are 4.0. This reflects that although Jilin University has a higher number of articles, the quality of the articles still needs improvement. Harvard University, despite having only 4 publications, has a high citation count of 130 and an average of 32.5 citations per article, which is the highest among all institutions. This indicates that Harvard University's research in this field has a high impact and recognition. By running VOSviewer, the institution network graph (Figure 5) was obtained, with a threshold set at 2, resulting in 35 nodes and 334 connections. The 35 institutions form 5 clusters.

3.5 Related journals in the field of imaging research of intraspinal schwannoma

A total of 82 journals have published literature related to intramedullary spinal cord tumor imaging research. Among them, the journal "World Neurosurgery" has the highest number of publications (26) and also ranks first in terms of citation count (113). Although the journal "Spine" has a relatively low number of publications, it has the highest average citations per article (11.8). The journals "Journal of Neurosurgery-Spine," "Neurosurgery," "European Spine Journal," "Spine," and "Acta Neurochirurgica" are all classified as JCR Q2 journals and have relatively high impact factors, with values of 3.6, 4.6, 3.1, 3.0, and 2.2, respectively. By setting a threshold of 2 in VOSviewer, the journal network graph (Figure 6) was obtained. Twenty-nine journals were included in the graph, forming 29 nodes and 227 connections, which were divided into 6 different clusters (see Table 5).

3.6 Keywords in the field of lumbar spinal stenosis and treatment

Keywords play an important role in an article as they not only summarize and reflect the core content of the article but also help

TABLE 4 Top 10 institutions in the field of imaging studies of spinal schwannoma.

No.	Institution	Articles	Citation	Average citations
1	Mayo Clinic	7	83	11.8
2	Capital Medical University	7	49	7.0
3	Jilin University	6	24	4.0
4	Harvard University	4	130	32.5
5	Kyushu University	4	31	7.75
6	University of Manchester	3	89	29.6
7	University of Toronto	3	73	24.3
8	Seoul University	3	35	11.7
9	The Seoul National University Hospital	3	35	11.7
10	Fudan University	3	10	3.3

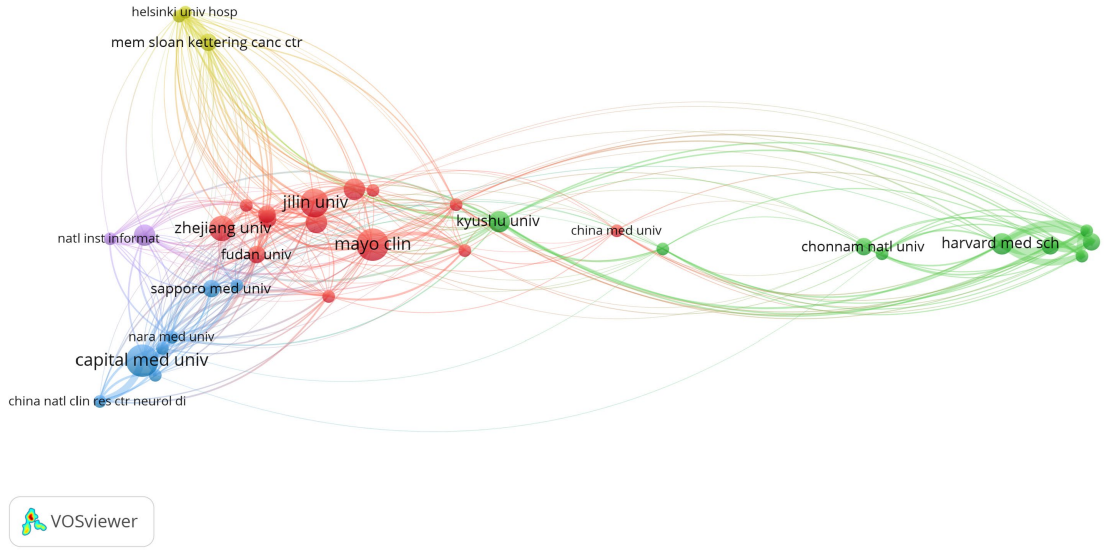

FIGURE 5
Institutional network diagram in the field of spinal schwannoma imaging research.

readers understand the research field and related concepts, thereby enhancing their understanding of the article. Table 6 lists the top 10 keywords with the highest frequency in the literature related to intramedullary spinal cord tumor imaging research. Among them, "Schwannoma" is the most frequently appearing keyword, with a total of 88 occurrences. "Tumors" and "Magnetic resonance imaging" rank second and third with frequencies of 27 and 26, respectively. By setting a threshold of 5 in VOSviewer, a keyword network graph was generated (Figure 7). A total of 53 keywords formed 53 nodes and 525 connections, divided into 5 different clusters. It is worth noting that "Schwannoma," "Tumors," "Magnetic resonance imaging," and "Surgery" became the core keywords in their respective clusters. Figure 8 illustrates the association between keyword frequency and time, where nodes closer to yellow indicate keywords that have been prominent in recent research. It can be observed that most keywords have appeared frequently in the literature from 2018 to 2023.

3.7 Outbreak words in the field of intraspinal schwannoma

Burst terms refer to the phenomenon where a specific keyword experiences a significant increase in frequency within a particular period. Figure 9 reflects the top 10 burst terms in the field of intramedullary spinal cord tumor imaging research over the past decade. Among them, the keyword "Cord" has the strongest burst intensity with a value of 2.65. The keywords "surgery," "resection," "schwannoma," and "case report" have the longest burst duration, consistently appearing at a high frequency for 3 years. Among them,

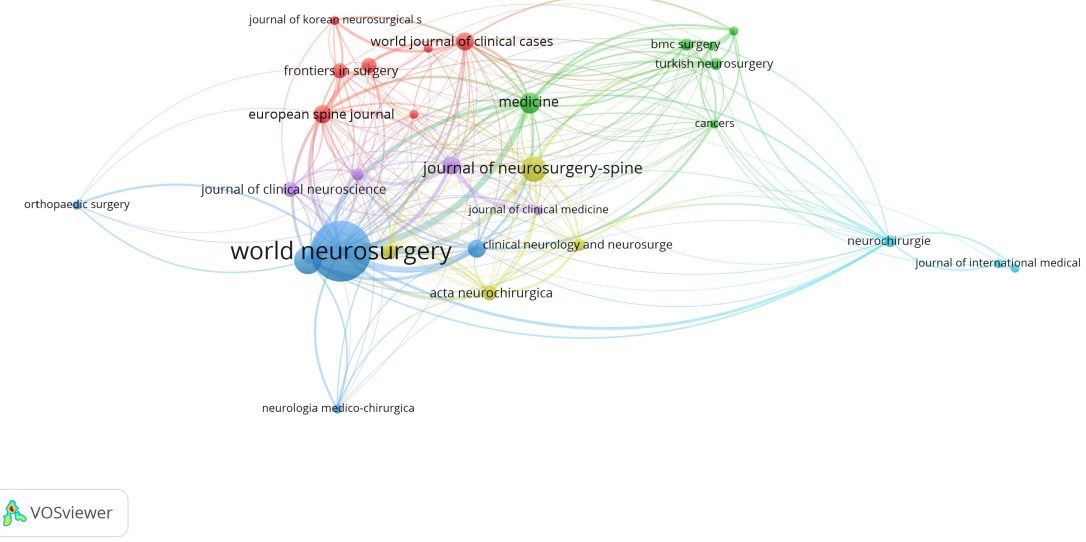

FIGURE 6
Network diagram of journals in the field of spinal schwannoma imaging research.

TABLE 5 Top 10 journals on imaging studies of spinal schwannoma.

No.	Journal	Articles	Citation	Average citations	JCR (2023)	IF (2023)
1	World Neurosurgery	26	113	4.3	3	2.1+
2	British Journal of Neurosurgery	9	20	2.2	4	1.5+
3	Journal of Neurosurgery-Spine	8	84	10.5	2	3.6
4	Medicine	6	13	2.1	4	1.6
5	Neurosurgery	5	45	9.0	2	4.6
6	European Spine Journal	5	52	10.4	2	3.1
7	Spine	5	59	11.8	2	3.0
8	World Journal of Clinical Cases	5	6	1.2	4	1.3
9	Oncology Letters	4	16	4.0	3	2.9
10	Acta Neurochirurgica	4	52	13.0	2	2.2

the keyword "tumor" had its first burst appearance in 2021, with a burst intensity of 2.49.

4 Discussion

4.1 Bibliometry

Web of Science, developed and maintained by Clarivate Analytics, is a comprehensive academic resource platform widely used across various disciplines. It features over 8,700 high-quality academic journals, conference proceedings, patents, and other literature sources (17). Web of Science offers robust search and filtering capabilities, enabling users to efficiently locate the academic literature they need. Additionally, it provides citation indexing, allowing researchers to track the citations received by specific articles, which facilitates an understanding of their academic impact and research trends within particular fields. Overall, the Web of Science serves as an essential resource for academic researchers, scientists, and students, supporting them in conducting literature reviews, exploring new research areas, and staying informed about the latest academic developments.

4.2 Status of global research in the field of schwannoma

From the perspective of publication volume, the average number of publications per year in this field is 17.9, which is relatively low compared to other fields. However, there has been a noticeable upward trend in the number of publications in this field over the past decade,

indicating that it is gradually gaining attention and recognition in the medical community. From a country perspective, China has almost the same publication volume (58) as the second and third-ranked countries, the United States (30) and Japan (29). This suggests that China has invested significant resources and efforts in research related to intramedullary spinal cord tumor imaging. Citation count is a reliable indicator of article quality. Similarly, the average citations per article from a country or institution can be used to evaluate the research quality and scientific level in that field. Among them, countries such as the United States and the United Kingdom, as well as institutions like Mayo Clinic and the University of Manchester, have the highest average citations per article, indicating their research level and quality are at a global top level. In contrast, although China has the highest number of articles, there is still a noticeable gap in terms of quality compared to developed countries in Europe and North America. In terms of authors, Japanese scholars have made significant contributions to this field. For example, in a retrospective study conducted in 2017, Kobayashi et al. (18) concluded that contrast-enhanced T1-weighted magnetic resonance imaging (MRI) is useful for predicting the proliferative activity and growth of intramedullary spinal cord tumors. These features are related to tumor enlargement and adhesion. The presence of an uneven pattern on contrast-enhanced T1-weighted images indicates tumor enlargement and adhesion. This pattern reflects the preoperative and postoperative motion status and recovery. In another study in 2023, Professor Shiro Imagama and his team developed an automated diagnostic system that uses deep learning with the You Only Look Once (YOLO) version 3 software, paired with MRI data, to accurately locate intramedullary spinal cord tumors. This system can detect incidental schwannomas on MRI scout images, reducing the workload of radiologists (19).

TABLE 6 Top 10 keywords in the field of imaging of intraspinal schwannoma.

No.	Keywords	Frequency of occurrence	Total connection strength
1	Schwannoma	82	88
2	Tumors	27	44
3	Magnetic resonance imaging	26	37
4	Spinal tumor	21	32
5	Surgery	19	26
6	Diagnosis	18	32
7	Meningioma	16	29
8	Outcomes	13	17
9	Features	12	19
10	Cauda-equina	12	18

4.3 Future trends in the field of schwannoma

Through the analysis of keywords and burst terms, we can gain insights into the research trends and emerging topics in a specific field. Schwannoma and magnetic resonance imaging (MRI) are undoubtedly the primary research focuses in the field of intramedullary spinal cord tumor imaging. MRI, a non-invasive medical imaging technique, plays a crucial role in generating detailed images of human tissue structures (20). It not only aids in accurate tumor localization but also provides valuable information about tumor shape, boundaries, internal structure, and relationship with

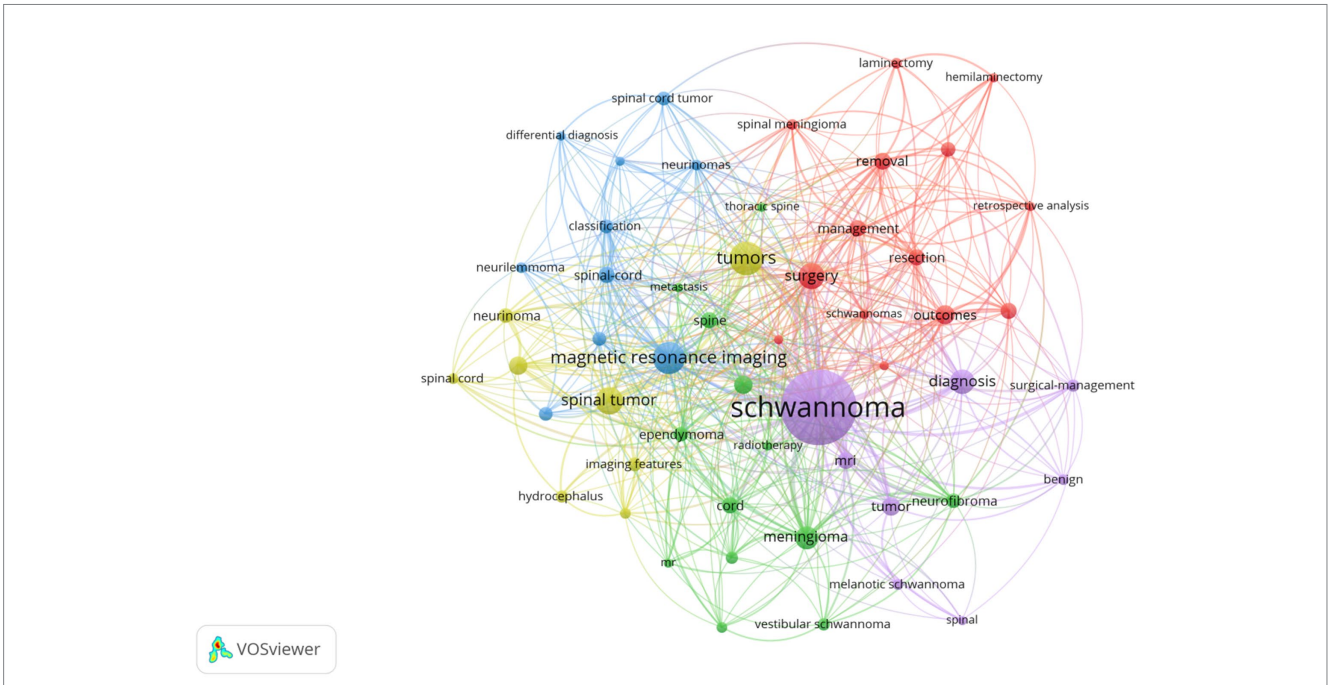

FIGURE 7
Clustering of keywords in the field of spinal schwannoma imaging research.

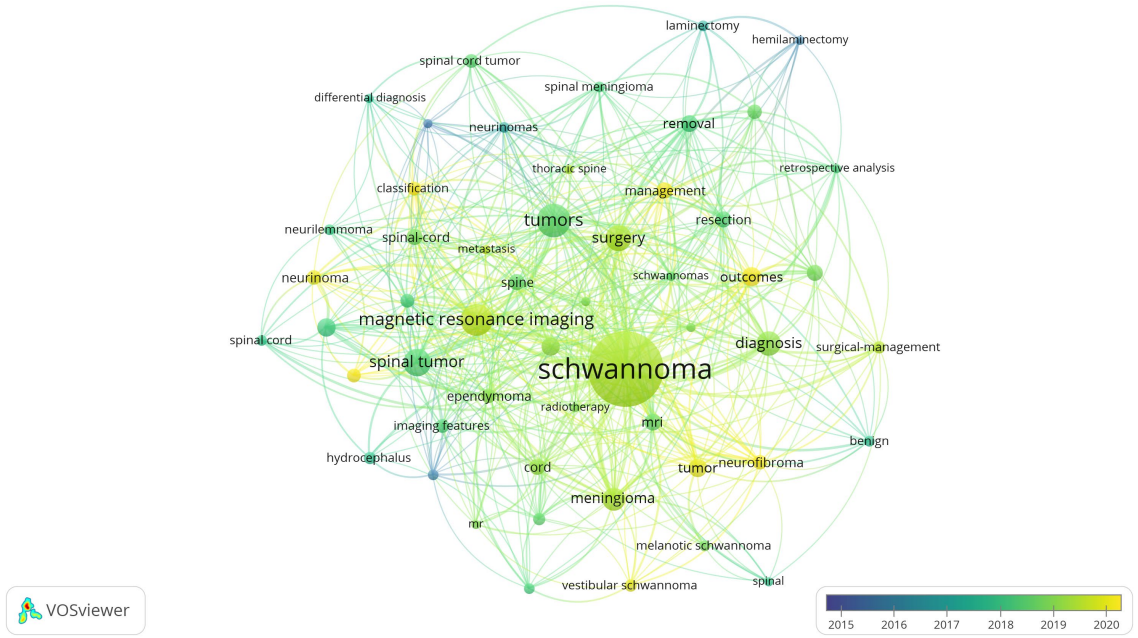

FIGURE 8
Keywords co-occurrence cluster map in the imaging field of spinal schwannoma (time superposition).

Top 10 Keywords with the Strongest Citation Bursts

Keywords	Year	Strength	Begin	End	2014 - 2023
mri	2015	1.62	2015	2017	
surgery	2016	2.12	2016	2019	
resection	2016	1.85	2016	2019	
vestibular schwannoma	2016	1.71	2016	2017	
cord	2018	2.65	2018	2019	
outcm	2018	1.68	2018	2019	
schwannoma	2014	2.17	2020	2023	
case report	2018	1.77	2020	2023	
surgical treatment	2020	1.56	2020	2023	
tumor	2021	2.49	2021	2023	

FIGURE 9
Atlas of top 10 outbreak words in the field of spinal schwannoma.

surrounding tissues (21). Distinguishing intramedullary spinal cord tumors from meningiomas has always been a challenging task in radiology (22). In a study evaluating the effectiveness of MRI in 764 cases of brain tumors, the sensitivity of MRI for schwannomas ranged from 90.7 to 92.6%, while for meningiomas, it ranged from 88.4 to 95.7% (23). Due to the similarity in imaging features between intramedullary spinal cord tumors and meningiomas, approximately 25% of schwannomas and meningiomas are difficult to differentiate in diagnosis (24, 25). In another study, researchers confirmed that the signal intensity ratio between intramedullary tumors and fat on T2-weighted images can accurately differentiate schwannomas from meningiomas (26). The preoperative identification of filum terminale ependymomas (FTE) and schwannomas poses significant challenges but is vital for the formulation of surgical plans and the assessment of prognoses. In a retrospective analysis, Gu et al. (27) identified that key elements include contrast-enhanced magnetic resonance imaging (MRI), convolutional neural networks (CNNs), filum terminale ependymoma, and schwannoma. 8F-FDG PET/CT is a sophisticated

medical imaging technique that integrates positron emission tomography (PET) and computed tomography (CT) and is extensively utilized in fields such as oncology, cardiology, and neuroscience. In a case report by Gültekin et al. (28), the team successfully diagnosed a patient with multiple sclerosis and liver metastasis using 8F-FDG PET/CT, with subsequent biopsy results corroborating their diagnosis. Additionally, numerous other case reports have demonstrated that as technology continues to evolve, the role of PET-CT in the management of nerve sheath tumors is becoming increasingly significant. The synergistic application of this technology enhances the diagnostic accuracy for nerve sheath tumors, aiding physicians in developing optimal treatment plans and ultimately improving patient outcomes. A populous country, China has a high incidence of intramedullary spinal cord tumors among spinal tumors (29). Imaging plays a crucial role in the clinical diagnosis of intramedullary spinal cord tumors. Surgery is the main treatment modality for intramedullary spinal cord tumors (2), and imaging plays a key guiding role in surgical treatment, helping surgeons determine the surgical approach, extent of resection, and protection of surrounding neural structures (30). Additionally, imaging can be used for postoperative follow-up and evaluation of treatment outcomes, monitoring tumor recurrence or progression (31). The imaging diagnosis of intramedullary spinal cord tumors remains a core issue in this field and is one of the main directions for future development. Therefore, improving the level of imaging diagnosis for intramedullary spinal cord tumors is an important task for healthcare professionals in China. Only through the combination of imaging and scientific research efforts can solid theoretical foundations be provided for clinical treatment, improving the level of care and enhancing the quality of patient prognosis.

4.4 Lack of the study

This study only includes relevant literature from the Web of Science Core database. Although this database has extensive coverage and includes a wide range of journals, there may still be some data omissions. Additionally, this study only includes English-language literature and may not capture high-quality non-English literature, which could introduce selection bias. Furthermore, the Web of Science Core database is continuously updated, so the analysis results are time-limited. However, the existing research still provides valuable insights and guidance for our research direction and design.

5 Conclusion

This article leverages bibliometric analysis of pertinent literature from the Web of Science core database to delve into the relationship between imaging studies and the clinical management of spinal intradural schwannomas. Through a comprehensive statistical analysis of an extensive body of literature, this study uncovers prevailing research trends, identifies hot topics, and maps out the knowledge landscape, thus significantly enriching the traditional literature review approach. Employing an interdisciplinary strategy, it promotes dialogue and cooperation among various fields, thereby broadening and deepening the scope of research into spinal intradural schwannoma imaging. Bibliometrics offers a swift and efficient means to process and analyze vast amounts of literature data, equipping researchers with timely and precise insights into the current state and directions of research. This method boosts research efficiency, minimizes repetitive studies, and fosters the rapid development and innovation of knowledge. Although spinal intradural schwannomas have not traditionally been a focal point in medical research, heightened international interest and investment have brought increased attention to this area. Nonetheless, there is a pressing need for enhancement in research quality, addressing prevailing issues such as the overall low quality of studies and a scarcity of mechanistic research. MRI remains the definitive diagnostic tool for spinal intradural schwannomas, with future research expected to concentrate on feature analysis, enhancement studies, and quantitative assessments, marking them as the next frontiers in research. Progress in these domains promises to raise the bar for diagnostic and therapeutic approaches to spinal intradural schwannomas, ultimately improving patient care and outcomes.

Data availability statement

The original contributions presented in the study are included in the article/supplementary materials, further inquiries can be directed to the corresponding author.

Author contributions

AA: Writing – original draft, Writing – review & editing. KS: Data curation, Writing – review & editing. HM: Conceptualization, Supervision, Writing – review & editing.

Funding

The author(s) declare that no financial support was received for the research, authorship, and/or publication of this article.

Conflict of interest

The authors declare that the research was conducted in the absence of any commercial or financial relationships that could be construed as a potential conflict of interest.

Publisher's note

References

1. Ram S, Vivek V, Shekhar R, Gabbita AC, Ganesh K. Giant cervicodorsal schwannoma. *J Exp Ther Oncol*. (2019) 13:155–8.

2. Ferreira A, Blanco CMB, Trindade JVC, Mattos G, Joaquim A. Surgical outcome of spinal schwannoma and neurofibroma. *Rev Assoc Med Bras*. (2023) 69:e20230190. doi: 10.1590/1806-9282.20230190

3. Alektoroff K, Moulopoulos LA, Papanagiotou P. Spinal tumors. *Radiologe*. (2021) 61:267–74. doi: 10.1007/s00117-021-00815-5

4. Garaud S, Boto J, Egervari K, Vargas MI. Extradural spinal meningioma mimicking a schwannoma: magnetic resonance imaging findings. *Can J Neurol Sci*. (2022) 49:467–9. doi: 10.1017/cjn.2021.120

5. Nakamae T, Kamei N, Tamura T, Maruyama T, Nakao K, Farid F, et al. Differentiation of the intradural extramedullary spinal tumors, schwannomas, and meningiomas utilizing the contrast ratio as a quantitative magnetic resonance imaging method. *World Neurosurg*. (2024) 188:e320–5. doi: 10.1016/j.wneu.2024.05.106

6. Arima H, Hasegawa T, Togawa D, Yamato Y, Kobayashi S, Yasuda T, et al. Feasibility of a novel diagnostic chart of intramedullary spinal cord tumors in magnetic resonance imaging. *Spinal Cord*. (2014) 52:769–73. doi: 10.1038/sc.2014.127

7. Ottenhausen M, Ntoulias G, Bodhinayake I, Ruppert FH, Schreiber S, Förschler A, et al. Intradural spinal tumors in adults-update on management and outcome. *Neurosurg Rev*. (2019) 42:371–88. doi: 10.1007/s10143-018-0957-x

8. Minhas AS, Oliver R. Magnetic resonance imaging basics. *Adv Exp Med Biol*. (2022) 1380:47–82. doi: 10.1007/978-3-031-03873-0_3

9. Harisinghani MG, O'Shea A, Weissleder R. Advances in clinical MRI technology. *Sci Transl Med*. (2019) 11:eaba2591. doi: 10.1126/scitranslmed.aba2591

10. Ahlawat S, Blakeley JO, Langmead S, Belzberg AJ, Fayad LM. Current status and recommendations for imaging in neurofibromatosis type 1, neurofibromatosis type 2, and schwannomatosis. *Skeletal Radiol*. (2020) 49:199–219. doi: 10.1007/s00256-019-03290-1

11. Morrison DR, Sorace AG, Hamilton E, Moore LS, Houson HA, Udayakumar N, et al. Predicting schwannoma growth in a tumor model using targeted imaging. *Otol Neurotol*. (2021) 42:e615–23. doi: 10.1097/MAO.0000000000003063

12. Wu F, Gao J, Kang J, Wang X, Niu Q, Liu J, et al. Knowledge mapping of exosomes in autoimmune diseases: a bibliometric analysis (2002–2021). *Front Immunol*. (2022) 13:939433. doi: 10.3389/fimmu.2022.939433

13. Wang B, Xing D, Zhu Y, Dong S, Zhao B. The state of exosomes research: a global visualized analysis. *Biomed Res Int*. (2019) 2019:1–10. doi: 10.1155/2019/1495130

14. van Eck NJ, Waltman L. Software survey: VOSviewer, a computer program for bibliometric mapping. *Scientometrics*. (2010) 84:523–38. doi: 10.1007/s11192-009-0146-3

15. Synnestvedt MB, Chen C, Holmes JH. CiteSpace II: visualization and knowledge discovery in bibliographic databases. *AMIA Annu Symp Proc*. (2005) 2005:724–8.

16. McGee S, Sipos T, Allin T, Chen C, Greco A, Bobos P, et al. A systematic review of the measurement properties of performance-based functional tests in patients with neck disorders. *BMJ Open*. (2019) 9:e031242. doi: 10.1136/bmjopen-2019-031242

17. Falagas ME, Pitsouni EI, Malietzis GA, Pappas G. PubMed, Scopus, Web of Science, and Google Scholar: strengths and weaknesses. *FASEB J*. (2008) 22:338–42. doi: 10.1096/fj.07-9492LSF

18. Kobayashi K, Imagama S, Ando K, Hida T, Ito K, Tsushima M, et al. Contrast MRI findings for spinal schwannoma as predictors of tumor proliferation and motor status. *Spine*. (2017) 42:E150–5. doi: 10.1097/BRS.0000000000001732

19. Ito S, Nakashima H, Segi N, Ouchida J, Oda M, Yamauchi I, et al. Automated detection and diagnosis of spinal schwannomas and meningiomas using deep learning and magnetic resonance imaging. *J Clin Med*. (2023) 12:5075. doi: 10.3390/jcm12155075

20. What is an MRI scan and what can it do? *Drug Ther Bull*. (2011) 49:141–4. doi: 10.1136/dtb.2011.02.0073

21. Wald LL. Ultimate MRI. *J Magn Reson*. (2019) 306:139–44. doi: 10.1016/j.jmr.2019.07.016

22. Neupane S, Kashyap A, Paudel S, Bhattarai G, Kharel SK, Adhikari A, et al. A rare case of schwannomatosis with meningioma: a case report. *Ann Med Surg*. (2024) 86:1724–8. doi: 10.1097/MS9.0000000000001738

23. Yan PF, Yan L, Zhang Z, Salim A, Wang L, Hu TT, et al. Accuracy of conventional MRIs for preoperative diagnosis of intracranial tumors: a retrospective cohort study of 762 cases. *Int J Surg*. (2016) 36:109–17. doi: 10.1016/j.ijsu.2016.10.023

24. Iwata E, Shigematsu H, Yamamoto Y, Kawasaki S, Tanaka M, Okuda A, et al. Preliminary algorithm for differential diagnosis between spinal meningioma and schwannoma using plain magnetic resonance imaging. *J Orthop Sci*. (2018) 23:408–13. doi: 10.1016/j.jos.2017.11.012

25. Zhai X, Zhou M, Chen H, Tang Q, Cui Z, Yao Y, et al. Differentiation between intraspinal schwannoma and meningioma by MR characteristics and clinic features. *Radiol Med*. (2019) 124:510–21. doi: 10.1007/s11547-019-00988-z

26. Takashima H, Takebayashi T, Yoshimoto M, Onodera M, Terashima Y, Iesato N, et al. Differentiating spinal intradural-extramedullary schwannoma from meningioma using MRI T_2 weighted images. *Br J Radiol*. (2018) 91:20180262. doi: 10.1259/bjr.20180262

27. Gu Z, Dai W, Chen J, Jiang Q, Lin W, Wang Q, et al. Convolutional neural network-based magnetic resonance image differentiation of filum terminale ependymomas from schwannomas. *BMC Cancer*. (2024) 24:350. doi: 10.1186/s12885-024-12023-0

28. Gültekin A, Aydoğmuş Ü, Arifoğlu H, Bir F, Yaylalı O. An intrathoracic schwannoma case in 18F-FDG PET/CT scan. *Hell J Nucl Med*. (2020) 23:206–8. doi: 10.1967/s002449912111

29. Ding Y, Zhu T. Progress in diagnosis and treatment of multiple schwannoma. *Chin J Neurosurg*. (2017) 33:426–9. doi: 10.3760/cma.j.issn.1001-2346.2017.04.028

30. Zhang E, Zhang J, Lang N, Yuan H. Spinal cellular schwannoma: an analysis of imaging manifestation and clinicopathological findings. *Eur J Radiol*. (2018) 105:81–6. doi: 10.1016/j.ejrad.2018.05.025

31. Merhemic Z, Stosic-Opincal T, Thurnher MM. Neuroimaging of spinal tumors. *Magn Reson Imaging Clin N Am*. (2016) 24:563–79. doi: 10.1016/j.mric.2016.04.007

frontiers | Frontiers in Oncology

TYPE Case Report
PUBLISHED 29 November 2024
DOI 10.3389/fonc.2024.1487835

OPEN ACCESS

EDITED BY
John Bianco,
Princess Maxima Center for Pediatric Oncology, Netherlands

REVIEWED BY
Joseph Louis Lasky,
Cure 4 The Kids, United States
Baraa Dabboucy,
Laval University, Canada

*CORRESPONDENCE
Mingfa Wang
wwwmingfa@163.com
Caicai Zhang
hy0206101@hainmc.edu.cn
Jigao Feng
fengjigao@hainmc.edu.cn

†These authors have contributed equally to this work

RECEIVED 28 August 2024
ACCEPTED 13 November 2024
PUBLISHED 29 November 2024

CITATION
Liu D, Li N, Zhu Y, Zhong Y, Deng G, Wang M, Zhang C and Feng J (2024) Case report: Pediatric intraventricular Rosai-Dorfman disease: clinical insights and surgical strategies in a decade-long observational study and literature review.
Front. Oncol. 14:1487835.
doi: 10.3389/fonc.2024.1487835

Case report: Pediatric intraventricular Rosai-Dorfman disease: clinical insights and surgical strategies in a decade-long observational study and literature review

Dayuan Liu[1†], Ning Li[1†], Yubo Zhu[1†], Yunxiang Zhong[1], Guolong Deng[1], Mingfa Wang[2*], Caicai Zhang[3*] and Jigao Feng[1,4*]

[1]Department of Neurosurgery, The Second Affiliated Hospital of Hainan Medical University, Haikou, Hainan, China, [2]Department of Pathology, The Second Affiliated Hospital of Hainan Medical University, Haikou, Hainan, China, [3]Department of Physiology, Hainan Medical University, Haikou, Hainan, China, [4]Department of Surgery, Hainan Vocational University of Science and Technology, Haikou, Hainan, China

Background: Rosai-Dorfman disease (RDD), or sinus histiocytosis with massive lymphadenopathy (SHML), is a rare benign disorder characterized by the proliferation of histiocytes of uncertain origin. Central nervous system (CNS) involvement, particularly intraventricular, is exceptionally rare and poses significant diagnostic challenges due to its non-specific clinical and radiographic presentation. This study aims to present a case of intraventricular RDD and review existing literature on its clinical features, treatment strategies, and prognosis.

Methods: We report the case of a five-year-old male with recurrent headaches and epilepsy caused by an intraventricular mass. The mass was surgically resected and histopathological examination was performed to confirm the diagnosis. A comprehensive literature review was conducted to identify similar cases of intraventricular RDD, focusing on clinical features, diagnostic methods, treatment strategies, and outcomes.

Results: Histopathological examination of the resected tumor revealed typical features of RDD, including large histiocytes, lymphocyte infiltration, and immunohistochemical positivity for CD68, S-100, and Vimentin. The patient remained asymptomatic ten years post-surgery with no recurrence of epilepsy or tumor. The literature review identified six similar cases, all of which showed favorable outcomes post-surgery, highlighting the self-limiting nature and favorable prognosis of intraventricular RDD following surgical resection.

Conclusion: Intraventricular RDD, though rare, should be considered in the differential diagnosis of intraventricular masses in pediatric patients. Surgical resection remains the primary treatment modality, and histopathological

confirmation is essential for accurate diagnosis. The prognosis is generally favorable with appropriate surgical intervention, although recurrence can occur, necessitating long-term follow-up. Further research is required to refine diagnostic criteria and explore adjuvant therapies for improved management of this rare CNS disorder.

KEYWORDS

Rosai-Dorfman disease (RDD), intraventricular tumor, pediatric epilepsy, central nervous system histiocytosis, surgery

1 Introduction

Sinus histiocytosis with massive lymphadenopathy (SHML), also known as Rosai-Dorfman disease (RDD), is a rare, benign disorder characterized by proliferative histiocytic activity of uncertain origin. Initially considered a non-neoplastic reactive histiocytic disease linked to autoimmunity (8), recent research has suggested an infectious theory, with some scholars proposing associations with specific infections such as cytomegalovirus, parvovirus B19, and Epstein-Barr virus (12, 14).

First described in 1969 by Rosai and Dorfman, the term RDD originated from their observation of four cases that demonstrated distinctive clinical presentations and histopathological features of histiocytic proliferative disease (1). The hallmark of RDD is the infiltration of sinus histiocytes in lymph nodes, typically presenting as painless lymphadenopathy (12, 14). Central nervous system (CNS)-RDD, particularly within ventricular systems, is exceptionally rare in clinical literature, with only a limited number of reported cases globally (3). Due to its low incidence rate and varied affected regions with associated pathological changes, alongside non-specific radiographic findings on CT and MRI scans, the potential for misdiagnosis or delayed diagnosis before definitive histopathological examination is considerable.

The disease predominantly affects children and young adults, with a peak incidence at around 20 years of age, and shows a higher prevalence in males than females. Related key manifestations include painless cervical lymphadenopathy, fever, weight loss, and non-specific symptoms resembling infection, such as elevated erythrocyte sedimentation rate (14). Some cases present with extranodal involvement without lymphadenopathy, affecting various organs, including the skin, nasal cavity, sinuses, eyelids, orbits, bones, and digestive system (11). In fewer than 5% of RDD cases, the disease involves the CNS, typically affecting sites like the suprasellar region, cerebral convexity, parasagittal region, cavernous sinus, and petroclival region. The most common CNS manifestation resembles a dural mass similar to meningioma (16, 23), and intraventricular involvement is exceptionally rare.

In the 2016 WHO classification of CNS tumors, RDD was categorized as a histiocytic tumor characterized by the infiltrative growth of non-neoplastic histiocytes in lymph nodes and extranodal sites (11). CNS involvement in RDD, termed CNS-RDD, is more frequently observed in older patients, with lesions typically found in locations such as the cerebellopontine angle, sellar region, and occipital lobe (5, 10). Clinical symptoms of CNS-RDD are non-specific and vary depending on the lesion's location, size, and impact on adjacent nerve function. Common symptoms include headaches, limb paralysis, sensory disturbances, and other neurological deficits. Lesions in the sellar region can lead to visual impairment and pituitary dysfunction similar to those seen in pituitary adenomas, while involvement of the ventricular system may result in obstructive hydrocephalus, potentially leading to coma and even death (15). RDD originating within the ventricles is rare, with only a few documented cases in the literature to date (6).

Currently, there is a lack of specific diagnostic methods for CNS-RDD. Due to its non-specific imaging characteristics, absence of distinctive histological features, or potential overlap with other concurrent lesions, RDD is frequently misdiagnosed as a tumor. Clinical cases often mimic meningiomas due to their solitary mass appearance, contributing to misdiagnosis in more than 90% of cases (9). The challenge of diagnosing RDD escalates when it presents as solitary lesions within the cerebral ventricles, as it lacks the typical features of dural-based lesions associated with this condition.

The aim of this study is to enhance understanding on intraventricular RDD by presenting a detailed case report and conducting a literature review, detailing the clinical manifestations, diagnostic challenges, treatment modalities and long-term outcomes associated with this rare CNS disorder, thereby aiding clinicians in recognizing and managing similar cases effectively.

2 Case description and methods

2.1 Patient profile

A five-year-old male child was admitted to our hospital on March 11, 2011, due to a primary complaint of recurring headaches and convulsions in the extremities that had persisted for over three years and intensified one day prior to admission. Before this period,

the child had experienced episodic headaches accompanied by limb rigidity and convulsions lasting approximately ten seconds before spontaneous resolution. Previously evaluated at a local hospital, an electroencephalogram (EEG) showed no significant abnormalities, while a cranial MRI revealed a space-occupying lesion in the right cerebral ventricle. Initial treatment with anti-epileptic medications resulted in symptom improvement, leading to discharge. However, the day before this admission, the child experienced a sudden onset of headache and vomiting, necessitating further evaluation at our facility. The patient had no significant familial medical history.

Upon admission, the child was conscious and responsive, with a Glasgow Coma Scale (GCS) score of E4V5M6 = 15. His cranial examination showed a normal-sized cranium with even hair distribution. Pupillary examination revealed equal and round bilateral pupils of approximately 3.0mm in diameter, responsive to light. No nystagmus or mouth angle deviation was observed, there was no neck resistance, and muscle strength and tone in all four limbs were normal. Pathological reflexes were not present.

2.2 Diagnostic investigation

The EEG showed mild abnormal electrical activity (Figure 1A), which normalized post-surgery (Figure 1B). Cranial MRI revealed a well-defined mass measuring approximately 59×50×46mm^3 in the anterior region of the right ventricle. The mass had clear margins, a lobulated appearance, low signal intensity on T1-weighted images, mixed high signal intensity on T2-weighted images, and significant enhancement with contrast. Bilateral lateral ventricles are dilated, especially the right ventricle, and high signals can be seen around the anterior horn of the lateral ventricle on T2-weighted images (Figure 2A). The results of blood tests, urinalysis and other investigations were within normal limits. Based on these, the preliminary diagnosis was right lateral ventricular tumor with obstructive hydrocephalus and secondary epilepsy.

2.3 Therapeutic intervention

A right frontal parietal craniotomy was conducted under general anesthesia with endotracheal intubation to resect the intraventricular tumor. Intraoperatively, the tumor was found to have a soft, purplish-red appearance, distinct from the surrounding brain tissues, and was encapsulated, measuring approximately 6cm×6cm. It was resected in sequential blocks, ensuring careful preservation of vasculature and avoiding venous injury. The excised tissue was then submitted for histopathological examination.

2.4 Literature assessment

A comprehensive search was conducted using databases such as PubMed, MEDLINE, and Scopus to perform the literature review. The keywords used included “Rosai-Dorfman Disease”, “intraventricular”, “central nervous system”, and “pediatric.” The study inclusion criteria encompassed case reports, clinical studies, and reviews published in peer-reviewed journals. Briefly, articles were screened for relevance based on the abstract, and full texts were analyzed to extract data on clinical features, diagnostic methods, treatment strategies, and outcomes of intraventricular RDD. Data synthesis and analysis focused on identifying patterns in presentation, management, and prognosis.

2.5 Statistical analysis

Descriptive statistics summarized patient demographics (age, gender, clinical presentation), tumor characteristics (location, size, MRI findings), treatment approaches (surgical methods, adjuvant therapies), and outcomes (follow-up duration, recurrence rates, symptom resolution).

3 Results

3.1 Postoperative pathology

The postoperative histopathological examination revealed a lesion composed of large histiocytes with round nuclei and prominent nucleoli. The lesion showed infiltration of lymphocytes and plasma cells, along with perivascular cuffing of lymphocytes in localized vascular areas. Immunohistochemical staining showed positivity for CD68, S-100, and Vimentin, partial positivity for GEAP, and a low Ki-67 proliferation index (<10%). CD1a staining was negative. Based on these findings, the lesion was diagnosed as consistent with RDD (Figures 3A–F).

3.2 Postoperative follow-up

A follow-up MRI performed two weeks post-surgery demonstrated near-total resection of the lesion, along with a low-signal lesion in the right frontal lobe, indicative of post-surgical changes, and evidence of encephalomalacia. Ventricular enlargement and cerebral edema showed improvement compared to previous scans (Figure 2B). A residual tumor was noted as a nodular enhancement at the genu of the corpus callosum on the right ventricle wall.

The patient did not receive postoperative radiotherapy or adjuvant therapy. Ten years post-surgery, the patient remained asymptomatic with no headaches or dizziness, and no recurrence of epilepsy. Follow-up cranial MRI revealed a reduction in the size of the nodular enhancement at the genu of the corpus callosum on the right ventricle wall compared to earlier scans (Figure 2C). There was no radiographic evidence of tumor recurrence. The patient’s growth and development were normal, and follow-up continued via telephonic consultations.

3.3 Literature review of RDD

Next, we summarized the clinical features of our case and reviewed other cases of intraventricular RDD (Table 1). As can be

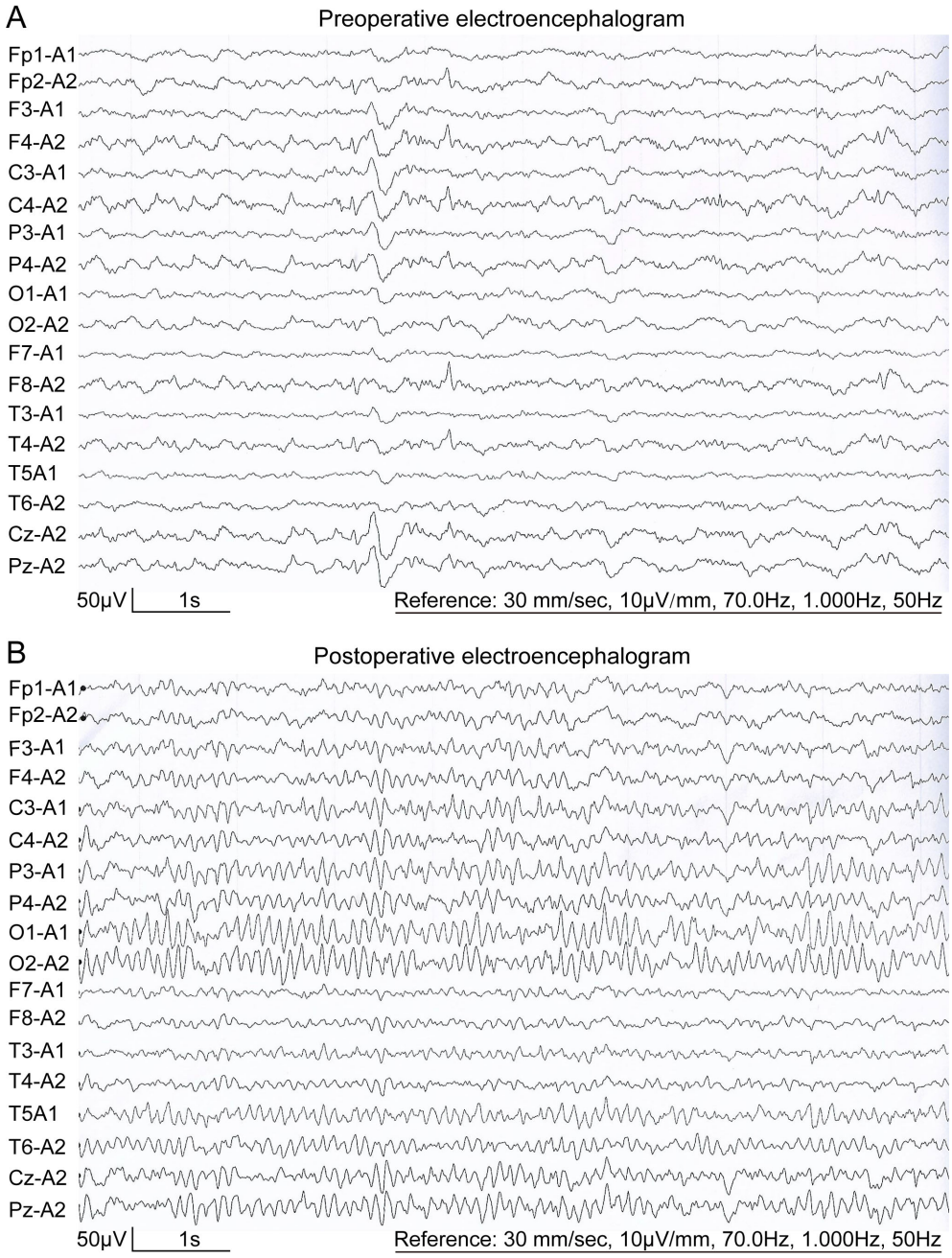

FIGURE 1
Eighteen-lead resting-state EEG of the patient. **(A)** Preoperative EEG of the patient showed sporadic spikes/sharp waves in the frontal and temporal lobes. **(B)** Postoperative EEG showed a normal EEG.

seen, each case showed pathological abnormalities mainly localized within the cerebral ventricles, affecting both the lateral and fourth ventricles, either as solitary or multifocal lesions (8).

Specifically, four cases involved a single intraventricular lesion, while the other two cases featured multiple lesion sites. According to the literature, most patients initially presented with symptoms indicative of increased intracranial pressure, such as headache and vomiting. Some also exhibited cognitive impairment and ataxia, depending on the locations invaded by the tumor. However, cases of ventricular RDD complicated by seizures were rare. In comparison with a case involving a child with RDD in the right ventricle and a lobulated enhancing mass in the fourth ventricle, our patient was slightly younger. They presented symptoms of supratentorial ventricular enlargement and obstructive hydrocephalus.

Clinical symptoms primarily included headache and dizziness, along with secondary epilepsy symptoms such as limb tetanic convulsions. These symptoms may be attributed to physiological blockage of cerebrospinal fluid circulation by the right ventricular tumor, leading to increased intracranial pressure, reduced cerebral blood flow perfusion causing cerebral ischemia and hypoxia, and subsequent epilepsy. Alternatively, compression of the frontal/temporal lobe by the ventricular tumor could induce corresponding lobar epilepsy symptoms.

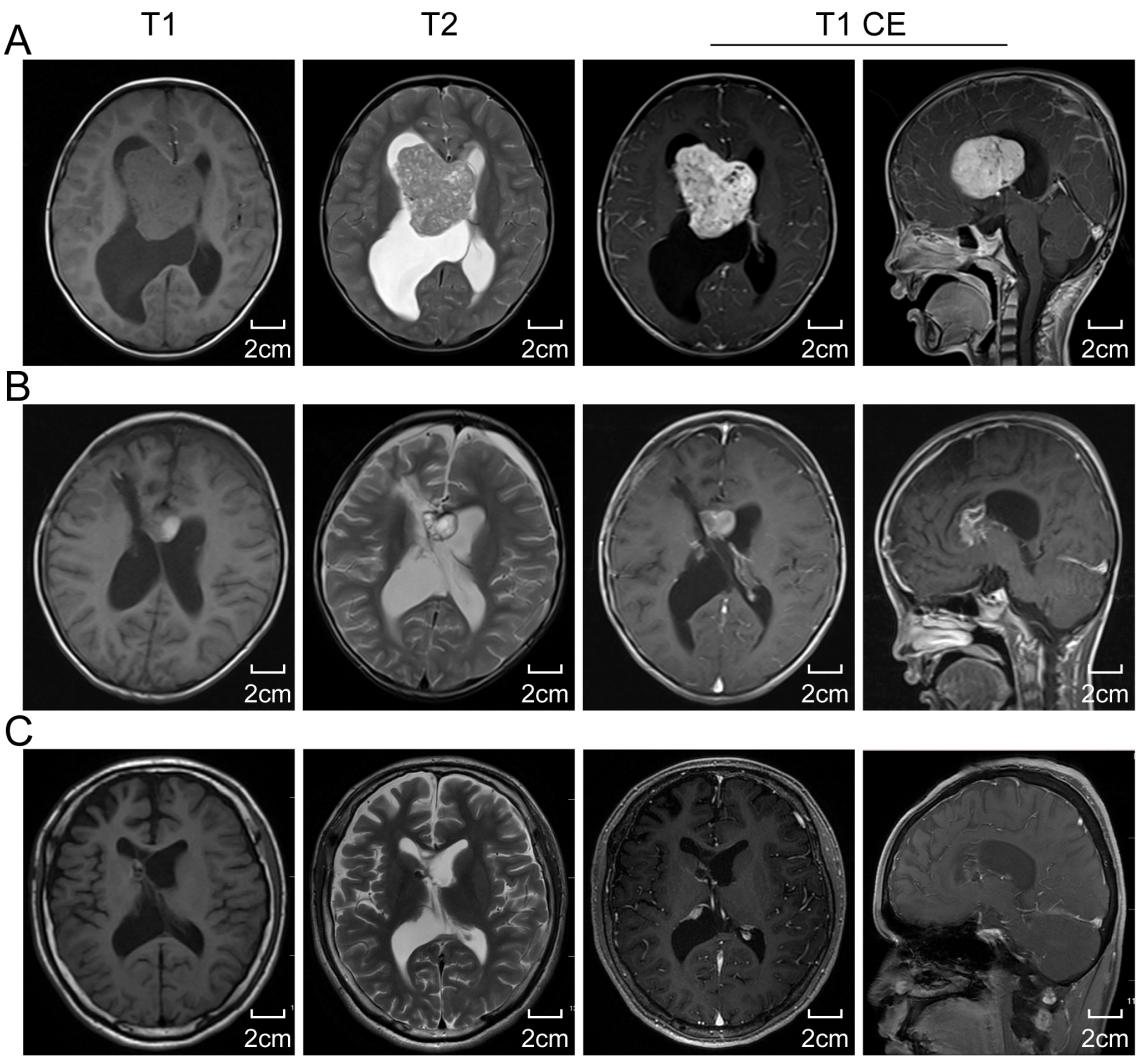

FIGURE 2
The cranial magnetic resonance imaging (MRI) results. **(A)** Preoperative standard MRI reveals a lesion within the lateral ventricle. The lesion presents as isointense with gray matter on T1-weighted images and hyperintense on T2-weighted images. Axial and sagittal views of enhanced T1-weighted images display uniformly enhanced intraventricular lesion, with obstructive hydrocephalus due to a blockage at the Monro foramen. **(B)** A two-week postoperative MRI follow-up suggests a subtotal resection of the tumor, with nodular enhancement indicating residual tumor within the ventricle at the genu of the corpus callosum. **(C)** A ten-year postoperative MRI follow-up indicates near disappearance of the intraventricular tumor and significant relief of hydrocephalus. T1 CE, T1-weighted contrast-enhanced imaging.

In our present case report, the patient did not have hepatosplenomegaly or other manifestations of extranodal lymph node diseases, suggesting it was an isolated intraventricular presentation of RDD, which is rare. Surgical treatment was performed on all six reported patients, and despite varying initial conditions and extents of tumor resection, most patients showed favorable outcomes. Compared to the literature review, additional benefits were observed in some patients who received post-surgical radiotherapy or steroid therapy.

4 Discussion

Our study presents a rare case of pediatric intraventricular RDD associated with epilepsy, managed successfully through surgical intervention. This case, along with five others documented in the literature, emphasizes the self-limiting nature of intraventricular RDD and its favorable prognosis following subtotal or total resection. Notably, all patients demonstrated significant clinical improvement post-surgery, with no recurrence or malignant progression observed during follow-up periods extending up to ten years.

The head MRI of our presented case revealed a lesion in the right ventricle characterized by irregular lobulated enhancement with well-defined borders, accompanied by ventricular enlargement and hydrocephalus. Initially, the clinical diagnosis considered choroid plexus papilloma, with meningioma also under consideration. However, unlike most choroid plexus papillomas, intracranial RDD typically shows high or isointense signals on T1-weighted MRI with clear boundaries. T2-weighted imaging usually

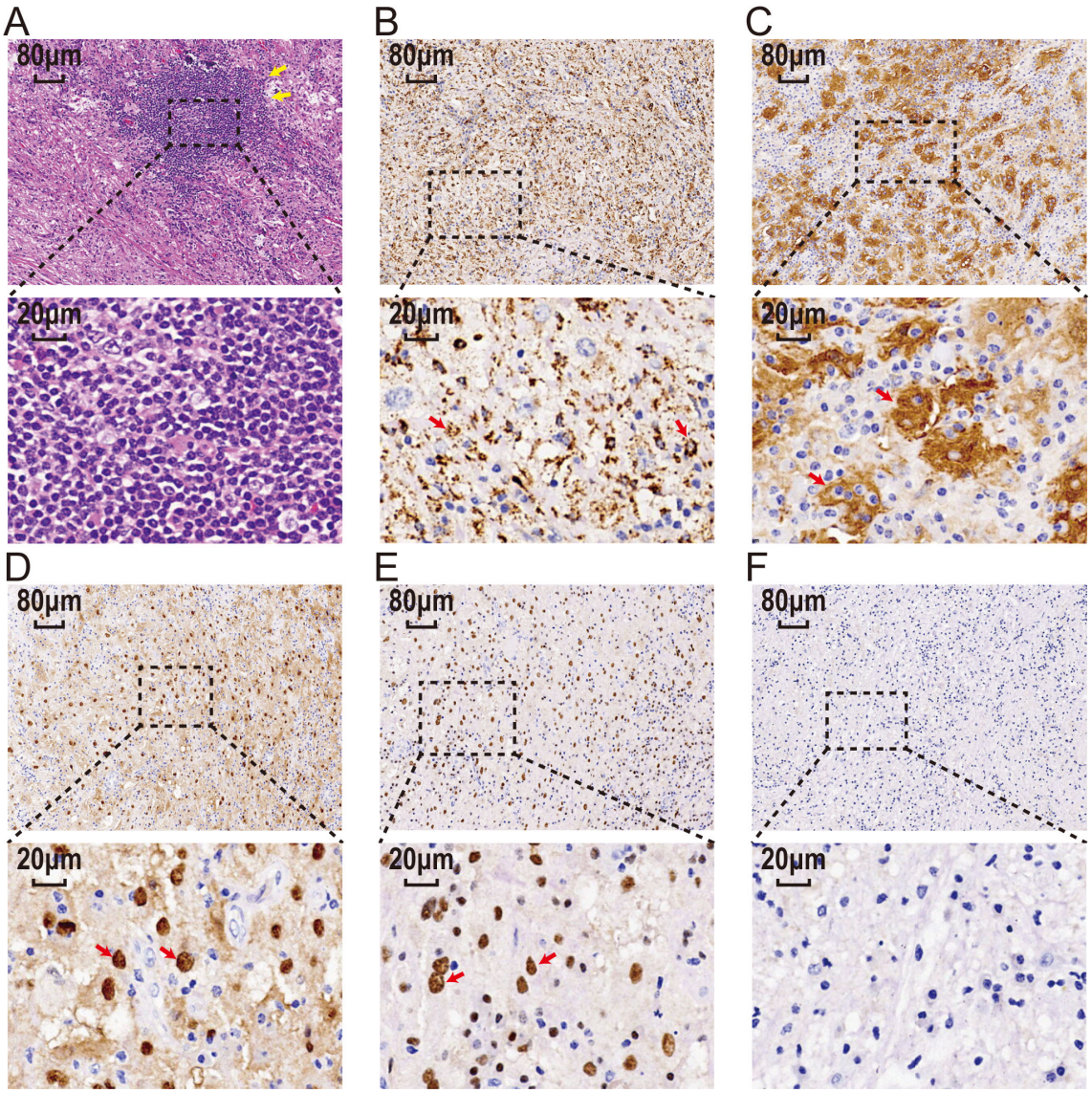

FIGURE 3
The histopathological examination results. **(A)** Hematoxylin-eosin stain of tissue sections shows atypical histiocytic cells with emperipolesis(yellow arrow). Large histicytes immunoreactive for CD68 **(B)**, S100 **(C)**, CyclinD1 **(D)**, and OCT2 **(E)** (red arrow) and immunonegatie for CD1a **(F)**. Scale bar: 20 μm and 80 μm. CD68, Cluster of Differentiation 68; S100, S100 protein; OCT2, Organic Cation Transporter 2; CD1a, Cluster of Differentiation 1a.

displays isointense signals, with areas of low signal intensity that enhance uniformly post-contrast. Some researchers suggest that these low-signal areas could result from free radicals produced during macrophage phagocytosis activity (19). However, such a phenomenon was not observed in our case, possibly due to the location of the lesion within the ventricles and inadequate lymphocyte aggregation. Therefore, differentiating RDD from other intraventricular tumors in adolescents, such as choroid plexus papillomas, ependymomas, subependymal giant cell astrocytomas, and central neurocytomas, is essential, and accurately diagnosing isolated intraventricular RDD remains a significant challenge for clinicians.

Recently, the new MRI sequences recommended for diagnosing RDD include diffusion tensor imaging, magnetic resonance susceptibility weighted imaging, and perfusion-weighted imaging (20). Meningiomas are characterized by a rich blood supply, whereas RDD shows varying degrees of vascularity (22). Therefore, magnetic resonance angiography (MRA), magnetic resonance venography (MRV), or angiography can aid in distinguishing between RDD and meningioma. However, due to the non-specific nature of clinical auxiliary examinations, accurately assessing the nature of the lesion based solely on clinical manifestations and imaging is extremely challenging, especially without prior tissue biopsy. Thus, histological diagnosis remains the gold standard for confirming RDD.

TABLE 1 Summary of the clinical features of cases with intraventricular Rosai-Dorfman disease.

Year/study	Gender/Age	Location	Clinical presentation	Surgery	Adjuvant therapy	Outcome	Follow-up
1998 (2)	F/40	Right lateral ventricle; Single lesion	Headache	Total resection	No	Asymptomatic	unknown
2015 (1)	F/2	Left lateral ventricle; Single lesion	Vomiting, fever	Subtotal resection	No	Asymptomatic	16months
2021 (15)	F/9	Bilateral lateral ventricles; Multiple lesions	Blurred vision, facial paralysis, giggle and cognitive impairment	Total resection	No	Asymptomatic	15 months
2022 (16)	M/8	Bilateral lateral ventricles; Multiple lesions	Nausea, vomiting and ataxia	Total resection	Radiotherapy/ chemotherapy	Asymptomatic	12 months
2021 (7)	M/30	The fourth ventricle; Single lesion	Vomiting, weight loss, dysphagia and vertigo	Resection	Chemotherapy	Remission	unknown
2024/This study	M/5	Right lateral ventricles; Single lesion	Seizures, headache	Subtotal resection	No	Asymptomatic	120 months

According to the extent of lesion involvement, RDD can be pathologically classified into three subtypes: nodal type, extranodal type, and mixed type involving both lymph nodes and extranodal organs (11). Low-power microscopic examination of pathological sections often reveals nodules of varying sizes with alternating pale and deeply stained areas. Eosinophilic granulocytes are rare, and histiocytes phagocytizing inflammatory cells, a phenomenon known as "emperipolesis", represent a typical pathological sign of RDD. However, about 35% of cases do not exhibit this feature due to extensive fibrous tissue and inflammatory cells obscuring typical histiocytic morphology (2, 13). When "emperipolesis" is not prominent, the diagnosis of RDD relies on specific immunohistochemical staining patterns: strong positive expression of S-100 protein and CD68, and negative expression of CD1a and GFAP in RDD histiocytes (24). The presence of inflammatory cells, predominantly composed of lymphocytes, further supports the diagnosis. Cases diagnosed as RDD on histopathology must also be differentiated from conditions such as Langerhans cell histiocytosis, lymphoplasmacyte-rich meningioma, malignant fibrous histiocytoma, chronic non-specific inflammation, and more (4). Additionally, distinguishing primary ventricular RDD from common childhood ventricular tumors like ependymoma, astrocytoma, choroid plexus papilloma, teratoma, and meningioma is crucial. In our case, presenting with headache, dizziness, and epilepsy symptoms, histopathological examination revealed sinus tissue proliferation resembling giant lymph node disease. Immunohistochemistry demonstrated strong positive staining for S-100 protein and CD68. Based on tissue morphology and immunohistochemical staining results, RDD in the ventricle was confirmed.

Due to the rarity of primary intracranial RDD, particularly ventricular RDD complicated by epilepsy, there are currently no established treatment guidelines. Surgical resection remains widely recognized as an effective therapeutic approach by most experts. Post-surgical pathological diagnosis provides crucial guidance for potential adjuvant therapies. RDD is classified as a non-neoplastic disorder, and patients who undergo complete resection generally have better prognoses. However, there is a risk of recurrence post-surgery, often correlated with the extent of resection. Therefore, complete lesion removal is recommended, accompanied by long-term patient follow-up. In recent years, some researchers have suggested that in cases where surgical resection is not feasible or as an adjunct to surgery, low-dose radiotherapy, hormone therapy, immunosuppressive therapy, or antiviral therapy may offer therapeutic benefits for RDD. However, such treatments are based on limited reported cases on CNS-RDD, necessitating further clinical validation and experience to establish their efficacy (18, 21). Moreover innovative advancements in the comprehension of molecular disturbances associated with RDD have furnished fresh insights for its therapeutic interventions (17). Specifically, alterations in the B-Raf Proto-Oncogene, Serine/Threonine Kinase (BRAF), mitogen-activated protein kinase (MAPK), A-Raf Proto-Oncogene, Serine/Threonine Kinase (ARAF), and Rat Sarcoma Viral Oncogene Homolog (RAS) pathways have been identified in RDD, presenting potential therapeutic targets (6). Several studies have demonstrated the responsiveness of RDD lesions to MAPK inhibitors, suggesting that targeting the MAPK pathways could offer a novel therapeutic strategy for RDD (7). However, further research is necessary to validate these targets in clinical trials and to explore other potential therapeutic targets within RDD.

In conclusion, this case report and literature review highlight the importance of considering RDD in the differential diagnosis of intraventricular tumors in pediatric patients. The favorable prognosis observed in intraventricular RDD cases suggests that individualized surgical interventions and vigilant postoperative monitoring can lead to excellent long-term outcomes. Future research could focus on refining diagnostic criteria and exploring potential adjuvant therapies to further improve management strategies for this rare but treatable condition.

Data availability statement

The original contributions presented in the study are included in the article/supplementary material. Further inquiries can be directed to the corresponding authors.

Ethics statement

The studies involving humans were approved by Ethics Committee of the Second Affiliated Hospital of Hainan Medical University. The studies were conducted in accordance with the local legislation and institutional requirements. Written informed consent for participation in this study was provided by the participants' legal guardians/next of kin. Written informed consent was obtained from the individual(s), and minor(s)' legal guardian/next of kin, for the publication of any potentially identifiable images or data included in this article.

Author contributions

DL: Writing – original draft, Investigation, Methodology. NL: Data curation, Writing – original draft. YBZ: Data curation, Writing – original draft. YXZ: Investigation, Writing – original draft. GD: Investigation, Writing – original draft. MW: Investigation, Writing – original draft. CZ: Writing – review & editing, Data curation. JF: Formal Analysis, Writing – review & editing.

Funding

The author(s) declare that no financial support was received for the research, authorship, and/or publication of this article.

Conflict of interest

The authors declare that the research was conducted in the absence of any commercial or financial relationships that could be construed as a potential conflict of interest.

Publisher's note

References

1. Abla O, Jacobsen E, Picarsic J, Krenova Z, Jaffe R, Emile JF, et al. Consensus recommendations for the diagnosis and clinical management of Rosai-Dorfman-Destombes disease. *Blood*. (2018) 131:2877–90. doi: 10.1182/blood-2018-03-839753

2. Andriko JA, Morrison A, Colegial CH, Davis BJ, Jones RV. Rosai-Dorfman disease isolated to the central nervous system: a report of 11 cases. *Mod Pathol*. (2001) 14:172–8. doi: 10.1038/modpathol.3880278

3. Antonius JI, Farid SM, Baez-Giangreco A. Steroid-responsive rosai-dorfman disease. *Pediatr Hematol Oncol*. (1996) 13:563–70. doi: 10.3109/08880019609030873

4. Azari-Yaam A, Abdolsalehi MR, Vasei M, Safavi M, Mehdizadeh M. Rosai-dorfman disease: A rare clinicopathological presentation and review of the literature. *Head Neck Pathol*. (2021) 15:352–60. doi: 10.1007/s12105-020-01183-7

5. Chen H, Zhou H, Song Z. Intracranial multifocal Rosai-Dorfman disease. *Neurol Neuroimmunol Neuroinflamm*. (2016) 3:e293. doi: 10.1212/NXI.0000000000000293

6. Cohen Aubart F, Idbaih A, Emile JF, Amoura Z, Abdel-Wahab O, Durham BH, et al. Histiocytosis and the nervous system: from diagnosis to targeted therapies. *Neuro Oncol*. (2021) 23:1433–46. doi: 10.1093/neuonc/noab107

7. Diamond EL, Durham BH, Ulaner GA, Drill E, Buthorn J, Ki M, et al. Efficacy of MEK inhibition in patients with histiocytic neoplasms. *Nature*. (2019) 567:521–4. doi: 10.1038/s41586-019-1012-y

8. González-Pacheco H, Salas-Villela RA, Carmona-Levario P, Manzur-Sandoval D, Mora-Cervantes R, Palma-Carbajal R, et al. Electrical storm in a patient with rosai-dorfman disease with intracardiac masses and myocardial infiltration. *Can J Cardiol*. (2020) 36:1326.e1313–15. doi: 10.1016/j.cjca.2020.03.004

9. Hingwala D, Neelima R, Kesavadas C, Thomas B, Kapilamoorthy TR, Radhakrishnan VV. Advanced MRI in Rosai-Dorfman disease: correlation with histopathology. *J Neuroradiol*. (2011) 38:113–7. doi: 10.1016/j.neurad.2010.09.002

10. Jiang Y, Jiang S. Intracranial meningeal rosai-dorfman disease mimicking multiple meningiomas: 3 case reports and a literature review. *World Neurosurg*. (2018) 120:382–90. doi: 10.1016/j.wneu.2018.09.060

11. Joshi SS, Joshi S, Muzumdar G, Turel KE, Shah RM, Ammbulkar I, et al. Cranio-spinal Rosai Dorfman disease: case series and literature review. *Br J Neurosurg*. (2019) 33:176–83. doi: 10.1080/02688697.2017.1329517

12. Jurić G, Jakić-Razumović J, Rotim K, Zarković K. Extranodal sinus histiocytosis (Rosai-Dorfman disease) of the brain parenchyma. *Acta Neurochir (Wien)*. (2003) 145:145–9. doi: 10.1007/s00701-002-1031-5

13. Kidd DP, Revesz T, Miller NR. Rosai-Dorfman disease presenting with widespread intracranial and spinal cord involvement. *Neurology*. (2006) 67:1551–5. doi: 10.1212/01.wnl.0000242893.55416.8e

14. Patwardhan PP, Goel NA. Isolated intraventricular rosai-dorfman disease. *Asian J Neurosurg*. (2018) 13:1285–7. doi: 10.4103/ajns.AJNS_134_18

15. Petrović D, Mihailović D, Petrović S, Zivković N, Mijović Z, Bjelaković B, et al. Asymptomatic flow of Rosai-Dorfman disease. *Vojnosanit Pregl*. (2014) 71:780–3. doi: 10.2298/VSP1408780P

16. Raslan O, Ketonen LM, Fuller GN, Schellingerhout D. Intracranial Rosai-Dorfman disease with relapsing spinal lesions. *J Clin Oncol*. (2008) 26:3087–9. doi: 10.1200/JCO.2007.15.7701

17. Ravindran A, Rech KL. How I diagnose rosai-dorfman disease. *Am J Clin Pathol*. (2023) 160:1–10. doi: 10.1093/ajcp/aqad047

18. Sasidharan A, Verma A, Epari S, Gupta T, Laskar S, Khanna N, et al. Symptomatic intracranial Rosai-Dorfman disease in the suprasellar region treated with conformal radiotherapy - A report of two cases and literature review. *Neurol India*. (2020) 68:489–92. doi: 10.4103/0028-3886.284371

19. Wang C, Kuang P, Xu F, Hu L. Intracranial Rosai-Dorfman disease with the petroclival and parasellar involvement mimicking multiple meningiomas: A case report and review of literature. *Med (Baltimore)*. (2019) 98:e15548. doi: 10.1097/MD.0000000000015548

20. Wang Q, Bradley K, Zhang M, Li S, Li X. Rosai-Dorfman disease of the breast: a clinicoradiologic and pathologic study. *Hum Pathol*. (2023) 141:30–42. doi: 10.1016/j.humpath.2023.08.009

21. Wang W, Sun J, Zhang W, Zhou D. Successful treatment of intracranial Rosai-Dorfman disease with cytarabine and dexamethasone: case report and review of literature. *Ann Hematol*. (2020) 99:1157–9. doi: 10.1007/s00277-020-03999-3

22. Woodcock RJ Jr., Mandell JW, Lipper MH. Sinus histiocytosis (Rosai-Dorfman disease) of the suprasellar region: MR imaging findings–a case report. *Radiology*. (1999) 213:808–10. doi: 10.1148/radiology.213.3.r99dc30808

23. Zhang X, Yin W, Guo Y, He Y, Jiang Z, Li Y, et al. Rosai-Dorfman disease of the central nervous system: A clinical, radiological, and prognostic study of 12 cases. *Front Oncol*. (2022) 12:1013419. doi: 10.3389/fonc.2022.1013419

24. Zhou B, Suster DI, Langer PD. Rosai-dorfman disease. *Ophthalmology*. (2023) 130:725. doi: 10.1016/j.ophtha.2022.08.009

Frontiers in Oncology

Advances knowledge of carcinogenesis and tumor progression for better treatment and management

The third most-cited oncology journal, which highlights research in carcinogenesis and tumor progression, bridging the gap between basic research and applications to imrpove diagnosis, therapeutics and management strategies.

Discover the latest Research Topics

See more →

Frontiers

Avenue du Tribunal-Fédéral 34
1005 Lausanne, Switzerland
frontiersin.org

Contact us

+41 (0)21 510 17 00
frontiersin.org/about/contact